NOTICE

The quality of this microform is heavily dependent upon the quality of the original thesis submitted for microfilming. Every effort has been made to ensure the highest quality of reproduction possible.

If pages are missing, contact the university which granted the degree.

Some pages may have indistinct print especially if the original pages were typed with a poor typewriter ribbon or if the university sent us an inferior photocopy.

Reproduction in full or in part of this microform is governed by the Canadian Copyright Act, R.S.C. 1970, c. C-30, and subsequent amendments.

AVIS

La qualité de cette microforme dépend grandement de la qualité de la thèse soumise au microfilmage. Nous avons tout fait pour assurer une qualité supérieure de reproduction.

S'il manque des pages, veuillez communiquer avec l'université qui a conféré le grade.

La qualité d'impression de certaines pages peut laisser à désirer, surtout si les pages originales ont été dactylographiées à l'aide d'un ruban usé ou si l'université nous a fait parvenir une photocopie de qualité inférieure.

La reproduction, même partielle, de cette microforme est soumise à la Loi canadienne sur le droit d'auteur, SRC 1970, c. C-30, et ses amendements subséquents.

Canada

NL-339 (r. 88/04) c

PETROCHEMISTRY OF THE WOODBURN LAKE GROUP KOMATIITIC SUITE, AMER LAKE, N.W.T., CANADA

By

Irvine R. Annesley

A Thesis
submitted to the School of Graduate Studies and Research
in Partial Fulfillment of the requirements
for the Degree of Doctor of Philosophy at
The University of Ottawa

Ottawa, Canada

NOTICE

The quality of this microform is heavily dependent upon the quality of the original thesis submitted for microfilming. Every effort has been made to ensure the highest quality of reproduction possible.

If pages are missing, contact the university which granted the degree.

Some pages may have indistinct print especially if the original pages were typed with a poor typewriter ribbon or if the university sent us an inferior photocopy.

Reproduction in full or in part of this microform is governed by the Canadian Copyright Act, R.S.C. 1970, c. C-30, and subsequent amendments.

AVIS

La qualité de cette microforme dépend grandement de la qualité de la thèse soumise au microfilmage. Nous avons tout fait pour assurer une qualité supérieure de reproduction.

S'il manque des pages, veuillez communiquer avec l'université qui a conféré le grade.

La qualité d'impression de certaines pages peut laisser à désirer, surtout si les pages originales ont été dactylographiées à l'aide d'un ruban usé ou si l'université nous a fait parvenir une photocopie de qualité inférieure.

La reproduction, même partielle, de cette microforme est soumise à la Loi canadienne sur le droit d'auteur, SRC 1970, c. C-30, et ses amendements subséquents.

ISBN 0-315-60553-7

UNIVERSITÉ D'OTTAWA
UNIVERSITY OF OTTAWA

ABSTRACT

Several metavolcanic-metasedimentary belts containing komatiites have been found in the Baker Lake region, N.W.T. In particular, a sequence of flows of komatiitic composition within the Woodburn Lake Group (WLG) show well preserved flow tops, polyhedral jointing, and spinifex textures, confirming their volcanic origin. The Woodburn Lake Group consists of a lower 2.8-3.0(?)Ga predominantly volcanic greenstone sequence and an upper platformal quartzite sequence. The lowermost rocks of the volcanic sequence comprise an essentially bimodal assemblage of komatiites-komatiitic basalts and dacites-rhyolites; intermediate rocks are rare. The uppermost rocks reflect a change in volcanic activity from komatiitic-tholeiitic to calc-alkaline in nature. This change is accompanied by an increase in sedimentation. The supracrustal succession is presently preserved as narrow linear belts within Late Archean (2.6 Ga) granitic to granodiorite plutons. Although there is no recognized pre-greenstone basement, the upper quartzite sequence suggests the presence of older sialic crust nearby.

The komatiites and komatiitic basalts (including high-Mg tholeiites) have been altered by greenschist grade regional metamorphism with complete replacement of primary mineralogy, but with excellent preservation of primary textures. The typical mineralogy of the komatiites is tremolite - antigorite - chlorite - Cr-magnetite and of the komatiitic basalts is amphibole -

chlorite - magnetite - plagioclase - epidote - quartz. The grade of metamorphism increases toward the margins of the WLG belts to amphibolite grade as a result of contact metamorphism by younger granitoids. Olivine-spinel geothermometry gives a temperature of 625°C for contact metamorphism of the komatiites.

Chemical variation diagrams of the komatiitic suites reflect variable degrees of element remobilization during alteration. Al, Ti, V, Cr, Ni, and Sc were immobile, whereas Na, K, Ca, Rb, Sr, and LREE exhibit variable mobility. Most ratios of incompatible elements (i.e. Zr, and LREE) show moderate to strong depletion of these elements in the komatiites and strong enrichment in the komatiitic basalts. The WLG komatiites are typical of the aluminum-undepleted type that characterizes Late Archean terrains. The WLG komatiitic basalts are geochemically similar to those from Kambalda (Australia), the Abitibi Greenstone Belt, and modern-day volcanic arcs.

Fractional crystallization explains the compositional variations within individual volcanic units, but does not explain adequately the differences between komatiites and komatiitic basalts. The Kambalda komatiitic basalts have been interpreted as resulting from crustal contamination and fractional crystallization of komatiitic magmas within an intra-continental setting. Quantitative modelling suggests derivation of the WLG komatiitic basalts by 20-40% crustal contamination of komatiitic magmas. Alternatively, the geochemical similarity to modern-day arc volcanics suggests an arc-related origin for the komatiitic

basalts.

REE patterns and inter-element ratios indicate that the mantle source region of the WLG komatiites underwent an early melting event, leaving it depleted in Zr and LREE. 30 to 40% partial melting of this source (assumed to be garnet lherzolite in composition) generated the komatiitic liquids.

The WLG is compositionally and lithologically similar to the Prince Albert Group and hence probably correlative.

Origin of the komatiitic suite in a continental margin arc-type environment is the favoured interpretation but an ensialic rifting model cannot be ruled out.

To Catherine

and

my parents

ACKNOWLEDGEMENTS

First and foremost I would like to thank Bill Heywood of the Geological Survey of Canada (G.S.C.) for introducing me to the geology of the Amer Lake map area and initiating this project. I am extremely greatful to Bill, Fred Taylor (G.S.C.), and Al Fraser (G.S.C.) for providing logistical support and encouragement throughout the duration of the field work. The competent field assistance of Maria Besso (1980) was much appreciated.

For the exchange of ideas in the field I would like to thank Bill Heywood, Mikkel Schau (G.S.C.), Fred Taylor, Al Fraser, Subhas Tella (G.S.C.), and most of all Ken Ashton (Queen's University). I was fortunate to have Ken show me some of his findings in proximity to the komatiites.

Next, I would like to thank my initial thesis supervisor, Calvin Pride of the University of Ottawa (U.O.), for providing financial support, exchanging ideas, and reviewing early parts of the text. Also, much gratitude is expressed to Ralph Kretz (U.O.), who inherited my project when Calvin Pride left the University of Ottawa for another career. Ralph Kretz improved the quality of this work and provided financial assistance for laboratory work. I acknowledge Ron Hartree (U.O.) who provided guidance for whole-rock chemical analyses by XRF and INAA. John Loop (U.O.) provided much advice and assistance in the determination of the REE by DCP-AES.

Subhas Tella, Mikkel Schau, and Andre Ciesielski arranged for the geochemical analyses determined at the G.S.C. laboratory. Subhas and Bill Heywood kindly provided access to field notes and maps. Ken Ashton graciously made available fields notes and maps, and geochemical data. Tony LeCheminant (G.S.C.) generously provided samples from the Aberdeen Lake region, and arranged for electron microprobe analyses of olivine and spinel.

Dave Kempson initiated me to the microprobe at Queen's University, and provided supervision during the microprobe work.

For discussion and review of parts or all of the text I would like to thank Fred Taylor, Ken Card (G.S.C.), Tom Frisch (G.S.C.), Mikkel Schau, Don Hogarth (University of Ottawa), Tony Fowler (U.O.), Ralph Kretz (U.O.), and Bob Baragar (G.S.C.). At this moment, I would like to extend my gratitude to Bob Baragar who endured the duration of the thesis and never lost patience with me. His suggestions made me reconsider some of my original ideas.

A special note of thanks goes to Jim Maley (formerly G.S.C.) who helped with computer aspects of the work. I acknowledge Sara Jane Barnes (University of Toronto) for providing some komatiite samples to monitor the determination of the REE analyses. Thanks to Subhas Tella for arranging the photoreduction of figures. Karyne Besso and Catherine Madore helped with drafting, and Catherine Madore typed parts of the final thesis draft. Acknowledgment and thanks are extended to the Geological Survey of Canada and the University of Ottawa for providing

laboratory facilities and financial support. Any shortcomings of the thesis lie solely with the author.

TABLE OF CONTENTS

LIST OF FIGURES

Figure

LIST OF TABLES

Table

LIST OF APPENDICES

Appendix

INTRODUCTION

1.1 STUDY AREA

The study area lies in the southeast quadrant (66H/1,2,7,8) of the Amer Lake map sheet, District of Keewatin; approximately 100 km north of Baker Lake, N.W.T. (Fig. 1). The size of the study area is approximately 50 km x 48 km. The area is readily accessible only by helicopter or small aircraft.

Rock exposure varies greatly from sporadic to nearly complete. Physiographically, the area is part of the barrenlands having subdued topography, treeless vegetation, numerous lakes, abundant intermittent streams, and a few major river systems. The climate of the region is severe and changes dramatically from season to season. The winters are long, cold, windy, dry, and sunless; the summers are short, warm, relatively wet, and nightless.

1.2 PREVIOUS STUDIES

Operation Baker, a reconnaissance mapping project (Wright, 1955 and 1967), outlined several NE-trending linear belts of mafic to ultramafic supracrustal rocks in the Amer Lake area. Later mapping between 1976 and 1981 (Heywood, 1977; Ashton, 1981 and 1982; Annesley, 1981a and 1981b; Tella and Heywood, 1983; Fraser, 1988) examined and defined these belts in detail and

Figure 1. Location map of thesis area. The black box indicates the SE corner of Amer Lake map area.

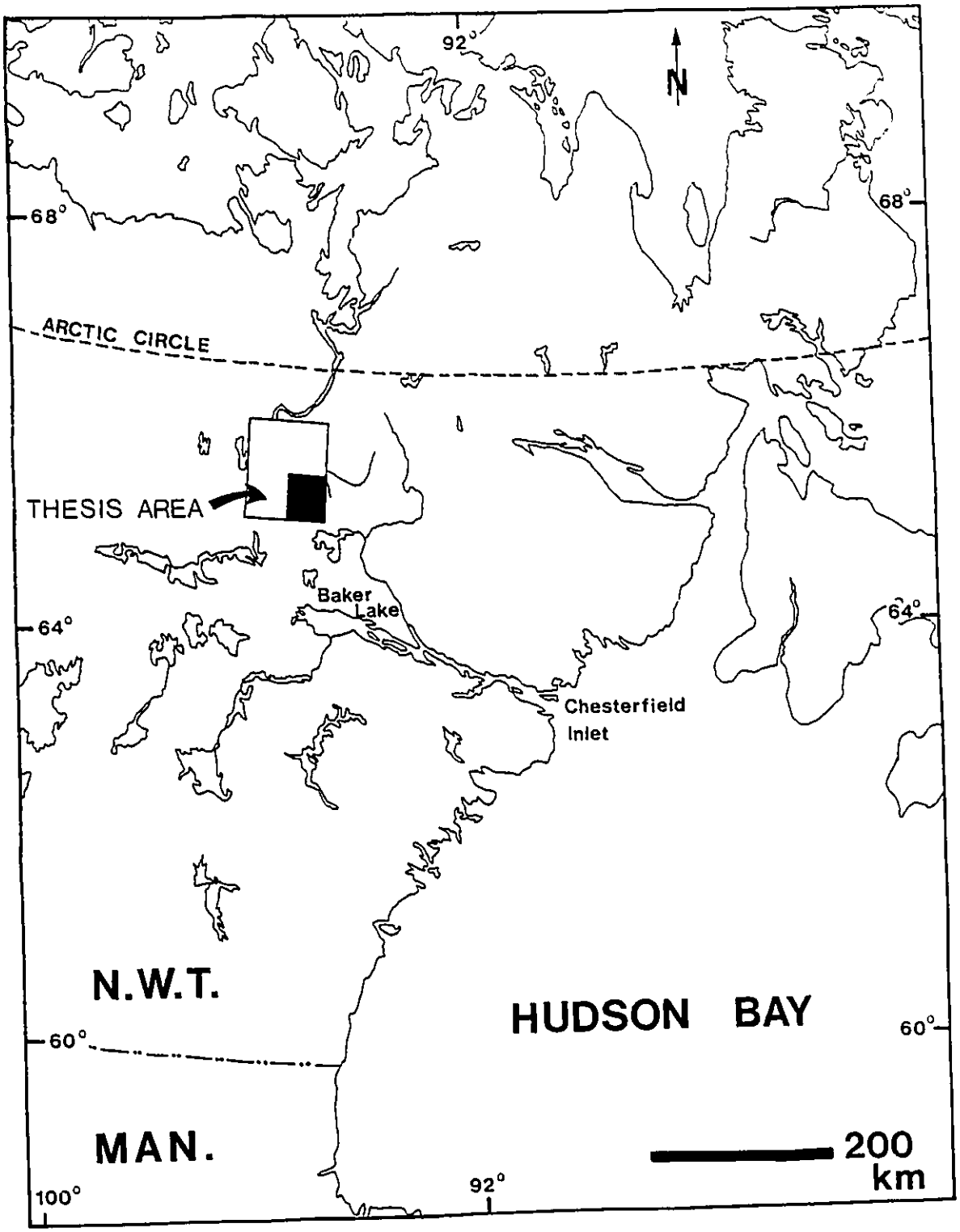
92°
N
68°
68°
ARCTIC CIRCLE
THESIS AREA
Baker Lake
64°
64°
Chesterfield Inlet
N.W.T.
HUDSON BAY
60°
60°
MAN.
200 km
100°
92°

documented the spectacular occurrences of spinifex-textured komatiites in the area. Figure 2 shows the location of these belts in the Amer Lake map sheet.

Ashton (1982) has named the supracrustal sequence that forms these belts the Woodburn Lake Group and has provided a description of the geology surrounding the komatiite occurrences within the Pipedream Lake belt. His work (Ashton, 1988), which focuses on the stratigraphy, age relationships, and correlation with units in adjacent regions, complements the present studies.

Annesley (1981a, 1981b) demonstrated the komatiitic nature of the mafic and ultramafic rocks in the SE Amer Lake area with a detailed description of their field characteristics, petrography, and major-trace element geochemistry. Most of the mafic and ultramafic rocks, recognized by the author, in the Pipedream Lake belt (Figs. 2 and 3) are of extrusive origin and are of similar mineralogy, morphology, textures, and geochemistry to mafic and ultramafic komatiitic flows seen within other Archean metavolcanic-metasedimentary belts (i.e. greenstone belts) such as the Abitibi Belt (Pyke et al., 1973). Two other belts in the Amer Lake area, informally named Esker Lake and No-name Lake, as well as part of the Woodburn Lake Group, consist of generally featureless, fine-grained mafic to ultramafic rocks of lower to middle amphibolite grade. These rocks show faint color banding and polyhedral jointing similar to the lava flows of the Pipedream Lake belt and are also considered to be of extrusive origin. Other occurrences of komatiites have been discovered

Figure 2. Location map of the metavolcanic-metasedimentary belts of the Woodburn Lake Group within the SE corner of the Amer Lake map area. See Figure 5 for geological map of this region.

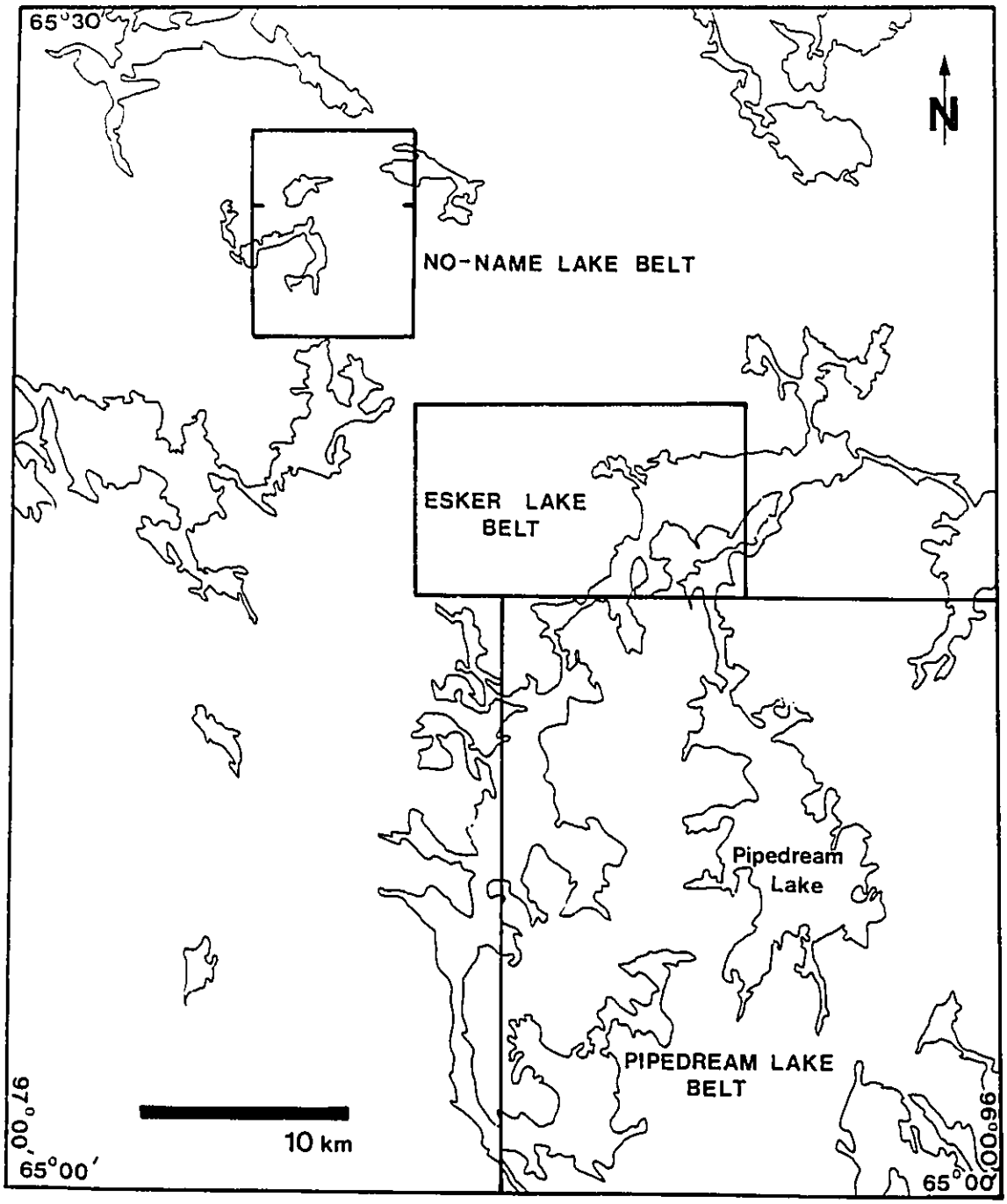
65°30'
N
NO-NAME LAKE BELT
ESKER LAKE BELT
Pipedream Lake
PIPEDREAM LAKE BELT
10 km
97°00'
96°00'
65°00'
65°00'

Figure 3. Location map of komatiitic rocks (black areas) in the southeast corner of the Amer Lake map area. Data from Heywood (1977), Annesley (1981a and 1981b), Ashton (1981 and 1982), Tella and Heywood (1983), and field work by Annesley (1978, 1980, 1981).

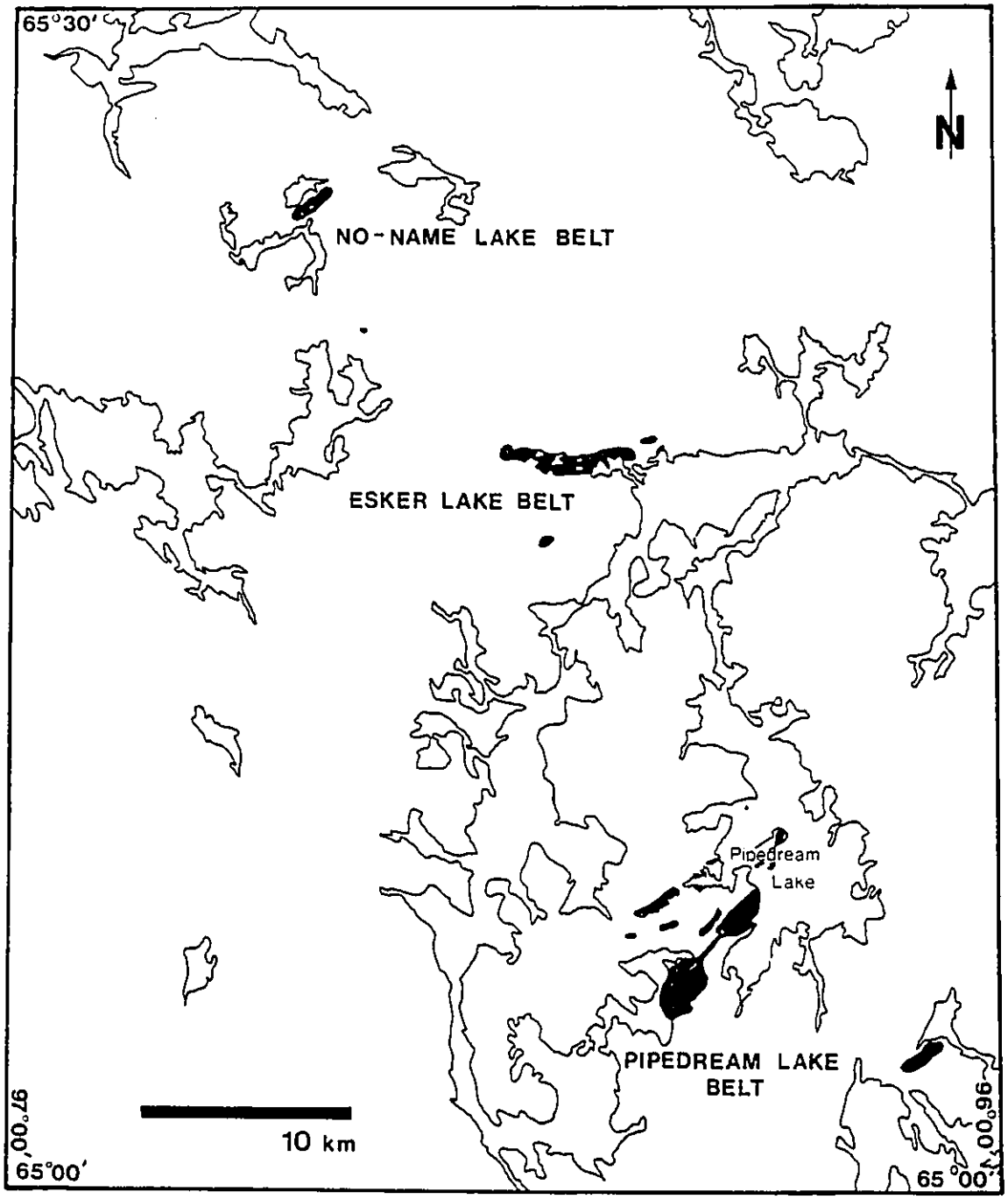
65°30'
N
NO-NAME LAKE BELT
ESKER LAKE BELT
Pipedream
Lake
PIPEDREAM LAKE
BELT
10 km
97°00'
65°00'
96°00'
65°00'

recently in adjacent map areas (Heywood and Schau, 1981; Taylor, 1985; Fraser, 1988; A.N. LeCheminant, pers. comm.) and these are thought to be stratigraphically equivalent . Fraser (1988) extended the Pipedream Lake belt and the Esker Lake belt a few kilometers eastward into the Woodburn Lake map sheet (56E/4,5).

Preliminary petrochemical studies were carried out by Annesley (1981b) on the komatiites of the Woodburn Lake Group; the present work was undertaken in order to resolve unanswered questions arising from the previous work and can be considered a detailed follow-up study of the komatiites of the Amer Lake area.

1.3 STATEMENT OF THE NATURE AND PURPOSE OF THE STUDY

Viljoen and Viljoen (1969a and b) recognized mafic and ultramafic lava flows in the Barberton Mountain Land, South Africa, and introduced the term komatiite to name this unusual group of rocks (i.e. a rock suite or class of rocks with a wide range of chemical compositions). They also introduced the terms, peridotitic komatiites and basaltic komatiites, to name and classify the volcanic rock types of this "komatiitic" suite. More recently, Arndt and Nisbet (1982a) suggested that the terminology of komatiites be more definitive. They proposed that the term komatiite(s) be simply redefined as an ultramafic volcanic rock(s), instead of the term being used to define a group name or magma series of komatiitic affiliation. Also, the magma series would be defined as the "komatiitic suite" and any

associated rocks would have the prefix "komatiitic" attached to their names. An excellent review (see section 4.3 for a summary) of the nomenclature of komatiites is presented in the Basaltic Volcanism Study Project (1981, p.6) and Arndt and Nisbet (1982b). Since their recognition, numerous detailed field, geochemical, isotopic, and geochronological studies have focussed on komatiites and their associated rocks (i.e. komatiitic basalts or basaltic komatiites) in an effort to understand their origin and evolution. Excellent summaries of this work are included in papers by Arndt et al. (1979), Nesbitt et al. (1979), and Arndt and Nisbet (eds., 1982). Several interesting theories have arisen from these studies, the most noteworthy being those involving the age, source material, and tectonic setting implications of komatiites.

Komatiites are generally thought to originate by large-scale partial melting of mantle material under high geothermal gradients (Viljoen and Viljoen, 1969a and b; Green, 1975; Green et al., 1975; Sun and Nesbitt, 1978; Nesbitt et al., 1979; Jahn et al., 1982; Nesbitt et al., 1982). The degree and type of partial melting, the composition of the source and residue, the temperature (T), pressure (P), and H_2O (i.e. quantity of) conditions during partial melting, the degree of modification of partial melt composition before, during, and after emplacement by various magmatic and postmagmatic processes, the tectonic setting, and the relevance of age in the formation of komatiites are all controversial (Jahn et al., 1980; Bickle, 1982; Allègre,

1982; Nisbet, 1982; Nesbitt et al., 1982; Jahn et al., 1982; Arndt, 1983; Nisbet and Fowler, 1983; Warren, 1984; Arndt, 1986b). Komatiites have been considered unique to the Archean until comparatively recently when Proterozoic and Phanerozoic examples have been found (Ganssar et al., 1979; Echeverria, 1980a and b; Schwarz and Fujiwara, 1977; Francis and Hynes, 1979; Baragar and Lamontagne, 1980). Still, they are considered to be largely an Archean phenomenon (Nesbitt et al., 1982). This unusual age distribution may be related to different tectonic and thermal conditions operating in the Archean (Nesbitt et al., 1982; Nisbet and Fowler, 1983; Arndt, 1983; Herzberg, 1983; Warren, 1984). Consequently, geochemical and petrological studies of komatiites may provide implications concerning the Earth's early evolutionary history. Even with the constraints given by komatiite petrogenesis, considerable controversy continues regarding the nature of processes operating in the Archean.

Various opinions are held about the evolution of Archean supracrustal sequences between 3.8 and 2.5 Ga. Over the years two major opposing hypotheses - ensimatic vs. ensialic - have surfaced regarding the origin and evolution of Archean metavolcanic-metasedimentary belts. Early models based upon ambiguous field evidence advocated an ensimatic origin similar to modern oceanic crust (Engel, 1968; Burke and Dewey, 1973; Glikson, 1972; Anhaeusser, 1971a and b, and 1973; Arth and Hanson, 1975; Glikson and Lambert, 1976; Condie and Hunter, 1976). Recently, De Wit (1986) and De Wit et al. (1986, 1987)

suggested that part of the Onverwacht Group in the Barberton Mountain Land represents an Archean ophiolite complex (i.e. Archean ocean floor). Since the early 1970's, more detailed mapping has revealed, in most Archean provinces, some metavolcanic-metasedimentary belts resting, seemingly directly, on older sialic crust (Bickle et al., 1975; Baragar and McGlynn, 1976; Henderson and Easton, 1977; Schau, 1982; among others). This field evidence has led to models in which early Archean volcanic rocks, including komatiites, erupted through sialic crust in an extensional environment. Variants of these hypotheses have emerged from time to time, but none have really gained general acceptance (Windley, 1977 and 1984; Condie, 1981 and 1982; Kroener, 1981, 1984 and 1985). This perplexing problem has resulted because well-preserved basement-supracrustal relationships have been recognized only for a few metavolcanic-metasedimentary belts (e.g. Belingwe Greenstone Belt and Yellowknife Greenstone Belt). The primary field relationships between the metavolcanic-metasedimentary belts and the gneissic granitoid rocks enclosing them, in most instances, have been masked or destroyed by deformation due to folding, faulting, and younger intrusions. Komatiites found within some of these belts, also, did not escape this strong deformation. Consequently, the lack of good preservation of komatiites in the early Archean has led to controversy over their alteration, classification, origin, and evolution.

The purpose of the present study is to elucidate the

petrogenesis of the Amer Lake komatiites, and to contribute to the resolution of problems concerning komatiite petrogenesis in general. This entails a comprehensive geochemical study in which the processes and effects of magmatic and postmagmatic conditions are examined and evaluated. Understanding and seeing through the postmagmatic changes (i.e. sea-water alteration, regional and contact metamorphism, and metasomatism) is an essential prerequisite to the identification of the range of primary mineralogical and chemical compositions typical of komatiites, and also to the classification of komatiites. The ability to identify and separate primary chemical trends from those resulting from postmagmatic processes will allow the establishment of rigid criteria necessary for the recognition of komatiites that have been variably metamorphosed and deformed. This in turn will permit valid comparisons of Archean komatiites and their associated volcanics with postulated modern-day equivalents. Ultimately, this will lead to an understanding of komatiite petrogenesis through time.

The chemical trends caused by alteration processes can only be identified and distinguished from those of magmatic processes if entire flow units and sequences of komatiites are systematically sampled and statistically analysed in areas of differing metamorphic grade. Samples must be examined carefully for specific alteration processes and for consistent/inconsistent compositional variations, within and between individual flows, in any effort to discriminate between primary and secondary chemical

trends. Ultimately, this leads to testing the extent of open system redistribution of elements. The Amer Lake area komatiites, found within belts showing different degrees of deformation and metamorphism, offer an excellent opportunity for solving some of these problems.

In summary, the main objectives of the present petrogenetic study are:

1) To carry out a comprehensive petrographic and geochemical study of the Woodburn Lake Group komatiites and some of the associated metavolcanic rocks.

2) To examine the present mineralogical and chemical composition of the komatiites in an effort to discriminate between primary magmatic processes and secondary alteration processes, and hence to determine the original magmatic composition of the rocks. This entails establishing the effects of alteration on the original composition, and possibly introducing new criteria for seeing through post-magmatic processes.

3) To examine the metamorphic history of the Woodburn Lake Group komatiites.

4) To compare the results and interpretations to those of other komatiite investigations.

5) To establish the petrogenesis of the Woodburn Lake Group komatiites and associated metavolcanics by correlating the primary chemical trends with their respective magmatic processes.

6) To propose possible tectonic environment(s) of komatiitic volcanism.

7) To discuss upper mantle compositions and conditions during the Archean and to compare the conditions of the Archean mantle beneath the Churchill Province to those of other Archean provinces.

REGIONAL GEOLOGY

2.1 GENERAL GEOLOGY

The study area lies in the south-central part of the northwestern Churchill Province which is a vast terrain of Precambrian rocks consisting of a great variety of lithologic units (Heywood, 1961 and 1967; Fraser, 1964; Wright, 1955 and 1967; Davidson, 1972; Heywood and Schau, 1978; Lewry et al., 1985). The geology of this region is known mainly from reconnaissance mapping; hence much of its character and evolution is poorly understood and constrained. However, the data base does indicate that the rocks have a complex history of polyphase deformation and low to high grade metamorphism, thought to be principally the product of the Early Proterozoic Hudsonian Orogeny about 1700-1900 Ma ago (Stockwell, 1982). This geological complexity has led to problems in unravelling the extent and exact nature of reworked Archean in the Churchill Province. Moore (1977), on the basis of limited geochronological data, suggested that both Archean basement and Early Proterozoic reworking was involved in the early evolution of the Churchill Province. A substantial increase of regional and detailed mapping in the last fifteen years has produced a more coherent picture of the Churchill Province. However, the character, evolution, and extent of the Archean basement and the Early Proterozoic Hudsonian Orogeny remains speculative and unresolved. The

division into Archean and/or Aphebian remains in many places questionable. More detailed studies and additional geochronological data are greatly needed to resolve the Archean and Proterozoic events of the Churchill Province.

The Churchill Province has been divided into subprovinces on the basis of lithologic-tectonic characteristics. These subprovinces have been called: fold belts, blocks, domains, zones, tectonic belts, basins, and by other designations (Davidson, 1972; Heywood and Schau, 1978; Lewry et al., 1985; amoung others). The present nomenclature and boundaries of the Churchill Province are tentative and somewhat controversial.

Heywood and Schau (1978) subdivided the northern part of the Churchill Province into three blocks - Queen Maud, Committee Bay, and Armit Lake - separated by major fault and mylonite zones. They suggested that the lithologic-tectonic features of each of the blocks are indicative of the different levels of the crust being exposed. They also suggested that predominant Hudsonian overprinting of the area can be explained by blockage of argon diffusion in mica during uplift of the blocks or during widespread shearing in the blocks. Fraser (1978) added a fourth block, the East Arm (i.e. Talston Block of Lewry et al., 1985), in the northwestern Churchill Province, to the lithologic-tectonic classification. A summary of the lithologic and/or tectonic similarities and differences defining these blocks is given in Tables 1a and 1b (from Heywood and Schau, 1978, and Fraser, 1978), respectively. The terrain of these four

Table 1a. Lithologic-tectonic characteristics of the Queen Maud, Committee Bay and Armit Lake blocks (from Heywood and Schau, 1978).

Table 1a (from Heywood and Schau, 1978)

Summary of main features of the Queen Maud, Committee Bay and Armit Lake blocks

	QUEEN MAUD BLOCK	COMMITTEE BAY BLOCK	ARMIT LAKE BLOCK
Paleozoic cover	Extensive in northeastern sector	Extensive in eastern sector	Extension in eastern sector
Diabase dykes	Rare, few in southern area	Common, widely spaced, continuous for tens to hundreds of kilometres	Rare, widely spaced
Granite, porphyritic (Nueltin type)	On eastern and western margins	Most in northeast trending zone in central part	Most common on eastern margin
Paleohelikian cover	Southeastern margin	At extreme northeast and southwest?	Western margin
Granite and gneiss	Local granite plutons. Local development of gneiss in Chantrey group	Gneiss developed from Penrhyn Group and preceding rocks. Local plutons. Augen gneiss developed from preceding plutons	Possible late pluton
Aphebian metasediment	Not reported	Chantrey, Amer, Hurwitz, Penrhyn groups	Hurwitz Group northeast of Baker Lake
Archean gneisses?	Archean? granites, gneisses and agmatites	Gneisses developed from Prince Albert Group and underlying gneisses. Intruded by large batholiths	Gneisses, in part of metasedimentary origin, granitic plutons
Anorthosite	Layers associated with gneisses	Small pods, deformed but appear discordant to Prince Albert Group and basement gneisses Possibly related to some gabbros.	Small stocks, deformed but discordant, at Baker Lake, Daly Bay, Walrus Island, Coats Island
Gabbro	Stocks, sills, dykes; possibly several ages	Small pods of several ages. Large sill-like bodies with anorthosite layers in eastern part	Small stocks of several ages, some large bodies with ultramafic affinities
Archean metasediments	Archean paragneiss and associated lime silicate gneiss	Prince Albert Group	Possibly granulites near Baker Lake. Quartzite of probable Archean age
Peridotite	Hornblendite associated with gneisses	Komatiite flows, sills, dykes in Prince Albert Group and derived gneisses; intrude older gneisses	Segregations in granulite terrane near Baker Lake
Basement gneisses	Layered grey gneiss, charnockitic gneiss	Grey gneiss, granite gneiss	Possibly charnockitic gneiss in Baker Lake area
Structural complexity	Insufficient data	Hudsonian deformation (possibly two) in Foxe Fold Belt; Kenoran deformation preserved in Committee fold belt; Pre-Prince Albert Group preserved in small areas	Hudsonian deformation? Kenoran deformation? Pre-Kenoran deformation?
Metamorphism general grade	Granulite and upper amphibolite facies, less commonly lower amphibolite	Predominantly amphibolite facies, ranges from greenschist to granulite	Amphibolite to granulite facies, granulite especially near northern and southern boundaries
Average chemical composition	Insufficient data. Small area same as average composition for shield gneiss	Similar to average gneiss composition of the Shield	Insufficient data
Gravity regional	Generally negative with Perry River Low and Boothia Peninsula high	Generally negative. High on Melville Peninsula over granulites and low over northeast trending granite belt. Wager Bay low is over Nueltin type granite	Negative at north and positive at south boundaries. Highs at Coral Harbour, Baker Lake, Daly Bay and Boas River. First three with granulite and anorthosite
Aeromagnetics regional	Generally above average for region strong linear pattern 100 km wide near Thelon Front	Generally below average for region	Generally above average, especially near margins
Radiometric data range (A-1.42)	K/A 1710-1880 m.y. mainly greater than 1710 m.y.	K/A 1500-2200 m.y. mainly 1600-1700 m.y. Rb/Sr 2280-2590 m.y.? Zr 2560-3060 m.y.	K/A 1660-1860 m.y. Rb/Sr 2070-3160 m.y.; 1730 m.y. on Dubawnt cover Zr 2660 m.y.
Topography	Back River Lowlands	Wager Plateau	Wager Plateau
LEVEL OF CRUST	"DEEP LEVEL CRUST"	"HIGH TO INTERMEDIATE LEVEL CRUST"	"INTERMEDIATE TO DEEP LEVEL CRUST"
Mapping	Reconnaissance scale only	Reconnaissance with detail in Hayes River-Kellett River, Mackar Inlet, Kingora River and the Penrhyn Group of Melville Peninsula	Reconnaissance with detail at Daly Bay, east end of Baker Lake, Amer Lake and Schultz Lake

Table 1b. Lithologic-metamorphic charteristics of the northwestern Churchill Province (from Fraser, 1978).

Table 1b(from Fraser, 1978)

Lithologic units and metamorphic events in the northwestern Churchill Province. Precise correlation between entries in adjacent columns is not implied.

	East Arm	Armit Lake	Queen Maud
Helikian	Mackenzie diabase dykes	Mackenzie diabase dykes	Mackenzie diabase dykes
		Northerly trending diabase dykes	Northerly trending diabase dykes
		Dubawnt Group	Dubawnt Group
	Et-then Group	Nonacho Group	
	TRANSCURRENT FAULTING	TRANSCURRENT FAULTING – MYLONITIZATION	TRANSCURRENT FAULTING – MYLONITIZATION
Aphebian	Diorite-monzonite laccoliths	Granite	Granite
	Great Slave Supergroup		
	East-northeast-trending diabase dykes	Northeast-trending diabase dykes	Northeast-trending diabase dykes
	MYLONITIZATION	MYLONITIZATION	MYLONITIZATION
	METAMORPHISM	METAMORPHISM	METAMORPHISM
	Wilson Island Group	Easterly trending mafic dykes	Easterly trending mafic dykes
Archean	Adamellite	Granite Anorthosite, gabbro	Granite Anorthosite, gabbro, norite
	METAMORPHISM	METAMORPHISM	METAMORPHISM
	Gneisses and migmatite	Tazin Group	Yellowknife Supergroup
		METAMORPHISM?	METAMORPHISM?

blocks consists mainly of Archean basement with abundant early Proterozoic granitoids and scattered Aphebian supracrustal successions.

Recently, Lewry et al. (1985) reviewed the major lithotectonic features of the western Churchill Province (i.e. west of Hudson Bay). They subdivided the northwestern Churchill Province into crustal blocks from interpretation of work by the Geological Survey of Canada and extrapolation from the southwestern Churchill Province. This subdivision is at odds with that proposed by Eade (1986) for the Southern District of Keewatin (i.e. south-central part of the northwestern Churchill Province). The work of Eade (1986) and Tella and Eade (1986) demonstrated that the Archean craton of the south-central part of the northwestern Churchill Province is divided into two major parts by the northeast-trending Tulemalu Fault Zone. Tella and Eade (1986) postulated that this major break is an extension of the Black River-Virgin River fault zones. Recently, Hoffman (1987a and b) has used this major crustal break as a province boundary zone in his interpretation of relations in the North American craton. Hoffman (1987a and b) subdivided the northwestern Churchill Province into the Rae (which includes the Queen Maud, Armit Lake, and Committee Bay blocks) and the Hearne Provinces on the basis of distinct sets of Archean greenstone belts within each province (see Fig.4).

Until comparatively recently, the only Archean rocks

Figure 4. Subdivision of the central northern Churchill Province (modified after Hoffman, 1987a and 1987b).

Solid black areas represent the Prince Albert, Woodburn Lake, and Ketyet River Groups.

Area with inverted V's signifies the Queen Maud uplift (part of Rae Province).

Area with inclined line-dot pattern indicates the Rae Province.

Area with horizontal line pattern represents the Hearne Province.

Area with stippled pattern indicates Proterozoic sedimentary fold belts south of the Rae and Hearne Provinces.

Solid black lines with or without arrows signify major crustal breaks.

Solid black "saw tooth" lines indicate low angle shear zones.

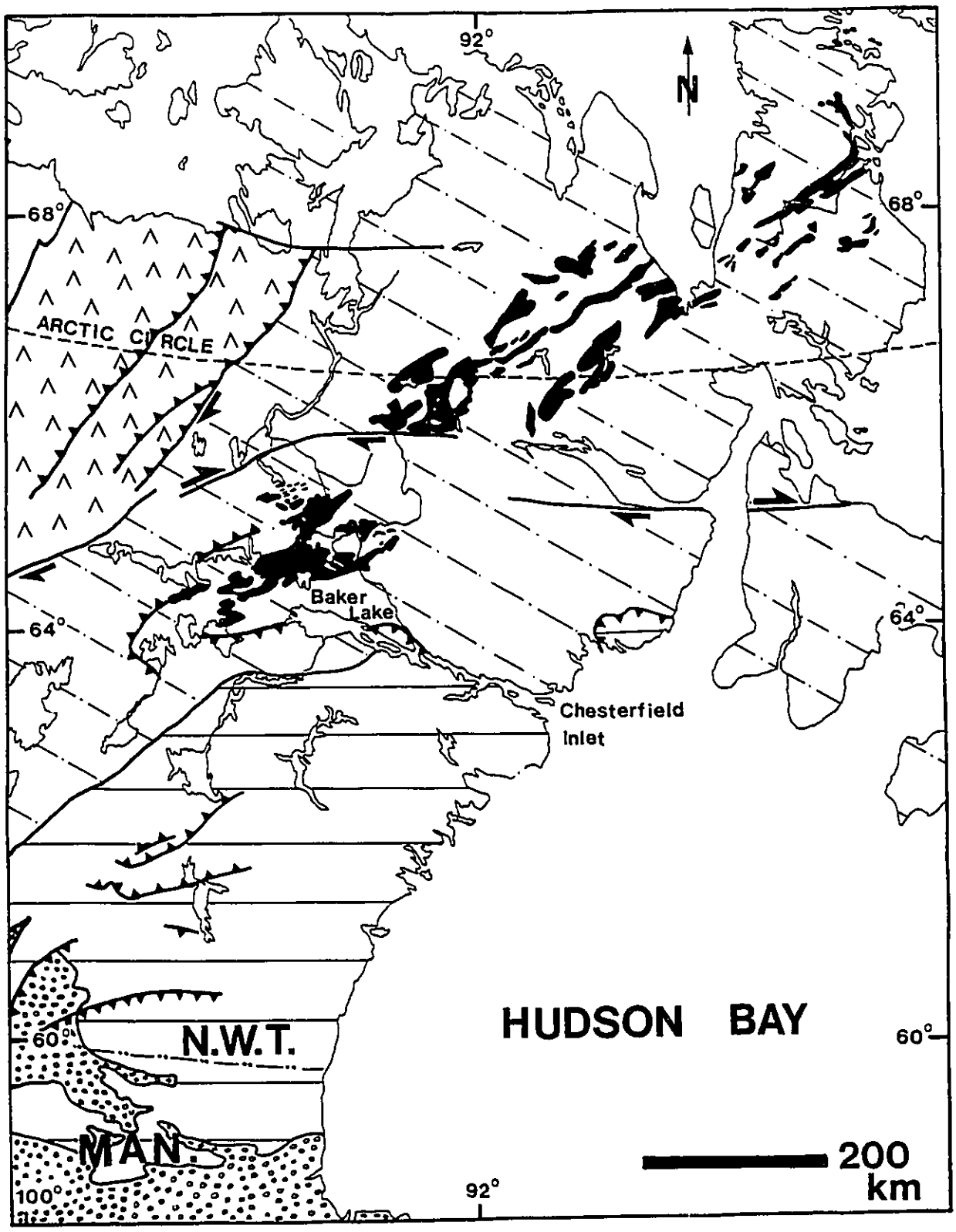
92°
N
68°
68°
ARCTIC CIRCLE
Baker
Lake
64°
64°
Chesterfield
Inlet
HUDSON BAY
60°
N.W.T.
60°
MAN.
100°
92°
200
km

recognized in the northern Churchill Province were the supracrustal rocks of the Kaminak Group of the Ennadai-Rankin Fold Belt and the Prince Albert Group of the Committee Bay Fold Belt (Wright, 1967; Davidson, 1970 and 1972; Heywood, 1961 and 1967). These supracrustal rocks are in many places older than the large tracts of granitic gneisses surrounding them, which consistently yield younger Rb-Sr and K-Ar isotopic ages. As a result, most of the Churchill Province was considered to be much younger than the Superior and Slave Provinces. Recent U-Pb zircon ages and Sm-Nd geochronology indicate that this is not the case and suggest that much of the Churchill Province is comparable in age to the Superior and Slave Provinces. Schau (1982) and Frisch (1982) have presented evidence to show that the Prince Albert Group in places overlies a basement complex which is at least 2.9 Ga old. Other recent studies (Tippett and Heywood, 1978; Annesley, 1981a and b; Ashton, 1981 and 1982; Heywood and Schau, 1981; Nadeau, 1981; Schau et al., 1982; Taylor, 1985; Fraser, 1988) have indicated a similar geologic setting in the Baker Lake region in which Archean metavolcanic-metasedimentary belts (i.e. Woodburn Lake Group and Ketyet River Group) possibly overlie an older sialic crust. Heywood (1981, pers. comm.) has obtained preliminary dates from gneisses in the Amer Lake region of 2441 and 2998 Ma. Tella et al. (1985) obtained a U-Pb zircon age of 2798 +24/-21 Ma from a dacite porphyry within one of the belts being studied by the author. Dating by Ashton (1985 and pers. comm.) on the granites intruding the Woodburn Lake Group gives a

minimum U-Pb zircon age of 2,598 +3/-2 Ma. Fraser (1988) has obtained a preliminary, minimum zircon age of 2,662 +78/-53 Ma from granulitic equivalents of the Woodburn Lake Group. These studies have also indicated, in most instances, that basement/supracrustal belt contacts and relationships are not known due to poor exposures, later granitic intrusions, folding, and/or faulting. Schau et al. (1982) speculated that the Prince Albert Group can be correlated with the Woodburn Lake and Ketyet River Groups to the southwest. Fraser (1988) has extended the Woodburn Lake Group northeastward in the Woodburn Lake map area with a corresponding increase in metamorphic grade from greenschist to granulite facies. Further studies between the two areas may find rocks of similar lithology and age that would allow a more positive correlation of the groups.

Archean rocks of the northwestern Churchill Province are unconformably overlain by Early Proterozoic (or Late Archean?) supracrustal sequences. Lord (1953) first noted the unconformities between Archean granite/greenstone terrains and overlying conglomeratic greywackes, which suggested an erosional period. Wright (1955) was the first to define and name these supracrustals as the Hurwitz Group, the main Aphebian supracrustal succession of the central part of the northern Churchill Province. Eade (1964 and 1966) and Bell (1970) redefined the subdivisions of the Hurwitz Group. Wright (1967) further suggested that the Hurwitz Group should include all metasedimentary belts dominated by white orthoquartzite; but

others (Bell, 1970 and 1971; Heywood, 1977) felt that usage of the Hurwitz should be restricted regionally to the area surrounding the type locality. Consequently, several major Aphebian supracrustal sequences in the northern Churchill Province have been separately identified as the Chantrey, Penrhyn, and Amer Groups. Heywood and Schau (1978) have suggested that some of the Aphebian sediments (i.e. Chantrey, Amer, Penrhyn, Hurwitz Groups) were deposited before or near the beginning of major faulting and mylonitization, whereas late Aphebian/Paleohelikian sediments (i.e. East Arm rocks, Bathurst Inlet rocks, and Dubawnt Group) were laid down during or after the major crustal movements. The Aphebian rocks and their Archean basement were subjected to strong polyphase deformation during this major Hudsonian event (1870 +/- 40 Ma, VanSchmus and Bowring, 1980). The principal loci of movement were major shear (e.g. Chantrey, Wager Bay, among others) and fault zones (Amer, Tulemalu (Hudsonian ?)) formed at relatively deep crustal levels. These shear and fault zones, in places, are known to have affected both Aphebian supracrustal sequences (e.g. Chantrey Group, Amer Group) and Hudsonian granites (e.g. I-type granitoids north of Wager Bay Shear Zone). However, it is not known whether these shear and fault zones originated as reactivation zones of major Archean features. The tectonic implications of the Hudsonian Orogeny in the northwestern Churchill Province have just recently begun to be unravelled (Heywood and Schau, 1978; Fraser, 1978; Patterson, 1981; Tella, 1984; Frisch et al., 1985;

Taylor, 1985; Eade, 1986; Henderson et al., 1986; LeCheminant et al., 1987b; Tella et al., 1986; Tella and Annesley, 1987 and 1988; Gordon, 1988; Fraser, 1988; among others).

The late Aphebian/Paleohelikian Dubawnt Group, consisting of continental sediments and volcanics, unconformably overlies the Archean and Aphebian rocks in parts of the south-central portion of the northwestern Churchill Province (Blake, 1980; LeCheminant et al., 1987a). Donaldson (1965) subdivided the Dubawnt Group into six formally named units. Blake (1980) added a seventh unit and suggested that a modern day analogue of the Dubawnt Group volcanism is the volcanic belt of southeast Papua, Papua New Guinea.

The basement complex and its cover rocks are cut by diabase and gabbro dykes and associated mafic intrusions of the 1282 Ma (Heaman and LeCheminant, 1988) Mackenzie dyke swarm (Donaldson, 1965 and 1969: Eade, 1976; Eade and Blake, 1977; Lecheminant et al., 1977; among others).

2.2 GEOLOGICAL SETTING OF THE WOODBURN LAKE GROUP KOMATIITES

The study area is characterized by several linear metavolcanic-metasedimentary belts which are resting on, or intruded by, an early Precambrian granite-gneiss complex (Tippett and Heywood, 1978; Tella and Heywood, 1983). The rock types and stratigraphy within the belts show many features typical of Archean greenstone belts in general, and especially of the Prince

Albert Group.

One major metavolcanic-metasedimentary belt, Pipedream Lake (Fig. 2), and two minor belts, Esker Lake and No-name Lake, with smaller outliers are present in the study area, and the rock units of these belts make up the Woodburn Lake Group. The stratigraphic sequence of these belts consists of metamorphosed mafic to felsic volcanics, komatiites, clastic and chemical sediments, and iron formation, all intruded by mafic to felsic plutonic rocks interpreted to be comagmatic. This sequence of rocks is bounded by a complex of older granitoid gneisses and younger intrusive granitoid bodies, as shown in Figure 5. Controversy exists over the origin and temporal relationships of the granitic terrain to the metavolcanic-metasedimentary belts. Since only intrusive and tectonic contacts are observed between the granites and greenstones, K.E. Ashton (pers. comm., 1985) assumes the granitic rocks are generally younger, whereas previous work by Tella and Heywood (1983) indicated that both an older plutonic basement complex and younger post orogenic granites are present. Zircon ages obtained by K.E. Ashton (pers. comm., 1985) on some of the granites suggest that only late Archean granites are present in the area. Possibly the present forms of the granites represent diapiric bodies formed as a consequence of mobilization during metavolcanic-metasedimentary belt formation as proposed elsewhere by Schwerdtner et al. (1978).

The rocks in the Pipedream Lake belt (see Fig. 6) occur

Figure 5. Geological map with legend of thesis area.
(with modifications, after Tella and Heywood, 1983)

GEOLOGIC MAP OF SE AMER LAKE AREA

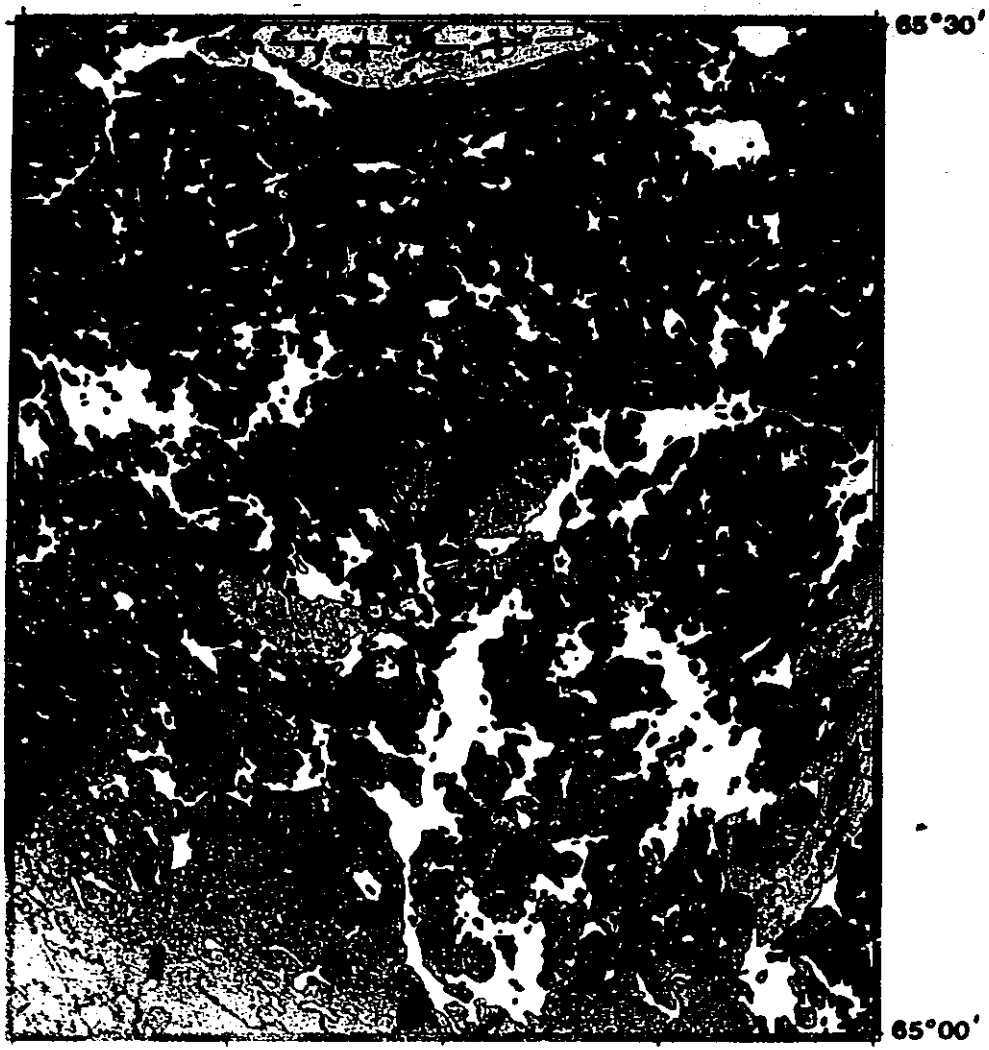

LEGEND

- Late Granitic Rocks
- Impure Sandstones
- Mudstone, Slate, Phyllite
- Carbonate
- Orthoquartzite
- Metavolcanics: intermediate to mafic
- Amphibolite
- Gabbro and Peridotite
- Granite: massive to foliated
- Foliated Granodiorite
- Augen Gneiss
- Granitoid Rocks: undifferentiated
- White Orthoquartzite
- Volcanogenic Metasediments
- Basaltic and Peridotitic Komatiites
- Metavolcanic Rocks: felsic to intermediate

---- Geological Contact
— — Fault
Thrust Fault
Syncline

5 0 5 10 m
5 0 5 10 15 km

From Tella and Heywood, 1983, with minor modifications

Figure 6. Geologic map of Pipedream Lake belt (after Ashton (1982) and Tella and Heywood (1983) with minor modifications). Rock units are given in Figure 6a.

Figure 6a. Legend to Figures 6 and 8.

Legend

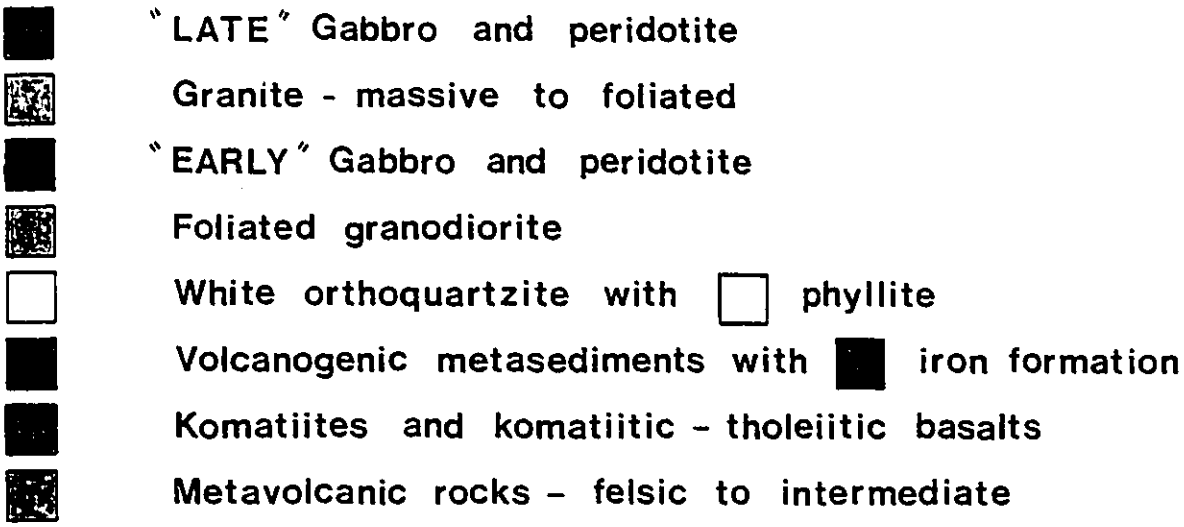

After Ashton (1982) and Tella and Heywood (1983) with minor modifications

within a tightly folded anticline which is overturned to the NW and plunges gently to the NE. Here, the Woodburn Lake Group has been divided into two major formations: Formation 1, a volcanic-sedimentary package consisting of a lower volcanic unit and upper volcaniclastic unit; and Formation 2, a sedimentary package consisting mainly of orthoquartzites (Ashton, 1982). A generalized section of the Woodburn Lake Group is shown in Figure 7. Formation 2 appears to lie unconformably on Formation 1 (See Fig. 7). Field work by the author under the supervision of Fraser (1988) supports this stratigraphic relationship.

Formation 1 consists of a succession of volcanic rocks that begins with a lower sequence of comagmatic felsic to intermediate flows, pyroclastics, and hypabyssal rocks. The basal contact of this lower sequence has not been observed. Ultramafic to mafic volcanism occurred after deposition of this basal sequence and produced komatiitic lavas. The ultramafic rocks are commonly color banded with alternating greyish-green and reddish-brown layers and are characterized by spinifex textures. Other ultramafic flows, characterized by extensive polyhedral jointing, are massive to pillowed and not color banded. A few poorly exposed mafic metavolcanics, mostly komatiitic basalts, and some related intrusives are associated with the komatiites. Overlying the komatiites is a sequence consisting of felsic metavolcanics overlain by metavolcaniclastics and more felsic to intermediate metavolcanics. This predominantly volcanic, lower unit is overlain conformably by an extensive volcanogenic assemblage

Figure 7. Generalized section of the formations of the Woodburn Lake Group within the Pipedream Lake belt.

Schematic Section of Formations of the Woodburn Lake Group

— Pipedream Lake Belt

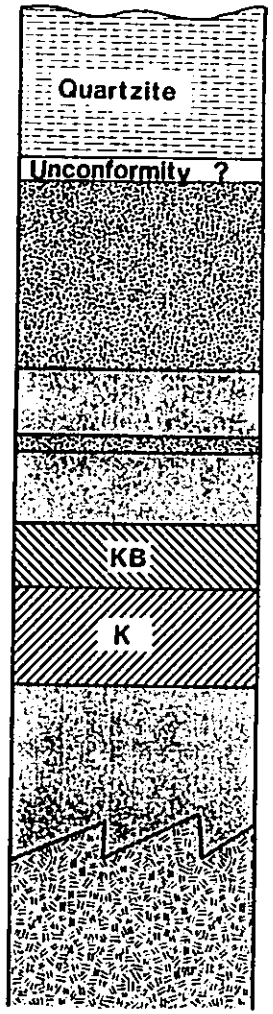

Quartzite, with minor meta-argillite, phyllite, biotite-quartz schist

Volcanogenic Sediments
- comprising pelitic schist, meta-BIF, meta-greywacke, volcaniclastic rocks

Felsic to Intermediate Metavolcanics and associated intrusive rocks; minor mafic metavolcanics

KB Komatiitic Basalts

K Komatiites

Intrusive Contact - Granite

Formation 2

Formation 1

(i.e. mixed sedimentary and tuffaceous) presently preserved as felsic to intermediate mica schists, banded metagreywackes, metavolcaniclastics, and chlorite-carbonate schists with thin horizons of iron formation and chert (Ashton, 1982).

Formation 2 is a distinctive sedimentary unit consisting of white, supermature, fine-grained orthoquartzites which crops out as topographically prominent, resistant ridges and plateaus. The thickness of this formation is unknown, but a minimum thickness of 1500 m is estimated. Bedding and other primary sedimentary features are rarely preserved. The proposed relationship of this formation to Formation 1 is speculative due to the lack of good contact exposures. The orthoquartzites of the Woodburn Lake Group exhibit many similarities to those of the Prince Albert Group but the uncertainty of their relative age and the apparent difference of their stratigraphic position to the komatiites makes correlation speculative. U-Pb zircon dating of the quartzites by Ashton (1985 and pers. comm.) yielded a complex data pattern indicative of a source possibly as old as 2.9 Ga.

The Esker Lake and No-name Lake belts, part of the Woodburn Lake Group, consist of narrow linear sequences of metavolcanic flows and possible tuffs. Similar rocks form small isolated outliers nearby. Figure 8 shows the geology of the Esker Lake belt. The metavolcanics are very fine-grained to fine-grained, massive to schistose, and moderately to strongly deformed. Locally they show amygdules and some poorly preserved pillows. They are most commonly intermediate to mafic in composition with

Figure 8. Geological map of the Esker Lake belt (after Tella and Heywood (1983) with minor modifications). Rock units are given in Figure 6a.

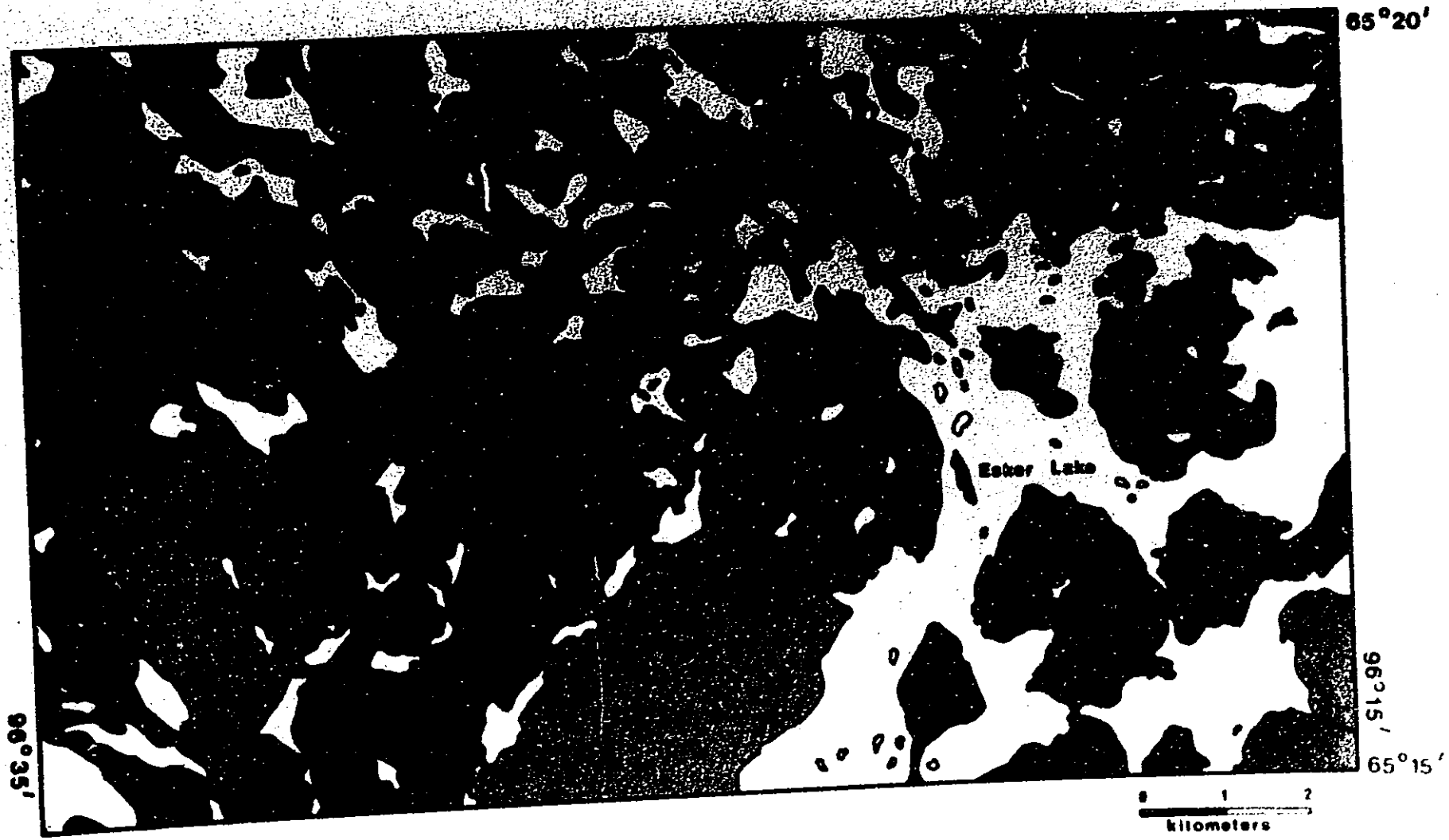
65°20'
Baker Lake
96°35'
96°15'
65°15'
0 1 2
kilometers

some intercalated ultramafic and felsic metavolcanic rocks (Fuller, 1977; Annesley, 1981b).

The ultramafic rocks of the Esker Lake and No-name Lake belts are very fine-grained, massive to schistose, and otherwise quite featureless. They are intensely deformed, altered, and recrystallized as shown by the presence of asbestos, serpentinite, "soapstone" (i.e. microscopic intergrowth of talc), and a strong northeast trending foliation. A few ultramafic units display distinct extrusive flow textures with minor spinifex. Moderately to strongly metamorphosed diorites and peridotites are associated with the metavolcanics and occur as scattered small intrusive bodies (i.e. similar to dioritic, gabbroic, and peridotitic units of the Pipedream Lake belt). Banded iron formation, consisting of alternating layers of hematite, magnetite, and silica, and metasediments similar to those of the volcanogenic unit of the Woodburn Lake Group in the Pipedream Lake belt occur along the southern margins of these two smaller belts. Structural and stratigraphic relationships of the rocks within these belts and the surrounding gneissic granitoid terrain are uncertain due to ambiguous field relations.

The rocks of the three belts and surrounding area are tightly and isoclinally folded around northeasterly-trending axes with overturned, subvertical to gently southerly-dipping axial planes. Normal and thrust faulting has occurred throughout the region. The details of the structural geology are beyond the scope of this study and can be found elsewhere (Ashton, 1981 and 1982;

Tella and Heywood, 1983; Fraser, 1988).

The rocks of the area have undergone regional metamorphism of lower greenschist to amphibolite grade and contact metamorphism of amphibolite grade by younger intruding granites.

FIELD AND PETROGRAPHIC CHARACTERISTICS OF THE KOMATIITES AND KOMATIITIC BASALTS

3.1 WOODBURN LAKE GROUP - PIPEDREAM LAKE BELT

The Woodburn Lake Group mafic to ultramafic metavolcanics are best exposed in the Pipedream Lake belt where they are associated with felsic to intermediate metavolcanics and metavolcaniclastics. They form hummocky, poorly to well exposed outcrops up to 75 m in local relief (Fig. 9a, 9b and 10a). The ultramafic rocks are predominantly komatiitic lava flows, but also locally form sills and dykes. Some komatiitic basalts are found along the southern boundary of the komatiites.

Individual ultramafic flows can be traced for up to 300 m but their full extent is not known. Some of the flows die out after only a few meters. Over these distances, individual flows display variable thicknesses because of the uneven surface(s) of underlying flow(s). Dykes of similar composition crosscut the flow units. Individual flows range from less than 0.5 m to 10 m thick with many in the 1.0 to 2.0 m range. They are identified as komatiitic lava flows by the following field criteria: flow top hyaloclastite and breccias, vesicular tops, rusty thick weathering rinds, spinifex textures (Figs. 10b, 11a, 12a, 13b), polyhedral jointing (Figs. 11b, 12b), and distinct contacts (Fig. 13a) between flow units. Most flow units show distinct

Figure 9a. A panoramic view of the field area looking south from field station AK-7. Large knob on the horizon is the best outcrop of komatiites in the region.

Figure 9b. A view of outcrop station AK-11 looking north from field station AK-7. Komatiites tend to form some of the more resistant ridges.

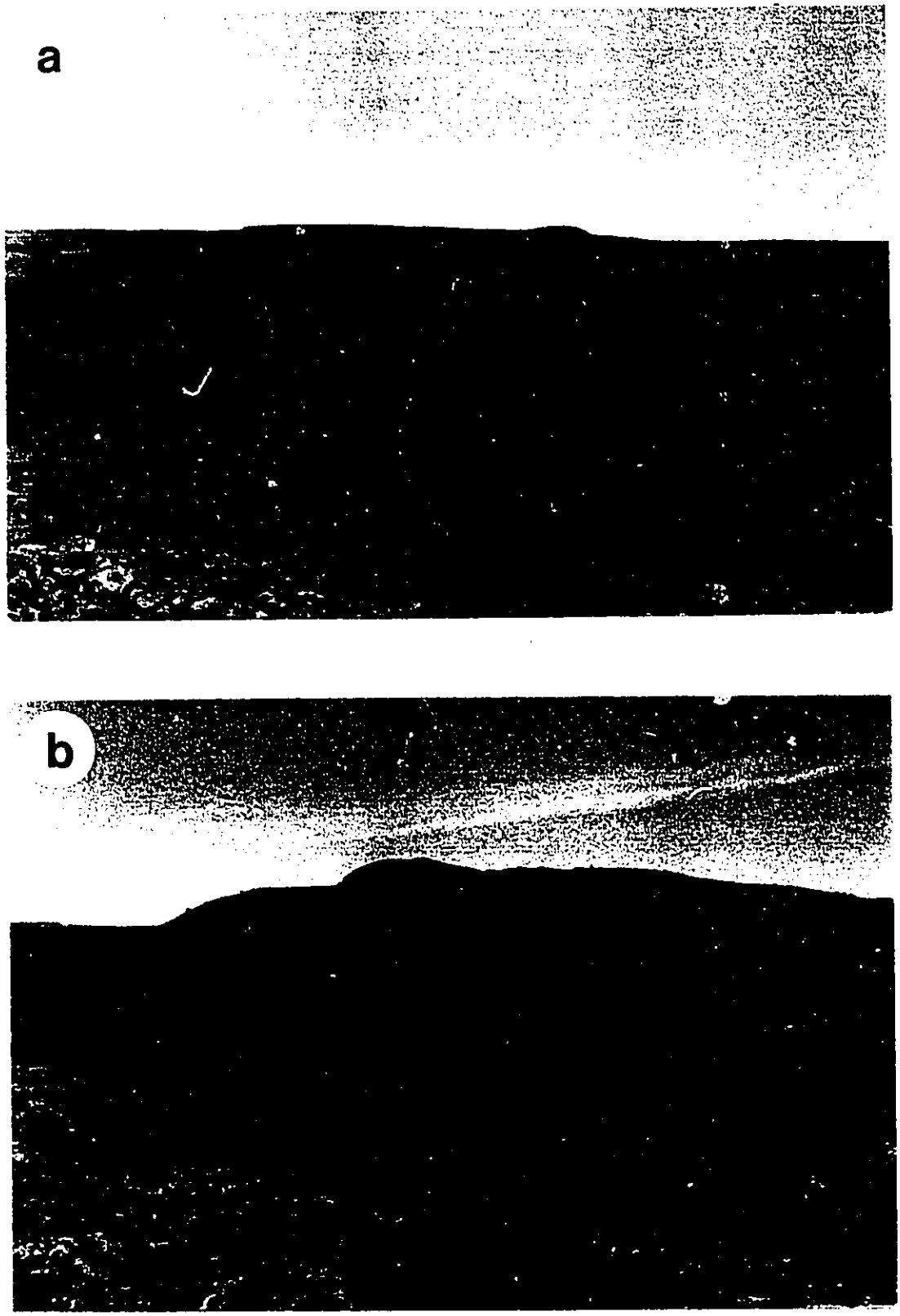
a
b

Figure 10a. A field photo of the best outcrop of predominantly spinifex-textured komatiites. Photo courtesy of G.S.C.

Figure 10b. A close-up shot of a komatiitic flow with a thick spinifex-textured zone. This zone coarsens downwards from left to right (tops to the left). Photo courtesy of G.S.C. Pencil used for scale is 15 cm in length.

a

Figure 11a. A close-up of the randomly oriented spinifex from Figure 9b (i.e. left-hand side of photo).

Figure 11b. The lower and central portion of a thick massive flow showing distinct polyhedral jointing.

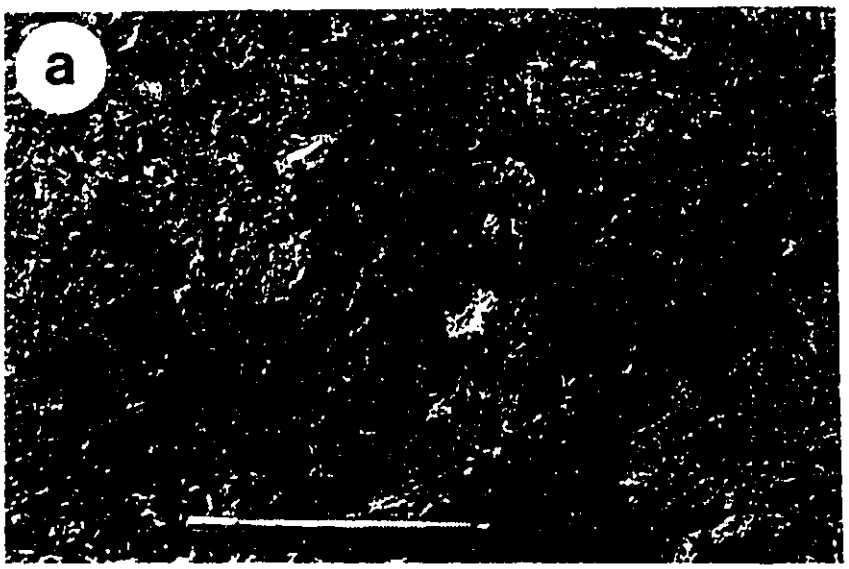
a


b

Figure 12a. A close-up of the spinifex texture from the K-35 sample locality.

Figure 12b. A close-up of the polyhedral jointing from the K-37 sample locality. The spacing of the polyhedral jointing is approximately 5 to 8 cm in diameter.


a
K-35

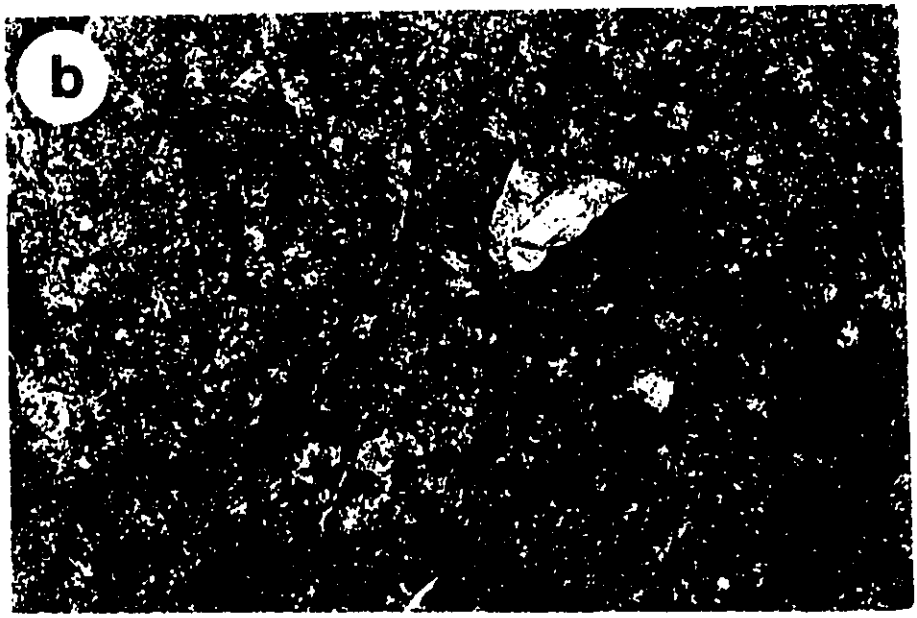
b

Figure 13a. A photograph of an outcrop showing the nature of flow units. Spinifex-textured A zones are dull dark greyish green and cumulate B zones are reddish brown. Tops is to the left (i.e. to the east) as indicated by fining upwards of spinifex texture. Hammerhead is positioned at the base of a cumulate zone.

Figure 13b. A close-up of the spinifex-textured A zone near the contact with the underlying cumulate B zone. Flow top direction is to the right (i.e. east).

a

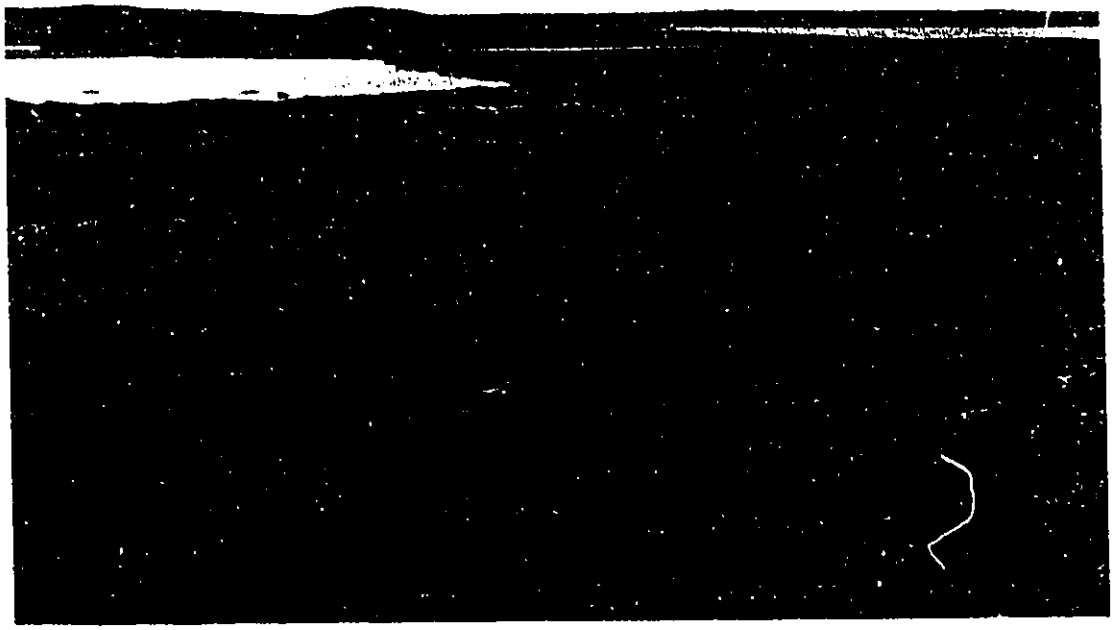

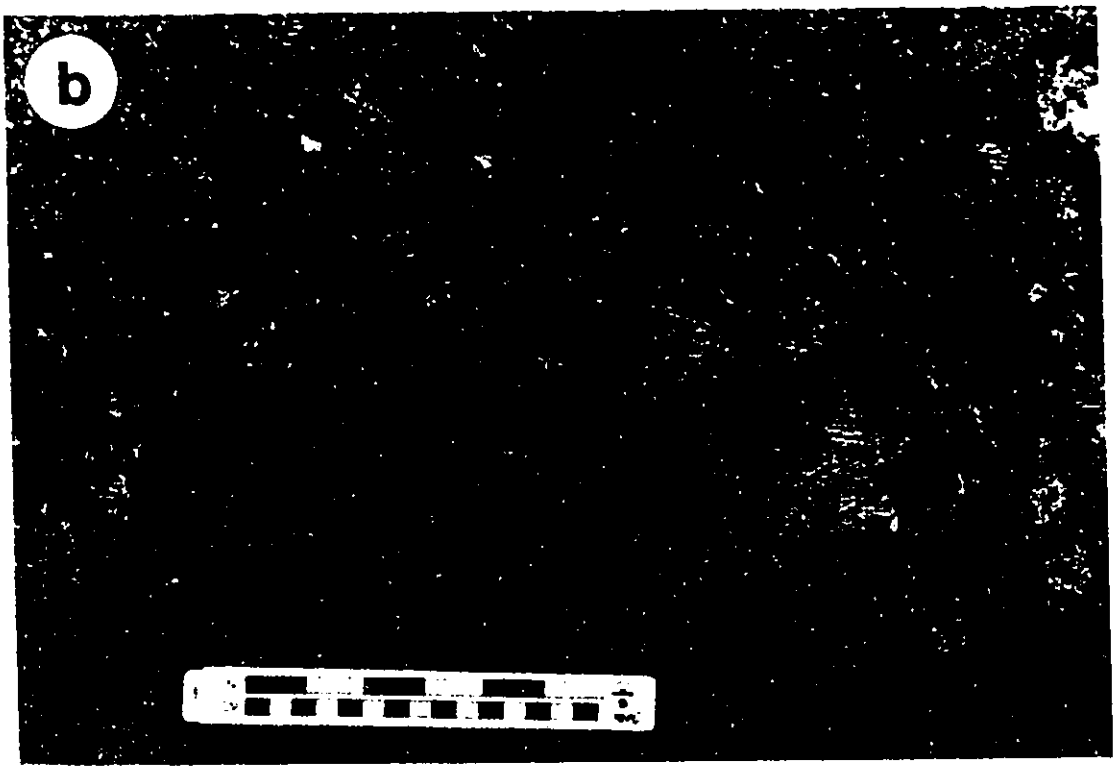

development of polyhedral cooling joints, which are as much as 8 cm in diameter in the quenched flow tops. Within the spinifex-textured flow units, the polyhedra are generally restricted to the flow tops and cummulate zones. These polyhedra display extensive alteration and a fragmental appearance with very fine-grained weathering rinds and coarser grained centers. Five types of flows have been positively identified: 1) ultramafic flows with thick (>0.5 m) spinifex-textured zones (Figs. 14a, 14b); 2) ultramafic flows with thin (<0.5 m) spinifex-textured zones and thick polyhedrally jointed bases; 3) ultramafic flows that are massive with polyhedral jointing throughout (Figs. 15a, 15b); 4) mafic to ultramafic (i.e. komatiitic basalt or pyroxenitic) flows with some large randomly oriented amphibole blades; and 5) pillowed ultramafic flows (Fig. 17a). In places the massive and more common spinifex-textured flows are interlayered. The presence of the fifth type of flow has been confirmed recently (Annesley, 1989 - unpublished data) in the SE Amer Lake map area (Fig. 16a). The author has also identified some pillowed ultramafic flows (Fig. 16b) within the Woodburn Lake map area (Fraser, 1988). The presence of pillows, along with hyaloclastite and interflow chemical sediments, indicates a subaqueous environment of eruption for the komatiites. Similar criteria for a subaqueous environment has been found in the Abitibi Greenstone Belt komatiites (Arndt et al., 1977 and Gelinas et al., 1977). Ultramafic volcaniclastic rocks have not been observed in the Woodburn Lake Group. Near

Figure 14a. One of the ultramafic flows with a thick spinifex -textured zone. Rusty brown cumulate B zone to the left is not totally exposed. Note the sharp contact with the overlying, dull dark greyish green spinifex-textured A zone (to the right). The asymmetry of the spinifex-textured zone indicates tops to the east (to the right in picture).

Figure 14b. A photograph of an outcrop showing ultramafic flows of types 1 and 2 across strike. Note the variable thickness of individual flows. Approximately twenty flow units are found on this outcrop. As in Figure 14a, contacts are sharp. Asymmetry within the flow units indicates tops to the NE (to the right in picture). These flow units are found approximately 200 meters south of the large knob shown in Figure 9a. Samples of the AK-21 to AK-24 series were collected from this locality.


a

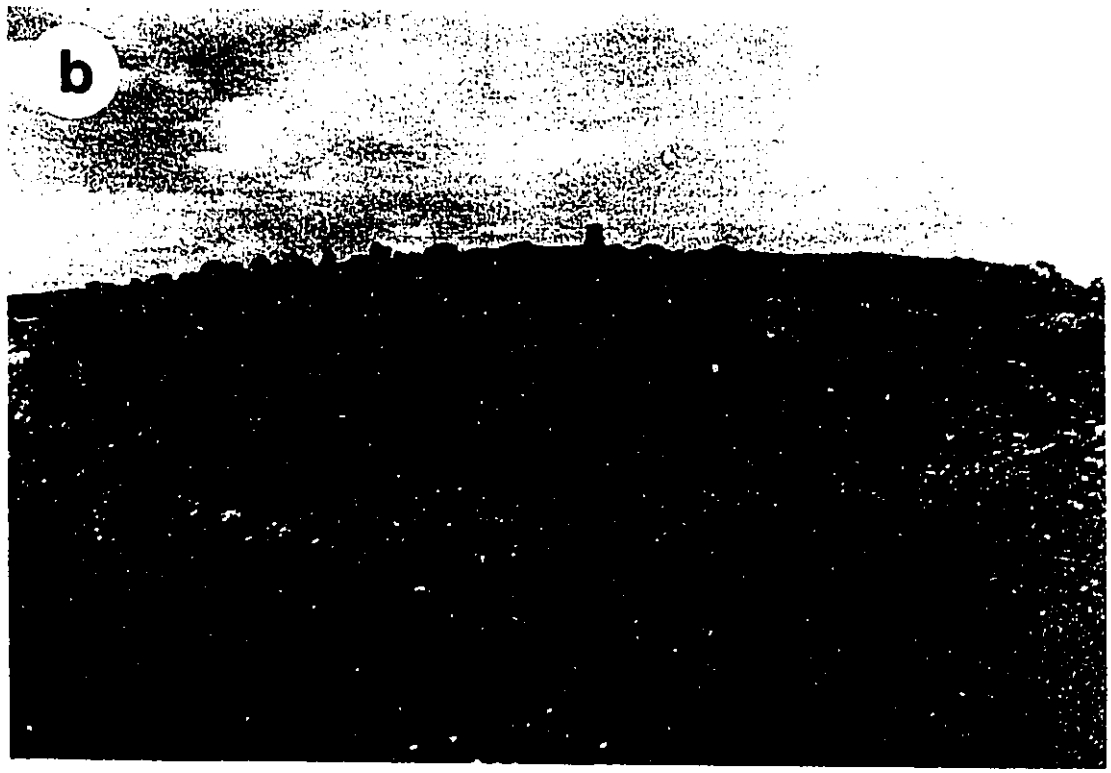
b

Figure 15a. Polyhedral jointing found within central portion of massive flow. Photo courtesy of Ken Ashton.

Figure 15b. More altered version of polyhedral jointing found within a massive flow. Photo courtesy of Ken Ashton. Field of view is approximatly 75 cm.

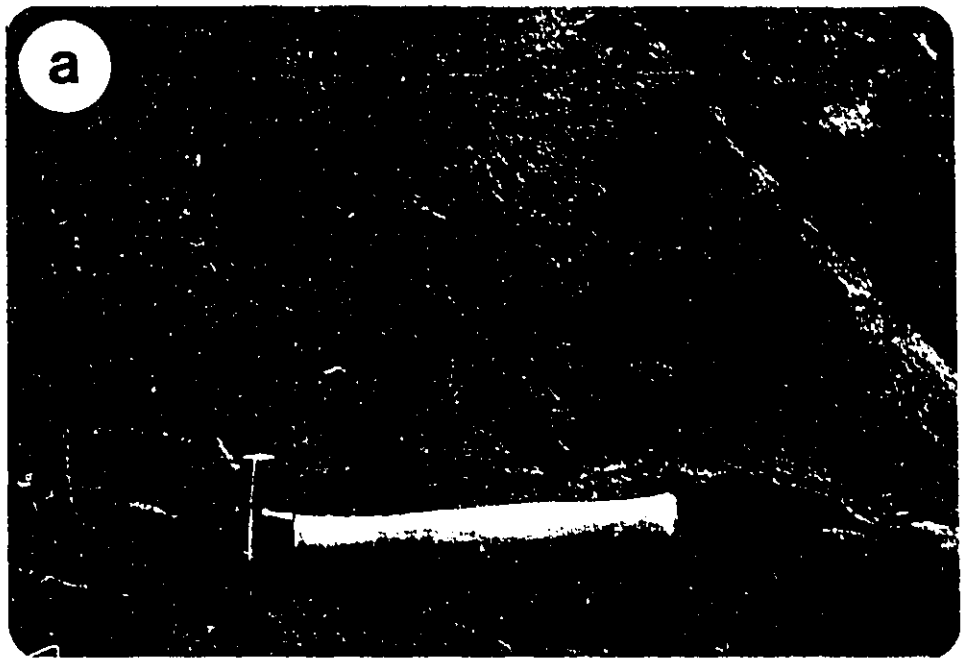
a

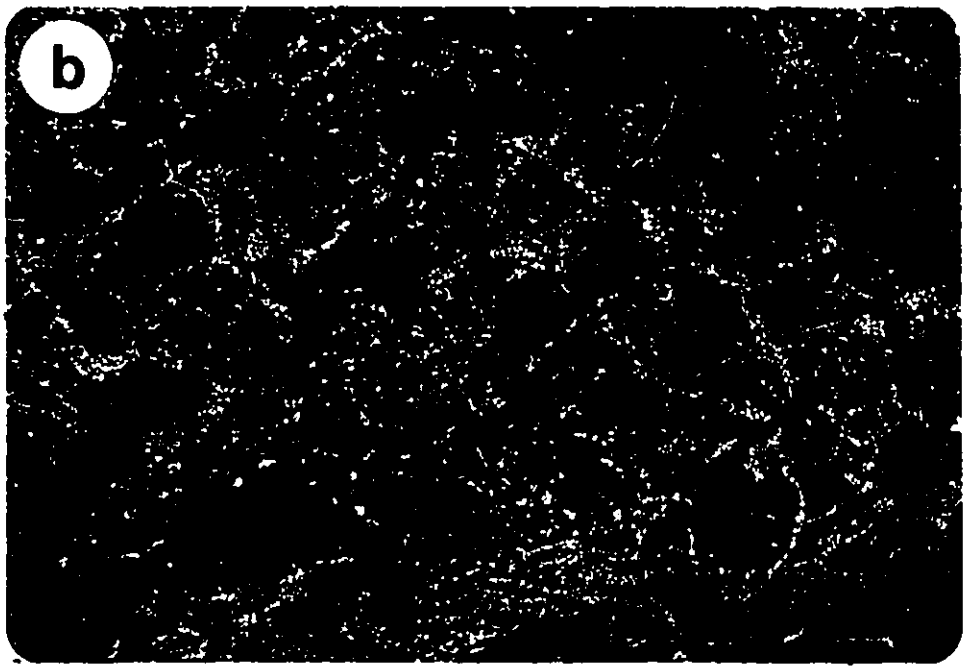
b

Figure 16a. An outcrop of ultramafic pillowed flows in the SW portion of the Pipedream Lake belt.

Figure 16b. Ultramafic pillowed flows found within the Woodburn Lake map area.

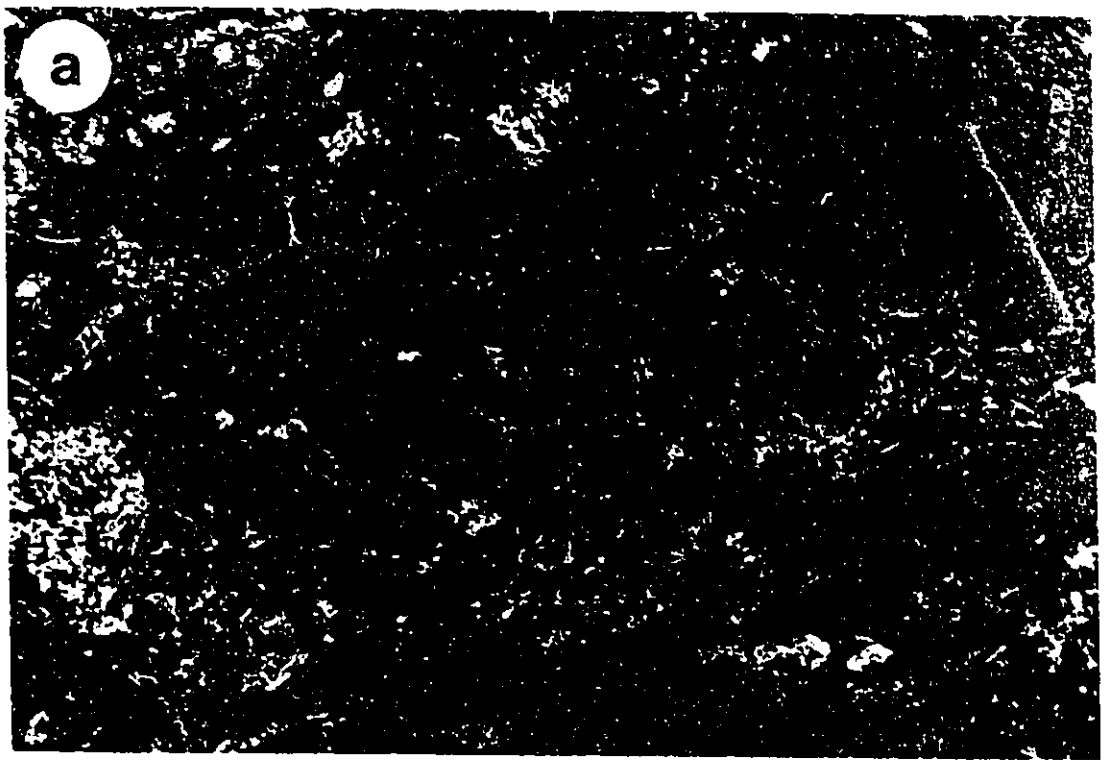
a


b

Figure 17a. Another convincing sample locality (AK-12) of ultramafic pillowed flows within the Pipedream Lake belt. The central portion of the pillows is defined by polyhedral jointing of large diameter. The polyhedra become smaller in diameter near the margin of the pillows. The field of view is 3 meters. The red pencil is oriented subparallel to the pillow margin.

Figure 17b. Details of the finer polyhedra in Figure 17a.

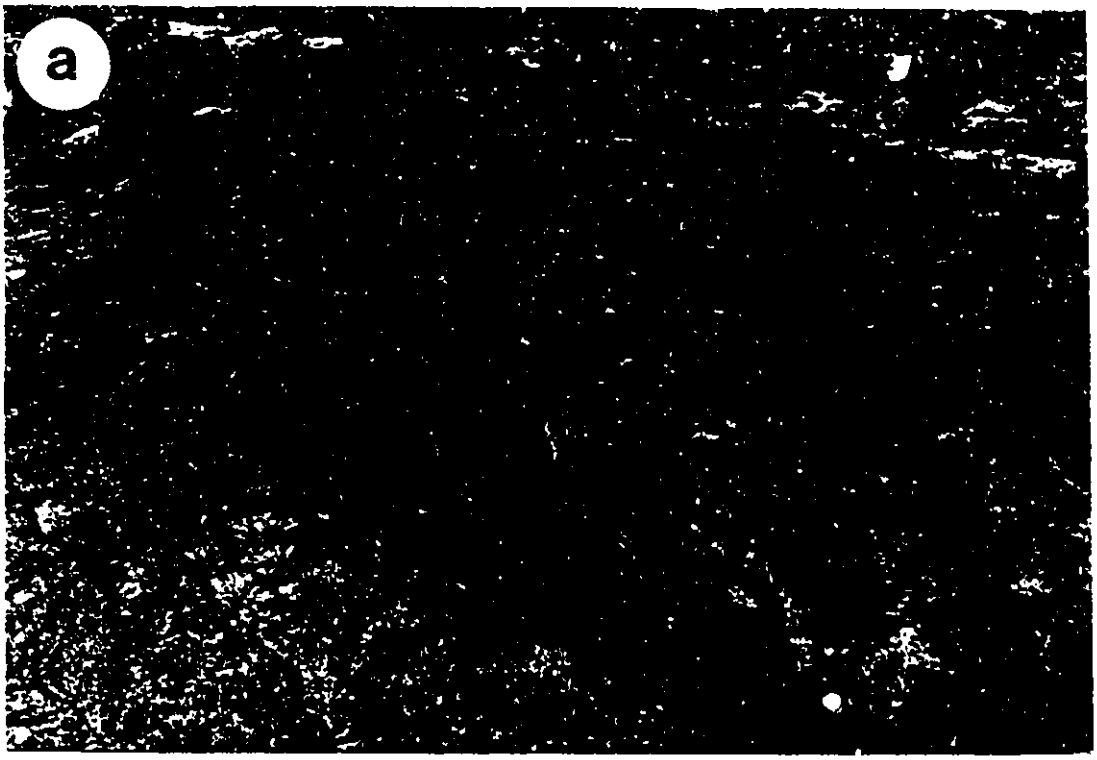
a

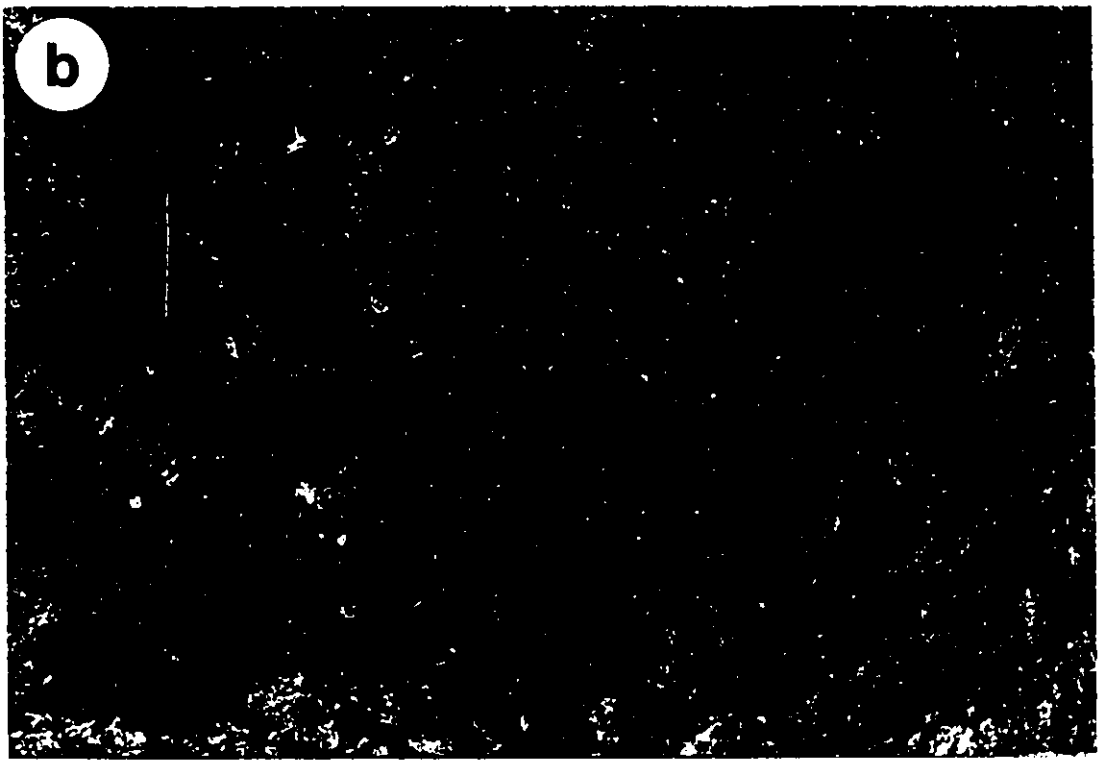
b

Figure 18a. Pervasive nodular porphyroblastic texture within massive ultramafic flows near a granite body on a small island uotcrop (AK-29 locality).

Figure 18b. A similar nodular porphyroblastic texture found within felsic metavolcanics near contact with granite body at AK-30 locality.

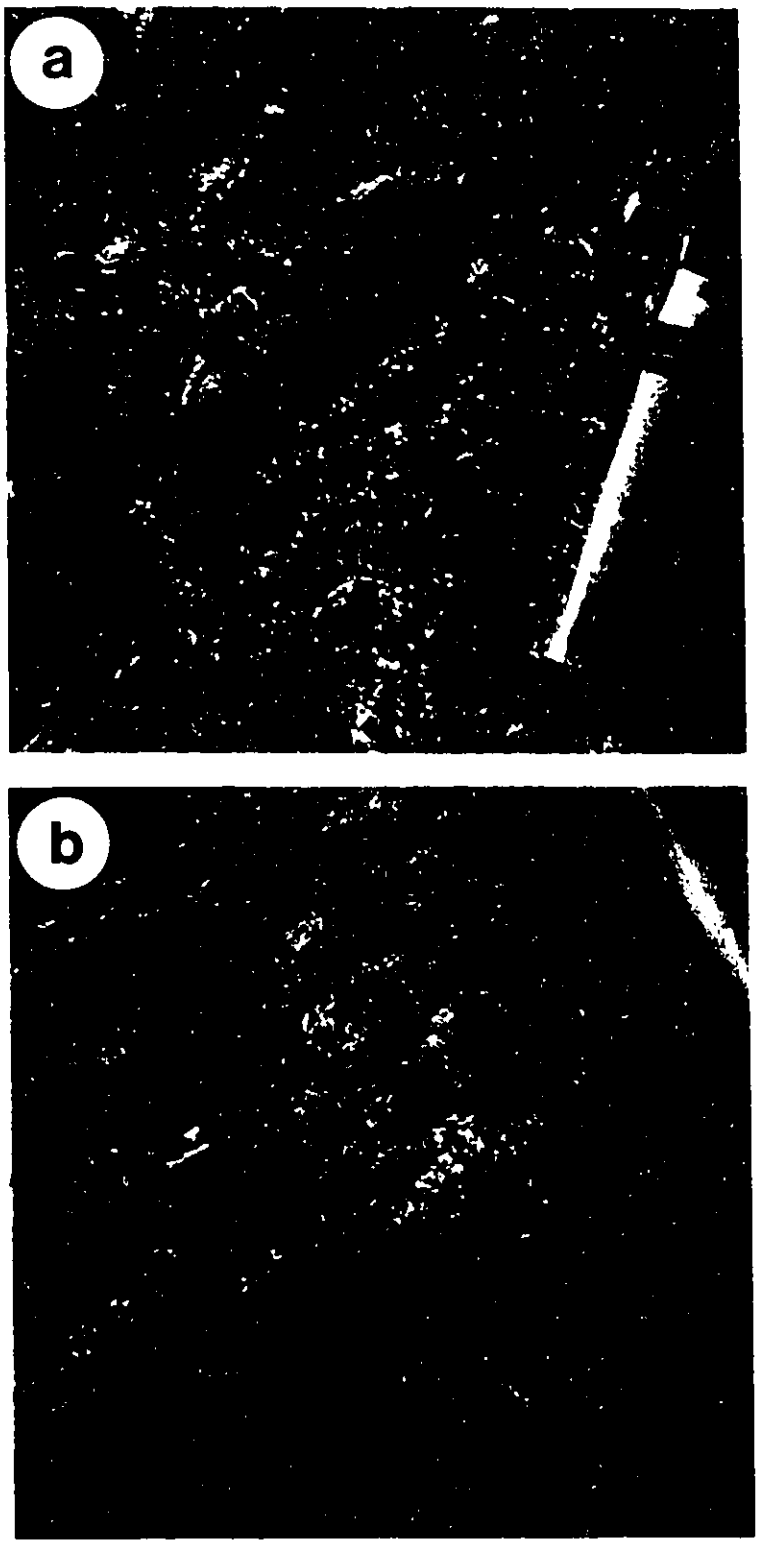
a
b

granitic contacts a pervasive nodular porphyroblastic texture (Figs. 18a and 18b) was observed in the ultramafic flows, as well as the felsic metavolcanics. This texture is similar to that observed by Oliver et al. (1972) in ultramafic rocks from Western Australia.

This study will use the nomenclature outlined by Donaldson (1974, 1976, and 1982) to describe rock textures and olivine morphology. Donaldson (1976) identified a total of ten shapes of olivine crystals. Of these, Donaldson (1982) described five of the more common types as observed by Nesbitt (1971) and others. These five types are as follows:

1) "Hopper olivine", equant to elongate crystals. These are equivalent to the "porphyritic spinifex" and "radiating spinifex" of Nesbitt (1971).
2) "Plate olivine", comprising two or more thinly tabular blades or plates that are stacked parallel or subparallel to one another. A group of similarly-oriented blades or plates, sometimes diverging slightly from a common nucleation site, comprise a "book" of plate olivine ("sheafs" or "booklets", Pyke et al., 1973). The intersection of these books commonly produces a complex olivine spinifex framework (i.e. intersecting upward-pointing cones of plate olivine with triangular inter-plate spaces). These are equivalent to the "plate spinifex" of Nesbitt (1971).

3) "Branching olivine", comprising the "linked parallel-growth" and "crystallographic branching" olivine types. These are probably equivalent to the "harrisitic spinifex" of Nesbitt (1971) and "chevron spinifex" of Arndt (1982a).
4) "Polyhedral olivine", equant to tabular, euhedral crystals.
5) "Granular olivine", equidimensional or subspherical crystals.

This study will also follow the flow type classification scheme used by Pyke et al. (1973) and Arndt et al. (1979).

3.1.1 ULTRAMAFIC FLOWS WITH A THICK SPINIFEX-TEXTURED ZONE

This type of flow consists of dull greenish-grey weathering spinifex-textured layers (A zone, after nomenclature of Pyke et al., 1973) and reddish-brown weathering massive cumulate layers (B zone). The thickness ratio of spinifex-textured layers to cumulate layers within flows varies greatly from < 0.1 to 0.6 between individual flows as well as along strike in individual flows. This variation is probably a reflection of different crystallization conditions; hence the need for flexible models to explain the formation of layering in komatiites. Nowhere does the spinifex-textured zone extend entirely across the flow unit. All of the spinifex-textured flows have chilled aphanitic tops (A_1

zone) displaying small polyhedra which in thin section consist of very fine-grained, randomly oriented, thin-bladed chlorite and/or tremolite pseudomorphs with magnetite after olivine, set in a chlorite/tremolite matrix after devitrified volcanic glass. No apparent pseudomorphs after clinopyroxene are observed in this chilled margin zone.

Underlying the chilled margin is the spinifex-textured zone (A_2 zone) which is characterized by an upper, randomly oriented region and a lower region with preferred orientation. The change in size and morphology of olivine pseudomorphs throughout the spinifex-textured zone is responsible for this characteristic layering in the spinifex-textured komatiites of the area. Usually, the layering shows up as fine-grained spinifex near the top and coarse-grained spinifex at the base of the zone. Although reversals occur locally, this predominant characteristic of spinifex coarsening downwards is employed in determining tops. In some spinifex-textured flows this increase in grain size is gradational (i.e. similar to that described by Pyke et al., 1973), whereas in other flows a distinct division of grain size is shown with an upper region of fine-grained randomly oriented spinifex and a lower region of coarse-grained platy spinifex (i.e. similar to that described by Lajoie and Gelinas, 1978). In general, the upper region is only a few centimeters thick, whereas the lower region can be several meters thick.

In the randomly oriented spinifex-textured region (Fig. 19a), fine-grained, elongated tremolite and/or chlorite (locally

Figure 19a. An example of the randomly oriented spinifex found within the upper portion of an ultramafic flow with a thick spinifex-textured zone. Large olivine pseudomorphs (now tremolite) set in a matrix of clinopyroxene needles (now tremolite) and glass (now chlorite). Other minerals present are magnetite and Cr-magnetite, which are found as large equant and small dendritic and cruciform crystals. Plane-polarized light, 10X. Sample K-42d.

Figure 19b. A photomicrograph of the lower region of preferred orientation of spinifex found within an ultramafic flow with a thick spinifex-textured zone. The spinifex is well developed, varying from alternating layers of plate olivine (now tremolite - light colored) and matrix (now chlorite and Cr-magnetite - dark colored) to geometric triangular forms of olivine pseudomorphs (now tremolite -light colored) oriented in a matrix of clinopyroxene needles (now tremolite), chromite dendrites (now Cr-magnetite and magnetite), and glass (now chlorite). Plane-polarized light, 10X. Sample K-6a.

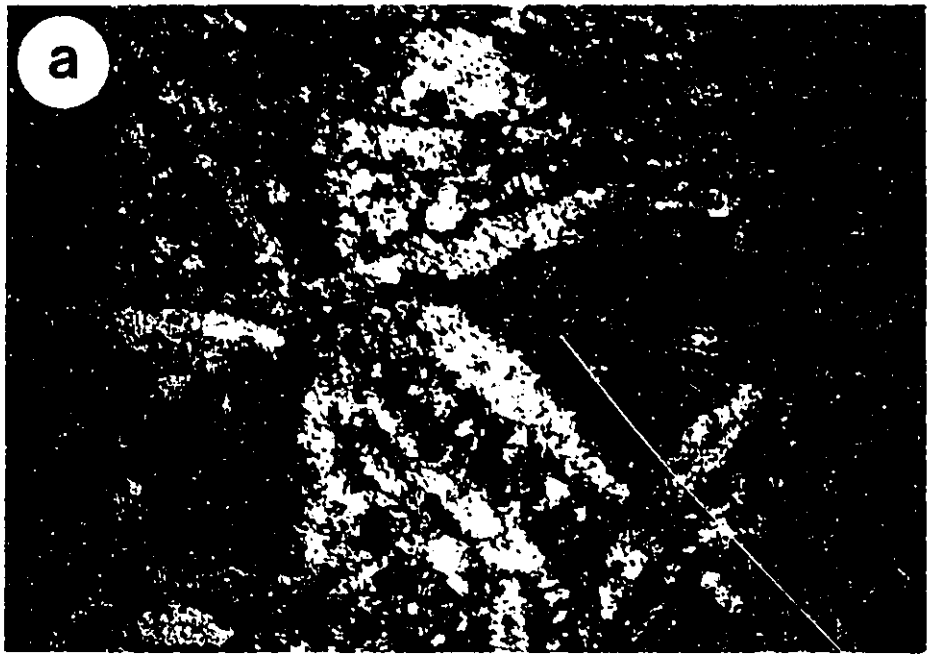
a


b

serpentine) pseudomorphs with magnetite after hopper olivine are found in a groundmass of chlorite, tremolite, Cr-magnetite and/or magnetite, and minor carbonate. These pseudomorphs after hopper olivine increase in size downwards into the lower region of preferred orientation (Fig. 19b). Also, in this upper, randomly oriented region, the pseudomorphs after hopper olivine commonly intersect to frame triangular spaces (Fig. 19a), consisting of anhedral microcrystals of tremolite and chlorite in a random arrangement. Downwards into the lower region of preferred orientation, the abundance and morphology of olivine changes from a few elongated pseudomorphs of hopper olivine to a multitude of thinly tabular pseudomorphs of plate olivine. The tremolite/chlorite, locally serpentine, pseudomorphs with magnetite after olivine are skeletal. Accompanying this change is an overall increase in the size of olivine pseudomorphs. Donaldson (1976, 1982) attributed this phenomenon to different cooling, growth, and nucleation conditions operating within individual flow units during crystallization. This would account, along with other factors such as eruption rates, flow rates, and ponding conditions, for the different types of flows produced by komatiitic lavas. "Books" of pseudomorphs after plate olivine become common downwards in this lower region of the spinifex-textured zone. These "books" are randomly to weakly oriented in the upper portion of the spinifex-textured zone, whereas they are oriented subperpendicular to the flow margins in the lower coarser grained portions of the spinifex-textured zone.

In general, downward through the spinifex-textured zone, the books become larger with an increase in the number and size of plates. The smaller, subrandomly oriented books consist only of a few closely packed, plate-like crystals set in a matrix of interplate material. The larger books consist of abundant, sub-parallel to parallel, closely packed, plate-like crystals surrounded by a matrix of interplate material. Commonly, chlorite and tremolite have replaced the serpentine pseudomorphs after olivine plates in a transverse fashion. Macroscopically, the plates or blades are up to 50 cm in length but microscopic observation suggests that the blades or plates are composed of numerous, small olivine crystals stacked end to end. The plates are .03 to 2.5 mm thick and they form books that are up to 15 cm thick. The largest blades and plates are found in the thickest books which in turn are found in the thickest flows. The spinifex blades are small in thin flows and large in thick flows (up to 50 cm in length).

The interplate and interblade areas are larger than that occupied by the olivine pseudomorphs (i.e. approximately a 55:45 ratio). These areas (Figs. 20a and 20b), originally composed of clinopyroxene, volcanic glass, and skeletal chromite and/or ferro-chromite with magnetite rims, have been altered in most cases to a recrystallized aggregate of tremolite, chlorite, and Cr-magnetite and/or magnetite. Fine-grained magnetite rims the spinifex blades in a ribbed manner. Tremolite shows cuspate, plumose, or feathery patterns pseudomorphic after clinopyroxene.

Figure 20a. A close-up of the interplate area within the geometric triangular forms. These areas were originally composed of clinopyroxene needles, volcanic glass, and dendritic to cruciform chromite and/or magnetite. Presently, these areas are a recrystallized aggregate of tremolite, chlorite, and magnetite that preserve the original igneous texture. Plane-polarized light, 40X. Sample AK-24b.

Figure 20b. Same field of view as Figure 20a but with crossed-polarized light.


a

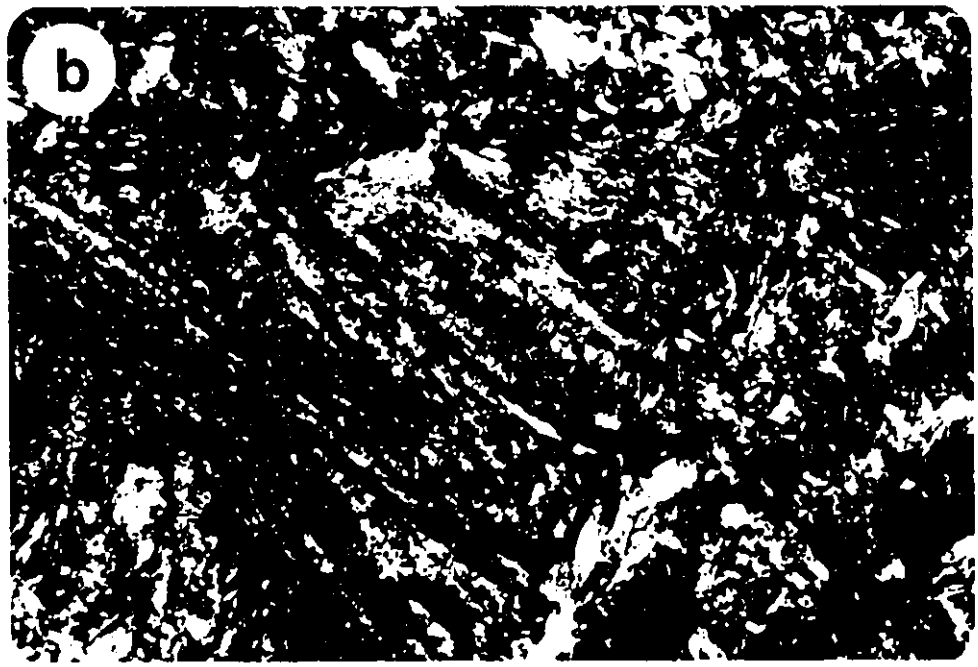
b

Commonly, the tremolite pseudomorphs after clinopyroxene have their long dimensions oriented perpendicular to the books of plate olivine. The clinopyroxene pseudomorphs are up to 1.5 mm in length within the coarser spinifex zones. Serpentine pseudomorphs (2.0 x 0.75 mm) after olivine phenocrysts (i.e. hopper olivine?) also occur in the coarser grained spinifex-textured zones within the interblade areas. In some flows minor plagioclase is present towards the base of spinifex-textured zones within the matrix as small microcrystals. Throughout the spinifex-textured zone, except at the chilled margin, Cr-magnetite and/or magnetite pseudomorphs after chromite and/or ferrochromite are found as equant to cruciform or dendritic crystals within the interplate and interblade areas. Quite possibly some of the magnetite was primary, that is, existing as mantles around chromite grains. Original glass is now represented by a very fine-grained matrix of tremolite and chlorite.

The spinifex zone shows a distinct, sharp, relatively planar contact (Fig. 21) with the top of the cumulate zone (B zone, nomenclature of Pyke et al., 1973), which consists of laminated tabular serpentine and/or tremolite pseudomorphs after olivine. This part of the B zone is referred to as the B_1 zone. It is generally narrow and foliated, and is not everywhere present. The B_1 zone grades into the major portion of the rubbly B zone which consists of solid (i.e. not hollow), equant- to tabular-shaped cumulate serpentine/tremolite/talc pseudomorphs with magnetite after olivine. Knobby peridotite, similar to the B_3 zone

Figure 21. An example of a distinct, sharp, relatively planar contact between the rusty brown cumulate B zone (to the left) and the dull dark greyish green spinifex-textured A zone (to the right). The B zone is distinctly foliated, parallel to to the contact, at this locality. However, the heavy lichen cover makes it difficult to discern in this photograph.

Figure 22a. Photomicrograph of cumulate zone showing serpentine-tremolite pseudomorphs of cumulate olivine grains set in a matrix of chlorite, tremolite, and dendritic magnetite (formerly clinopyroxene, glass, and chromite (?)). Note the euhedral form of some of the olivine pseudomorphs. Plane-polarized light, 10X. Sample K-41.

Figure 22b. Same field of view as Figure 22a but with crossed-polarized light.


a


b

described by Pyke et al. (1973), was not observed. The cumulate zone in thin section (Figs. 22a and 22b) shows a weak to moderate foliation. Approximately 60-80 percent of the zone is composed of olivine pseudomorphs. The serpentine pseudomorphs with magnetite after olivine display various shapes and sizes: from elongate to equant shaped grains which average 1.0-1.5 mm in maximum dimension. Along with the altered olivine, up to 5 percent pseudomorphs of clinopyroxene phenocrysts occur in the upper portions of the cumulate zone. The interstitial area, originally mostly glass and clinopyroxene, as observed by others, consists of fine-grained tremolite pseudomorphs after clinopyroxene set in a fine-grained felt-like mass of chlorite, fibrous amphibole, and magnetite. The grain size within the cumulate zone of most spinifex-textured flows generally increases downwards from the top to the middle portion of the cumulate zone, and then decreases to the base of the cumulate zone which is commonly brecciated as reported elsewhere by Pyke et al. (1973). This basal portion consists of an aphanitic groundmass of serpentine, amphibole, and magnetite with scattered microphenocrysts of serpentine pseudomorphic after olivine. No pseudomorphs of clinopyroxene phenocrysts are apparent in this basal portion of the cumulate zone, which is similar to the flow top.

In contact metamorphic zones, these layered spinifex-textured flows are overprinted by "nodular-like" porphyroblasts. Accompanying this textural change is a change from greenschist

Figure 23a. Spinifex-textured A zone of a komatiite flow showing the typical form of olivine development on the outcrop surface. AK-7 sample locality.

Figure 23b. The typical form in outcrop of the spinifex-textured A zone of a komatiite flow in the contact metamorphic zones. Note the distribution and shape of the "nodular-like" porphyroblasts of olivine with spinel. Photograph film box used for scale is 5.5 cm in length. AK-8 sample locality.


a

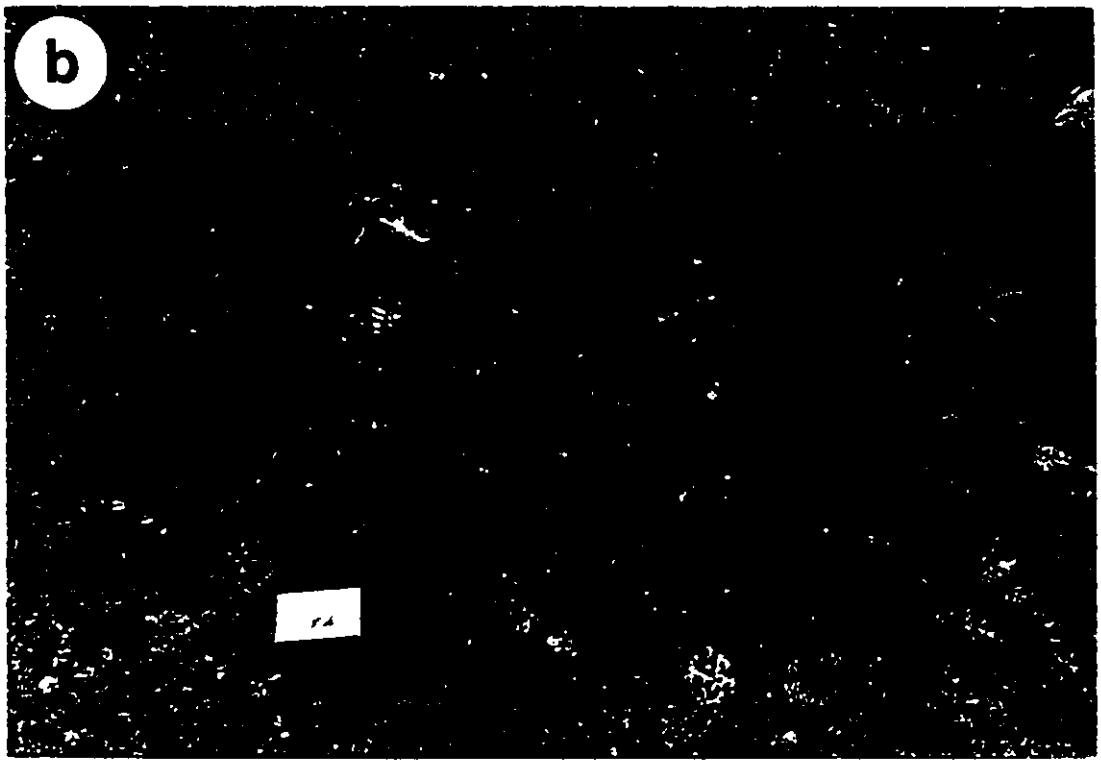
b

facies mineralogy to amphibolite facies mineralogy (Figs. 23a and 23b; also see Chapter 5).

3.1.2 ULTRAMAFIC FLOWS WITH THIN SPINIFEX-TEXTURED ZONES

This flow type consists of a polyhedrally jointed A_1 zone, an A_2 zone with limited spinifex, and an underlying polyhedrally jointed cumulate B zone; no B_1 foliated zone is present. These flows display weathered surfaces similar to the flows with thick spinifex-textured zones. Most of the spinifex is randomly oriented and grades sharply into the olivine cumulate zone. The thickness of the A_2 zone is less than 40 cm, averaging 10-15 cm. No spinifex schlieren such as those at Munro Township (Arndt et al., 1977) were observed. Microscopically, the textures and mineralogy are similar to those observed in the flows with thick spinifex-textured zones.

3.1.3 MASSIVE ULTRAMAFIC FLOWS

The massive flows are very fine-grained to fine-grained and relatively homogeneous throughout. An outstanding feature of these flows is the pervasive and unique polyhedral jointing which is closely spaced at the flow centers. These flows contain rounded or polyhedral, pseudomorphed olivine grains set in a completely altered matrix derived from clinopyroxene, glass, and chromite. This texture is similar in appearance to the rubbly

cumulate layers of spinifex-textured flows. The olivine grains of massive flows are less closely packed than those of the cumulate zone and make up approximately 55 percent of the rock. These olivine pseudomorphs are medium-grained, solid, and equant- to tabular-shaped. They are concentrated in the flow centers, and are finer-grained and less common at the flow margins. The olivine grains have been replaced totally by serpentine/tremolite and magnetite, and the groundmass of clinopyroxene, glass, and chromite and/or ferrochromite has been replaced respectively by tremolite, chlorite, and Cr-magnetite and/or magnetite. In the contact metamorphic zones, olivine and spinel has replaced in varying degrees this greenschist facies mineralogy (Figs. 24a and 24b).

3.1.4 KOMATIITIC (PYROXENITIC) AND THOLEIITIC BASALT FLOWS

Komatiitic and tholeiitic basalt flows are fine- to medium-grained with a dull, dark green weathering color. On outcrops, it was not possible to distinguish between komatiitic basalts and tholeiitic basalts, although the komatiitic basalts appeared to be more porphyritic after comparing textures with chemistry. An outstanding feature of these flows is the relatively large randomly oriented tremolite pseudomorphs after prismatic solid (i.e. not skeletal), skeletal, and radiating pyroxene phenocrysts. The tremolite pseudomorphs are set in a completely altered matrix pseudomorphic after clinopyroxene,

Figure 24a. A photomicrograph of clear neoblastic olivine and dull dark green spinel grains (lower right hand corner) set in a fine-grained matrix of chlorite and randomly oriented blades of tremolite and anthophyllite with minor magnetite. Plane-polarized light, 10X. Sample AK-12b, from a porphyroblastic, contact metamorphosed massive flow.

Figure 24b. A photomicrograph of the same rock as Figure 24a, but another field of view and cross-polarized light, 10X.


a

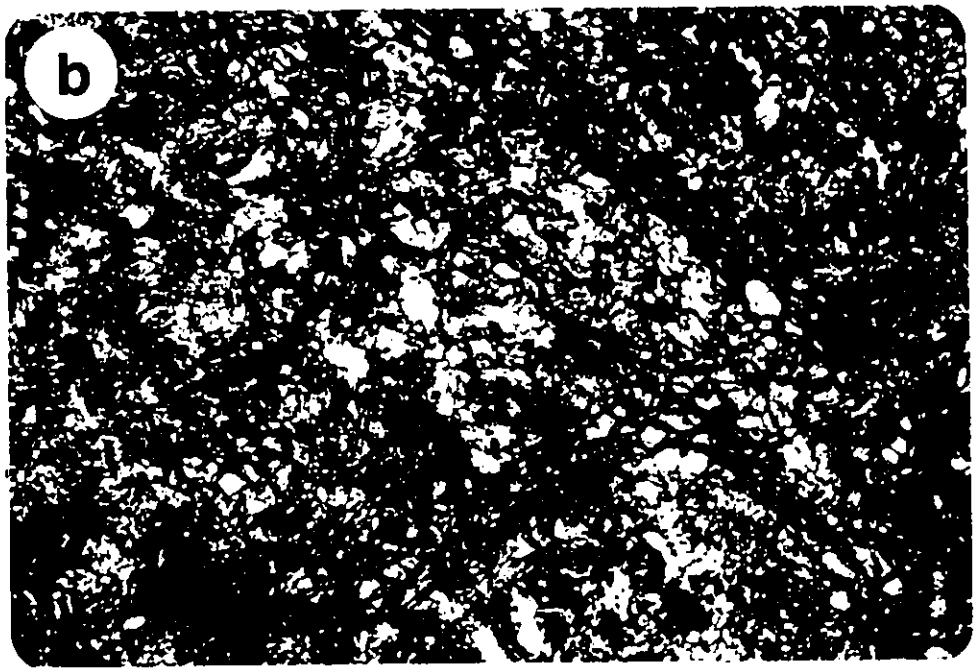
b

possible plagioclase, and glass. This texture is weakly subophitic. These flows are commonly polyhedrally jointed but massive otherwise.

3.1.5 STRATIGRAPHIC RELATIONSHIPS

The contacts of the komatiites and komatiitic basalts with the other adjacent supracrustal rocks of the Pipedream Lake belt are poorly preserved. The maximum stratigraphic thickness of the steeply dipping komatiitic flows is uncertain but is estimated to be no greater than 1000 m. Stratigraphic relationships are not conclusive, but field evidence (i.e. spinifex textures and relict pillows as top indicators) seems to indicate that a relatively thick basal section of felsic to intermediate lava flows and fragmental rocks is overlain by komatiites and komatiitic basalts. Komatiitic basalts apparently overlie the komatiites and are in turn overlain by felsic to intermediate metavolcanics, which in turn are overlain by an upper volcanogenic sequence, as shown previously in Figure 6.

3.2 WOODBURN LAKE GROUP - ESKER LAKE AND NO-NAME LAKE BELTS

Petrographically, some of the rocks from the Esker Lake belt are similar texturally to those described above, but are less well-preserved due to a higher degree of alteration, metamorphism, and deformation. Fuller (1977) described the

No-name Lake belt metavolcanics and some of these also resemble komatiites from the Pipedream Lake belt, even though the rocks have undergone amphibolite grade regional metamorphism and large-scale deformation.

3.2.1 ULTRAMAFIC KOMATIITES

The ultramafic komatiitic flows are exposed in low, rubbly, hummocky outcrops with few recognizable primary features. The rocks are quite homogeneous, very fine-grained to fine-grained, and soft; and have been altered to tremolite, serpentine, and talc. They have a thick, rusty brown to dull, dark green weathering rind, and are greenish grey, light green, or dark green on fresh surfaces. In places, alternating massive, rusty brown layers and schistose, greyish-green layers are present, and these represent the cumulate zones and spinifex-textured zones, respectively. A closely to widely spaced fracture pattern, filled with magnetite, is present in some of the flows and is presumed to be deformed polyhedral joints. Flows are up to 5 m thick with rare spinifex textures. Some of these ultramafic rocks consist of fine grained serpentine/tremolite/talc pseudomorphs after olivine set in a matrix of very fine-grained skeletal, plumose, and/or cuspate tremolite pseudomorphs after clinopyroxene, and chlorite after glass. More commonly, these ultramafic komatiites have been strongly deformed and altered to a very fine- to fine-grained randomly oriented aggregate of

variable metamorphic assemblages which are dependent upon the metamorphic conditions. Fuller (1977) observed olivine and enstatite as well as possible anthophyllite and cordierite in several thin sections of No-name Lake ultramafics, which is indicative of upper amphibolite grade. No relict textures of spinifex were found, but some cumulate textures were preserved in the least deformed rocks. The cumulate rocks consist of serpentine/tremolite/talc pseudomorphs after olivine set in a groundmass of tremolite and chlorite.

3.2.2 KOMATIITIC BASALTS AND HIGH-MG THOLEIITIC BASALTS

Komatiitic basalts and associated tholeiitic basalts occur chiefly as massive flows and are rarely pillowed. Flows are less than 5 m thick. Hand specimens show the rocks to be homogeneous, dense, aphanitic to fine-grained, and generally lacking in primary volcanic textures. The rocks have been moderately to strongly metamorphosed and deformed. Pyroxene spinifex textures are not preserved or do not occur in these komatiitic to tholeiitic basalts.

Petrographically, these rocks consist of acicular, dendritic, and cuspated clinopyroxene microphenocrysts, and rare clinopyroxene and olivine phenocrysts set in a very fine-grained groundmass of densely intergrown microlites of plagioclase and pyroxenes with devitrified glass. The rare olivine crystals have been pseudomorphically altered to tremolite or serpentine. The

clinopyroxenes have been replaced by fibrous tremolite or chlorite, or hornblende at higher metamorphic grades; the plagioclase altered to epidote, albite, and carbonate; and the devitrified glass to chlorite. The majority of the basalts are aphyric and without any primary textures, and have been moderately metamorphosed to a very fine-grained felty aggregate of various metamorphic mineral assemblages which include actinolite or hornblende, epidote, zoisite, chlorite, tremolite, albite, or carbonate. Some of the least altered rocks show faint relict subophitic textures.

WHOLE-ROCK GEOCHEMISTRY

4.1 SAMPLE LOCATION AND SELECTION

The majority of analysed samples, lettered R, K and AK, were collected by the author while working for the Geological Survey of Canada under the supervision of W.W. Heywood (1978), F.C. Taylor (1980), and J.A. Fraser (1981). Other samples, marked S and F, within the thesis area were collected by S. Tella (1978) and R. Fuller (1976), respectively, while working for W.W. Heywood. Ken Ashton provided some samples of the volcanogenic suite (Note: refer to Ashton (1988) for location of these samples). Other komatiite and basalt samples and analyses from adjacent map areas were provided by M. Schau (Prince Albert Group), F.C. Taylor (Ketyet River Group) and A.N. LeCheminant (Aberdeen Lake). The sample localities within the Pipedream Lake, Esker Lake, and No-name Lake belts are shown in Figures 25, 26, and 27, respectively. The large number of samples analyzed in the Pipedream Lake belt make it necessary to subdivide the belt into four geographic sectors.

In most instances, the freshest possible samples were collected on the basis of textural preservation and obvious alteration. Some highly altered/deformed samples were also collected in order to look at the problem of alteration.

Figure 25. Location map of sample localities within the Pipedream Lake belt. See Figure 6 for details of the geology of the Pipedream Lake belt.

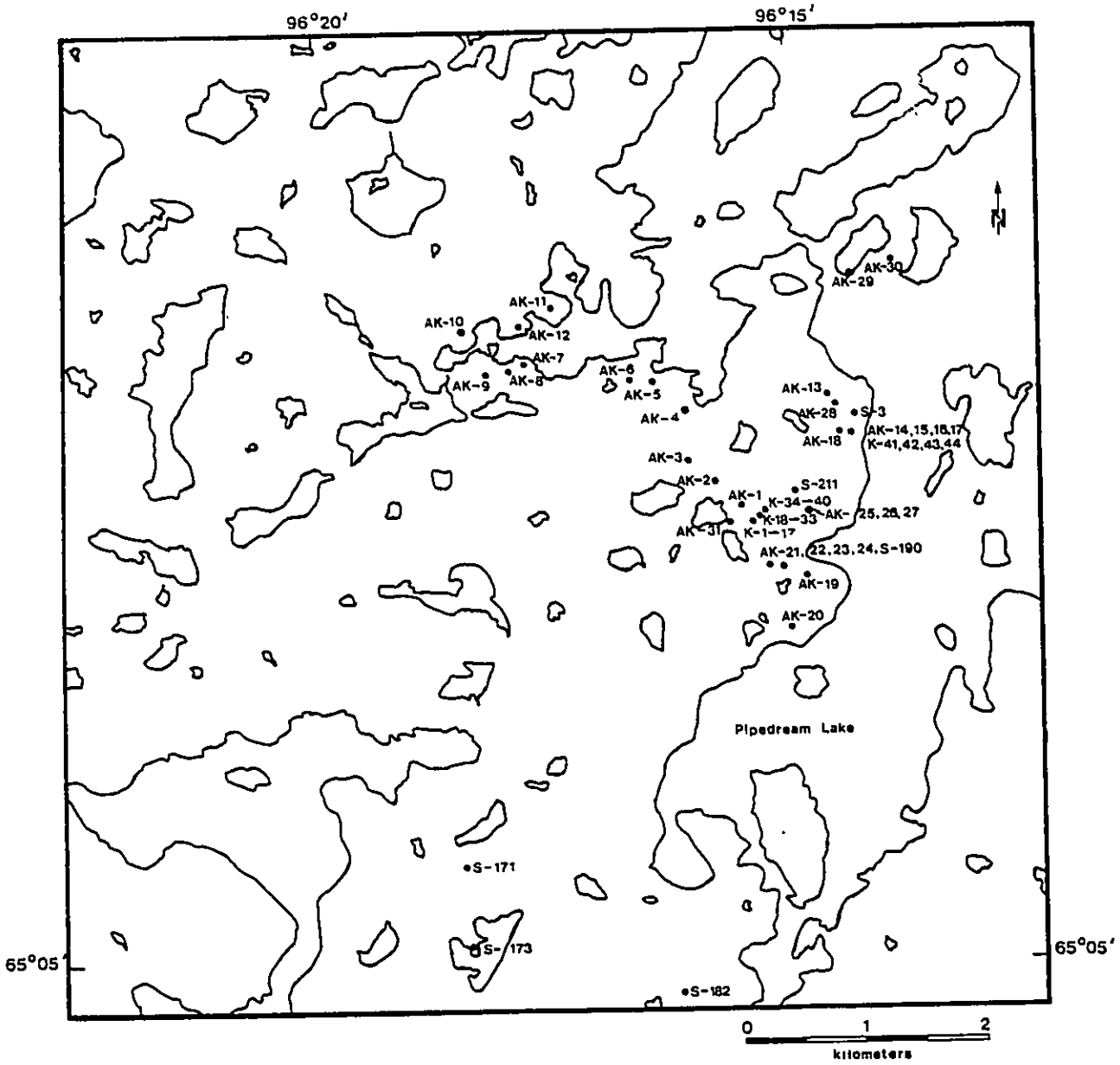
96°20′
96°15′
65°05′
65°05′
N
AK-30
AK-29
AK-11
AK-10
AK-12
AK-7
AK-6
AK-9
AK-8
AK-5
AK-4
AK-13
AK-28
S-3
AK-14,15,16,17
K-41,42,43,44
AK-18
AK-3
AK-2
S-211
AK-1
K-34-40
AK-25,26,27
K-18-33
AK-31
K-1-17
AK-21,22,23,24,S-190
AK-19
AK-20
Pipedream Lake
S-171
S-173
S-182
0
1
2
kilometers

Figure 26. Location map for the samples of the Esker Lake belt used in this study. See Figure 8 for details of the geology of the Esker Lake belt.

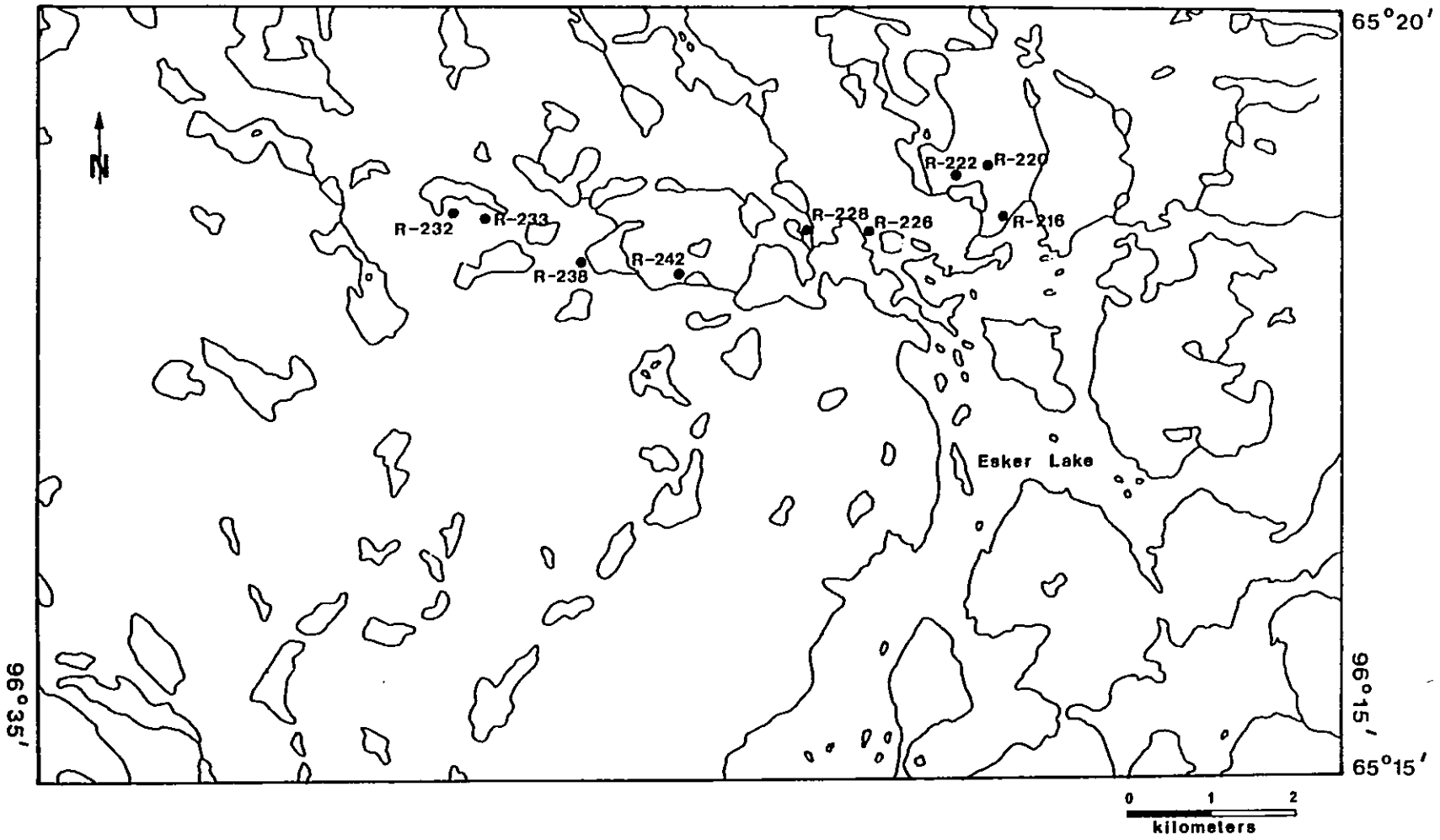
65°20′
96°35′
96°15′
65°15′
N
R-222
R-220
R-232
R-233
R-228
R-226
R-216
R-242
R-238
Esker Lake
0
1
2
kilometers

Figure 27. Location map of the komatiite samples within the No-name Lake belt analysed by Fuller (1977) and used in this study. Refer to Figure 2 for location of this belt relative to the Pipedream Lake and Esker Lake belts. Details of the geology can be obtained from Fuller (1977).

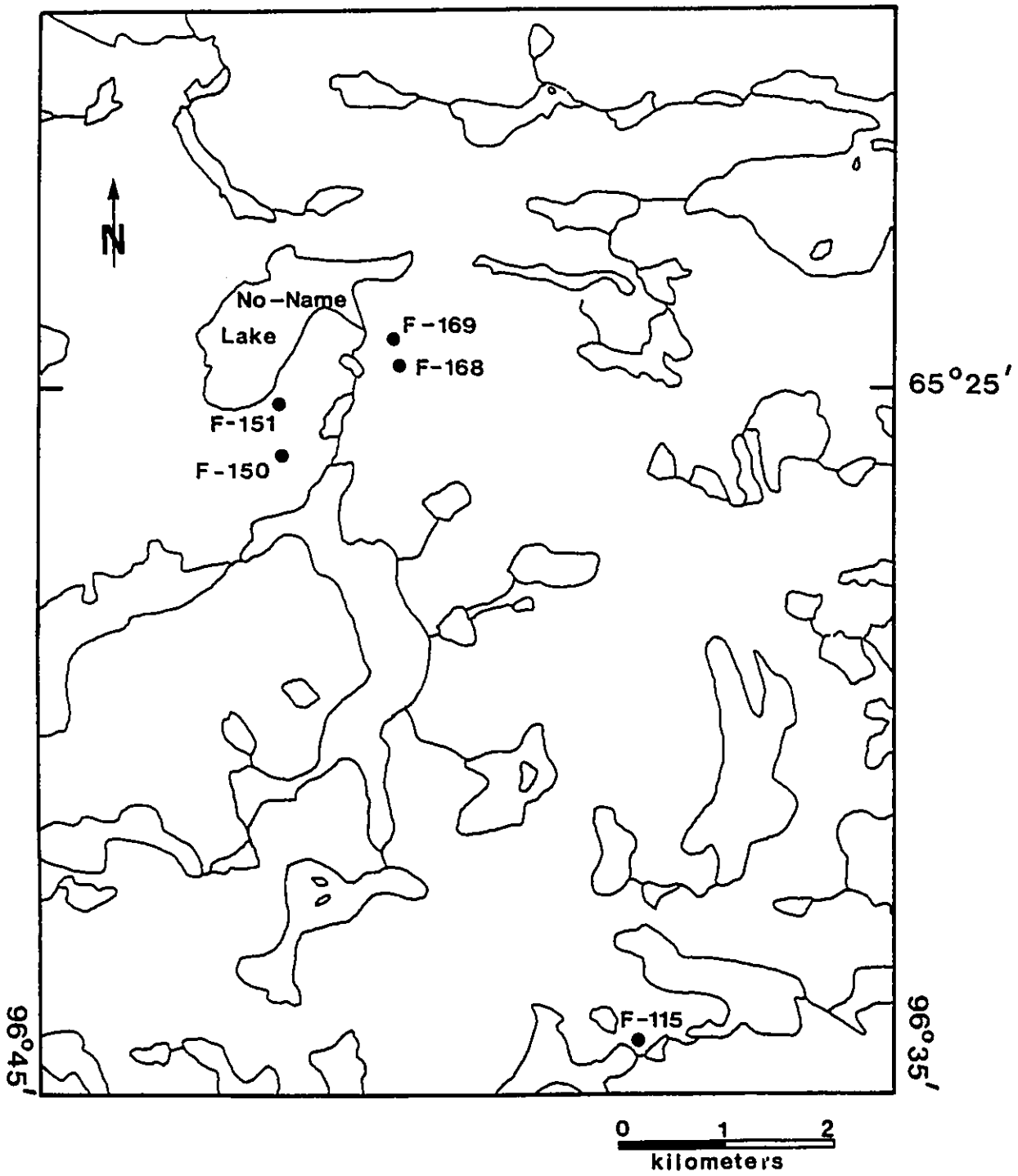
N
No-Name
Lake
F-169
F-168
F-151
F-150
F-115
65°25′
96°45′
96°35′
0
1
2
kilometers

4.2 ANALYTICAL METHODS AND CHEMICAL DATA

Major elements and trace elements (Cr, Nb, Ni, Rb, Sr, V, Y, Zn, Zr) were determined by X-ray fluorescence (XRF) at the University of Ottawa for all of the Woodburn Lake Group samples; except samples K326A, K347, K759c, K006a, K567d, K793, and F-115, of Ashton (1988) and samples F-150c, F-150f, and F-169a of Fuller (1978). Analyses were carried out with a Philips 1410 automated X-ray fluorescence unit using fused disks ($Li_2B_4O_7$, $LiCO_3$, and the sample), a Cr tube, and the technique of alpha coefficients described by DeJongh (1975). Total iron was determined as Fe and expressed as Fe_2O_3 by the XRF technique. FeO was determined by rapid wet chemistry on 20 samples. Precision and accuracy obtained from replicate analyses and analyses of USGS standards are given in Tables 2a, 2b, and 2c. Chemical data of a representative suite of komatiites and komatiitic basalts are shown in Table 3. A complete listing of chemical data, including inter-element ratios and CIPW norms, is presented in Appendices B1.a to B1.f.

Duplicate XRF analyses of major and trace (Ba, Cr, Ni, Rb, Sr, Zn, Zr) elements of 52 of these samples were made at the Geological Survey of Canada (G.S.C.). Analysis of FeO, H_2O_{Tot}, CO_{2Tot}, and S were made by rapid chemical methods. Fe_2O_3 was calculated using $Fe_2O_3 = Fe_2O_3$ (XRF) - 1.11136 * FeO (determined by wet chemistry). In addition, atomic absorption (AA) analyses of B, Ba, Co, Cr, Cu, Ni, Sr, and V of these 52 samples were made

Table 2a – Precision of whole-rock analyses

	DR-N (15)	2s
SiO2	53.84	+/- 0.38
TiO2	1.83	+/- 0.01
Al2O3	17.65	+/- 0.17
Fe2O3*	9.73	+/- 0.12
MnO	0.21	+/- 0.01
MgO	4.23	+/- 0.12
CaO	6.98	+/- 0.04
Na2O	3.05	+/- 0.18
K2O	1.74	+/- 0.03
P2O5	0.15	+/- 0.04
Cr	44	+/- 7
Nb	5	+/- 6
Ni	18	+/- 8
Rb	71	+/- 4
Sr	388	+/- 5
V	222	+/- 13
Y	29	+/- 4
Zn	146	+/- 9
Zr	131	+/- 4

2s = confidence limit presented as 2.0 times standard deviation

Note: mean of 15 DR-N analyses listed in Table 2b; 8 analyses from DR-N(1) disk, 6 analyses from DR-N(2) disk, and 1 analysis from R-N(A).

Table 2b - Accuracy and precision of major and trace elements for standard samples of silicate rocks

	DR-N(1)	DR-N(1)	DR-N(1)	DR-N(1)	DR-N(1)	DR-N(1)	DR-N(1)	DR-N(1)	DR-N(2)	DR-N(2)	DR-N(2)
SiO2	53.02	53.50	53.16	53.05	52.93	53.05	53.14	53.21	53.02	53.00	52.50
TiO2	1.03	1.03	1.03	1.03	1.03	1.03	1.04	1.03	1.03	1.03	1.03
Al2O3	17.74	17.79	17.61	17.64	17.69	17.63	17.65	17.67	17.60	17.74	17.49
Fe2O3T	9.71	9.77	9.74	9.73	9.72	9.72	9.74	9.73	9.50	9.70	9.60
MnO	0.21	0.21	0.21	0.21	0.21	0.21	0.21	0.21	0.22	0.21	0.21
MgO	4.26	4.26	4.22	4.19	4.26	4.23	4.21	4.26	4.20	4.20	4.10
CaO	6.96	7.03	6.99	6.90	7.00	6.97	6.97	6.90	7.01	7.00	6.99
Na2O	2.91	3.17	3.14	3.01	3.07	2.90	3.11	2.80	3.10	3.04	3.09
K2O	1.74	1.75	1.74	1.74	1.74	1.74	1.74	1.74	1.76	1.74	1.75
P2O5	0.13	0.10	0.16	0.12	0.10	0.13	0.14	0.16	0.16	0.14	0.16
S	0.03	0.03	0.03	0.03	0.03	0.03	0.03	0.03	0.01	0.01	0.01
Total	97.74	98.72	98.03	97.73	97.86	97.72	97.90	97.90	97.85	97.97	97.89
Cr	50	44	44	46	47	47	42	45	39	39	44
Nb	61	5	5	3	4	5	3	1	13	3	7
Ni	20	15	22	20	24	25	19	17	15	19	14
Rb	74	75	70	69	72	69	72	60	74	72	72
Sr	387	392	387	380	389	386	380	383	390	392	387
V	210	207	225	217	215	220	222	224	233	225	216
Y	29	25	20	31	29	30	20	29	30	20	32
Zn	153	145	150	140	144	151	144	143	147	140	153
Zr	131	132	134	133	132	132	129	130	132	129	133

Table 2b (continued)

	DR-N(2)	DR-N(2)	DR-N(2)	DR-N(A)	Mean (15)	Variance (15)	Std-Dev (15)	COV(*100) (15)	2s (15)	DR-N (RV)
SiO2	53.05	52.90	53.05	52.89	53.04	0.03556	0.189	0.4	0.38	52.90
TiO2	1.04	1.03	1.04	1.05	1.03	0.00004	0.006	0.6	0.01	1.09
Al2O3	17.69	17.46	17.60	17.72	17.65	0.00742	0.086	0.5	0.17	17.56
Fe2O3T	9.78	9.76	9.74	9.80	9.73	0.00350	0.059	0.6	0.12	9.72
MnO	0.21	0.21	0.21	0.22	0.21	0.00001	0.003	1.6	0.007	0.22
MgO	4.21	4.13	4.13	4.37	4.23	0.00342	0.059	1.4	0.12	4.41
CaO	6.98	6.96	6.98	6.97	6.98	0.00034	0.019	0.3	0.04	7.07
Na2O	3.20	3.00	3.00	3.00	3.05	0.00765	0.087	2.9	0.18	3.00
K2O	1.75	1.73	1.74	1.69	1.74	0.00022	0.015	0.9	0.03	1.70
P2O5	0.17	0.14	0.13	0.15	0.15	0.00033	0.018	12.2	0.04	0.25
S	0.01	0.02	0.01	0.03	0.02	0.00009	0.009	41.0	0.02	?
Total	98.09	97.34	97.63	97.98	97.84					98.00
Cr	37	50	42	43	44	14	3.7	8.4	7	42
Nb	6	6	3	6	5	0.5	2.9	62	6	6?
Ni	17	18	14	10	18	15	3.9	22	8	16
Rb	71	71	71	68	71	4.3	2.1	2.9	4	70
Sr	388	389	387	393	388	6.2	2.5	0.6	5	400
V	215	224	226	230	222	44	6.6	3.0	13	230
Y	29	29	29	34	29	3.8	2.0	6.7	4	30?
Zn	150	144	140	147	146	19	4.4	3.0	9	145
Zr	128	130	128	135	131	4.3	2.1	1.6	4	125

Note: RV means recommended values as reported in G.S.C. Paper 83-15 - 'Studies in "Standard Samples" of silicate rocks and minerals 1969-1982' (Abbey, 1983). The accuracy or degree of conformity of the measured standard values is established by comparing these values to their recommended values (RV). The precision or reproducibility of measured standard values is given by the mean and 2s of these values.

Table 2b (continued)

	GA(1)	GA(1)	Mean (2)	GA (RV)	BCR-1	BCR-1	Mean (2)	Mean (DP-14)	2s (DP-14)	BCR-1 (RV)
SiO2	70.12	70.19	70.15	69.96	54.48	54.57	54.53	54.65	0.63	54.53
TiO2	0.34	0.34	0.34	0.38	2.22	2.20	2.21	2.25	0.02	2.26
Al2O3	14.83	14.85	14.84	14.51	13.68	13.60	13.64	13.68	0.18	13.72
Fe2O3T	2.80	2.80	2.80	2.77	13.69	13.68	13.69	13.51	0.23	13.41
MnO	0.09	0.09	0.09	0.09	0.18	0.18	0.18	0.18	0.10	0.18
MgO	0.83	0.84	0.84	0.95	3.41	3.38	3.40	3.44	0.18	3.48
CaO	2.43	2.45	2.44	2.45	7.01	7.01	7.01	6.95	0.08	6.97
Na2O	3.61	3.62	3.62	3.55	3.36	3.33	3.35	3.30	0.23	3.38
K2O	4.12	4.10	4.11	4.03	1.75	1.75	1.75	1.72	0.02	1.70
P2O5	0.11	0.09	0.10	0.12	0.34	0.33	0.34	0.36	0.05	0.36
S	bl	0.01	0.01	0.02?	0.07	0.08	0.08	0.03	0.02	0.04?
Total	99.28	99.38	99.33	98.83	100.19	100.11	100.18	100.07		99.95
Cr	12	10	11	12	36	44	40	29	15	15
Nb	9	8	9	10?	12	9	11	-	-	19?
Ni	15	18	17	7	bl	bl	bl	bl	-	10
Rb	172	170	171	175	41	46	44	48	7	47
Sr	297	297	297	310	382	390	386	384	13	330
V	31	30	31	38	410	416	413	-	-	420
Y	19	20	20	21	34	38	36	41	1	40
Zn	102	79	91	80	127	155	141	119	10	125
Zr	149	149	149	150	185	181	183	171	9	185

Table 2b (continued)

	G-2	G-2 (RV)	GSP-1	GSP-1 (RV)	SY-2(1)	SY-2(1) (RV)
SiO2	69.24	69.22	66.98	67.32	60.16	60.10
TiO2	0.47	0.48	0.65	0.66	0.13	0.14
Al2O3	15.38	15.40	14.95	15.20	12.23	12.12
Fe2O3T	2.70	2.69	4.28	4.30	6.30	6.28
MnO	0.04	0.03	0.04	0.04	0.31	0.32
MgO	0.66	0.75	0.82	0.97	2.58	2.70
CaO	1.94	1.96	2.00	2.03	7.90	7.98
Na2O	4.18	4.06	2.77	2.81	4.31	4.34
K2O	4.53	4.46	5.56	5.51	3.56	4.48
P2O5	0.13	0.13	0.28	0.28	0.35	0.43
S	bl	0.01?	0.01	0.03?	bl	0.01
Total	99.27	99.19	98.34	99.23	97.83	98.90
Cr	13	5	13	8	12	12
Nb	bl	13?	21	23?	20	23?
Ni	14	4	12	9	25	10
Rb	170	170	250	250	216	220
Sr	369	400	229	240	262	275
V	36	36	47	54	45	52
Y	bl	11	21	29	135	130
Zn	87	84	109	105	264	250
Zr	315	300	560	500	277	280

Table 2c - Precision of komatiite (whole-rock) analyses.

	komatiite average (n=5 duplicate analyses)		S	2S	V(100)
SiO2	43.28	+/-	0.16	0.32	3.8
TiO2	0.29	+/-	0.006	0.012	2.1
Al2O3	6.99	+/-	0.11	0.22	1.6
Fe2O3	10.89	+/-	0.09	0.18	0.9
MnO	0.17	+/-	0.00	0.00	0.0
MgO	26.44	+/-	0.23	0.46	0.9
CaO	5.62	+/-	0.06	0.12	1.0
Na2O	0.64	+/-	0.09	0.18	13.5
K2O	0.04	+/-	0.003	0.09	7.5
P2O5	bl	+/-	-	-	-
Cr	2758	+/-	64	128	2.3
Nb	bl	+/-	-	-	-
Ni	1484	+/-	45	90	3.0
Rb	bl	+/-	-	-	-
Sr	4	+/-	2	4	48.0
V	172	+/-	9	18	5.0
Y	17	+/-	3	6	19.4
Zn	76	+/-	19	38	24.4
Zr	11	+/-	1	2	9.1

S = confidence limit presented as 1.0 standard deviation
2S = confidence limit presented as 2.0 standard deviation
V = S/mean
bl = below detection limit
- = not determined

Table 3 - Representative analyses of komatiites and high-Mg (komatiitic to tholeiitic) basalts from the Woodburn Lake Group

	K-44g	AK-14a	AK-14b	AK-14c	AK-14d	K-24	R-242a	R-242b	R-220d	R-222
SiO2	43.87	42.76	41.66	43.53	42.14	41.93	42.77	41.54	51.35	46.93
TiO2	0.30	0.29	0.24	0.30	0.29	0.24	0.37	0.25	1.09	0.66
Al2O3	6.97	6.90	5.65	7.32	6.92	5.89	8.44	6.21	13.58	13.69
Fe2O3T	10.55	11.09	10.87	10.20	11.63	10.71	11.58	10.64	8.07	12.29
Fe2O3	nd	4.26	2.84	3.09	4.90	nd	2.81	4.15	nd	nd
FeO	nd	6.15	7.23	6.40	6.06	nd	7.89	5.84	nd	nd
MnO	0.16	0.17	0.15	0.16	0.15	0.17	0.16	0.16	0.08	0.16
MgO	25.42	26.39	29.85	25.91	25.49	31.04	23.83	29.34	13.82	13.35
CaO	6.40	5.29	3.20	6.21	5.73	3.86	6.30	4.34	2.57	6.22
Na2O	0.70	0.73	0.40	0.76	0.29	0.27	0.44	0.51	3.24	2.41
K2O	0.02	0.08	0.02	0.07	bl	0.02	0.01	0.10	0.14	1.01
P2O5	bl	bl	bl	bl	bl	bl	bl	bl	0.22	bl
H2O(GSC)-(LOI)	5.60	6.60	8.60	6.10	6.30	6.90	(5.78)	(7.57)	(5.56)	(3.42)
CO2(GSC)	0.20	0.20	0.40	0.10	0.10	0.20	nd	nd	nd	nd
Total	98.84	100.50	101.12	100.66	99.04	100.43	99.68	100.66	99.72	100.14
B (AA-GSC)	19	bl	19	16	21	22	nd	nd	nd	nd
Ba (AA-GSC)	12	26	17	15	19	17	nd	nd	nd	nd
Ba (XRF-UW)	nd	nd	nd	nd	nd	nd	16	16	135	157
Co (INAA)	89	71	99	80	68	95	nd	nd	nd	nd
Cr (XRF)	2682	2637	2600	2865	2736	2849	2357	2672	475	738
Cu (AA-GSC)	5	24	72	11	13	23	nd	nd	nd	nd
Nb (XRF-UW)	nd	nd	nd	nd	nd	nd	3	3	13	4
Ni (XRF)	1395	1463	1882	1320	1296	1961	986	1839	287	207
Rb (XRF)	bl	1	bl	bl	bl	bl	bl	bl	9	42
Sr (XRF)	7	3	1	3	5	3	17	17	287	299
V (XRF)	166	163	123	183	184	139	180	160	182	302
Y (ICP-GSC)	6	7	5	6	6	6	10	6	21	16
Zn (XRF)	51	61	87	82	57	64	114	101	109	78
Zr (XRF)	11	13	11	11	12	6	21	9	129	43
Sc (INAA)	27	27	21	28	27	23	nd	nd	nd	nd
La (ICP-GSC)	0.7	1.4	0.8	0.7	0.6	1.2	1.3	nd	nd	3.0
Ce (ICP-GSC)	1.5	2.7	1.7	1.6	1.8	2.4	3.4	nd	nd	7.1
Nd (ICP-GSC)	2.5	3.2	2.6	2.5	2.6	2.7	4.8	nd	nd	7.3
Sm (ICP-GSC)	0.5	0.3	0.3	0.2	0.5	0.4	0.5	nd	nd	1.8
Eu (ICP-GSC)	0.2	0.2	0.1	0.2	0.2	0.2	0.2	nd	nd	0.5
Gd (ICP-GSC)	0.8	1.1	0.8	1.0	0.9	0.9	1.6	nd	nd	2.5
Dy (ICP-GSC)	1.3	1.4	1.0	1.2	1.2	1.2	1.9	nd	nd	3.0
Er (DCP-UO)	1.2	1.1	1.1	1.1	1.2	1.2	nd	nd	nd	nd
Yb (ICP-GSC)	0.5	0.7	0.4	0.5	0.6	0.6	0.9	nd	nd	1.5

Komatiites (spinifex-textured) - K-44g (possible liquid composition), AK-14c, AK-14d (possible liquid composition), R-242a
Komatiites (cumulate) - AK-14a (base of cumulate zone), AK-14b, K-24, R-242b
bl = below detection limit; nd = not determined

Table 3 (continued)

	R-232b	R-232c	R-233	AK-20	AK-31
SiO2	44.15	53.34	46.22	50.97	50.71
TiO2	1.84	1.14	0.57	0.65	0.56
Al2O3	14.50	13.80	12.03	11.05	12.43
Fe2O3T	11.68	10.05	12.15	15.10	11.05
Fe2O3	nd	nd	nd	nd	nd
FeO	nd	nd	nd	nd	nd
MnO	0.15	0.14	0.25	0.17	0.18
MgO	8.96	7.09	12.73	8.74	12.72
CaO	6.51	5.26	9.04	9.30	6.55
Na2O	2.59	3.93	2.00	1.66	3.20
K2O	2.42	1.39	1.60	1.10	0.00
P2O5	0.16	0.10	bl	bl	bl
H2O(GSC)-(LOI)	(4.86)	(1.80)	(2.45)	nd	nd
CO2(GSC)	nd	nd	nd	nd	nd
Total	97.82	98.04	99.12	97.90	97.40
B (AA-GSC)	nd	nd	nd	nd	nd
Ba (AA-GSC)	nd	nd	nd	nd	nd
Ba (XRF-UW)	364	432	286	nd	nd
Co (INAA)	nd	nd	nd	nd	nd
Cr (XRF)	151	245	1033	370	1093
Cu (AA-GSC)	nd	nd	nd	nd	nd
Nb (XRF-UW)	8	8	4	nd	nd
Ni (XRF)	185	143	301	130	353
Rb (XRF)	55	42	66	60	bl
Sr (XRF)	182	372	221	140	117
V (XRF)	147	140	278	209	255
Y (ICP-GSC)	23	14	15	12	10
Zn (XRF)	94	190	161	60	91
Zr (XRF)	52	112	31	45	45
Sc (INAA)	nd	nd	nd	27	nd
La (ICP-GSC)	17	nd	1.4	4.9	3.2
Ce (ICP-GSC)	32	nd	3.7	9.6	7.9
Nd (ICP-GSC)	20	nd	5.2	10	6.0
Sm (ICP-GSC)	3.8	nd	0.8	1.1	1.4
Eu (ICP-GSC)	1.4	nd	0.4	0.7	0.5
Gd (ICP-GSC)	5.0	nd	2.1	2.4	2.0
Dy (ICP-GSC)	4.6	nd	2.5	2.9	2.6
Er (DCP-UO)	nd	nd	nd	nd	nd
Yb (ICP-GSC)	1.5	nd	1.3	1.5	1.1

High-Mg basalts (komatiitic to tholeiitic) - R-220d, R-222, R-232b, R-232c,R-233, AK-20, AK-31

at the same laboratory. Analytical precision and accuracy at the G.S.C. laboratory are presented in Table 4.

In addition, Sc and Co were determined for 102 samples using instrumental neutron-activation analysis (INAA). Also, Cr, Ni, and FeO_{Tot} were checked at the same time by this method. The samples were irradiated at McMaster University using a Slowpoke II reactor and were measured using a Ge-Li detector at the University of Ottawa.

Sixty samples were analysed for REE (La, Ce, Nd, Sm, Eu, Dy, Er, Yb) by direct current plasma - atomic emission spectroscopy (DCP-AEC) at the University of Ottawa (Appendix B2) using a procedure described in Appendix C1. Analytical precision and accuracy of this method are presented in Tables 5a and 5c. The REE (La, Ce, Nd, Sm, Eu, Gd, Dy, Yb, and Y) concentrations were checked on duplicate sets of 15 of the above 60 samples by inductively coupled argon plasma - atomic emission spectroscopy (ICAP-AES) at the Geological Survey of Canada (Appendix B2). Analytical uncertainties are given in Tables 5a and 5b. In addition, REE (La, Ce, Nd, Sm, Eu, Tb, Yb) analyses were checked on another 14 samples by INAA using the procedure described above.

Difficulties were encountered with the REE determinations due to the detection limit of the analytical methods, and the low concentration of REE present in the samples (i.e. especially the komatiites with 1X to 5X chondritic values). Analytical precision by DCP-AEC and ICAP-AES is excellent, as shown by close agreement

Table 4 - Analytical reliability of results for
major and trace elements at G.S.C. laboratory

Major Elements by Wavelength-Dispersive XRF

	Abs(+/- %)	Rel(+/- %)	Det(%)
SiO2	.40	1	.40
TiO2	.02	1	.02
Al2O3	.40	1	.40
Cr2O3	.02	1	.02
Fe2O3	.10	1	.10
FeO	.20	2	.20
MnO	.01	2	.01
MgO	.10	1	.10
CaO	.10	1	.10
Na2O	.50	1	.50
K2O	.05	1	.05
H2OT	.10	5	.10
CO2T	.05	3	.05
P2O5	.02	1	.02
S	.04	5	.04

Trace Elements by Wavelength-Dispersive XRF

	Abs(+/- ppm)	Rel(+/- %)	Det(ppm)
Ba	20	1	20
Ni	30	10	30
Rb	20	1	20
Sr	20	10	20
Zn	20	10	20
Zr	20	10	20

Abs = absolute analytical error
Rel = relative analytical error
Det = detection limit

Note: 2s = (abs + rel). For example, if SiO_2 is 50.00 wt%, then 2s for this value is 0.90 wt%.

Table 5a - Accuracy (i.e. comparison of measured values by ICP and DCP with recommended values (RV)) of REE for standard samples of silicate rocks

	STM-1 (ICP)	STM-1 (ICP)	STM-1 (DCP)	STM-1 (DCP)	STM-1 (RV)	G-2 (ICP)	G-2 (ICP)	G-2 (DCP)	G-2 (DCP)	G-2 (RV)
La	130	130	150	150	150	84	83	96	99	92
Ce	240	240	276	274	260	160	150	172	179	160
Nd	82	83	85	83	78	57	52	56	56	58?
Sm	11	12	11	-	13	6.8	5.7	6.8	6.9	7.2
Eu	3.4	3.4	3.5	3.5	3.7	1.4	1.2	1.3	1.4	1.4
Gd	8.6	8.6	-	-	10?	3.8	2.8	4.0	3.4	5?
Dy	8.1	7.8	8.2	7.9	-	2.1	1.1	2.0	2.0	2.3
Er	-	-	4.1	4.1	-	-	-	0.9	1.0	1.3
Yb	3.9	4.0	3.7	3.2	4.3	0.5	-	0.8	0.8	0.9
Y	43	45	-	-	46?	9.6	-	-	-	11

	MRG-1 (ICP)	MRG-1 (ICP)	MRG-1 (DCP)	MRG-1 (DCP)	MRG-1 (DCP)	MRG-1 (DCP)	MRG-1 (DCP)	MRG-1 (DCP)	MRG-1 (DCP)	MRG-1 (DCP)	MRG-1 (RV)
La	8.3	8.7	-	-	-	-	-	9.9	9.5	9.7	10?
Ce	24	25	31	34	29	29	30	23	24	-	25?
Nd	24	24	15	14	16	16	15	-	-	18	19?
Sm	3.0	3.9	3.1	4.4	3.3	3.4	3.4	-	-	2.2	5?
Eu	1.4	1.5	1.2	1.2	1.2	1.1	1.1	1.3	1.1	1.2	1.4?
Gd	4.5	4.5	3.9	3.8	3.5	3.6	3.6	-	-	-	-
Dy	3.2	3.1	2.0	1.9	2.2	2.1	2.1	2.7	2.7	2.7	3?
Er	-	-	1.8	1.7	1.2	1.1	1.1	1.8	1.8	1.9	-
Yb	0.8	0.8	-	-	-	-	-	0.6	0.6	0.8	1?
Y	13	14	-	-	-	-	-	-	-	-	16?

	RGM-1 (ICP)	RGM-1 (ICP)	RGM-1 (DCP)	RGM-1 (DCP)	RGM-1 (DCP)	RGM-1 (DCP)	RGM-1 (DCP)	RGM-1 (RV)
La	21	22	-	-	20	20	27	23?
Ce	43	44	46	49	50	48	-	48?
Nd	21	21	14	17	21	20	21	19?
Sm	3.2	3.9	3.0	3.5	3.1	2.9	2.5	4.3?
Eu	0.6	0.6	0.4	0.5	0.6	0.6	0.6	0.7?
Gd	3.6	3.6	2.8	3.3	-	-	-	-
Dy	3.8	3.6	1.9	2.7	3.4	2.9	2.8	-
Er	-	-	1.6	2.0	2.2	2.2	2.1	-
Yb	2.4	2.4	-	-	1.3	1.3	1.3	2.5?
Y	22	23	-	-	-	-	-	25?

Table 5a (continued)

	BHVO-1 (ICP)	BHVO-1 (ICP)	BHVO-1 (DCP)	BHVO-1 (DCP)	BHVO-1 (DCP)	BHVO-1 (DCP)	BHVO-1 (DCP)	BHVO-1 (DCP)	BHVO-1 (DCP)	BHVO-1 (DCP)	BHVO-1 (DCP)	BHVO-1 (RV)
La	18	15	-	-	16	16	16	16	16	14	14	17?
Ce	37	37	46	40	39	36	-	-	-	-	46	39
Nd	30	28	21	20	25	25	25	24	25	26	25	24
Sm	4.5	6.2	4.7	4.7	-	-	4.5	3.9	-	-	4.6	6.1
Eu	2.1	2.1	1.7	1.7	2.1	1.8	1.7	1.7	1.7	2.0	-	2.0
Gd	6.4	6.5	5.3	5.2	6.7	7.1	6.1	6.3	5.7	-	-	6.0
Dy	5.5	5.4	3.4	3.3	4.5	4.4	5.3	4.5	5.1	4.5	4.6	5?
Er	-	-	2.4	2.3	2.9	2.7	2.3	3.0	2.8	2.8	2.4	-
Yb	1.9	2.0	-	-	1.3	1.3	1.4	1.2	1.2	1.4	-	1.9
Y	25	27	-	-	-	-	-	-	-	-	-	27

	SDC-1 (ICP)	SDC-1 (ICP)	SDC-1 (RV)	NIM-G (ICP)	NIM-G (ICP)	NIM-G (RV)	NIM-P (DCP)	NIM-P (DCP)	NIM-P (DCP)	NIM-P (DCP)	NIM-P (RV)
La	40	39	42	99	100	105?	2.5	2.0	2.3	2.2	2?
Ce	85	87	92	180	190	200	-	-	-	-	4.6?
Nd	44	45	38	75	77	68?	-	-	-	-	-
Sm	7.7	8.2	8.3?	12	14	16	-	-	-	-	-
Eu	1.6	1.6	1.7?	0.3	0.4	0.4?	0.1	0.1	0.1	0.1	0.2?
Gd	7.0	7.1	7.2?	14	15	-	-	-	-	-	-
Dy	6.8	6.5	-	19	18	15	0.4	0.4	0.5	0.3	-
Er	-	-	-	-	-	-	0.8	0.8	0.8	1.1	-
Yb	3.6	3.6	4.2	13	13	14	0.4	0.5	0.5	0.7	0.6?
Y	36	38	42?	120	130	145	-	-	-	-	6?

	JB-1 (ICP)	JB-1 (ICP)	JB-1 (RV)	AGV-1 (DCP)	AGV-1 (RV)	BCR-1 (DCP)	BCR-1 (RV)	BIR-1 (DCP)	BIR-1 (RV)
La	38	37	36?	42	36	26	27	0.8	0.7?
Ce	63	65	67?	73	71	-	53	-	1.6?
Nd	28	29	21?	34	37?	-	26?	2.6	-
Sm	4.3	4.7	4.8?	-	5.9	5.4	6.5	-	1.0?
Eu	1.4	1.5	1.5?	1.7	1.6?	2.0	2.0	0.4	0.6?
Gd	4.1	4.8	-	-	5.5?	-	1.6?	-	-
Dy	2.8	4.2	4?	3.5	3.5?	6.6	7?	2.3	3.7?
Er	-	-	-	1.9	1.2?	3.3	3.5?	2.0	-
Yb	-	1.8	2.1?	1.8	1.9	3.6	3.4	1.3	1.7?
Y	-	22	26?	-	19	-	40	-	16?

Table 5b - Analytical reliability (precision) of results for Rare Earth Elements (REE's) at the G.S.C. Laboratories.

Rare Earth Elements by DCP

	Abs(+/- ppm)	Rel(+/- %)	Det(ppm)
La	.5	5	.5
Ce	.5	5	.5
Nd	.5	5	.5
Sm	.3	5	.3
Eu	.1	5	.1
Gd	.2	5	.2
Dy	.2	5	.2
Yb	.1	5	.1
Y	1.0	5	1.0

Table 5c - Analytical reliability (precision) of results for Rare Earth Elements (REE's) at the University of Ottawa geochemical laboratory.

Rare Earth Elements by DCP

	Abs(+/- ppm)	Rel(+/- %)	Det(ppm)
La	.5	5	.5
Ce	2.0	10	2.0
Nd	.5	5	.5
Sm	.3	5	.3
Eu	.1	5	.1
Gd	.5	10	.5
Dy	.5	5	.5
Er	.5	5	.5
Yb	.5	5	.5

(i.e. low standard deviation) between duplicate analyses (Table 5b and Appendix B2). However, the accuracy (i.e. the deviation between determined and accepted values of standard silicate rocks) ranges from acceptable (<2 standard deviations) to unacceptable (>2 standard deviations) at these chondritic levels by comparison with standard silicate rocks (Table 5a). For example, careful examination of the Nd and Sm values of standard silicate rocks determined by ICP shows the Nd values to be consistently higher than and the Sm values consistently lower than recommended values (from Abbey, 1983). The deviation of Nd and Sm values appears to be an analytical problem that is more noticeable with samples that have low REE totals. This suggests that the analytical problem is masked by high concentrations of REE. The consistently higher Nd values might be the result of a spectral overlap by another element, and the consistently lower Sm values might be the consequence of an improper background correction. Values of La and Nd by DCP are considered to be good, the same with values of La, Ce, Gd, and Dy by ICP. The values for La, Sm, Eu, and Yb determined by INAA are considered to be fair to good. The values of Dy, Er, and Yb by DCP are consistently higher or lower than recommended values of standards that have low concentrations of these elements (i.e. NIM-P, BIR-1, BHVO-1). Correction factors of 1.33, 0.85, and 1.25 have been determined for DCP values of Dy, Er, and Yb, respectively, on the basis of these consistently higher and lower values of U.S.G.S. standards. These correction factors can be applied to

the determined DCP values of Dy, Er, and Yb of the komatiite samples. Similarly, a correction factor of 1.2 can be applied to the Yb value determined by ICP. The problems with Nd, Sm (<0.5 ppm), and Eu (<0.3 ppm) by ICP and Ce (<7.5 ppm), Sm (<0.5 ppm), and Eu (<0.3 ppm) by DCP are attributed to analytical detection levels, background correction/matrix problems, and spectral interferences. Hence, the REE chondrite-normalized profiles (Figs. 28a to 28l) are shown with the sets of raw data (i.e. not corrected by the determined correction factors) of different analytical techniques, so as not to mislead the reader. These REE chondrite-normalized profiles are considered approximate and can be used as a comparison with other komatiite occurrences. However, only a few of the REE (i.e. La (ICP, DCP), Ce (ICP), Nd (DCP), Sm(INAA), Eu(INAA), Gd(ICP), Dy(ICP), and Yb (DCP)) can be used with any degree of confidence in petrogenetic modelling.

Thirty three samples of the Woodburn Lake Group were previously analysed for major and trace elements at the University of Windsor. Trace elements (Ba, Co, Cr, Nb, Ni, Rb, Sr, Y, Zr) were determined on pressed powder pellets. Analytical procedures and uncertainties are described by Annesley (1981b). These samples were run again for major and trace elements at the University of Ottawa.

Values obtained for most majors and traces are consistent between most laboratories. Values obtained for Na_2O (XRF-G.S.C.), P_2O_5 (XRF-University of Ottawa), Y (XRF-University of Ottawa), V and Y (AA-G.S.C.), and Co, Cr, Ni, and V (XRF-University of

Figure 28a. Chondrite-normalized REE plots of two cumulate zone samples from an ultramafic flow with a thick spinifex-textured zone. The position of the samples within the flow is shown in Figure 50.

Note: The symbol index in Figures 28a to 28l indicates the analytical methods used in determining the REE. The chosen REE profile is established on the basis of the accuracy of each method for a particular REE. Normalizing values are from Jahn et al. (1980).

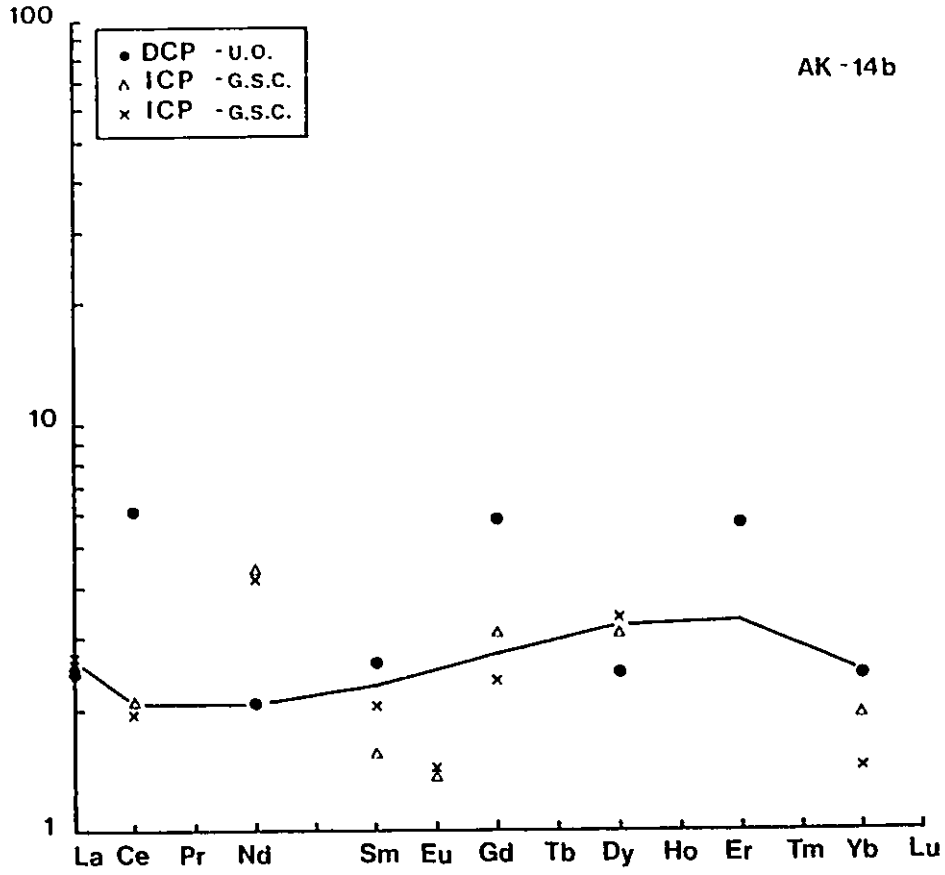
100
10
1
• DCP - U.O.
△ ICP - G.S.C.
× ICP - G.S.C.
AK - 14b
La Ce Pr Nd Sm Eu Gd Tb Dy Ho Er Tm Yb Lu

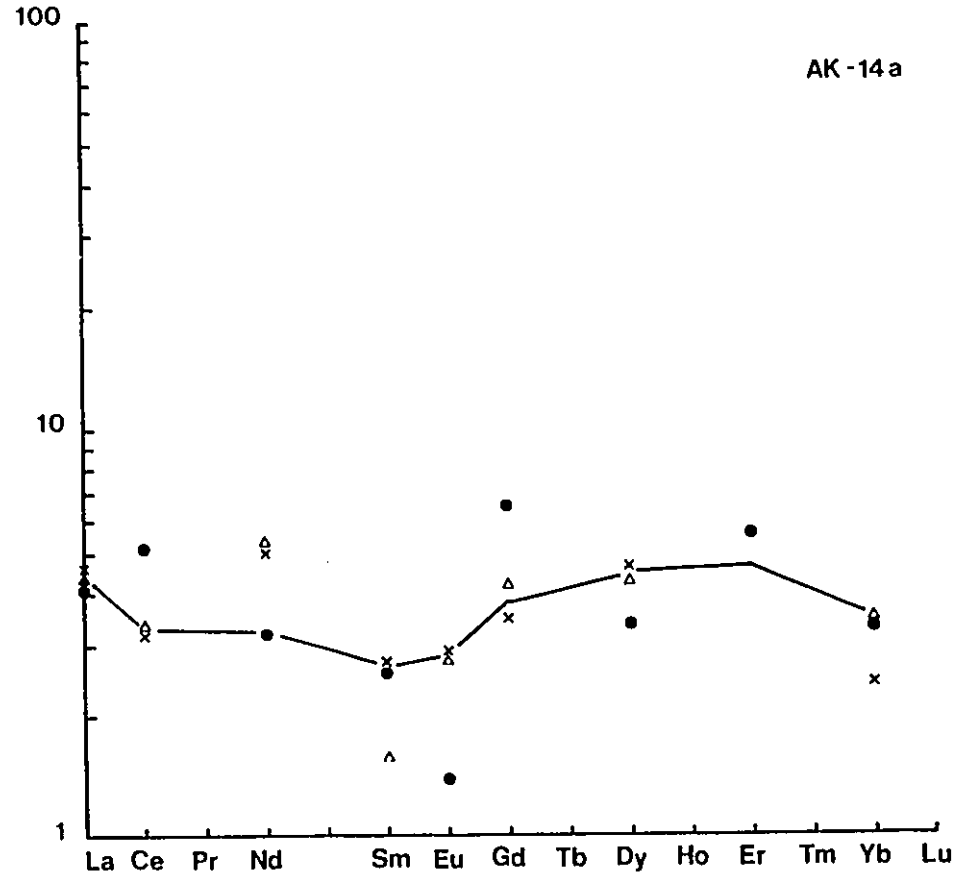
100
10
1
AK - 14a
La Ce Pr Nd Sm Eu Gd Tb Dy Ho Er Tm Yb Lu

Figure 28b. Chondrite-normalized REE plots of two spinifex-textured zone samples from the same flow as Figure 28a. Sample position within the flow is shown in Figure 50.

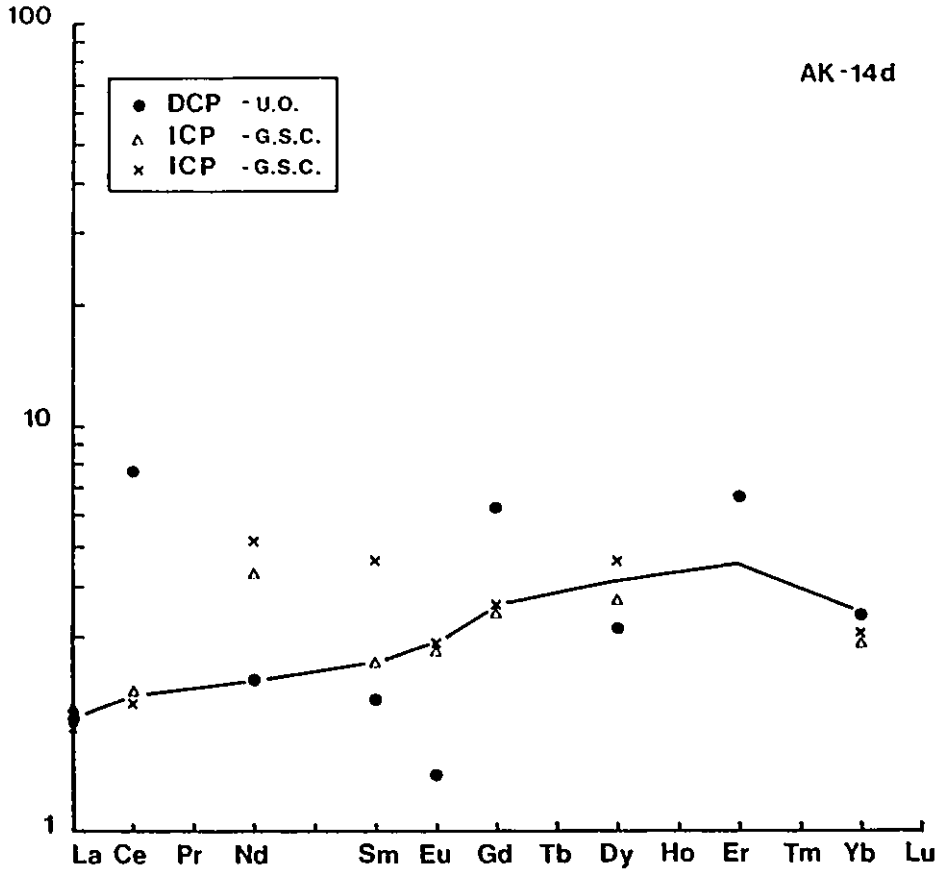
100
10
1
DCP - U.O.
ICP - G.S.C.
ICP - G.S.C.
AK-14d
La Ce Pr Nd Sm Eu Gd Tb Dy Ho Er Tm Yb Lu

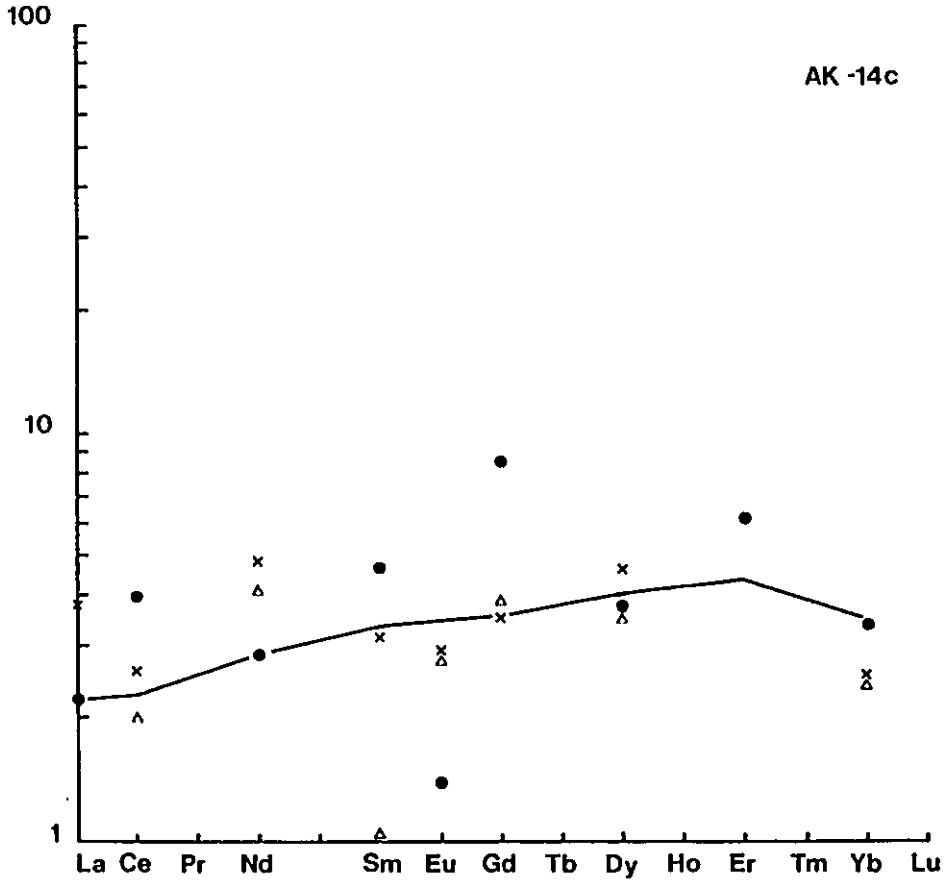
100
10
1
AK-14c
La Ce Pr Nd Sm Eu Gd Tb Dy Ho Er Tm Yb Lu

Figure 28c. Chondrite-normalized REE plots of the flow top (K-44g) and the middle portion of the cumulate zone from an ultramafic flow with a thick spinifex-textured zone.

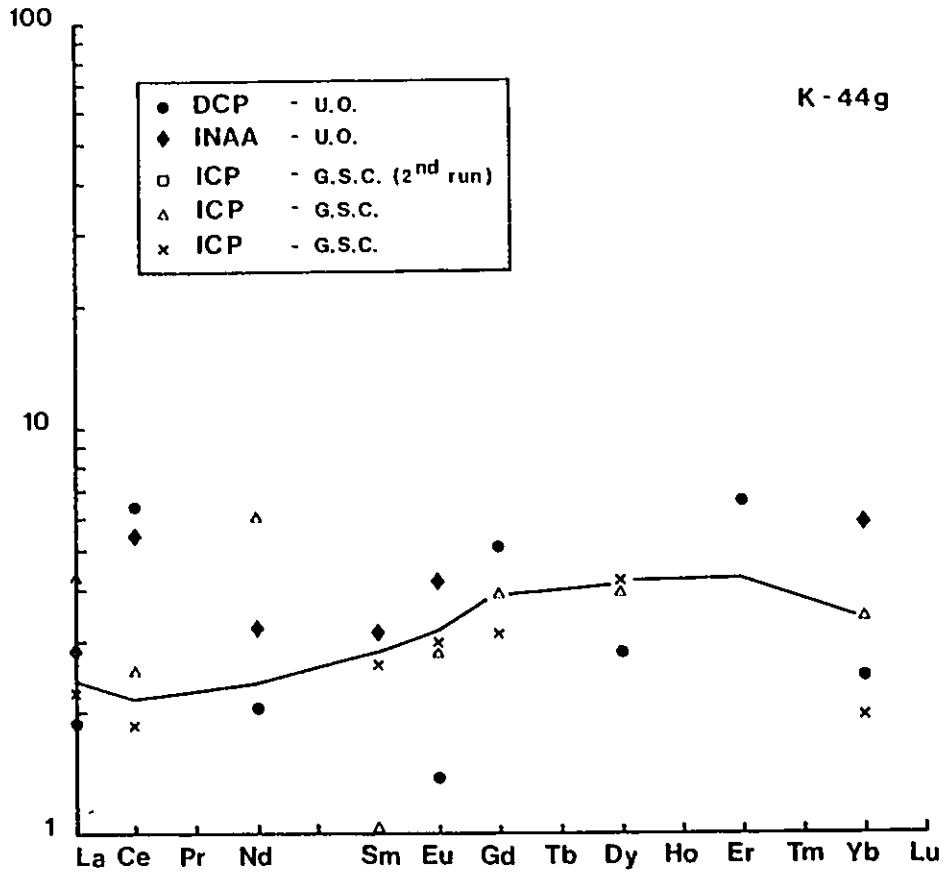
100
10
1
DCP - U.O.
INAA - U.O.
ICP - G.S.C. (2nd run)
ICP - G.S.C.
ICP - G.S.C.
K-44g
La Ce Pr Nd Sm Eu Gd Tb Dy Ho Er Tm Yb Lu

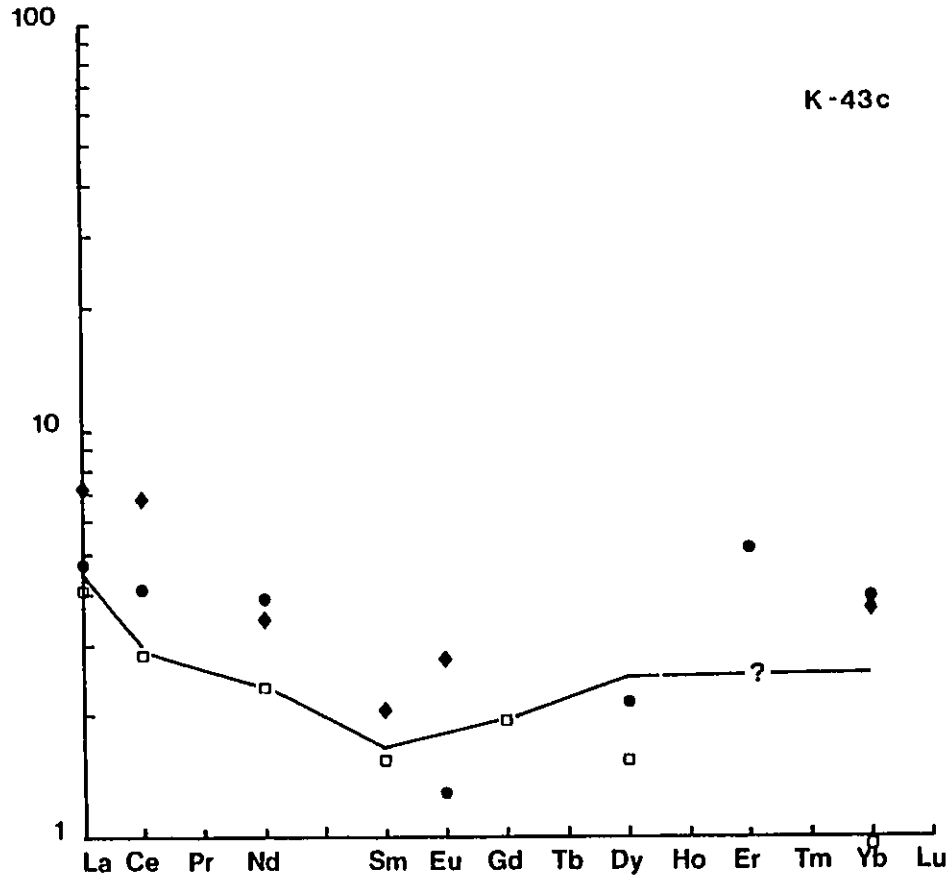
100
10
1
K-43c
?
La Ce Pr Nd Sm Eu Gd Tb Dy Ho Er Tm Yb Lu

Figure 28d. Chondrite-normalized REE plots of a contact metamorphosed komatiite (AK-12b) and a spinifex-textured komatiite (K-42a). The position of K-42a within the spinifex-textured zone is shown in Figure 50.

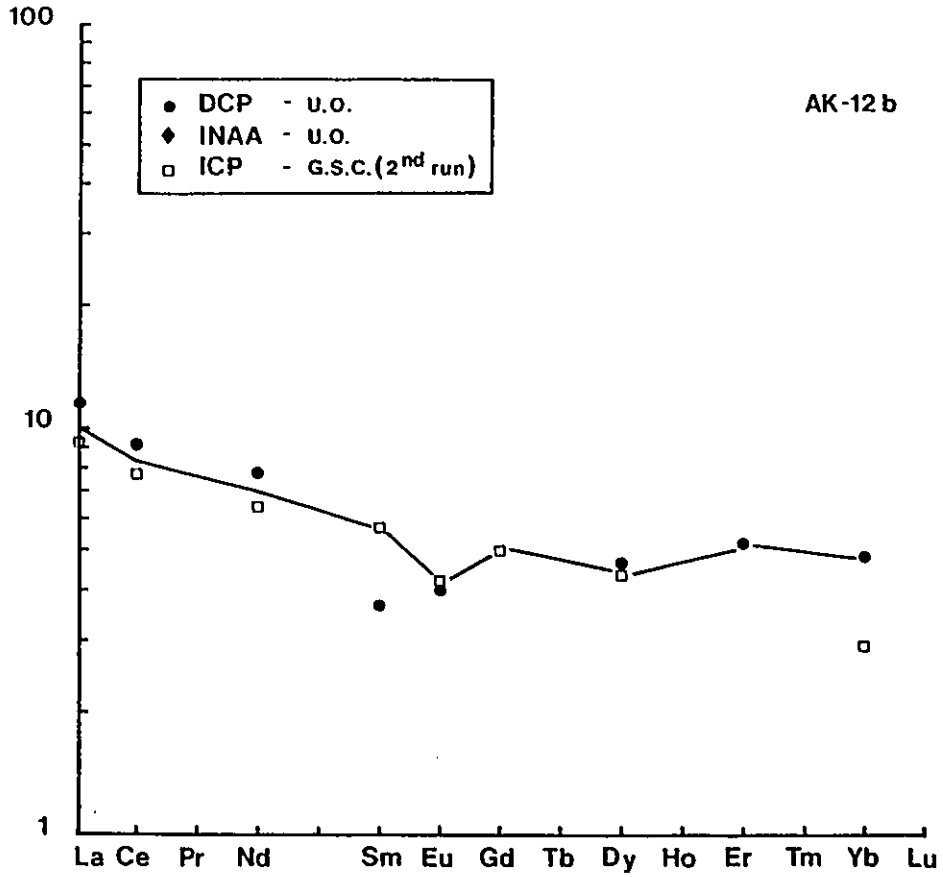
100
10
1
DCP - U.O.
INAA - U.O.
ICP - G.S.C.(2nd run)
AK-12 b
La Ce Pr Nd Sm Eu Gd Tb Dy Ho Er Tm Yb Lu

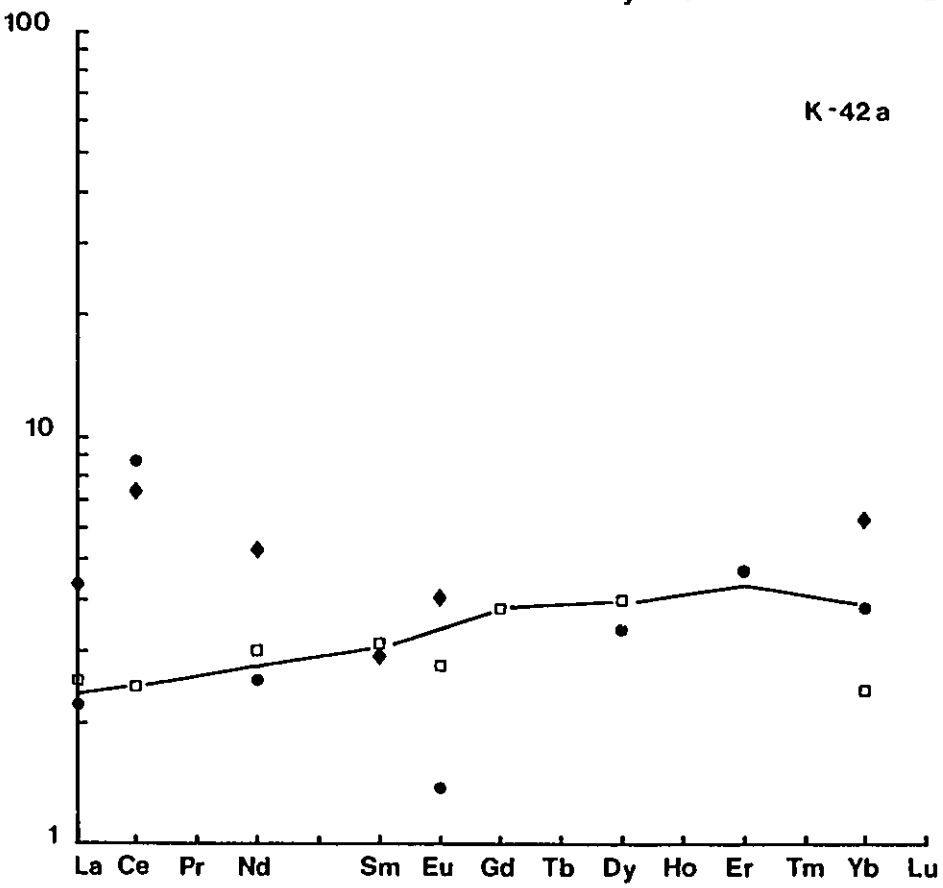
100
10
1
K-42 a
La Ce Pr Nd Sm Eu Gd Tb Dy Ho Er Tm Yb Lu

Figure 28e. Chondrite-normalized REE plots of two other komatite samples from the Pipedream Lake belt.

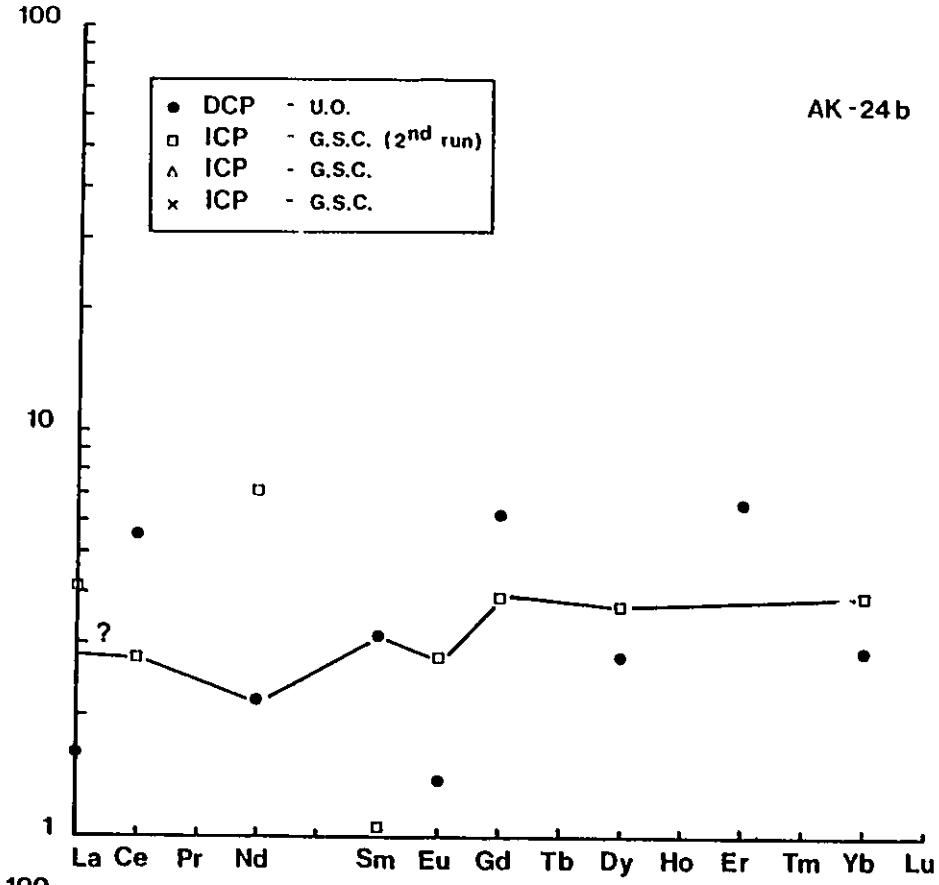
100
10
1
DCP - U.O.
ICP - G.S.C. (2nd run)
ICP - G.S.C.
ICP - G.S.C.
AK-24b
?
La Ce Pr Nd Sm Eu Gd Tb Dy Ho Er Tm Yb Lu

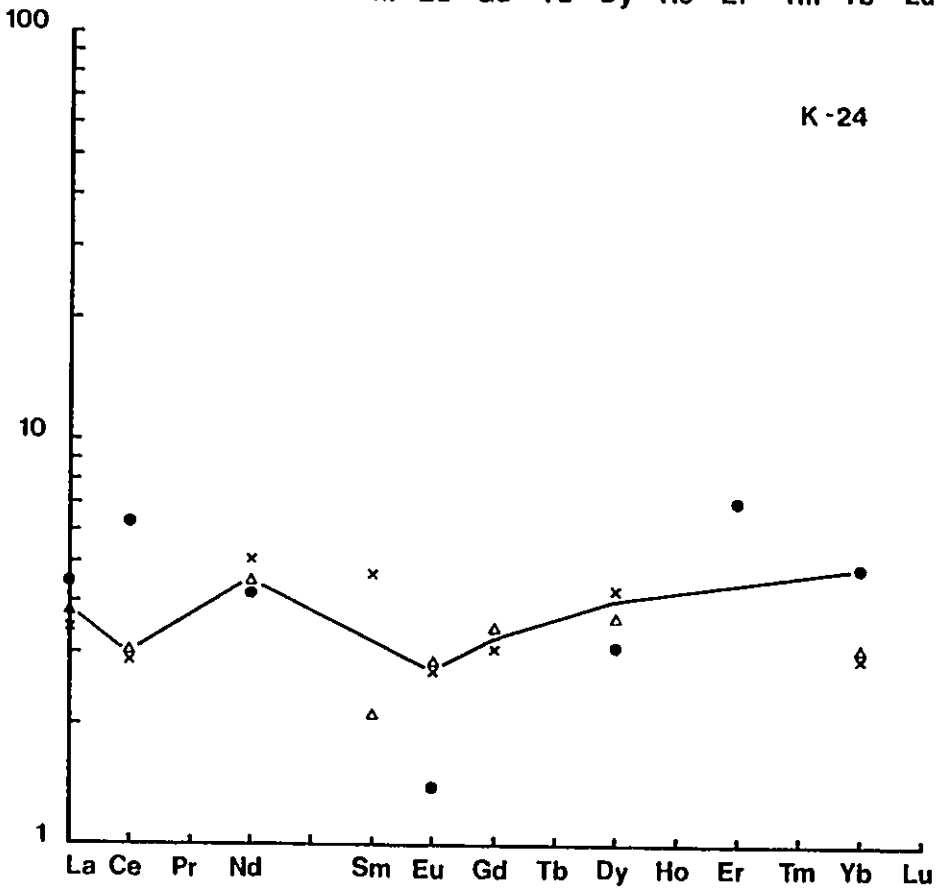
100
10
1
K-24
La Ce Pr Nd Sm Eu Gd Tb Dy Ho Er Tm Yb Lu

Figure 28f. Chondrite-normalized REE plots of a komatiitic basalt (R-233) and a spinifex-textured komatiite (R-242a) from the Esker Lake belt.

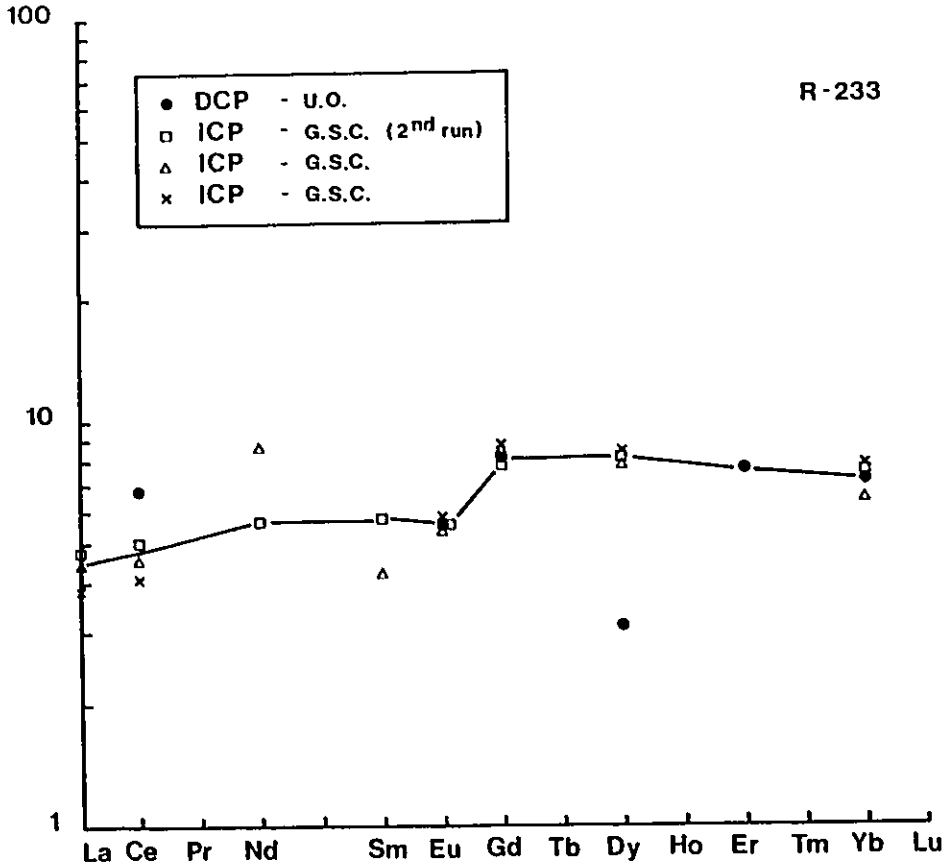
100
10
1
DCP - U.O.
ICP - G.S.C. (2nd run)
ICP - G.S.C.
ICP - G.S.C.
R-233
La Ce Pr Nd Sm Eu Gd Tb Dy Ho Er Tm Yb Lu

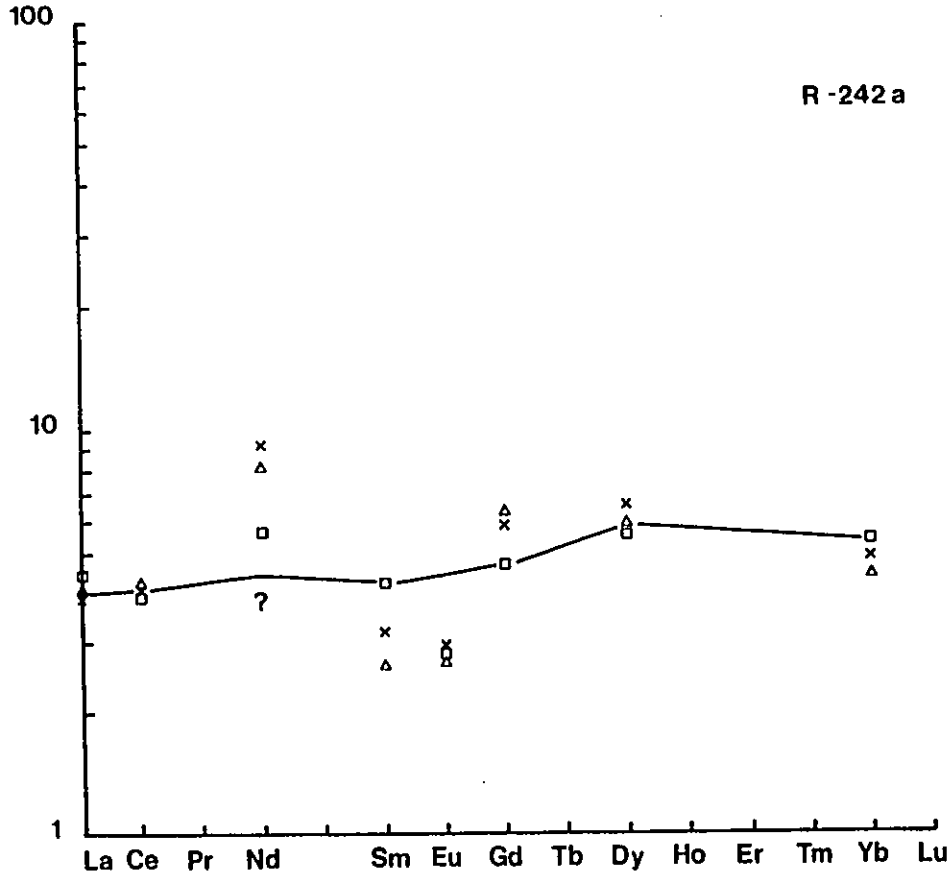
100
10
1
R-242a
?
La Ce Pr Nd Sm Eu Gd Tb Dy Ho Er Tm Yb Lu

Figure 28g. Chondrite-normalized REE plots of a komatiitic basalt (AK-31) and a high-Mg tholeiitic basalt (AK-20) from the Pipedream Lake belt.

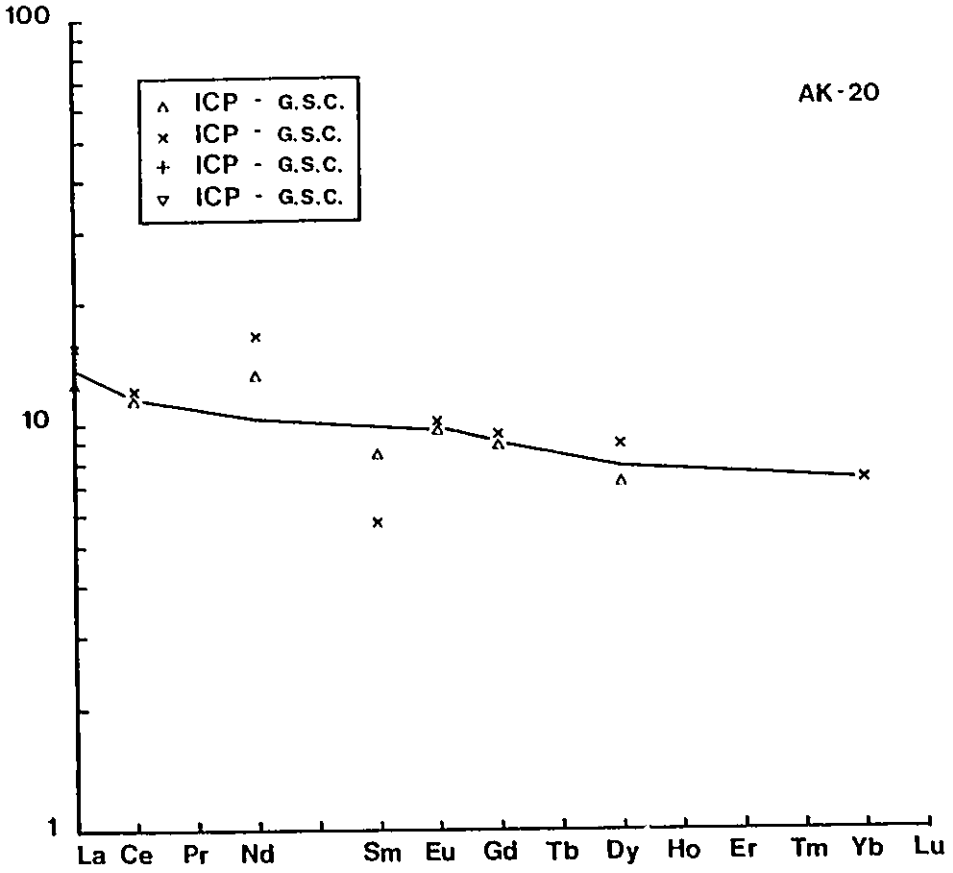
100
10
1
ICP - G.S.C.
ICP - G.S.C.
ICP - G.S.C.
ICP - G.S.C.
AK-20
La Ce Pr Nd Sm Eu Gd Tb Dy Ho Er Tm Yb Lu

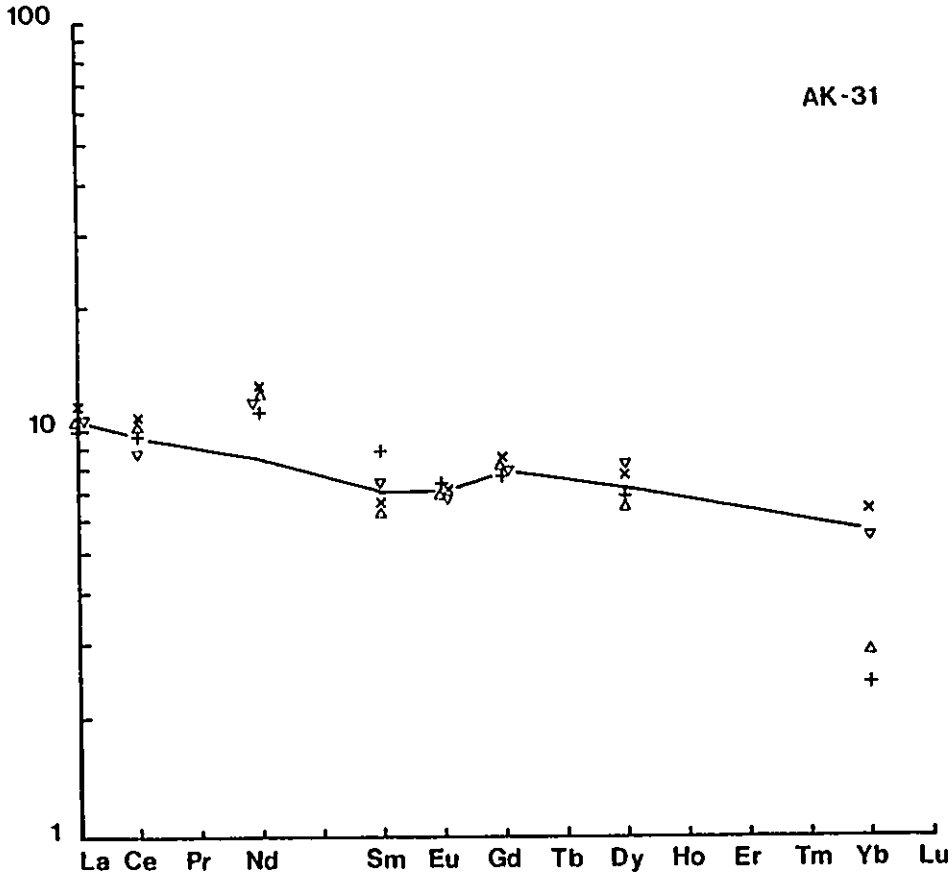
100
10
1
AK-31
La Ce Pr Nd Sm Eu Gd Tb Dy Ho Er Tm Yb Lu

Figure 28h. Chondrite-normalized REE plots of a komatiitic basalt (R-222) and a tholeiitic basalt (R-232b) from the Esker Lake belt.

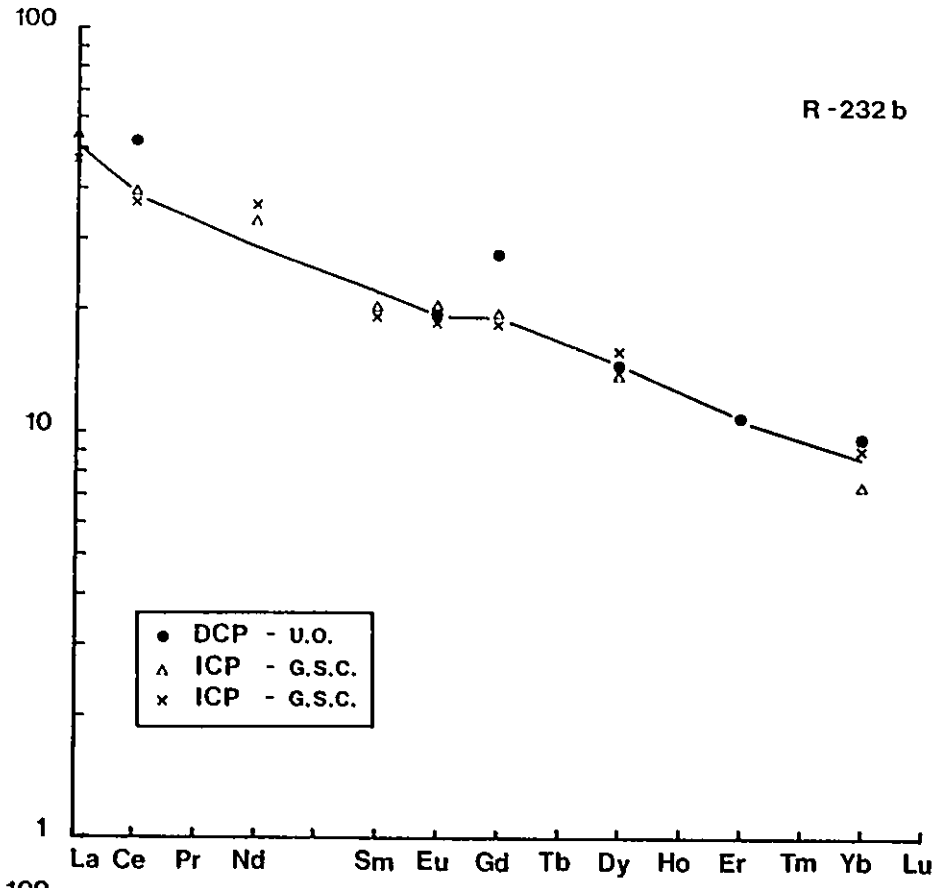
100
10
1
R-232b
DCP - U.O.
ICP - G.S.C.
ICP - G.S.C.
La Ce Pr Nd Sm Eu Gd Tb Dy Ho Er Tm Yb Lu

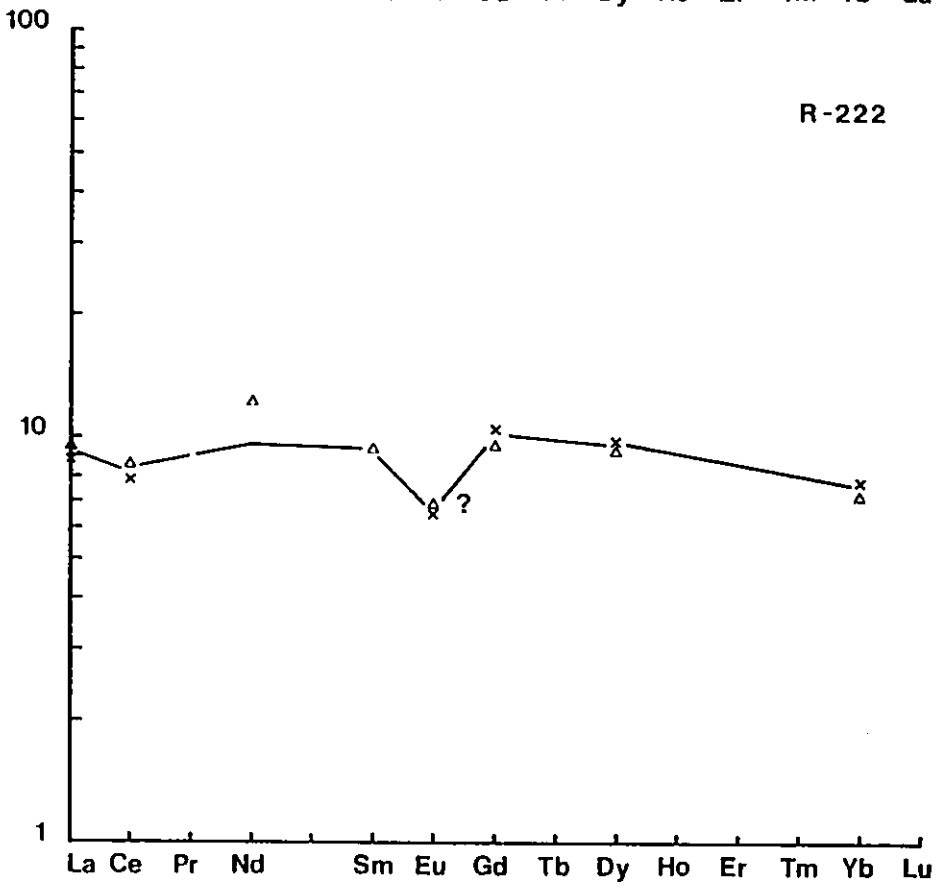
100
10
1
R-222
?
La Ce Pr Nd Sm Eu Gd Tb Dy Ho Er Tm Yb Lu

Figure 28i. Chondrite-normalized REE plots of an andesite (AK-6a) from the Woodburn Lake Group and a basaltic andesite (T-8) from the Ketyet River Group.

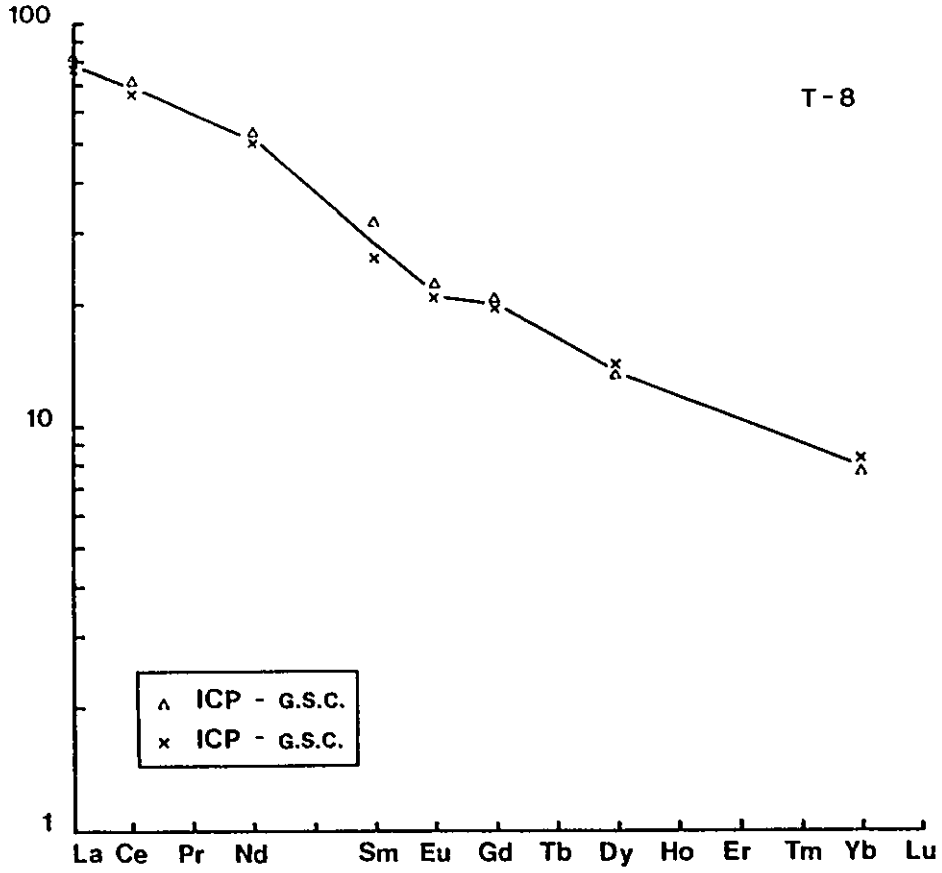
100
10
1
T-8
ICP - G.S.C.
ICP - G.S.C.
La Ce Pr Nd Sm Eu Gd Tb Dy Ho Er Tm Yb Lu

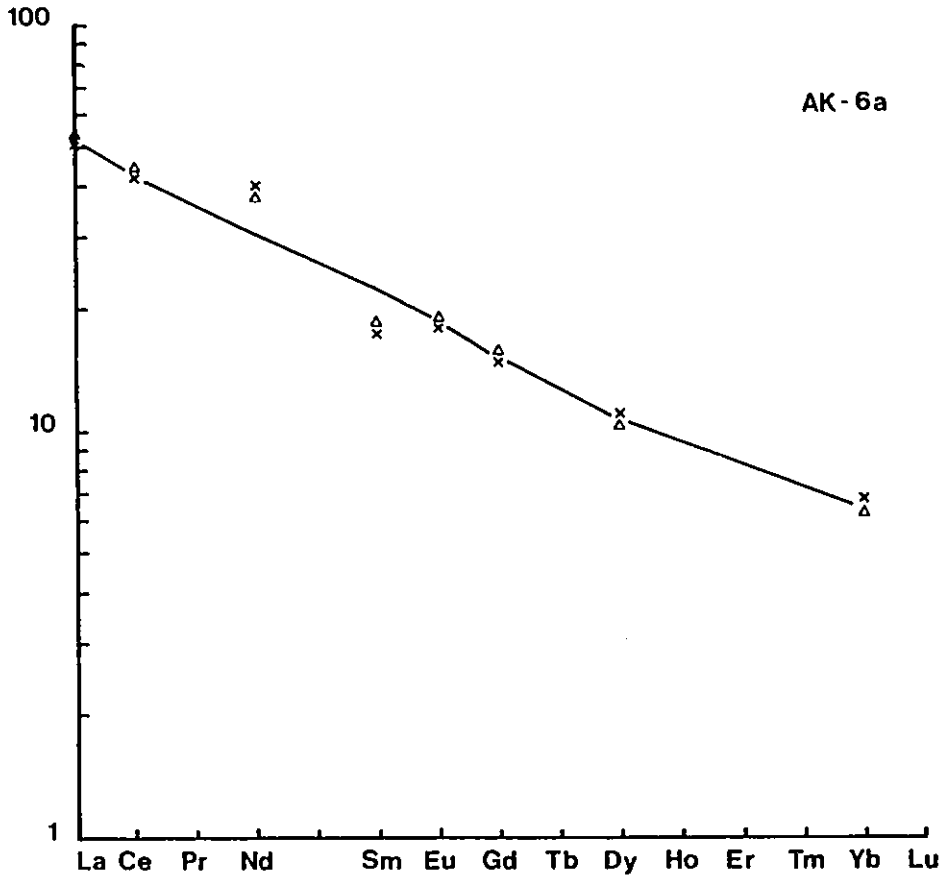
100
10
1
AK-6a
La Ce Pr Nd Sm Eu Gd Tb Dy Ho Er Tm Yb Lu

Figure 28j. Chondrite-normalized REE plots of a high-Mg tholeiitic basalt (T-13) and a high-Fe tholeiitic basalt (T-4) from the Ketyet River Group.

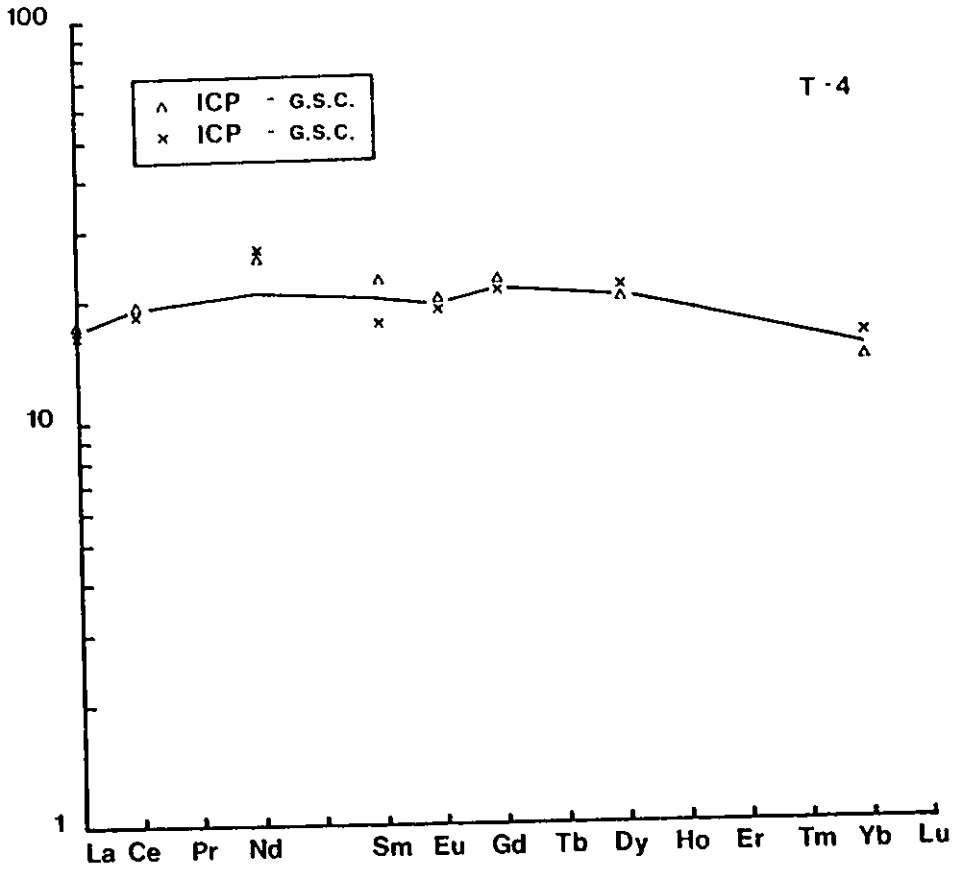
100
10
1
ICP - G.S.C.
ICP - G.S.C.
T-4
La Ce Pr Nd Sm Eu Gd Tb Dy Ho Er Tm Yb Lu

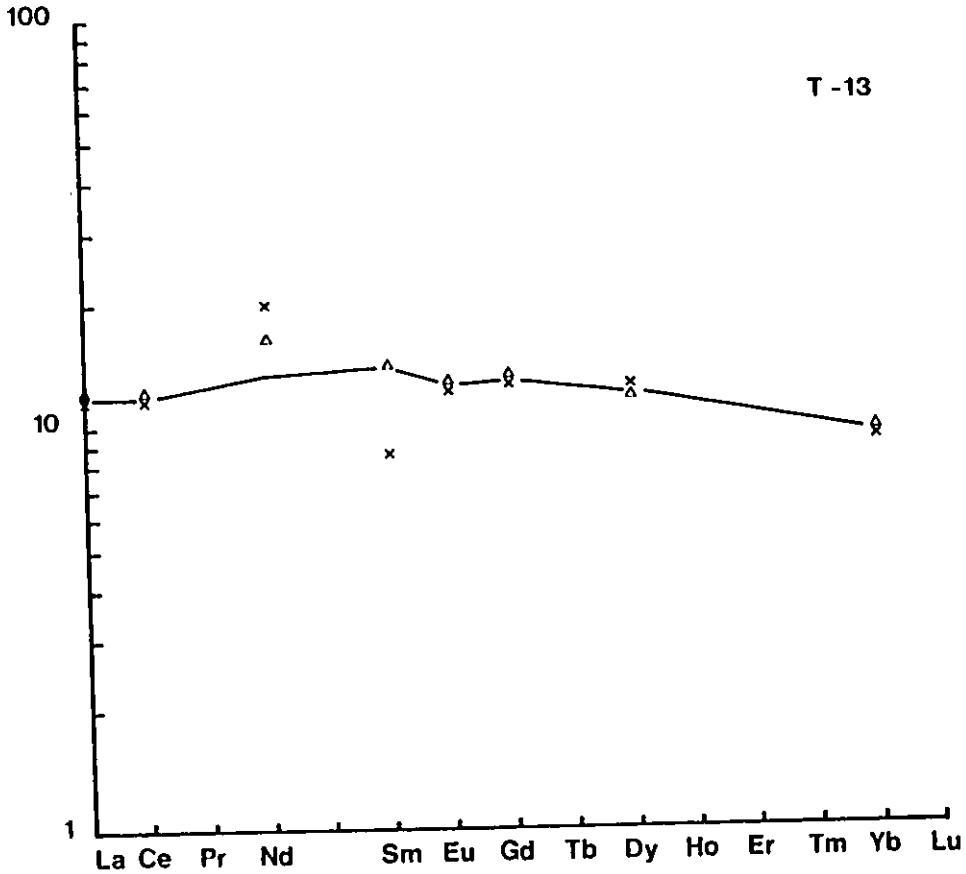
100
10
1
T-13
La Ce Pr Nd Sm Eu Gd Tb Dy Ho Er Tm Yb Lu

Figure 28k. Chondrite-normalized REE plots of two Prince Albert Group komatiites.

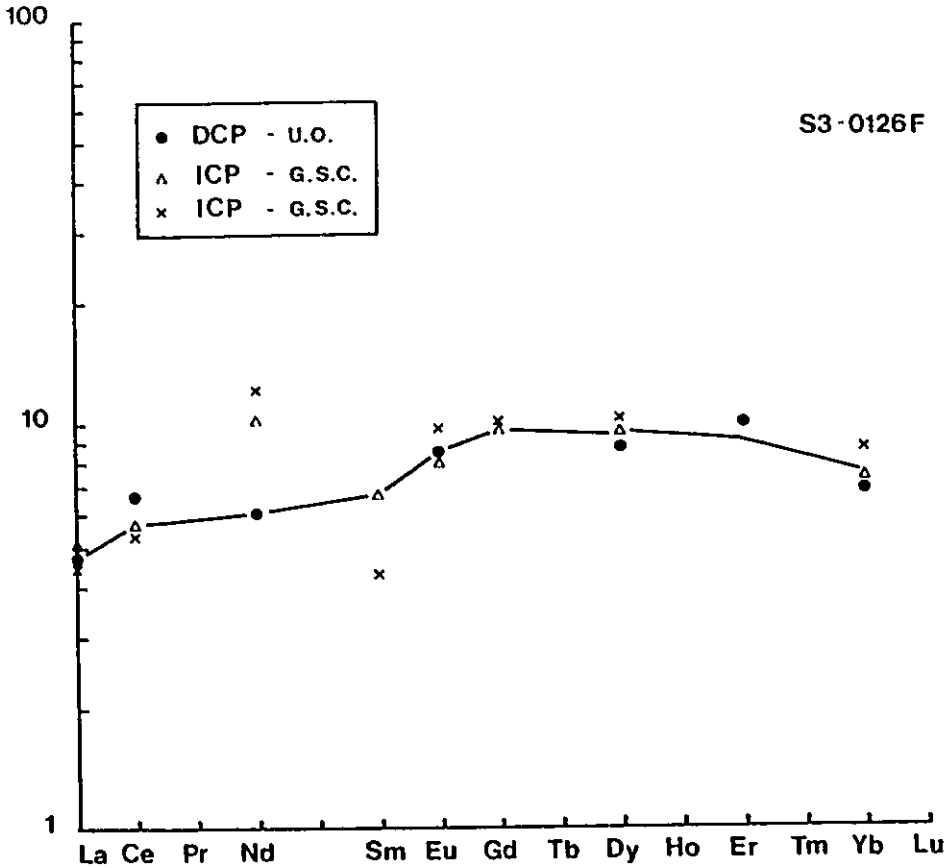
100
10
1
DCP - U.O.
ICP - G.S.C.
ICP - G.S.C.
S3-0126F
La Ce Pr Nd Sm Eu Gd Tb Dy Ho Er Tm Yb Lu

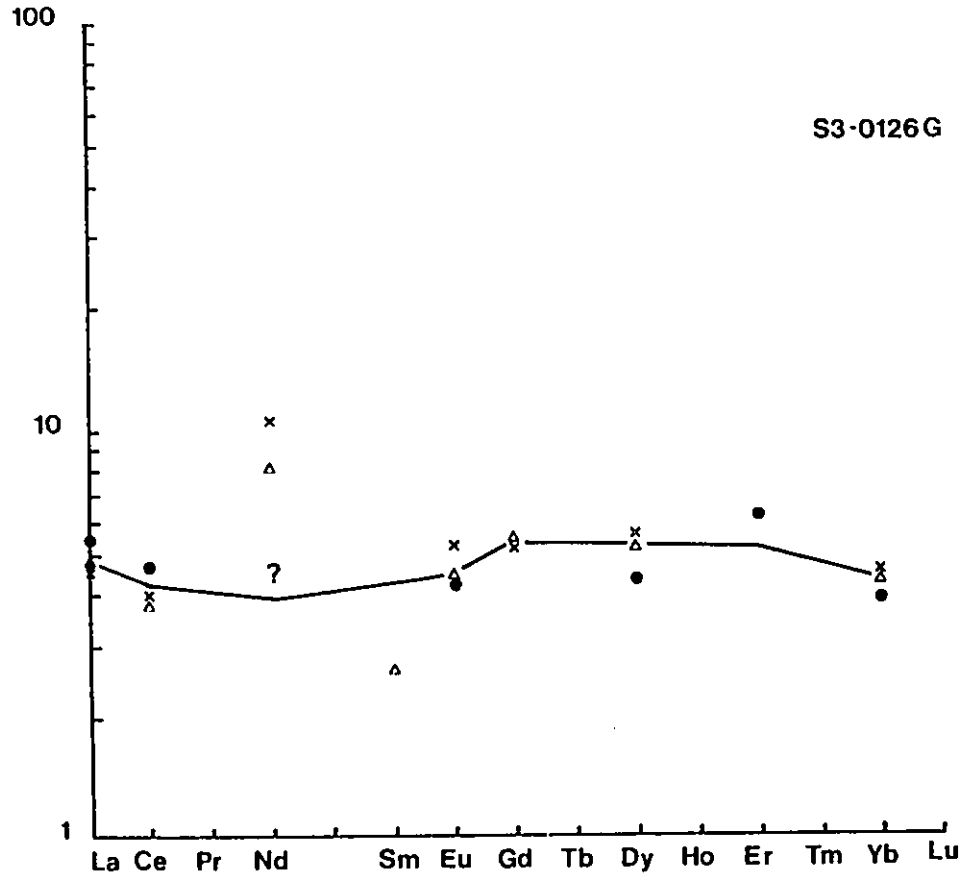
100
10
1
S3-0126G
?
La Ce Pr Nd Sm Eu Gd Tb Dy Ho Er Tm Yb Lu

Figure 281. Chondrite-normalized REE plots of a high-SiO_2 rhyolite (AK-9) and a low-SiO_2 rhyolite (AK-2) from the Pipedream Lake belt.

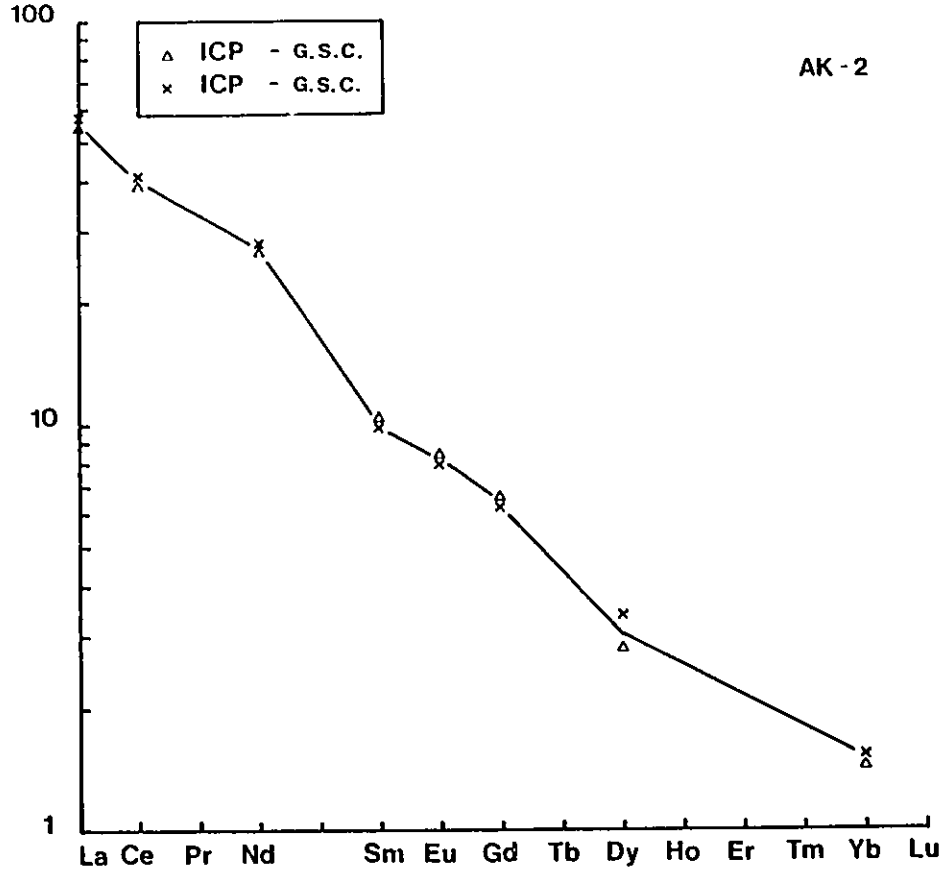
100
10
1
Δ ICP - G.S.C.
× ICP - G.S.C.
AK-2
La Ce Pr Nd Sm Eu Gd Tb Dy Ho Er Tm Yb Lu

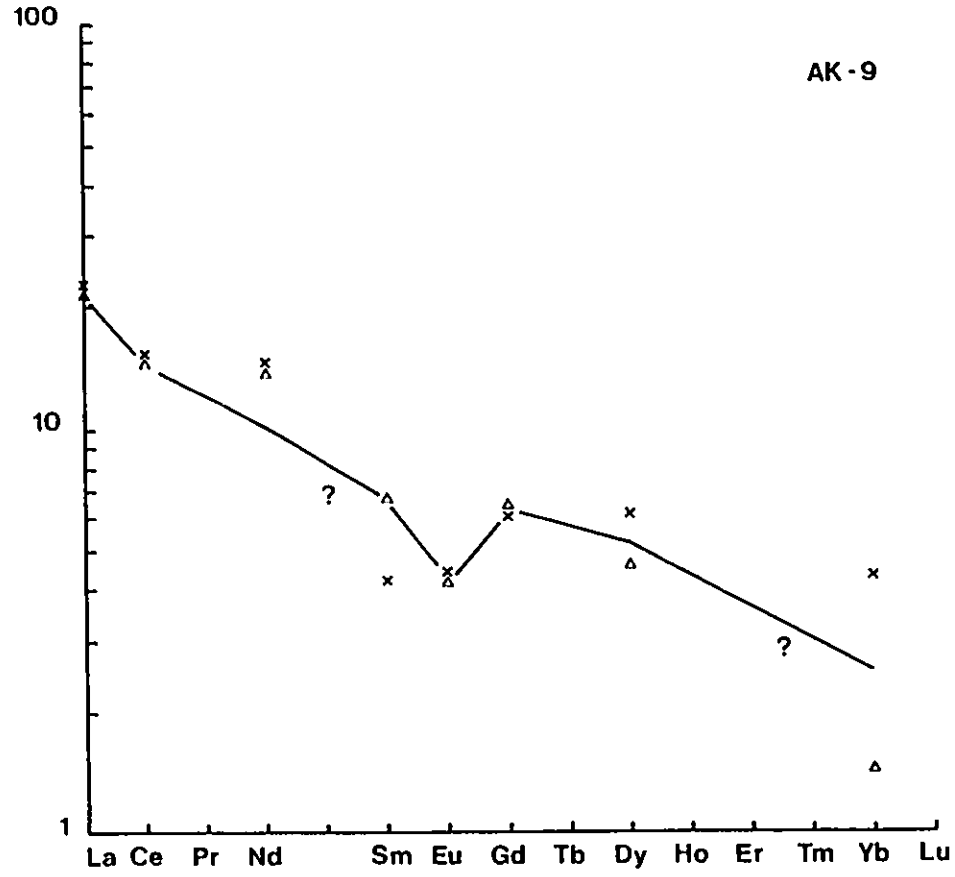
100
10
1
AK-9
?
?
La Ce Pr Nd Sm Eu Gd Tb Dy Ho Er Tm Yb Lu

Windsor), are considered to be too high or too low on the basis of comparison with other techniques and laboratories. For example, the discrepancy in Y-values is shown in Table 6. The Y determinations by ICP (G.S.C.) and XRF (U.W. - pressed powders) are considered superior because the determined Y values are higher than the detection limits of the analytical method. Also, it should be noted that the Y-values determined by XRF (U.O.) are unacceptable for mafic and ultramafic rocks and acceptable for felsic rocks (AK-2, AK-6a, and AK-9) at low detection levels. This is indicative of a matrix problem, which is enhanced near analytical detection levels.

Chemical results of some Prince Albert Group and Ketyet River Group (Aberdeen Lake) komatiites, analysed by the author and Schau (1982) are presented in Appendices B3 and B4 to supplement the data and to be used for comparison. Three of the Prince Albert Group komatiites were analysed for REE and Y at the G.S.C. A few of the intercalated calc-alkaline suite of rhyolites and dacites were analysed and are listed in Appendix B5. These will be used in conjunction with the komatiites to aid in the interpretation of the tectonic environment of the area. Some mafic metavolcanics, analysed by Taylor (1985), are found in Appendix B6 and will be used for comparison and interpretation. Three of these samples were also analysed for REE and Y.

Table 6 - Comparison of Y determinations from different laboratories

XRF (UO)	AA (GSC)	ICP (GSC)	ICP (GSC)	XRF (UW)		
AK-14a		18	22	7.4	6.8	nd
AK-14b		16	21	4.8	4.8	nd
AK-14c		17	22	6.0	6.3	nd
AK-14d		17	26	6.2	6.1	nd
AK-20		8	nd	9.2	15	nd
AK-31		23	nd	13	12	nd
AK-31(dup)		nd	nd	9.1	7.9	nd
K-24		18	28	6.6	6.5	nd
K-44g		17	28	6.8	5.2	nd
AK-2		7	nd	4.6	4.5	nd
AK-6a		16	26	17	16	nd
AK-9		9	21	5.6	9.9	nd
R-222		25	nd	16	16	18
R-232b		30	nd	22	24	27
R-233		20	nd	14	15	15
R-242a		16	nd	9.5	9.7	10
S3-0126F		21	nd	17	18	nd
S3-0126G		21	nd	9.6	9.4	nd
S3-0126H		13	nd	7.4	13	nd

4.3 GEOCHEMICAL CLASSIFICATION AND TERMINOLOGY OF KOMATIITES AND KOMATIITIC BASALTS

The classification of mafic and ultramafic extrusive rocks of Archean and Proterozoic greenstone belts has evolved since the discovery of komatiites and is based on their field, textural, and chemical characteristics (Viljoen and Viljoen, 1969a and b; Brooks and Hart, 1972; Naldrett and Arndt, 1976; Arndt et al., 1977; Nesbitt et al., 1979; Arndt and Nisbet, 1982a).

The proof of being komatiitic in nature depends on a) field characteristics - the presence of spinifex, b) demonstrating the high-Mg, ultramafic chemical composition of the rocks, and c) establishing that the rock was once a liquid (i.e. not a cumulate). Viljoen and Viljoen (1969a) strongly emphasized a high CaO/Al_2O_3 weight percent ratio for confirmation of a komatiitic composition. They also subdivided komatiites into peridotitic komatiites and basaltic komatiites. Brooks and Hart (1974), based on other occurrences, refined the komatiite definition (i.e. including basaltic types) to mean extrusive rocks with SiO_2 less than 53%, MgO greater than 9%, TiO_2 less than 0.9%, K_2O less than 0.5% and CaO/Al_2O_3 greater than 1.0. Arndt (1976) and Arndt et al. (1977) found that a CaO/Al_2O_3 of 1.0 still excluded the Munro Township komatiites. Nisbet et al. (1977) suggested CaO/Al_2O_3 ratios close to or greater than chondritic (i.e. 0.82). Nesbitt and Sun (1976), Nesbitt et al. (1979), Schau (1977), and Arndt et al. (1977) suggested that the CaO/Al_2O_3 ratio greater than 1.0 is

not characteristic of most komatiitic suites. Nesbitt et al. (1979) proposed that peridotitic komatiites be classified either as aluminum-depleted or as aluminum-undepleted. Subsequently, Nesbitt et al. (1982) suggested that the CaO/Al_2O_3 ratio of peridotitic komatiites is a function of age and is reflected by high CaO/Al_2O_3 ratios in the early Archean and lower (i.e. chondritic) CaO/Al_2O_3 ratios in the late Archean.

It appears that the low $FeO^*/(FeO^* + MgO)$ ratio, the low TiO_2 content, the low alkalies, the high MgO content, and the high Ni and Cr values are the most important chemical parameters in identifying komatiites. Most workers now agree on the chemical parameters defining the komatiitic suite, however subdivisions within the suite are not universally agreed upon. The 1979 Penrose conference on komatiites redefined komatiite to mean an ultramafic volcanic rock with greater than 18% MgO by weight (Arndt and Nisbet, 1982a). This MgO content is somewhat arbitrary but was taken to represent a compositional gap which appears in several provinces between the distribution of analyses of ultramafic lavas (i.e. peridotitic and pyroxenitic) and associated mafic lavas. St.-Seymour et al. (1983) suggested that this gap is variable and is dependant upon the volcanic suite under consideration. Also, this new definition is too restrictive in that it excludes high level intrusive rocks derived from komatiitic magmas (i.e. sills and dykes).

Critical to the komatiite classification is whether or not komatiites represent a magma series. Arndt et al. (1977)

suggested that peridotitic (MgO > 20%), pyroxenitic (12% < MgO < 20%), and basaltic (8% < MgO < 12%) komatiites form a magma series. Francis and Hynes (1979) concurred that a komatiitic trend merges into a tholeiitic trend, whereas Nesbitt et al. (1979) suggested that peridotitic komatiites, basaltic komatiites, and tholeiitic basalts are distinctive primitive magmas. More recently, Arndt and Nisbet (1982a) have concluded that komatiites constitute the ultramafic part of the komatiitic magma series.

A confusing situation currently exists in that it may be difficult to distinguish between komatiitic basalts and tholeiitic basalts at the low-Mg end of the komatiitic suite. More commonly used chemical variation diagrams such as an AFM plot show low-Mg members of the komatiitic suite falling within the tholeiitic compositional field with no clear distinction between komatiitic and tholeiitic basalts. Several geochemical diagrams have been developed for discriminating komatiitic and tholeiitic rocks. Arndt (1975 and 1976), Arndt et al. (1977), and Naldrett and Goodwin (1977) advocated an Al_2O_3 versus $FeO^*/(FeO^* + MgO)$ diagram for distinguishing tholeiitic lavas from komatiitic lavas. Arndt et al. (1977) also used SiO_2 - TiO_2 and MgO - TiO_2 diagrams to effectively separate tholeiitic basalts from komatiitic basalts within the same stratigraphic level. Jensen (1976) developed the Jensen Cation Diagram to distinguish komatiitic rocks from other subalkalic volcanic rocks. Jensen uses 10% MgO by weight as the dividing line between the

tholeiitic and komatiitic fields and 20% MgO by weight as the dividing line between peridotitic and basaltic komatiites and these have been transposed to his Cation Diagram.

This study will use the combined nomenclature of Arndt et al. (1977) and Arndt and Nisbet (1982a) and several of the above mentioned diagrams to classify the Woodburn Lake Group rocks.

4.4 CLASSIFICATION OF THE WOODBURN LAKE GROUP ULTRAMAFIC AND ASSOCIATED MAFIC (High-Mg) METAVOLCANICS

Before classifying the rocks the author notes that, in the majority of samples, the present chemistry clearly reflects primary values for most elements. Evidence that the original chemical composition has not been greatly affected by interaction with seawater or during metamorphism is considered in Section 4.5 and Chapter 5.

The author (Annesley, 1981a and 1981b) demonstrated the komatiitic and tholeiitic nature of the Woodburn Lake Group ultramafic and mafic metavolcanics by use of variation diagrams (pp. 69-71 and 74-80, 1981b).

The present study supports the previous work of the author. All the komatiite samples plot within the tholeiitic field of the AFM diagram (Fig. 29). Most of the mafic to ultramafic metavolcanics analyzed in the current study have greater than 18% MgO by weight on an anhydrous basis, which places them in the komatiite field (Arndt and Nisbet, 1982a). The remainder of

Figure 29a. Symbol legend. Letters and symbols shown on all of the chemical plots in this thesis correspond to the rock type subdivisions (i.e. including suites, areas, and belts) as outlined in this legend.

Symbol Legend

A Area 1
B Area 2
C Area 3
D Area 4

Pipedream Lake belt 

E Esker Lake and No-Name Lake belts ▲

Woodburn Lake Group komatiites

- △ Spinifex-textured zone
- ● Cumulate zone
- ◆ Pillowed flows
- □ Massive flows - base to middle
- ■ Massive flows - flow top
- × Flow top
- ○ Massive flows - undifferentiated
- ◇ Serpentinites

F Woodburn Lake Group High-Mg basalts ◆

- ■ Komatiitic basalt
- ▼ High-Mg tholeiitic basalt

G Prince Albert Group komatiites ▼

H Ketyet River Group basalts ■

I Aberdeen Lake Group komatiites □

J Woodburn Lake Group calc-alkaline volcanic suite ◇

Figure 29b. Standard AFM ($Na_2O + K_2O$ vs FeO_T and MgO) diagram showing the positions of analyses of the different rock types of the Woodburn Lake Group. The solid curved line divides the diagram into a tholeiitic field (upper) and a calc-alkaline field (lower), after Irvine and Baragar (1971). Letters and symbols as in symbol legend on p.102.

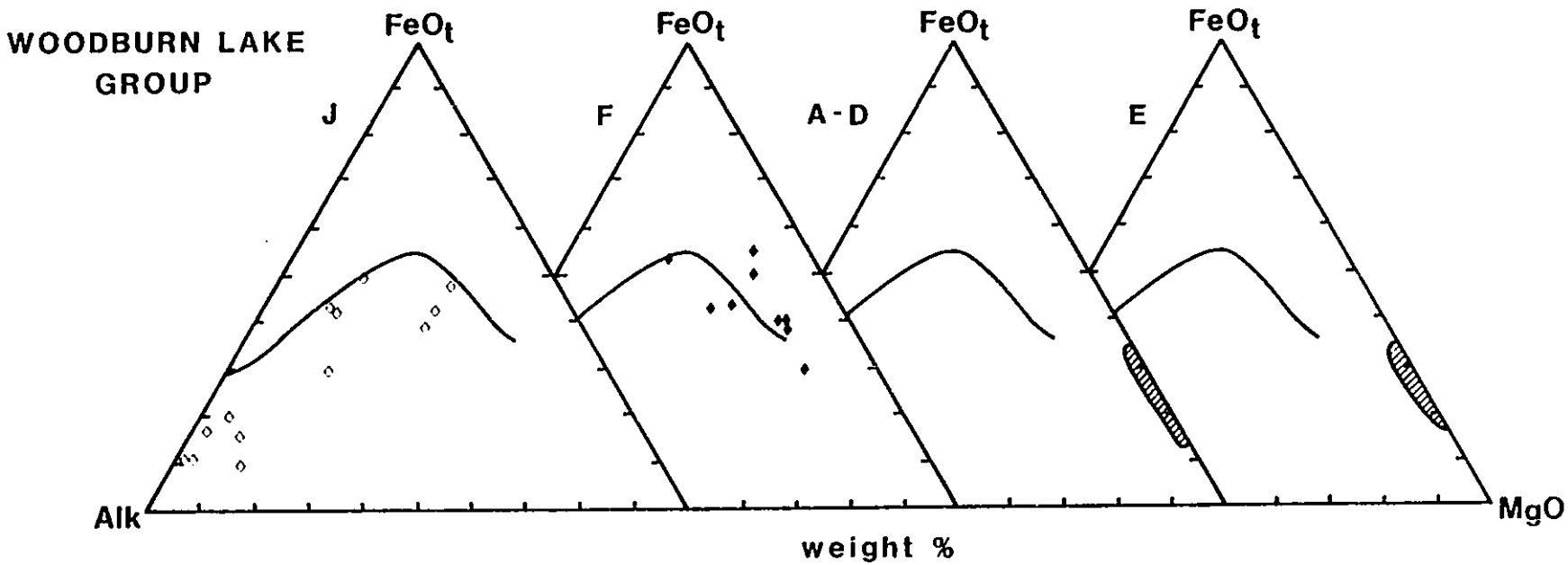
WOODBURN LAKE GROUP
FeOt
FeOt
FeOt
FeOt
J
F
A-D
E
Alk
MgO
weight %

samples with 8 - 18% MgO by weight are komatiitic and tholeiitic basalts and most of these are from the Esker Lake belt. According to the classification of Arndt et al. (1977), the rocks of this study are peridotitic komatiites (> 18 % MgO), pyroxenitic komatiites (12 - 18% MgO), and basaltic komatiites (8 - 12% MgO). Most of the rocks display komatiitic affinities as shown in FeO^*/FeO^* + MgO vs. Al_2O_3 (Fig. 30), TiO_2 vs. SiO_2, TiO_2 vs. MgO, and TiO_2 vs. Al_2O_3 weight % plots because of the lower TiO_2 and FeO^*/FeO^* + MgO contents exhibited by komatiites. These plots show that the mafic metavolcanics straddle the komatiitic and tholeiitic fields. In the Jensen Cation Plot (Fig. 31) and the AMC (Al_2O_3-MgO-CaO) ternary plot (Fig. 32) the major chemical variations of the Woodburn Lake Group komatiites and basalts clearly show a trend from peridotitic komatiite to komatiitic basalt to tholeiitic basalt. The AMC plot and Jensen Cation Plot show a pattern typical of most komatiitic suites in which the fractional crystallization of olivine followed by clinopyroxene controls the trend . It is apparent from the AMC diagram that the CaO/Al_2O_3 ratio of most of the komatiites is less than one and that some inflection points are present. One of these shows up as a curvature near the MgO apex which will be shown later to be the result of CaO migration during serpentization. The major inflection point within the peridotitic komatiites is of great interest and suggests not only olivine fractionation but also olivine and clinopyroxene fractionation (Section 4.8) within some samples.

Figure 30. $FeO^{*} / FeO^{*} + MgO$ vs. Al_2O_3 weight % plot showing some of the principal mafic and ultramafic volcanic components of the Woodburn Lake (A - F), Ketyet River (H), and Prince Albert (G) Groups. Note the difference between the Woodburn Lake Group basalts (F) and the Ketyet River Group basalts (H). The fields are after Naldrett and Goodwin (1977) and Nesbitt et al. (1979).

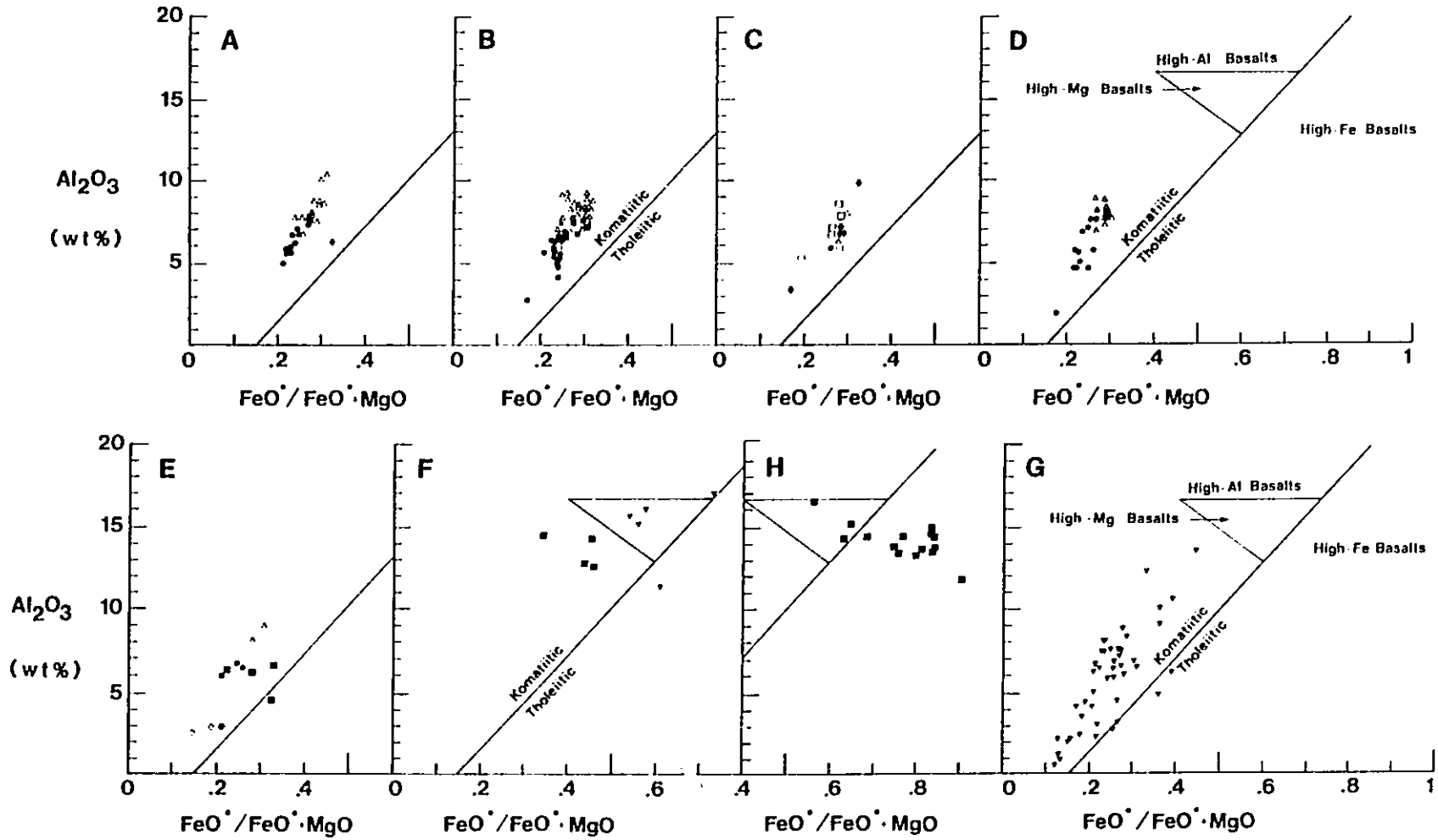
A
B
C
D
E
F
H
G
Al_2O_3
(wt%)
FeO^*/FeO^*+MgO
Komatiitic
Tholeiitic
High-Al Basalts
High-Mg Basalts
High-Fe Basalts

Figure 31. Jensen Cation Plot showing the distribution of the Woodburn Lake Group (A - D, E, J, and F), Ketyet River Group (I and H) and Prince Albert Group (G) volcanics. The fields shown in far left plot are from Jensen (1976).

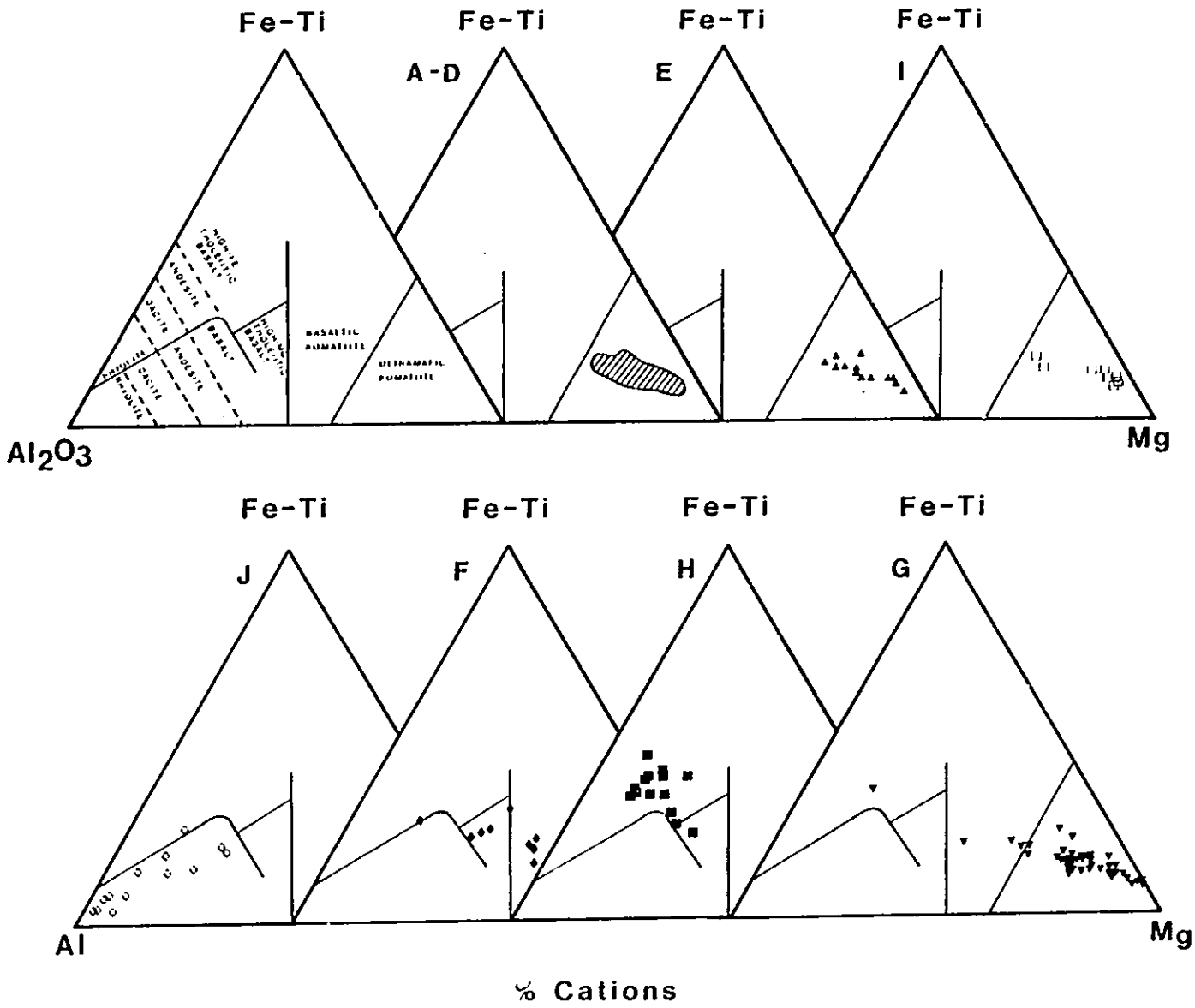
Fe-Ti
Fe-Ti
Fe-Ti
Fe-Ti
A-D
E
I
BASALTIC KOMATIITE
KOMATIITIC BASALT
ANDESITE
DACITE
RHYOLITE
BASALT
ANDESITE
DACITE
HIGH-Mg TOLEIITIC BASALT
BASALTIC KOMATIITE
ULTRAMAFIC KOMATIITE
Al2O3
Mg
Fe-Ti
Fe-Ti
Fe-Ti
Fe-Ti
J
F
H
G
Al
Mg
% Cations

Figure 32. AMC (Al_2O_3-MgO-CaO) ternary plot showing the distribution of analyses of the mafic and ultramafic volcanics of the Woodburn Lake (A - D, E, and F), Ketyet River Group (H and I), and Prince Albert (G) Groups. The fields shown in far left plot are from Arndt et al. (1977).

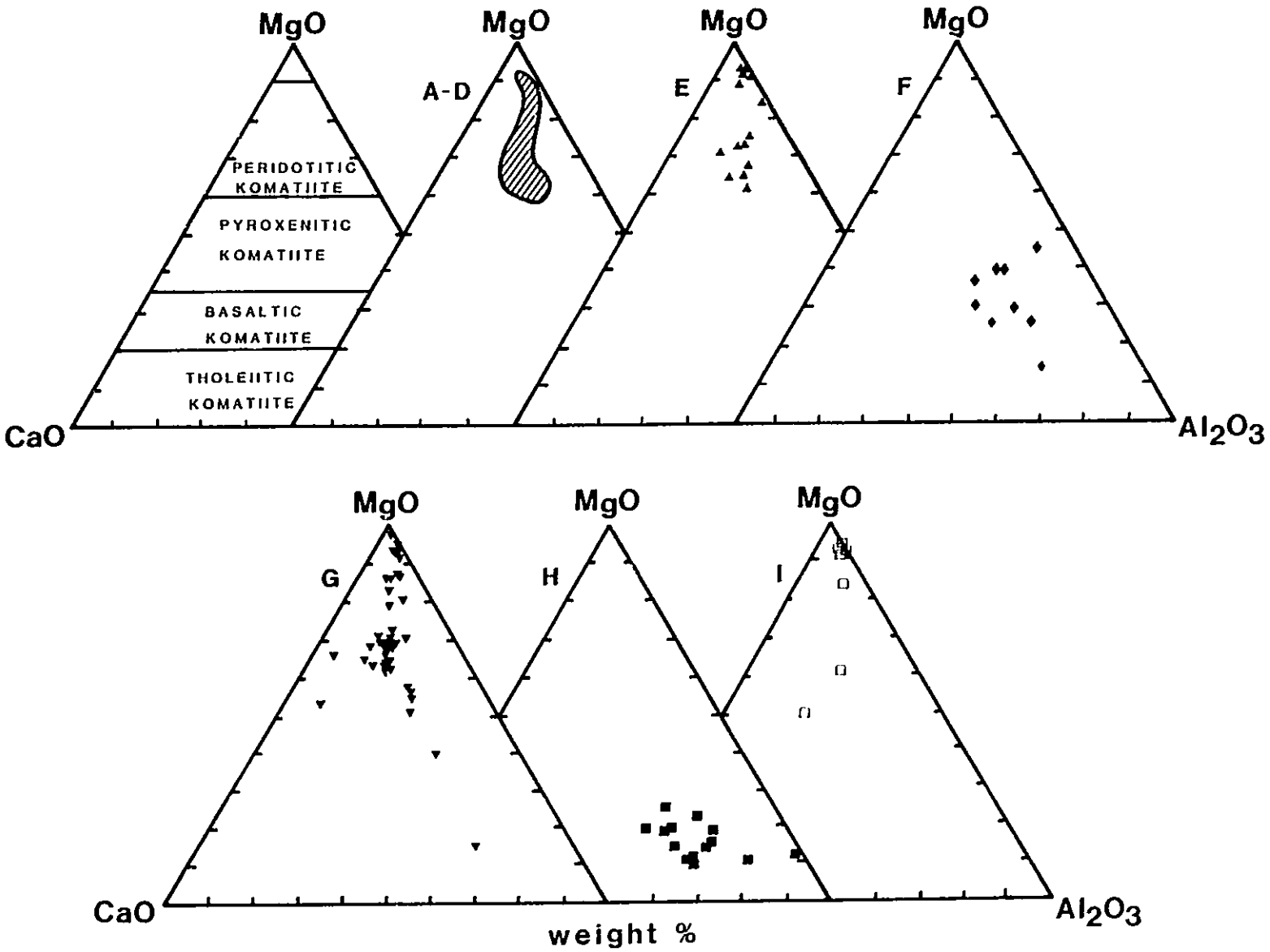
MgO
MgO
MgO
MgO
A-D
E
F
PERIDOTITIC KOMATIITE
PYROXENITIC KOMATIITE
BASALTIC KOMATIITE
THOLEIITIC KOMATIITE
CaO
Al2O3
MgO
MgO
MgO
G
H
I
CaO
Al2O3
weight %

4.5 ALTERATION

One of the major problems in determining the igneous processes operating during the petrogenetic history of Archean metavolcanic suites is the possibility that the rocks have undergone notable changes in chemical composition during alteration processes. It is widely accepted that most mafic and ultramafic volcanics and especially those older than a few hundred million years have undergone some mineralogical and chemical modification. This mineralogical and chemical modification depends greatly upon the environment of emplacement (e.g. sea floor) and the deformation history. The older the rocks are, the greater the probability that they have been involved in more geologic processes than the younger rocks, hence they have a greater chance of being deformed and altered. This modification of primary mineralogy has raised the question of how significant has mineralogical alteration been in modifying the original chemistry, and hence creating anomalous chemical trends. This problem of chemical modification has been the subject of considerable research in the last 15 years, especially involving recent sea-floor basalts (i.e. MORB). Studies on present-day MORB show that chemical exchange has taken place between seawater and basalt. Most Archean basalts and komatiites have formed in a submarine environment like that of MORB, given the presence of pillow morphologies, hyaloclastite breccia, polyhedral jointing, and marine interflow sediments. An oxygen isotope study

by Beatty and Taylor (1982) also supports a subaqueous environment for komatiites. The alteration (i.e. a change in the original chemical composition) problem is especially complicated in the case of Archean basalts and komatiites, which have commonly had the effects of regional and contact metamorphism superimposed on the effects of seawater alteration.

Recent studies (Seyfried et al., 1988; among others) on the problem of anomalous chemical trends have shown that certain elements (K, Na, Rb, Sr, Ba) are extremely mobile in volcanic rocks during alteration processes. Pearce and Cann (1973) suggested that other elements such as Al, Ti, Zr, Y, Sc, Nb, V, Cr, and REE are immobile. More recent studies have shown that this is not always the case (Thompson, 1973; Frey et al., 1974; Smith and Smith, 1976; Wood et al., 1976; Hellman and Henderson, 1977; Condie et al., 1977; Smith and Erlank, 1978; Mottl and Holland, 1978; Humphris and Thompson, 1978a and b; Humphris et al., 1978; Ludden and Humphris, 1978; Ludden and Thompson, 1978; Hellman et al., 1979; Ludden and Thompson, 1979; Menzies et al., 1979; Beswick, 1982 and 1983; Ludden et al., 1982; Ludden and Gelinas, 1982; Gelinas et al., 1982; Staudigel and Hart, 1983). In metavolcanic rocks of the Barberton Mountain Land, Condie et al. (1977) demonstrated that Ti, P, Zr, Ca, Fe^{2+}, Fe^{3+}, Y, and Cr have been mobile in places. Sun and Nesbitt (1978) suggested that light REE are more prone to redistribution than the heavy REE. Hellman et al. (1979) identified and subdivided REE mobility into four major types of variable elemental mobility, La, Ce, and

Eu being especially vulnerable. Ludden et al. (1982) studied some Archean pillow basalts in detail and found K, Rb, and Sr to be mobile, Zr, Y, Ti and REE to be immobile, and other elements exhibiting variable degrees of mobility. Beswick (1983), from the study of a single komatiite flow, found Zr, Y, and LREE to be mobile. In a study of komatiite flows from the Abitibi Greenstone Belt, Barnes (1985) concluded that Na, K, Ca, Sr, Rb, and Ba have been disturbed during seafloor alteration and metamorphism.

There are several approaches presently being utilized to overcome the problem of alteration within metavolcanic rocks. Most commonly, the freshest samples are selected on the assumption that metavolcanic rocks exhibiting the best preservation of primary mineralogy and textures have been least affected by alteration processes. Alternatively, Gelinas et al. (1977) used the volatile and alkali contents in conjunction with textural observations to select rock samples which are least altered. This method is not satisfactory for studying komatiites since komatiites, characteristically, have high water contents by virtue of their metamorphic mineralogy. This problem of knowing which samples to pick for analyzing, when there is no pristine material available for comparison, is difficult because of a number of factors critical to the geochemistry. These factors include: 1) the effect of primary mineralogy and chemistry on the presently observed mineralogy and chemistry.

2) the effect of secondary mineralogy on the presently observed chemistry.

3) the effects of the volume and chemistry of fluid phases that may have migrated through the rocks.
4) the effects of textural variations (i.e. the presence or absence of glass, and the morphology of primary minerals in the original rock).

These factors would explain the conflicting results in the above mentioned studies as to the mobilities of many elements. For example, this is shown in the study by Condie et al. (1977) whereby relatively immobile elements such as Ti and Y show variable mobility that is dependent upon the alteration process (i.e. epidotization, carbonatization, etc.) All these alteration studies on volcanic rocks suggest that it is probably unrealistic to make generalizations concerning element mobilities without considering all of the above mentioned factors. Each case study may be applicable only to the rocks of the area under consideration. Another possibility is that komatiites react differently than other volcanic rocks, especially since their original mineralogy, textures, and chemistry are so different.

Nesbitt and Sun (1976) and Sun and Nesbitt (1978), after analyzing well preserved samples from a metavolcanic suite, found that certain elemental ratios are relatively constant and chondritic in nature; thus indicating their primary or primitive nature. Nesbitt et al. (1979, p. 170) reiterated this approach with the following guidelines for identifying and classifying altered rocks: "a search for regularities in the geochemistry and the belief that there should be consistency of elemental ratios

in magmatic liquids which cannot be matched by metamorphic processes".

Studies on modern and ancient seafloor pillowed basalts (Ludden and Thompson, 1978 and 1979; Baragar et al., 1979; Ludden and Gelinas, 1982), where primary sample homogeneity is known, have shown that the problem of alteration can be successfully resolved by comparing subsamples with different alteration mineralogy. This approach is not applicable to komatiites since komatiites show major primary textural and geochemical heterogeneity. Ludden and Gelinas (1982) evaluated the effects of alteration and metamorphism on the geochemistry of komatiites and komatiitic basalts by using a normalization process based upon the least mobile elements. Their method is formulated on the premise that abundances of elements which do not show a covariance with the least mobile elements (e.g. Al, Ti, Zr) have been modified. Elements should show a covariance on the basis of element incompatibility with respect to igneous processes (i.e. partial melting and fractional crystallization). This approach is similar to that used by Nesbitt et al. (1979), Glikson (1979), Barnes et al. (1983), among others. The degree of depletion or enrichment of some elements can be estimated using the (element/TiO_2)-normalization method of Staudigel and Hart (1983).

Pearce (1968) introduced molecular proportion ratio (MPR) diagrams (Note: more recently called Pearce element ratio (PER) diagrams) to alleviate the misleading interpretations of oxide-oxide weight percent (Harker-type) diagrams. Harker

diagrams (wt%) are misleading because of a) the closure effect imposed on chemical analyses by summing to 100 wt% and b) the difficulty of relating wt% to mineral compositions. Chemical data presented on a wt% basis become difficult to interpret since the true elemental variations are not preserved (Pearce, 1968). Beswick and Soucie (1978) suggested a modified graphical version of Pearce's (1968) ratio diagrams to examine elemental ratios of altered metavolcanic rocks. These diagrams are constructed by plotting two oxides in molecular proportions normalized to a third oxide. This approach examines observed trends within altered metavolcanics for consistent ratios which are similar to those, and therefore indicative, of primary magmatic processes that produced the rocks. Beswick (1982), Paktunc (1984a), and Barnes (1985) have used these diagrams to evaluate the effects of alteration on their komatiite data. Paktunc (1984a) suggested caution when using these diagrams, since they have a tendency of enhancing correlations. Recently, Rollinson and Roberts (1986) and Butler (1986) have tried to analyze the statistical validity of these MPR diagrams. They stated that these diagrams may produce spurious correlations and/or may greatly enhance the correlations that are present. Rollinson and Roberts (1986) strongly condemn the use of these ratio diagrams on statistical grounds. They suggested that a high correlation coefficient does not necessarily indicate a petrologically significant relationship of the element ratio pairs under consideration. Butler (1986) suggested the use of molecular proportion ratio

diagrams without common denominators or numerators for petrological modelling.

Pearce (1987) has considered and discussed the critical comments made by Rollinson and Roberts (1986). He pointed out that the assumptions made by Rollinson and Roberts (1986) are not correct, because the selected boundaries of their modelling does not match the boundaries of natural mineralogical systems. Nicholls (1988) has examined the statistics of MPR diagrams and concluded that these diagrams are statistically valid. He pointed out that a valid Pearce diagram consists of 1) molecular proportion ratios with a common denominator, the denominator being a conserved constituent (i.e. incompatible elements) and 2) the contribution made by the variance of the common denominator is much less than the one made by the variance of the numerator. Nicholls (1988) also showed that the statistical testing performed by Rollinson and Roberts (1986) and Butler (1986) is erroneous, since they did not use a "conserved denominator". According to Pearce (1987, p.529), a valid trend on a Pearce diagram has a "significant (non-zero) y-intercept and a meaningful slope". Pearce (1987, p.529) stated that a spurious correlation trend on a Pearce diagram needs to pass through "the origin and the average composition of the data set". Nicholls (1988) pointed out the unusual case where a valid trend does pass through the zero intercept. This takes place when the numerators of the two ratios under consideration remain in constant proportion for all samples of the igneous rock suite. Pearce

(1987, p.529) concluded that the use of Pearce-type MPR diagrams is a powerful technique to decipher original magmatic trends through "the veil of metamorphic overprinting". Nicholls (1988) also concluded that Pearce-type MPR diagrams accurately portray the magmatic processes that created the inhomogeneous magmatic trends of igneous rock suites.

Both Pearce (1987) and Nicholls (1988) used the Fortran 77 computer program of Russell (1986) for least squares analysis of Pearce-type MPR diagrams. The author used a modified version of this program to look at the Woodburn Lake Group komatiitic suite. This approach to recognizing element mobility in altered volcanics shows that the Woodburn Lake Group komatiites have distributions of whole-rock compositions that are consistent with primary magmatic processes. The results of least squares linear regression, presented in Table 7, shows that the chemical data for spinifex-textured flows lie along two distinct trends and one variable trend. This information was obtained by plotting molecular proportions of SiO_2 and FeO^* + MgO (FeO^* represents total iron) normalized to elements incompatible with olivine. The two distinct trends have slopes of 1:1 and 1:2. These trends can be related to the spinifex-textured zone and cumulate zone, respectively. The trend of the cumulate zone samples is consistent with olivine-only fractionation. This is confirmed by comparing the Woodburn Lake Group komatiites (Figs. 33a, 33b, and 33c) to fresh komatiites from Zimbabwe (Nisbet et al., 1987). As shown in Figures 33d, 33e, and 33f, the Zimbabwe komatiites all

Table 7 - Summary of least squares linear regression of Pearce element ratio diagrams

	Tony's Flow	WLG komatiites - Area 1		WLG komatiites - Area 2		WLG komatiites - Area 3	WLG komatiites - Area 4		WLG komatiites -Esk-L/No-L	WLG komatiitic basalts
		spin	cum	spin	cum		spin	cum		
Y= Si/Ti X=(Fe+Mg)/Ti										
intercept (b)	95.07	0.09	91.64	28.16	86.07	67.78	-19.12	94.71	61.66	28.35
sigma (+/-)	2.02	12.61	9.92	9.27	4.70	10.88	9.32	12.86	8.16	9.88
slope (M)	0.51	0.93	0.49	0.77	0.50	0.55	1.00	0.52	0.55	1.33
sigma (+/-)	0.01	0.07	0.03	0.05	0.01	0.04	0.05	0.03	0.01	0.21
correlation coefficient	0.999	0.966	0.976	0.947	0.989	0.970	0.990	0.985	0.997	0.921
n =	7	16	13	33	32	14	14	12	10	9
Y=Si/Al X=(Fe+Mg)/Al										
intercept (b)	3.01	-0.03	2.92	0.75	2.27	2.21	-0.43	2.28	2.70	2.09
sigma (+/-)	0.01	0.37	0.36	0.27	0.11	0.27	0.18	0.24	0.38	0.45
slope (M)	0.50	0.94	0.43	0.77	0.51	0.52	0.98	0.54	0.50	0.66
sigma (+/-)	0.01	0.07	0.04	0.05	0.01	0.03	0.03	0.02	0.03	0.29
correlation coefficient	1.000	0.962	0.946	0.939	0.992	0.977	0.994	0.994	0.981	0.650
n =	7	16	13	33	32	14	14	12	14	9
Y=Si/Mn X=(Fe+Mg)/Mn										
intercept (b)	314.92	47.04	177.23	65.15	141.45	67.79	18.01	170.74	141.72	92.72
sigma (+/-)	9.20	45.87	38.65	25.41	18.17	33.83	19.70	34.64	28.27	67.52
slope (M)	0.00	0.79	0.38	0.72	0.41	0.64	0.85	0.36	0.50	1.58
sigma (+/-)	0.03	0.14	0.09	0.07	0.05	0.10	0.06	0.09	0.04	0.34
correlation coefficient	0.986	0.840	0.786	0.872	0.950	0.885	0.960	0.793	0.958	0.870
n =	7	16	13	33	32	14	14	12	14	9
Y=Si/Ca X=(Fe+Mg)/Ca										
intercept (b)	3.43	2.10	1.74	1.68	1.94	2.84	1.34	2.87	2.62	1.46
sigma (+/-)	0.09	0.28	0.14	0.16	0.19	0.33	0.33	0.25	1.04	1.22
slope (M)	0.46	0.63	0.67	0.67	0.65	0.57	0.71	0.61	0.62	1.71
sigma (+/-)	0.02	0.04	0.01	0.02	0.01	0.02	0.05	0.00	0.01	0.28
correlation coefficient	0.997	0.974	0.999	0.983	0.997	0.991	0.980	1.000	0.999	0.918
n =	7	16	13	33	32	14	14	12	14	9

Table 7 (continued)

	Tony's Flow	WLG komatiites - Area 1		WLG komatiites - Area 2		WLG komatiites - Area 3	WLG komatiites - Area 4		WLG komatiites -Esk-L/No-L	WLG komatiitic basalts
		spin	cum	spin	cum		spin	cum		
Y=Si/Na X=(Fe+Mg)/Na										
intercept (b)	14.58	1.67	8.88	0.28	11.95	11.55	0.14	3.37	23.98	3.09
sigma (+/-)	1.39	0.59	1.47	0.42	2.67	2.98	1.03	4.32	6.83	1.29
slope (M)	0.46	0.38	0.66	0.90	0.66	0.63	0.90	0.76	0.51	1.38
sigma (+/-)	0.06	0.02	0.02	0.00	0.01	0.04	0.02	0.01	0.05	0.24
correlation coefficient	0.963	0.998	0.995	1.000	0.996	0.977	0.997	0.998	0.941	0.987
n =	7	16	13	33	31	14	14	12	13	9
Y=Si/K X=(Fe+Mg)/K										
intercept (b)	239.51	-16.20	123.11	57.48	176.01	98.46	8.37	428.61	189.29	5.55
sigma (+/-)	31.60	18.30	56.14	19.75	70.76	79.87	13.97	281.27	246.42	3.92
slope (M)	0.72	0.96	0.72	0.87	0.72	0.71	0.89	0.70	0.63	1.05
sigma (+/-)	0.04	0.02	0.02	0.01	0.02	0.04	0.01	0.08	0.08	0.04
correlation coefficient	0.992	0.998	0.995	0.997	0.989	0.984	1.000	0.957	0.951	0.999
n =	7	15	13	33	26	14	14	9	9	9
Y=Si/P X=(Fe+Mg)/P										
intercept (b)	1103.30	-	-	-	-	-	-	-	-	-
sigma (+/-)	124.52	-	-	-	-	-	-	-	-	-
slope (M)	0.57	-	-	-	-	-	-	-	-	-
sigma (+/-)	0.05	-	-	-	-	-	-	-	-	-
correlation coefficient	0.978	-	-	-	-	-	-	-	-	-
n =	7	-	-	-	-	-	-	-	-	-
Y=Si/Ba X=(Fe+Mg)/Ba										
intercept (b)	104.48	-11.38	14.40	-8.98	44.71	18.74	-	-	87.31	0.03
sigma (+/-)	33.05	11.75	20.48	13.61	16.13	12.50	-	-	18.76	3.96
slope (M)	0.86	0.97	0.75	0.93	0.70	0.75	-	-	0.60	1.46
sigma (+/-)	0.05	0.03	0.06	0.03	0.02	0.03	-	-	0.01	0.24
correlation coefficient	0.993	0.995	0.976	0.994	0.993	0.996	-	-	0.999	0.939
n =	7	15	11	12	14	7	-	-	10	7

Table 7 (continued)

	Tony's Flow	WLG komatiites - Area 1		WLG komatiites - Area 2		WLG komatiites - Area 3	WLG komatiites - Area 4		WLG komatiites -Esk-L/No-L	WLG komatiitic basalts
		spin	cum	spin	cum		spin	cum		
Y=Si/Co (Fe+Mg)/Co										
intercept (b)	-	-0.16	-2.17	2.52	0.60	16.31	0.84	11.11	-	-
sigma (+/-)	-	1.11	5.07	1.93	1.33	6.07	0.92	10.73	-	-
slope (M)	-	0.94	0.87	0.84	0.79	0.24	0.87	0.41	-	-
sigma (+/-)	-	0.03	0.14	0.05	0.04	0.21	0.03	0.38	-	-
correlation coefficient	-	0.992	0.883	0.991	0.983	0.495	0.996	0.432	-	-
n =	-	15	13	7	15	6	8	7	-	-
Y=Si/Cr X=(Fe+Mg)/Cr										
intercept (b)	1.08	-0.03	0.53	0.05	0.01	0.48	-0.08	0.57	-0.06	-4.69
sigma (+/-)	0.39	0.09	0.10	0.07	0.01	0.09	0.04	0.22	0.19	1.80
slope (M)	-0.17	0.97	0.27	0.85	0.78	0.34	1.01	0.22	0.86	3.77
sigma (+/-)	0.46	0.11	0.10	0.09	0.00	0.10	0.05	0.22	0.13	0.28
correlation coefficient	-0.161	0.916	0.645	0.865	1.000	0.704	0.988	0.297	0.891	0.981
n =	7	16	13	33	32	14	14	12	14	9
Y=Si/Cu X=(Fe+Mg)/Cu										
intercept (b)	-	-3.33	14.49	3.06	11.36	-1.21	-	-	-	-
sigma (+/-)	-	2.01	4.53	1.73	6.00	10.02	-	-	-	-
slope (M)	-	0.95	0.72	0.86	0.73	0.87	-	-	-	-
sigma (+/-)	-	0.01	0.01	0.02	0.04	0.05	-	-	-	-
correlation coefficient	-	1.000	0.999	0.999	0.987	0.997	-	-	-	-
n =	-	15	10	5	11	4	-	-	-	-
Y=Si/Ni X=(Fe+Mg)/Ni										
intercept (b)	-1.00	0.16	-0.91	0.01	-0.57	-0.12	0.00	-0.59	-0.21	-14.27
sigma (+/-)	0.16	0.13	0.09	0.11	0.15	0.10	0.09	0.29	0.20	3.10
slope (M)	1.96	0.86	1.37	0.91	1.16	0.93	0.86	1.20	0.98	4.16
sigma (+/-)	0.06	0.06	0.05	0.05	0.09	0.05	0.04	0.19	0.10	0.30
correlation coefficient	0.997	0.963	0.992	0.953	0.914	0.985	0.986	0.897	0.943	0.983
n =	7	16	13	33	32	14	14	12	14	9

Table 7 (continued)

	Tony's Flow	WLG komatiites - Area 1		WLG komatiites - Area 2		WLG komatiites - Area 3	WLG komatiites - Area 4		WLG komatiites -Esk-L/No-L	WLG komatiitic basalts
		spin	cum	spin	cum		spin	cum		
Y=Si/Rb X=(Fe+Mg)/Rb										
intercept (b)	640.60	-	-	-	-	21.05	-	-	-	20.11
sigma (+/-)	242.57	-	-	-	-	46.00	-	-	-	21.49
slope (M)	0.78	-	-	-	-	0.87	-	-	-	1.87
sigma (+/-)	0.09	-	-	-	-	0.02	-	-	-	0.22
correlation coefficient	0.975	-	-	-	-	0.998	-	-	-	0.960
n =	6	-	-	-	-	8	-	-	-	8
Y=Si/Sr X=(Fe+Mg)/Sr										
intercept (b)	53.82	18.83	68.87	20.77	33.31	29.98	-2.79	27.68	70.84	3.07
sigma (+/-)	4.15	11.46	50.82	3.62	14.47	4.69	2.19	18.36	23.17	1.85
slope (M)	0.54	0.91	0.74	0.87	0.75	0.62	0.91	0.75	0.58	1.67
sigma (+/-)	0.04	0.01	0.02	0.00	0.01	0.01	0.01	0.01	0.03	0.17
correlation coefficient	0.986	1.000	0.996	1.000	0.999	1.000	1.000	0.999	0.995	0.964
n =	7	16	10	32	25	11	13	10	7	9
Y=Si/V X=(Fe+Mg)/V										
intercept (b)	0.48	-0.37	4.96	0.53	4.91	3.64	-0.59	5.19	4.48	2.17
sigma (+/-)	0.35	0.60	0.37	0.08	0.28	0.98	0.32	0.56	0.54	4.34
slope (M)	0.49	0.97	0.52	0.87	0.52	0.60	0.95	0.54	0.53	1.75
sigma (+/-)	0.02	0.05	0.02	0.00	0.01	0.06	0.03	0.02	0.02	0.79
correlation coefficient	0.994	0.981	0.992	1.000	0.991	0.951	0.995	0.993	0.997	0.640
n =	7	16	13	33	32	14	14	12	10	9
Y=Si/Y X=(Fe+Mg)/Y										
intercept (b)	381.65	-	-	-	-	-	-	-	-	37.31
sigma (+/-)	35.62	-	-	-	-	-	-	-	-	34.13
slope (M)	0.51	-	-	-	-	-	-	-	-	1.79
sigma (+/-)	0.07	-	-	-	-	-	-	-	-	0.22
correlation coefficient	0.960	-	-	-	-	-	-	-	-	0.952
n =	7	-	-	-	-	-	-	-	-	9

Table 7 (continued)

	Tony's Flow	WLG komatiites - Area 1		WLG komatiites - Area 2		WLG komatiites - Area 3	WLG komatiites - Area 4		WLG komatiites -Esk-L/No-L	WLG komatiitic basalts
		spin	cum	spin	cum		spin	cum		
Y=Si/Zn X=(Fe+Mg)/Zn										
intercept (b)	-	1.25	-0.04	-1.74	1.11	-1.08	-0.34	-6.32	4.83	7.91
sigma (+/-)	-	1.50	5.03	0.36	0.57	3.35	0.49	3.36	5.54	4.27
slope (M)	-	0.90	1.00	0.95	0.76	0.89	0.91	0.94	0.59	1.50
sigma (+/-)	-	0.03	0.11	0.00	0.01	0.10	0.01	0.03	0.15	0.26
correlation coefficient	-	0.990	0.935	1.000	0.999	0.932	0.999	0.994	0.818	0.908
n =	-	16	13	30	31	14	14	12	10	9
Y=Si/Zr X=(Fe+Mg)/Zr										
intercept (b)	141.07	4.42	108.03	19.90	101.17	72.32	-3.90	142.27	91.09	22.39
sigma (+/-)	3.65	12.90	24.83	7.90	12.01	22.53	6.60	26.35	11.08	6.05
slope (M)	0.45	0.92	0.58	0.85	0.62	0.62	0.91	0.55	0.55	1.40
sigma (+/-)	0.02	0.04	0.05	0.02	0.01	0.06	0.02	0.04	0.01	0.13
correlation coefficient	0.997	0.986	0.962	1.000	0.993	0.951	0.997	0.978	0.998	0.971
n =	7	16	13	33	31	14	14	12	8	9
Y=Si/Sc X=(Fe+Mg)/Sc										
intercept (b)	-	-0.68	34.43	3.49	33.97	29.22	-3.69	31.16	-	-
sigma (+/-)	-	4.75	3.79	1.95	5.38	5.35	2.85	5.03	-	-
slope (M)	-	0.94	0.46	0.86	0.45	0.51	0.95	0.51	-	-
sigma (+/-)	-	0.07	0.04	0.02	0.06	0.05	0.04	0.04	-	-
correlation coefficient	-	0.962	0.966	0.998	0.917	0.966	0.989	0.981	-	-
n =	-	16	13	8	14	9	13	10	-	-

Figure 33a. Pearce element ratio diagrams of SiO_2/TiO_2 vs. $(FeO^* + MgO)/TiO_2$ and SiO_2/Al_2O_3 vs. $(FeO^* + MgO)/Al_2O_3$ of WLG komatiites (Area 1).

Note: (for Figs. 33a, 33b, and 33c)
Solid lines are regression lines through the analyses of the spinifex-textured zone and the cumulate zone samples. Statistics of these lines, as well as those of other Woodburn Lake Group komatiites and high-Mg basalts, are presented in Table 7. Dashed lines represent the molar proportions of SiO_2 to $(FeO^* + MgO)$ in olivine (1:2) and clinopyroxene (2:1). Rock compositions related through olivine fractionation will define a slope of 0.5, whereas those related through clinopyroxene fractionation will define a slope of 2.0. Consequently, rock compositions that result from both olivine and clinopyroxene fractionation will define slopes between 0.5 and 2.0. Note that the latter case appears to be the situation with the spinifex-textured zone samples.

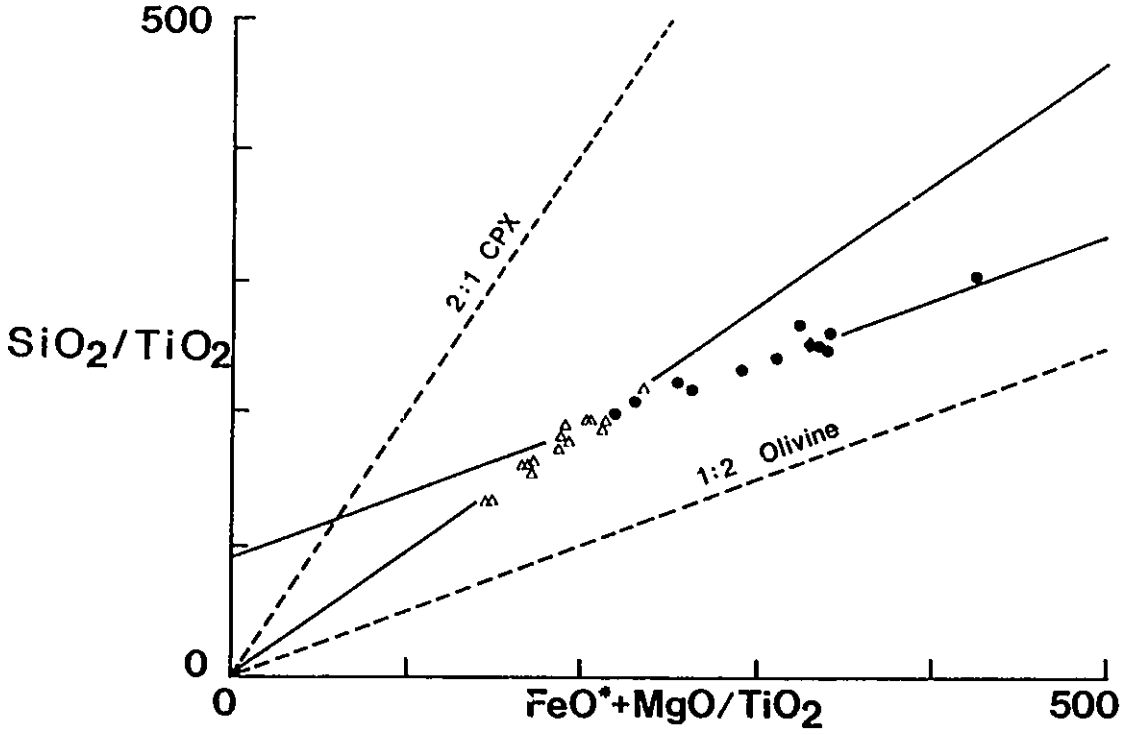
500
SiO_2/TiO_2
2:1 CPX
1:2 Olivine
0
0
FeO^*+MgO/TiO_2
500

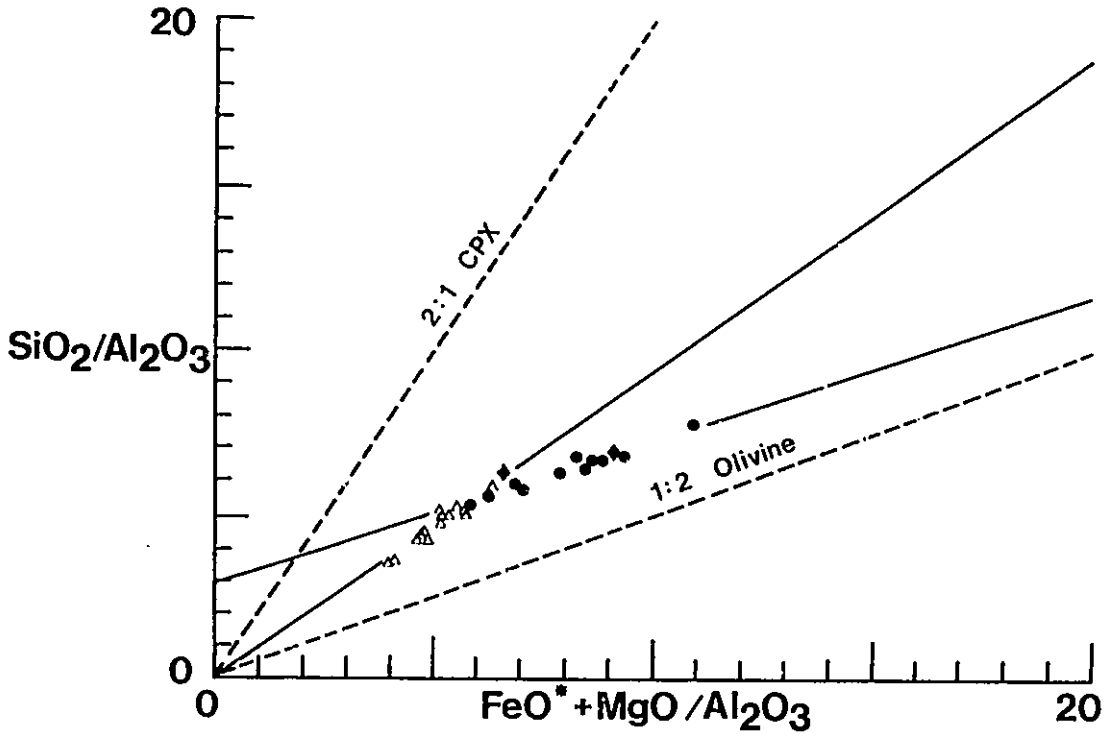
20
SiO_2/Al_2O_3
2:1 CPX
1:2 Olivine
0
0
FeO^*+MgO/Al_2O_3
20

Figure 33b. Pearce element ratio diagrams (Pearce, 1968) of SiO_2/CaO vs. FeO^* + MgO/CaO and SiO_2/Sr vs. (FeO^* + MgO)/Sr of Woodburn Lake Group komatiites (Area 1).

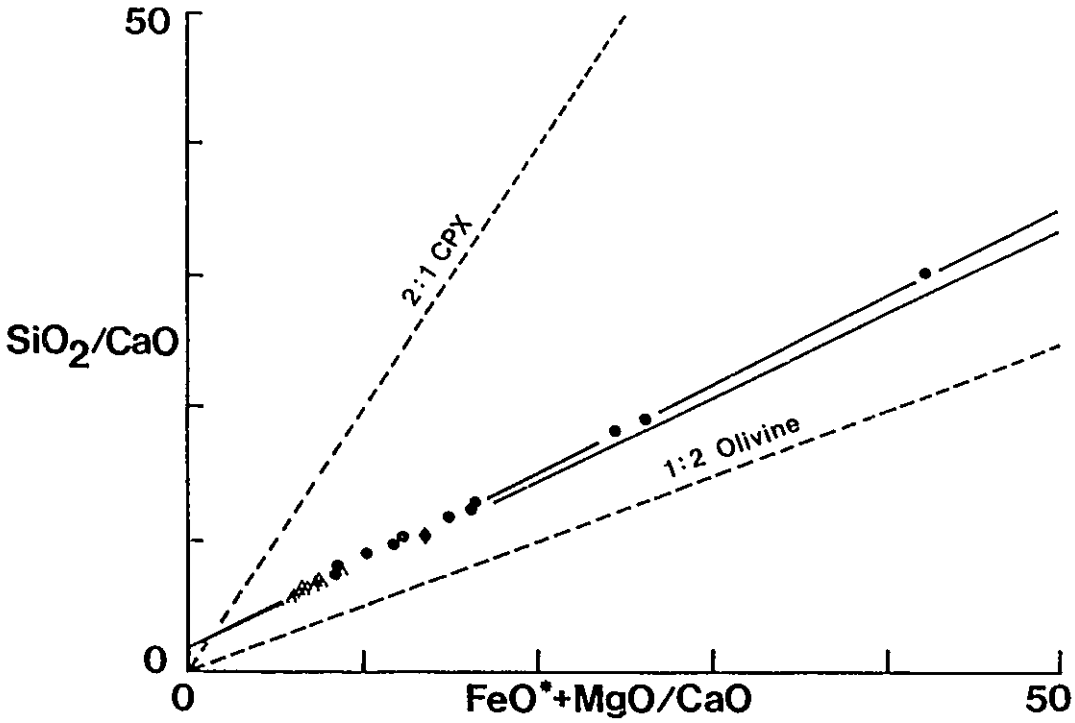
50
SiO_2/CaO
2:1 CPX
1:2 Olivine
0
0
FeO*+MgO/CaO
50

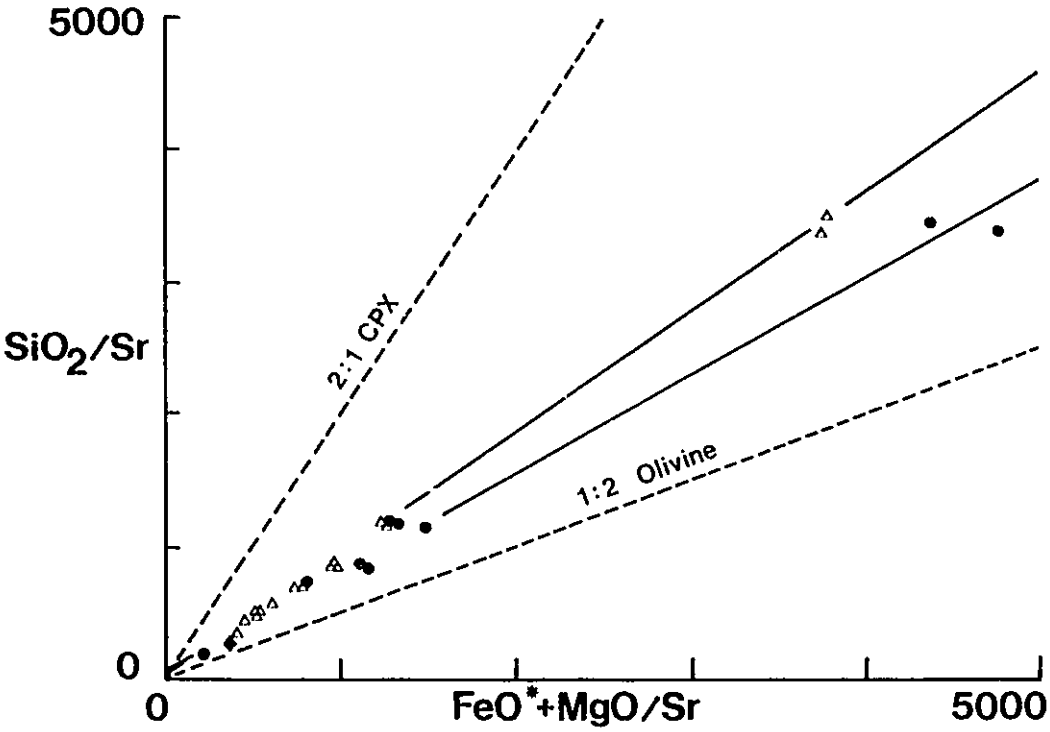
5000
SiO_2/Sr
2:1 CPX
1:2 Olivine
0
0
FeO*+MgO/Sr
5000

Figure 33c. Pearce element ratio diagrams (Pearce, 1968) of SiO_2/V vs. $(FeO^* + MgO)/V$ and SiO_2/Zr vs. $FeO^* + MgO/Zr$ of Woodburn Lake Group komatiites (Area 1).

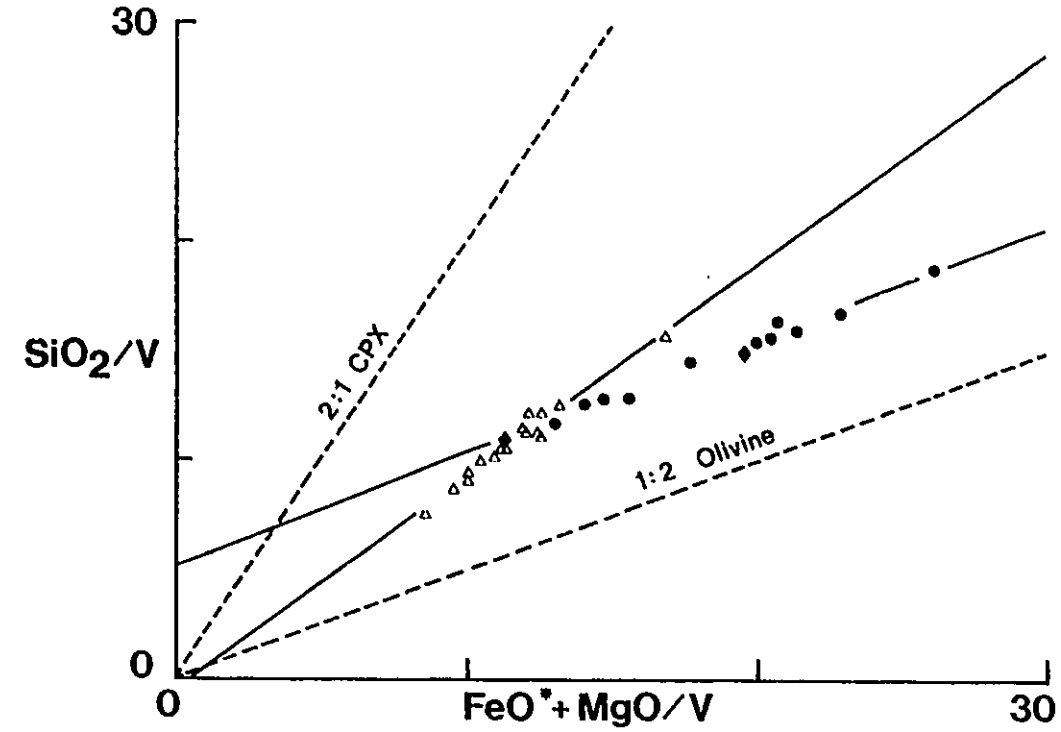
30
SiO_2/V
0
0
FeO^*+MgO/V
30
2:1 CPX
1:2 Olivine

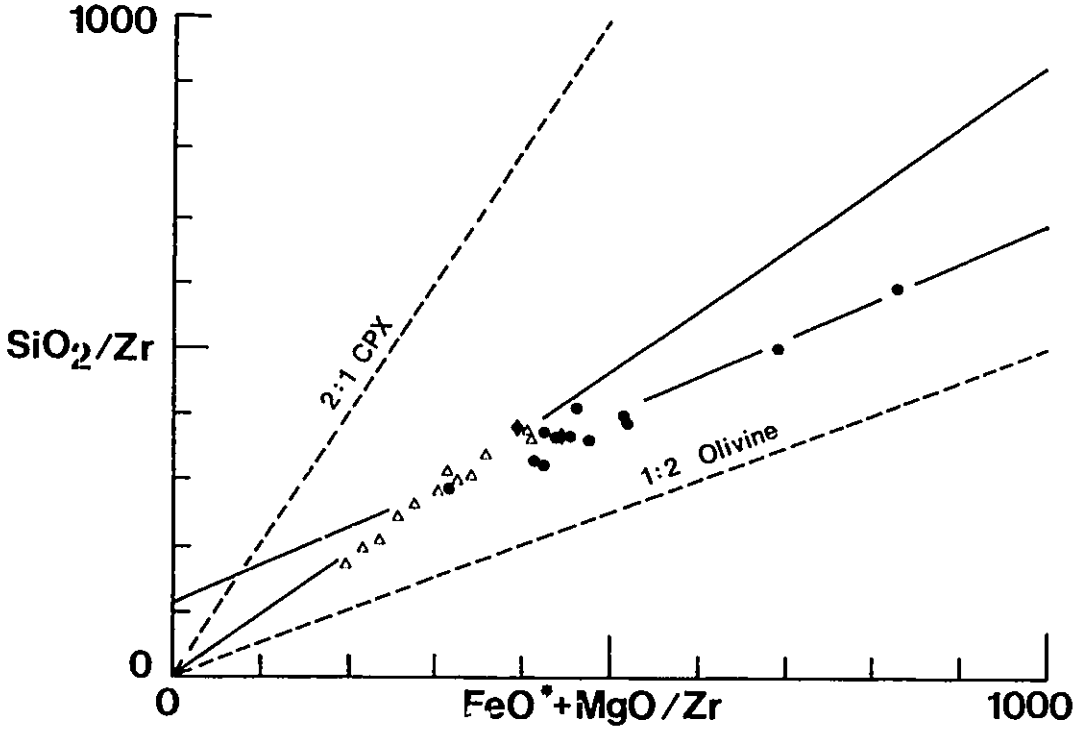
1000
SiO_2/Zr
0
0
FeO^*+MgO/Zr
1000
2:1 CPX
1:2 Olivine

Figure 33d. Pearce element ratio diagrams (Pearce, 1968) of SiO_2/TiO_2 vs. $(FeO^* + MgO)/TiO_2$ and SiO_2/Al_2O_3 vs. $(FeO^* + MgO)/Al_2O_3$ for Tony's Flow (Nisbet et al., 1987).

Note: (for Figs. 33d, 33e, and 33f)
Solid line is a regression line through the data points of Tony's Flow. Symbols are triangles for spinifex-textured samples and closed circles for cumulate samples. Statistics of the regression line are found in Table 7 for comparison with the Woodburn Lake Group komatiites. Dashed lines represent the molar proportions of SiO_2 to $FeO^* + MgO$ in olivine, 1:2 and clinopyroxene, 2:1. Note that the trend of the data points of Tony's Flow is parallel to the olivine trend. This agrees with Nisbet et al.'s (1987) interpretation of olivine-controlled fractionation.

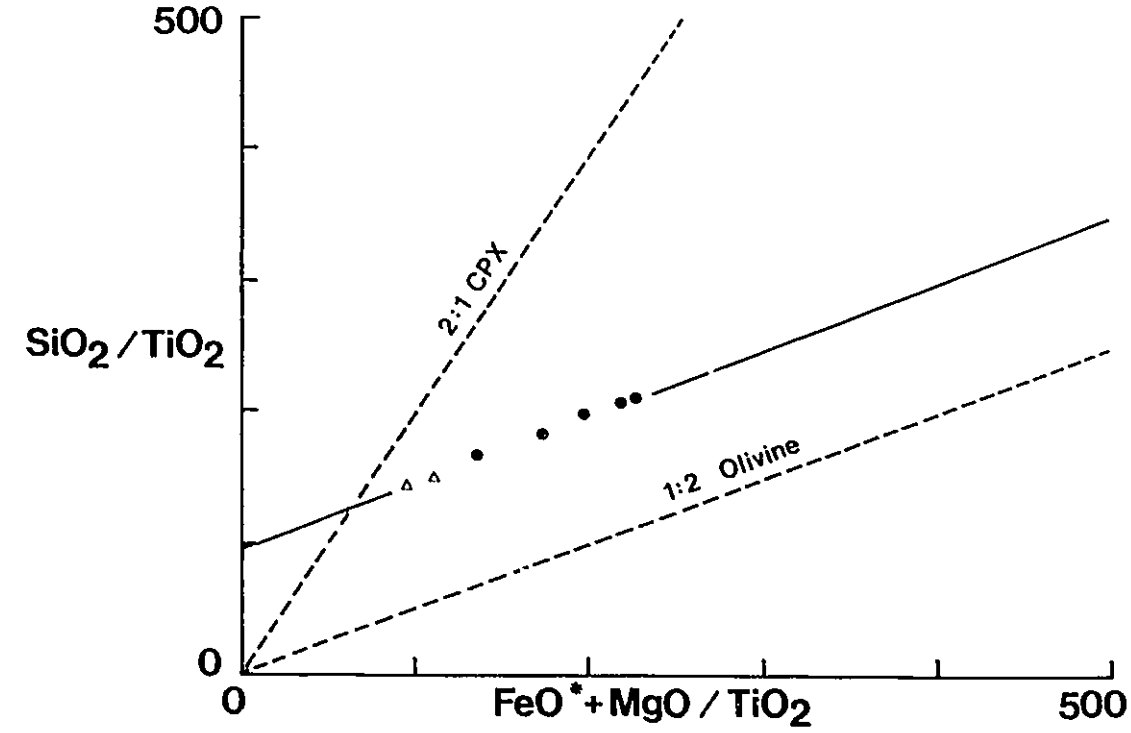
500
SiO_2 / TiO_2
2:1 CPX
1:2 Olivine
0
0
$FeO^* + MgO / TiO_2$
500

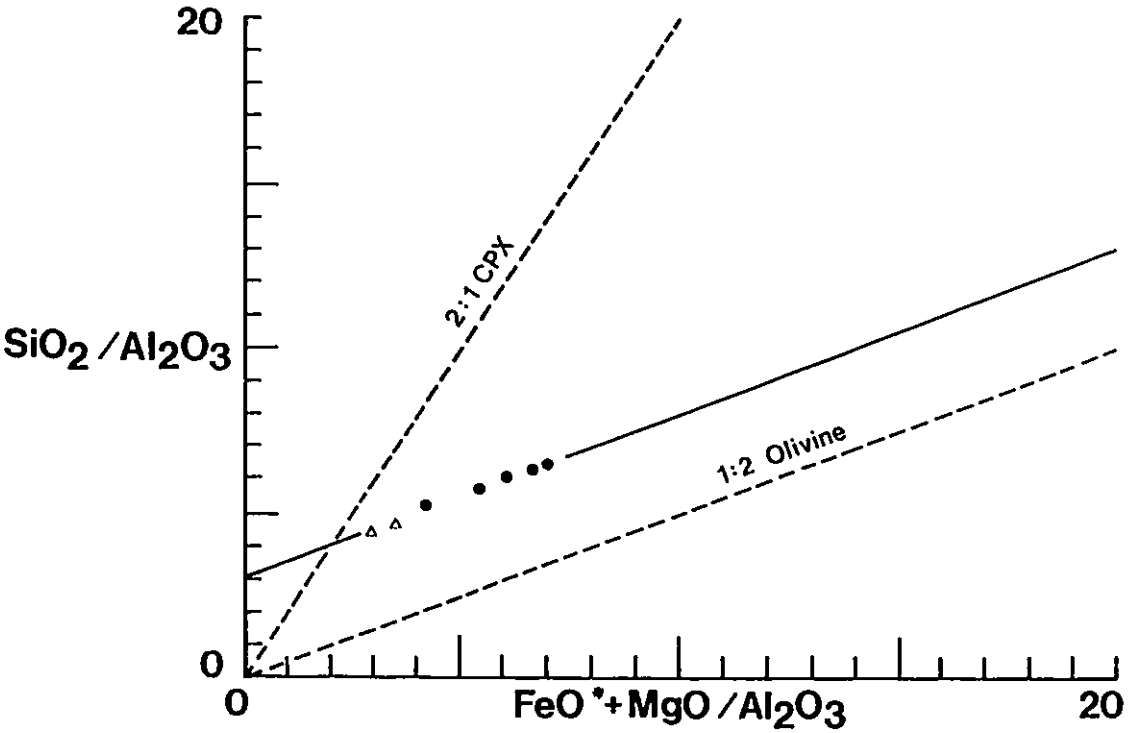
20
SiO_2 / Al_2O_3
2:1 CPX
1:2 Olivine
0
0
$FeO^* + MgO / Al_2O_3$
20

Figure 33e. Pearce element ratio diagram (Pearce, 1968) of SiO_2/CaO vs. (FeO^* + MgO)/CaO and SiO_2/Rb vs. (FeO^* + MgO)/Rb for Tony's Flow (Nisbet et al., 1987).

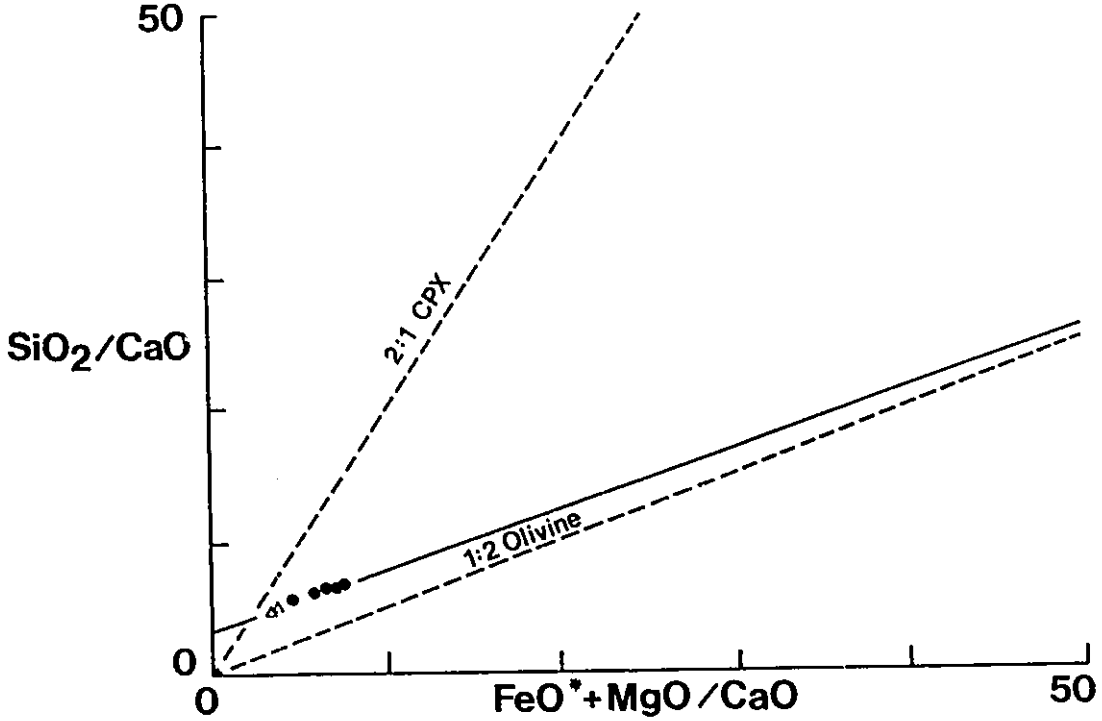
50
SiO_2/CaO
2:1 CPX
1:2 Olivine
0
0
FeO^*+MgO/CaO
50

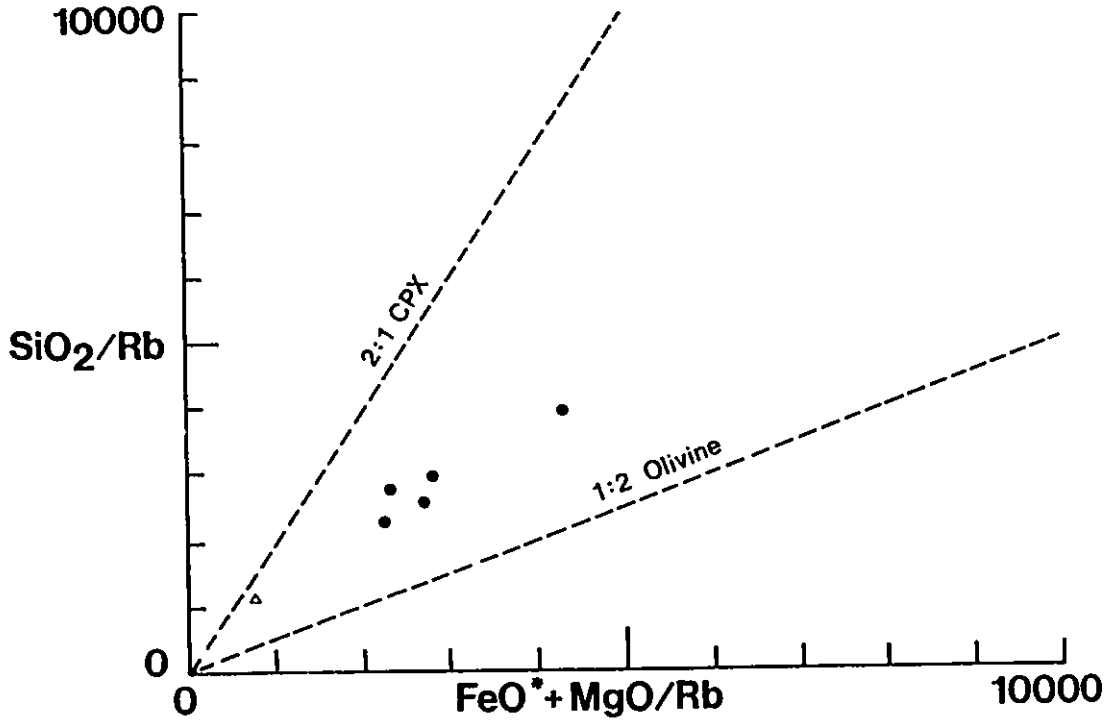
10000
SiO_2/Rb
2:1 CPX
1:2 Olivine
0
0
FeO^*+MgO/Rb
10000

Figure 33f. Pearce element ratio diagram (Pearce, 1968) of SiO_2/V vs. (FeO^* + MgO)/V and SiO_2/Zr vs. (FeO^* + MgO)/Zr for Tony's Flow (Nisbet et al. 1987).

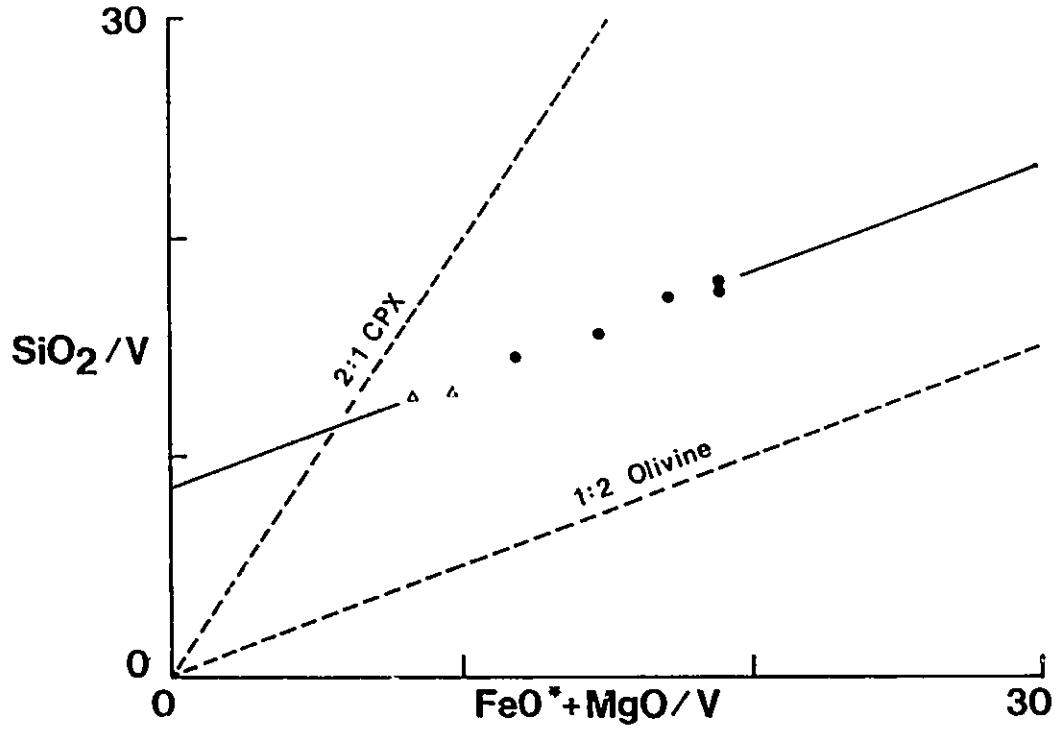
30
SiO_2 / V
0
2:1 CPX
1:2 Olivine
0
FeO^*+MgO / V
30

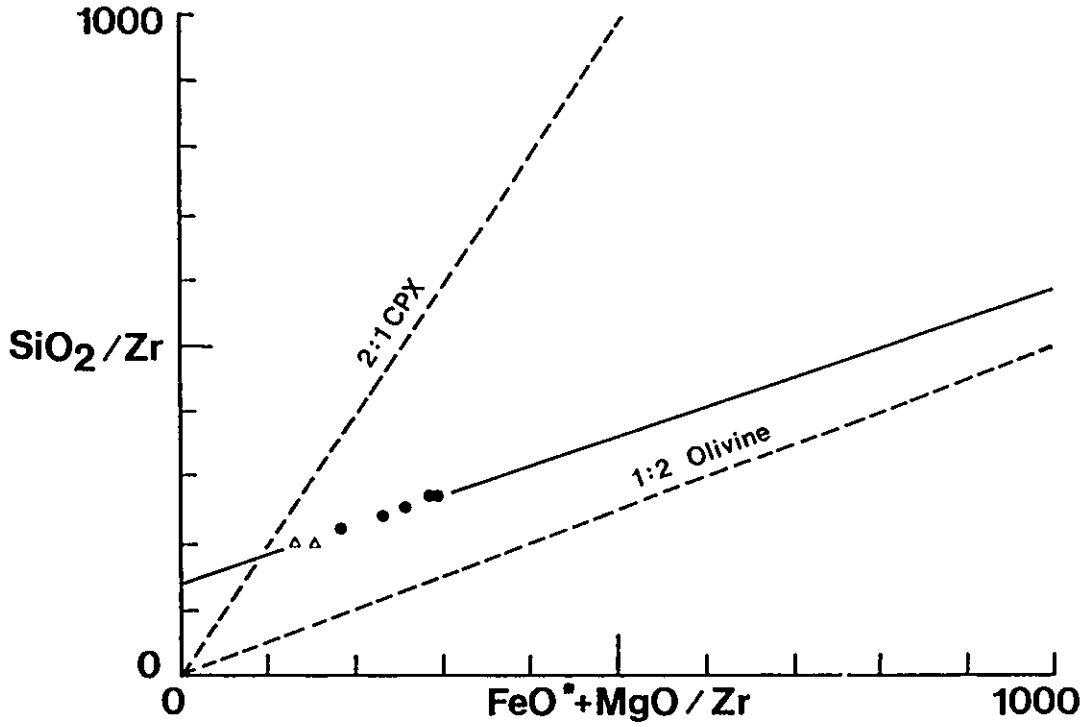
1000
SiO_2 / Zr
0
2:1 CPX
1:2 Olivine
0
FeO^*+MgO / Zr
1000

plot along an olivine control line when using incompatible normalizing oxides and elements versus molecular proportions of SiO_2 and FeO^* + MgO. The other distinct trend with a slope of 1:1 is thought to represent a 50:50 fractionating ratio of olivine and clinopyroxene. However, in most instances, the data of this trend have a zero intercept. This would appear to present a problem, but as mentioned above, this zero intercept can indicate one of two things:

a) a non-conserved oxide or element

or b) numerators (i.e. SiO_2 and FeO^* + MgO) in constant proportion throughout the igneous rock suite.

The author opines that the numerators are in constant proportion throughout the igneous rock suite. The molecular proportions of SiO_2 and (FeO^* + MgO) within the spinifex-textured zones would not be expected to have a large variation during the crystallization history of the flow unit. However, the more likely reason for the zero intercept is that the oxide or element used as the denominator is not conserved. This does not necessarily mean that the 1:1 trend lines with a zero intercept are not valid. Instead, these trend lines are possibly indicating that the oxide or element used as the denominator is compatible with at least one of the mineral phase(s) involved in the differentiation process(es) illustrated on the MPR diagram. For example in Figure 33a, where TiO_2 and Al_2O_3 are used as the common denominator, the trend line of the spinifex-textured zone

goes through the origin. This is expected because TiO_2 and Al_2O_3 are highly compatible with clinopyroxene. Hence, when clinopyroxene joins the liquidus with olivine and chromite, oxides or elements that are compatible with clinopyroxene will generate MPR trend lines which plot through the origin. This conclusion is consistent with the data presented in molecular proportion ratio (MPR) diagrams by Canil (1987). Also, a re-examination of the data of Barnes (1985, Figures 8, 9, 11) show the spinifex-textured samples having a 1:1 slope and a zero-intercept. The other trend of high variability falls somewhere between the two distinct trends. The normalizing oxides/elements (e.g. CaO) that give trends deviating from the two distinct trends (i.e. fan-shaped arrays, scatter, or rotation from 1:1 or 1:2 slopes) are considered to have been remobilized during secondary processes.

On this basis, TiO_2, Al_2O_3, FeO^*, MgO, SiO_2, MnO, Sc, V, Ni, Cr, Zr, and heavy REE contents of the komatiites and komatiitic to tholeiitic basalts are considered, in most instances within the Pipedream Lake and Esker Lake belts, to be essentially immobile. For example, Al_2O_3, Sc, and V show the coherent behavior of immobile elements when plotted versus TiO_2 (Fig. 34). Hence, they maintain constant ratios (i.e. conserved constituents) over a wide range of compositions. Zr shows some variable scatter when plotted versus other immobile oxides/elements such as TiO_2 (Fig. 34) or MgO (Figs. 38, 42, 44, 46 in Section 4.6), but this can be explained by the analytical

Figure 34. Plot of immobile oxides/elements (Al_2O_3, V, Sc, and Zr) versus TiO_2 (wt%) of komatiites from the Pipedream Lake belt (Areas 1, 2, 3, and 4 designated, respectively, as A, B, C, and D, see legend on p.102). Solid lines represent the chondritic ratio (wt%) of the plotted oxides/elements.

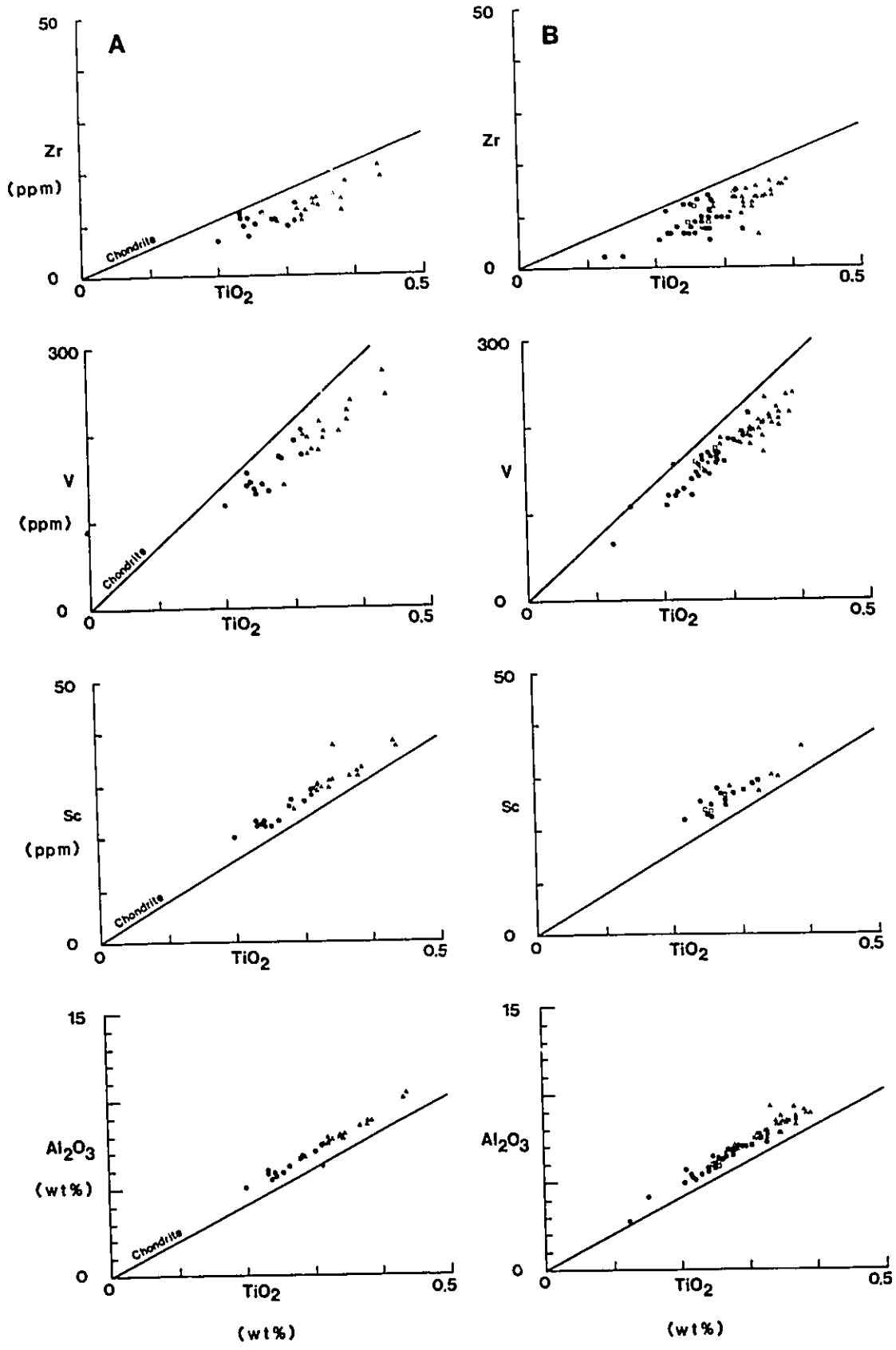
A
B
50
0
Zr
(ppm)
Chondrite
0
TiO2
0.5
300
V
(ppm)
Sc
(ppm)
15
Al2O3
(wt%)
(wt%)

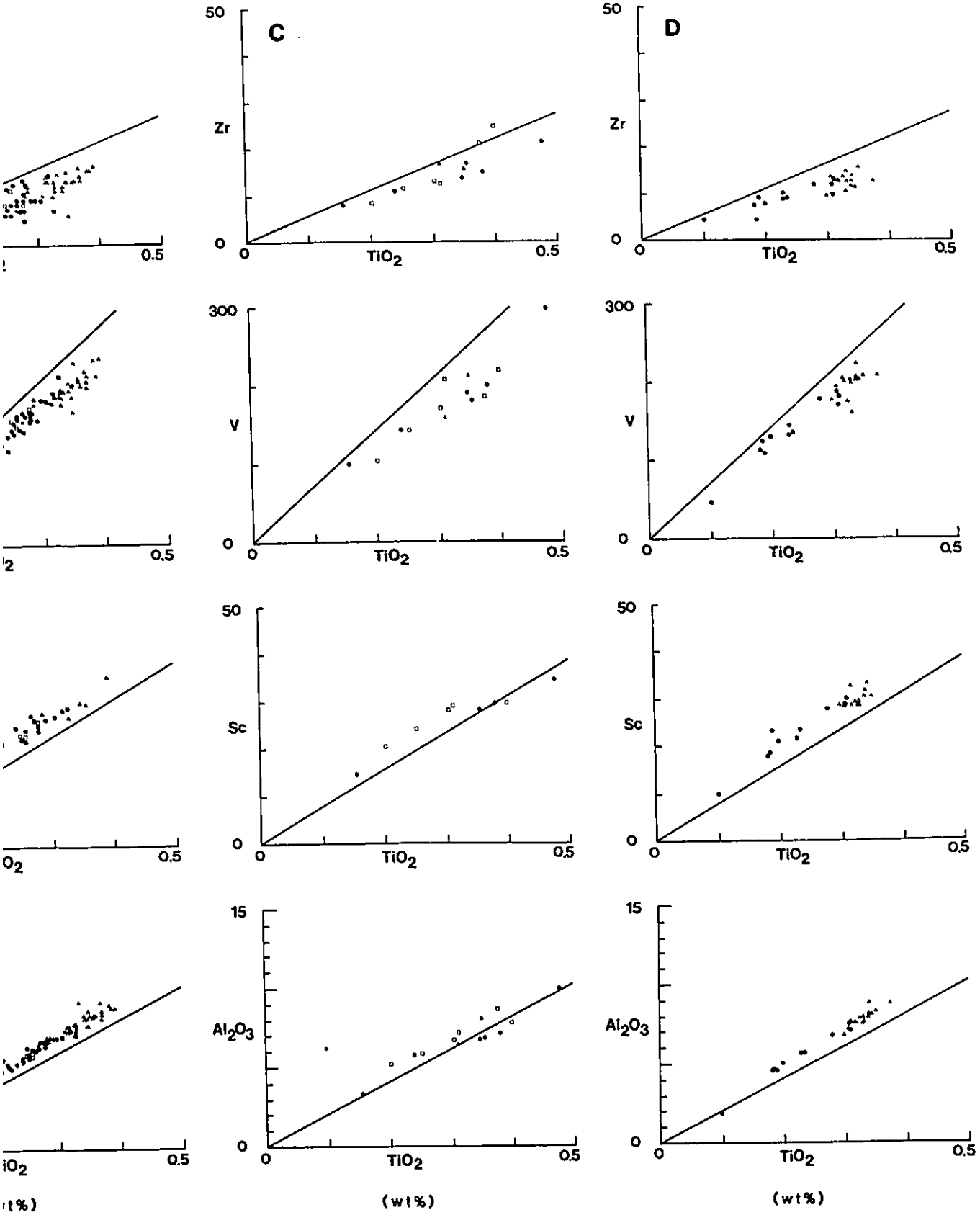
C
D
50
Zr
0
0.5
TiO_2
300
V
Sc
15
Al_2O_3
(wt%)

imprecision of Zr, especially within the cumulate zone samples, at these low (i.e. <20 ppm) concentrations. Co, Cu, Na_2O, K_2O, Rb, Sr, Ba, and light REE are found to be mobile to varying degrees, but all, except Co, show a relatively consistent, negative correlation with MgO. K_2O, Ba, Sr, and to a lesser degree Na_2O, exhibit a large scatter when plotted against a relatively immobile element, Zr (Fig. 35); indicative of secondary processes. P_2O_5, S, Nb, and Y were analyzed but are not treated here because of the poor analytical precision associated with their extremely low values. The coherent nature of CaO with some of the relatively immobile oxides/elements suggests that CaO has not been mobile. However, it is possible that CaO contents in the Woodburn Lake Group komatiites have been tightly constrained by an alteration process that is a function of composition, hence resulting in a systematic rotation of trend lines (see next paragraph).

In view of the importance placed on the geochemical trends of MgO, CaO, Al_2O_3, TiO_2, and REE in petrogenetic modelling of komatiites, another approach will be used to assess the nature of alteration processes on the present chemistry of the komatiites. This approach consists of plotting MgO, CaO, Al_2O_3, and La/Yb against H_2O, CO_2, and FeO/Fe_2O_3 (Figs. 36a, 36b, 36c, and 36d). FeO/Fe_2O_3 is also plotted against H_2O and CO_2 (Fig. 36e). H_2O correlates positively with MgO, La/Yb, and FeO/Fe_2O_3, and negatively with CaO and Al_2O_3. CO_2 to a lesser degree, also, shows the same positive trends with MgO, La/Yb, and FeO/Fe_2O_3,

Figure 35. Plot of large lithophile oxides/elements versus Zr. (ppm) of komatiites from the Pipedream Lake belt (Areas 1, 2, 3, and 4). Note the high degree of scatter of all plots, except to a lesser degree the Na_2O versus Zr plot.

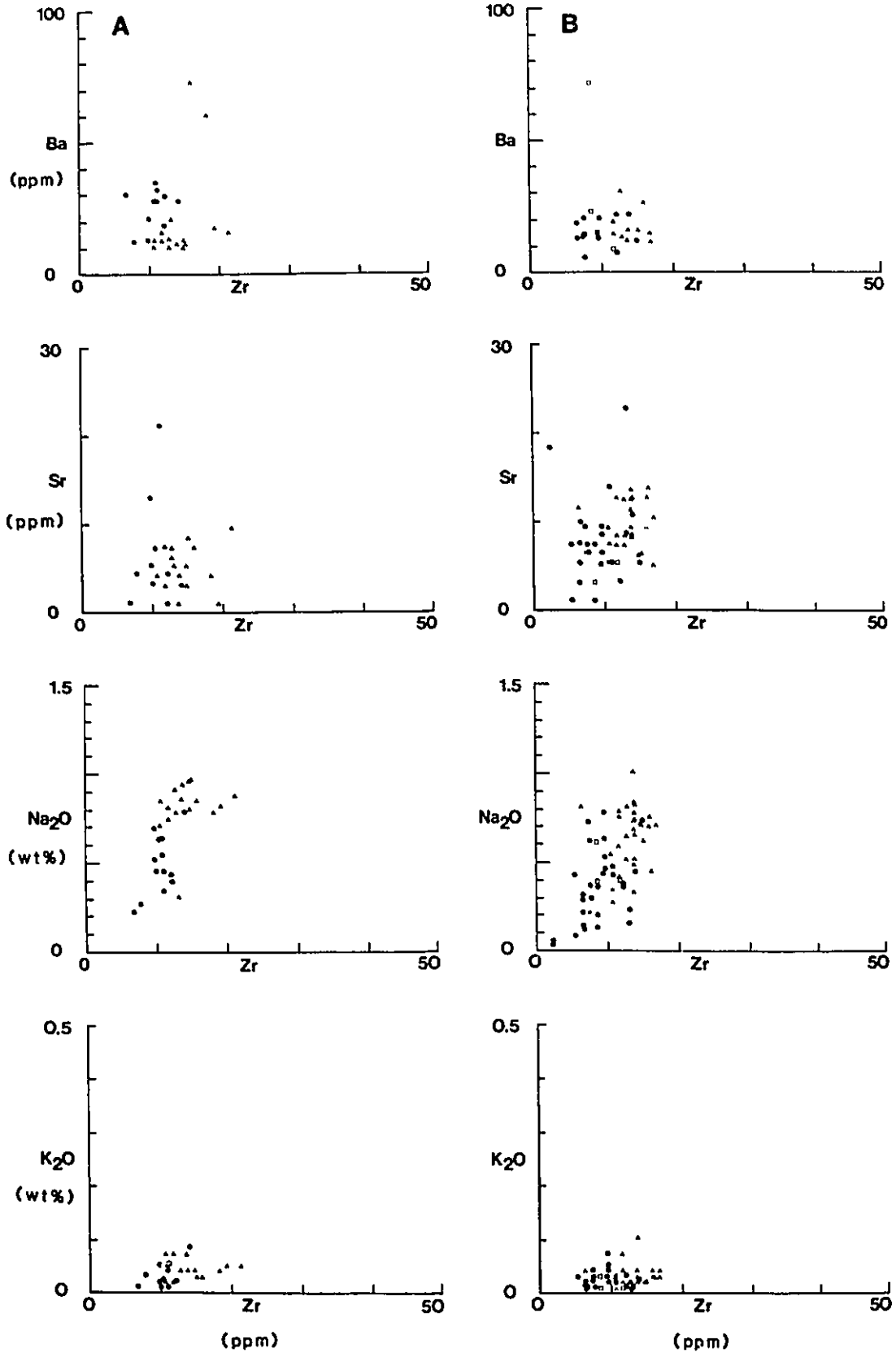
A
B
100
Ba
(ppm)
0
Zr
50
30
Sr
1.5
Na_2O
(wt%)
0.5
K_2O

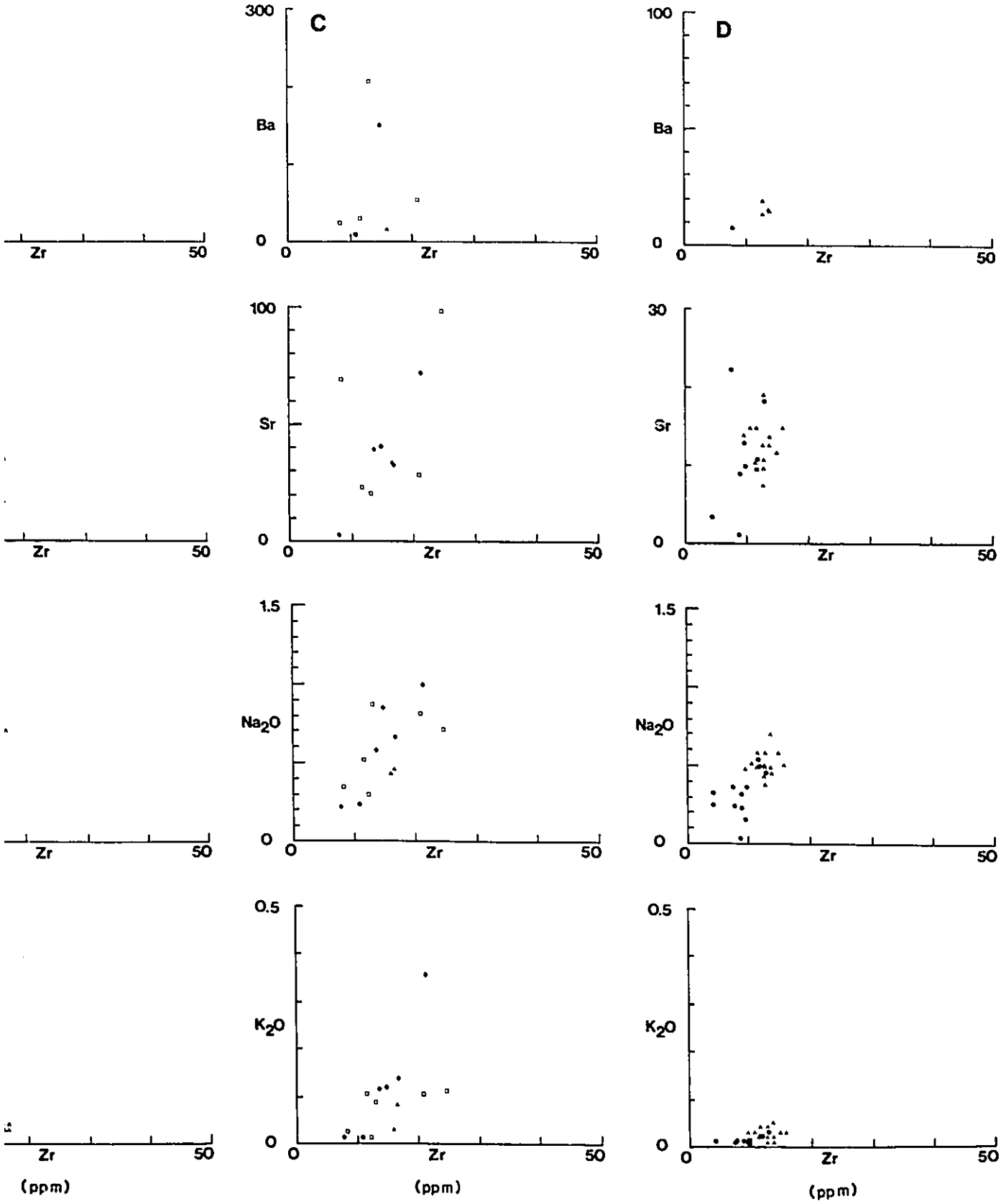
C
D
300
100
Ba
0
Zr
50
100
30
Sr
1.5
Na_2O
0.5
K_2O
(ppm)

Figure 36a. MgO plotted against H_2O, CO_2, and FeO/Fe_2O_3 for those Woodburn Lake Group komatiitic samples with determinations of FeO, Fe_2O_3, CO_2, and H_2O.

Open star - represents sheared komatiite (AK-3)
Closed star - represents contact metamorphosed komatiites (AK-7a and AK-12b)
Open triangle - represents spinifex-textured zone
Closed circle - represents cumulate zone

Note: For Figures 36a, 36b, 36c, 36d, and 36e the oxides and elements have not been recalculated on an anhydrous basis.

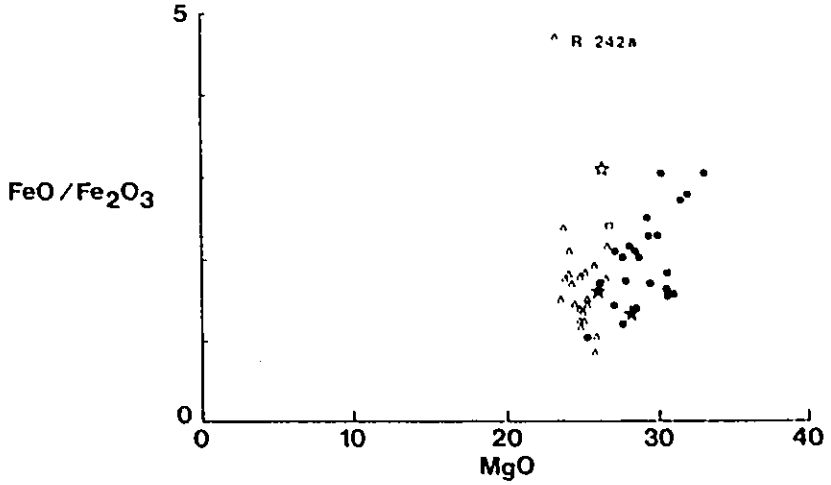
5
0
FeO / Fe2O3
0
10
20
30
40
MgO

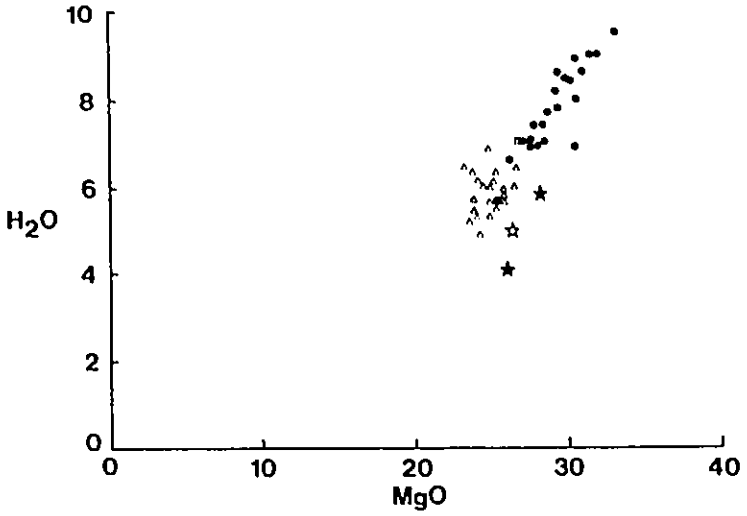
10
8
6
4
2
0
H2O
0
10
20
30
40
MgO

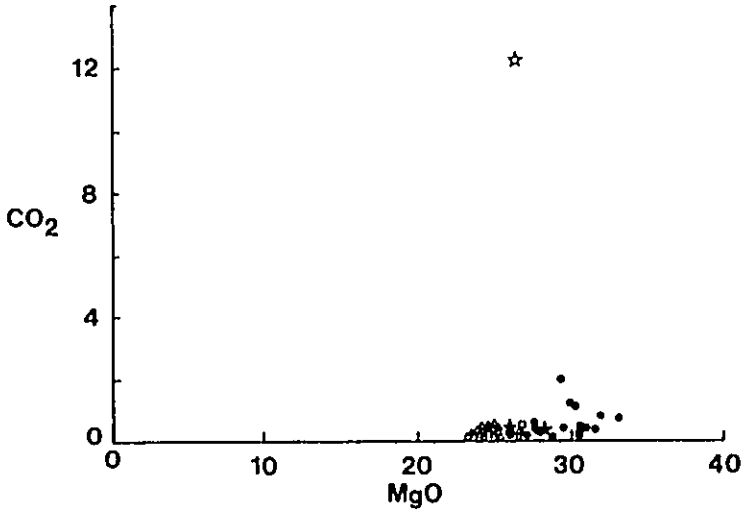
12
8
4
0
CO2
0
10
20
30
40
MgO

Figure 36b. CaO plotted against H_2O, CO_2, and FeO/Fe_2O_3 for those Woodburn Lake Group komatiitic samples with determinations of FeO, Fe_2O_3, CO_2, and H_2O.

Open star - represents sheared komatiite (AK-3)
Closed star - represents contact metamorphosed komatiites (AK-7a and AK-12b)
Open triangle - represents spinifex-textured zone
Closed circle - represents cumulate zone

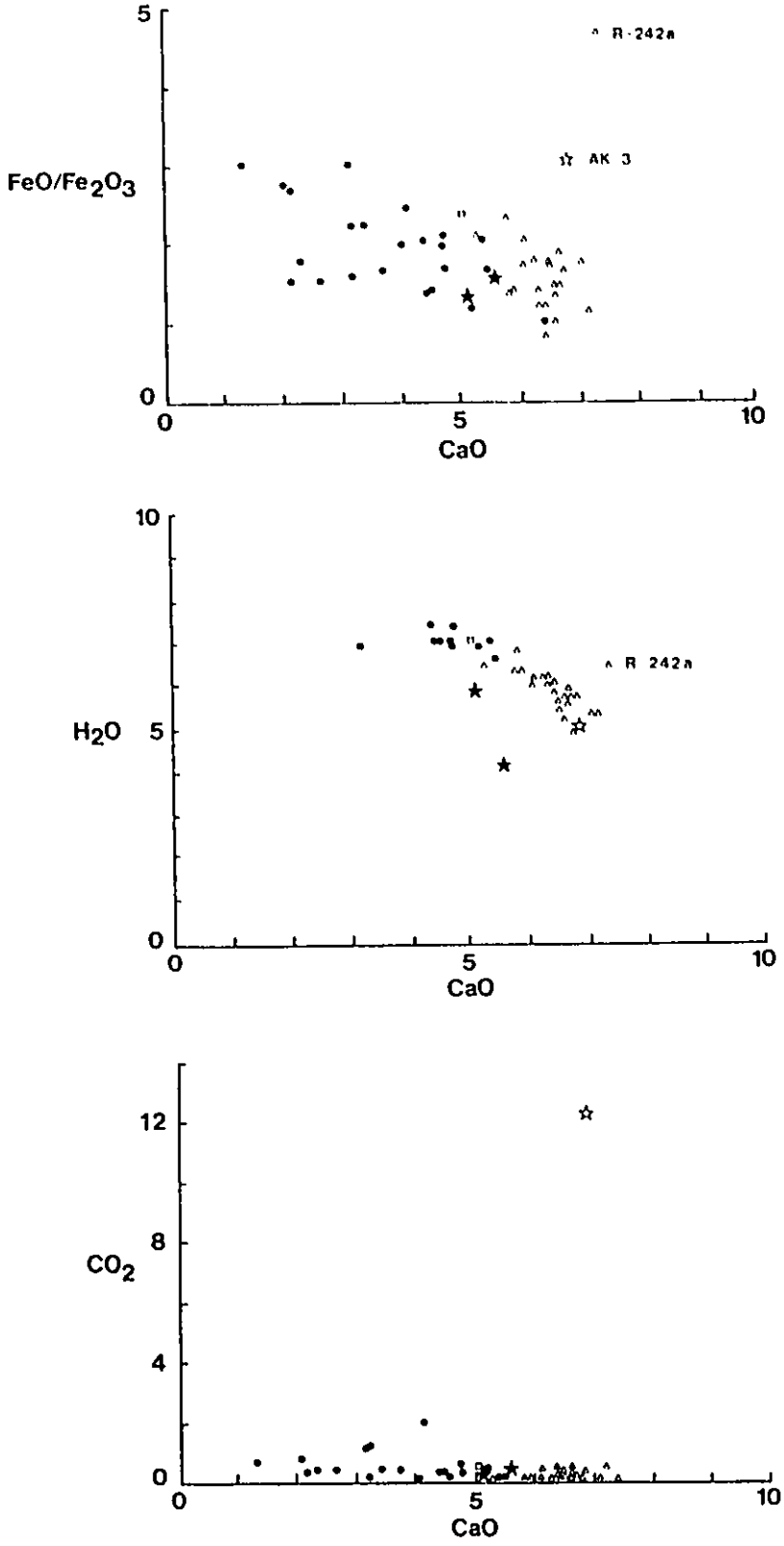
5
0
FeO/Fe2O3
R-242a
AK 3
0
5
10
CaO
10
5
0
H2O
R 242a
0
5
10
CaO
12
8
4
0
CO2
0
5
10
CaO

Figure 36c. Al_2O_3 plotted against H_2O, CO_2, and FeO/Fe_2O_3 for those Woodburn Lake Group komatiitic samples with determinations of FeO, Fe_2O_3, CO_2, and H_2O.

Open star - represents sheared komatiite (AK-3)
Closed star - represents contact metamorphosed komatiites (AK-7a and AK-12b)
Open triangle - represents spinifex-textured zone
Closed circle - represents cumulate zone

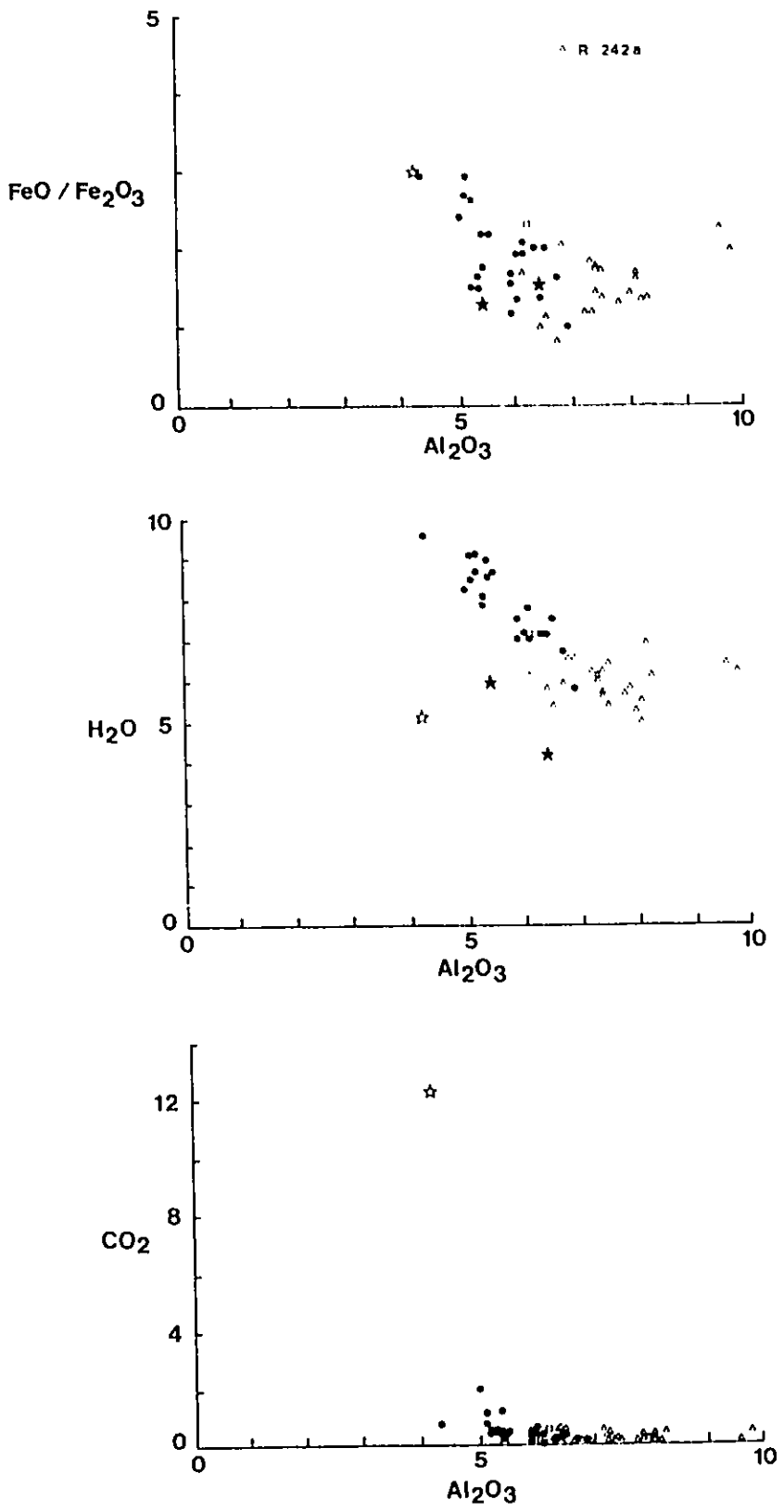
R 242a
FeO / Fe2O3
Al2O3
H2O
Al2O3
CO2
Al2O3
0
5
10
12
8
4

Figure 36d. La/Yb plotted against H_2O, CO_2, and FeO/Fe_2O_3 for those Woodburn Lake Group komatiitic samples with determinations of FeO, Fe_2O_3, CO_2, and H_2O.

Open star - represents sheared komatiite (AK-3)
Closed star - represents contact metamorphosed komatiites (AK-7a and AK-12b)
Open triangle - represents spinifex-textured zone
Closed circle - represents cumulate zone

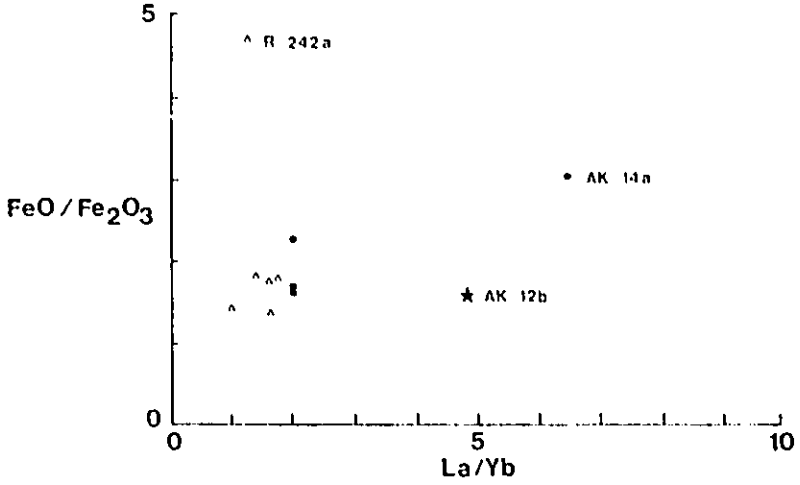
5
R 242a
AK 14a
AK 12b
FeO / Fe2O3
0
0
5
10
La/Yb

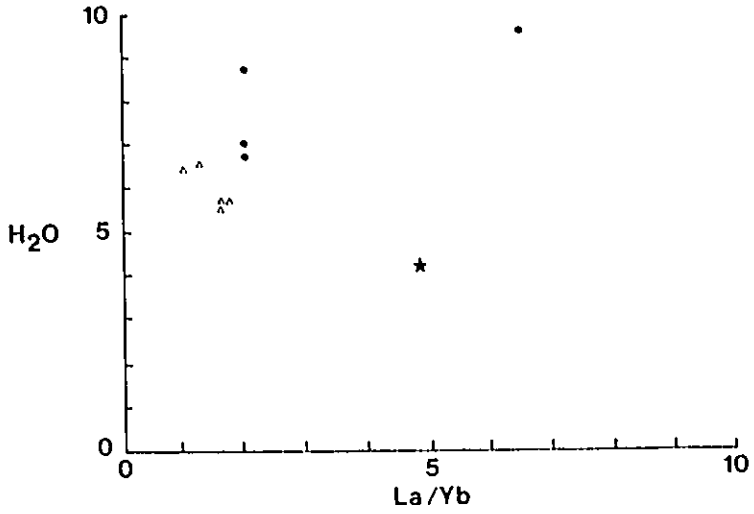
10
H2O
5
0
0
5
10
La/Yb

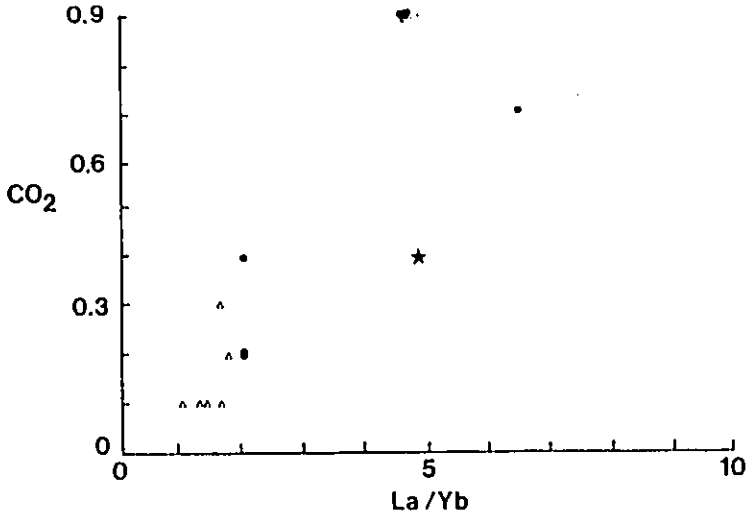
0.9
0.6
CO2
0.3
0
0
5
10
La/Yb

Figure 36e. FeO/Fe_2O_3 plotted against H_2O and CO_2 for those Woodburn Lake Group komatiitic samples with determinations of FeO, Fe_2O_3, CO_2, and H_2O.

Open star - represents sheared komatiite (AK-3)
Closed star - represents contact metamorphosed komatiites (AK-7a and AK-12b)
Open triangle - represents spinifex-textured zone
Closed circle - represents cumulate zone

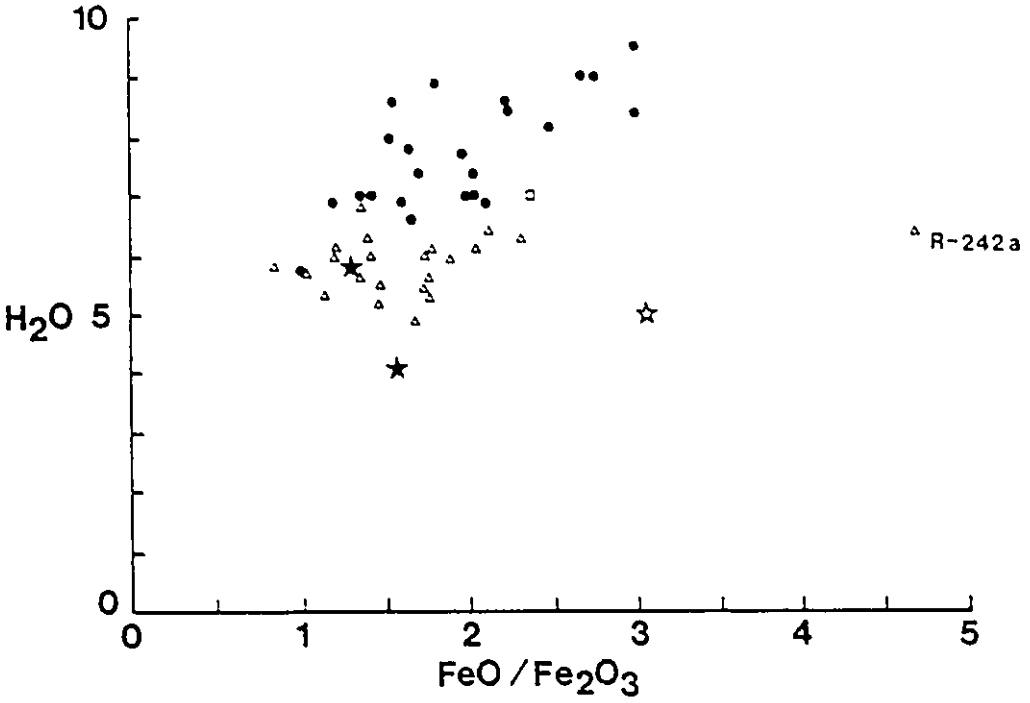
10
H_2O 5
0
0
1
2
3
4
5
FeO / Fe_2O_3
R-242a

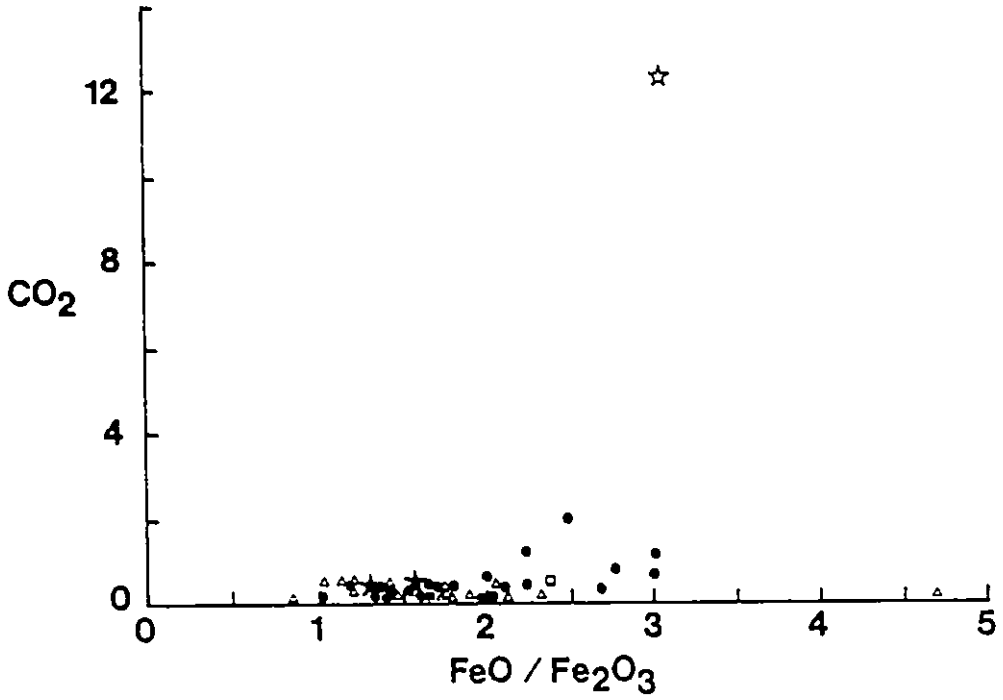
12
8
CO_2
4
0
0
1
2
3
4
5
FeO / Fe_2O_3

and negative trends with CaO and Al_2O_3. These trends are definitely produced by an alteration process since it is known that fresh komatiites have low H_2O (volatile) contents (see data of Nisbet et al., 1987). The volatile contents of the Woodburn Lake Group komatiites exhibit a positive correlation with increasing MgO contents, which is consistent with the increasing serpentine content of the komatiites with increasing MgO and decreasing CaO and Al_2O_3 contents. However, the decrease of CaO in the cumulate zone samples is more rapid than the corresponding decrease of Al_2O_3. This increased rate of decrease of CaO relative to Al_2O_3 is accompanied by higher FeO/Fe_2O_3 and La/Yb ratios, higher H_2O contents, and in some instances higher CO_2 contents. The process of serpentinization would account for most of these variations; i.e. the higher contents of H_2O, the addition of light REE, and the leaching of CaO in the olivine-rich, cumulate zone samples. Evidence for this serpentinization process would be the oxidation of FeO to Fe_2O_3 and the formation of magnetite. The reaction responsible for this is:

$$3(FeO) + H_2O = Fe_3O_4 + H_2$$

However, this appears not to be the case, since according to the H_2O vs FeO/Fe_2O_3 diagram serpentinization is negatively correlated with oxidation. This increase in oxidation state of Fe from the cumulate zone upwards into the spinifex-textured zone suggests a strong element of igneous influence. However, this

apparent problem can be resolved by remembering that the primary (i.e. unaltered) spinifex-textured zones contained abundant chromite relative to the cumulate zone. Now the spinifex-textured zones contain Cr-magnetite and these are relicts of chromite which have probably been altered to magnetite during serpentinization. This would explain the higher FeO/Fe_2O_3 ratios in the cumulate zones. Therefore, the original mineralogy and chemistry has a controlling factor on the degree of oxidation.

The major element chemistry of the komatiites in the No-name Lake belt (Fuller, 1977) is similar to that from the other two belts.

The overall low mobility of elements within analysed samples of the Woodburn Lake Group komatiites and associated basalts can probably be explained as a result of: 1) low CO_2 infiltration, 2) low water/rock ratios, 3) fluid chemistry of neutral pH (rock-dominated system, H^+ neutralized, K and Ca released) and 4) low degree of bulk rock deformation (refer to Seyfried et al., 1988 for details). Only those samples with high CO_2 contents (e.g. AK-3) or those having undergone a high degree of serpentinization (e.g. R-216 which probably formed in a seawater-dominated system) or contact metamorphism (e.g. AK-8b) show some mobility of the relatively immobile elements.

4.6 MAJOR AND TRACE ELEMENT CHEMISTRY OF THE WOODBURN LAKE GROUP KOMATIITIC SUITE

The compositions of the komatiites are quite variable as they range between 25 and 40 wt.% MgO and display the characteristic CaO/Al_2O_3 ratios, low TiO_2 and K_2O values. The basal cumulate units of spinifex-textured flows and strongly altered, massive to schistose soapstones of deformed flows (i.e. from the Esker Lake belt) are the most magnesian-rich komatiites of the area. The less magnesian-rich komatiites are represented by spinifex-textured zones of flows, massive units, and pillowed flows of the area (see Table 3 and Appendices B1.a - B1.e). The komatiitic basalts and tholeiitic basalts, cropping out mostly within the Esker Lake belt, exhibit much lower MgO values, lower CaO/Al_2O_3 ratios, and higher TiO_2 and K_2O values than the komatiites. They are predominantly olivine normative tholeiites with compositions similar to Archean low-K tholeiites (see Table 3 and Appendix B1.f).

The variation diagrams of MgO versus other major and trace elements of the komatiites are shown in Figures 37 to 46. The degree of correlation varies beween different elements but is overall quite consistent from belt to belt. Scatter about these trends, especially Na_2O, K_2O, Rb, Sr, and Ba, are attributable to alteration, as mentioned in the previous section. SiO_2, TiO_2, Al_2O_3, FeO^*, MnO, and CaO exhibit a coherent, weak to strong, negative correlation with MgO, suggestive of a fractionation trend. The negative covariant trends, CaO-MgO and Na_2O-MgO, suggest that CaO and Na_2O have been mobile at least within the cumulate zone, since if olivine is the only major phase that has

Figure 37. Oxide (wt%) versus MgO (wt%) variation diagrams of Area 1 komatiites. The solid line represents a regression line through the analyses of the spinifex-textured zone. The dashed line is a regression line through the data points of the cumulate zone.

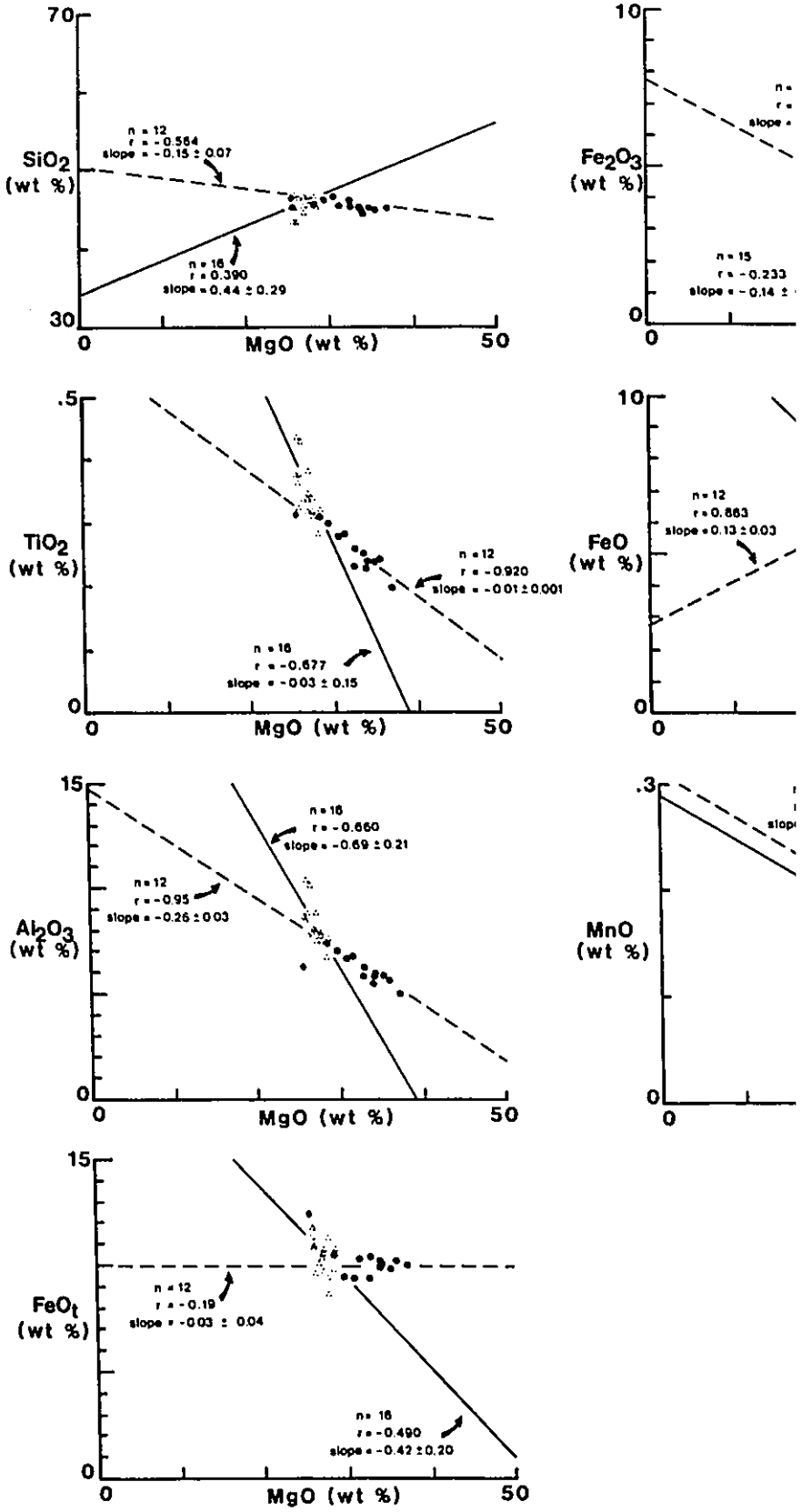
70
30
0
50
MgO (wt %)
SiO2 (wt %)
n = 12
r = -0.564
slope = -0.15 ± 0.07
n = 16
r = 0.390
slope = 0.44 ± 0.29
10
0
Fe2O3 (wt %)
n = 15
r = -0.233
slope = -0.14 ±
.5
TiO2 (wt %)
n = 12
r = -0.920
slope = -0.01 ± 0.001
n = 16
r = -0.677
slope = -0.03 ± 0.15
FeO (wt %)
n = 12
r = 0.863
slope = 0.13 ± 0.03
15
Al2O3 (wt %)
n = 16
r = -0.660
slope = -0.69 ± 0.21
n = 12
r = -0.95
slope = -0.26 ± 0.03
.3
MnO (wt %)
FeOt (wt %)
n = 12
r = -0.19
slope = -0.03 ± 0.04
n = 16
r = -0.490
slope = -0.42 ± 0.20

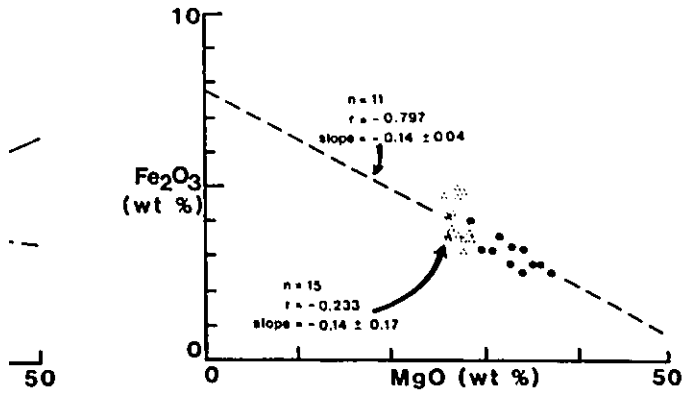
10
0
50
Fe_2O_3 (wt %)
n = 11
r = -0.797
slope = -0.14 ± 0.04
n = 15
r = -0.233
slope = -0.14 ± 0.17
0
MgO (wt %)
50

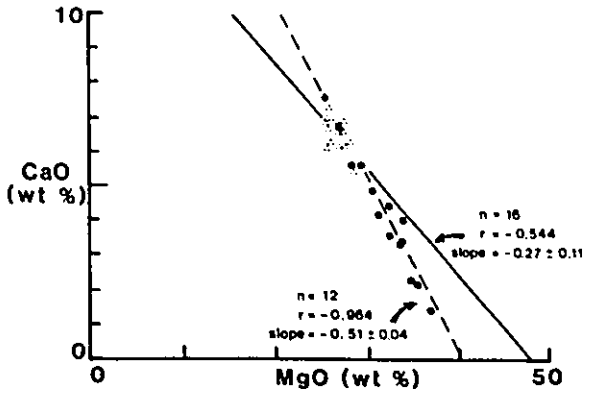
10
0
CaO (wt %)
n = 16
r = -0.544
slope = -0.27 ± 0.11
n = 12
r = -0.964
slope = -0.51 ± 0.04
0
MgO (wt %)
50

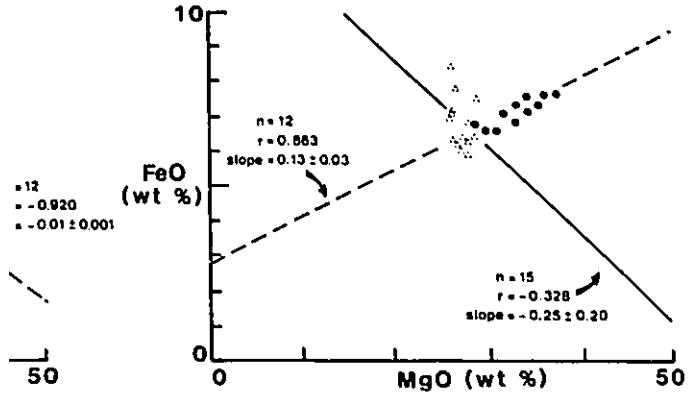
10
0
50
FeO (wt %)
n = 12
r = 0.883
slope = 0.13 ± 0.03
n = 15
r = -0.328
slope = -0.25 ± 0.20
0
MgO (wt %)
50

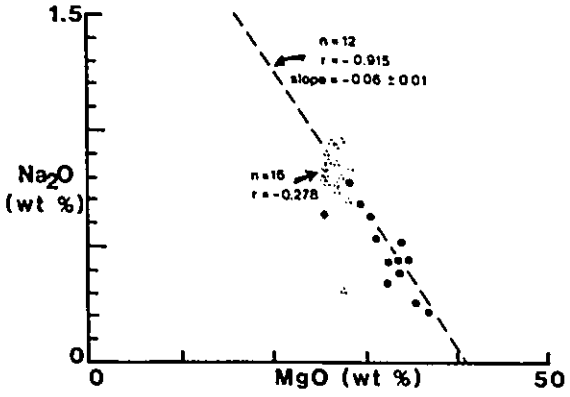
1.5
0
Na_2O (wt %)
n = 12
r = -0.915
slope = -0.06 ± 0.01
n = 16
r = -0.278
0
MgO (wt %)
50

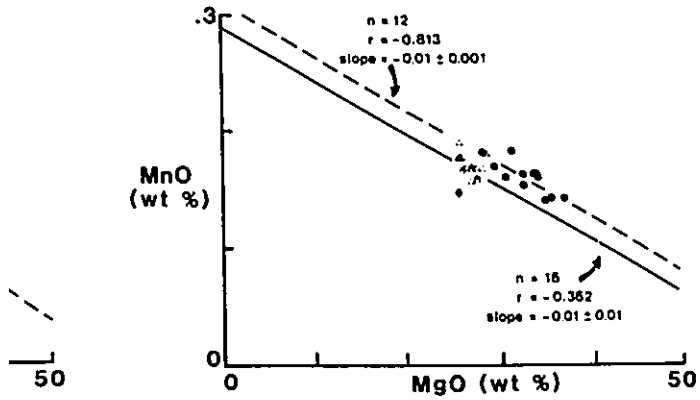
.3
0
50
MnO (wt %)
n = 12
r = -0.813
slope = -0.01 ± 0.001
n = 16
r = -0.362
slope = -0.01 ± 0.01
0
MgO (wt %)
50

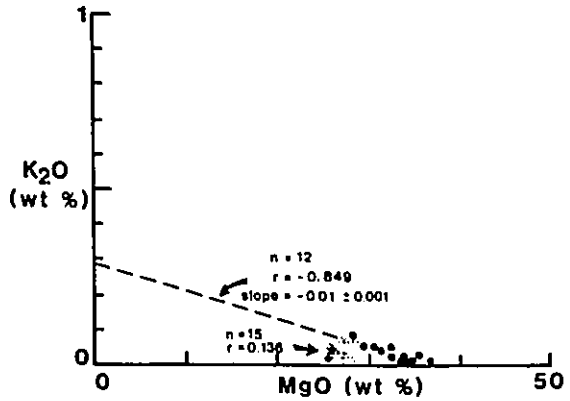
1
0
K_2O (wt %)
n = 12
r = -0.849
slope = -0.01 ± 0.001
n = 15
r = -0.136
0
MgO (wt %)
50

Figure 38. Variation diagrams of MgO (wt%) versus trace elements (ppm) of Area 1 komatiites.

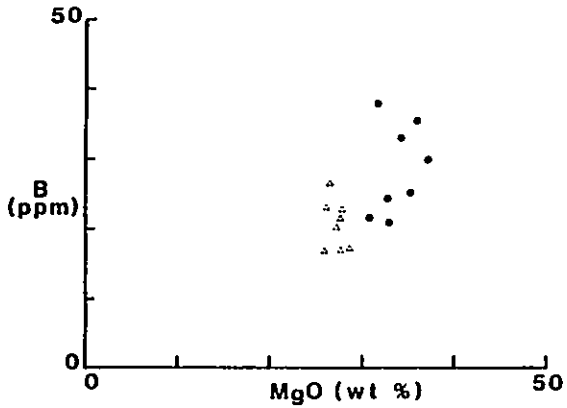
50
B
(ppm)
0
0
MgO (wt %)
50

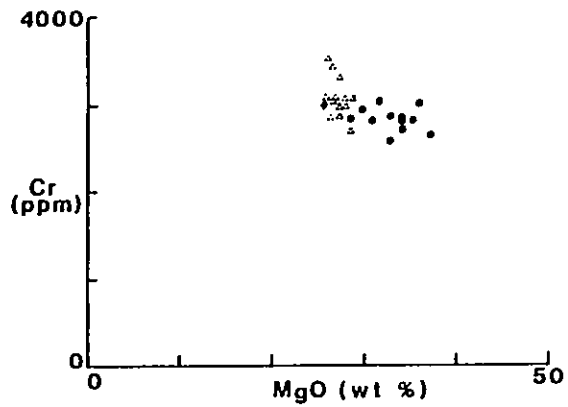
4000
Cr
(ppm)
0
0
MgO (wt %)
50

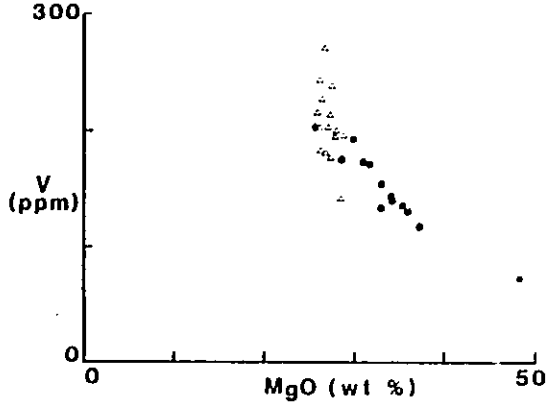
300
V
(ppm)
0
0
MgO (wt %)
50

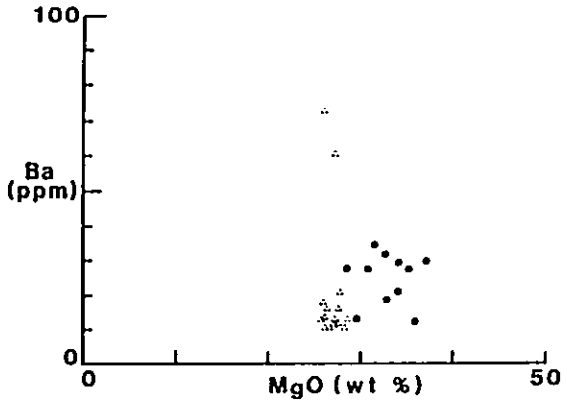
100
Ba
(ppm)
0
0
MgO (wt %)
50

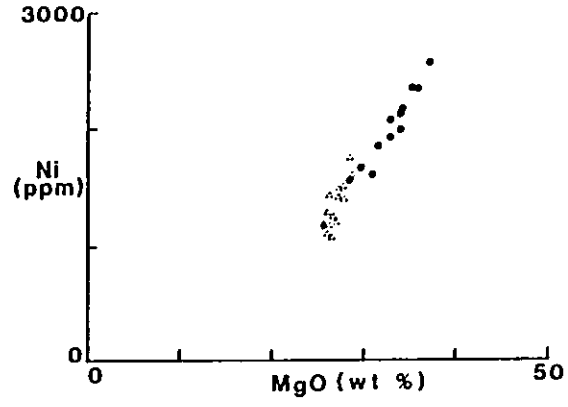
3000
Ni
(ppm)
0
0
MgO (wt %)
50

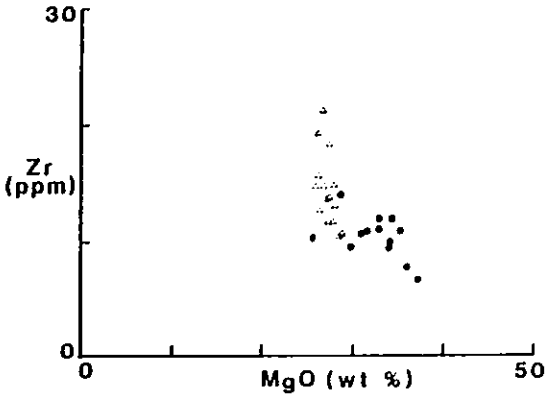
30
Zr
(ppm)
0
0
MgO (wt %)
50

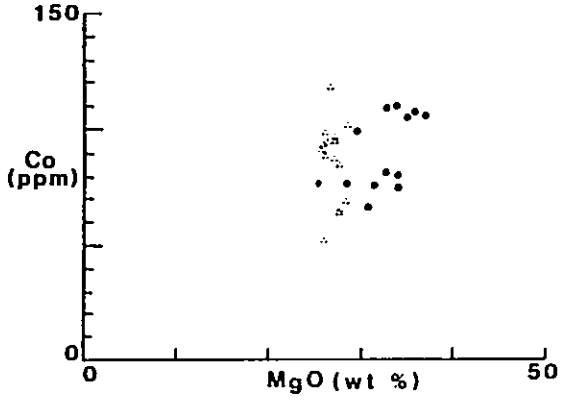
150
Co
(ppm)
0
0
MgO (wt %)
50

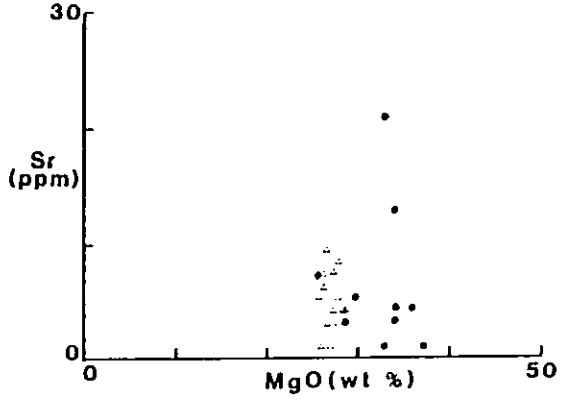
30
Sr
(ppm)
0
0
MgO (wt %)
50

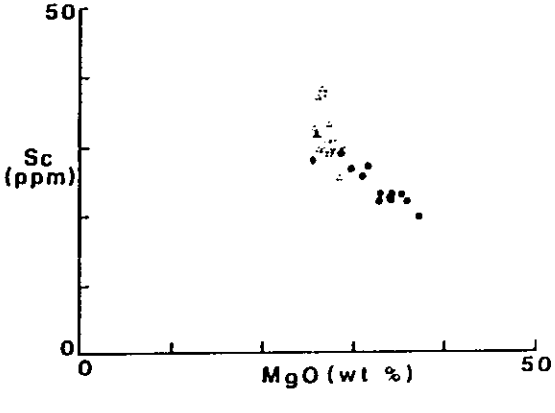
50
Sc
(ppm)
0
0
MgO (wt %)
50

Figure 39. Oxide (wt%) versus MgO (wt%) variation diagrams of Area 2 komatiites. The solid line represents a regression line through the analyses of the spinifex-textured zone and the massive flow unit. The dashed line is a regression line through the data points of the cumulate zone.

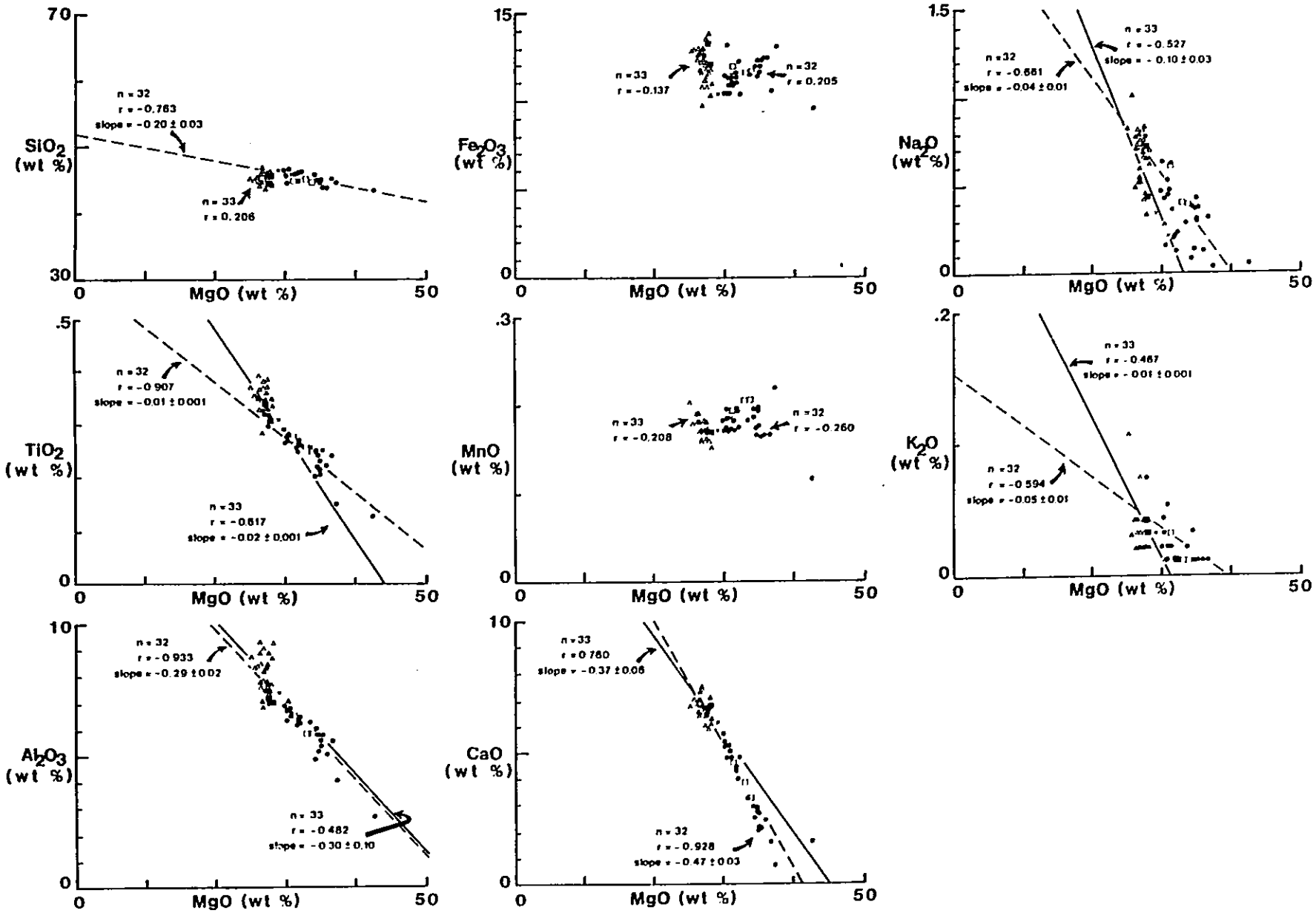
70
30
SiO2 (wt %)
n = 32
r = -0.763
slope = -0.20 ± 0.03
n = 33
r = 0.206
0
MgO (wt %)
50
15
0
Fe2O3 (wt %)
n = 33
r = -0.137
n = 32
r = 0.205
1.5
Na2O (wt %)
n = 33
r = -0.527
slope = -0.10 ± 0.03
n = 32
r = -0.681
slope = -0.04 ± 0.01
.5
TiO2 (wt %)
n = 32
r = -0.907
slope = -0.01 ± 0.001
n = 33
r = -0.617
slope = -0.02 ± 0.001
.3
MnO (wt %)
n = 33
r = -0.208
n = 32
r = -0.260
.2
K2O (wt %)
n = 33
r = -0.467
slope = -0.01 ± 0.001
n = 32
r = -0.594
slope = -0.05 ± 0.01
10
Al2O3 (wt %)
n = 32
r = -0.933
slope = -0.29 ± 0.02
n = 33
r = -0.482
slope = -0.30 ± 0.10
CaO (wt %)
n = 33
r = 0.760
slope = -0.37 ± 0.06
n = 32
r = -0.928
slope = -0.47 ± 0.03

Figure 40. Variation diagrams of MgO (wt%) versus trace elements (ppm) of Area 2 komatiites.

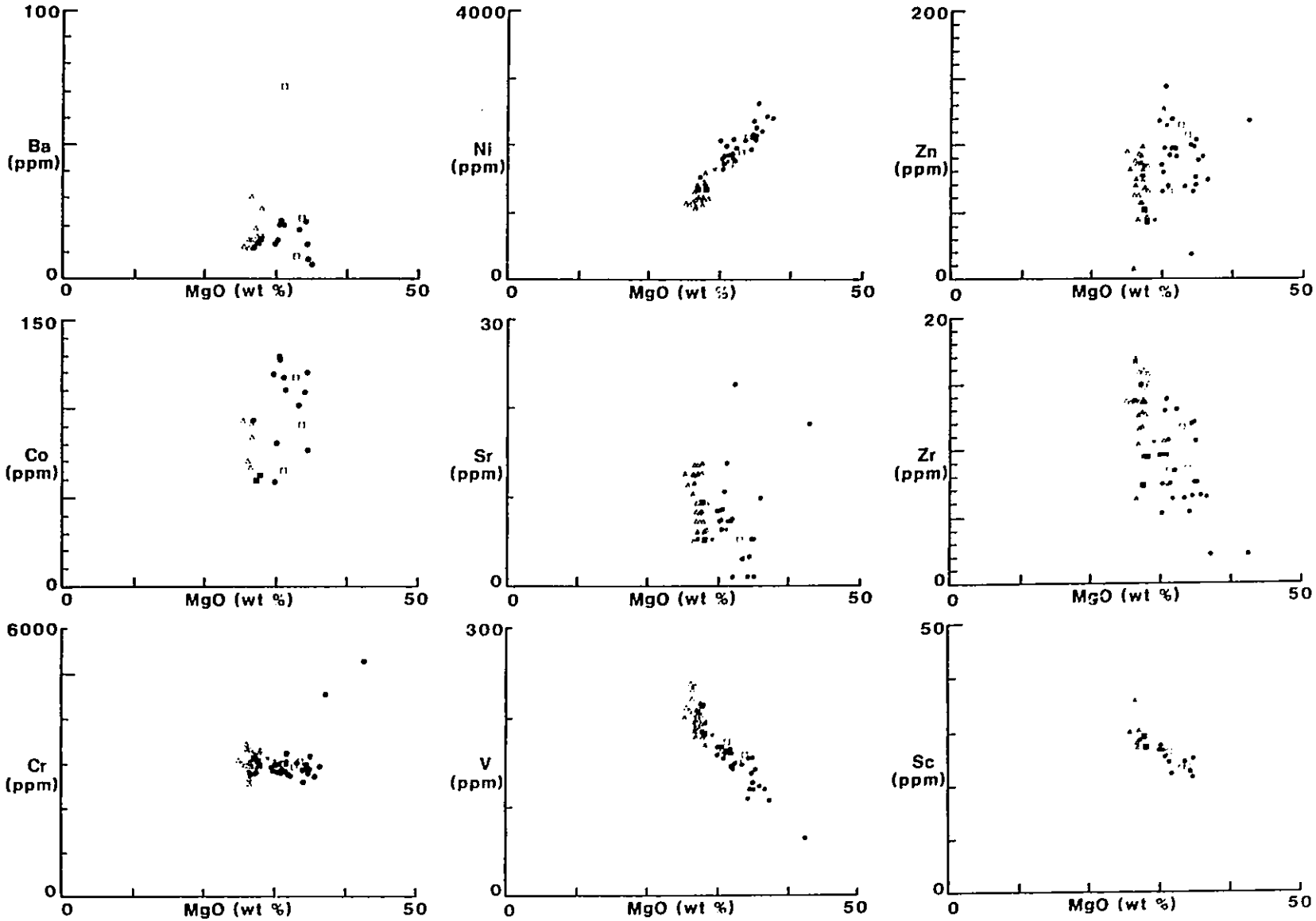
100
Ba
(ppm)
0
0
MgO (wt %)
50
4000
Ni
(ppm)
0
0
MgO (wt %)
50
200
Zn
(ppm)
0
0
MgO (wt %)
50
150
Co
(ppm)
0
0
MgO (wt %)
50
30
Sr
(ppm)
0
0
MgO (wt %)
50
20
Zr
(ppm)
0
0
MgO (wt %)
50
6000
Cr
(ppm)
0
0
MgO (wt %)
50
300
V
(ppm)
0
0
MgO (wt %)
50
50
Sc
(ppm)
0
0
MgO (wt %)
50

Figure 41. Oxide (wt%) versus MgO (wt%) variation diagrams of Area 3 komatiites. The solid line is a regression line through the data points.

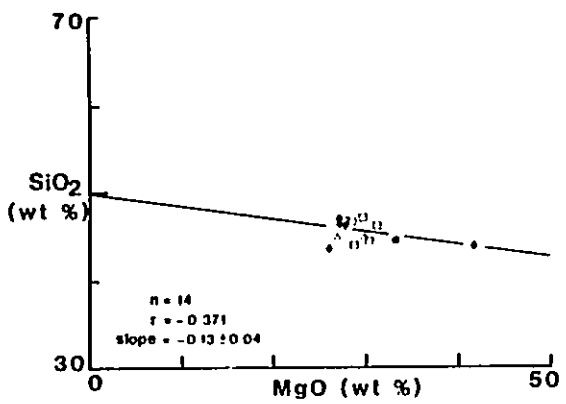
70
30
SiO_2 (wt %)
n = 14
r = -0.371
slope = -0.13 ± 0.04
0
MgO (wt %)
50

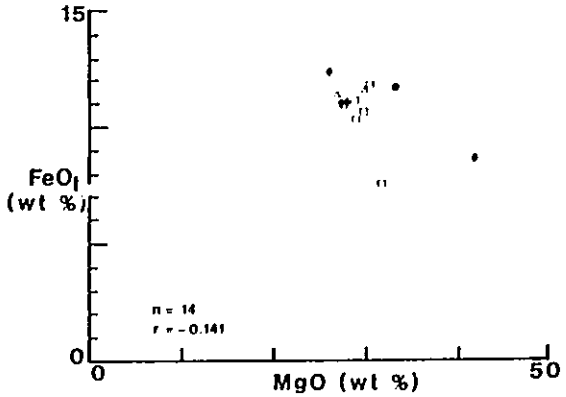
15
0
FeO_t (wt %)
n = 14
r = -0.141
0
MgO (wt %)
50

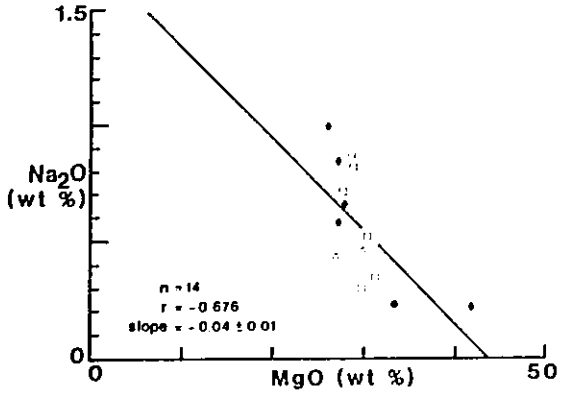
1.5
0
Na_2O (wt %)
n = 14
r = -0.676
slope = -0.04 ± 0.01
0
MgO (wt %)
50

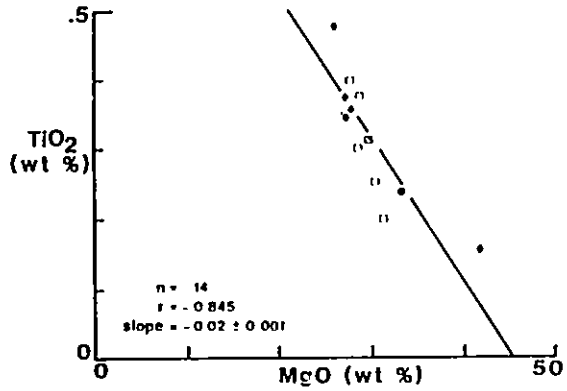
.5
0
TiO_2 (wt %)
n = 14
r = -0.845
slope = -0.02 ± 0.001
0
MgO (wt %)
50

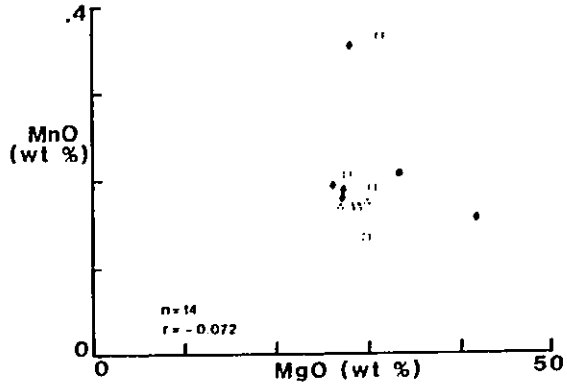
.4
0
MnO (wt %)
n = 14
r = -0.072
0
MgO (wt %)
50

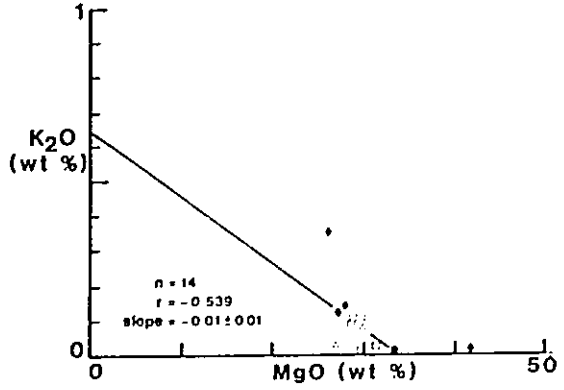
1
0
K_2O (wt %)
n = 14
r = -0.539
slope = -0.01 ± 0.001
0
MgO (wt %)
50

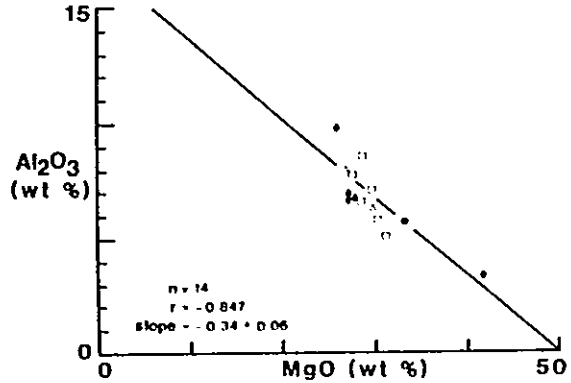
15
0
Al_2O_3 (wt %)
n = 14
r = -0.847
slope = -0.34 ± 0.06
0
MgO (wt %)
50

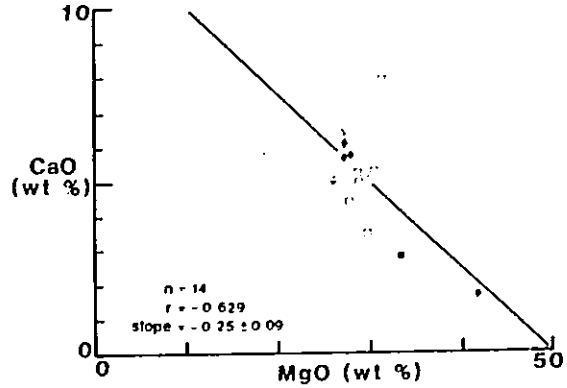
10
0
CaO (wt %)
n = 14
r = -0.629
slope = -0.25 ± 0.09
0
MgO (wt %)
50

Figure 42. Variation diagrams of MgO (wt%) versus trace elements (ppm) of Area 3 komatiites.

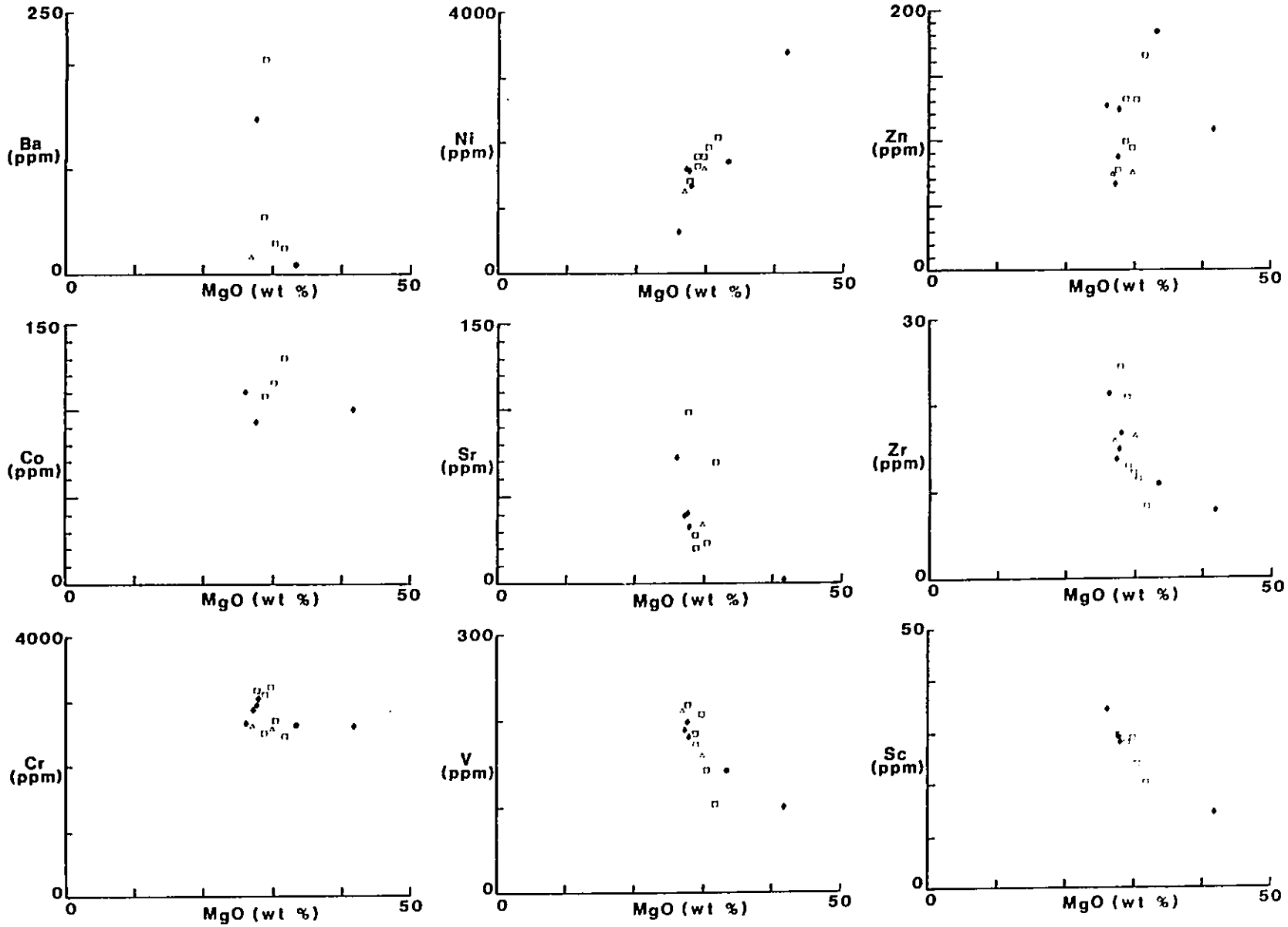
250
Ba
(ppm)
0
0
MgO (wt %)
50
4000
Ni
(ppm)
0
0
MgO (wt %)
50
200
Zn
(ppm)
0
0
MgO (wt %)
50
150
Co
(ppm)
0
0
MgO (wt %)
50
150
Sr
(ppm)
0
0
MgO (wt %)
50
30
Zr
(ppm)
0
0
MgO (wt %)
50
4000
Cr
(ppm)
0
0
MgO (wt %)
50
300
V
(ppm)
0
0
MgO (wt %)
50
50
Sc
(ppm)
0
0
MgO (wt %)
50

Figure 43. Oxide (wt%) versus MgO (wt%) variation diagrams of Area 4 komatiites. The solid line represents a regression line through the analyses of the spinifex-textured zone. The dashed line is a regression line through the data points of the cumulate zone.

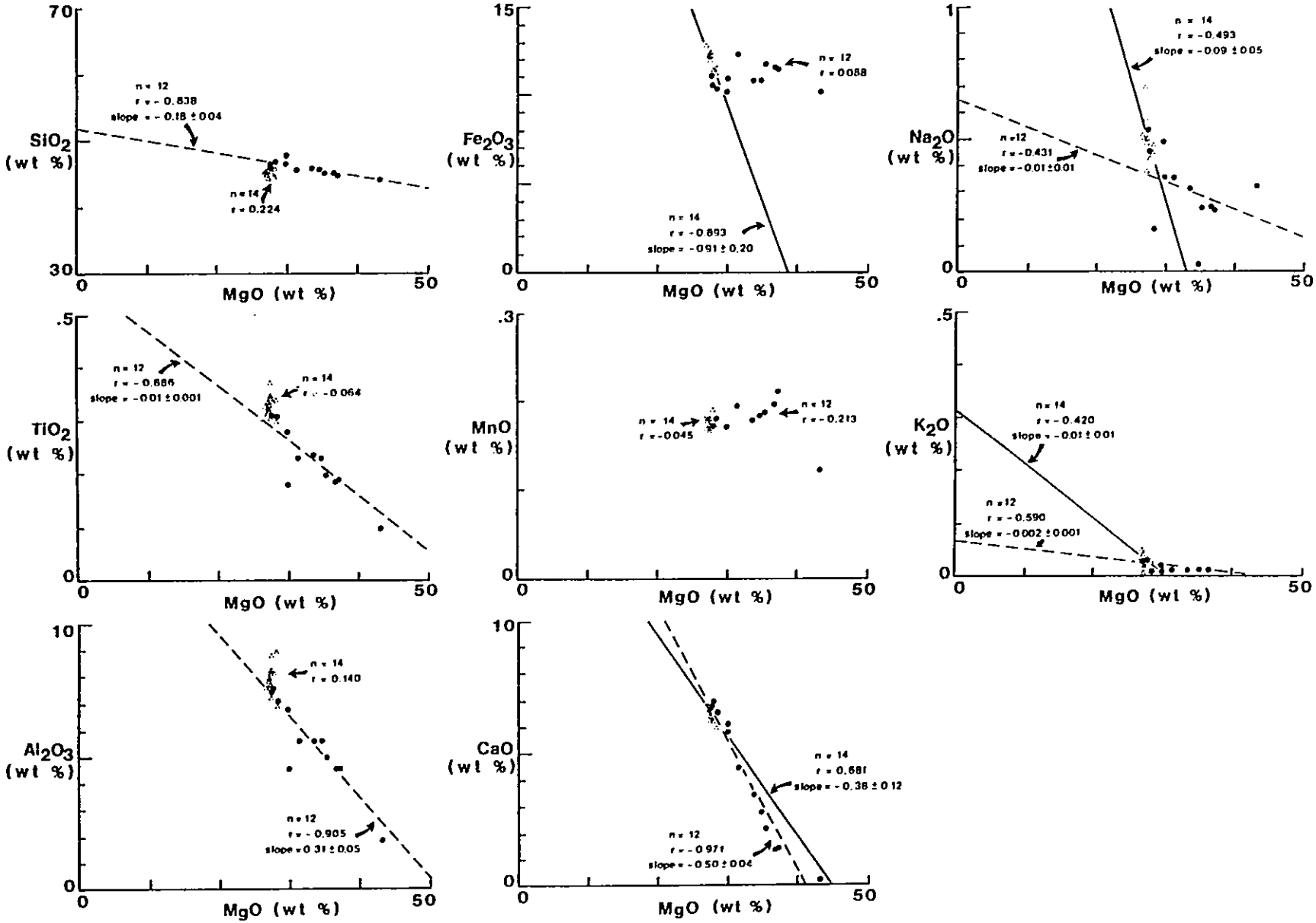
70
30
SiO2 (wt %)
n = 12
r = - 0.838
slope = - 0.18 ± 0.04
n = 14
r = 0.224
0
50
MgO (wt %)
15
0
Fe2O3 (wt %)
n = 12
r = 0.088
n = 14
r = - 0.893
slope = - 0.91 ± 0.20
0
50
MgO (wt %)
1
0
Na2O (wt %)
n = 14
r = - 0.493
slope = - 0.09 ± 0.05
n = 12
r = - 0.431
slope = - 0.01 ± 0.01
0
50
MgO (wt %)
.5
0
TiO2 (wt %)
n = 12
r = - 0.886
slope = - 0.01 ± 0.001
n = 14
r = - 0.064
0
50
MgO (wt %)
.3
0
MnO (wt %)
n = 14
r = - 0.045
n = 12
r = - 0.213
0
50
MgO (wt %)
.5
0
K2O (wt %)
n = 14
r = - 0.420
slope = - 0.01 ± 0.01
n = 12
r = - 0.590
slope = - 0.002 ± 0.001
0
50
MgO (wt %)
10
0
Al2O3 (wt %)
n = 14
r = 0.140
n = 12
r = - 0.905
slope = 0.31 ± 0.05
0
50
MgO (wt %)
10
0
CaO (wt %)
n = 14
r = 0.681
slope = - 0.38 ± 0.12
n = 12
r = - 0.971
slope = - 0.50 ± 0.04
0
50
MgO (wt %)

Figure 44. Variation diagrams of MgO (wt%) versus trace elements (ppm) of Area 4 komatiites.

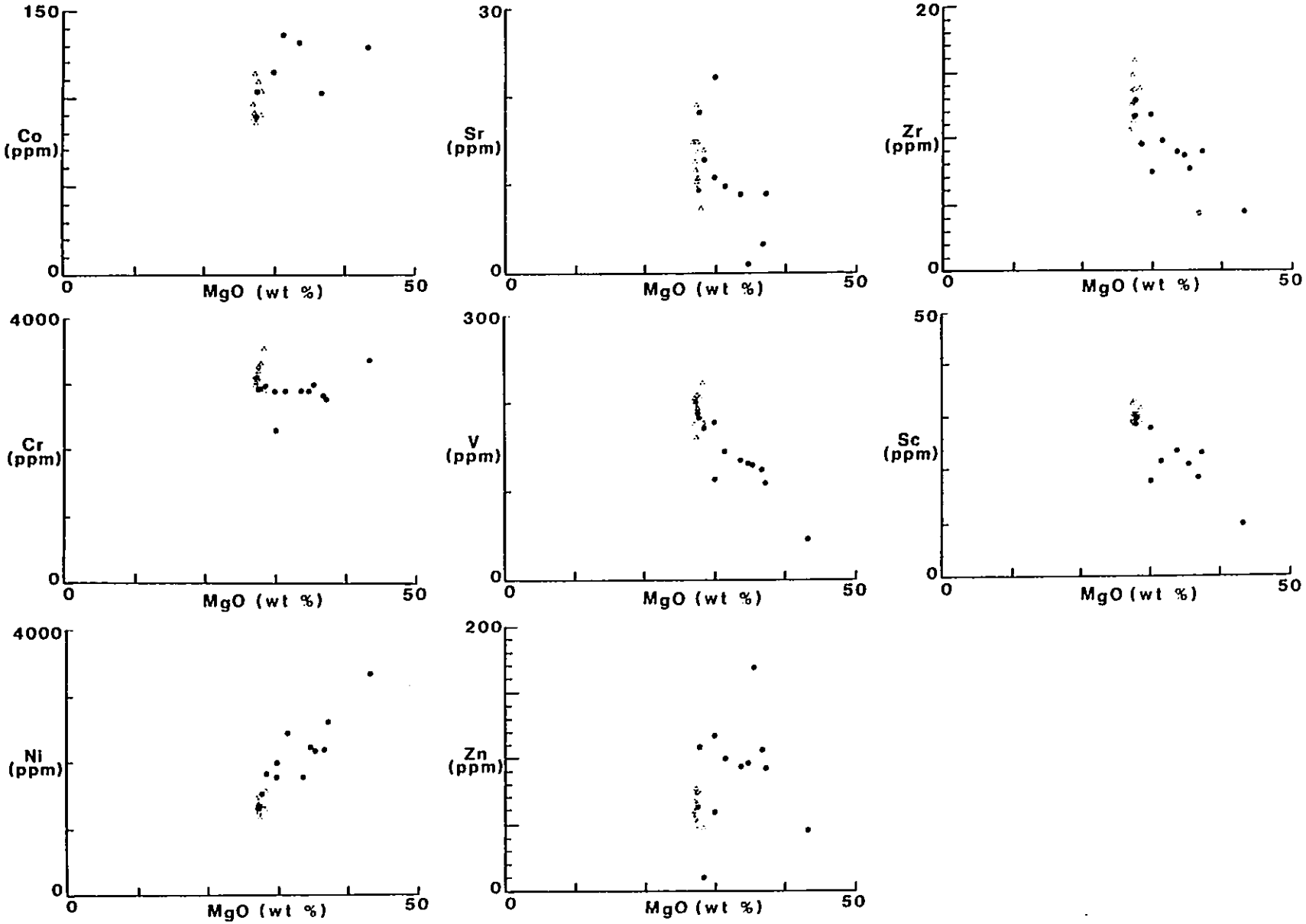
150
Co
(ppm)
0
0
MgO (wt %)
50
30
Sr
(ppm)
0
0
MgO (wt %)
50
20
Zr
(ppm)
0
0
MgO (wt %)
50
4000
Cr
(ppm)
0
0
MgO (wt %)
50
300
V
(ppm)
0
0
MgO (wt %)
50
50
Sc
(ppm)
0
0
MgO (wt %)
50
4000
Ni
(ppm)
0
0
MgO (wt %)
50
200
Zn
(ppm)
0
0
MgO (wt %)
50

Figure 45. Oxide (wt%) versus MgO (wt%) variation diagrams of komatiites from the Esker Lake and No-name Lake belts. The solid line is a regression line through the data points.

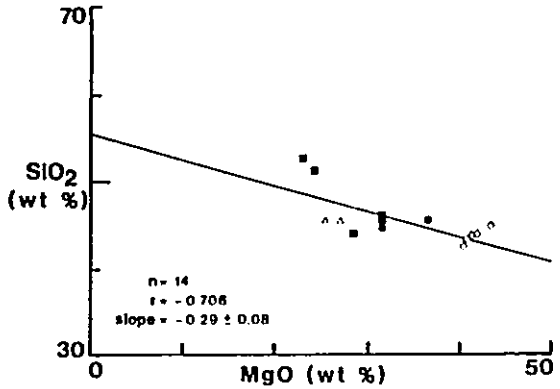
70
30
SiO_2 (wt %)
n = 14
r = -0.706
slope = -0.29 ± 0.08
0
MgO (wt %)
50

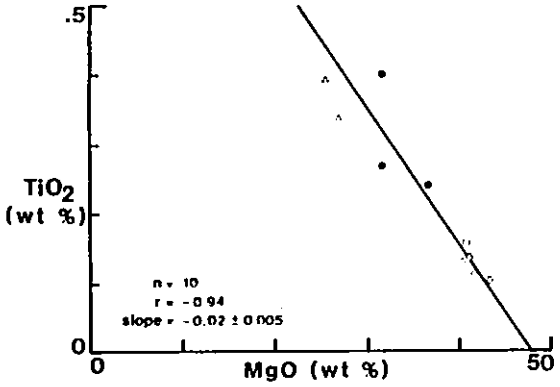
.5
0
TiO_2 (wt %)
n = 10
r = -0.94
slope = -0.02 ± 0.005
0
MgO (wt %)
50

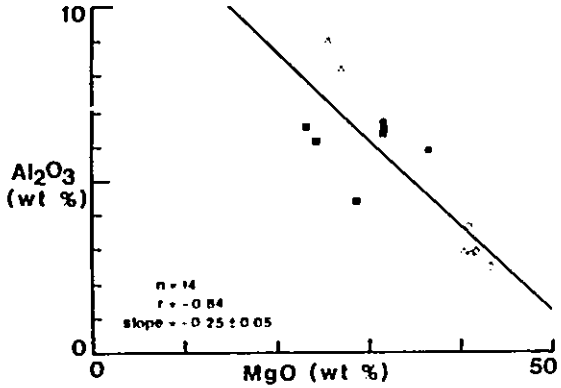
10
0
Al_2O_3 (wt %)
n = 14
r = -0.84
slope = -0.25 ± 0.05
0
MgO (wt %)
50

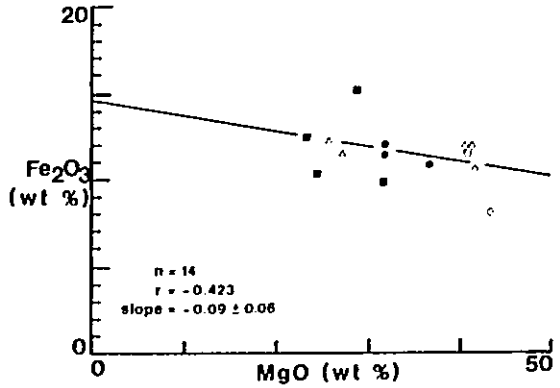
20
0
Fe_2O_3 (wt %)
n = 14
r = -0.423
slope = -0.09 ± 0.06
0
MgO (wt %)
50

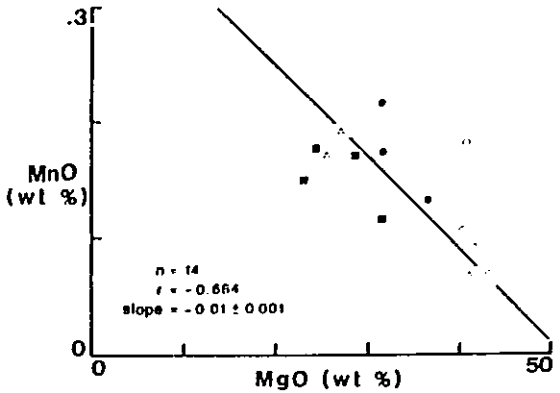
.3
0
MnO (wt %)
n = 14
r = -0.664
slope = -0.01 ± 0.001
0
MgO (wt %)
50

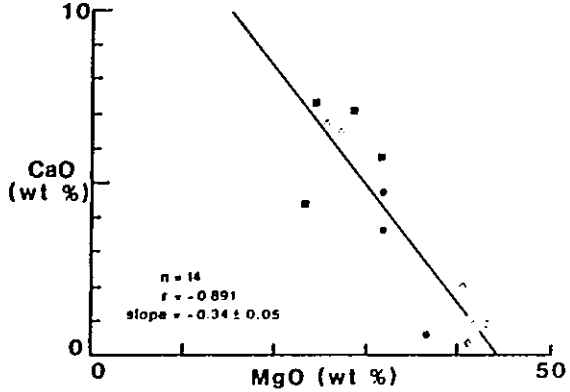
10
0
CaO (wt %)
n = 14
r = -0.891
slope = -0.34 ± 0.05
0
MgO (wt %)
50

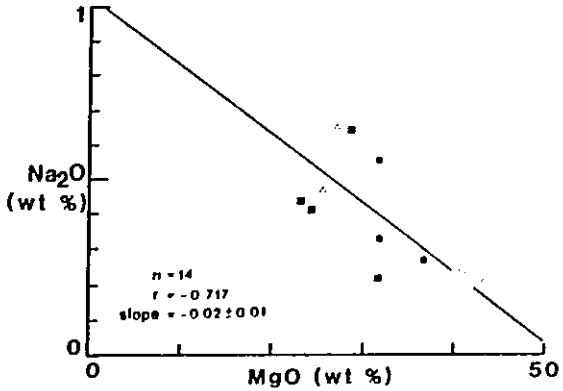
1
0
Na_2O (wt %)
n = 14
r = -0.717
slope = -0.02 ± 0.01
0
MgO (wt %)
50

Figure 46. Variation diagrams of MgO (wt%) versus trace elements (ppm) of komatiites in Esker Lake and in No-name Lake belts.

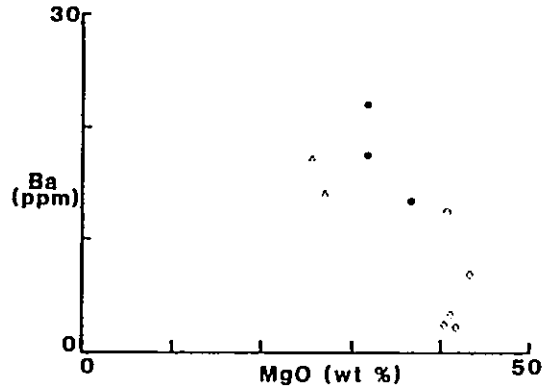
30
Ba
(ppm)
0
0
MgO (wt %)
50

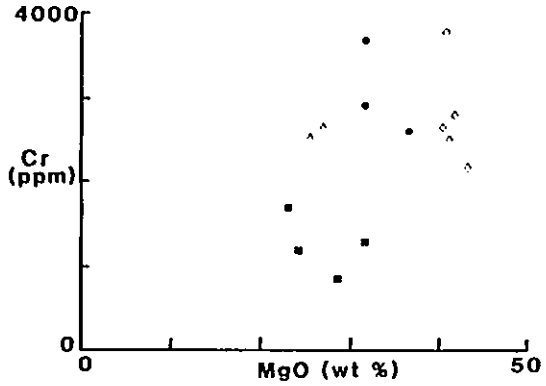
4000
Cr
(ppm)
0
0
MgO (wt %)
50

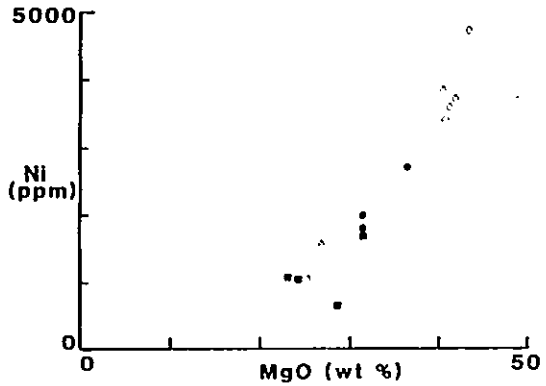
5000
Ni
(ppm)
0
0
MgO (wt %)
50

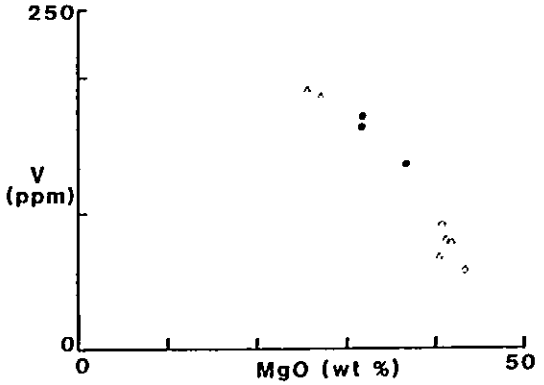
250
V
(ppm)
0
0
MgO (wt %)
50

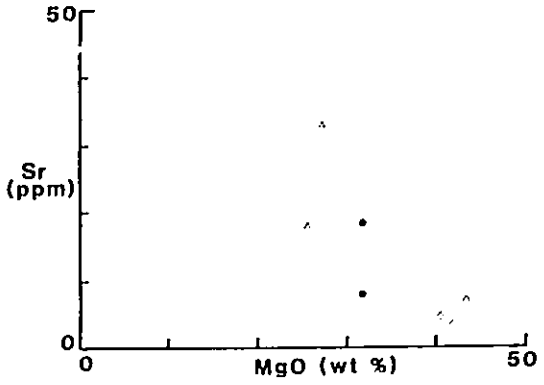
50
Sr
(ppm)
0
0
MgO (wt %)
50

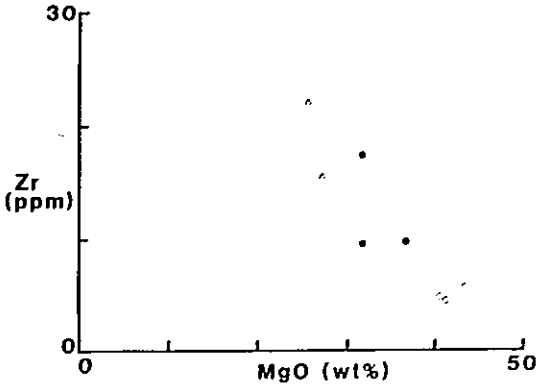
30
Zr
(ppm)
0
0
MgO (wt%)
50

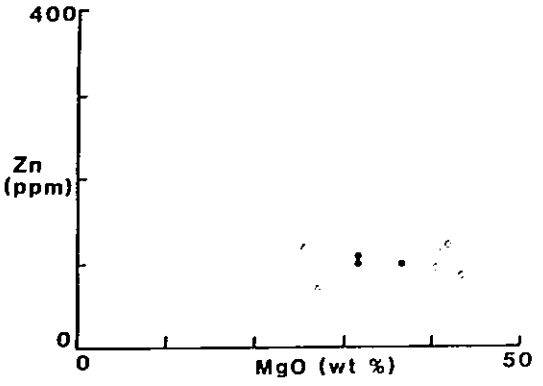
400
Zn
(ppm)
0
0
MgO (wt %)
50

crystallized, then CaO, Na_2O, Al_2O_3, and TiO_2 should intercept the MgO axis at the same point. A positive covariance is well established between MgO and Ni and less so in the case of Co. This follows from the dominance of olivine separation for the major part of the fractionation trend (Fig. 29b) since MgO, Ni, and Co, are compatible in the olivine structure. V and Sc exhibit a similar but negative coherent correlation with MgO, hence behaving like incompatible elements during olivine fractionation. It should be noted here that all the oxides and elements incompatible with olivine, except CaO and Na_2O , show an inflection point between the cumulate and spinifex-textured zone samples when plotted against MgO. This is attributed to a primary phenomenon, not alteration, probably combined olivine and clinopyroxene fractionation in the formation of spinifex-textured flows (Section 4.7). Zr also shows a negative correlation with MgO. Trace elements such as Sr, Rb, and Ba exhibit much scatter when plotted versus MgO but show an overall negative correlation trend that is consistent with their incompatible nature. The plots with CaO and Na_2O do not show an inflection point because of the preferential loss of CaO and Na_2O in the B zone.

Cr values show a pattern that is not characteristic of olivine-only fractionation when plotted versus MgO. The cumulate zone samples exhibit a trend that does not lie on an olivine control line, and the spinifex textured zone samples lie on a trend that cuts the olivine control line. These trends must be the result of a Cr-rich phase extracting Cr from the melt.

Chromite and clinopyroxene are the two possibilities on the basis of chemical considerations and petrographic observations. Geochemical data from other studies (Cattell and Arndt, 1987) show that equal proportions of olivine and clinopyroxene fractionation (highly unlikely based on major elements) or 98:2 proportions of olivine and chromite fractionation can explain the spinifex-textured trend. The above mentioned inflection point and petrographic observations indicate that olivine, clinopyroxene, and chromite were the major crystallizing phases involved in the formation of the spinifex-textured zones of the Woodburn Lake Group komatiites. A rough approximation of proportions would be 70:28:2 of olivine, clinopyroxene, and chromite, respectively.

Therefore, the Cr-MgO trend of the spinifex-textured flows suggest that only olivine plus minor chromite were the liquidus phases for at least part of the early period of fractionation. As the liquid evolved, olivine was joined by clinopyroxene and increasing proportions of chromite on the liquidus. Cattell and Arndt (1987) have demonstrated that there is a definite relationship between whole rock Cr content and chromite morphology in spinifex-textured zone samples. On this basis they suggest that the dendritic chromite forms in a manner similar to olivine spinifex blades. Petrographic observations of the Woodburn Lake Group komatiites indicate a similar relationship between chromite morphology and the Cr contents of the rock. Also, there appears to be a relationship between whole-rock chemistry and clinopyroxene morphology which indicates that

clinopyroxene may have evolved similarly.

The REE distributions of the Woodburn Lake Group komatiites are not uniform. Two patterns can be distinguished: a) one with variably enriched light REE and undepleted heavy REE, and 2) the other with weakly to moderately depleted light REE and undepleted to weakly depleted heavy REE (See Figs. 28a to 28f for chondrite-normalized REE profiles of representative samples). The variable light REE enrichment - flat heavy REE pattern is caused by alteration processes, probably selective light REE enrichment by sea-water or a change in oxidation state during progressive metamorphism. Evidence for the latter situation is suggested by the change in FeO/Fe_2O_3 ratios during serpentinization, as mentioned above. This is also supported by the increase in La/Yb ratios with increasing H_2O and CO_2 contents (Fig. 36b). The second pattern is thought to be characteristic of the parent magma and its source.

Some of the more important element ratios are listed in Appendices B1.a - B1.f. V/Sc, Al/Sc, Ti/Sc, Ti/V, Al_2O_3/TiO_2, CaO/TiO_2, and CaO/Al_2O_3 ratios of the komatiites are close to chondritic, except for cumulate zone samples where CaO has been mobile. Al/Zr and Sc/Zr ratios of the komatiites (except cumulate samples) are higher than chondritic values. The small deviations from chondritic values for ratios involving TiO_2 (Ti) are thought to be analytical error, although they may reflect minor depletion of TiO_2 in the source. These ratios indicate that the source of the komatiites had chondritic values of Al2O3, CaO, V, and Sc.

Since the rocks are depleted in Zr and light REE relative to chondrite, and possibly to a lesser degree TiO_2, they are indicative of a source depleted in these elements, assuming that the source was chondritic in nature.

The normative mineralogy of the Woodburn Lake Group ultramafic and mafic volcanics is shown in Appendices B1.a - B1.f. The majority of the rocks are olivine normative. The normative mineralogy of the komatiites suggests the presence of modal plagioclase but only minor quantities are present in the spinifex-textured zones. This is explained by the normative plagioclase component being tied up within the glass, as indicated by probe analyses of glass elsewhere (Arndt et al.,1977 and Arndt, 1986, among others). The normative plagioclase component can also partly be explained by the Ca-Tschermak molecule in clinopyroxene. The variable ratio of normative plagioclase and pyroxene in the komatiites suggests, indirectly, a change in the ratio of glass to pyroxene across flow units, as mentioned by Barnes (1985). Petrographic observations of the Woodburn Lake Group komatiites support this. Normative corundum values are found within the cumulate zone samples and this can be explained by the loss of CaO and/or Na_2O.

The Woodburn Lake Group komatiitic-tholeiitic (high-Mg) basalts range from 15% to 5% MgO (see Appendix B1.f and Fig. 47). Their major element compositions are similar in some respects to those of low-K tholeiites, but they have variable SiO_2 contents, ranging from 44% to 54%. In most instances, they also exhibit

Figure 47. Oxide (wt%) versus MgO (wt%) variation diagrams of the Woodburn Lake Group high-Mg basalts. The solid line is a regression line through the data points.

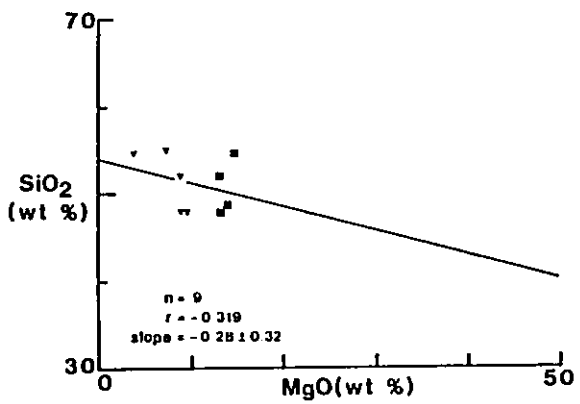
70
30
SiO_2 (wt %)
n = 9
r = -0.319
slope = -0.28 ± 0.32
0
MgO(wt %)
50

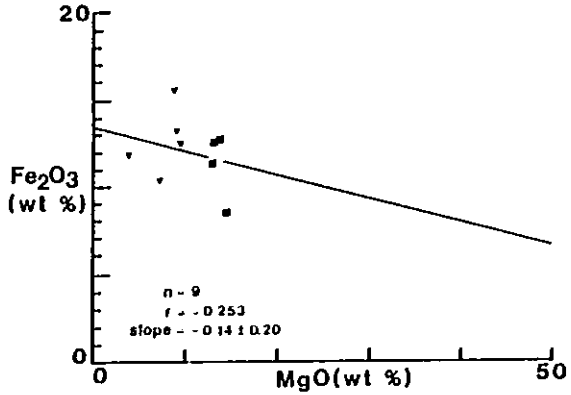
20
0
Fe_2O_3 (wt %)
n = 9
r = -0.253
slope = -0.14 ± 0.20
0
MgO(wt %)
50

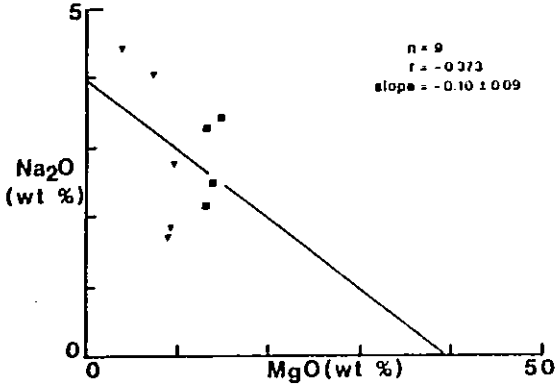
5
0
Na_2O (wt %)
n = 9
r = -0.373
slope = -0.10 ± 0.09
0
MgO(wt %)
50

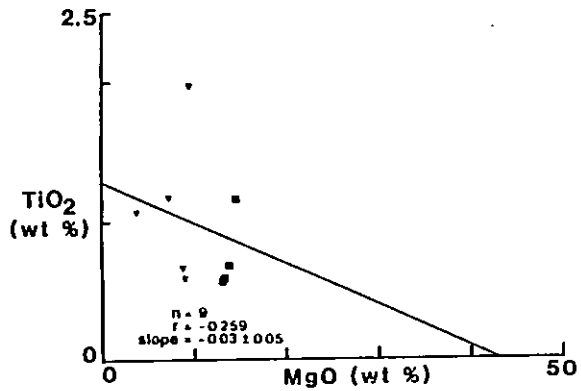
2.5
0
TiO_2 (wt %)
n = 9
r = -0.259
slope = -0.03 ± 0.05
0
MgO (wt %)
50

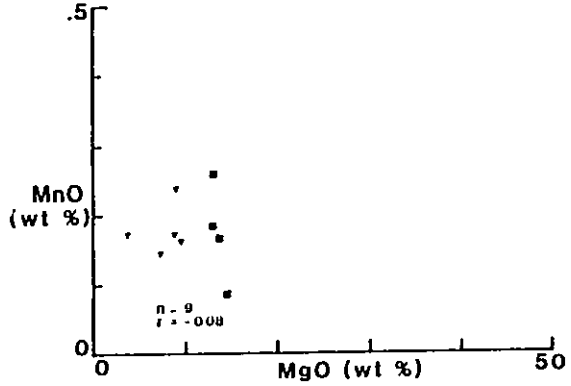
.5
0
MnO (wt %)
n = 9
r = -0.08
0
MgO (wt %)
50

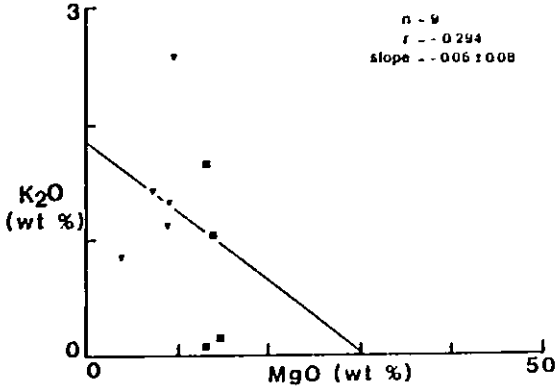
3
0
K_2O (wt %)
n = 9
r = -0.294
slope = -0.05 ± 0.08
0
MgO (wt %)
50

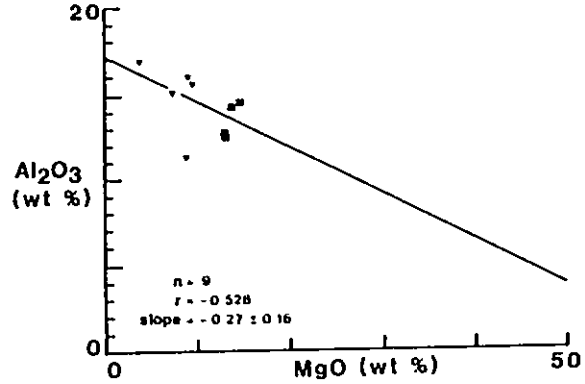
20
0
Al_2O_3 (wt %)
n = 9
r = -0.528
slope = -0.27 ± 0.16
0
MgO (wt %)
50

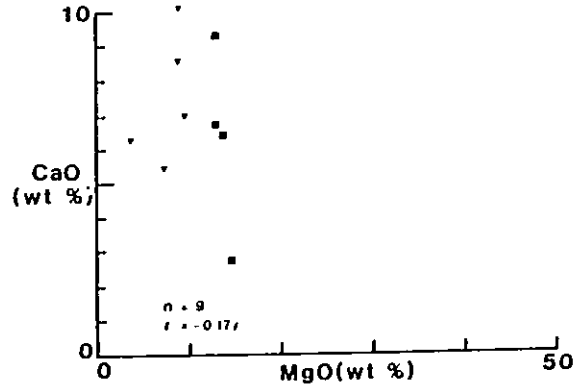
10
0
CaO (wt %)
n = 9
r = -0.17
0
MgO(wt %)
50

lower TiO_2 and higher FeO contents at similar MgO values when compared to low-K tholeiites. The trace element concentrations (see Appendix B1 and Fig. 48) of these rocks clearly distinguish them from komatiites and typical Archean tholeiites (see Basaltic Volcanism Study Project, 1981). In particular, the LREE are weakly to strongly enriched when compared to the komatiites (see Figs. 28a-28h). Most of the highly incompatible elements (eg. LREE, Zr) are markedly enriched relative to more compatible elements (eg. Ni). They appear to be transitional between komatiites and Archean tholeiites, as shown on the Jensen Cation Plot (Fig. 31). They are also distinctly different from the basalts of the Ketyet River Group, as shown in some chemical discrimination diagrams (Figs. 31, 32, and 49). The Ketyet River Group basalts are more Fe-rich and Ti-rich than the Woodburn Lake Group high-Mg basalts. This is suggestive of different magmatic processes and/or different source regions. Most of the Woodburn Lake Group komatiitic-tholeiitic basalts are olivine-normative tholeiites (see Appendix B1.f). Their normative mineralogy suggests the modal presence of olivine, clinopyroxene, orthopyroxene (?), chromite, and plagioclase. Possibly these minerals have played an important role in the fractionation history of these rocks (i.e. derived from komatiitic parents). will be tested in the petrogenetic modelling of Chapter 6.

4.7 COMPARISON WITH OTHER ARCHEAN KOMATIITIC SUITES

Figure 48. Variation diagrams of MgO (wt%) versus trace elements (ppm) of the Woodburn Lake Group high-Mg basalts.

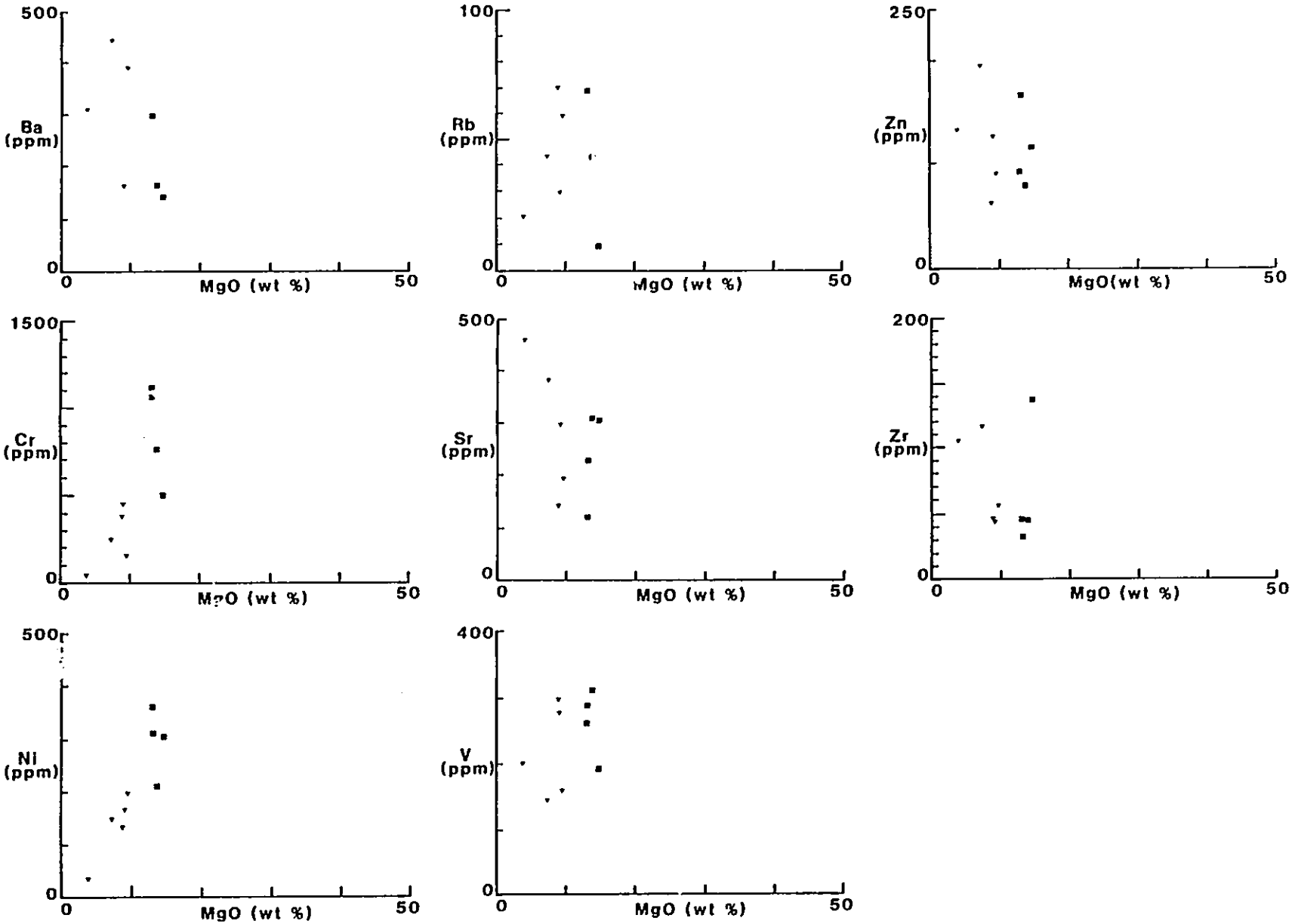
500
Ba (ppm)
0
0
MgO (wt %)
50
100
Rb (ppm)
0
0
MgO (wt %)
50
250
Zn (ppm)
0
0
MgO(wt %)
50
1500
Cr (ppm)
0
0
MgO (wt %)
50
500
Sr (ppm)
0
0
MgO (wt %)
50
200
Zr (ppm)
0
0
MgO (wt %)
50
500
Ni (ppm)
0
0
MgO (wt %)
50
400
V (ppm)
0
0
MgO (wt %)
50

Figure 49. A comparison of the Woodburn Lake Group komatiitic and tholeiitic basalts (F) and the Ketyet River Group basalts (H) using chemical classification diagrams for common volcanic rocks (color index (CI) versus normative anorthite content (AN) from Irvine and Baragar, 1971; $Na_2O + K_2O$ (Alk) versus SiO_2 from Cox et al., 1979).

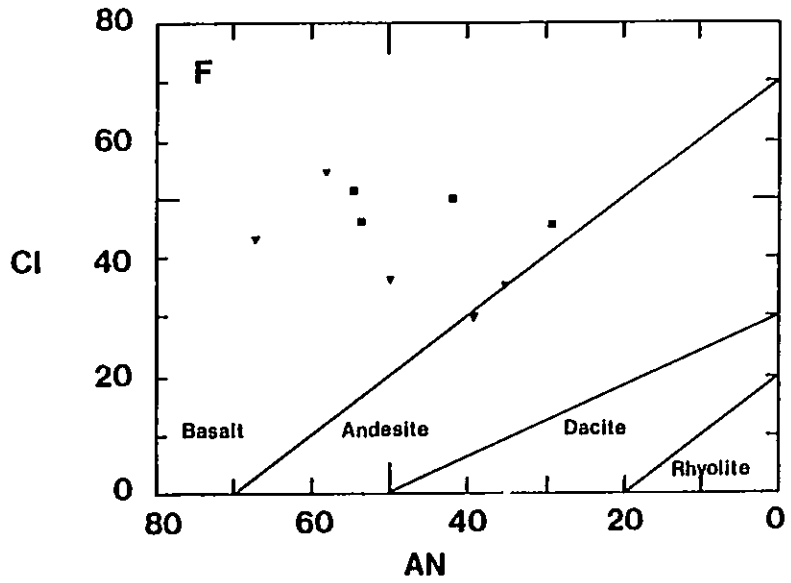
F
Cl
AN
Basalt
Andesite
Dacite
Rhyolite
80
60
40
20
0

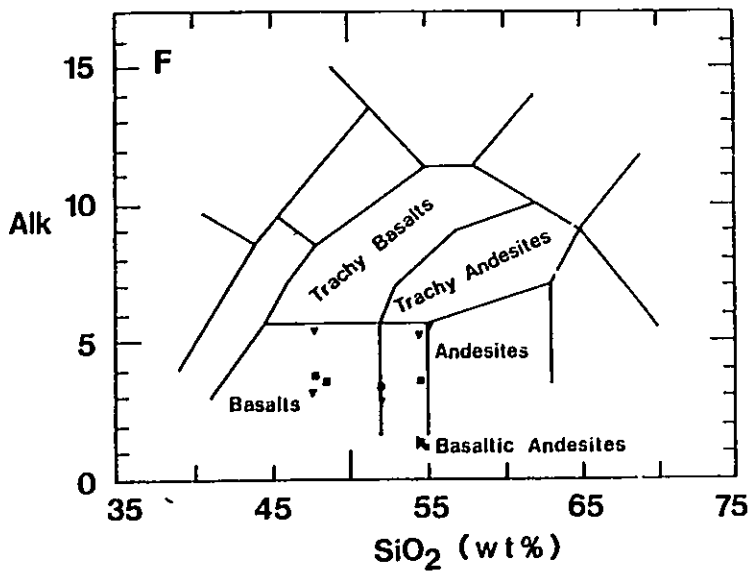
F
Alk
SiO2 (wt%)
Trachy Basalts
Trachy Andesites
Andesites
Basalts
Basaltic Andesites
15
10
5
0
35
45
55
65
75

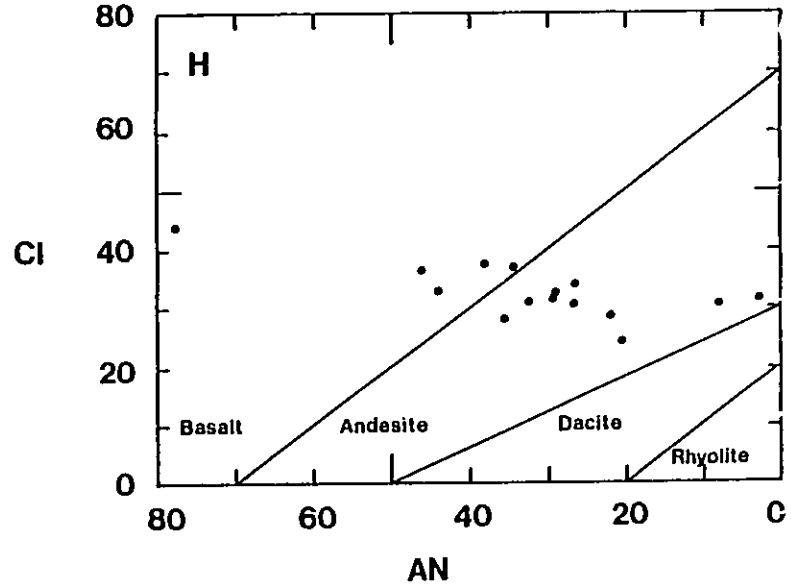
H
Cl
AN
Basalt
Andesite
Dacite
Rhyolite
80
60
40
20
0

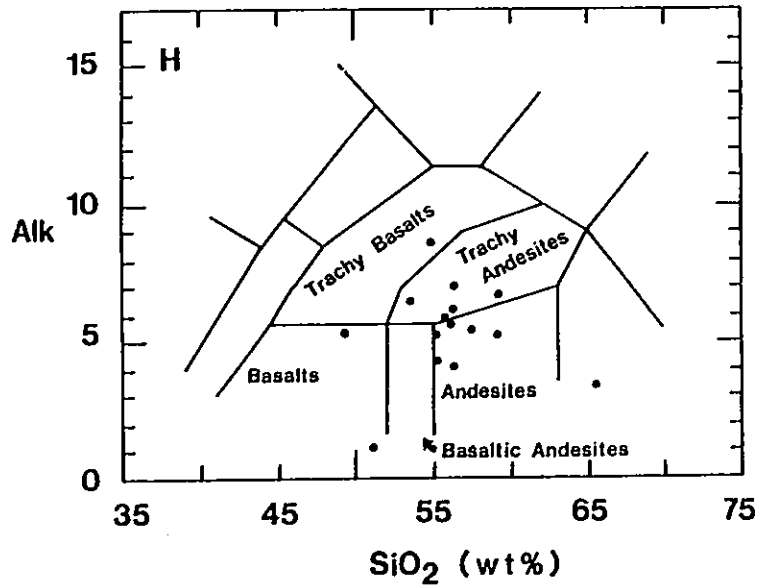
H
Alk
SiO2 (wt%)
Trachy Basalts
Trachy Andesites
Basalts
Andesites
Basaltic Andesites
15
10
5
0
35
45
55
65
75

The geochemical characteristics of the Woodburn Lake Group komatiites and associated basalts are shown in Tables 8, 9, and 10 along with similar rocks from some other Archean suites and modern-day tectonic environments. The Woodburn Lake Group komatiites exhibit similar chemical compositions to other Late Archean komatiites, especially to those of the Abitibi Greenstone Belt. Table 10 shows that the Woodburn Lake Group komatiites have close to chondritic ratios of most elements but these ratios indicate that moderately to highly incompatible elements such as LREE , Zr, and possibly Ti have been depleted relative to chondrite (e.g. Al/Zr ratios are generally greater than chondrite (i.e. 1825); Appendices B1.a to B1.e). The Woodburn Lake Group komatiites that do not show LREE mobility are typically LREE depleted as observed in most other Archean suites. The Woodburn Lake Group komatiites are aluminum-undepleted since most of the samples exhibit CaO/Al_2O_3 ratios close to unity (Nesbitt et al., 1979). Nesbitt et al. (1979) proposed that there are two types of komatiites: 1) aluminum-undepleted with CaO/Al_2O_3 ratios close to 1.0 and with chondritic values for ratios of the high field strength elements (i.e. ratios involving Ti, Al, Sc, V, Y, and Lu) and 2) aluminum-depleted with CaO/Al_2O_3 ratios greater than 1.0 and Al_2O_3/TiO_2, Sc/Zr, and Ti/Zr ratios being less than chondritic. Some of the other ratios also support the aluminum-undepleted nature of the Woodburn Lake Group komatiites. The ratios also indicate that the Woodburn Lake Group komatiites have been depleted in Zr and light REE, and possibly TiO_2 to a

Table 8 - Comparison of some chemical data of komatiites from different komatiitic suites

Group or Locality	WLG	WLG	WLG	WLG	PAG	PAG	PAG	PAG	Munro	Munro	Munro	Munro
Sample #	K-43b	K-44g	R-242b	R-242a	74-72	74-73	74-74	74-75	SA-2039	SA-2048	P9-119	P9-118
SiO2	40.70	43.80	41.54	42.77	39.80	43.90	41.46	43.77	41.20	44.20	40.80	41.40
TiO2	0.25	0.33	0.25	0.37	0.22	0.26	0.16	0.31	0.17	0.26	0.14	0.33
Al2O3	5.10	7.40	6.21	8.44	4.61	7.00	4.02	7.40	4.84	7.12	3.70	6.40
Fe2O3*	2.50	3.40	4.15	2.81	4.10	4.20	9.55	8.85	10.10	11.30	8.20	12.40
FeO*	6.90	6.00	5.84	7.89	5.70	5.00	-	-	-	-	-	-
MnO	0.14	0.16	0.16	0.16	0.16	0.15	0.20	0.18	0.20	0.20	0.15	0.24
MgO	32.00	24.80	29.34	23.83	32.40	26.20	32.34	26.60	32.10	25.10	35.10	25.60
CaO	2.04	6.54	4.34	6.30	2.71	7.15	3.55	6.87	4.04	7.39	3.28	5.90
Na2O	bl	0.10	0.51	0.44	0.10	0.10	0.04	0.13	0.20	0.00	0.07	0.06
K2O	0.04	0.05	0.10	0.01	0.14	0.14	0.01	0.02	0.02	0.06	0.10	0.07
P2O5	0.01	0.02	bl	bl	0.04	0.04	bl	bl	-	-	-	-
CO2	0.00	0.20	-	-	0.50	bl	-	-	-	-	-	-
H2O(LOI)	9.00	5.60	(7.57)	(5.70)	9.30	6.10	(10.00)	(5.90)	6.90	3.10	9.30	7.40
Total	99.48	98.40	100.01	98.00	99.00	100.30	101.33	100.11	99.85	99.53	100.04	99.00
Ba	11	12	16	16	8	5	19	19	-	-	-	-
Cr	2707	2682	2672	2357	2400	2700	2220	2700	-	-	1762	3000
Ni	2120	1395	1839	986	1900	1200	1020	1200	-	-	2290	1470
Rb	bl	bl	bl	bl	5	6	1	1	-	-	3	3
Sr	4	7	17	17	10	10	2	13	-	-	6	3
V	110	166	160	100	63	84	-	-	-	-	-	-
Y	-	7	6	10	-	-	2	4	-	-	-	-
Zn	89	51	101	114	60	40	-	-	-	-	54	101
Zr	7	11	9	21	45	32	9	14	-	-	-	-
Sc	20	27	-	-	-	-	-	-	-	-	-	-
CaO/Al2O3	0.40	0.88	0.70	0.80	0.59	1.01	0.88	0.93	0.83	1.04	0.89	0.86
CaO/TiO2	8.2	19.8	17.4	19.0	12.3	27.5	22.2	22.2	23.8	28.4	23.4	17.9
Al2O3/TiO2	20.4	22.7	24.8	22.8	21.0	27.2	25.1	23.9	28.5	27.4	26.4	19.4

Single values of Fe2O3* or FeO* = Total Fe expressed as Fe2O3 or FeO, respectively

WLG (K-43b, K-44g, R-242b, R-242a) - this study of the Woodburn Lake Group komatiitic suite
PAG (74-72, 74-73, 74-74, 74-75) - Prince Albert Group komatiites, Frisch (1982)
Munro (SA-2039, SA-2048, P9-119, P9-118) - Munro Township komatiites, Arndt et al. (1977)

Note: Every pair of two samples in this table represents a cumulate zone (high MgO) and a spinifex-textured zone, (low MgO) respectively, from individual komatiite flows at the different localities

Table 9 - Comparison of chemical data of the Woodburn Lake Group komatiitic basalts with other basalts of ancient and modern volcanic suites

Group or Locality	WLG	WLG	WLG	PAG	PAG	Munro-T	Kambalda	Kambalda	Gorgona-I	Troodos
Sample #	AK-20	AK-31	R-233	256	AVG (n=11)	C126	22	21	AVG (n=4)	AM-26b
SiO2	50.97	50.71	46.22	52.70	49.60	51.02	49.74	52.30	44.20	53.05
TiO2	0.65	0.56	0.57	0.45	0.94	0.61	0.65	0.55	0.66	0.54
Al2O3	11.05	12.43	12.03	8.60	14.40	12.20	14.33	12.42	12.00	14.51
Fe2O3*	15.18	11.05	12.15	0.50	-	11.60	-	11.24	3.20	8.36
FeO*	-	-	-	8.70	11.70	-	10.52	-	8.20	-
MnO	0.17	0.18	0.25	0.21	0.21	0.19	0.18	0.18	0.18	0.17
MgO	8.74	12.72	12.73	14.10	8.20	12.20	12.85	9.77	15.90	10.05
CaO	8.30	6.55	9.04	8.50	10.30	8.50	9.77	10.39	10.10	10.70
Na2O	1.66	3.20	2.00	1.20	2.40	3.39	1.82	1.46	1.13	1.74
K2O	1.10	0.00	1.60	0.33	0.30	0.09	0.06	0.46	0.02	0.15
P2O5	bl	bl	bl	0.36	0.00	0.07	0.06	0.06	0.06	0.06
CO2	-	-	-	0.30	-	-	0.00	-	-	-
H2O(LOI)	-	-	(2.45)	4.10	(1.00)	(2.55)	(2.51)	(1.60)	4.00	0.73
Total	97.90	97.40	99.12	100.35	99.13	100.00*	100.00*	100.55	99.65	100.06
Ba	-	-	286	450	94	102	20	-	bl	15
Cr	370	1093	1033	550	297	1089	1057	872	1250	540
Ni	130	353	301	250	162	285	335	163	710	149
Rb	60	bl	66	bl	14	2	1	12	bl	4
Sr	140	117	221	30	94	73	84	220	50	71
V	209	255	270	170	-	237	224	197	256	133
Y	12	9	14	-	21	17	20	10	14	12
Zn	60	91	161	60	-	-	-	74	57	62
Zr	45	45	31	-	59	30	59	63	30	32
Sc	27	-	-	-	-	30	34	33	31	-

Single values of Fe2O3* or FeO* = Total Fe expressed as Fe2O3 or FeO, respectively

WLG (AK-20, AK-31, R-233) - komatiitic basalts, Woodburn Lake Group - this study
PAG (256) - komatiitic basalt, Prince Albert Group - M. Schau (G.S.C., unpublished data)
PAG (AVG) - average basalt, Prince Albert Group - Frisch (1982)
Munro-T (C126) - komatiitic basalt - Arndt and Nesbitt (1984)
Kambalda (22) - komatiitic basalt - Arndt and Jenner (1986)
Kambalda (21) - siliceous high magnesian series basalt - Redman and Keays (1985)
Gorgona-I (AVG) - komatiitic basalt - Gansser et al. (1979)
Troodos (AM-266) - boninite - Flower and Levine (1987)
Bl = below detection limit; - = not determined

Table 9 (continued)

Group or Locality	Cape Vogel	Cape Vogel	New Zealand	Huronian	Aleutian
Sample #	46.2	6	AVG (n=6)	AVG (n=14)	AVG (n=21)
SiO2	55.62	58.34	52.26	52.20	49.39
TiO2	0.48	0.42	0.18	0.85	0.65
Al2O3	9.95	11.42	12.84	14.10	14.80
Fe2O3*	2.17	-	2.96	13.20	-
FeO*	6.74	9.46	6.11	-	8.86
MnO	0.18	0.18	0.17	0.23	0.17
MgO	11.78	12.02	10.97	5.54	11.82
CaO	5.38	6.66	10.43	7.17	10.80
Na2O	1.28	1.07	1.43	2.89	2.17
K2O	0.46	0.38	0.12	0.55	0.72
P2O5	0.09	0.04	0.09	0.09	0.16
CO2	-	-	-	-	-
H2O(LOI)	5.39	-	-	-	-
Total	99.52	100.00*	97.56	96.82	99.54
Ba	-	34	63	205	197
Cr	910	735	1133	182	946
Ni	227	212	224	94	409
Rb	-	9	5	41	7
Sr	-	96	39	206	448
V	-	211	-	155	230
Y	-	9	8	27	13
Zn	-	-	-	84	-
Zr	84	62	9	81	46
Sc	-	36	-	-	36

Single values of Fe2O3* or FeO* = Total Fe expressed as Fe2O3 or FeO, respectively

Cape Vogel (46.2) - boninite - Walker and Cameron (1983)
Cape Vogel (6) - high-Mg andesite - Jenner (1981)
New Zealand (AVG) - boninite - Wood (1980)
Huronian (AVG) - tholeiitic basalt, Thessalon Formation - Jolly (1987), Table 2
Aleutian (AVG) - high-Mg basalts, Aleutian Arc - Myers (1988), Table 4, analysis 7

Table 10 - Comparison of inter-element ratios from different komatiitic suites

	Ti/Zr	Ti/Y	Ti/Sc	Ti/V	Zr/Sc	Zr/Y	Al2O3/TiO2	CaO/Al2O3	(La/Yb)N
Chondrite	110	275	78	10	0.7	2.5	20	0.82	1.0
Churchill Province									
WLG - komatiites	120-180	240-280	60-72	9-12	0.3-0.7	1.5-2.2	23-25	0.5-1.2	0.5-1.5
WLG - kom.basalts	50-212	230-325	144*	12-50	0.6*	2.1-8.0	8-27	0.2-0.8	0.8-7.0
PAG - komatiites	110-150	200-300	60-95	10-14	0.5-0.9	1.5-2.1	12-33	0.2-1.3	0.5-1.5
PAG - basalts	(96)	(269)	-	-	-	(2.8)	(15)	(0.5)	-
Abitibi Greenstone Belt									
Pyke Hill - komatiites	(120)	(210)	(74)	(14)	0.65-0.8	(1.7)	(23)	0.7-1.25	0.35-0.5
Fred's Flow	(122)	(245)	(98)	(16)	(0.80)	(1.9)	(20)	-	-
Cycle I - basalts	(115)	(134)	(97)	(16)	(0.84)	(2.1)	(20)	-	-
Cycle II - basalts	(87)	(216)	(130)	(19)	(1.49)	(2.5)	(17)	-	-
Lamotte - komatiites	110-160	214-230	98-105	-	0.7-0.9	-	17-19	0.8-1.3	0.30-0.6
Destor - kom. basalts	83-106	202-230	115-130	-	0.8-1.3	-	15-19	0.5-2.0	0.7-3.1
Western Australia									
Yilgarn - komatiites	(110)	(275)	-	-	-	(2.5)	(20)	(1.0)	0.6-1.0
Mt.White - kom. basalt	(100)	(240)	-	-	-	(2.4)	(19)	0.6-0.9	1.0-3.4
Zimbabwe									
Belingwe - komatiites	124-129	270-330	-	14-15	-	2.1-2.7	20-21	1.0-1.1	-

WLG = Woodburn Lake Group
PAG = Prince Albert Group

( ) = average values
* = ratio based on one sample

Data sources for PAG are Frisch (1982), Schau (1982), and this study
Data sources for Abitibi Greenstone Belt and Western Australia are given in Ludden and Gelinas (1982) and Arndt and Nesbitt (1982)
Data source for Zimbabwe is Nisbet et al. (1987)

lesser degree; hence similar to those from Munro Township (Barnes, 1985).

The Woodburn Lake Group komatiitic to tholeiitic basalts have geochemical characteristics that set them apart from many Archean tholeiitic basalt sequences. Their MgO contents (5-15%) are higher and their moderately to highly incompatible elements are enriched relative to more compatible elements (e.g. Ti/Sc, Zr/Y). Tables 9 and 10 show that they are similar to the type B Hanging Wall basalts of Kambalda (Arndt and Jenner, 1986) and the komatiitic basalts from Destor Township (Ludden and Gelinas, 1982). The Woodburn Lake Group komatiitic basalts also show some similarities to modern day boninites (Table 9 - Cape Vogel) which suggests a possible arc-related origin (See Section 6.4).

Schau (1982), on the basis of lithological and structural similarities, suggested that the Woodburn Lake and Prince Albert Groups are correlative. A comparison of some representative chemical data and various inter-element ratios (summarized in Table 10 and shown in Figures 30-32) of the different rock types from within the two groups shows that the two groups are extremely similar. These chemical data support the lithological, structural, and geochronological similarities outlined by Schau (1982) and Ashton (1985). The Ketyet River Group is also thought to be correlative on the basis of field characteristics (Schau, 1982), but the only chemistry available for comparison is that of some basalts (Appendix B6 from Taylor, 1985) which appear to be unique (i.e. high Fe - tholeiites) to the region. Some ultramafic

rocks, including a layered sill, from the Aberdeen Lake region exhibit komatiitic affinities (Appendix B4) with rare spinifex textures. They are most likely an extension of the Woodburn Lake Group (A.N. LeCheminant, pers. comm., 1984).

4.8 CHEMICAL VARIATIONS WITHIN AND BETWEEN INDIVIDUAL KOMATIITIC FLOWS

Since the komatiitic flow units within the Pipedream Lake belt are extremely well preserved, detailed sampling was conducted at five localities. Cross sections showing flow type and morphology, and chemical variations across flow units are presented in Figures 50 and 51. The chemistry of the individual samples has already been presented in Appendix B1. The chemical profiles reveal fairly consistent trends within each of the flow types. These profiles differ between one another in a manner consistent with the previously described flow morphology and petrography of the different flow types (Chapter 3).

The chemical profiles of spinifex-textured flows reveal the following: a) patterns in each flow that are virtually identical to one another, which suggests minimal redistribution of elements during alteration,

b) a sharp contact between the spinifex-textured zone and the cumulate zone, with elements incompatible with olivine (e.g. Al_2O_3, TiO_2) being enriched in the spinifex-textured zone and elements compatible

Figure 50. Variation of MgO, NiO, Cr_2O_3, TiO_2, CaO, H_2O, and CaO/Al_2O_3 (anhydrous values except for H_2O) through some layered komatiitic flows of Area 1. Scale bar is representative of both vertical and horizontal distance in the diagrammatic section through the komatiitic flows. Horizontal lines mark the boundaries of flow units. Tops is up as indicated by the asymmetry within the flow units. The stippled pattern represents the cumulate zone, whereas the variable "herringbone" pattern represents the spinifex-textured zone.

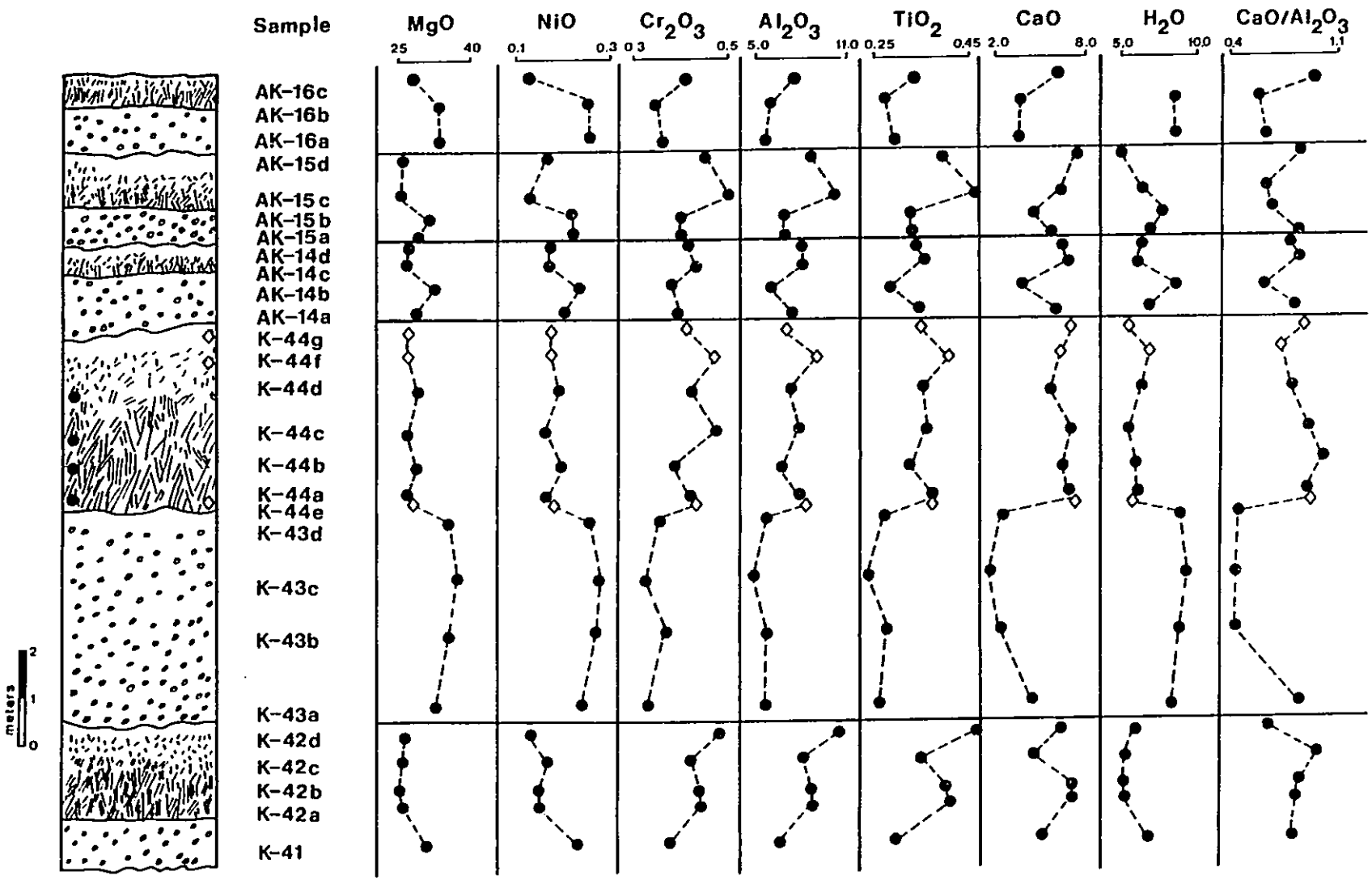
Sample
MgO
25
40
NiO
0.1
0.3
Cr_2O_3
0.3
0.5
Al_2O_3
5.0
11.0
TiO_2
0.25
0.45
CaO
2.0
8.0
H_2O
5.0
10.0
CaO/Al_2O_3
0.4
1.1
AK-16c
AK-16b
AK-16a
AK-15d
AK-15c
AK-15b
AK-15a
AK-14d
AK-14c
AK-14b
AK-14a
K-44g
K-44f
K-44d
K-44c
K-44b
K-44a
K-44e
K-43d
K-43c
K-43b
K-43a
K-42d
K-42c
K-42b
K-42a
K-41
meters
2
1
0

Figure 51. Variation of MgO, NiO, Cr_2O_3, Al_2O_3, TiO_2, CaO, H_2O, and CaO/Al_2O_3 (anhydrous values except for H_2) through some layered and massive komatiitic flows of the Area 2. Scale bar represents vertical distance through flow units. Horizontal lines mark the boundaries of flow units. Note that the average thickness of these flow units is less than those shown in Figure 50. Tops is up in the figure as indicated by the asymmetry of the flow units. The polygonal-shaped pattern represents either polyhedral jointed massive flows or cumulate zones (K-34). The variable "herringbone" pattern represents the spinifex-textured zone.

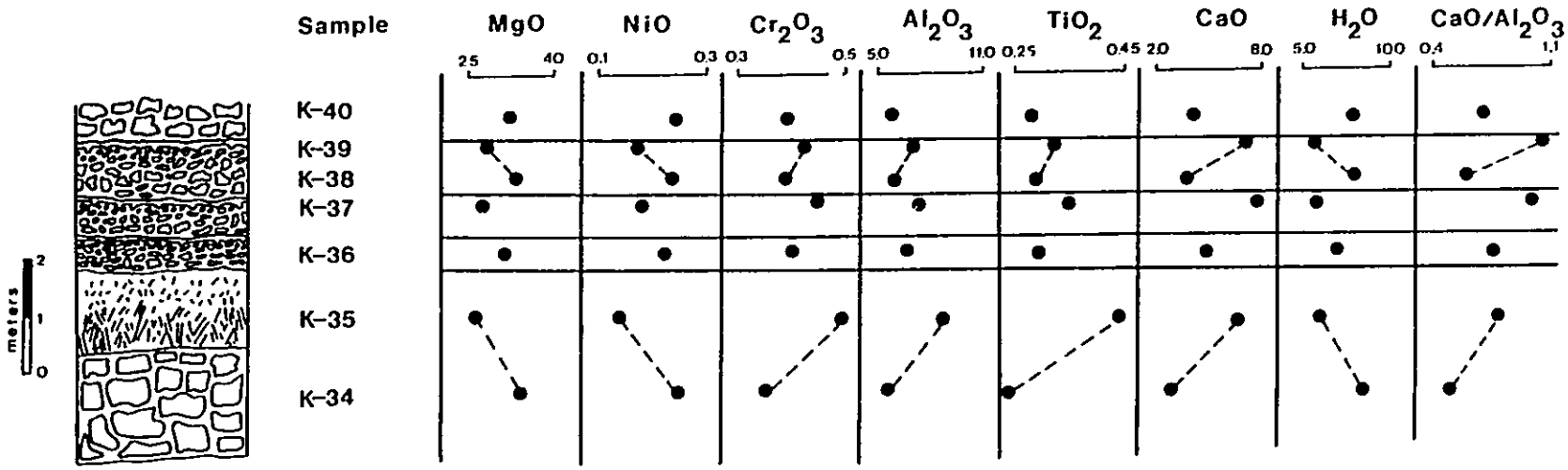
Sample
MgO
NiO
Cr_2O_3
Al_2O_3
TiO_2
CaO
H_2O
CaO/Al_2O_3
25
40
0.1
0.3
0.3
0.5
5.0
11.0
0.25
0.45
2.0
8.0
5.0
10.0
0.4
1.1
K-40
K-39
K-38
K-37
K-36
K-35
K-34
meters
2
1
0

with olivine (e.g. MgO, Ni, Co) being enriched in the cumulate zone,

c) a progressive change across the cumulate zone with the interior portion having enriched contents of elements compatible with olivine,

d) some similarities of bulk composition between the upper margin and the lower margin of the flow,

e) a zig-zag pattern in the spinifex-textured zone, which is probably indicative of the evolving fractionated liquid compositions generated during post-eruptive flow differentiation in an open system. However, magma pulses, onsurface crustal contamination, and/or analytical error could also explain all or part of the zig-zag pattern,

f) convincing evidence that olivine has accumulated in the lower part relative to the upper part of the flow.

The chemical contrast between the spinifex-textured zones and cumulate zones is in general not as great in flows with thin spinifex-textured zones or in thin flows. An interpretation of the within- and between-flow variations follows in Chapter 6.2.2

The chemical profiles across massive flows, although based on fewer samples, differ from those of spinifex-textured flows and are suggestive of different crystallization (i.e. physiochemical) conditions. Their profiles show a progressive increase of

elements compatible with the olivine structure (eg. MgO, Ni) from the flow margins to the flow interior. The highest content of compatible elements and lowest content of incompatible elements occurs at approximately 2/5 of the flow thickness from the base.

4.9 GEOCHEMICAL RESULTS OF THE WOODBURN LAKE GROUP CALC-ALKALINE SUITE, AND A COMPARISON TO OTHER SUITES

The chemical data from 13 representative samples (Appendix B5) show that the calc-alkaline volcanic suite ranges from basaltic andesite to rhyolite. The rocks have been divided on the basis of volatile-free SiO_2 contents into basaltic andesites (52-56 wt%), andesites (56-62 wt%), dacites (62-70 wt%), and rhyolites (70-80 wt%). All of the samples fall into the calc-alkaline field of the AFM plot (Fig. 29) and the Jensen Cation Plot (Fig. 31). In the Jensen Cation Plot, the two andesite samples fall into the basalt field, hence the classification of these rocks as basaltic andesite. On these diagrams the rhyolites merge into the dacites and the dacites into the andesites. The chemical data of representative samples (i.e. proportional to the estimated areal extent mapped in the field) suggest that the rhyolites and dacites are the most abundant rocks of this volcanic suite, in agreement with the field mapping.

Rhyolites, dacites, and andesites of the Woodburn Lake Group are quite similar in major and trace elements (Tables 11a, 11b,

and 11c) to those from the Prince Albert Group (Frisch, 1982), the Marda Complex (Hallberg et al., 1976), averages of the Superior Province (Goodwin, 1977), and the Michipicoten Greenstone Belt (Sylvester et al., 1987). Such compositional comparisons are necessary in order to interpret the origin and tectonic environment of the Woodburn Lake Group volcanic suite. Using such an approach, Frisch (1982) and Sylvester et al. (1987) suggested that possible modern tectonic analogues are continental-margin arc and island- and continental-arc for the Woodburn Lake Group and Michipicoten Greenstone Belt, respectively. Using a modified version of Table 2 of Sylvester et al. (1987), it can be argued that the rhyolites of the Woodburn Lake Group and Prince Albert Group are most similar to those of subduction-related continental intra-arc regions (Table 11d). Sylvester et al. (1987) came to a similar conclusion for the rhyolite ash flow tuffs of the Michipicoten Greenstone Belt. This is at odds with Fryer and Jenner's (1978) suggestion that the Prince Albert Group rhyolites were generated by partial melting of intra-continental sialic crust.

Table 11a - Comparison of some chemical data of rhyolites from different volcanic suites

Sample #	AK-9	AK-2	1	2	3	4	5	6 (n=11)	7 (n=7)	8 (n=143)
SiO2	75.83	70.99	73.40	74.40	73.70	77.40	71.70	73.20	72.00	73.04
TiO2	0.01	0.31	0.29	0.30	0.30	0.05	0.11	0.50	0.76	0.31
Al2O3	13.85	15.85	13.60	12.90	13.60	12.90	12.00	12.00	13.70	14.24
Fe2O3*	1.02	1.90	-	0.90	0.90	0.20	0.70	4.04	3.60	1.44
FeO*	-	-	2.60	-	-	0.30	0.90	-	-	0.54
MnO	0.02	0.03	0.04	0.10	0.06	0.26	0.05	0.03	0.04	0.07
MgO	0.15	1.02	1.33	0.30	0.70	0.26	2.41	0.37	0.42	0.47
CaO	0.52	0.69	1.96	0.50	0.94	0.13	2.44	0.71	1.60	1.36
Na2O	3.33	6.40	3.10	4.00	3.92	3.50	1.90	2.21	2.14	3.76
K2O	3.97	1.62	2.30	3.90	2.31	2.43	2.67	5.67	3.06	4.70
P2O5	bl	0.09	0.09	0.04	0.13	0.02	0.03	0.17	0.15	0.08
H2O(LOI)	-	-	(1.00)	0.80	1.07	1.10	2.00	-	-	-
Total	98.70	98.10	99.79	98.04	97.71	98.55	96.91	98.90	97.56	100.01
Ba	1100	-	460	1216	470	970	410	2634	473	957
Co	-	-	-	-	-	1	1	-	-	3
Cr	10	12	7	10	9	1	2	5	7	3
Ni	17	41	9	7	10	bl	bl	5	5	3
Rb	115	30	64	116	-	45	99	175	130	100
Sr	121	250	79	131	107	100	140	117	177	249
V	bl	34	22	8	55	-	-	45	45	20
Y	-	-	45	30	-	-	-	30	30	29
Zn	22	23	14	-	0	-	-	55	52	-
Zr	50	111	264	291	210	50	220	229	215	217
Sc	1	-	-	-	-	2	2	-	-	-
Al2O3+CaO/ (FeO*+Alkalis)	1.75	1.62	1.93	1.55	2.06	2.03	2.37	1.10	1.00	1.50

Single values of Fe2O3* or FeO* = Total Fe expressed as Fe2O3 or FeO, respectively

AK-9 - high silica (>75%) rhyolite - Woodburn Lake Group, this study
AK-2 - low silica (70-75%) rhyolite - Woodburn Lake Group, this study
1 - average metarhyolite, Prince Albert Group - Frisch (1982), Table 14
2 - average rhyolite, Marda Complex, Western Australia - Hallberg et al. (1976), Table 2, analyses 17-33
3 - average rhyolite, Superior Province - Goodwin (1977), Table IV
4,5 - high- and low-silica rhyolites, respectively, Michipicoten greenstone belt - Sylvestor et al. (1987), Table 1, analyses 5 and 4, respectively
6 - average low-silica, high-LILE, low-LREE rhyolites, Huronian Supergroup, Thessalon Formation - Jolly (1987), Table 2
7 - average low-silica, low-LILE, high-LREE rhyolite, Huronian Supergroup, Thessalon Formation - Jolly (1987), Table 2
8 - average orogenic rhyolite, western U.S.A. - Ewart (1979), p. 44

Table 11a (continued)

Sample #	9 (n=83)	10 (n=4)	11 (n=2)	12 (n=6)	13	14	15 (n=36)
SiO2	74.92	72.53	75.23	72.78	78.86	74.81	69.97
TiO2	0.25	0.21	0.22	0.23	0.11	0.13	0.73
Al2O3	13.47	13.66	13.34	13.88	12.02	14.56	12.32
Fe2O3*	1.01	1.11	1.51	1.58	0.76	1.22	3.91
FeO*	0.89	0.84	0.15	0.47	-	-	1.18
MnO	0.06	0.07	0.03	0.04	0.04	0.04	0.09
MgO	0.32	0.23	0.21	0.28	0.16	0.38	0.86
CaO	1.57	1.26	0.64	0.87	0.45	0.91	1.98
Na2O	3.18	4.45	3.34	3.48	4.57	2.48	2.68
K2O	3.27	4.48	5.30	5.64	3.13	6.08	4.47
P2O5	0.05	0.03	0.04	0.04	0.04	0.05	0.21
H2O(LOI)	-	-	-	-	(0.51)	(2.01)	(1.45)
Total	98.99	98.87	100.01	99.29	100.65	102.59	99.85
Ba	849	800	770	1052	791	1010	686
Co	2	20	2	3	-	-	-
Cr	1	69	5	2	4	4	6
Ni	2	8	bl	2	4	4	6
Rb	111	124	174	187	-	127	201
Sr	113	59	88	89	-	102	100
V	9	14	9	14	8	3	-
Y	24	47	43	39	21	27	75
Zn	-	48	29	45	13	24	-
Zr	159	225	291	262	94	115	317
Sc	-	4	-	1	1	1	-
Al2O3+CaO/ (FeO*+Alkalis)	1.82	1.39	1.38	1.35	1.49	1.61	1.21

Single values of Fe2O3* or FeO* = Total Fe expressed as Fe2O3 or FeO, respectively

9 - average rhyolite, Taupo Volcanic Zone, New Zealand - Ewart (1979), p. 44
10 - average rhyolite, Casma Group, the Peruvian Andes - Pitcher et al. (1985), Appendix 3
11 - average high-silica rhyolite, Calipuy Group, the Peruvian Andes, Pitcher et al. (1985), Appendix 2, samples V173, and V183b
12 - average low-silica rhyolite, Calipuy Group, the Peruvian Andes, Pitcher et al. (1985), Appendix 2, samples V11, V12, V175, V177, V180, V182
13 - high-silica rhyolite, Old Red Sandstone Formation, Scotland - Thirlwall (1983), Table 2, sample OC128
14 - low-silica rhyolite, Old Red Sandstone Formation, Scotland - Thirlwall (1983), Appendix 2, sample OC111
15 - low-silica rhyolite, Palmas type, Parana Plateau, Brazil - Bellieni et al. (1986), Table 2

Table 11b - Comparison of some chemical data of dacites from different volcanic suites

Sample #	AK-5a	AK-6c	1	2	3	4	5	6 (n=133)	7 (n=24)	8 (n=6)	9 (n=5)
SiO2	63.65	62.25	67.30	63.20	66.70	62.70	61.10	66.21	65.57	66.55	65.51
TiO2	0.45	0.45	0.58	0.70	0.52	0.59	0.64	0.63	0.60	0.40	0.52
Al2O3	14.63	14.81	14.90	14.40	14.90	14.90	17.20	16.34	14.15	15.37	15.77
Fe2O3*	4.83	6.26	-	1.60	-	1.30	2.00	2.93	1.63	3.13	1.50
FeO*	-	-	4.90	4.70	4.30	3.00	3.30	1.05	6.03	1.21	2.73
MnO	0.11	0.20	0.09	0.10	0.10	0.07	0.07	0.09	0.16	0.07	0.10
MgO	2.30	1.85	2.40	2.80	1.85	4.50	2.75	1.17	1.92	2.53	1.75
CaO	3.76	4.96	3.15	4.30	3.02	1.98	3.49	3.14	5.85	4.85	3.55
Na2O	2.57	5.00	2.90	3.70	4.16	5.20	5.70	4.11	3.02	3.52	3.63
K2O	3.64	0.65	2.24	2.20	1.52	1.05	1.93	4.11	0.91	2.27	2.55
P2O5	0.12	0.10	0.18	0.20	0.17	0.25	0.18	0.23	0.16	0.10	0.15
H2O(LOI)	-	-	(1.40)	1.80	1.57	1.70	1.40	-	-	1.71	-
Total	95.26	96.61	100.04	99.70	98.81	97.25	99.76	100.00*	100.00*	100.00*	97.76
Ba	-	-	667	792	315	980	590	1587	167	450	585
Co	26	31	-	-	-	11	14	8	14	-	14
Cr	101	40	56	59	44	16	14	16	16	56	83
Ni	62	75	34	53	23	-	-	16	6	43	362
Rb	135	18	80	60	-	24	50	113	13	63	93
Sr	233	429	107	256	198	90	480	537	251	315	294
V	94	78	64	91	102	-	-	63	96	80	77
Y	-	-	-	24	-	-	-	31	26	17	29
Zn	55	81	52	65	72	-	-	68	106	-	76
Zr	97	107	191	217	217	160	200	247	53	143	179
Sc	14	10	-	-	-	8	11	-	-	13	11

Single values of Fe2O3* or FeO* = Total Fe expressed as Fe2O3 or FeO, respectively
100.00* = recalculated to 100% volatile-free

AK-5a, AK-6c - dacites, Woodburn Lake Group calc-alkaline suite - this study
1 - average metadacite, Prince Albert Group - Frisch (1982), Table 11
2 - average dacite, Morda Complex, Western Australia - Hallberg et al. (1976), Table 11, analyses 8-16
3 - average dacite, Superior Province, Goodwin (1977), Table IV
4, 5 - dacites, Michipicoten greenstone belt - Sylvester et al. (1987), Table 1, analyses 3 and 7
6 - average orogenic dacite, western U.S.A. - Ewart (1979), p. 34
7 - average dacite, Tonga-Kermadec Islands, Taupo Volcanic Zone - Ewart (1979), p.34
8 - dacite, Tauhara, Taupo Volcanic Zone - Reid and Cole (1983), Table III, analysis 5
9 - average dacite, Casma Group, the Peruvian Andes - Pitcher et al. (1985), Appendix 3

Table 11c - Comparison of some chemical data of andesites from different volcanic suites

Sample #	AK-6a	K006A	1	2	3	4	5	6	7	8
SiO2	58.32	56.00	58.10	58.70	55.99	56.10	59.99	58.45	58.70	57.05
TiO2	1.08	0.66	0.84	0.81	0.91	0.75	1.23	1.14	1.02	1.17
Al2O3	16.10	15.80	15.20	14.90	15.60	14.40	16.18	16.50	16.47	15.18
Fe2O3*	9.41	1.70	1.90	1.90	2.01	10.80	6.82	6.53	2.91	3.62
FeO*	-	5.90	6.70	5.70	5.90	-	-	-	4.01	4.05
MnO	0.15	0.16	0.16	0.11	0.16	0.16	0.06	0.09	0.13	0.11
MgO	2.61	5.69	4.80	4.80	4.87	5.15	2.83	4.22	2.64	3.60
CaO	4.40	6.74	6.10	6.60	5.88	5.70	5.16	5.81	6.21	5.85
Na2O	2.86	3.40	3.20	3.50	3.67	4.47	4.13	4.17	3.49	3.95
K2O	2.99	1.03	1.62	1.20	1.11	0.26	2.44	2.20	2.14	2.03
P2O5	0.08	0.14	0.19	0.24	0.21	0.09	0.39	0.27	0.23	0.27
H2O(LOI)	-	2.20	1.40	1.90	2.54	1.18	(0.79	(0.96	-	-
Total	98.10	99.42	100.11	99.56	98.85	99.14	100.02	100.34	97.95	96.88
Ba	600	-	350	744	358	215	844	620	559	453
Co	12	-	-	-	-	-	-	-	19	29
Cr	20	205	34	116	111	307	113	96	25	69
Ni	30	-	40	76	61	68	83	46	bl	22
Rb	140	54	46	36	-	44	-	-	69	62
Sr	509	480	132	378	242	449	-	-	324	173
V	76	-	185	133	232	143	144	113	169	181
Y	-	-	-	-	-	29	20	25	32	35
Zn	129	-	80	57	80	84	73	65	88	93
Zr	110	92	130	196	145	134	231	220	193	191
Sc	13	-	-	-	-	-	18	18	-	-

Single values of Fe2O3* or FeO* = Total Fe expressed as Fe2O3 or FeO, respectively

AK-6a - andesite, Woodburn Lake Group calc-alkaline suite - this study
K006a - andesite, Woodburn Lake Group calc-alkaline suite - Ashton (1988)
1 - average metaandesite, Prince Albert Group - Frisch (1982), Table 10
2 - average andesite, Marda Complex, Western Australia - Hallberg et al. (1976), Table 11, analyses 1-7
3 - average andesite, Superior Province - Goodwin (1977), Table IV
4 - andesite, Huronian Supergroup, Thessalon Formation - Jolly (1987), Table 1, sample 4282c (least iron-rich of 3 representative samples)
5 - andesite, Old Red Sandstone Formation - Thirlwall (1983), Table 2, sample OC131
6 - andesite, Old Red Sandstone Formation - Thirlwall (1983), Table 2, sample OC141
7 - andesite, Calipuy Group, the Peruvian Andes, Fortaleza traverse - Pitcher et al. (1985), Appendix 2, sample V170
8 - andesite, Calipuy Group, the Peruvian Andes, Fortaleza traverse - Pitcher et al. (1985), Appendix 2, sample V179

Table 11d - Comparison of some inter-element ratios of the Woodburn Lake Group rhyolite with other rhyolites of modern and ancient volcanic suites (with modification after Sylvester et al. (1987); references in Sylvester et al., except where noted)

Average compositions with standard deviations

A. Extension-related intracontinental rift- or hot-spot related volcanic suites

Locality	SiO2 range	Na2O + K2O		Al2O3 + CaO		FeO*		(Al2O3 + CaO)/ (Na2O + K2O + FeO*)	
SiO2 interval		70-75	>75	70-75	>75	70-75	>75		
Trans-Pecos volcanic Province, Texas (n=4)	69-75	9.29 (0.63)	-	13.22 (1.25)	-	3.89 (1.12)	-	0.76 - 1.25	
Rio Grande rift, Jemez Mountains, N. Mexico (n=9)	75-78	-	8.44 (0.41)	-	12.72 (0.49)	-	0.99 (0.25)	1.21 - 1.43	
Yellowstone Plateau volcanic field (n=5)	75-77	-	8.60 (0.17)	-	13.20 (0.41)	-	1.53 (0.25)	1.24 - 1.37	
Palmas lavas, Parana Plateau, Brazil (n=36) - Bellini et al., 1986	69-72	7.26 (0.25)		14.53 (0.32)		4.77 (0.52)		1.21 (avg)	
B. Subduction-related, continental intra-arc volcanic suites									
Oligocene sheets, San Juan volcanic field, Colorado(n=12)	69-75	8.82 (0.99)	-	16.84 (1.09)	-	1.95 (0.60)	-	1.34 - 2.05	
Taupo volcanic zone, New Zealand (n=6)	69-78	7.23 (0.06)	7.74 (0.23)	15.27 (0.53)	14.07 (0.19)	1.80 (0.45)	1.23 (0.13)	1.57 - 1.71	
Mid-Tertiary sequence, Sierra Madre Occidental, Mexico (n=6)	71-75	7.45 (0.27)	-	16.09 (0.76)	-	1.89 (0.26)	-	1.62 - 1.85	
Calipuy Group, the Peruvian Andes (n=6) - Pitcher et al., 1985	71-76	9.18 (0.35)	8.64 (0.70)	14.85 (0.21)	13.98 (0.18)	1.91 (0.20)	1.51 (0.05)	1.26-1.47	1.35-1.42
Casma Group, the Peruvian Andes (n=4) - Pitcher et al., 1985	71-74	9.03 (0.32)		15.09 (0.24)		1.86 (0.24)		1.27 - 1.56	
C. Archean greenstone belts									
Unit FV1, Michipicoten Greenstone Belt (n=11)	70-78	6.86 (0.92)	5.28 (1.09)	17.15 (0.46)	13.92 (0.64)	2.53 (0.60)	1.63 (0.34)	1.69-2.4	1.67-2.28
Unit FV3, Michipicoten Greenstone Belt (n=8)	70-78	6.44 (2.03)	6.12 (1.00)	17.15 (1.55)	14.32 (1.09)	3.35 (0.40)	0.93 (0.41)		
Woodburn Lake Group, - this study (n=6)	70-77	7.14 (1.48)	6.61 (0.65)	17.24 (1.66)	14.91 (0.20)	1.70 (0.07)	0.90 (0.22)	1.62-2.38	1.66-2.74

METAMORPHIC PETROLOGY

5.1 INTRODUCTION

The komatiites and associated high-Mg basalts of the SE Amer Lake map area are preserved as metamorphic assemblages ranging in grade from greenschist to amphibolite. The metavolcanics exhibit a wide range of bulk compositions and igneous textures, which will be shown to play an important role in controlling the metamorphic mineral assemblages that are present. The degree of metamorphism varies from one belt to another. The greenschist facies of regional metamorphism predominates within the Pipedream Lake belt, except in the contact aureoles of intruding granites where the grade is amphibolite facies. The contact metamorphic aureoles have not been mapped in detail, thus the thermal metamorphic zonation sequence put forth by Evans (1977) cannot be verified. The Esker Lake belt exhibits metamorphic assemblages representative of upper greenschist to amphibolite facies. Petrographic work by Fuller (1977) on the No-Name Lake belt metavolcanics indicates metamorphism under upper greenschist to middle amphibolite conditions. There appears to be an increase in regional metamorphic grade from south to north. This is consistent with Fraser's work (1988) to the east where metamorphic grade increases northwards from subgreenschist to granulite conditions.

This study concentrated on the metamorphic conditions of the

komatiites and associated high-Mg basalts found within the Pipedream Lake belt because of its superior state of preservation (i.e. more outcrop and larger areal extent). As mentioned before, regional and contact metamorphism, and possibly sea-water alteration, have destroyed the original mineralogy, but primary textures are well preserved in the Pipedream Lake belt and to a much lesser degree within the other belts.

5.2 MINERAL ASSEMBLAGES

The mineral assemblages and corresponding textures of the rocks of this study are for the most part typical of komatiites and related rocks seen elsewhere under similar conditions (Jolly, 1980 and 1982; Auvray et al., 1982; among others). The mineral assemblages found in this study are listed in Table 12 and their locations shown in Figure 52. The mineralogy of the Woodburn Lake Group komatiites is simple: 1) antigorite, tremolite and/or actinolite, chlorite, and Cr-magnetite in the greenschist zone, 2) antigorite, talc, tremolite and/or hornblende, chlorite, and Cr-magnetite in the lower amphibolite zone and 3) olivine, tremolite, chlorite, talc, minor anthophyllite, spinel and Cr-magnetite in the contact metamorphic zone. Olivine, anthophyllite, and spinel become members of the mineral assemblages in contact metamorphic zones. Olivine, orthopyroxene, clinopyroxene, cordierite and anthophyllite are found within the No-Name Lake belt but it is not known whether

Table 12 - Representative mineral assemblages of the Woodburn Lake Group komatiitic suite

	Ol	Tr/ Act	Act/ Hbl	Ath	Chl	Srp	Tlc	Sp	Mag	Cr-Mag	Cb	Pl	Ep	Qtz	Bt
Pipedream Lake belt															
Komatiites (greenschist facies)															
- spinifex-textured zone	-	+	-	-	+	+,tr	-	-	+	+	tr	tr	-	-	-
- cumulate zone	-	+	-	-	+	+	tr	-	+	-	tr	-	-	-	-
- massive flow unit	-	+	-	-	+	+	-	-	+	+	tr	-	-	-	-
- pillowed flow unit	-	+	-	-	+	+	-	-	+	+	tr	-	-	-	-
Komatiites (contact metamorphism)															
- spinifex-textured zone	+	+	-	-	+	-	tr	+	+	-	-	-	-	-	-
- cumulate zone	+	+	-	+	+	+,tr	tr	+	+	-	-	-	-	-	-
- massive flow unit	+	+	-	+	+	-	-	+	+	+	-	-	-	-	-
- pillowed flow unit	+	+	-	+	+	-	-	+	+	+	-	-	-	-	-
Komatiitic Basalts	-	-	+	-	+	-	-	-	+	+	-	+	+	tr	-
	-	-	+	-	+	-	-	-	tr	-	-	-	+	+	-
	-	-	+	-	+	-	-	-	+	+	tr	+	+	tr	-
Esker Lake belt															
Komatiites (greenschist/amph.)															
- spinifex-textured zone	-	+	-	-	+	tr,+	tr	-	+	+	tr	-	-	-	-
- cumulate zone	-	+	-	-	+	+	tr	-	+	+	tr	-	-	-	-
- undifferentiated	-	tr	-	-	+	+	+	-	+	+	tr,+	-	-	-	-
- contact metamorphosed	+	+	-	+	+	tr	-	+	+	-	tr	-	-	-	-
High-Mg Basalts (komatiitic to tholeiitic)															
- undifferentiated	-	+	-	-	+	-	-	-	+	+	+	+	+	tr	-
	-	tr	+	-	+	-	-	-	-	-	tr	+	+	+	tr
	-	-	+	-	+	-	-	-	-	-	-	+	+	+	-
	-	+	+	-	-	-	-	-	+	-	-	+	+	tr	-
No-Name Lake belt															
Komatiites - undifferentiated	+(*)	+	-	tr	+	+	tr	-	+	+	-	-	-	-	-
(from Fuller, 1978)	-	tr	-	-	+	-	+	-	-	-	tr	-	-	-	-
	-	-	+	+	+	tr	+	-	+	+	-	tr	-	-	-
	-	-	-	-	+	+	+	-	+	+	-	-	-	-	-
	-	+	-	-	+	+	-	-	+	+	+	tr	-	-	+
	-	+	+	-	-	-	-	-	+	+	tr	-	-	-	+
	-	-	-	-	+	-	+	-	+	-	tr	+	-	-	-
	-	+	+	tr	+	-	-	-	+	+	+	-	-	-	-

Note: (*) = olivine coexisting with 2 pyroxenes

+ = present, tr = trace amounts, and - = not present

Ol = olivine; Ath = anthophyllite; Tr/Act = tremolite/actinolite; Act/Hbl = actinolite/hornblende; Chl = chlorite; Srp = serpentine; Tlc = talc; Sp = spinel; Mag = magnetite; Cr-Mag = Cr-magnetite; Cb = carbonate; Pl = plagioclase; Ep = epidote; Qtz = quartz; Bt = biotite

Figure 52. Location of metamorphic assemblages in Pipedream Lake belt.

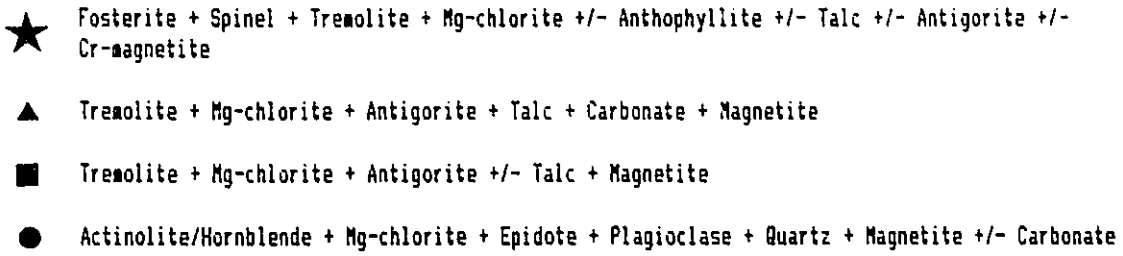

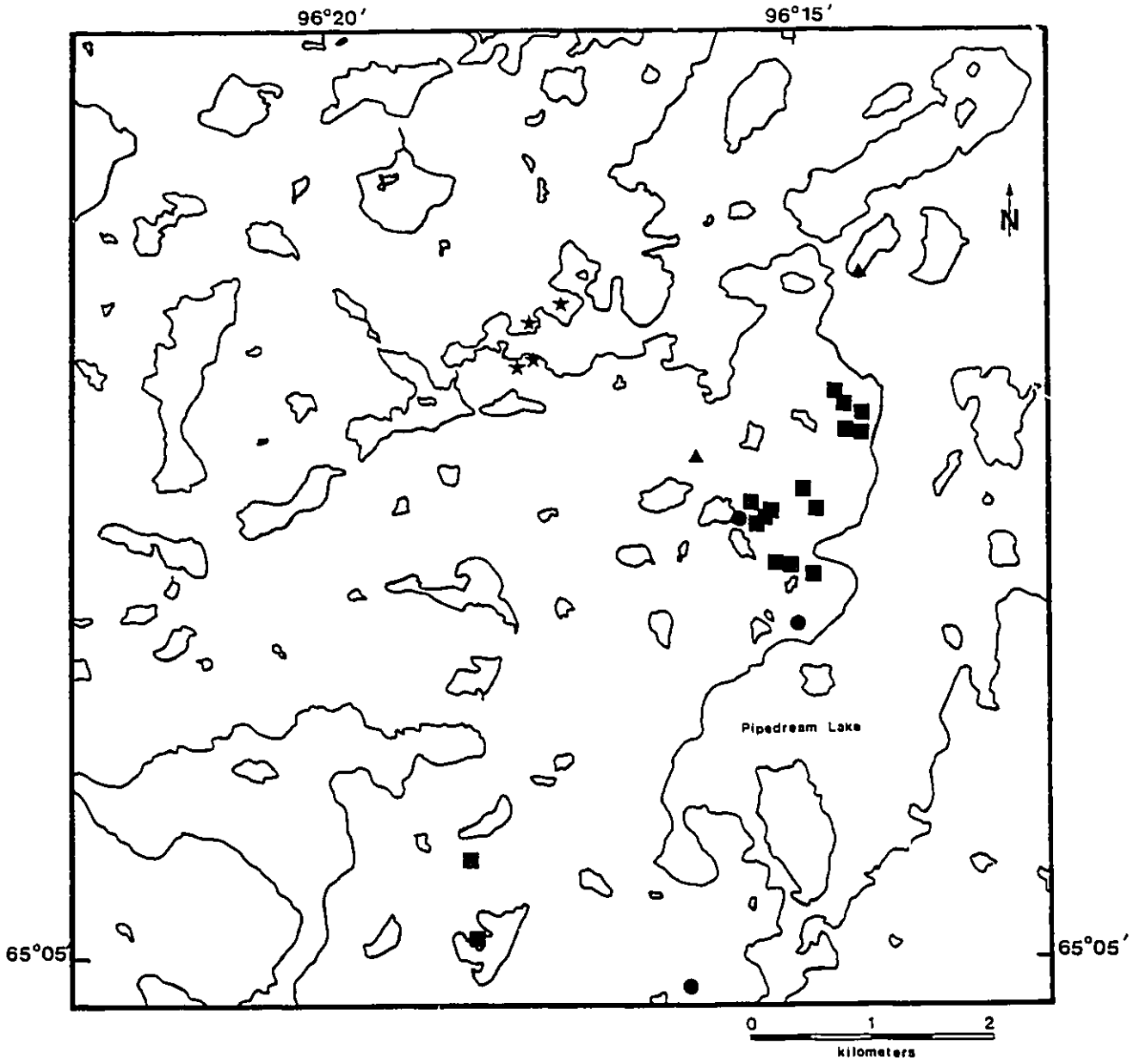
96°20′
96°15′
N
Pipedream Lake
65°05′
65°05′
0
1
2
kilometers

they are part of a regional or contact metamorphic mineral assemblage. The proportions of each of the greenschist facies minerals in some of the komatiites have been calculated using the least squares mixing method (Bryan et al., 1968) with mineral probe data and whole rock analysis. This has provided a semi-quantitative estimate of the proportions of metamorphic minerals (Table 13), which agrees in general with the modal estimates from petrographic observations.

Evans (1977) has shown that the bulk chemical compositions of ultramafic rocks can be correlated with the mineral assemblages of different metamorphic grade on a CSM ($CaO-SiO_2-MgO$) molecular diagram (Fig. 53). Plotting of the Woodburn Lake Group mafic and ultramafic metavolcanics on this diagram shows the komatiites positioned half way along the SiO_2 - MgO join and the high-Mg basalts positioned two third up along SiO_2 - MgO join. When compared to the different fields established by Jolly (1982) for the Abitibi metavolcanics, most of the Woodburn Lake Group metavolcanics, especially the cumulate zone samples, plot away from the CaO apex (Fig. 53). This agrees with previous observations (e.g. low $CaO\backslash Al_2O_3$ ratios) that calcium has been removed from the cumulate zone samples during serpentinization.

5.3 MINERAL CHEMISTRY

Olivine and spinel analyses were obtained at the Geological Survey of Canada with a MAC 400 electron microprobe equipped with

Figure 53. CSM ($CaO-SiO_2-MgO$) diagram of the Woodburn Lake Group and Ketyet River Group volcanic rocks. Upper left diagram shows the fields of average Abitibi Greenstone Belt volcanic rocks (from Jolly, 1982). In general, there is good agreement, except that the most magnesian-rich Woodburn Lake Group volcanic rocks (i.e. the cumulate zone samples) plot further away from the CaO apex than Jolly's accumulates.

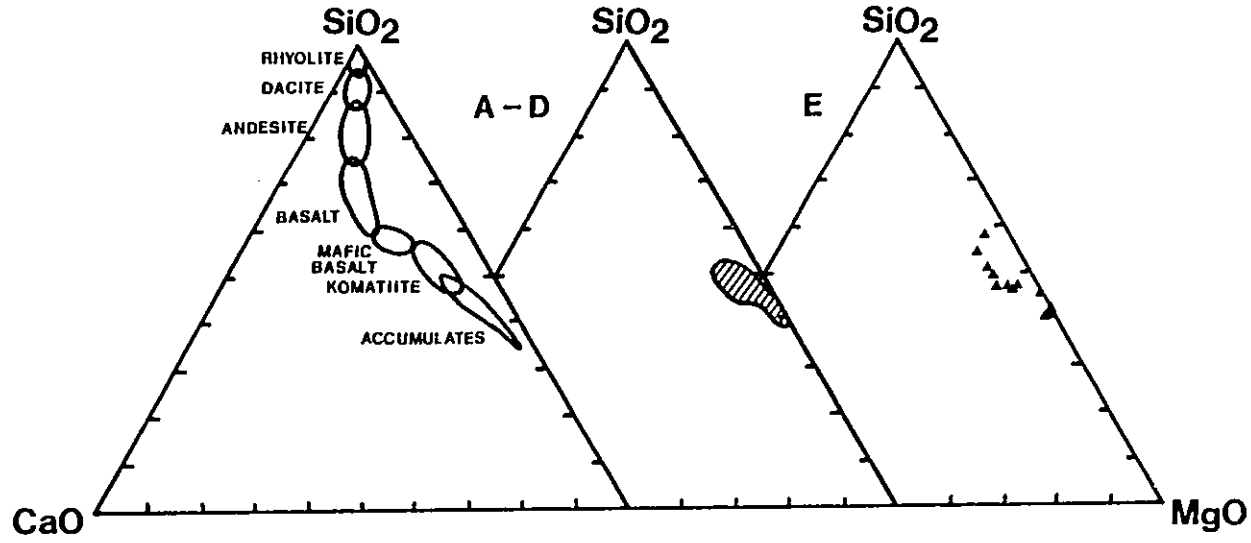
SiO2
SiO2
SiO2
RHYOLITE
DACITE
ANDESITE
BASALT
MAFIC
BASALT
KOMATIITE
ACCUMULATES
A – D
E
CaO
MgO

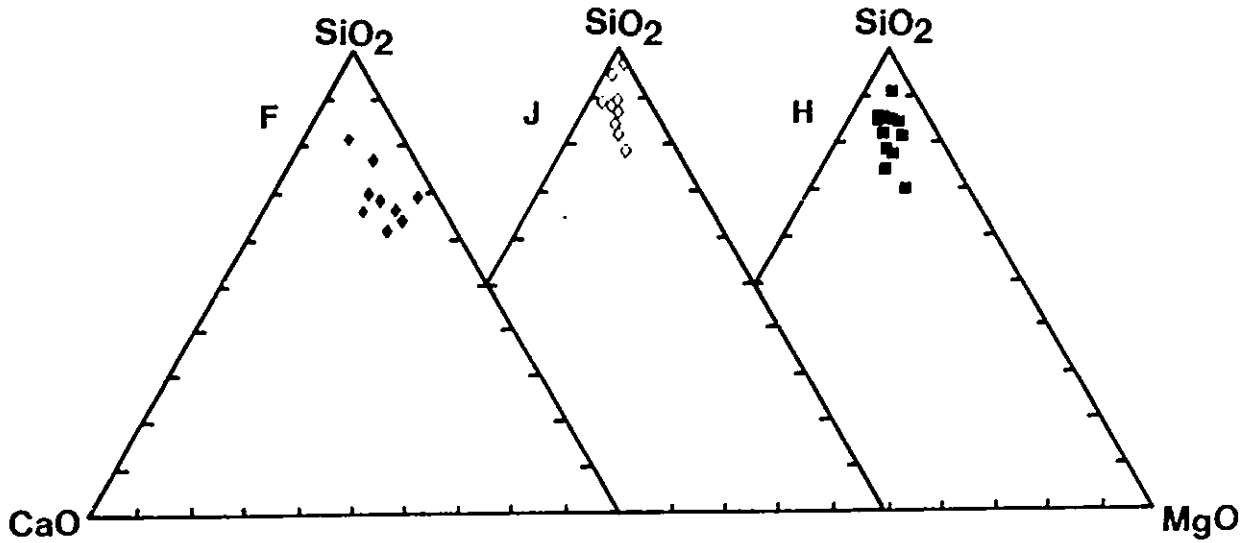
SiO2
SiO2
SiO2
F
J
H
CaO
MgO

mole %

Table 13 - A comparison of observed and calculated mineral proportions for a spinifex-textured flow unit.

		Tr/Act	Chl	Srp	Cr-Mag/Mag
K-43a	Obs.	13	10	65	10
	Cal.	28	25	41	5
K-43b	Obs.	15	5	67	10
	Cal.	12	18	64	5
K-43c	Obs.	20	10	55	8
	Cal.	7	15	72	5
K-43d	Obs.	30	20	40	10
	Cal.	6	28	61	5
K-44a	Obs.	65	25	5	5
	Cal.	50	33	11	5
K-44b	Obs.	65	15	10	10
	Cal.	43	26	27	5
K-44c	Obs.	67	20	3	10
	Cal.	54	32	9	5
K-44d	Obs.	55	25	10	10
	Cal.	63	18	15	4
K-44e	Obs.	50	30	10	10
	Cal.	51	28	18	3
K-44f	Obs.	55	35	5	5
	Cal.	48	31	18	3
K-44g	Obs.	55	15	20	10
	Cal.	56	26	13	5

Note: mineral proportions were calculated using a least squares mixing method (Bryan et al., 1969) with whole-rock chemistry (data from Appendix B1.a) and mineral chemistry (data from Tables 16 to 19).

an energy dispersive Kevex system and automated for data reduction. Similarly, tremolite, chlorite, serpentine, and opaques were analyzed at Queen's University with an ARL model AMX microprobe equipped with an energy dispersive detector set up and supervised by P.L. Roeder, M.I. Corlett, and Dave Kempson. Operating conditions were 20 kV, 0.2 uA and 15 kV, 0.5 uA, respectively. Counting times of 100 to 120 seconds were used. Bence-Albee corrections were applied in calculating weight percent oxides. Natural and synthetic standards were used for calibration. All the minerals analyzed are from samples of the Pipedream Lake belt. Oxide totals of 98 - 102 wt% were considered acceptable for analyses of anhydrous minerals; whereas hydrous mineral determinations were acceptable, if they fell in the 98 - 102 wt% range after the addition of average water content for the mineral in question. Exceptions to this are as follows - for chlorite: K-44f, K-44g, and K-6a; for amphibole: K-44d and K-6a; for serpentine: K-43a and for magnetite: K-43b and K-44f. These analyses are listed only for rough comparisons with the same minerals in other samples. Ferric iron content of spinel was calculated from total iron by assuming spinel stoichiometry. Mineral analyses are listed in Tables 14 to 19. The amphibole, chlorite, serpentine, and opaque mineral compositions are representative of regional metamorphism, whereas the olivine and spinel compositions are from the contact metamorphic zone. Sample locations are shown in Figure 25.

Table 14 - Olivine microprobe analyses

	AK-12c n=4	AK-7a n=5	AK-7a n=3	AK-12b n=7
SiO2	38.39	39.54	42.24	39.16
Al2O3	bl	bl	1.99	bl
Cr2O3	0.04	0.03	0.08	0.06
FeO*	18.21	18.97	15.83	18.47
MnO	0.21	0.17	0.12	0.16
MgO	41.09	42.08	37.33	41.66
NiO	0.22	-	-	-
CaO	0.03	bl	2.04	bl
Total	98.18	100.79	99.64	99.50
#Si+4	0.999	1.003	1.094	1.005
T-site	0.999	1.003	1.094	1.005
#Al+3	0.000	0.000	0.061	0.000
#Cr+3	0.001	0.001	0.002	0.001
#Fe+2	0.396	0.402	0.343	0.396
#Mn+2	0.005	0.004	0.003	0.003
#Mg+2	1.594	1.591	1.441	1.594
#Ni+2	0.005	-	-	-
#Ca+2	0.001	0.000	0.057	0.000
Y-site	2.001	1.997	1.906	1.995
#TOTAL	3.000	3.000	3.000	3.000
Charge	7.999	8.006	8.251	8.011
#Mg/(Fe+Mg)	0.801	0.798	0.808	0.801

Olivine formula calculated on the basis of 3 cations
FeO* = total Fe expressed as FeO
bl = below detection level
- = not determined
= molecular

Table 15 - Spinel microprobe analysis

	AK-12c n=8
SiO2	0.34
TiO2	0.03
Al2O3	63.38
Cr2O3	1.54
Fe2O3	1.92
FeO	16.16
MnO	0.09
MgO	16.93
CaO	0.01
NiO	0.35
ZnO	0.40
Total	101.15
#Si+4	0.009
#Ti+4	0.001
#Al+3	1.913
#Cr+3	0.031
#Fe+3	0.037
Y-site	1.991
#Fe+2	0.346
#Mn+2	0.002
#Mg+2	0.646
#Ca+2	0.000
#Ni+2	0.007
#Zn+2	0.008
X-site	1.009
Cations	3.000
#Cr/(Al+Cr+Fe^{3+})	0.015
#Al/(Al+Cr+Fe^{3+})	0.966
#Fe^{3+}/(Al+Cr+Fe^{3+})	0.019
#Fe^{2+}/(Fe^{2+}+Mg)	0.349
#Mg/(Fe^{2+}+Mg)	0.651

Spinel formula calculated on the basis of 3 cations and 4 oxygens

Fe^{3+}/Fe^{2+} calculated from FeO* (total Fe expressed as FeO) on the basis of 3 cations and no vacancies in spinel stoichiometry

= molecular

Table 16 - Chlorite microprobe analyses

	K-43a	K-43b n=4	K-43c	K-43d	K-44a n=2	K-44c n=6	K-44e n=4	K-44f n=3	K-44g	K-6a n=2	K-8
SiO2	33.15	33.96	34.16	36.05	31.49	31.66	31.16	30.71	30.49	31.95	36.56
TiO2	0.11	0.05	bl	bl	0.04	0.07	0.03	0.03	0.10	0.03	0.06
Al2O3	13.33	13.56	12.99	11.33	16.75	15.11	17.14	16.29	16.34	13.22	11.56
Cr2O3	0.56	0.75	0.60	0.61	0.34	0.63	0.36	0.61	0.49	0.31	0.40
Fe2O3	-	-	-	-	-	-	-	-	-	-	-
FeO*	8.13	8.71	7.38	6.98	8.65	10.97	6.36	8.41	7.17	7.26	7.68
MnO	0.08	0.09	0.12	bl	0.15	0.12	0.13	0.08	0.16	0.10	0.21
MgO	31.17	30.70	31.52	28.93	29.60	29.55	30.87	29.23	29.45	29.02	27.55
NiO	0.22	0.11	bl	bl	bl	0.10	bl	bl	bl	bl	bl
CaO	bl	0.43	0.20	2.17	0.05	0.38	0.12	0.09	0.06	0.29	2.94
Na2O	bl	bl	bl	0.12	bl	bl	0.20	bl	bl	0.42	bl
K2O	-	-	-	-	-	-	-	-	-	-	-
H2O	-	-	-	-	-	-	-	-	-	-	-
Total	86.75	88.36	86.97	86.13	87.04	88.59	86.38	85.45	84.26	82.60	86.96
#Si+4	3.218	3.243	3.287	3.499	3.050	3.061	3.016	3.033	3.034	3.251	3.531
#Al IV	0.782	0.757	0.713	0.501	0.950	0.939	0.984	0.967	0.966	0.749	0.469
T-site	4.000	4.000	4.000	4.000	4.000	4.000	4.000	4.000	4.000	4.000	4.000
#Al VI	0.743	0.772	0.760	0.795	0.961	0.783	0.972	0.929	0.950	0.825	0.847
#Ti+4	0.008	0.004	0.008	0.008	0.003	0.005	0.002	0.002	0.007	0.002	0.004
#Cr+3	0.043	0.057	0.046	0.047	0.026	0.049	0.028	0.047	0.039	0.026	0.031
#Fe+3	-	-	-	-	-	-	-	-	-	-	-
#Fe+2	0.660	0.699	0.594	0.566	0.700	0.892	0.491	0.695	0.597	0.618	0.620
#Mn+2	0.007	0.008	0.010	0.008	0.012	0.010	0.010	0.007	0.013	0.009	0.017
#Mg+2	4.511	4.373	4.522	4.185	4.272	4.263	4.454	4.304	4.369	4.394	3.967
#Ni+2	0.017	0.008	0.008	0.008	0.008	0.008	0.008	0.008	0.008	0.008	0.008
#Ca+2	0.008	0.043	0.021	0.226	0.005	0.039	0.012	0.010	0.006	0.032	0.304
#Na+1	0.008	0.008	0.008	0.023	0.008	0.008	0.038	0.008	0.008	0.081	0.008
#K+1	-	-	-	-	-	-	-	-	-	-	-
O-site	5.998	5.961	5.953	5.841	5.979	6.048	6.009	5.993	5.981	5.988	5.791
#Total	9.998	9.961	9.953	9.841	9.979	10.048	10.009	9.993	9.981	9.988	9.791
#O-2	14.000	14.000	14.000	14.000	14.000	14.000	14.000	14.000	4.000	14.000	14.000
#Mg/(Fe+Mg)	0.872	0.862	0.884	0.881	0.859	0.827	0.901	0.861	0.880	0.877	0.865

Chlorite formula calculated on the basis of 14 oxygens
Note: impurities are present in K-43d and K-8, as indicated by their anomalous CaO values
FeO* = Total Fe expressed as FeO
bl = below detection level
- = not determined
= molecular

Table 17 - Amphibole microprobe analyses

	K-43c	K-44a n=3	K-44c n=7	K-44d	K-44e n=4	K-44f n=2	K-44g	K-6a n=2	K-8
SiO2	57.26	54.30	54.76	49.70	54.38	50.54	52.26	55.47	56.71
TiO2	0.08	0.08	0.16	0.07	0.20	0.22	0.27	0.04	bl
Al2O3	bl	1.70	2.97	4.51	3.51	5.07	3.33	0.49	0.47
Cr2O3	0.13	0.25	0.25	0.17	0.24	0.30	0.36	0.16	0.15
Fe2O3	-	-	-	-	-	-	-	-	-
FeO*	3.27	8.09	5.33	5.92	4.76	5.69	5.48	3.43	3.65
MnO	bl	0.23	0.26	bl	0.17	0.31	0.11	0.16	0.26
MgO	24.01	21.46	21.70	25.43	21.86	20.92	22.54	22.49	21.88
NiO	bl	0.05	0.06	bl	0.05	bl	bl	bl	bl
CaO	12.76	12.08	11.80	7.91	12.08	11.80	10.67	12.18	12.60
Na2O	bl	0.95	1.26	0.93	1.52	2.03	1.38	0.61	0.45
K2O	-	-	-	-	-	-	-	-	-
H2O	-	-	-	-	-	-	-	-	-
Total	97.51	99.19	98.54	94.64	98.76	96.07	96.48	95.02	96.17
#Si+4	7.886	7.574	7.576	7.148	7.502	7.235	7.486	7.865	7.941
#Al IV	0.000	0.264	0.424	0.764	0.495	0.765	0.556	0.081	0.059
#Fe+3	0.000	0.000	0.000	0.000	0.000	0.000	0.000	0.000	0.000
#Ti IV	0.008	0.000	0.000	0.008	0.003	0.000	0.029	0.004	0.000
T-site	7.994	7.838	8.000	7.920	8.000	8.000	8.001	7.950	8.000
#Al VI	0.000	0.015	0.040	0.000	0.075	0.090	0.000	0.000	0.019
#Fe+3	0.000	0.000	0.000	0.000	0.000	0.000	0.000	0.000	0.000
#Ti+4	0.000	0.009	0.017	0.000	0.018	0.024	0.000	0.000	0.000
#Al+3	0.000	0.000	0.000	0.000	0.000	0.000	0.000	0.000	0.000
#Cr+3	0.014	0.028	0.027	0.019	0.026	0.034	0.040	0.017	0.017
#Mg+2	4.930	4.463	4.475	4.981	4.496	4.464	4.762	4.754	4.567
#Ni+2	0.000	0.005	0.007	0.000	0.005	0.000	0.000	0.000	0.000
#Fe+2	0.056	0.480	0.434	0.000	0.380	0.389	0.198	0.229	0.397
#Mn+2	0.000	0.000	0.000	0.000	0.000	0.000	0.000	0.000	0.000
#Ca+2	0.000	0.000	0.000	0.000	0.000	0.000	0.079	0.000	0.000
M1,2,3	5.000	5.000	5.000	5.000	5.000	5.000	5.000	5.000	5.000
#Mg+2	0.000	0.000	0.000	0.471	0.000	0.000	0.000	0.000	0.000
#Fe+2	0.321	0.464	0.182	0.712	0.169	0.292	0.451	0.177	0.030
#Mn+2	0.000	0.028	0.031	0.000	0.020	0.038	0.013	0.019	0.031
#Ca+2	1.679	1.494	1.738	0.817	1.771	1.663	1.536	1.804	1.890
#Na+1	0.000	0.014	0.049	0.000	0.040	0.007	0.000	0.000	0.049
M4-site	2.000	2.000	2.000	2.000	2.000	2.000	2.000	2.000	2.000
#Ca+2	0.284	0.411	0.011	0.402	0.015	0.023	0.084	0.045	0.000
#Na+1	0.000	0.242	0.289	0.259	0.366	0.555	0.379	0.169	0.073
#K+1	-	-	-	-	-	-	-	-	-
A-site	0.284	0.653	0.300	0.661	0.381	0.578	0.463	0.214	0.073
#Total	15.098	15.392	15.320	15.582	15.382	15.578	15.456	15.166	15.073
#O-2	23.000	23.000	23.000	23.000	23.000	23.000	23.000	23.000	23.000

Table 18 - Serpentine microprobe analyses

	K-43a	K-43b	K-43c	K-43d n=3	K-44d	K-44g n=2	AK-7a
SiO2	40.10	41.31	41.50	41.35	37.35	44.42	39.36
TiO2	bl	bl	bl	bl	bl	0.04	bl
Al2O3	2.82	3.02	2.32	2.40	9.09	1.85	0.43
Cr2O3	0.18	0.21	0.37	0.13	0.18	0.29	0.48
Fe2O3	-	-	-	-	-	-	-
FeO*	10.31	9.40	8.62	8.45	8.39	8.77	13.33
MnO	0.10	0.18	0.10	0.15	0.23	0.17	bl
MgO	38.67	33.36	33.87	32.64	32.82	38.59	32.35
NiO	bl	0.26	0.16	bl	bl	bl	bl
CaO	3.43	bl	bl	1.31	3.85	2.83	1.39
Na2O	bl	bl	bl	0.20	bl	bl	1.14
Total	84.61	88.34	86.94	86.32	88.11	98.94	87.78
#Si+4	4.002	3.933	3.994	4.012	3.553	4.181	3.818
#Al IV	0.000	0.067	0.006	0.000	0.447	0.000	0.050
T-site	4.002	4.000	4.000	4.012	4.000	4.181	3.868
#Al VI	0.332	0.272	0.257	0.275	0.572	0.204	0.000
#Ti+4	0.000	0.000	0.000	0.000	0.000	0.003	0.000
#Cr+3	0.014	0.016	0.028	0.010	0.014	0.021	0.038
#Fe+3	-	-	-	-	-	-	-
#Fe+2	0.860	0.748	0.694	0.687	0.667	0.694	1.085
#Mn+2	0.008	0.015	0.008	0.012	0.019	0.013	0.000
#Mg+2	4.563	4.820	4.860	4.730	4.654	4.311	4.389
#Ni+2	0.000	0.020	0.012	0.000	0.000	0.000	0.000
#Ca+2	0.046	0.000	0.000	0.102	0.005	0.277	0.148
#Na+1	0.000	0.000	0.000	0.038	0.000	0.000	0.220
O-site	5.823	5.890	5.860	5.853	5.931	5.523	6.380
#Total	9.825	9.990	9.860	9.865	9.931	9.704	10.248
#O-2	14.000	14.000	14.000	14.000	14.000	14.000	14.000
#Mg/(Fe+Mg)	0.841	0.866	0.875	0.873	0.875	0.861	0.818

Serpentine formula calculated on the basis of 14 oxygens

FeO* = total Fe expressed as FeO
bl = below detection level
- = not determined
= molecular

Table 19 - Magnetite and Cr-magnetite microprobe analysis

	K-43b n=1	K-44a n=1	K-44c n=1	K-44e n=4	K-44f n=2	AK-12c n=5
SiO2	5.28	0.37	0.42	0.62	4.11	2.18
TiO2	bl	0.13	bl	0.16	0.11	0.03
Al2O3	1.21	0.14	0.20	0.21	0.75	1.22
Cr2O3	1.94	10.51	7.86	14.84	6.66	0.14
Fe2O3	60.10	56.71	61.55	50.37	50.49	63.99
FeO	28.18	30.93	31.74	30.21	29.75	30.08
MnO	0.34	0.45	0.29	0.45	0.28	0.01
MgO	6.60	0.13	0.22	0.35	3.18	2.68
CaO	0.72	0.06	0.10	0.10	0.56	0.01
NiO	0.23	bl	bl	0.04	bl	0.03
ZnO	bl	bl	bl	bl	bl	0.08
Na2O	bl	bl	0.13	0.27	0.16	bl
Total	104.60	99.43	102.38	97.86	95.89	100.45
#Si+4	0.180	0.014	0.016	0.024	0.156	0.081
#Ti+4	0.000	0.004	0.000	0.005	0.003	0.001
#Al+3	0.049	0.006	0.009	0.010	0.034	0.053
#Cr+3	0.052	0.319	0.230	0.456	0.200	0.004
#Fe+3	1.540	1.639	1.723	1.464	1.442	1.779
Y-site	1.821	1.982	1.978	1.959	1.834	1.918
#Fe+2	0.802	0.993	0.987	0.981	0.943	0.930
#Mn+2	0.010	0.015	0.009	0.015	0.009	0.000
#Mg+2	0.335	0.007	0.012	0.020	0.180	0.148
#Ca+2	0.026	0.002	0.004	0.004	0.023	0.000
#Ni+2	0.006	0.000	0.000	0.001	0.000	0.001
#Zn+2	0.000	0.000	0.000	0.000	0.000	0.002
#Na+1	0.000	0.000	0.009	0.020	0.011	0.000
X-site	1.179	1.018	1.022	1.041	1.166	1.082
#TOTAL	3.000	3.000	3.000	3.000	3.000	3.000
Charge	8.001	7.998	7.974	7.862	7.974	7.998

Structural formulas with adjusted Fe3+/Fe2+ calculated on the basis of 3 cations, 4 oxygen atoms, and no vacancies

FeO* = total Fe expressed as FeO
bl = below detection level
- = not determined
= molecular

5.3.1 Olivine

Metamorphic olivines, found within the komatiitic lavas, occur as small pale green grains up to 1.0 mm in size. They form an equigranular mosaic texture. This is at odds with field observations where large porphyroblasts, up to 5.0 cm are found in the contact metamorphic zones (see Fig. 20). Petrographic observations suggest that these fine olivine grains may have formed by recrystallization and/or deformational processes from former olivine porphyroblasts (i.e. megacrysts) and their groundmass. This second (?) generation of olivine is called neoblast, after the terminology of Mercier and Nicolas (1975). In places, the olivine neoblasts are partly replaced by serpentine, iddingsite, and magnetite. Metamorphic olivine from a massive or pillowed (?) komatiitic flow (AK-12b and AK-12c) and a porphyroblastic massive komatiitic flow (AK-7a) were analyzed (Table 14). The composition of the olivine in sample AK-12b is quite uniform, ranging from Fo_{79} to Fo_{81}. It should be noted that the Mg/Mg+Fe ratio of the olivine is somewhat lower than that of the host rock. The olivine grains contain small amounts of Cr (<0.05 wt% Cr_2O_3), Ni (<0.29 wt% NiO), and Mn (<0.22 wt% MnO). The small amounts of these three elements are at or below the detection limits of the analytical method and therefore can not be used with any degree of confidence. In general, the olivine is compositionally homogeneous. Although no zoning was observed, it is possible that thin zones at crystal margins were not detected.

Primary olivine was not observed in the Woodburn Lake Group komatiites, but an estimation of the primary olivine composition can be calculated by using the distribution coefficient equation of Roeder and Emslie (1970) on estimated liquid compositions. As described in Chapter 6, these calculations suggest that primary olivines for the Woodburn Lake Group komatiites ranged from Fo_{90} to Fo_{94}. Use of these estimated compositions supports the view that the metamorphic olivine is less magnesian than the original magmatic olivine. This is consistent with the results of St-Seymour and Francis (1980), who found metamorphic olivine in the range Fo_{60-65}. They concluded that metamorphic olivine in komatiites appears to have a lower fosterite content than primary olivine in the same rocks. This is probably a function of metamorphic crystallization conditions. A Fe-rich olivine is more likely to be stable at lower temperatures than a Mg-rich igneous olivine.

5.3.2 Spinel

Spinels are found in close proximity with olivine (Fig. 24). They occur as fine anhedral grains of green hercynite-pleonaste with thin opaque rims of magnetite and/or Cr-magnetite. The compositions of spinel cores (Table 15), coexisting with olivine in one sample (AK-12b), are relatively uniform, being an Al-Mg-Fe spinel with the mole fraction of Cr (Y^{Sp}_{Cr}) ranging from 0.010 to 0.019. Based upon Evans's work (1977) these spinel compositions

would be stable under amphibolite conditions.

5.3.3 Amphibole

The compositions of the analyzed amphiboles (Table 17), based on 9 samples, are calcic with low Al_2O_3 and TiO_2. The amphiboles contain very small amounts of Ni (<0.2 wt% NiO) and Cr (<0.45 wt% Cr_2O_3). The Al_2O_3, SiO_2, and alkali contents are quite variable, whereas the MgO and CaO contents are relatively constant. This variability may reflect the amphibole structure offering a more convenient exchange site for elements during metamorphism than coexisting chlorite, serpentine, and magnetite. Even so, there appears to be a systematic change from the cumulate zone (K-43c) upwards through the spinifex-textured zone (K-44a to K-44g). This change is not as regular as the ones shown by chlorite (Table 16) and magnetite and Cr-magnetite (Table 19). They may be classified as tremolite or actinolite, and actinolitic hornblende or magnesio-hornblende using the IMA classification (Leake, 1978), which depends upon their Mg/(Mg+Fe) ratios and Al_2O_3 contents.

5.3.4 Chlorite

Most of the analyzed chlorites are magnesian with approximately 3.2 silicon, 0.7 iron, and 1.6 aluminum atoms per 14 oxygens (Table 16). On this basis, they are classified as clinochlore (Deer et al., 1966). Small amounts of Ni and Cr are

present (up to 0.5 wt%). The Mg/(Mg+Fe) ratio is almost identical to coexisting amphibole and serpentine. Even more noticeable than within the amphiboles, there is a systematic change in composition from the base of the cumulate zone (K-43a) upwards into and through the spinifex-textured zone (K-44a to K-44g). The chlorites in the spinifex-textured zones have lower SiO_2, higher Al_2O_3, and possibly lower CaO contents than those of the cumulate zones.

5.3.5 Serpentine

The analyzed serpentine minerals are identified as antigorite on the basis of textural and chemical data. There is very little variation in antigorite compositions except for those that are partially altered to chlorite or tremolite. One possible exception is the relative abundance of Ni in antigorite of the cumulate samples (K-43a to K-43d) versus antigorite of spinifex-textured zone samples (K-44d and K-44g). The Mg/(Mg+Fe) ratio of antigorite is close to that of the bulk rock. Antigorite of this composition with relatively high FeO contents has been reported in other komatiite occurrences (Blais and Auvray, 1987).

5.3.6 Cr-magnetite and Magnetite

The analyzed opaque minerals (Table 19) are chromian-rich magnetite and magnetite. As mentioned in Chapter 3, textural

evidence indicates that the magnetite crystals appear as pseudomorphs after chromite and/or ferrochromite and as a breakdown product of original olivine grains (i.e. the oxidation of FeO in olivine to Fe_2O_3 during serpentinization). Likewise, textural and mineralogical evidence indicates that the Cr-magnetite grains are a replacement of primary chromite and/or ferrochromite (i.e. pseudomorphic recrystallization). They are highly variable in composition with Cr and Fe ranging between <0.2 and 15 wt% Cr_2O_3 and 65 and 90 wt% FeO. The limited number of analyses suggest that the variation changes with position in flow units. The Cr-rich variety being found within spinifex-textured zones.

5.4 Olivine-Spinel Geothermometry

Olivine-spinel geothermometry has been applied to co-existing olivine-spinel from within a massive komatiitic flow. The iron-magnesium exchange equilibrium between co-existing olivine and spinel was first investigated by Irvine (1965, 1967). Irvine demonstrated that the empirical distribution coefficient for Fe-Mg exchange between olivine and spinel,

$$K_D = X^{Ol}_{Mg} \times X^{Sp}_{Fe} / X^{Ol}_{Fe} \times X^{Sp}_{Mg},$$

where X = mole fraction,

varies with temperature but is also a function of the mole fractions of trivalent ions i, $Y^{Sp}_i = i/Cr+Al+Fe^{3+}$.

Jackson (1969) attempted to calibrate this geothermometer based on limited thermochemical data. Use of his calibrated geothermometer on natural assemblages did not compare well to values produced by other geothermometers. More recently, Evans and Frost (1975), Frost (1975), and Medaris (1975) pointed out that the Mg-Fe exchange equilibrium between olivine and spinel is strongly temperature dependent and is in agreement with Fe-Mg partitioning of natural olivine-spinel pairs that equilibrated under isothermal conditions. Evans and Frost (1975) proposed a tentative graphical version of this geothermometer based on natural olivine-spinel pairs. Since then, other distinct calibrations of this geothermometer have been proposed based upon natural assemblages, thermochemical data, experimental data or a combination of these (Fujii, 1977; Engi, 1978; Roeder et al., 1979; Fabries, 1979). Ozawa (1983) examined some of these geothermometers as possible indicators of thermal histories recorded in peridotites. He found that the geothermometers calibrated by Fabries (1979) and Evans and Frost (1975) give similar results and are quite reliable, whereas those of Fujii (1977) and Roeder et al. (1979) are unacceptable for various reasons. Fabries (1979), Engi and Evans (1980), and Paktunc (1984b) have also challenged the Roeder et al. (1979) geothermometer and found it to be unreliable, probably because the free energy values for their end-member spinels are not correct (Fabries, 1979). Paktunc (1984b) found that the geothermometer of Fabries (1979) provided fairly reasonable

temperature estimates for komatiitic rocks from the Thompson belt.

Application of Fabries version of the olivine-spinel geothermometer to the Woodburn Lake Group olivine-spinel pair gives temperature estimates of 690°C to 780°C. These temperatures are unreasonable for the temperature of the high level granite responsible for contact metamorphism. The mineral assemblages of the contact aureole also suggest lower temperatures. The presence of Mg-chlorite and the absence of anthophyllite and enstatite places an upper limit of 650°C at 2 kb on contact metamorphism (Berman et al., 1987).

This unreasonable temperature estimate may indicate that complete equilibrium was not achieved between olivine and spinel. Alternatively, a more viable explanation is offered by the experimental and thermodynamic analysis of olivine-spinel pairs by Engi (1983). Engi conclusively shows that 1) olivine and spinel are nonideal thus making K_D dependent upon the bulk magnesium content (X_{Mg}) of the system, 2) the isotherms of ln K_D versus Y^{Sp}_{Cr} are not linear, 3) the non-linearity is mainly a function of the spinel speciation, and 4) the shape and position of the isotherms are highly dependent on the "bulk composition of the system" (i.e. the proportion of magnesium to iron content of the ultramafic rock suite being studied). This explains why so many recalibrations of this geothermometer have taken place. Engi (1983) has recalibrated the olivine spinel geothermometer on the basis of the bulk X_{Mg} of the system under consideration. He has

left room for further refinement by new experimental, thermodynamic, and natural mineral data.

The first step in applying the geothermometer of Engi (1983) is to define 1) the modal proportion (r) or ratio of olivine to spinel in the rock and 2) the whole rock composition of the olivine-spinel mineral assemblage being studied. According to Table 4 of Engi (p.63) the Woodburn Lake Group olivine-spinel pairs fall within the "L1" type. Then the ln K_D and the Y^{Sp}_{Cr} were calculated for the olivine-spinel pairs. Plotting of these values on a ln K_D versus Y^{Sp}_{Cr} diagram (Fig. 54, from Engi, 1983) shows them lying close to the 600°C isotherm. Corrections for pressure and Y_{Fe+++} are neglible since the assumed pressure is 2 to 3 kbar and Y_{Fe+++} <0.03. This temperature estimate is consistent with the mineral assemblages present. Further detailed sampling of the contact aureoles and more probe work might show a range of temperatures from greenschist facies to 650°C. The peak temperature of contact metamorphism of the Woodburn Lake Group komatiites and associated high-Mg basalts is 625°C +/- 25°C based on olivine-spinel pairs. This temperature is similar to that estimated by Irving and Ashley (1976) and Ashley et al. (1979) for some ultramafic hornfels in Australia.

5.5 METAMORPHIC REACTIONS AND PHYSICAL CONDITIONS OF METAMORPHISM

The mineral assemblages and textures of the Woodburn Lake Group komatiitic and high-Mg basaltic rocks indicate that a

Figure 54. Diagram of the logarithm of the distribution coefficient of Mg - Fe exchange equilibrium in olivine and spinel versus the $Cr/(Cr + Al + Fe^{3+})$ in spinel (from Engi, 1983). Isotherms between 600°C and 1400°C are calculated by Engi (1983) from several sources of data. The olivine-spinel pair of this study plots close to the 600°C isotherm and this is in agreement with the estimates from the mineral assemblages present.

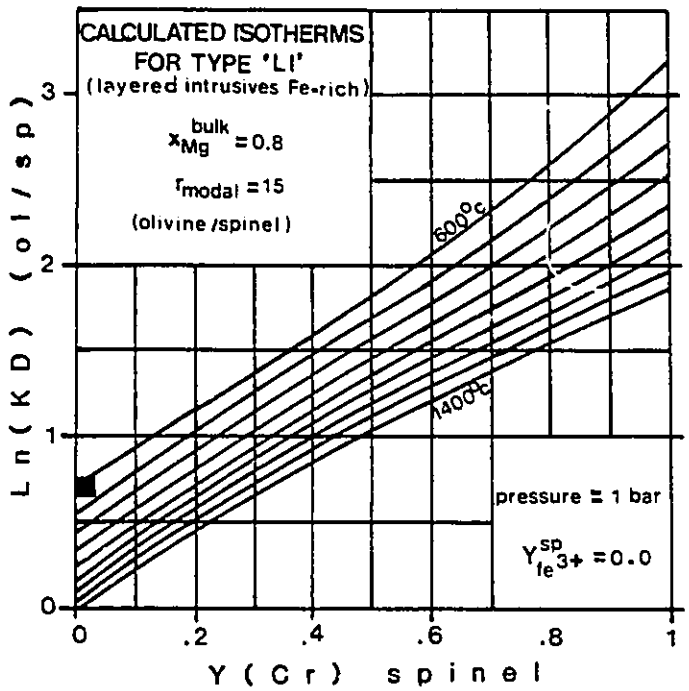
CALCULATED ISOTHERMS
FOR TYPE 'LI'
(layered intrusives Fe-rich)
$x_{Mg}^{bulk} = 0.8$
$r_{modal} = 15$
(olivine/spinel)
600°C
1400°C
pressure = 1 bar
$Y_{Fe^{3+}}^{sp} = 0.0$
Ln(KD) (ol/sp)
Y (Cr) spinel
0
1
2
3
.2
.4
.6
.8

series of complex hydration and dehydration reactions occurred during sea-water alteration, regional metamorphism and contact metamorphism. An evaluation of these reactions in completely altered rocks requires the recognition of pseudomorphs of the original minerals and the difficult task of estimating the proportions of fine-grained metamorphic minerals. The komatiite flows are more suited than the high-Mg basalts to the investigation of the metamorphic conditions since, as mentioned above, their textures are better preserved and their secondary mineralogy is simpler (Table 12).

Metamorphic mineral changes of the Woodburn Lake Group komatiites proceeded in three stages: 1) the first stage is a hydration event involving the breakdown of olivine and glass by water, possibly sea-water, percolating through them, 2) the second stage is a partially overprinting dehydration event (i.e. regional metamorphism) involving chemical changes of previously formed metamorphic minerals, and 3) the third stage is a hydration contact metamorphic event that produced higher temperature minerals, including tourmaline. It is not known whether these processes represent separate phases of alteration or are a gradual progression of changes during increasing pressure and temperature conditions. It is difficult to evaluate the changes during sea-water alteration since no primary minerals remain and no metamorphic isograds are observed.

Based upon the present mineralogy and the work of Jolly (1980 and 1982), Evans (1977), and St-Seymour and Francis (1980), the

following synopsis of mineral changes are given. Olivine was probably serpentinized during sea-water alteration to chrysotile and/or lizardite, and magnetite. During regional metamorphism these serpentine minerals were converted to antigorite and/or chlorite depending upon how much chemical interaction took place with other minerals. Further metamorphism resulted in the conversion of antigorite and chlorite to tremolite, especially near normative plagioclase-rich areas (i.e. matrix) in which Al is readily available for the mineral reactions. Clinopyroxene was probably only partially serpentinized (i.e. bastite) during sea-water alteration. With increasing metamorphism clinopyroxene was converted entirely to tremolite. The matrix most probably was completely devitrified during sea-water alteration. Continuing metamorphism caused conversion to chlorite. Chromite was most likely little affected by sea-water alteration. Progressive metamorphism resulted in a change to Cr-magnetite. Contact metamorphism then caused the chlorite - tremolite - antigorite - Cr-magnetite assemblage to become recrystallized and promoted the growth of olivine and spinel.

The following mineral reactions are considered to have taken place at various stages during alteration and metamorphism of the Woodburn Lake Group komatiites (Note: calculated from data given in Berman et al., 1987). The alteration assemblages would vary greatly depending upon the bulk composition of the rock, the proportions and composition of reactants available and their different reactivities.

1) $2(2MgO{\cdot}SiO_2) + 3H_2O = (MgO{\cdot}2Mg(OH)_2{\cdot}2SiO_2) + Mg(OH)_2 + H_2$
Fosterite Water Serpentine Brucite

2) $2(2FeO{\cdot}SiO_2) + 3H_2O = (FeO{\cdot}2Fe(OH)_2{\cdot}2SiO_2) + Fe(OH)_2 + H_2$
Fayalite Water Fe-Serpentine Fe-Brucite

3) $4(2FeO{\cdot}SiO_2) + 5H_2O + 2O_2 = (FeO{\cdot}2Fe(OH)_2{\cdot}2SiO_2) + 2Fe(OH)_2 + (FeO{\cdot}Fe_2O_3) + 2SiO_2 + 2H_2$
Fayalite Water Fe-Serpentine Fe-Brucite Magnetite Quartz

4) $5(2MgO{\cdot}SiO_2) + 5Al_2O_3 + 10SiO_2 + 10H_2O = 5(Mg(OH)_2{\cdot}MgO{\cdot}Al_2O_3{\cdot}3SiO_2) + 5H_2$
Fosterite Alumina Silica Water Chlorite

5) $17(MgO{\cdot}2Mg(OH)_2{\cdot}2SiO_2) = (17MgO{\cdot}31Mg(OH)_2{\cdot}34SiO_2) + 3Mg(OH)_2$
Chrysotile Antigorite Brucite

6) $(4Mg(OH)_2{\cdot}MgO{\cdot}Al_2O_3{\cdot}3SiO_2) + 5SiO_2 + 2CaO = (2CaO{\cdot}4MgO{\cdot}Mg(OH)_2{\cdot}8SiO_2) + 3H_2O + Al_2O_3$
Chlorite Silica Lime Tremolite Water Alumina

7) $4(CaO{\cdot}MgO{\cdot}2SiO_2) + MgO + H_2O = (2CaO{\cdot}4MgO{\cdot}MgOH)_2{\cdot}8SiO_2) + 2CaO$
Ca-Pyroxene Tremolite Lime

8) $2(CaO{\cdot}Al_2O_3{\cdot}2SiO_2) + 9(2MgO{\cdot}SiO_2) + 2(MgO{\cdot}CaO{\cdot}2SiO_2) + 10H_2O + 5SiO_2 =$
Glass Olivine Ca-Pyroxene Water Quartz

$2(4Mg(OH)_2{\cdot}MgO{\cdot}Al_2O_3{\cdot}3SiO_2) + 2(2CaO{\cdot}4MgO{\cdot}Mg(OH)_2{\cdot}8SiO_2)$
Chlorite Tremolite

The observed mineral assemblages of the Woodburn Lake Group komatiites and associated basalts indicate that the peak temperature of regional metamorphism was upper greenschist to lower amphibolite facies with a maximum temperature of 400°C to 450°C. Greenschist facies appears to be the most common since the dominant mineral assemblage is tremolite + chlorite + antigorite + Cr-magnetite. This agrees with macroscopic mineral assemblages observed in the associated metasediments by Ashton (1982). Ashton (1982) found kyanite - chlorite - white mica - quartz and chloritoid - chlorite - white mica - quartz in the quartzites and

phyllitic schists, respectively. Fraser (1988) found andalusite, sillimanite, and garnet in the metasediments associated with the Woodburn Lake Group volcanics, indicative of lower to middle amphibolite grade. Fraser (1988) also found kyanite in the quartzites and suggested that this indicates "temperatures typical of greenschist or subgreenschist metamorphism" in the low-pressure portion of the kyanite stability field (i.e. moderate pressure).

The Woodburn Lake Group komatiitic assemblages can be represented in the system $MgO-CaO-SiO_2-Al_2O_3-H_2O-CO_2$. Chlorite is found in all of the ultramafic rocks, thus being stable over the P-T-X conditions under consideration. Therefore the Al_2O_3 component can be eliminated by projecting from chlorite. Most of the rocks have very low content of CO_2 and therefore they can be expressed in the $MgO-CaO-SiO_2-H_2O$ system (Turner, 1981). This is shown in Figure 55. The dominant mineral assemblage of tremolite + chlorite + antigorite + Cr-magnetite suggests the maximum and minimum temperatures of most of the komatiitic rocks. The chrysotile to antigorite reactions generally occur at temperatures less than 300°C, whereas the antigorite to olivine reactions occur between 400°C and 500°C depending upon the presence (curve 1, Figure 55) or absence (curve 3, Figure 55) of brucite. The breakdown of high-temperature serpentine (curve 3) takes place by the reaction:

$$\text{antigorite} = \text{forsterite} + \text{talc} + H_2O$$

at temperatures of 500°C to 550°C and pressure of 1 kb to 5 kb

Figure 55. A PT diagram for the $MgO-CaO-SiO_2-H_2O$ system (after Turner, 1981 and Jölly, 1982) showing the stability relationships among fosterite (Fo), enstatite (En), anthophyllite (Ath), diopside (Di), tremolite (Trm), actinolite (Act), brucite (Br), hornblende (Hb), talc (Tc), and quartz (Qz).

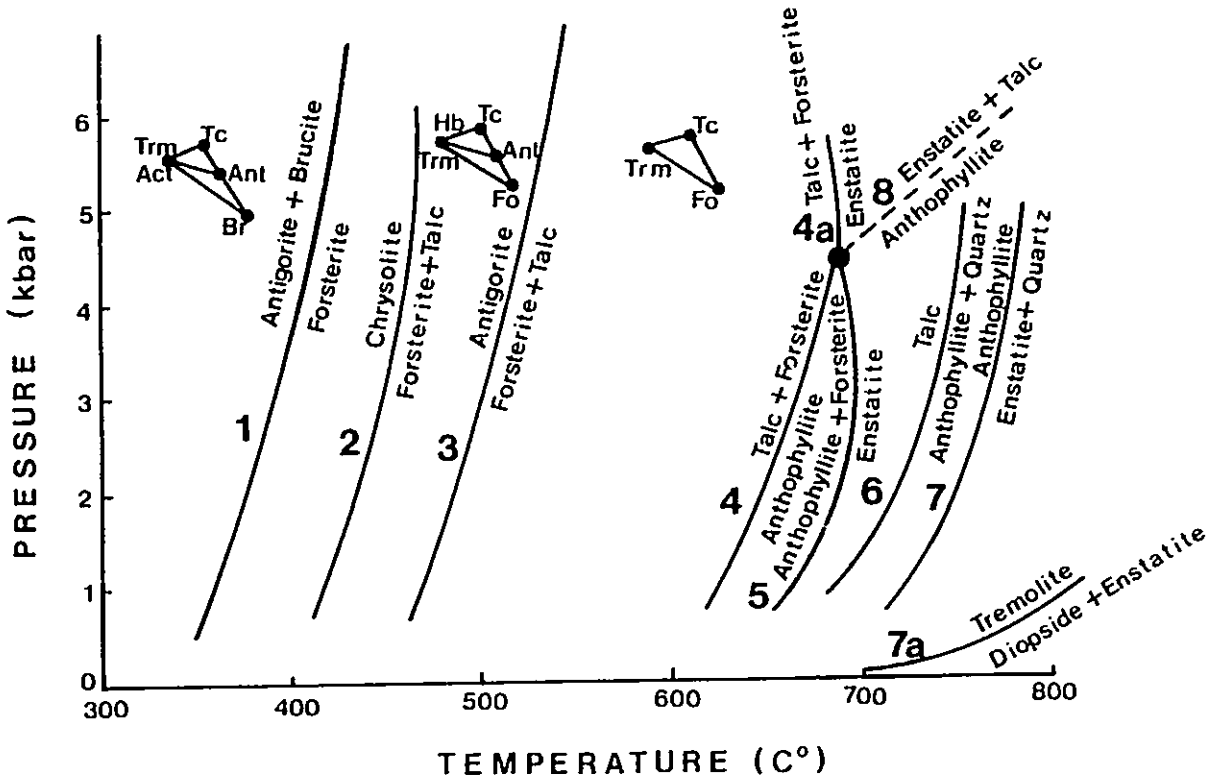
PRESSURE (kbar)
TEMPERATURE (C°)
0
1
2
3
4
5
6
300
400
500
600
700
800
Trm
Tc
Act
Ant
Br
Hb
Fo
1
Antigorite + Brucite
Forsterite
2
Chrysolite
Forsterite+Talc
3
Antigorite
Forsterite+Talc
4
Talc + Forsterite
Anthophyllite
4a
5
Anthophyllite +Forsterite
6
Enstatite
7
Talc
Anthophyllite + Quartz
7a
Tremolite
Diopside +Enstatite
8
Enstatite + Talc
Anthophyllite
Anthophyllite
Enstatite+ Quartz

(Turner, 1981). The presence of abundant tremolite indicates that CaO is an important chemical constituant of these rocks. Diopside was not observed in these rocks although it should be stable relative to tremolite at temperatures below 450°C. However, the content of Ca relative to Si and Al in the original rock appears to control the presence and absence of tremolite.

Locally, CO_2 is abundant in the rocks. The Al_2O_3 component can be treated as above. In a similar manner, tremolite can account for most of the calcium in the rocks (Gole et al., 1987). Therefore the rocks can be represented in the $MgO-SiO_2-H_2O-CO_2$ system, as shown in Figure 56. Talc is found in some of the rocks, especially replacing antigorite in the cumulate zone rocks. This is suggestive of temperatures between 375°C and 500°C, since no forsterite is present in the dominant mineral assemblage. The presence of talc is attributed to an influx of CO_2 from the surrounding rocks since the rocks with talc have, in general, higher CO_2 contents. Probably associated with this CO_2 influx is a metasomatic introduction of SiO_2 since talc-rich assemblages have higher silica contents.

In summary, the ultramafic mineral assemblages constrain the peak regional metamorphic conditions to 400°C to 450°C, relatively low pressure, and relatively water-rich fluid.

Contact metamorphism has significantly reconstituted some of the ultramafic rocks by transforming antigorite - chlorite - tremolite dominated assemblages to olivine - spinel - anthophyllite (minor) - chlorite - tremolite - antigorite - talc

Figure 56. An isobaric $TX_{H2O-CO2}$ diagram for the $MgO-SiO_2-H_2O-CO_2$ system at 2 kb and 3 kb (from Berman et al., 1987) showing the stability relationships among fosterite (Fo), enstatite (En), anthophyllite (Ath), talc (tc), antigorite (Atg), magnesite (Mst), and quartz (Qz).

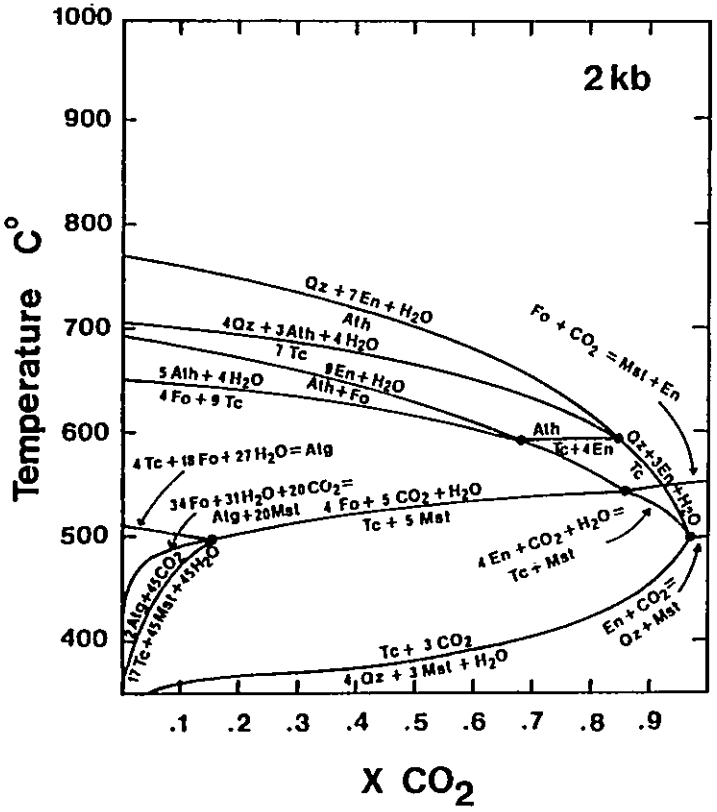
2 kb
Temperature C°
X CO2
1000
900
800
700
600
500
400
.1
.2
.3
.4
.5
.6
.7
.8
.9
Qz + 7 En + H2O
Ath
4 Qz + 3 Ath + 4 H2O
7 Tc
9 En + H2O
Ath + Fo
5 Ath + 4 H2O
4 Fo + 9 Tc
Fo + CO2 = Mst + En
Ath
Tc + 4 En
Qz + 3 En + H2O
Tc
4 Tc + 18 Fo + 27 H2O = Alg
34 Fo + 31 H2O + 20 CO2 =
Alg + 20 Mst
4 Fo + 5 CO2 + H2O
Tc + 5 Mst
4 En + CO2 + H2O =
Tc + Mst
En + CO2 =
Qz + Mst
Tc + 3 CO2
4 Qz + 3 Mst + H2O
Alg + 45 CO2
17 Tc + 45 Mst + 45 H2O

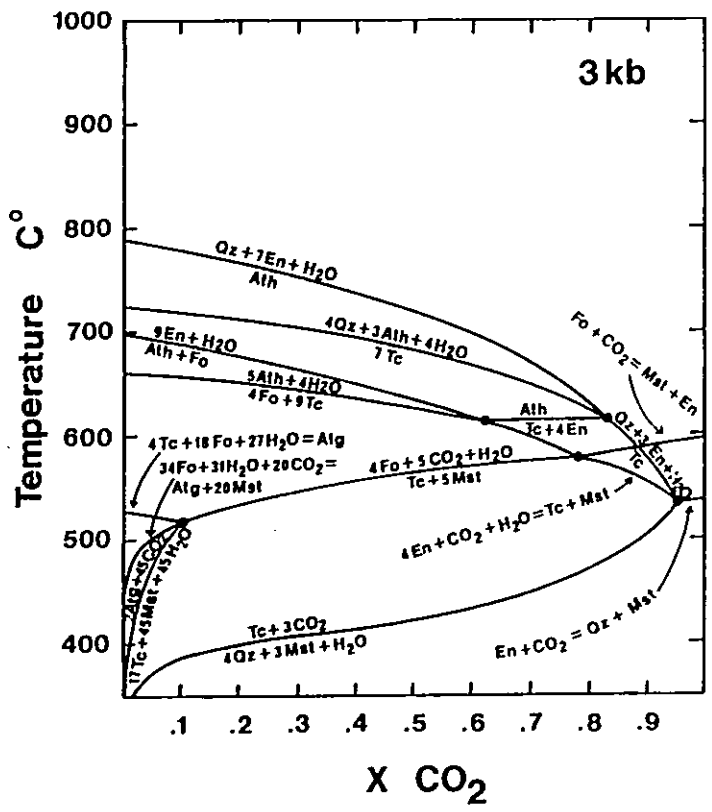
3 kb
Temperature C°
X CO2
1000
900
800
700
600
500
400
.1
.2
.3
.4
.5
.6
.7
.8
.9
Qz + 7 En + H2O
Ath
4 Qz + 3 Ath + 4 H2O
7 Tc
9 En + H2O
Ath + Fo
5 Ath + 4 H2O
4 Fo + 9 Tc
Fo + CO2 = Mst + En
Ath
Tc + 4 En
Qz + 3 En + H2O
Tc
4 Tc + 18 Fo + 27 H2O = Alg
34 Fo + 31 H2O + 20 CO2 =
Alg + 20 Mst
4 Fo + 5 CO2 + H2O
Tc + 5 Mst
4 En + CO2 + H2O = Tc + Mst
En + CO2 = Qz + Mst
Tc + 3 CO2
4 Qz + 3 Mst + H2O
Alg + 45 CO2
17 Tc + 45 Mst + 45 H2O

assemblages. The minor presence of anthophyllite and the absence of enstatite suggests temperatures less than 680°C (curve 4, Figure 55) and pressures less than 4 kb (curve 4a, Figure 55). This temperature estimate agrees with that determined with the olivine-spinel geothermometer.

PETROGENESIS OF THE WOODBURN LAKE GROUP KOMATIITES AND KOMATIITIC-THOLEIITIC BASALTS

6.1 INTRODUCTION

In this chapter, the field and petrographic observations and the chemical data presented in the previous chapters will be used to evaluate and model the petrogenetic history of the Woodburn Lake Group komatiitic and tholeiitic rocks. Petrographic observations and chemical data demonstrate that all the Woodburn Lake Group rocks have been affected by hydrous secondary alteration. The previous chapters on alteration and metamorphism have indicated some minor element mobility with varying amounts of H_2O added to the rocks. In most instances, alteration has involved the addition of H_2O only, without changing the ratios between elements. Consequently, the chemical variations shown within and between the komatiites, komatiitic basalts, and tholeiites are considered mostly to be primary. These differences in primary chemical characteristics are the result of one or, more likely, a combined effect of several of the following igneous processes : a) partial melting, b) pre-eruptive fractional crystallization, c) post-eruptive fractional crystallization, d) crustal assimilation, and e) magma mixing. Each of these processes will be considered along with possible differences in source mineralogy and chemistry, and implications

of tectonic environment in the following discussion.

6.2 PETROGENESIS OF THE KOMATIITES

Most of the compositional variation observed within the Woodburn Lake Group komatiitic lavas is the result of post-eruptive processes and this is substantiated by petrographic observations and chemical profiles through the lava flows. These processes include in-situ crystal growth, crystal settling, and crystal accumulation (i.e. within-flow differentiation - Donaldson, 1982; Barnes et al., 1983; Lesher et al., 1984; Barnes, 1985; Arndt, 1986a; among others). The products of these processes are best seen within the spinifex-textured komatiites. Before modelling these processes one must establish with some degree of confidence the composition of the initial komatiitic liquid and the liquidus minerals. This will be attempted before modelling the fractional crystallization processes.

6.2.1. COMPOSITION OF THE INITIAL KOMATIITIC LIQUID AND THE LIQUIDUS OLIVINE

No primary minerals were found in the Woodburn Lake Group komatiites due to alteration and metamorphism. This restricts somewhat the modelling of post-eruptive fractional crystallization within the Woodburn Lake Group komatiitic flows. Other studies on the basis of relict igneous minerals, microprobe

data, textural criteria, and whole rock chemical trends (Arndt, 1986a; among others) indicate that olivine and minor oxides and sulfides are the predominant liquidus phases of komatiites. The direct correlation between MgO and NiO and the inverse correlation between MgO and Al_2O_3, TiO_2, V, and Sc exhibit the type of pattern characteristic of olivine fractionation. Also, as previously mentioned, the AMC diagram (Fig. 32) is most easily explained by olivine fractionation, followed by olivine plus clinopyroxene fractionation. Experimental studies by Arndt (1976 and 1977) of natural komatiitic melts indicate that olivine and chromite are on the liquidus at 1.0 atmosphere.

The forsterite content of the Woodburn Lake Group liquidus olivine was deduced by two methods used by other researchers (Bickle et al., 1977; Barnes et al., 1983, Barnes, 1985). The first method assumes that the trend lines on XY plots of MgO versus elemental oxides and trace elements incompatible with the olivine structure (i.e. Al_2O_3, TiO_2, V, Sc) are mixing lines between olivine and the melt from which it crystallized. Hence, the intercept on the MgO axis is the estimated MgO content (i.e. forsterite content) of the olivine. On this basis, the MgO content of the olivine was estimated to be 50-53 wt% (Fo_{91-93}). Alternatively, the composition of the liquidus olivine can be calculated using the olivine-liquid Fe-Mg distribution constant ($K^{Ol/Liq}_D$ of Fe-Mg = 0.30) of Roeder and Emslie (1970) on a initial liquid of known composition. Chill margins and upper portions of spinifex-textured zones are the usual candidates for

initial liquid composition (Arndt et al., 1977; Arndt, 1986a). Chill margins to estimate the initial liquid composition are not always present. Arndt et al. (1977), Smith et al. (1980), Barnes (1983), and Barnes (1985), among others, found that randomly oriented spinifex-textured zone samples have compositions which closely approximate the chill margins and thus can be inferred to represent the initial liquid composition. Smith et al. (1980) also suggested using a weighted average of the entire flow to approximate the initial liquid. This second approach was tried on some randomly oriented spinifex-textured samples and this resulted in olivine compositions of Fo_{90-94}, close to the values determined by MgO intercept method. Estimated forsterite contents are approximately the same within all of the Woodburn Lake Group belts.

6.2.2 MODEL OF COOLING AND FRACTIONATION OF THE WOODBURN LAKE GROUP KOMATIITIC LAVAS

The characteristics of komatiite lava flows are well known and have been described in detail (Nesbitt, 1971; Pyke et al., 1973; Lewis and Williams, 1973; Arndt et al., 1977 and 1979; Smith et al., 1980; Arndt and Nesbitt, 1982b; Smith and Erlank, 1982; Beswick, 1983; Barnes et al., 1983; Viljoen et al., 1983; Barnes, 1985; Arndt, 1986a; Arndt and Jenner, 1986). Spinifex-textured komatiite flows are unique among the various flow types and have only been studied in detail in the Abitibi

Greenstone belt (Pyke et al., 1973; Arndt et al., 1977; Lajoie and Gelinas, 1978; Beswick, 1983; Arndt, 1986a) and the Barberton Mountain Land (Smith et al., 1980 and Viljoen et al., 1983). The generalized patterns of textural and compositional layering shown within spinifex-textured komatiite flows are well summarized by Donaldson (1982). As pointed out by many, there are variations and exceptions to this layering classification. Donaldson (1982) presented the petrologic problems of producing spinifex-textured layered flows and reviewed the various crystallization models on the origin of layering within komatiite lava flows. Donaldson (1982) also outlined the factors responsible for generating the layering and causing the differences in flow units, locally and regionally. He stated that several variants of crystallization history are possible within a single flow unit (i.e. along strike).

Until recently, research on layered komatiites suggested that the cumulate zone (B-zone) formed by gravitational settling of olivine crystals and the spinifex-textured zone represented frozen liquids. Bickle (1982) suggested that convective velocities within cooling komatiite lava flows, most likely, are greater than olivine settling velocities. Experimental work by Turner et al. (1986) confirms this and suggests that another mechanism is necessary to explain the formation of the cumulate zone. Donaldson (1982), Barnes et al. (1983), and Barnes (1985) hypothesized that the major portion of the spinifex-textured zone does not represent frozen liquid, but instead is a crescumulate

resulting from stalactite growth of olivine and/or pyroxene into an evolving liquid.

Up until 1982, most crystallization models of layered komatiites considered that the flows solidify under nearly static conditions. Recent work by Barnes et al. (1983), Huppert et al. (1984), Barnes (1985), Huppert and Sparks (1985a), Kinzler and Grove (1985), and Arndt (1986a) provides evidence that conditions were both static and dynamic (i.e. turbulent) during flowage, cooling, and crystallization of komatiitic lavas. Mass balance calculations by Barnes et al. (1983) and Barnes (1985) suggest that the B_2-zone should be half as thick as the A_3-zone but field observations show the two zones to be of similar thickness. These observations point towards either an open system (i.e. magma replenishment) or abundant intratelluric olivines being carried by the flow. Barnes (1985) concluded that the spinifex-textured and cumulate zones formed during quiescent periods between episodic magma influxes along lava tubes. Huppert and Sparks (1985a) and Turner et al. (1986) have experimentally investigated the cooling and crystallization of komatiitic lava flows and shown that spinifex textures form by constitutional supercooling as a result of compositional convection. Their experiments (Turner et al., 1986) provide an alternative mechanism to crystal settling and intertelluric olivines in forming the cumulate zones. They envisaged the cumulate zone forming as a consequence of progressive enrichment of olivine grains in an ever decreasing, lower convective layer during development of a nearly

static upper spinifex zone. This model also assumes an upward migration and accumulation of differentiated liquid. Arndt (1986a) has similarly explained the differentiation (i.e. layering) differentiation (i.e. layering) of komatiitic lava flows, but entirely by the convective redistribution of olivine phenocrysts and the crystallization of trapped liquid. Both these models alleviate the above mentioned problem inferred by the mass balance calculations of Barnes (1985).

The effects of fractional crystallization on the chemistry of the initial liquid during emplacement of the Woodburn Lake Group komatiites have been calculated. The effects were calculated by modelling major element variations within several flow units. Initial models assumed: a) olivine of Fo_{92-93} composition (refer to Appendix D1 for source of mineral data used in mass balance calculations) as the only fractionating phase and b) an initial liquid composition represented by chill margins or randomly oriented spinifex-textured samples. The least-squares linear mixing method of Bryan et al. (1969) was used to calculate the amount of olivine that fractionated from the A-zone and accumulated into the B-zone (e.g. AK-15c and AK-15d). Those elements which are considered to be extremely mobile were not used in the calculations. The results (Table 20) show that olivine fractionation can explain reasonably well the major and trace element variations shown between the spinifex-textured zone and the cumulate zone, and across the cumulate zone, but not those within the spinifex-textured zone. Modelling of the B-zone

Table 20a. Results of mass balance fractional crystallization calculations involving olivine in the formation of spinifex-textured flows.

INPUT DATA:

	PARENT	FOR-92	DAUGHTER
SiO_2	45.12	40.30	45.46
TiO_2	0.36	0.00	0.29
Al_2O_3	8.39	0.00	6.91
FeO	11.03	7.97	10.50
MnO	0.18	0.16	0.17
MgO	25.62	51.13	28.92
CaO	6.94	0.25	5.53
Na_2O	0.84	0.00	0.67
K_2O	0.03	0.00	0.05
Cr_2O_3	0.43	0.17	0.39

(PARENT - MINERALS = DAUGHTER)

PARENT: AK-15d (upper portion of spinifex-textured zone)
DAUGHTER: AK-15a (base of cumulate zone)

	SOLUTION	% CUMULATE
AK-15d	1.000	
FOR-92	0.148	100.000
AK-15a	1.148	

R SQUARED = 0.990 (sum (calculated - observed)^2)

	PARENT ANALYSIS	DAUGHTER ANALYSIS	DAUGHTER CALC.	WEIGHTED RESID.
SiO_2	45.12	45.46	45.04	0.42
TiO_2	0.36	0.29	0.32	-0.03
Al_2O_3	8.39	6.91	7.41	-0.50
FeO	11.03	10.50	10.77	-0.27
MnO	0.18	0.17	0.18	-0.01
MgO	25.62	28.92	29.20	-0.29
CaO	6.94	5.53	6.17	-0.63
Na_2O	0.84	0.67	0.74	-0.07
K_2O	0.03	0.05	0.03	0.03
Cr_2O_3	0.43	0.39	0.40	-0.01

Table 20b. Results of mass balance fractional crystallization calculations involving olivine in the formation of spinifex-textured flows.

INPUT DATA:

	PARENT	FOR-92	DAUGHTER
SiO_2	45.12	40.30	45.16
TiO_2	0.36	0.00	0.28
Al_2O_3	8.39	0.00	6.63
FeO	11.03	7.97	10.43
MnO	0.18	0.16	0.18
MgO	25.62	51.13	31.04
CaO	6.94	0.25	4.19
Na_2O	0.84	0.00	0.54
K_2O	0.03	0.00	0.04
Cr_2O_3	0.43	0.17	0.40

(PARENT - MINERALS = DAUGHTER)

PARENT: AK-15d (upper portion of spinifex-textured zone)
DAUGHTER: AK-15b (middle portion of cumulate zone)

	SOLUTION	% CUMULATE
AK-15d	1.000	
FOR-92	0.269	100.000
AK-15b	1.269	

R SQUARED = 2.379 (sum (calculated - observed)^2)

	PARENT ANALYSIS	DAUGHTER ANALYSIS	DAUGHTER CALC.	WEIGHTED RESID.
SiO_2	45.12	45.16	44.70	0.45
TiO_2	0.36	0.28	0.29	-0.01
Al_2O_3	8.39	6.63	6.72	-0.09
FeO	11.03	10.43	10.53	-0.10
MnO	0.18	0.18	0.18	0.01
MgO	25.62	31.04	31.38	-0.33
CaO	6.94	4.19	5.62	-1.42
Na_2O	0.84	0.54	0.68	-0.14
K_2O	0.03	0.04	0.03	0.02
Cr_2O_3	0.43	0.40	0.38	0.02

Note: Discrepancy in CaO is due to CaO leaching as discussed in Chapter 4.

Table 20c. Results of mass balance fractional crystallization calculations involving olivine in the formation of spinifex-textured flows.

INPUT DATA:

	PARENT	FOR-92	DAUGHTER
SiO_2	45.12	40.30	43.25
TiO_2	0.36	0.00	0.43
Al_2O_3	8.39	0.00	10.26
FeO	11.03	7.97	11.78
MnO	0.18	0.16	0.19
MgO	25.62	51.13	25.58
CaO	6.94	0.25	6.07
Na_2O	0.84	0.00	0.81
K_2O	0.03	0.00	0.05
Cr_2O_3	0.43	0.17	0.48

(PARENT - MINERALS = DAUGHTER)

PARENT: AK-15d (upper portion of spinifex-textured zone)
DAUGHTER: AK-15c (lower portion of spinifex-textured zone)

	SOLUTION	% CUMULATE
AK-15d	1.000	
FOR-92	0.003	100.000
AK-15c	1.003	

R SQUARED = 6.777 (sum (calculated - observed)^2)

	PARENT ANALYSIS	DAUGHTER ANALYSIS	DAUGHTER CALC.	WEIGHTED RESID.
SiO_2	45.12	43.25	44.05	-0.80
TiO_2	0.36	0.43	0.35	0.08
Al_2O_3	8.39	10.26	8.17	2.09
FeO	11.03	11.78	10.76	1.02
MnO	0.18	0.19	0.17	0.02
MgO	25.62	25.58	25.10	0.48
CaO	6.94	6.07	6.76	-0.69
Na_2O	0.84	0.81	0.82	-0.01
K_2O	0.03	0.05	0.03	0.02
Cr_2O_3	0.43	0.48	0.42	0.06

Table 20d. Results of mass balance fractionational crystallization calculations involving olivine in the formation of spinifex-textured flows.

INPUT DATA:

	PARENT	FOR-92	DAUGHTER
SiO_2	45.37	40.30	45.87
TiO_2	0.31	0.00	0.32
Al_2O_3	7.45	0.00	7.71
FeO	11.27	7.97	9.67
MnO	0.16	0.16	0.17
MgO	27.45	51.13	27.30
CaO	6.17	0.25	6.54
Na_2O	0.31	0.00	0.80
K_2O	0.00	0.00	0.07
Cr_2O_3	0.41	0.17	0.41

(PARENT - MINERALS = DAUGHTER)

PARENT: AK-14d (upper portion of spinifex-textured zone)
DAUGHTER: AK-14c (lower portion of spinifex-textured zone)

	SOLUTION	% CUMULATE
AK-14d	1.000	
FOR-92	-0.008	100.000
AK-14c	0.992	

R SQUARED = 3.222 (sum (calculated - observed)^2)

	PARENT ANALYSIS	DAUGHTER ANALYSIS	DAUGHTER CALC.	WEIGHTED RESID.
SiO_2	45.37	45.87	45.52	0.34
TiO_2	0.31	0.32	0.32	0.00
Al_2O_3	7.45	7.71	7.53	0.18
FeO	11.27	9.67	11.33	-1.65
MnO	0.16	0.17	0.16	0.01
MgO	27.45	27.30	27.32	-0.01
CaO	6.17	6.54	6.23	0.31
Na_2O	0.31	0.80	0.32	0.49
Cr_2O_3	0.41	0.41	0.41	-0.00

Table 20e. Results of mass balance fractional crystallization calculation involving olivine in the formation of spinifex-textured flows.

INPUT DATA:

	PARENT	FOR-92	DAUGHTER
SiO_2	45.37	40.30	45.06
TiO_2	0.31	0.00	0.26
Al_2O_3	7.45	0.00	6.11
FeO	11.27	7.97	10.58
MnO	0.16	0.16	0.16
MgO	27.45	51.13	32.28
CaO	6.17	0.25	3.55
Na_2O	0.31	0.00	0.43
K_2O	0.00	0.00	0.02
Cr_2O_3	0.41	0.17	0.38

(PARENT - MINERALS = DAUGHTER)

PARENT: AK-14d (upper portion of spinifex-textured zone)
DAUGHTER: AK-14b (central portion of cumulate zone)

	SOLUTION	% CUMULATE
AK-14d	1.000	
FOR-92	0.259	100.000
AK-14b	1.259	

R SQUARED = 2.375 (sum (calculated - observed)^2)

	PARENT ANALYSIS	DAUGHTER ANALYSIS	DAUGHTER CALC.	WEIGHTED RESID.
SiO_2	45.37	45.06	44.07	0.36
TiO_2	0.31	0.26	0.25	0.01
Al_2O_3	7.45	6.11	5.98	0.13
FeO	11.27	10.58	10.69	-0.10
MnO	0.16	0.16	0.16	-0.00
MgO	27.45	32.28	32.54	-0.26
CaO	6.17	3.55	5.00	-1.46
Na_2O	0.31	0.43	0.25	0.18
Cr_2O_3	0.41	0.38	0.36	0.01

by olivine accumulation is good, except for CaO values, but this is easily explained by CaO depletion during serpentinization. Correction for CaO, by assuming CaO/Al_2O_3 has a chondrite value, results in a near-perfect fit.

Some of the spinifex-textured zones (e.g. AK-14c and AK-15c) show poor matches between observed and estimated compositions. It was noted earlier that an inflection point between the spinifex-textured zone and the cumulate zone samples is present in the variation diagrams. Figure 57 illustrates the common situation that exists between the spinifex-textured zone and cumulate zone samples on plots of MgO versus other elements incompatible with olivine. The diagram shows that the spinifex-textured zone samples define a trend that is significantly different from the trend of the cumulate zone samples. In most instances, the trend of the spinifex-textured zone samples is consistently rotated away from the cumulate trend to the point where it intercepts the MgO axis between 30 and 35 wt% MgO.

This change in slope of trend lines is believed to represent a real igneous process, since the migration of elements like Ti, Al, V, Sc, among others, has been shown as minimal. One must now consider the possibility of another phase crystallizing with olivine because if alteration and metamorphism were the cause, then both the spinifex-textured and the cumulate zones should be affected in an unsystematic manner. The chemical data of the Woodburn Lake Group komatiites supports another phase

Figure 57. Schematic representation of the very different trends defined by the spinifex-textured zone samples and the cumulate zone samples, on oxide and/or element vs MgO (wt%) variation diagrams. Olivine and CPX fields represent the compositions of olivine and clinopyroxene, respectively, found in komatiites (See Appendix D1 for references).

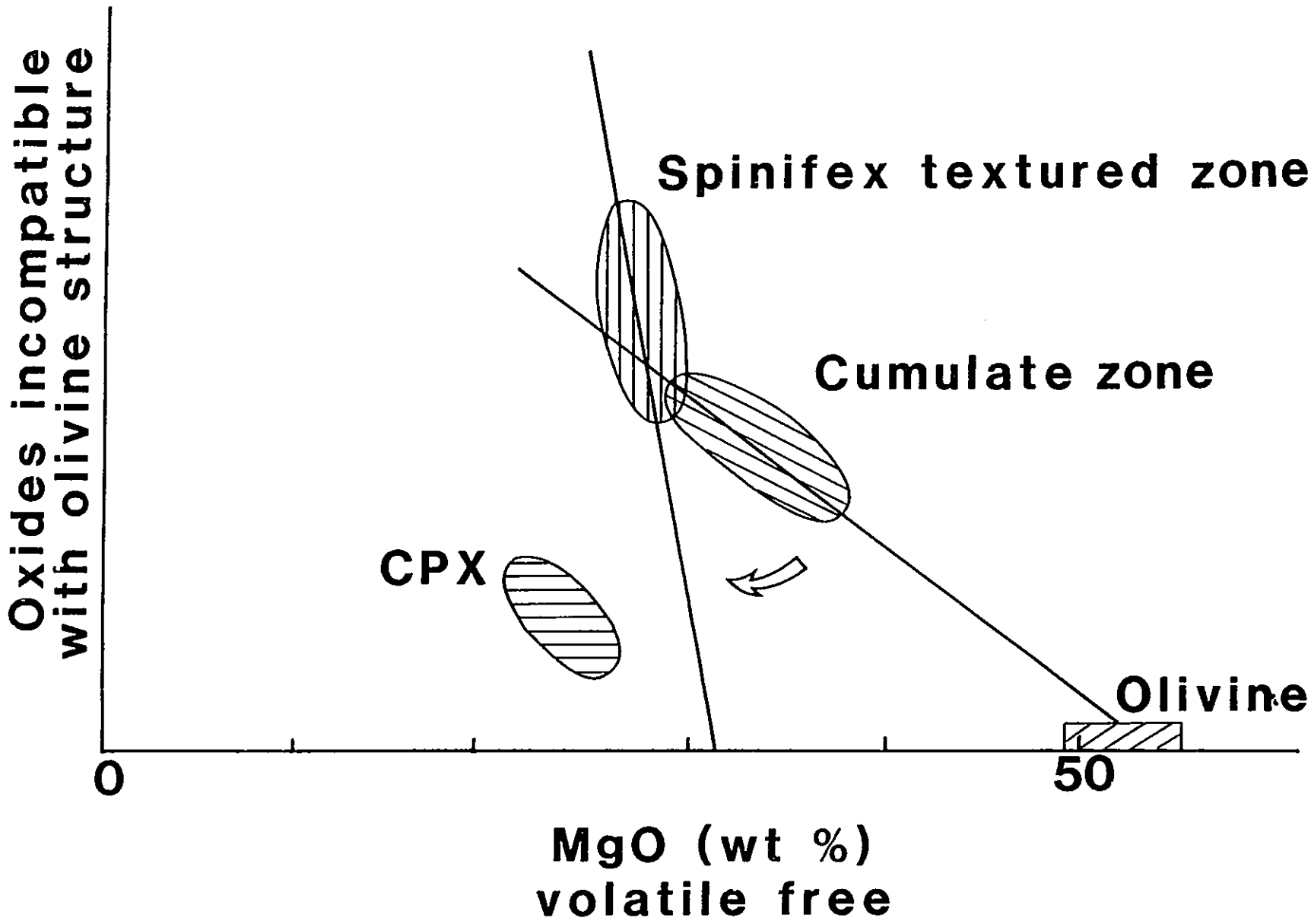
Oxides incompatible with olivine structure
Spinifex textured zone
Cumulate zone
CPX
Olivine
0
50
MgO (wt %) volatile free

crystallizing later with olivine since the geochemical profiles across flows do not show the drastically lower MgO contents at the base of the spinifex-textured zones, which would indicate that only olivine was fractionating out. Petrographic observations also suggest another phase. This phase is most likely sub-calcic or calcic pyroxene (i.e. pigeonite or augite) since skeletal and acicular outlines of clinopyroxene were observed.

Further consideration of this change in slope of trend lines on Figure 57 shows that a line drawn between hypothetical olivine and pyroxene compositions would intercept the spinifex-textured zone trend line. This point would represent the average composition of olivine and pyroxene being removed. Application of the lever rule would give the percentages of olivine and pyroxene crystallizing at that point in time (Note: in the figure this would be approximatly 30% olivine and 70% clinopyroxene). An approximate liquid line of descent is shown since no original mineralogy is present to accurately constrain this line. This liquid line of descent is steeper than the one controlled only by olivine fractionation. Additional calculations (see Table 21) with sub-calcic or calcic pyroxene joining olivine (analyses from Barnes, 1985, and Barnes et al., 1983) as a fractionating phase give better fits between observed and estimated compositions of the spinifex-textured zones.

Some trace elements were used to test the validity of the olivine only fractionation model versus the olivine and

Table 21. Results of mass balance fractional crystallization calculations involving olivine plus clinopyroxene in the formation of spinifex-textured flows.

INPUT DATA:

	PARENT	FOR-92	AUG	DAUGHTER
SiO_2	45.13	40.30	51.13	43.25
TiO_2	0.36	0.00	0.22	0.43
Al_2O_3	8.39	0.00	3.51	10.26
FeO	11.03	7.97	9.26	11.78
MnO	0.18	0.16	0.22	0.19
MgO	25.62	51.13	20.90	25.58
CaO	6.94	0.25	12.99	6.07
Na_2O	0.84	0.00	0.00	0.81
K_2O	0.03	0.00	0.00	0.05
Cr_2O_3	0.43	0.17	0.77	0.48

(PARENT - MINERALS = DAUGHTER)

PARENT: AK-15d (upper portion of spinifex-textured zone)
DAUGHTER: AK-15c (lower portion of spinifex-textured zone)

	SOLUTION	% CUMULATE
AK-15d	1.000	
FOR-92	-0.039	15.937
AUG	-0.205	84.063
AK-15c	0.756	

R SQUARED = 0.452 (sum (calculated - observed)^2)

	PARENT ANALYSIS	DAUGHTER ANALYSIS	DAUGHTER CALC.	WEIGHTED RESID.
SiO_2	45.13	43.25	43.47	-0.22
TiO_2	0.36	0.43	0.42	0.01
Al_2O_3	8.39	10.26	10.10	0.16
FeO	11.03	11.78	11.61	0.17
MnO	0.18	0.19	0.16	0.03
MgO	25.62	25.58	25.43	0.15
CaO	6.94	6.07	5.60	0.47
Na_2O	0.84	0.81	1.11	-0.30
K_2O	0.03	0.05	0.04	0.01
Cr_2O_3	0.43	0.48	0.34	0.13

sub-calcic or calcic pyroxene fractionation model. Calculated trace elements were obtained using the following Rayleigh fractionation equation: C = Co/F or F = Co/C, where F is the % melt and C is the concentration of the trace element. In most cases, good agreement was found between observed and calculated trace elements, except Cr, thus supporting the olivine plus sub-calcic or calcic pyroxene fractional crystallization model. The variation between the observed and calculated Cr values can not be explained by clinopyroxene alone because of the unreasonably high proportion of clinopyroxene needed. Therefore, another Cr-rich phase must be responsible for fractionating Cr. As mentioned earlier, this phase is chromite. Modelling calculations suggest 1 - 2 wt% crystallization of chromite to explain the Cr variation and this is in agreement with petrographic and other geochemical data.

Until recently, most komatiite research (Donaldson, 1982; Barnes, 1985; Arndt, 1986a; among others) stated that only olivine and possibly chromite fractionated from komatiitic liquids and clinopyroxene from komatiitic basaltic liquids. Campbell and Arndt (1982) suggested the metastable crystallization of low-Ca pyroxene within clinopyroxene spinifex-textured flows as the result of supercooling. Barnes (1985) alternatively explained the presence of low-Ca pyroxene by suggesting olivine fractionation is predominant until the pyroxene liquidus phase boundary is reached, at which point both olivine and low-Ca pyroxene crystallize. Experimental work by

Kinzler and Grove (1985) supports Barnes' explanation and suggests that magma mixing and crustal assimilation/contamination may also play important roles in the fractional crystallization history of komatiitic flows. Recent work by Blais et al. (1987) demonstrated that low-Ca pyroxene does indeed fractionate from komatiitic liquids. They suggested that the physico-chemical conditions operating within a flow unit dictate whether olivine alone or olivine plus clinopyroxene fractionates from komatiitic liquids. This thesis agrees with the results of Blais et al. (1987). The author feels that some of the komatiite occurrences elsewhere should be re-examined in light of these new findings.

The lack of preserved primary minerals makes it impossible to monitor closely the manner in which the composition of magma, as represented by the Woodburn Lake Group lava flows, changes as the spinifex-textured zone forms. However, it is possible, using the models of Donaldson (1982), Barnes (1985), and Arndt (1986a) with petrographic observations and geochemical profiles across flows, to formulate a general model for the development of the spinifex-textured komatiite flows.

The model proposed is as follows (Fig. 58a and b). The komatiite lava is emplaced as flows or tubes under highly turbulent conditions (Huppert et al., 1984). Upper and lower chill margins form. Heat is transported efficiently to the flow tops due to the turbulent nature of the flow. This prevents a thick chill margin from forming. Spinifex-textured olivine starts to crystallize from this cooler roof, only after the flow

Figure 58a. Schematic diagram representing the formation of a komatiite flow from the Woodburn Lake Group. Position within evolving flow unit dictates the type of ultramafic flow that is produced.

Figure 58b. Details of crescumulate growth of spinifex blades into convecting liquid. "Depleted" means olivine-depleted, hence depleted in those elements compatible with the olivine structure.

A.

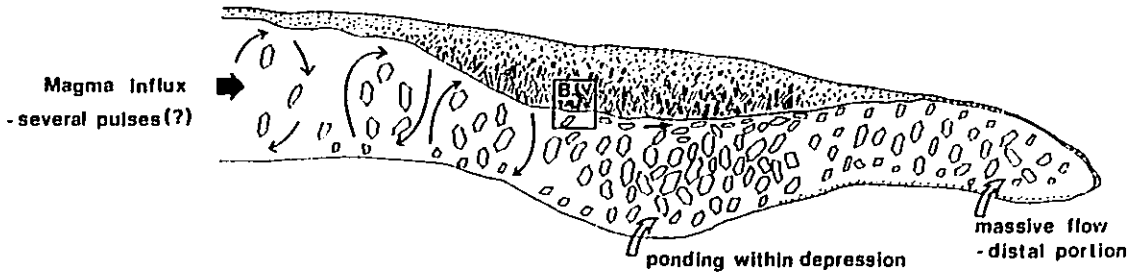
Magma influx
- several pulses(?)
B.V.
massive flow
- distal portion
ponding within depression

B.

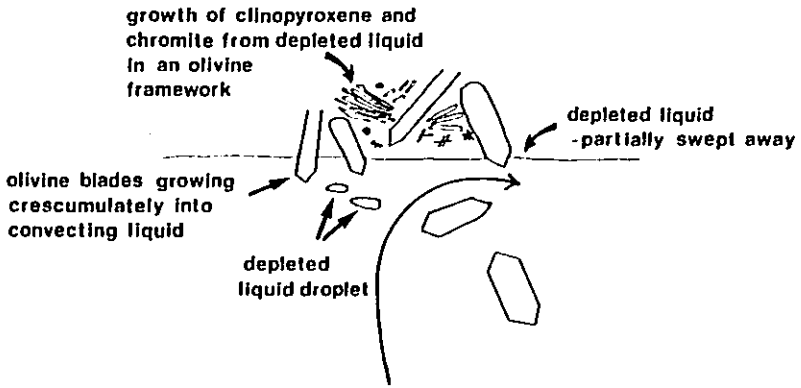
growth of clinopyroxene and chromite from depleted liquid in an olivine framework
depleted liquid
- partially swept away
olivine blades growing crescumulately into convecting liquid
depleted liquid droplet

conditions decrease in intensity due to ponding or back up of magma behind a solidified flow front (Arndt, 1986a). The spinifex-textured zone grows as a crescumulate (Barnes, 1985) from the top downwards into convecting liquid (Fig.58b). In this manner a framework of olivine is built with some evolved liquid trapped inside. Some of this olivine-depleted liquid is possibly mixed with the lower convecting liquid. This depleted trapped liquid reaches a point where olivine, clinopyroxene and chromite crystallize and finally only clinopyroxene and chromite crystallize. Meanwhile, in the lower part of the flow, olivine phenocrysts are fractionating out and growing as equant to elongate grains. The turbulent nature of the flow keeps the olivine phenocrysts in suspension. These olivine phenocrysts continue to crystallize as the spinifex-textured zone grows thicker, but they become relatively more abundant in a continuously decreasing volume of convecting liquid. According to Arndt (1986a) when the relative abundance of olivine phenocrysts in the remaining liquid exceeds 50%, convection stops and the flow freezes. This model is consistent in explaining the upward increase in MgO content across the cumulate zone. One can imagine that some olivine phenocrysts do settle out into a lowermost layer which would solidify through time (Marsh and Maxey, 1985). Furthermore, the olivine phenocrysts grow with time and this would explain the upward increase in size and abundance through the cumulate zone.

This proposed model assumes that the flow operated as a

closed system. However the chemical variations within the Woodburn Lake Group komatiites (see Figs.49 and 50), across some of the flows, indicate that this may not be the case. The zig-zag patterns in the spinifex-textured zone may possibly indicate periodic, new, small batches of primitive magma that mix with the convective magma. This would result in higher MgO and Ni contents and slightly lower incompatible element values. However, this is difficult to document without closer sampling intervals and primary mineralogy. A new pulse of magma would result, in many instances, in a change in forsterite content of the olivine. Also, the zig-zag pattern would probably show more as a step-like pattern. Another possibility is that the zig-zag pattern shows the effects of crustal contamination on the komatiitic lavas. This crustal contamination could have taken place en route to the surface or on the surface over which the komatiites flowed. A possibility of the latter situation is given by the REE chemistry of sample AK-13a which is found close to the rhyolites.

6.2.3 PARTIAL MELTING

In order to understand the effects of partial melting on the chemistry of the initial komatiitic liquids of the Woodburn Lake Group, several processes and factors must be considered. These factors and processes include: a) the chemical, physical, and thermal conditions of the source material, b) the degree, depth, and physico-chemical conditions of partial melting, c) the

chemical and physical nature of komatiitic liquids, d) the degree of fractional crystallization that may have taken place en route to the surface, and e) the degree and kind of crustal contamination that may have occurred (Note: the role of post-eruptive fractional crystallization has been discussed). It is necessary to determine to what degree each process and factor contributed to the present chemistry. It is especially important, if possible, to understand the petrogenetic history of the initial liquid en route to the surface. Otherwise, one will not know if the initial liquid erupted on the surface is primary or not. An extensive review of the "state of the art" of komatiite petrogenesis will be presented first, followed by the petrogenetic modelling and discussion of the Woodburn Lake Group komatiites.

The origin of komatiites has been discussed in great detail over the last 18 years (Arndt, 1986b; Arndt et al., 1986a; and Nisbet, 1987). Investigations of komatiite petrogenesis has provided some clues to the nature and evolution of the Earth's early crust and mantle. Arndt (1986b) clearly pointed out the problems associated with using komatiites as "mantle probes". Chondrite data and spinel- and garnet-lherzolite data (summarized in Basaltic Volcanism Study Project, 1981) suggest an upper mantle of peridotitic composition (Palme and Nickel, 1985; Herzberg and O'Hara, 1985; Anderson and Bass, 1986; Takahashi, 1986). It is assumed with some degree of certainty that komatiitic magmas represent partial melts generated in the

Earth's upper mantle (Arndt, 1975; Green, 1975; O'Hara et al., 1975; Nesbitt and Sun, 1976; Bickle et al., 1977; among others).

Most researchers agree that komatiitic liquids with MgO contents of 24 to 32% erupted during Archean time (Arndt et al., 1977; Nesbitt et al., 1979; Bickle, 1982 and 1986) but Elthon (1986) estimated the most magnesian liquids to be 25% MgO. Bickle (1982) has presented strong evidence in support of the compositions of noncumulate komatiite samples being similar in composition to the liquids from which they crystallized. More recent work by Campbell and Arndt (1983), Barnes et al. (1983), Kinzler and Grove (1985), Barnes (1985), and Arndt (1986a) conclusively shows that the spinifex-textured samples have a MgO content (i.e. a higher modal olivine content) variably higher than the liquid from which the spinifex-textured olivines crystallized. This is a result of incorporating a small proportion of excess (0-30 wt%) olivine. Therefore most spinifex-textured samples, especially those of thick flows, are not representative of initial liquid composition. Consequently, Barnes (1985) and Arndt (1986a) suggested that only the upper chill zone and randomly oriented spinifex-textured samples are representative of initial liquid composition of komatiitic flows. Still, there remains the possibility that these liquids fractionated olivine within the volcanic conduits system or further upslope prior to flow differentiation or that seawater alteration changed their composition after crystallization. However, when the chill margin composition is compared to liquid

compositions, inferred from their relict liquidus olivine, there is very little or no difference. The most magnesian chill margin sample observed in komatiites is about 30% MgO, which is substantially higher than the MgO content theoretically deduced by Elthon (1986). As mentioned above, the MgO content of the Woodburn Lake Group komatiitic liquid is 27-30%.

Early experimental studies showed that komatiites have unusually high liquidus temperature (>1650°C under dry conditions) at 1 atm and low pressures (Green, 1975; Green et al., 1975; Arndt, 1976). These physical properties along with chemical properties make komatiites distinct from other lava types and introduce several constraints on their petrogenesis. Green (1975) suggested that high temperatures are necessary for the extrusion of ultramafic lavas and the formation of spinifex-textured flows. Cawthorn (1975), assuming specific conditions, showed that a mantle source at 1950°C is required to produce ultramafic lavas of 1650°C. Nesbitt and Sun (1976) agreed with this value by proposing 1900°C as the temperature necessary for komatiitic liquid genesis. To reach these temperatures they suggested that a depth of at least 200 km is needed.

Recent experimental studies on high pressure minerals and rock types (Green, 1981; Takahashi and Scarfe, 1985; Ohtani, 1984 and 1985; Takahashi, 1986) also confirmed that komatiites have unusually high liquidus temperatures (1500°C - 2000°C), low viscosities, and high densities at pressures from 1 atm to 100 kbar. This new data introduces several constraints, as well

as generating new problems, in the study of the petrogenesis of komatiites (excellently summarized by Nisbet, 1982; Takahashi, 1986; and Arndt, 1986b).

Since their discovery, many models have been proposed to explain the origin of komatiitic liquids. Early researchers of komatiites thought that they were generated by high degrees of partial melting (40-100%) of mantle material at pressures of <30 kbar to 200 kbar and temperatures from 1600°C to 2200°C. This hypothesis was invoked because of their high liquidus temperature and their chemical similarity to mantle peridotites (Green, 1975; Green et al., 1975; Cawthorn, 1975; Arndt, 1976; Nesbitt and Sun, 1976; Nesbitt et al., 1979; among others). If a high degree of partial melting is a prerequisite to produce a komatiitic liquid, then it is necessary that the partial melt fraction exceeded 40% by volume. Theoretical and experimental data (Arndt, 1977; Walker et al., 1980; Stolper et al., 1981; McKenzie, 1984; among others) shows that a partial melt of mantle peridotite will segregate from its source instantaneously when the degree of partial melting rises above a critical level (i.e. 10-30% by volume). If komatiites come from the same low pressure source as basalts, then the high temperature of komatiites also requires a large volume of basalts to be produced. The low pressure in this part of the mantle would favour basaltic liquids to separate from residual peridotites after 20-40% partial melting (Jacques and Green, 1980; Stolper, 1980; Takahashi and Kushiro, 1983).

McKenzie (1984) recognized this problem of trying to produce

komatiites by melting that part of the mantle which is the source of mid-ocean ridge basalts. McKenzie (1984) believed that komatiites are generated at greater depths than basalts, since magmas produced at higher pressures are more magnesian than those of lower pressures. According to O'Hara (1968) and O'Hara et al. (1975) low degrees of partial melting take place at high pressures. This initial or low degree of partial melting hypothesis has recently provided a second hypothesis on the degree of partial melting that is necessary in explaining the origin of komatiites (Herzberg, 1983; Herzberg and O'Hara, 1985; Takahashi and Scarfe, 1985; Takahashi, 1986; among others).

Arndt (1977) pointed out that it would be difficult to prevent magma separation and ascent before the degree of partial melting of the mantle source reaches a high percentage. Instead, Arndt (1977) proposed a multistage melting model in which komatiitic liquids were generated from a mantle peridotitic composition after several cycles of partial melting and melt extraction. In this model an olivine tholeiite is produced after the first cycle of melting, then a komatiitic basalt fraction after more melting, and finally a komatiitic liquid from a small amount of melting. Arndt considered this model as a better alternative to explain the differences in MgO contents, CaO/Al_2O_3 and MgO/FeO ratios, and light REE patterns between the tholeiitic and komatiitic rocks of Munro Township. Arndt's model also permits olivine and clinopyroxene to be in equilibrium with the first liquid, and garnet to be partially or completely consumed

into the melt. The complete melting of garnet would result in aluminum being depleted relative to calcium in the refractory residue, hence an abnormally high CaO/Al_2O_3 rich liquid would result with further melting. Therefore, the extremely high CaO/Al_2O_3 ratios of the South Africa komatiites could be explained by Arndt's model.

Nesbitt et al. (1979) disagreed with Arndt's model of explaining the abnormally high CaO/Al_2O_3 ratios of the Barberton Mountain Land komatiites. They postulated instead that Al partitioning and clinopyroxene melting result in a buffering of the CaO/Al_2O_3 ratio of the liquid, hence a lower CaO/Al_2O_3 ratio.

Arndt (1977) believed and Nesbitt et al. (1979) concurred that the garnet peridotitic source of komatiites has lost a melt fraction, which is more felsic than the source. The evidence for a previous melt fraction is the light REE depleted patterns of komatiites (Arndt et al., 1977; Arth et al., 1977; Sun and Nesbitt, 1978; Whitford and Arndt, 1978). There are differences of opinion on the volume and composition of this melt fraction. Arndt (1977) argued that there was a large melt fraction, whereas Nesbitt et al. (1979) believed that the melt fraction represented only a small percentage of melting or alternatively, if a large percentage melting was involved, there must have been a high percentage of melt retention. Their evidence for a small volume of melt is the presence of nearly chondritic values for the Al_2O_3/TiO_2 and CaO/TiO_2 ratios, and the light REE patterns of komatiites. This small volume change of a light REE enriched

liquid would only cause changes in the light REE contents of the komatiite source, since only incompatible elements and light REE were lost in this process. Otherwise, if a large degree of melting occurred, then, according to Nesbitt et al. (1979), retention would have to be high in order to explain the similarity of komatiitic and chondritic values of Al_2O_3/TiO_2 and CaO/TiO_2.

Nesbitt et al. (1979) agreed with part of Arndt's (1977) model in that it explains the relatively low CaO/Al_2O_3 (about 1.0) ratios of aluminum-undepleted peridotitic komatiites. By comparing the chondritic values of CaO/TiO_2 and Al_2O_3/TiO_2 to those of komatiites, they showed that CaO/Al_2O_3 values of komatiites (about 1.0) should be close to chondritic (0.82). The higher CaO/Al_2O_3 ratio could be explained by a CaO/TiO_2 ratio in komatiites that is greater than chondritic, or as suggested by Purvis (1978), a lower Al_2O_3/TiO_2 ratio (i.e. implying an aluminum-depleted source material). Nesbitt et al. (1979) suggested that sequential melting processes may explain the high CaO/Al_2O_3 ratio, based upon the light REE data of ultramafic komatiites (Sun and Nesbitt, 1978). In the case of abnormally high CaO/Al_2O_3 ratios (greater than 1.5), they proposed that the loss of garnet from the source material causes Al depletion (Green, 1975).

Nesbitt et al. (1979), on the basis of geochemical data, clearly established that komatiites fall into two distinct types, those with high CaO/Al_2O_3 ratios (Al-depleted) and those with

ratios close to one (Al-undepleted). Nesbitt et al. (1982) pointed out that the bulk of Archean komatiites are Al-undepleted, whereas the Al-depleted type commonly occur in the early Archean and may reflect an age significance. However, recent work in the Barberton Greenstone Belt, South Africa (Smith and Erlank, 1982) and the Abitibi Greenstone Belt (Cattell et al., 1984; Cattell, 1987; and Cattell and Arndt, 1987) conclusively documents contemporaneous occurrence of both types in Early Archean and Late Archean sequences, respectively. Even if the CaO/Al_2O_3 ratio does not reflect age differences, the two komatiite types indicate specific magma generation processes (i.e. garnet separation) or melting of different mantle sources (i.e. a layered or heterogeneous mantle). Gruau (1983) documented a third, less common type of komatiite that is Al-enriched.

Nesbitt et al. (1982) suggested that an early Archean mantle process, possibly garnet separation, generated a garnet-depleted "shallow mantle zone". Melting of this zone resulted in Al-depleted (Barberton-type) komatiites. Melting during the Late Archean, because of a decreasing geothermal gradient, resulted in melting of deeper mantle sources and the formation of Al-undepleted (Yilgarn-type) komatiites. This model seems unrealistic because komatiites would form at similar or shallower depths than tholeiites, which contradicts the depths postulated for the high temperatures required in komatiite genesis (i.e. if one assumes that komatiites and tholeiites are primary magmas). Other variants of a mineralogically and chemically layered mantle

have been proposed. Palme and Nickel (1985) suggested that the chemical data from komatiites supports CaO/Al_2O_3 fractionation in the Earth's early mantle through mantle differentiation. They reviewed the literature and established that most Archean komatiites (i.e. Al-undepleted) have CaO/Al_2O_3 ratios close to 1.0, which is approximately 20% higher than the chondritic ratio of 0.82. They hypothesized that this slightly higher than chondritic CaO/Al_2O_3 ratio is the result of a small amount (approx. 4%) of garnet separation after large-scale melting of the mantle in the Early Archean. This fractionation took place at 300-500 km and resulted in a layered mantle, from which a variety of magma types are possible. Recent experimental work by Ohtani et al. (1986) supports the hypothesis that the primordial upper mantle had a higher than chondritic CaO/Al_2O_3 ratio. They suggested that this is the result of majorite (i.e. a complex garnet mineral) fractionation in the lower part of the upper mantle by partial melting. Ohtani (1984) suggested, on the basis of experimental melting data and theoretical considerations of the melting curves of silicate minerals at high pressures, that chemical layering occurred within the primordial upper mantle. This stratification of the mantle was produced by separation of garnet and fractionation of picritic liquid from ascending diapirs at depths of 200-500 km. The critical factors in Ohtani's model are a) the increasing of melt densities with increasing pressure and b) the convergence of melt densities and mineral densities with increasing pressure.

Another concept that has surfaced from examining the densities of mantle minerals and magma at high pressures is one of magma oceans existing in the mantle during Archean time. This magma ocean may have formed and accumulated in the mantle at depths where mantle mineral densities are less than magma densities. Two types of magma ocean have been proposed: one that solidified early in Archean time and produced a layered mantle, and a second that survived to late Archean time. Anderson (1981 and 1982) believed that a magma ocean froze soon after its formation, which resulted in an upper garnet-depleted layer and a lower garnet-enriched layer. Gruau et al. (1986) surmised that the 3 types of komatiites in the Barberton Mountain Land indicate a solidified magma ocean by 3.5 Ga. Alternatively, Nisbet and Walker (1982) advocated the existence of a magma ocean from 4.5 to 2.6 Ga that evolved through time, and was the source of the different types of komatiites. Ohtani (1985), using experimental melting curves of mantle minerals and geophysical constraints, also proposed a model suggesting that the upper mantle represents the product of a magma ocean which fractionated from the whole mantle. Recent experimental work by Agee and Walker (1986) supports "the existence of an Archean subterranean magma ocean".

Another interpretation used to explain the different chemical types of komatiites is selective separation of garnet during partial melting of rising mantle diapirs (Green, 1975; Sun and Nesbitt, 1978; Jahn et al., 1982; Ohtani, 1984; Arndt, 1986b). Arndt (1986b) suggested that all three types of komatiites (i.e.

Al-depleted, Al-enriched, and Al-undepleted) can be generated using a modified model of Ohtani (1984). Others have also postulated that komatiites are simply derived from "plumes" or "diapirs" that rose from deep levels of the crust (Jarvis and Campbell, 1983; Campbell and Jarvis, 1984; Takahashi and Scarfe, 1985; Takahashi, 1986). These diapirs may have originated at thermal boundary layers, such as the one at 670 km between the lower and upper mantle (Jarvis and Campbell, 1983).

Recent investigations of the shape of the mantle's melting curves strongly suggest that the mantle's solidus and liquidus converge closely with increasing pressure (Stolper et al., 1981; Herzberg, 1983; Herzberg and O'Hara, 1985; Takahashi, 1986; Takahashi and Scarfe, 1985; Scarfe and Takahashi, 1986; Herzberg, 1986; Herzberg et al., 1986; Walker, 1986; Herzberg, 1987). Herzberg and O'Hara (1985) reviewed the major element geochemistry of 61 komatiites and 83 mantle peridotites. Plotting of this data in CMAS (O'Hara plots) space defines a trend that is not due entirely to a primary olivine control process. They (p.541) suggested that this trend possibly represents a "pressure-induced compositional trace of eutectic liquids in equilibrium with mantle assemblages from 40 to 150 kbar". They also postulated that the upper mantle was produced from the whole mantle as an ultrabasic partial melt with the transition zone and lower mantle representing the complementary eclogite and pyroxenite residua. Anderson and Bass (1986) came to a similar conclusion on the basis of geochemical and geophysical evidence.

They believed that chemical stratification of the mantle is a natural result of large scale melting in the Early Archean mantle. According to Walker (1986), thermodynamic constraints on the convergence of the mantle's solidus and liquidus require that the bulk composition of the mantle peridotite is very close to eutectic melt composition at the pressure of convergence. Herzberg et al. (1986) demonstrated from melting experiments at 50-80 kbar that komatiites could have been produced by either small or large scale partial melting of an upper mantle peridotitic source. O'Hara (1986, in Arndt et al., 1986a) suggested that the melting processes at high pressures are complex, with the degree of melting probably varying from a maximum to a minimum within the melt zone. Therefore the magmas rising from these melt zones are probably mixed melts.

Another plausible scenario to explain the distinct chemical types of komatiites is that of crustal contamination and/or mantle contamination. The problem of contamination is very complex, since it is difficult to estimate the total contribution made by 1) variable degrees of partial melting, 2) polybaric fractional crystallization, 3) heterogeneous mantle source compositions, 4) mantle contamination (i.e. before or during ascent), and 5) crustal contamination to the final chemical composition of the magma. Komatiitic liquids exhibit high temperatures and low viscosities (Nisbet, 1982), and most probably ascend and flow turbulently through and onto the continental crust (Huppert and Sparks, 1985a and b). Recent

experimental modelling (Huppert and Sparks, 1985a and b), and geologic and geochemical considerations (Sparks, 1986) have shown that crustal contamination may explain the close spatial and temporal proximity of komatiites, komatiitic basalts, and tholeiitic basalts. Recent work on komatiitic basalts from Munro Township, Ontario (Cattell, 1987), and Kambalda, Western Australia (Arndt and Jenner, 1986) has conclusively demonstrated their generation as highly contaminated komatiites. Initial ratios of Pb support this hypothesis (Cattell et al., 1984; Dupre et al., 1984). This mechanism will be discussed further in Section 6.3. However, in this section, an attempt will be made to explain the Al-undepleted, Al-depleted, and Al-enriched komatiites by lower crustal and/or mantle contamination instead of by different source regions or specific magma generation processes.

Recently, Sparks (1986) has reviewed the role of crustal contamination in magma genesis through time. Sparks (1986) pointed out that komatiitic liquids may be contaminated by rocks of similar composition (i.e. garnet pyroxenites or pyroxenites) within the lower crust. Contamination by such material could possibly explain the Al-depleted and Al-enriched komatiites. However, when HREE and other trace elements (V, Sc, among others) are considered, it becomes difficult to explain all the chemical variations (i.e. depletion and enrichment) entirely by crustal contamination. It is more appealing to explain the three chemical types of komatiites by variations in the mantle, either because

of a heterogeneous mantle, or because of contamination of the komatiitic liquids as they ascended through a vertically heterogeneous (i.e. layered) or a laterally heterogeneous mantle. Bickle et al. (1977) and Cox (1978) proposed similar mechanical mixing models to explain the variations within and between komatiitic suites. The variations between different komatiite magmas is explained by different mixing lines between the initial melt and the assimilated mantle material. There exist many possible mantle compositions for the assimilated solid material such as overlying mantle material (i.e. garnet lherzolite (Bickle et al., 1977), among others) or residual material (Cox, 1978) or a combination of these. Smith and Erlank (1982) appealed to the assimilation of overlying mantle material to explain the geochemical trends of their type II komatiites. This mechanism is attractive, but the hypothesis of Ca/Al fractionation in the Earth's mantle (Palme and Nickel, 1985), either by garnet fractionation (Ohtani, 1985) or by extensive partial melting to form a magma ocean that froze in the early history of the Earth (Herzberg and O'Hara, 1985), is more convincing. Also, the process of garnet fractionation during the komatiite generation event appears to be necessary to explain some of the differences in komatiite types. This is supported by the Hf isotope data of Gruau et al. (1986). However, additional high-quality data is needed from detailed isotopic, petrological, high-pressure geophysical, and geological studies in order to understand the processes of magma generation in the Archean mantle and

continental crust.

In summary, the recent experimental work indicates that komatiites represent initial, low to moderate degree, partial melts (i.e. direct) of mantle peridotite of varying compositions at pressures from 50 kbar to 140 kbar at high temperatures.

What are the implications of the major and trace element geochemistry of the Woodburn Lake Group komatiites on the composition of their source region, the extent and depth of melting, etc.?

The Woodburn Lake Group komatiites are characterized by nearly chondritic CaO/Al_2O_3, Al_2O_3/TiO_2, and CaO/TiO_2 ratios for non-cumulate samples. These characteristics are typical of the aluminum-undepleted type of komatiite (Nesbitt et al., 1979) which is common in Late Archean terrains. Other inter-element ratios (Table 10 and Fig. 34) and REE plots (Fig. 28a and 28b) of the Woodburn Lake Group komatiites indicate that their source has been depleted in Zr, LREE, and possibly to a lesser degree, TiO_2. This is consistent with other occurrences of Al-undepleted komatiites that show light REE depletion with TiO_2/Zr ratios greater than chondritic. This agrees with the observation of Sun et al. (1979) that Zr is more incompatible than TiO_2 during mantle melting. This previous mantle melting event is also indicated by Ti/Sc and Ti/Y ratios being less than the chondritic value. Further support for a previous melting event is the CaO/Al_2O_3 ratio of the Woodburn Lake Group komatiites, which is close to 1.0. This value is approximatively 20% higher than

chondritic and can be explained by a small percentage of garnet fractionation in an earlier mantle melting event (Palme and Nickel, 1985). Also supportive to this previous event is a slight HREE fractionation in the REE patterns of the komatiites (Figs. 28a and 28b).

A previous melting event is compatible with the model of Herzberg and O'Hara (1985), which would project the source region of the Woodburn Lake Group komatiites as a frozen partial melt. Plotting of the Woodburn Lake Group komatiites on CMAS projections (O'Hara plots - Figs. 59-62), using the predicted phase boundaries of O'Hara (1968) and Herzberg and O'Hara (1985), suggests derivation of the komatiites as initial melts of a garnet lherzolite at pressures of 50-60 kbar. The displacement of the spinifex-textured komatiites from the lherzolite eutectic (Fig. 61) implies that the komatiites were in equilibrium with a harzburgite residua. This shift away from the eutectic requires the complete melting of clinopyroxene in the source, followed by melting of an aluminous phase, most likely garnet. Not that this melting of an aluminous phase might be difficult to distinghish from melting at a lower pressure. Even so, garnet did not play a major role in the generation of the Woodburn Lake Group komatiites, since the komatiites do not exhibit a molar trend of 3:1 in Figure 63a. Further support of garnet not being involved in their petrogenesis is their nearly constant ratios of Al_2O_3/TiO_2. Also, non-cumulate komatiitic samples exhibit relatively constant, nearly chondritic (approx. 1.0) CaO/Al_2O_3

Figure 59. CMAS diagram (O'Hara, 1968) showing the projection of the Woodburn Lake Group komatiites and high-Mg basalts from or towards diopside onto the C_3A-S-M plane (wt%). The phase boundaries and equilibria divides are from O'Hara (1968). Mineral abreviations are: Pl - plagioclase, Opx - orthopyroxene, Ol - olivine, Ga - garnet. The index shows the position of the C_3A-S-M plane in the CMAS tetrahedron.

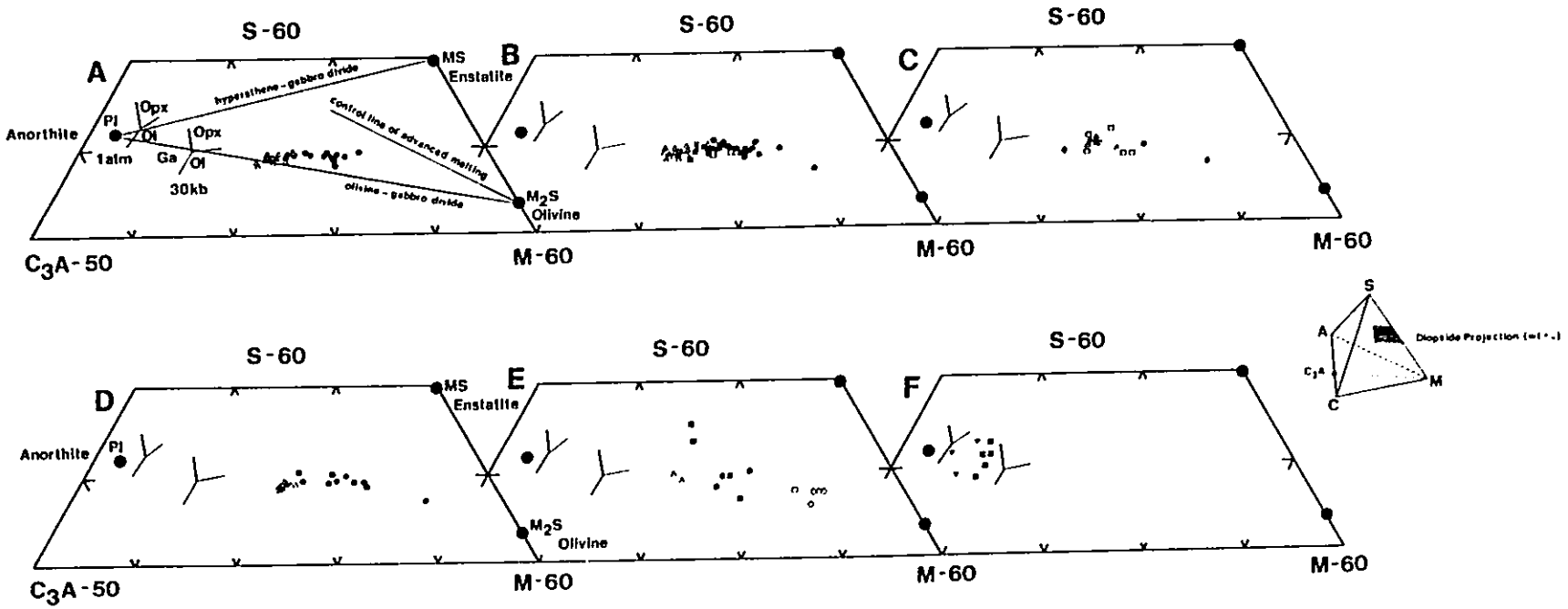
S-60
A
MS
Enstatite
B
S-60
C
S-60
Anorthite
Pl
Opx
Ol
hypersthene - gabbro divide
Opx
Ga
Ol
1atm
30kb
olivine - gabbro divide
control line of advanced melting
M2S
Olivine
C3A-50
M-60
M-60
M-60
D
S-60
MS
Enstatite
E
S-60
F
S-60
Anorthite
Pl
M2S
Olivine
C3A-50
M-60
M-60
M-60
S
A
C3A
C
M
Diopside Projection

Figure 60. CMAS diagram (O'Hara, 1968) showing the projection of the Woodburn Lake Group komatiites and high-Mg basalts from or towards diopside onto the CA-S-M plane (wt%). The one atmosphere and 30 kilobar phase boundaries are from O'Hara (1968). Predicted eutectics for 40, 60, 80, 100, and 150 kilobars are from Herzberg and O'Hara (1985). The star symbols represent proposed cosmochemical compositions of bulk crust and mantle. The outlined area marks the position of the lower mantle transition zone (Herzberg and O'Hara, 1985). The index shows the position of the CA-S-M plane in the CMAS tetrahedron.

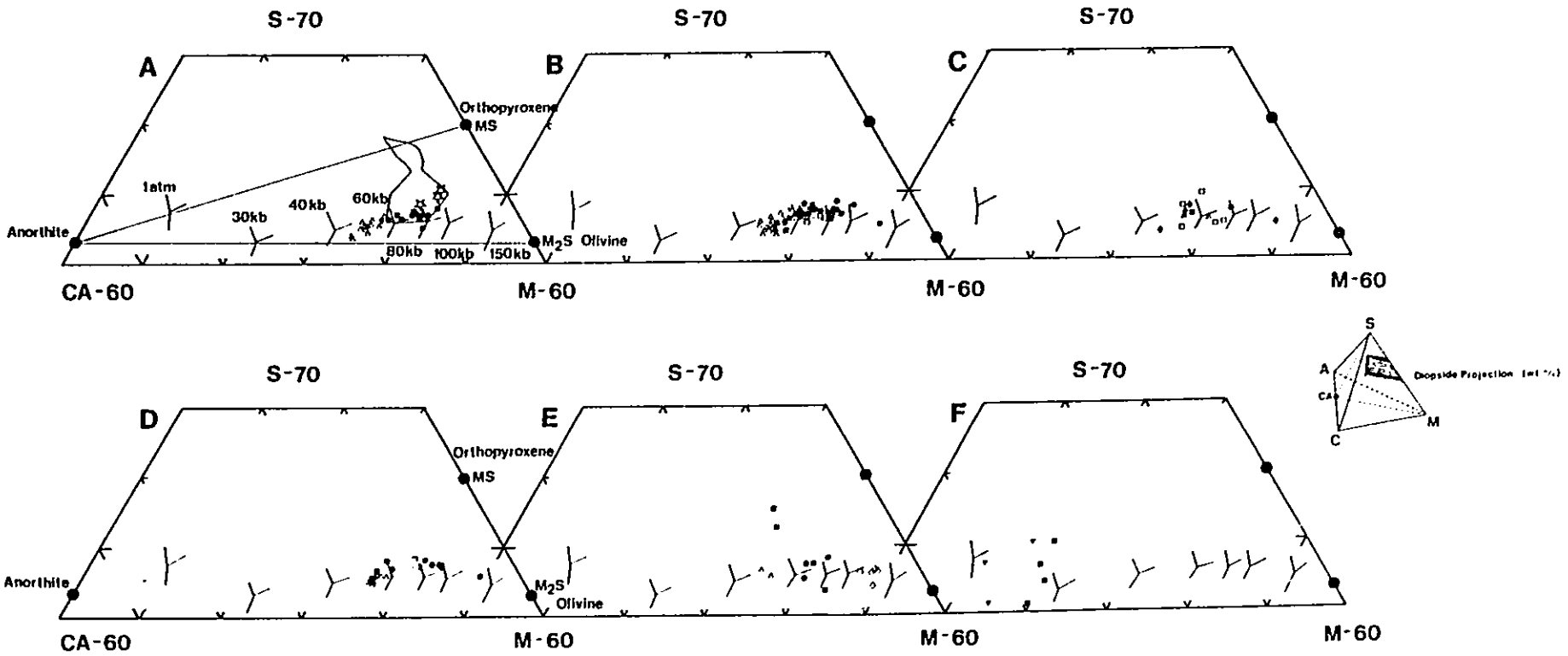
S-70
S-70
S-70
A
B
C
Orthopyroxene
MS
1atm
30kb
40kb
60kb
80kb
100kb
150kb
Anorthite
M2S Olivine
CA-60
M-60
M-60
M-60
S
A
CA
C
M
Diopside Projection (wt %)
S-70
S-70
S-70
D
E
F
Orthopyroxene
MS
Anorthite
M2S
Olivine
CA-60
M-60
M-60
M-60

Figure 61. CMAS diagram (O'Hara, 1968) showing the projection of the Woodburn Lake Group komatiites and high-Mg basalts from or towards enstatite onto the C_2S_3-A_2S_3-M_2S plane (wt%). The one atmosphere and 30 kilobar phase equilibria are from O'Hara (1968). The predicted eutectics for 40, 60, 80, 100, and 150 kilobars are from Herzberg and O'Hara (1985). Mineral abreviations are: Ol - olivine, Cpx - clinopyroxene, Pl - plagioclase, Ga - garnet. The index shows the position of the C_2S_3-A_2S_3-M_2S plane in the CMAS diagram.

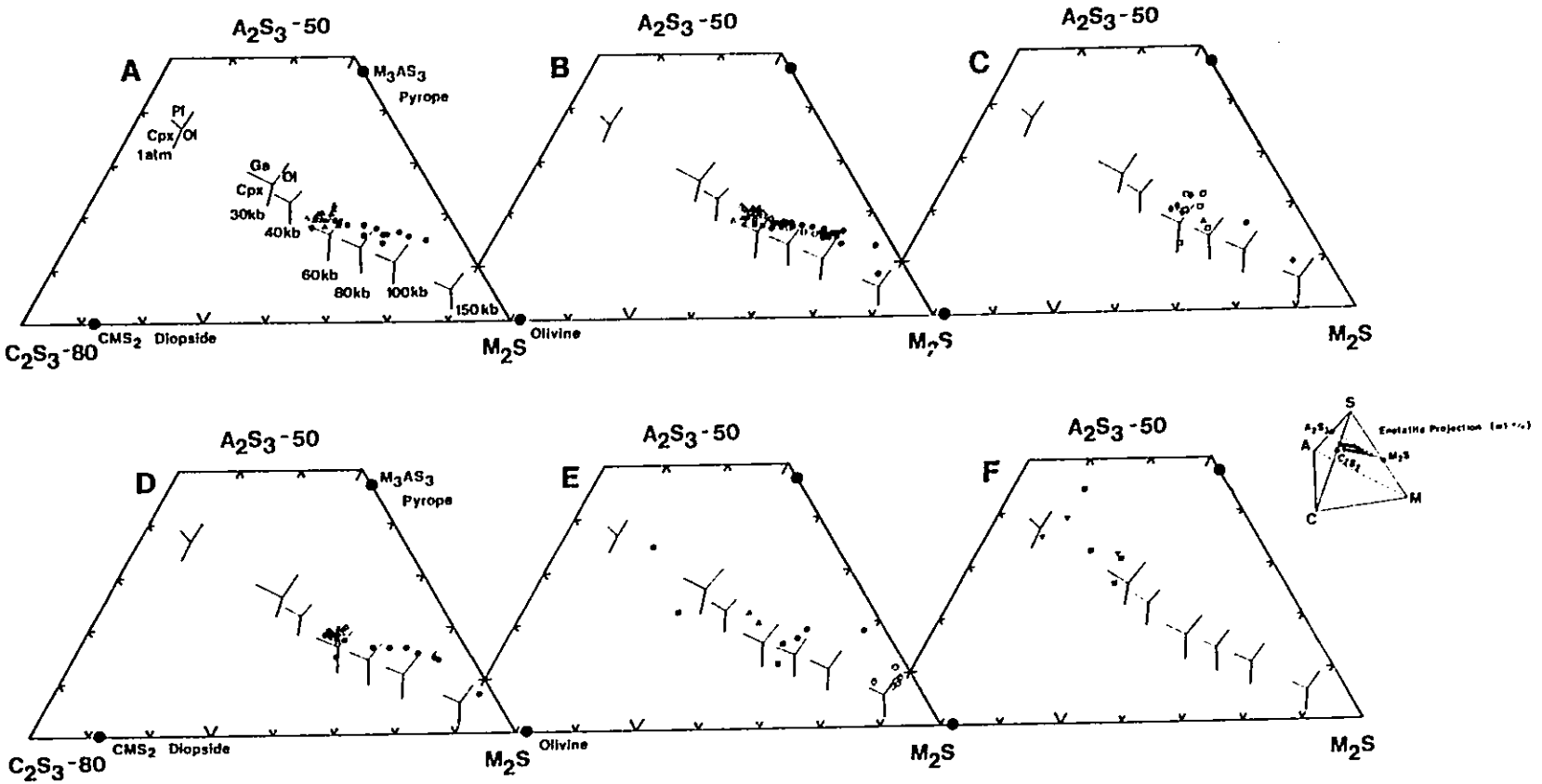
A
B
C
D
E
F
A_2S_3-50
M_3AS_3
Pyrope
Pl
Cpx/Ol
1atm
Ga
Ol
Cpx
30kb
40kb
60kb
80kb
100kb
150kb
C_2S_3-80
CMS_2 Diopside
M_2S
Olivine
S
A
C
M

Figure 62. CMAS diagram (O'Hara, 1968) showing the projection of the Woodburn Lake Group komatiites and high-Mg basalts from or towards olivine onto the CS-A-MS plane (wt%). The phase boundaries are from O'Hara (1968). Mineral abreviations as in Figure 61. The index shows the position of the CS-A-MS plane in the CMAS tetrahedron.

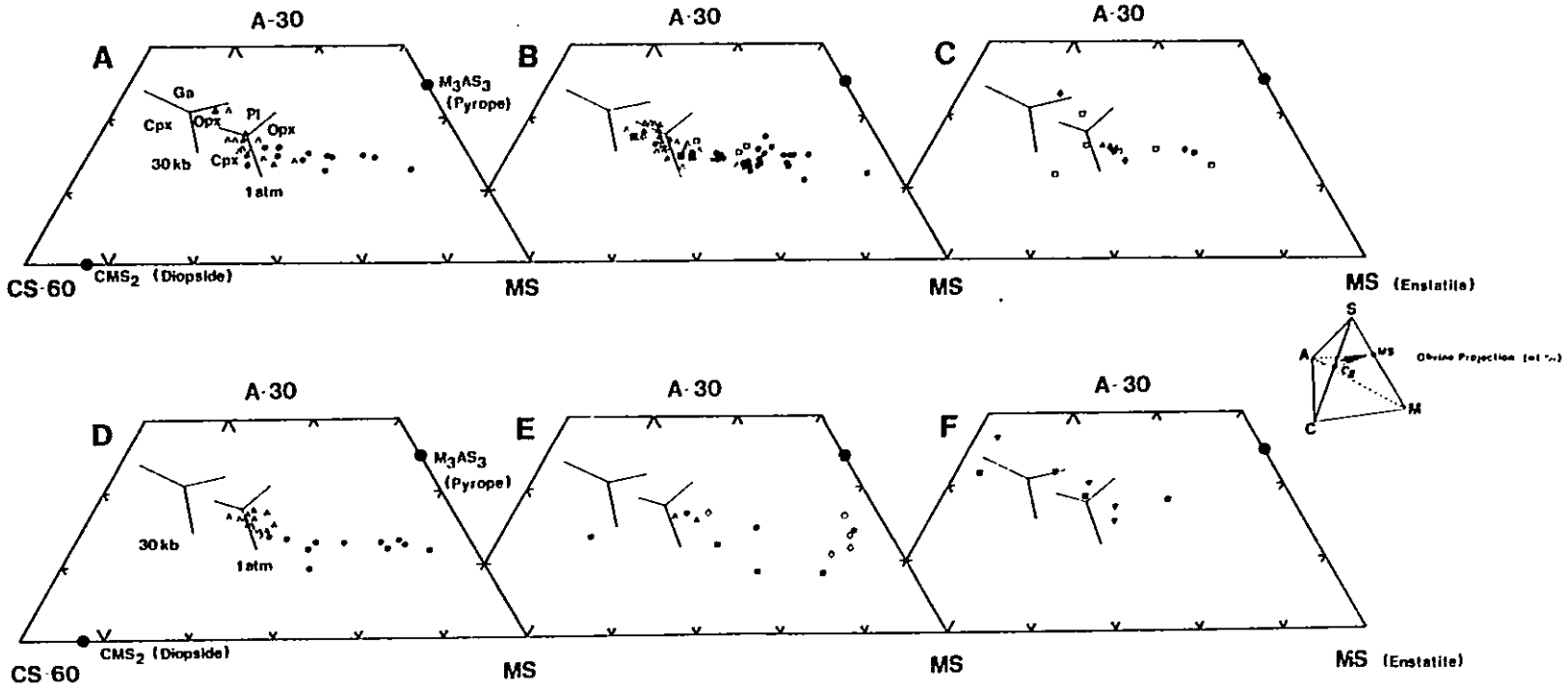
A-30
A
B
C
D
E
F
Ga
Cpx
Opx
Pl
Opx
30 kb
Cpx
1 atm
M_3AS_3 (Pyrope)
CS-60
CMS_2 (Diopside)
MS
MS (Enstatite)
S
A
MS
M
C
Olivine Projection

Figure 63. Pearce element ratio diagrams (Pearce, 1968) for Al_2O_3/TiO_2 vs. MgO/TiO_2, MgO/TiO_2 vs. FeO_T/TiO_2, and MgO/CaO vs. FeO_T/CaO of the representative suite (Table 3) of Woodburn Lake Group komatiites and high-Mg basalts. Solid lines represent fractionation control lines for the indicated minerals. Note the fairly constant Al_2O_3/TiO_2 for the komatiites in the far left diagram. Also note that the high-Mg basalts fall along the garnet control line, but this may also be explained by assimilation of continental crust by the parental magma.

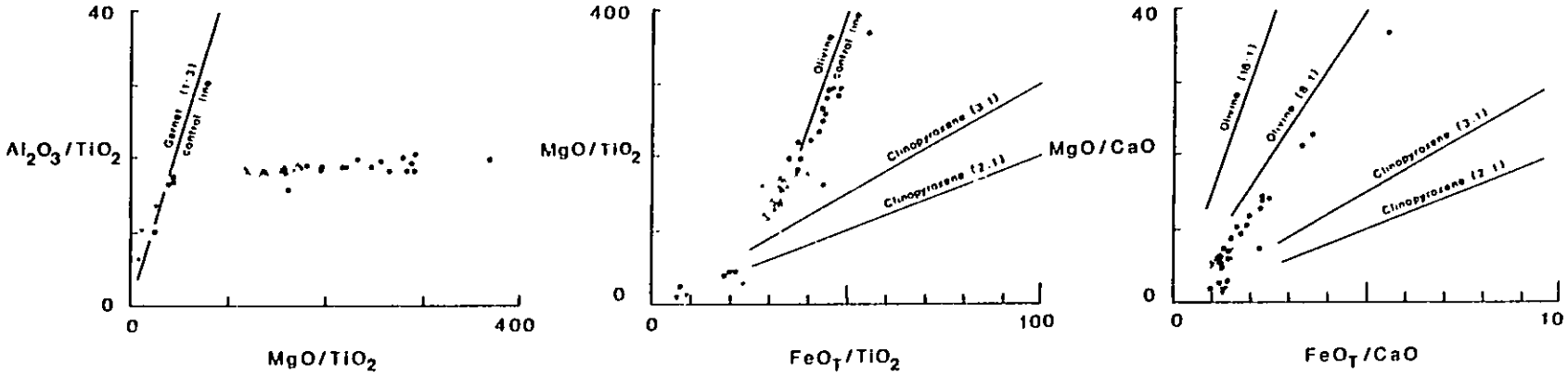
40
0
400
Al_2O_3/TiO_2
MgO/TiO_2
Garnet (1:3)
control line
400
0
100
MgO/TiO_2
FeO_T/TiO_2
Olivine
control line
Clinopyroxene (3:1)
Clinopyroxene (2:1)
40
0
10
MgO/CaO
FeO_T/CaO
Olivine (10:1)
Olivine (8:1)
Clinopyroxene (3:1)
Clinopyroxene (2:1)

ratios, which predicates against garnet involvement during the partial melting event that produced the komatiitic liquids. Additional proof that garnet has not greatly affected the chemistry of the komatiites during their genesis is shown in the Pearce element ratio plots (Figs. 63a, 63b, and 63c). The 1:1 slopes (Figs. 33a, 33b, and 33c) of the spinifex-textured samples are explained by combined olivine and clinopyxene fractionation (Chapter 4), not garnet or orthopyroxene involvement.

What is the proof that partial melting is responsible for generating the Woodburn Lake Group komatiites? According to Arth (1976) and Hanson (1978) the relative behavior of highly compatible trace elements such as Ni and Cr to an incompatible element such as Zr reflects partial melting or differentiation processes. In Figures 64 and 65 (from the Woodburn Lake Group) komatiites plot in an area indicating high degrees of partial melting in their genesis. This estimate of degree of partial melting is probably high since the diagram does not take into account a source depleted in Zr.

Hanson and Langmuir (1978) used the olivine saturation surface determined by Roeder and Emslie (1970) to estimate the melting and residual fields for batch melting of the mantle. In using their plot (Fig. 66) of molar MgO versus molar FeO, the Woodburn Lake Group komatiites fall within the 30-50% field of melting of a model garnet-lherzolite mantle (i.e. pyrolite composition). The temperatures given on this diagram are for 1 atmosphere and according to Langmuir and Hanson (1980) they

Figure 64. Plot of Zr versus Ni contents in the Woodburn Lake Group komatiites and komatiitic-tholeiitic basalts. Curves A and B are calculated batch melting curves from Rajamani et al. (1985). Curve A corresponds to melting of a mantle source with 2000 ppm Ni and 7.8 ppm Zr at 1850°C and 50 kb, whereas curve B corresponds to melting of the same source at 1575°C and 25 kb. In calculating the batch melting curves, Rajamani et al. (1985) assumed that the bulk distribution coefficient (D) for Ni remains constant over the melting interval and D for Zr is zero (i.e. incompatible). Curves C and D are calculated fractional crystallization curves for olivine from two different respective melts (Rajamani et al., 1985). The calculated fractionation curves take into consideration the changes in olivine composition and temperature as crystallization proceeds. If pyroxene and plagioclase become crystallizing phases with olivine, then inflection points would appear because of an increase in Zr concentration relative to Ni (i.e. Zr becomes compatible). Tics indicate 5 % intervals of olivine fractionation.

The dotted field represents the position of the Woodburn Lake Group spinifex-textured komatiites.

The solid boxes and the solid inverted triangles designate komatiitic basalts and high-Mg tholeiitic basalts, respectively.

The position of the high-Mg basalts with low Zr abundances suggest that they would be related to the komatiites mostly by olivine fractionation.

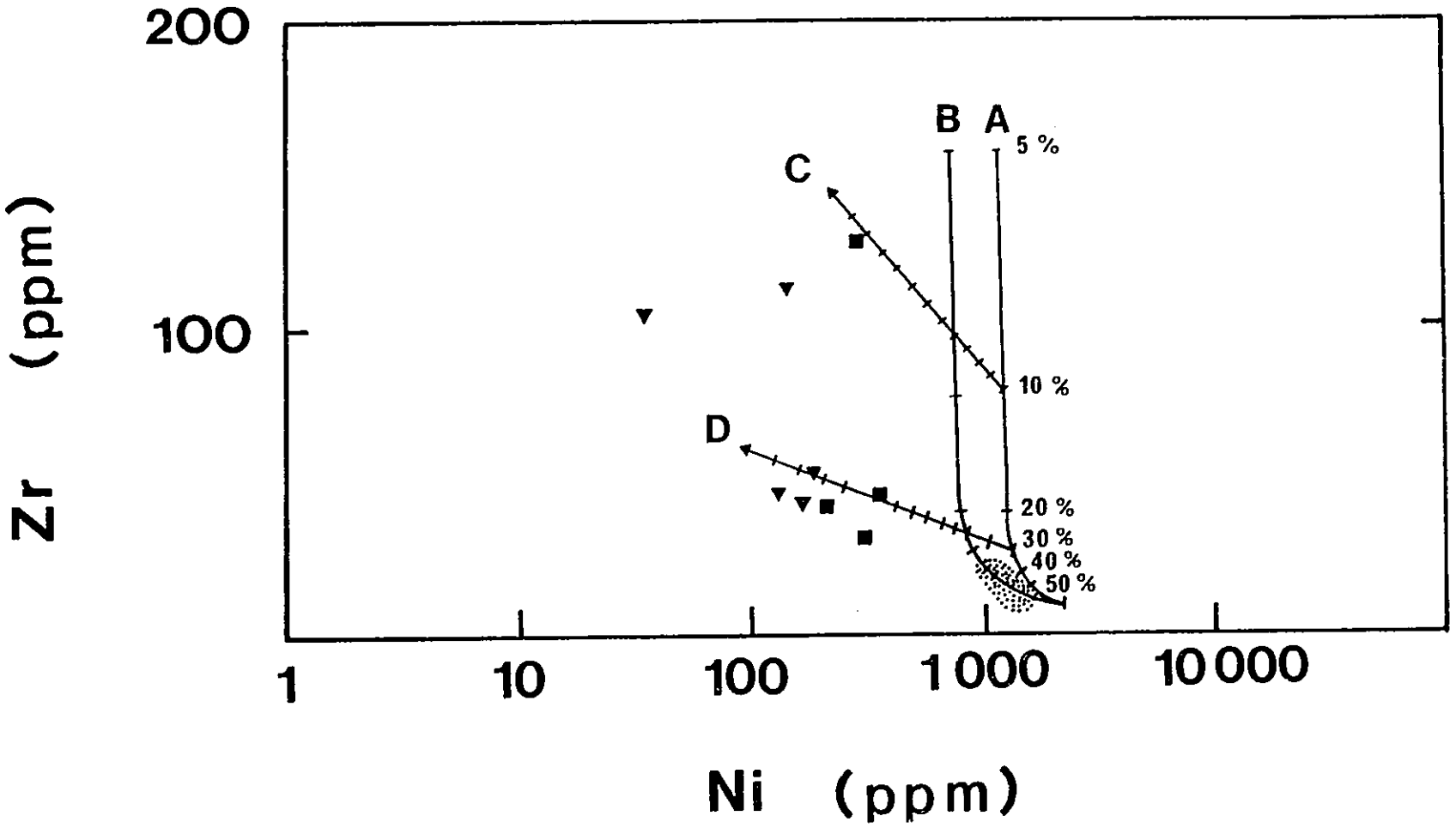
200
100
Zr (ppm)
B
A
5 %
C
10 %
D
20 %
30 %
40 %
50 %
1
10
100
1 000
10 000
Ni (ppm)

Figure 65. Plot of Zr versus molar Fe contents in the Woodburn Lake Group komatiites and komatiitic-tholeiitic basalts. Curves A and B are calculated batch melting curves from Rajamani et al. (1985). Curve A corresponds to melting of a mantle source with 5.65 cation % Fe and 7.8 ppm Zr ar 1850°C and 50 kb, whereas curve B corresponds to melting a mantle source with 7.5 cation % Fe and 7.8 ppm Zr at 1850°C and 50 kb. As in Figure 64, Zr is assumed to be incompatible. Curves with arrows are calculated fractional crystallization trends for olivine from representative parental melts. These parental magmas were generated by 10 % and 25 % batch melting of the mantle source.
This diagram suggests that olivine fractionation from komatiitic liquids cannot produce the high-Mg basalts. The position of the high-Mg basalts suggests either a) low to moderate (15-25 %) degrees of partial melting of a different source or b) contamination of komatiitic liquids with a contaminant low in FeO.

Symbols as in Figure 64.

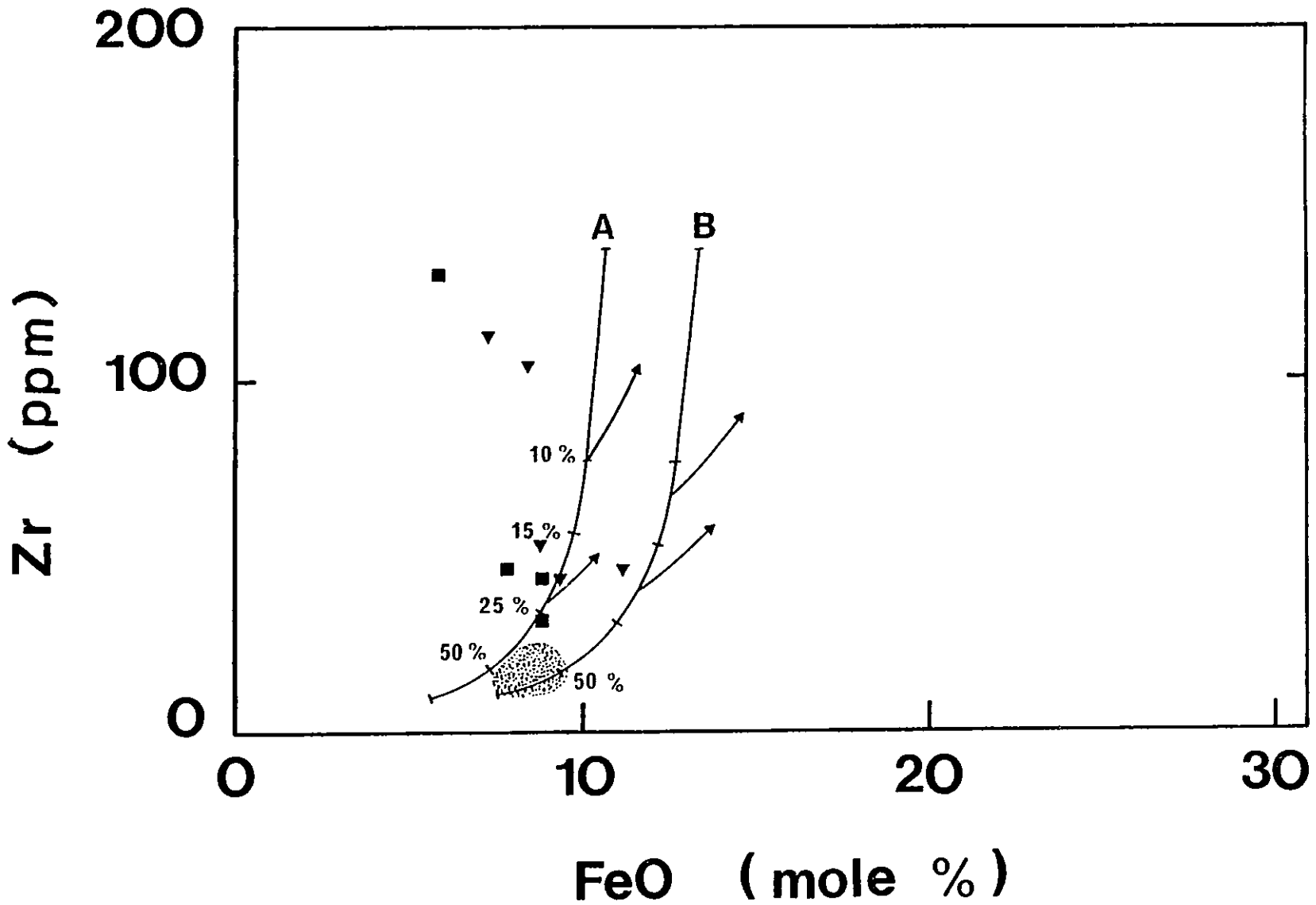
200
100
0
Zr (ppm)
A
B
10 %
15 %
25 %
50 %
50 %
0
10
20
30
FeO (mole %)

Figure 66. Variation diagram ("Sail" diagram, Hanson and Langmuir, 1978) of MgO plotted against FeO (cation mole %) of the Woodburn Lake Group komatiites and komatiitic-tholeiitic basalts. Symbols as in Figure 64. The lower (melt) and upper (residue) contoured fields are from Hanson and Langmuir (1978) calculations for batch melting of the mantle, using the olivine saturation surface of Roeder and Emslie (1970). The composition of the upper mantle (Pyrol) used in the calculations is 38.9 wt% MgO and 7.6 wt% FeO. The curved lines without tics in the lower field indicate the percent of partial melting of this mantle source. The horizontal lines in the lower field designate the position of isotherms, which are pressure dependent. The two curved lines with tics in the lower field indicate the fractional crystallization trend of olivine. The tics indicate 5% intervals of olivine fractionation. The temperatures given are for one atmosphere. Temperatures at higher pressures are calculated by increasing the temperature along an isotherm by 5°C per kb.

The position of the komatiites indicates that they could be generated by 25 to 55% partial melting of pyrolite source. The position of the high-Mg basalts indicates that they are derived magmas which must have experienced fractional crystallization since leaving their upper mantle source. Olivine fractionation is a possibility, however, the scatter is consistent with other phases fractionating.

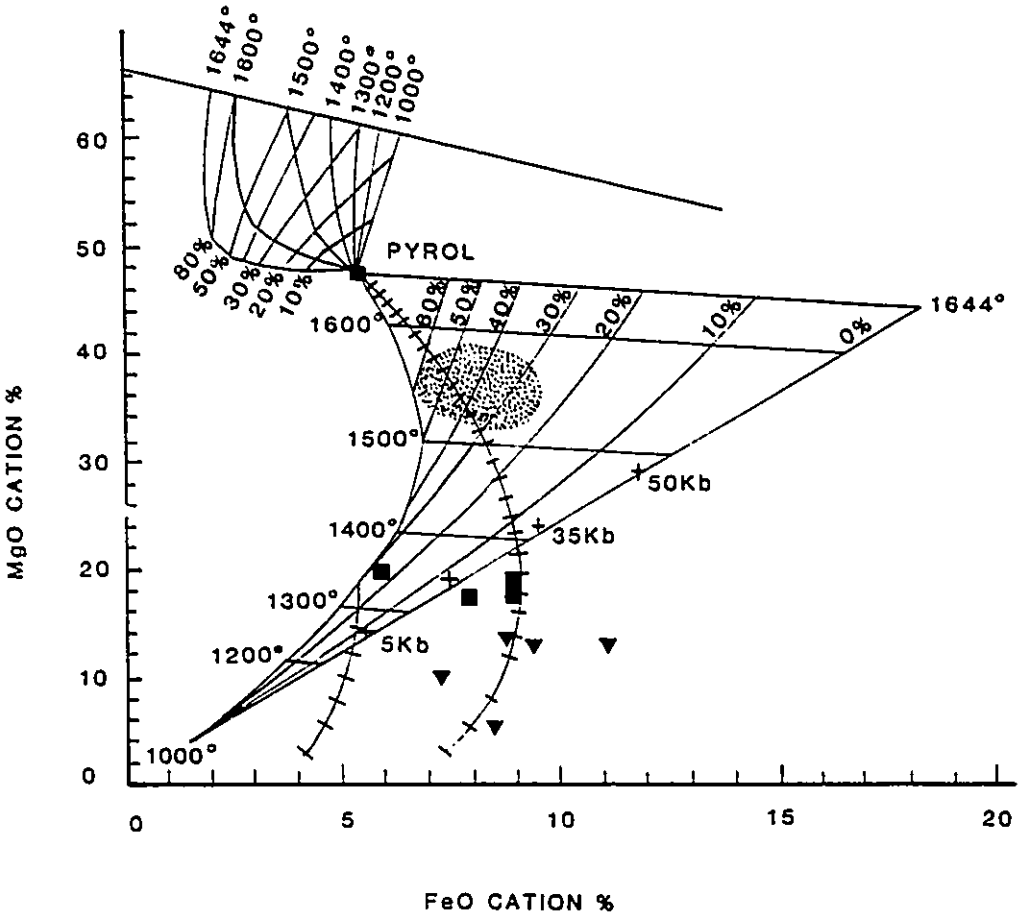
1644°
1600°
1500°
1400°
1300°
1200°
1000°
PYROL
80%
50%
30%
20%
10%
1600°
60%
50%
40%
30%
20%
10%
0%
1644°
1500°
50Kb
1400°
35Kb
1300°
1200°
5Kb
1000°
MgO CATION %
FeO CATION %
0
10
20
30
40
50
60
0
5
10
15
20

should be increased by 5°C per kbar. Therefore at 50 kbar the temperature estimate for the Woodburn Lake Group komatiites is 1800°C.

Francis et al. (1983) have also proposed that a field of possible melt compositions can be calculated in Al-Si space for any given mantle composition. This regularity of the systematics of Al and Si is related to temperature, pressure, and degree of partial melting, similar to the "sail-like" diagram of Mg-Fe space proposed by Hanson and Langmuir (1978). On this diagram (Fig. 67), the Woodburn Lake Group komatiites plot in a field that is indicative of pressures greater than 30 kbar, temperatures between 1600°C and 1700°C, and degrees of partial melting ranging from 30-40%. These estimates agree fairly well with those from the Mg-Fe diagram. The slight discrepancy of estimates between the two diagrams probably reflects the sensitivity of temperature, pressure, and degree of partial melting to the bulk composition of the mantle source.

6.3 PETROGENESIS OF THE KOMATIITIC AND THOLEIITIC BASALTS

Sequences of highly magnesian (6-18% MgO) basaltic lavas are spatially associated with komatiites (>18% MgO) in many Archean greenstone belts (Arndt et al. 1977; Arndt and Nisbet, 1982; among others). A recurring question is whether the close spatial and temporal proximity is the result of a common origin. Many researchers (Arndt et al., 1977; Nisbet and Chinner, 1981;

Figure 67. "Sail-like" diagram (Francis et al., 1983) in Al-Si space (cation %) of the Woodburn Lake Group komatiites and komatiitic-tholeiitic basalts. Symbols as in Figure 64. Vertical lines indicate the pressure in kilobars. Solid curved lines designate the position of isotherms and dashed curved lines indicate the percent of partial melting. Francis et al. (1983) calculated the "Sail-like" field of possible melt compositions in Al-Si space by applying the results of melting experiments to the work of Hanson and Langmuir (1978).

The position of the Woodburn Lake Group komatiites (dotted field) and komatiitic-tholeiitic basalts (symbols) in Al-Si space agrees with their position in Mg-Fe space (Fig. 66).

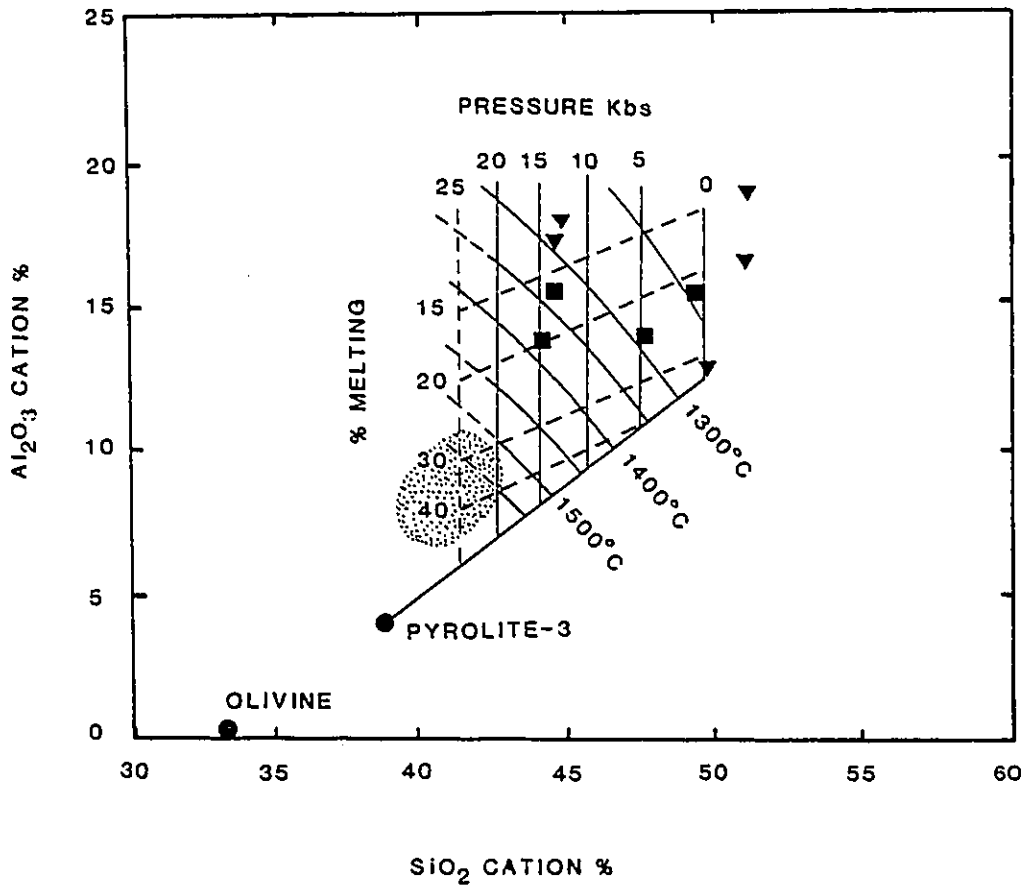
PRESSURE Kbs
20 15 10 5 0
25
15
20
30
40
% MELTING
1300°C
1400°C
1500°C
PYROLITE-3
OLIVINE
25
20
15
10
5
0
30
35
40
45
50
55
60
Al_2O_3 CATION %
SiO_2 CATION %

Cameron and Nisbet, 1982; Arndt and Nesbitt, 1982a; Aitken and Echeverria, 1984; Arndt and Nesbitt, 1984; Arndt and Jenner, 1986; Cattell, 1987) have discussed this problem, and many solutions have been proposed.

The geochemical differences between komatiites and komatiitic-tholeiitic basalts have been explained by 1) fractional crystallization (Arndt et al., 1977; Nisbet and Chinner, 1981), 2) varying degrees of partial melting (Arndt et al.,1977), 3) a combined effect of varying degrees of partial melting and fractional crystallization (St.-Seymour et al., 1983; Canil, 1987), 4) magma mixing (Arndt and Nesbitt, 1984), 5) different source regions (Nesbitt et al., 1979; Arndt and Nesbitt, 1984; Canil, 1987), and 6) combined assimilation-fractional crystallization (AFC - Longhi et al., 1983; Huppert et al., 1984; Kinzler and Grove, 1985; Arndt and Jenner, 1986; Cattell, 1987; among others).

The major element chemistry of most komatiitic-tholeiitic basalts suggests their derivation from an ultramafic parent liquid by fractional crystallization of olivine and clinopyroxene at low pressures. Nisbet and Chinner (1981) suggested that under special conditions (i.e. an extensional event) komatiites would erupt to the surface without being contaminated and/or undergoing fractional crystallization. Later, after a magma chamber had formed, the komatiitic liquids would fractionate by double diffusive processes and erupt more evolved komatiitic-tholeiitic basalts. The volcanic suite would consist of unfractionated

komatiites and more evolved komatiitic-tholeiitic basalts with a compositional gap. St.-Seymour et al. (1983) investigated a similar compositional gap between peridotitic-pyroxenitic komatiites and tholeiitic basalts. They found that the compositional gap did not exist between komatiites and komatiitic basalts, but instead between komatiitic basalts (i.e. pyroxenitic komatiites) and tholeiitic basalts. They suggested that the peridotitic and pyroxenitic komatiites represent a continuous magmatic series related by varying degrees of partial melting. The composition of the basalts is controlled by fractional crystallization of a komatiitic parental magma.

Arndt and Nesbitt (1984) also examined a compositional gap between komatiites and komatiitic basalts from Munro Township. They concluded, on the basis of trace element data, that the two magma types could not be related by low pressure fractionation. Instead, they appealed to independent melting of sources of different compositions. They proposed other possibilities such as 1) the same source with some pyroxene as a residual phase and 2) fractional crystallization at high pressures. They also suggested that some of the more magnesian (16-18% MgO) komatiitic basalts are the result of magma mixing between komatiite and komatiitic basalt liquids.

Recently, Canil (1987) examined some komatiites, komatiitic basalts, high-Mg tholeiitic basalts and high-Fe tholeiitic basalts. He concluded that the komatiitic basalts and high-Mg tholeiitic basalts are unrelated to the komatiites and require

partial melting of a different source. In addition, he postulated a third source for generating the high-Fe tholeiitic basalts. This work by Canil (1987) is suggestive of komatiitic basalts being primary melts.

Alternatively, recent experimental modelling (Huppert et al., 1984; Huppert and Sparks, 1985a and 1985b), field evidence (Arndt and Jenner, 1986; Cattell, 1987), isotopic data (Compston et al., 1986; Cattell, 1987) and geochemical modelling (Longhi et al., 1983; Arndt and Jenner, 1986; Arndt et al., 1986b; Cattell, 1987; Cattell and Arndt, 1987) is strongly suggestive of komatiitic basalts forming by combined crustal assimilation-fractional crystallization (AFC) of komatiitic liquids. The experimental modelling conducted by Huppert and Sparks (1985a and 1985b) indicates that komatiites ascend through continental crust and flow on the surface under extremely hot, turbulent conditions. Under these conditions, the komatiites can be contaminated with up to 40% continental crust en route to the surface, and up to 10% underlying country rock on the surface. Modelling of the contamination process (AFC) by Arndt and Jenner (1986), Cattell (1987), and Longhi et al. (1983) indicated 12%, 7-25%, and 30-50% crustal contamination, respectively. These model calculations are in excellent agreement with the experimental modelling results.

6.3.1 DERIVATION OF THE WOODBURN LAKE GROUP KOMATIITIC-THOLEIITIC BASALTS

Compositional and classification plots (Figs. 29 to 32) of the Woodburn Lake Group komatiites and komatiitic-tholeiitic basalts indicate that the komatiitic-tholeiitic basalts may be related to the komatiites by fractional crystallization. For example in the AMC plot (Fig. 32) the komatiites are end members on the liquid line of descent from komatiite to tholeiitic basalt. Petrographic observations and geochemical evidence, as mentioned in Section 6.2.2, indicate that the differences within the komatiites can be explained by olivine, chromite, and clinopyroxene fractionation. Since the trends through the komatiites can be projected through the komatiitic basalts, it is thought that the komatiitic basalts are related to the komatiites by a similar process.

Arndt (1976) studied the phase relations of a komatiitic liquid at a pressure of 1 atmosphere. He found that clinopyroxene appears as a liquidus phase only when the liquid had <9 wt% MgO. Whitford and Arndt (1978) came to a similar conclusion in that significant amounts of augite crystallized only in liquids with <10 wt% MgO. More recent work by Kinzler and Grove (1985) has clearly demonstrated that clinopyroxene appears on the liquidus surface only after the liquid has <12 wt% MgO. These phase equilibria studies suggest that clinopyroxene would have little or no effect on the fractionation process responsible for

generating the Woodburn Lake komatiitic basalts from komatiitic liquids. This appears to be at odds with chemical modes and petrographic observations of the komatiitic basalts. However, these phase equilibria studies do not negate the possibility that clinopyroxene fractionation played an important role in generating the tholeiitic basalts from komatiitic basalts.

One way of testing whether fractional crystallization processes are responsible for the komatiitic-tholeiitic basalt formation is by using Pearce element ratio diagrams. On several of these plots (Figs. 63a, 63b, and 63c), the komatiitic basalts could be derived from the komatiites by olivine plus clinopyroxene fractionation. The slopes of the compositional trends are indicative of trends along an olivine plus clinopyroxene controlled liquid line of descent. The compositional trend lines of the tholeiitic basalts in Figure 63 suggest mainly a clinopyroxene controlled liquid line of descent. This indicated fractionation model was then tested by using a least squares mixing program. The mixing tests were conducted by choosing a parental magma from some of the komatiite samples assumed to be the most primitive, and allowing the computer to simulate the fractionation process. The computer program tried to reproduce the daughter magma from combinations of one of the komatiites presumed to be an initial komatiitic liquid and varying proportions of mineral phases (i.e. olivine, clinopyroxene, and chromite). Cr_2O_3 and NiO were run as minor elements in the mixing program because of their high

concentrations in the komatiites and komatiitic basalts. Trace elements were modelled by a sub-routine program to calculate daughter-magmatic liquid concentrations. The results of some of these mass balance, mixing calculations are given in Table 22. These results show that fractionating large proportions of olivine and clinopyroxene and minor amounts of chromite and/or plagioclase from the komatiites accounts for some of the major and trace elements in the komatiitic basalts. Similarly, it is shown that fractionating large proportions of clinopyroxene from the komatiitic basalts can produce some of the major and trace element values of the high-Mg tholeiitic basalts (Table 22b).

However, these results show that there are problems with generating the komatiitic basalts solely by a combination of olivine, clinopyroxene, and chromite fractionation of a komatiitic liquid. The large variation in chondrite-normalized REE plots of the high-Mg basalts is not reconciled by fractional crystallization processes only. Figure 63a suggests garnet involvement in their petrogenesis, however this aluminous trend could also be due to fractionation of orthopyroxene or assimilation of continental crust.

In addition to phase equilibrium considerations, as mentioned previously, geochemical characteristics of the Woodburn Lake Group komatiitic-tholeiitic basalts clearly negates their derivation from a komatiitic liquid by low pressure fractional crystallization. The Woodburn Lake Group komatiitic-tholeiitic basalts are enriched in highly incompatible elements (i.e. LREE,

Table 22a. Results of mass balance, fractional crystallization calculations to produce komatiitic-tholeiitic basalts from a komatiitic liquid.

INPUT DATA:

	PARENT	FOR-92	AUG-1	CHR-1	DAUGHTER
SiO_2	45.13	40.30	51.00	0.31	48.56
TiO_2	0.36	0.00	0.33	0.42	0.68
Al_2O_3	8.39	0.00	3.73	15.53	14.17
FeO	11.03	7.97	8.45	26.84	11.44
MnO	0.18	0.16	0.18	0.00	0.17
MgO	25.62	51.13	17.88	9.29	13.81
CaO	6.94	0.25	16.90	0.00	6.44
Na_2O	0.84	0.00	0.00	0.00	2.49
K_2O	0.03	0.00	0.00	0.00	1.05
Cr_2O_3	0.43	0.17	0.52	46.61	0.11

(PARENT - MINERALS = DAUGHTER)

PARENT: AK-15d (upper portion of spinifex-textured zone)
DAUGHTER: R-222 (komatiitic basalt)

	SOLUTION	% CUMULATE
AK-15d	1.000	
FOR-92	-0.295	61.509
AUG-1	-0.167	34.828
CHR-1	-0.018	3.663
R-222	0.520	

R SQUARED = 8.730 (sum (calculated - observed)^2)

	PARENT ANALYSIS	DAUGHTER ANALYSIS	DAUGHTER CALC.	WEIGHTED RESID.
SiO_2	45.13	48.56	47.67	0.89
TiO_2	0.36	0.68	0.58	0.10
Al_2O_3	8.39	14.17	14.45	-0.29
FeO	11.03	11.44	13.11	-1.66
MnO	0.18	0.17	0.19	-0.03
MgO	25.62	13.81	14.25	-0.44
CaO	6.94	6.44	7.80	-1.37
Na_2O	0.84	2.49	1.63	0.87
K_2O	0.03	1.05	0.06	0.98
Cr_2O_3	0.43	0.11	-1.02	1.13

Table 22b. Results of mass balance, fractional crystallization calculations to produce komatiitic-tholeiitic basalts from a komatiitic liquid.

INPUT DATA:

	PARENT	FOR-92	AUG	PLAG60	DAUGHTER
SiO_2	45.13	40.30	51.13	52.47	47.63
TiO_2	0.36	0.00	0.22	0.00	1.99
Al_2O_3	8.39	0.00	3.51	29.67	15.64
FeO	11.03	7.97	9.26	0.00	11.34
MnO	0.18	0.16	0.22	0.00	9.67
MgO	25.62	51.13	20.90	0.00	9.67
CaO	6.94	0.25	12.99	12.24	7.02
Na_2O	0.84	0.00	0.00	4.29	2.79
K_2O	0.03	0.00	0.00	0.35	2.61
Cr_2O_3	0.43	0.17	0.77	0.00	0.02

(PARENT - MINERALS = DAUGHTER)

PARENT: AK-15d (upper portion of spinifex-textured zone)
DAUGHTER: R-232b (high-Fe tholeiitic basalt)

	SOLUTION	% CUMULATE
AK-15d	1.000	
FOR-92	-0.310	77.116
AUG	-0.165	41.146
PLAG60	0.073	-18.262
R-232b	0.598	

R SQUARED = 17.442 (sum (calculated - observed)^2)

	PARENT ANALYSIS	DAUGHTER ANALYSIS	DAUGHTER CALC.	WEIGHTED RESID.
SiO_2	45.13	47.63	46.61	1.03
TiO_2	0.36	1.99	0.55	1.44
Al_2O_3	8.39	15.64	16.65	-1.01
FeO	11.03	11.34	11.69	-0.35
MnO	0.18	0.16	0.15	0.01
MgO	25.62	9.67	10.41	-0.74
CaO	6.94	7.02	9.35	-2.32
Na_2O	0.84	2.79	1.93	0.86
K_2O	0.03	2.61	0.09	2.52
Cr_2O_3	0.43	0.02	0.41	-0.39

Table 22c. Results of mass balance, fractional crystallization calculations to produce tholeiitic basalts from a komatiitic basalt liquid.

INPUT DATA:

	PARENT	FOR-83	AUG-1	PLAG-70	MT-1	DAUGHTER
SiO_2	49.40	39.34	51.01	51.26	0.00	55.45
TiO_2	0.60	0.00	0.33	0.00	7.28	1.19
Al_2O_3	12.25	0.33	3.73	30.53	0.00	14.34
FeO	10.62	14.95	8.46	0.00	91.67	9.40
MnO	0.28	0.22	0.18	0.00	0.00	0.15
MgO	13.34	44.96	17.88	0.00	0.00	7.37
CaO	8.67	0.20	16.90	13.23	0.00	5.47
Na_2O	2.06	0.00	0.00	3.82	0.00	4.09
K_2O	1.53	0.00	0.00	0.17	0.00	1.44
Cr_2O_3	0.17	0.00	0.52	0.00	0.00	0.04

(PARENT - MINERALS = DAUGHTER)

PARENT: R-233 (komatiitic basalt)
DAUGHTER: R-232c (high-Mg tholeiitic basalt)

	SOLUTION	% CUMULATE
R-233	1.000	
FOR-83	-0.132	23.661
AUG-1	-0.235	41.939
PLAG-70	-0.164	29.314
MT-1	-0.028	5.087
R-232c	0.440	

R SQUARED = 5.333 (sum (calculated - observed)^2)

	PARENT ANALYSIS	DAUGHTER ANALYSIS	DAUGHTER CALC.	WEIGHTED RESID.
SiO_2	49.40	55.45	55.22	0.23
TiO_2	0.60	1.19	0.72	0.46
Al_2O_3	12.25	14.34	14.63	-0.29
FeO	10.62	9.40	9.44	-0.04
MnO	0.28	0.15	0.48	-0.33
MgO	13.34	7.37	7.55	-0.18
CaO	8.67	5.47	5.88	-0.42
Na_2O	2.06	4.09	3.30	0.79
K_2O	1.53	1.44	3.45	-2.01
Cr_2O_3	0.17	0.04	0.12	-0.08

Zr, and Ba) relative to more compatible elements (i.e. HREE, Ti, and Y). The geochemical contrast between low Zr/Y, high Ti/Zr, and LREE depleted komatiites and high Zr/Y, low Ti/Zr and LREE enriched komatiitic-tholeiitic basalts cannot be explained by the fractional crystallization of olivine, clinopyroxene, and chromite. This is because the compositional "jump" is too large for fractionation to concentrate the values of Ti, Zr, and LREE, relative to the major elements, in the residual liquid. Another mechanism other than clinopyroxene fractionation may better explain the compositional "jump" between komatiites and komatiitic basalts.

Garnet fractionation is another possibility indicated by the position of the komatiitic-tholeiitic basalts on the CMAS diagrams (Figs. 59 to 62) and the Al_2O_3/TiO_2 versus MgO/TiO_2 plot (Figs. 63a, 63b, and 63c). However, the compositional trends of komatiitic-tholeiitic basalts on other molecular proportion ratio plots indicate that garnet has not played a major role in their evolution. Other researchers have appealed to variable degrees of partial melting of the same source to explain the transition from komatiites to komatiitic basalts (St.-Seymour et al., 1983). Canil (1987) proposed that his komatiitic basalts and high-Mg tholeiitic basalts were generated from a different source than komatiites. He explained his transition between komatiitic basalts and high-Mg tholeiitic basalts by variable degrees of partial melting of a clinopyroxene-bearing source or by fractional crystallization of clinopyroxene from komatiitic

basalt liquids.

The Woodburn Lake Group komatiitic-tholeiitic basalts cannot be primary melts because they do not fall within the melt fields that can coexist with mantle compositions in Figures 67 and 66 (i.e. plots of molar Al_2O_3 versus SiO_2 and molar FeO versus MgO). The position of the komatiitic-tholeiitic basalts on CMAS projections (Figs. 59-62) suggests that their compositions are controlled by a process that takes place between 1 atmosphere and 30 kbar. As mentioned above, this process is probably combined assimilation-fractional crystallization (AFC) of komatiitic liquids within a crustal magma chamber. This hypothesis of generating LREE enriched komatiitic basalts from LREE depleted komatiites has strong support from recent work by Arndt and Jenner (1986) and Cattell (1987). The degree of AFC that has take place probably dictates the position of compositional gaps within komatiitic suites.

The Woodburn Lake Group komatiitic-tholeiitic basalts were modelled for the hypothesis of their generation from komatiitic magmas by combined olivine-clinopyroxene fractionation and continental crustal assimilation. The composition of the contaminant(s) is not known, since continental crust is not found in the intermediate area. Possible contaminants are a) gneisses, similar in composition to the Brown River Gneisses (Schau, 1982) of the Prince Albert Group, and b) felsic-intermediate metavolcanics that underlie the komatiites. Mass balance calculations of this AFC process are shown in Table 23. These

Table 23a. Mass balance, assimilation-fractional crystallization calculations (AFC) to model the generation of komatiitic-tholeiitic basalts.

INPUT DATA:

	PARENT	FOR-92	AUG-1	CHR-1	AK-2	DAUGHTER
SiO_2	45.12	40.30	51.00	0.31	71.84	51.97
TiO_2	0.36	0.00	0.33	0.42	0.31	0.57
Al_2O_3	8.39	0.00	3.73	15.53	15.23	12.74
FeO	11.03	7.97	8.45	26.84	1.73	10.19
MnO	0.18	0.16	0.18	0.00	0.03	0.18
MgO	25.62	51.13	17.88	9.29	1.03	13.04
CaO	6.94	0.25	16.90	0.00	0.70	6.71
Na_2O	0.84	0.00	0.00	0.00	6.48	3.28
K_2O	0.03	0.00	0.00	0.00	1.64	0.08
Cr_2O_3	0.43	0.17	0.52	46.61	0.00	0.16

(PARENT - MINERALS = DAUGHTER)

PARENT: AK-15d (upper portion of spinifex-textured zone)
DAUGHTER: AK-31 (komatiitic basalt)
CONTAMINANT: AK-2 (low-SiO_2 rhyolite)

	SOLUTION	% CUMULATE
AK-15d	1.000	
FOR-92	-0.259	165.304
AUG-1	-0.082	52.418
CHR-1	-0.004	2.272
AK-2	0.188	-119.994
AK-31	0.843	

R SQUARED = 0.872 (sum (calculated - observed)^2)

	PARENT ANAL.	DAUGHTER ANAL.	DAUGHTER CALC.	WEIGHTED RESID.
SiO_2	45.12	51.97	52.01	-0.04
TiO_2	0.36	0.57	0.47	0.11
Al_2O_3	8.39	12.74	12.89	-0.15
FeO	11.03	10.19	10.04	0.1[illegible]
MnO	0.18	0.18	0.15	0.04
MgO	25.62	13.04	13.03	0.01
CaO	6.94	6.71	6.64	0.07
Na_2O	0.84	3.28	2.44	0.84
K_2O	0.03	0.08	0.40	-0.32
Cr_2O_3	0.43	0.16	0.20	-0.04

Table 23b. Mass balance, assimilation-fractional crystallization calculations (AFC) to model the generation of komatiitic-tholeiitic basalts.

INPUT DATA:

	PARENT	FOR-90	AUG-1	AK-2	DAUGHTER
SiO_2	46.53	39.70	50.99	71.84	54.48
TiO_2	0.32	0.00	0.33	0.31	1.16
Al_2O_3	7.39	0.00	3.73	15.23	14.41
FeO	9.61	9.56	8.45	1.73	7.70
MnO	0.17	0.00	0.18	0.03	0.08
MgO	26.96	50.23	17.88	1.03	14.66
CaO	6.79	0.30	16.90	0.70	2.73
Na_2O	0.74	0.00	0.00	6.48	3.44
K_2O	0.02	0.00	0.00	1.64	0.15
Cr_2O_3	0.40	0.20	0.52	0.00	0.07

(PARENT - MINERALS = DAUGHTER)

PARENT: K-44g (upper portion of spinifex-textured zone)
DAUGHTER: R-220d (komatiitic basalt)
CONTAMINANT: AK-2 (low-SiO_2 rhyolite)

	SOLUTION	% CUMULATE
K-44g	1.000	
FOR-90	-0.246	67.771
AUG-1	-0.306	84.241
AK-2	0.189	-52.012
R-220d	0.636	

R SQUARED = 0.881 (sum (calculated - observed)^2)

	PARENT ANAL.	DAUGHTER ANAL.	DAUGHTER CALC.	WEIGHTED RESID.
SiO_2	46.53	54.48	54.51	-0.04
TiO_2	0.32	1.16	0.43	0.72
Al_2O_3	7.39	14.41	14.34	0.07
FeO	9.61	7.70	7.84	-0.13
MnO	0.17	0.08	0.19	-0.10
MgO	26.96	14.66	14.61	0.06
CaO	6.79	2.73	2.62	0.10
Na_2O	0.74	3.44	3.09	0.35
K_2O	0.02	0.15	0.52	-0.37
Cr_2O_3	0.40	0.07	0.30	-0.23

Table 23c. Mass balance, assimilation-fractional crystallization calculations (AFC) to model the generation of komatiitic-tholeiitic basalts.

INPUT DATA:

	PARENT	FOR-92	AUG-1	PLAG-60	CHR-1	667636	DAUG
SiO_2	45.13	40.30	51.00	52.47	0.31	64.63	54.49
TiO_2	0.36	0.00	0.33	0.00	0.42	0.76	1.16
Al_2O_3	8.39	0.00	3.73	29.67	15.53	17.24	14.41
FeO	11.03	7.97	8.45	0.00	26.84	3.35	7.71
MnO	0.18	0.16	0.18	0.00	0.00	0.07	0.08
MgO	25.62	51.13	17.88	0.00	9.29	1.87	14.66
CaO	6.94	0.25	16.90	12.24	0.00	3.88	2.73
Na_2O	0.84	0.00	0.00	4.29	0.00	5.21	3.44
K_2O	0.03	0.00	0.00	0.35	0.00	1.98	0.15
Cr_2O_3	0.43	0.17	0.52	0.00	46.61	0.00	0.07

(PARENT - MINERALS = DAUGHTER)

PARENT: AK-15d (upper portion of spinifex-textured zone)
DAUGHTER: R-220d (komatiitic basalt)
CONTAMINANT: 667636 (Brown River Gneiss)

	SOLUTION	% CUMULATE
AK-15d	1.000	
FOR-92	-0.033	-10.836
AUG-1	-0.350	-116.080
PLAG-60	-0.012	-3.860
CHR-1	-0.004	-1.421
667636	0.700	232.198
R-220d	1.302	

R SQUARED = 1.206 (sum (calculated - observed)^2)

	PARENT ANALYSIS	DAUGHTER ANALYSIS	DAUGHTER CALC.	WEIGHTED RESID.
SiO_2	45.13	54.49	54.45	0.04
TiO_2	0.36	1.16	0.60	0.56
Al_2O_3	8.39	14.41	14.44	-0.03
FeO	11.03	7.71	7.76	-0.06
MnO	0.18	0.08	0.12	-0.04
MgO	25.62	14.66	14.68	-0.02
CaO	6.94	2.73	2.79	-0.06
Na_2O	0.84	3.44	3.42	0.02
Cr_2O_3	0.43	0.07	0.03	0.04

Table 23d. Mass balance, assimilation-fractional crystallization calculations (AFC) to model the generation of komatiitic-tholeiitic basalts.

INPUT DATA:

	PARENT	FOR-92	AUG-1	CHR-1	AK-2	DAUGHTER
SiO_2	45.12	40.30	51.00	0.31	71.84	48.56
TiO_2	0.36	0.00	0.33	0.42	0.31	0.68
Al_2O_3	8.39	0.00	3.73	15.53	15.23	14.17
FeO	11.03	7.97	8.45	26.84	1.73	11.44
MnO	0.18	0.16	0.18	0.00	0.03	0.17
MgO	25.62	51.13	17.88	9.29	1.03	13.81
CaO	6.94	0.25	16.90	0.00	0.70	6.44
Na_2O	0.84	0.00	0.00	0.00	6.48	2.49
K_2O	0.03	0.00	0.00	0.00	1.64	1.05
Cr_2O_3	0.43	0.17	0.52	46.61	0.00	0.11

(PARENT - MINERALS = DAUGHTER)

PARENT: AK-15d (upper portion of spinifex-textured zone)
DAUGHTER: R-222 (komatiitic basalt)
CONTAMINANT: AK-2 (low-SiO_2 rhyolite)

	SOLUTION	% CUMULATE
AK-15d	1.000	
FOR-92	-0.268	72.411
AUG-1	-0.175	47.453
CHR-1	-0.005	1.306
AK-2	0.078	-21.170
R-222	0.630	

R SQUARED = 0.949 (sum (calculated - observed)^2)

	PARENT ANAL.	DAUGHTER ANAL.	DAUGHTER CALC.	WEIGHTED RESID.
SiO_2	45.12	48.56	48.66	-0.10
TiO_2	0.36	0.68	0.52	0.17
Al_2O_3	8.39	14.17	13.94	0.22
FeO	11.03	11.44	11.64	-0.20
MnO	0.18	0.17	0.16	0.00
MgO	25.62	13.81	13.71	0.11
CaO	6.94	6.44	6.21	0.23
Na_2O	0.84	2.49	2.13	0.36
K_2O	0.03	1.05	0.25	0.79
Cr_2O_3	0.43	0.11	0.10	0.02

Table 23e. Mass balance, assimilation-fractional crystallization calculations (AFC) to model the generation of komatiitic-tholeiitic basalts.

INPUT DATA:

	PARENT	FOR-90	AUG-1	CHR-1	PLAG60	AK-2	DAUGH
SiO_2	45.12	39.70	50.99	0.31	52.46	71.85	52.29
TiO_2	0.36	0.00	0.33	0.42	0.00	0.31	0.67
Al_2O_3	8.39	0.00	3.73	15.53	29.67	15.23	11.34
FeO	11.03	9.56	8.45	26.84	0.00	1.73	14.01
MnO	0.18	0.00	0.18	0.00	0.00	0.03	0.17
MgO	25.62	50.23	17.88	9.29	0.00	1.03	8.97
CaO	6.94	0.30	16.90	0.00	12.24	0.70	8.60
Na_2O	0.84	0.00	0.00	0.00	4.29	6.48	1.70
K_2O	0.03	0.00	0.00	0.00	0.35	1.64	1.13
Cr_2O_3	0.43	0.20	0.52	46.61	0.00	0.00	0.05

(PARENT - MINERALS = DAUGHTER)

PARENT: AK-15d (upper portion of spinifex-textured zone)
DAUGHTER: AK-20 (high-Mg tholeiitic basalt)
CONTAMINANT: AK-2 (low-SiO_2 rhyolite)

	SOLUTION	% CUMULATE
AK-15d	1.000	
FOR-90	-0.402	76.111
AUG-1	-0.071	13.434
CHR-1	-0.006	1.104
PLAG60	-0.135	25.615
AK-2	0.086	-16.264
AK-20	0.472	

R SQUARED = 0.794 (sum (calculated - observed)^2)

	PARENT ANALYSIS	DAUGHTER ANALYSIS	DAUGHTER CALC.	WEIGHTED RESID.
SiO_2	45.12	52.29	52.31	-0.02
TiO_2	0.36	0.67	0.78	-0.11
Al_2O_3	8.39	11.34	11.32	0.02
FeO	11.03	14.01	13.98	0.03
MnO	0.18	0.17	0.35	-0.18
MgO	25.62	8.97	8.96	0.01
CaO	6.94	8.60	8.56	0.04
Na_2O	0.84	1.70	1.74	-0.04
K_2O	0.03	1.13	0.27	0.86
Cr_2O_3	0.43	0.05	0.08	-0.03

Table 23f. Mass balance, assimilation-fractional crystallization calculations (AFC) to model the generation of komatiitic-tholeiitic basalts.

INPUT DATA:

	PARENT	FOR-92	AUG-1	PLAG-60	CHR-1	667642	DAUG
SiO_2	45.12	40.30	51.00	52.47	0.31	64.17	55.44
TiO_2	0.36	0.00	0.33	0.00	0.42	1.05	1.18
Al_2O_3	8.39	0.00	3.73	29.67	15.53	16.27	14.34
FeO	11.03	7.97	8.45	0.00	26.84	3.71	9.40
MnO	0.18	0.16	0.18	0.00	0.00	0.05	0.15
MgO	25.62	51.13	17.88	0.00	9.29	2.42	7.37
CaO	6.94	0.25	16.90	12.24	0.00	4.30	5.47
Na_2O	0.84	0.00	0.00	4.29	0.00	4.95	4.08
K_2O	0.03	0.00	0.00	0.35	0.00	2.07	1.44
Cr_2O_3	0.43	0.17	0.52	0.00	46.61	0.00	0.04

(PARENT - MINERALS = DAUGHTER)

PARENT: AK-15d (upper portion of spinifex-textured zone)
DAUGHTER: R-232c (high-Mg tholeiitic basalt)
CONTAMINANT: 667642 (Brown River Gneiss)

	SOLUTION	% CUMULATE
AK-15d	1.000	
FOR-92	-0.325	488.123
AUG-1	-0.175	262.656
PLAG-60	-0.096	143.364
CHR-1	-0.004	6.371
667642	0.533	-800.513
R-232c	0.933	

R SQUARED = 0.821 (sum (calculated - observed)^2)

	PARENT ANALYSIS	DAUGHTER ANALYSIS	DAUGHTER CALC.	WEIGHTED RESID.
SiO_2	45.12	55.44	55.52	-0.08
TiO_2	0.36	1.18	0.92	0.26
Al_2O_3	8.39	14.34	14.38	-0.04
FeO	11.03	9.40	9.33	0.07
MnO	0.18	0.15	0.13	0.02
MgO	25.62	7.37	7.32	0.05
CaO	6.94	5.47	5.31	0.16
Na_2O	0.84	4.08	3.28	0.80
K_2O	0.03	1.44	1.18	0.26
Cr_2O_3	0.43	0.04	0.08	-0.04

results indicate that the komatiites could have been contaminated by either of the two contaminants. Where and when did this contamination-fractional crystallization process take place? Two scenarios are possible: 1) within an open system magma chamber in the lower portions of the continental crust, or 2) en route through the pre-existing volcanic pile. The range of compositions of the komatitic - tholeiitic basalts suggests the former. Continued fractionation of the komatiitic basalt liquid (13-15 wt% MgO) en route to the surface would explain the observed range of compositions.

6.4 TECTONIC ENVIRONMENT

Numerous and varied models have been advocated for the evolution of granite-greenstone terrains in the Archean. These models have been described in detail by Windley (1977, 1984), Condie (1981 and 1982), and Kroener (1981, 1984 and 1985). Most of these models can be categorized into two groups; a) subduction-related settings or b) intracontinental rifting settings.

Models of the subduction-related settings consider a plate-style tectonic mechanism as being responsible for the origin of greenstone belts. These models assume a simatic-sialic transformation from production of oceanic crust to subduction, horizontal collisional tectonism, and back-arc basin formation in oceanic or Andean-type magmatic arcs. Models of the

intracontinental rifting settings assume an initial sialic crust, followed by formation of greenstone belts in rifts or linear downsags of the crust. Continuation of mantle processes and downsagging causes vertical, gravity-driven tectonism to operate. This results in partial melting of the crust, diapirism and plutonism, deformation, crustal stacking, metamorphism, and uplift. The final product is a granite-greenstone terrain.

A typical Archean granite-greenstone terrain is characterized by komatiitic, tholeiitic, and calc-alkaline volcanics, related clastic and chemical sedimentary rocks, and adundant granitoids. Most Archean greenstone belts contain few intermediate volcanics, and are typically bimodal in composition (Ayres and Thurston, 1985). When andesites and dacites are found, they generally show a calc-alkaline affinity. Recent work, excellently summarized by Ayres and Thurston (1985) and Nisbet (1987), indicates the presence of sialic crust either underneath or along the margin of greenstone belts. This implies that the sialic crust acted as a basement to the greenstone belts. Good evidence for such a setting is provided by the Belingwe Formation, Rhodesia (Bickle et al., 1975) and the Pongola Sequence, South Africa (Armstrong et al., 1982 and 1986). Since good geological evidence has led many workers to favour intracontinental rifting models for the origin of greenstone belts (Schau, 1977; Baragar and McGlynn, 1978; Kroener, 1981 and 1984; Henderson, 1981; Ayres and Thurston, 1985; among others), many geologists have rejected oceanic island-arc and continental-arc models for greenstone belt

formation.

Although intracontinental rifting models are much in favour, subduction-related models have not lost their appeal. It has been noted that the general stratigraphy of most greenstone belts is inverted when compared to typical continental rifts (Armstrong et al., 1986; Hoffman, 1986). In typical continental rifts the major volcanic sequence overlies the sedimentary sequence, such as in the Pongola Sequence. In addition, recent isotopic data suggests that most granitoids are younger than the greenstone belts with which they are associated.

Langford and Morin (1976) proposed a convergent plate tectonic setting with successive accretion of island arcs to explain the tectonic style within the Superior Province. Similarly, Blackburn (1980) suggested a plate convergent model for the Wabigoon greenstone belt on the basis of its similarities to modern island arcs. Percival and Stern (1984) suggested that the Quetico metasedimentary belt is analogous to modern-day back-arc basins such as the sea of Japan. Card (1986 and pers. comm.) and Hoffman (1986) suggested that greenstone belts represent ancient, magmatic-arc accretionary complexes, comparable to the Western Pacific region. Further support of applying this model to Archean greenstone belts is given by Sylvester et al. (1987) and Ludden et al. (1986). Sylvester et al. (1987) suggested that the major geological features of the Late Archean (2744-2696 Ma) Michipicoten greenstone belt and the geochemical characteristics of its volcanic rocks are similar to

those found in Cenozoic convergent plate margins. This convergent plate margin setting varied laterally from an immature oceanic island arc to a more mature continental marginal arc. Ludden et al. (1986) came to a similar conclusion for the Abitibi greenstone belt, whereby the northern part represents an older continental marginal arc and the southern part represents a later series of rift basins within continental crust.

What is the tectonic environment and significance of the komatiites and komatiitic basalts from the Woodburn Lake Group greenstone belt? These rocks form an unique association with the overlying quartzites. This association is unusual in that the quartzites represent crustal stability and the mafic-ultramafic volcanics indicate extension (rifting?). This association has been found elsewhere in Canada (Schau, 1977, 1982; Frisch, 1982; Taylor, 1985; Wood and Thurston, 1986; Donaldson and Dekemp, 1987; Roscoe and Donaldson, 1988), South Africa (Armstrong et al., 1982 and 1986), and India (Srinivasan and Ojakangas, 1985). Most researchers have suggested that this association indicates that of komatiites and/or tholeiitic basalts were emplaced on a tectonically stable sialic crust. This is because many authors regard quartz arenites as being formed in a stable tectonic environment. Intensive research in recent years has shown that quartz arenites can also occur in less stable tectonic environments (Mack, 1984; Velbel, 1985; Dorsey, 1988; Chandler, 1988). This work clearly indicates that generalizations on the relationship between sandstone (i.e. in this case quartzites)

petrography and depositional/tectonic environments must be treated with caution. Mack (1984) and Velbel (1985) have provided modern and ancient examples of mature sandstones which have experienced and recorded one to three tectonic settings, and these are:

1) a depositional setting corresponding to the source area (provenance) tectonics.
2) a depositional setting reflecting the sedimentary transportation environment, and which may not be related to the provenance source.
3) a tectonically transported depositional setting, whereby the sandstone petrography represents the tectonics of the source and depositional setting, but not the structural setting.

The origin and interpretation of quartz arenites must take into consideration provenances, depositional basins, and tectonic processes within the same geological model. If the geological history of an area is not understood, than sandstone petrography can only provide information on the tectonics of the source area.

U-Pb age dating of zircons from a quartz porphyry underlying the quartzites and an intrusive granodiorite give ages of 2798 +24/-21 Ma (Tella et al., 1985) and 2598 +3/-2 Ma (Ashton, 1985), respectively, and bracket the age of the Woodburn Lake Group quartzites. The minimum age of detrital zircons in the quartzite is 2875 Ma, which Ashton (pers. comm.) believes is suggestive of an intracontinental setting for the metavolcanic-metasedimentary

package. However, Ashton (1988) pointed out that there are too many unknowns to pin down the tectonic environment, although he favours the continental rifting environment.

In this study, the author feels that the evidence from the Woodburn Lake Group greenstone belts may possibly be more indicative of a continental marginal arc environment rather than an intracontinental rifting environment. Again, it should be pointed out that either environment is possible.

The major geologic features of the Woodburn Lake Group greenstone belts are:

1) bimodal volcanism (i.e. komatiite-basalt and dacite-rhyolite),
2) voluminous calc-alkaline felsic-intermediate volcanics (pyroclastic?) with chemistry similar to Cenozoic continental-arc and island-arc sequences, and the Michipicoten greenstone belt,
3) some pillowed lavas, indicative of a subaqueous environment,
4) oxide facies chemical sediments, indicative of a shallow-water environment, and probably chemical precipitates related to volcanism,
5) komatiitic-tholeiitic basalts with chemistry similar to modern-day mafic volcanics, either island arc or oceanic in nature (Fig. 68), although the Ketyet River Group basalts have continental affinities,

Figure 68. Discrimination diagrams using a) MgO, FeO, and Al_2O_3 (wt%, Pearce et al. 1977) and b) Zr, Ti/100 and Sr/2 (ppm, Pearce and Cann, 1973) to indicate the tectonic environment of the Woodburn Lake Group komatiitic-tholeiitic basalts and the Ketyet River Group tholeiitic basalts. A comparison of Woodburn Lake Group basalts (upper left) and the Ketyet River Group basalts (lower left) indicates different tectonic environments, ocean ridge and floor vs continental, respectively. However, in the Zr - Ti/100 - Sr/2 diagram the Woodburn Lake Group komatiitic-tholeiitic basalts plot along the boundary between the island arc and calc-alkali basalt fields.

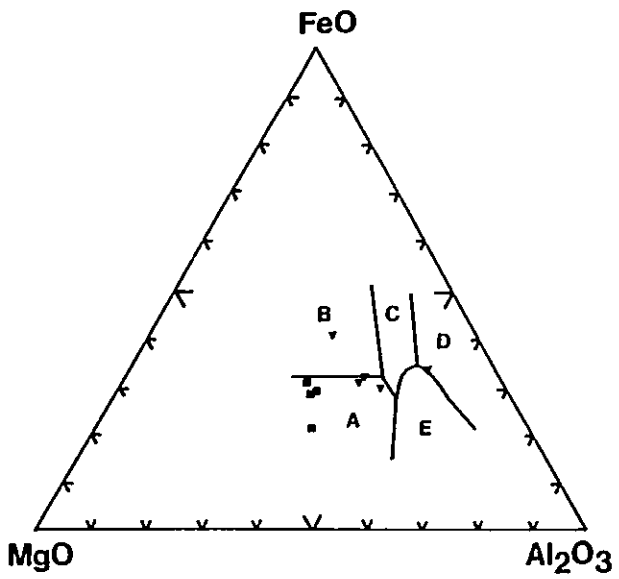

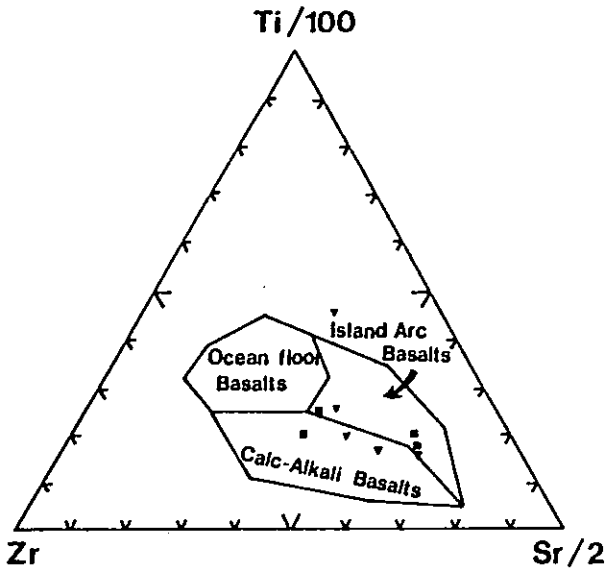

(ppm)

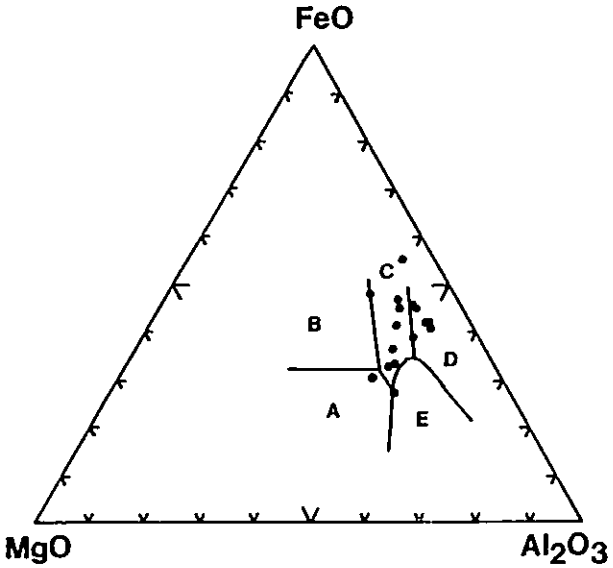

(weight %)

A Ocean Ridge and Floor
B Ocean Island
C Continental
D Spreading Center Island
E Orogenic

6) clastic sediments (i.e. volcanoclastic in part),

7) upper platformal sequence of quartzites, indicative of nearby continental crust, but with no clear indicators of the environment of formation (i.e. aeolian, tidal, fluvial, or resedimented),

8) abundant faulting; imbricate thrusting (north-west verging ?),

9) an unconformity (?) between the quartzites and the underlying volcanics,

10) no evidence of gneissic basement to the metavolcanic metasedimentary belts,

11) extreme stratigraphic diversity within the Woodburn Lake Group supracrustal belts,

12) no evidence of a major rift.

Except for the occurrence of komatiites, these geological features are similar to those presented by Sylvester et al. (1987) for the Michipicoten greenstone belt. Sylvester et al. (1987) provided compelling evidence for the Taupo-Kermadec-Tonga volcanic zone (Ewart et al., 1977) being a representative Cenozoic analogue of the Michipicoten greenstone belt. The Taupo-Kermadec-Tonga volcanic zone is characterized by 1) oceanic island arc basalts, 2) continental arc rhyolites, and 3) clastic sediments. This volcanic zone varies laterally from an immature oceanic island arc to a mature continental arc.

According to this model, the komatiites and komatiitic-tholeiitic basalts would form the lower parts in

immature continental marginal arcs, possibly a rifted continental margin or back-arc basin. The calc-alkaline volcanics would form as the upper parts of mature arcs or back arcs. Archean greywackes (i.e. turbidites) would represent trench, inter-arc, or fan deposits. The quartzites would represent late fluvial-alluvial sedimentary sequences during late rift-phase sedimentation of mature back-arcs or island arcs. The late granites would represent the roots of arc systems, similar to modern arcs. The reason(s) for komatiites not being produced in the modern environment is probably the result of the Archean tectonic and geothermal environment being different from that of today.

The plate tectonic model for the Woodburn Lake Group is a practical starting place for developing and interpreting the tectonic environment of the Woodburn Lake Group. However, it should be pointed out that there are weaknesses to this model and these are:

1) modern plate-margin arc systems are not small-scale tectonic systems, whereas most greenstone belts appear to be small-scale,
2) the tectonic elements of modern tectonic settings are reasonably well understand, however this is not the case with the tectonic elements of Archean terrains,
3) too much emphasis is placed on one rock suite (i.e. komatiites); need for detailed mapping of the rest of the Woodburn Lake Group supracrustal belt; komatiites and

quartzites may be indicative of one or more tectonic environments,

4) not being able to find a modern analogue of komatiites, however, this may only be a function of the Archean geothermal gradient and not of a specific tectonic environment.

It has been proposed that the Woodburn Lake Group is correlative to the Prince Albert Group and the Ketyet River Group (Schau, 1982). The author suggests that the name, Woodburn Lake Group, should incorporate the Ketyet River Groups. Instead of having three separate groups (Fig. 69), there would be two groups correlated across a major tectonic break. Eventually, one group name might be used as a supergroup. The lithological and structural complexity of the Woodburn Lake Group, Prince Albert Group, and Ketyet River Group can easily be explained as a melange of magmatic rocks, subduction complexes, and volcaniclastics of many different arc systems. The northwest Pacific region, where accretion is ongoing and far from complete, provides an excellent analogue to this complicated lithologic and structural complex. The only difference being that the northwest Pacific has not undergone the later stages of plutonism and compressional and horizontal tectonism that cause crustal stacking, uplift, erosion, and cratonic stabilization. A comparison of the Woodburn Lake Group, Ketyet River Group, and Prince Albert Group with the northwest Pacific Basin region, on similar scales (Fig. 70), shows a more evolved continental-arc

Figure 69. Regional distribution of Prince Albert, Woodburn Lake, and Ketyet River Groups (represented by black areas).

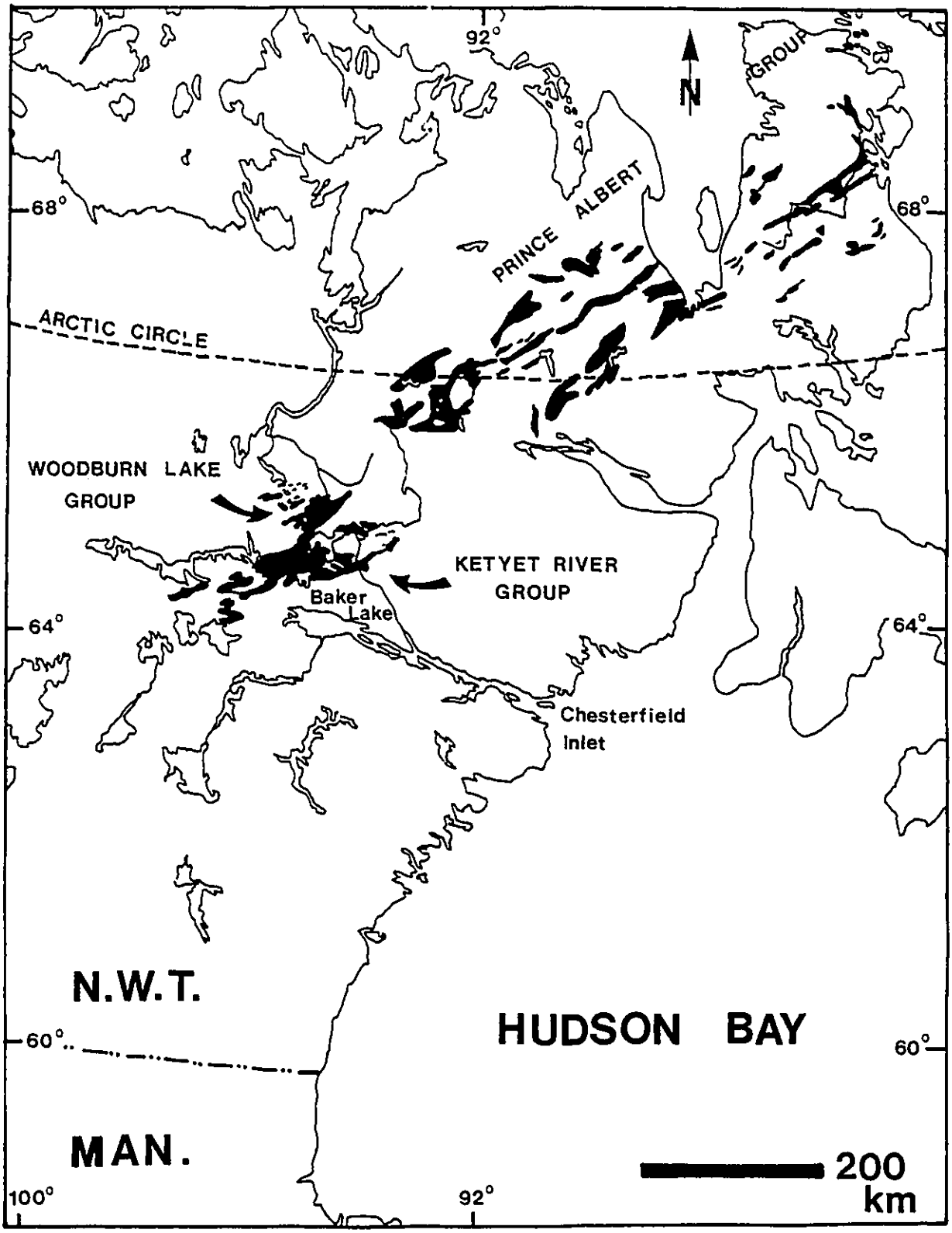
92°
N
GROUP
68°
PRINCE ALBERT
68°
ARCTIC CIRCLE
WOODBURN LAKE
GROUP
KETYET RIVER
GROUP
Baker
Lake
64°
64°
Chesterfield
Inlet
N.W.T.
HUDSON BAY
60°
60°
MAN.
200
km
100°
92°

Figure 70. Comparison of scale and patterns of tectonic system of the Central Northern Churchill Province with those of the northern Pacific Basin and the Tonga-Kermadec-Taupo region.

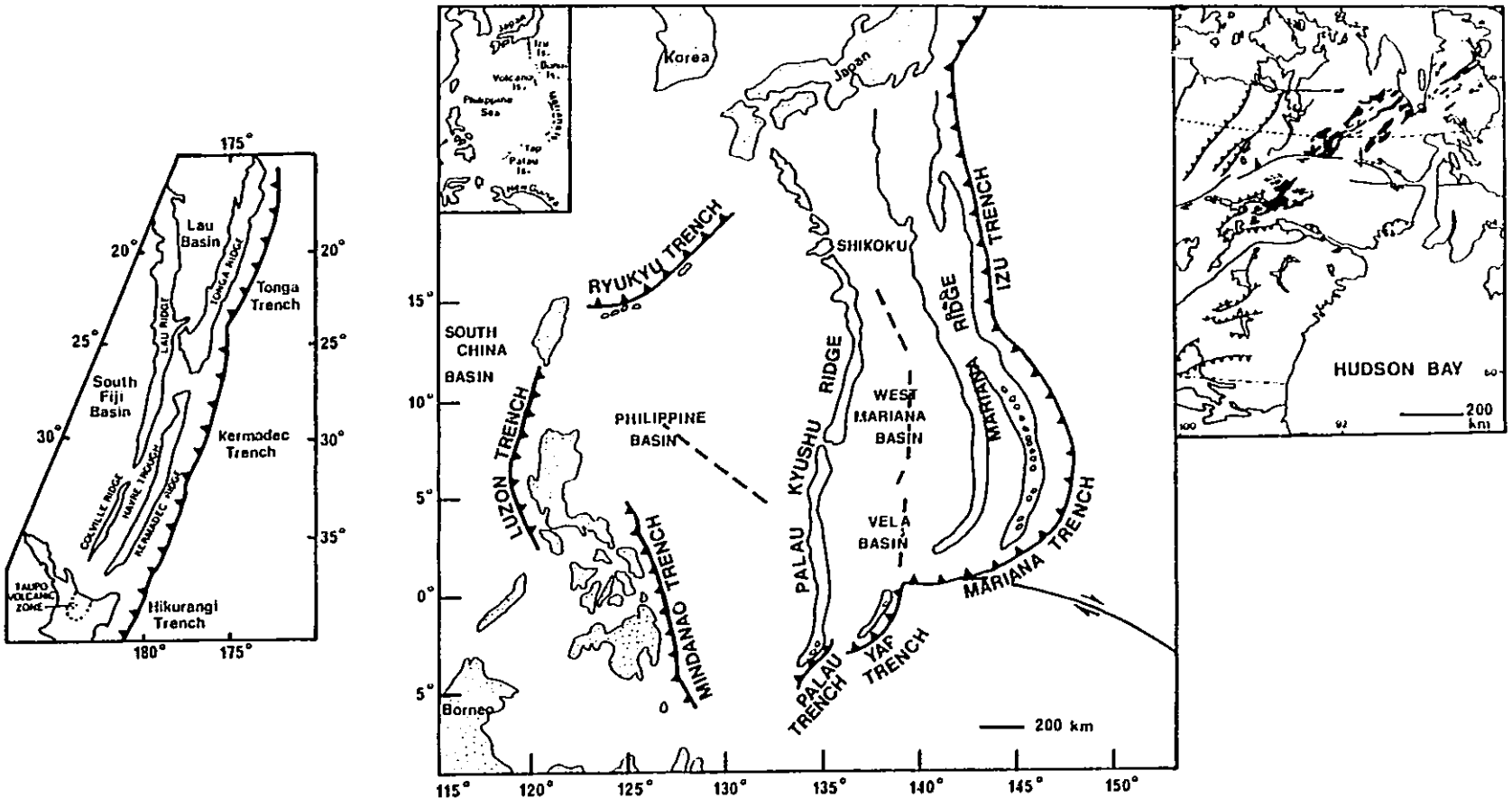
175°
20°
25°
30°
35°
180°
175°
Lau Basin
Tonga Trench
South Fiji Basin
Kermadec Trench
LAU RIDGE
TONGA RIDGE
COLVILLE RIDGE
HAVRE TROUGH
KERMADEC RIDGE
TAUPO VOLCANIC ZONE
Hikurangi Trench
Korea
Japan
Philippine Sea
Volcano Is.
Izu Is.
Bonin Is.
Yap
Palau Is.
New Guinea
RYUKYU TRENCH
SHIKOKU
IZU TRENCH
RIDGE
MARIANA
SOUTH CHINA BASIN
PHILIPPINE BASIN
WEST MARIANA BASIN
LUZON TRENCH
MINDANAO TRENCH
PALAU KYUSHU RIDGE
VELA BASIN
MARIANA TRENCH
PALAU TRENCH
YAP TRENCH
Borneo
200 km
115°
120°
125°
130°
135°
140°
145°
150°
15°
10°
5°
0°
5°
HUDSON BAY
200 km

and island-arc complex versus a much less evolved analogue.

Further detailed mapping, structural and sedimentological studies, geochemical results, and isotopic work are needed to test the tectonic models proposed for the Woodburn Lake Group and its correlative supracrustal belt, the Prince Albert Group.

CONCLUSIONS AND CONTRIBUTIONS TO THE LITERATURE

1. The Woodburn Lake Group komatiites are aluminum-undepleted, similar to other Late Archean occurrences. They exhibit the typical field characteristics observed elsewhere.

2. The Woodburn Lake Group komatiitic-tholeiitic basalts are LREE and LILE-enriched, similar to those from Kambalda, Australia, and the Abitibi Greenstone Belt, Canada.

3. The major and trace-element geochemistry of the komatiites and komatiitic-tholeiitic basalts has not been significantly changed by alteration processes.

4. The komatiites and komatiitic-tholeiitic basalts have been regionally metamorphosed to greenschist and lower amphibolite grade. Locally, contact metamorphism by intruding granites has taken place at the margins of the Woodburn Lake Group belts. Olivine-spinel geothermometry gives a temperature estimate of 625°C.

5. The compositional variations shown within the volcanic units can be explained by fractional crystallization, but the differences between the komatiites and komatiitic basalts are not adequately explained by this process.

6. Most of the fractional crystallization within the komatiites took place at the surface.

7. Use of Pearce type diagrams suggest that this fractional crystallization process is not solely due to olivine separation, but also to varying degrees of olivine, clinopyroxene, and chromite fractionation.

8. Quantitative modelling suggests the generation of the Woodburn Lake Group komatiitic basalts by 20-40% crustal contamination of the initial komatiitic liquids.

9. The chemical characteristics of the Woodburn Lake Group komatiites indicate that their mantle source region underwent an earlier melting event, leaving it depleted in Zr, LREE, and to a lesser degree, TiO_2.

10. The Woodburn Lake Group komatiites were derived from a garnet lherzolite source by 30-40% partial melting at a pressure of 50-60 kbar and a temperature of 1700-1800°C.

11. The bimodal assemblage of komatiite - basalt and dacite - rhyolite possibly reflects a lateral variation within the tectonic environment.

12. It is advocated that the Woodburn Lake Group komatiites, komatiitic-tholeiitic basalts, dacites, and rhyolites were erupted in a continental marginal arc environment, which was extensional and partly subaqueous.

13. It is proposed that the Woodburn Lake Group, Ketyet River Group, and Prince Albert Group all belong to the same group, and should be named as a supergroup.

REFERENCES

Abbey, S. (1983)
Studies in "standard samples" of silicate rocks and minerals 1969-1982. Geological Survey of Canada, Paper 83-15, 114 p.

Agee, C. and Walker, D. (1986)
Experimental static compression and olivine flotation in ultrabasic silicate liquid. EOS, Transaction American Geophysical Union 67, p.409.

Aitken, B.G. and Echeverria, L.M. (1984)
Petrology and geochemistry of komatiites and tholeiites from Gorgona Island, Colombia. Contributions to Mineralogy and Petrology 86, pp. 94-105.

Allègre, C.J. (1982)
Genesis of Archean komatiites in a wet ultramafic subducted plate. In Komatiites, N.T. Arndt and E.G. Nisbet, (eds.), George Allen and Unwin, London, pp. 495-500.

Anderson, D.L. (1981)
A global geochemical model for the evolution of the mantle. in Evolution of the Earth, R.J. O'Connell and W.S. Fyfe (eds.), Geodynamics Series, volume 5, American Geophysical Union, Washington, D.C., pp. 6-18.

Anderson, D.L. (1982)
Isotopic evolution of the mantle: a model. Earth and Planetary Science Letters 57, pp. 13-24.

Anderson, D.L. and Bass, J.D. (1986)
Transition region of the Earth's upper mantle. Nature 320, pp. 321-328.

Anhaeusser, C.R. (1971a)
Cyclic volcanicity and sedimentation in the evolutionary development of Archean greenstone belts of shield areas. Geological Society of Australia, Special Publication 3, pp. 103-119.

Anhaeusser, C.R. (1971b)
The Barberton Mountain Land, South Africa - a guide to the understanding of the Archaean geology of western Australia. Geological Society of Australia, Special Publication 3, pp. 103-119.

Anhaeusser, C.R. (1973)
The evolution of the early Precambrian crust of southern Africa. Philosophical Transactions of the Royal Society of London, Series A, 273, pp. 359-388.

Annesley, I.R. (1981a)
Field characteristics, petrology, and geochemistry of the Amer Lake ultramafic metavolcanics, District of Keewatin. In Current Research, Part A, Geological Survey of Canada, Paper 81-1A, pp. 275-279.

Annesley, I.R. (1981b)
A field, petrographic and chemical investigation of the Amer Lake mafic and ultramafic komatiites and associated mafic volcanic rocks. Unpublished M.Sc. thesis, University of Windsor, Windsor, Ontario, 159 p.

Armstrong, N.V. Hunter, D.R. and Wilson, A.H. (1982)
Stratigraphy and petrology of the Archean Nsuze Group, northern Natal and southeastern Transvaal, South Africa. Precambrian Research 19, pp. 75-107.

Armstong, N.V., Wilson, A.H. and Hunter, D.R. (1986)
The Nsuze Group, Pongola Sequence, South Africa: geochemical evidence for Archean volcanism in a continental setting. Precambrian Research 34, pp. 175-203.

Arndt, N.T., (1975)
Ultramafic rocks of Munro Township and their volcanic setting. Unpublished Ph.D. thesis, University of Toronto, Toronto, Ontario.

Arndt, N.T. (1976)
Melting relations of ultramafic lavas (komatites) at one atmosphere and high pressure. Carnegie Institution of Washington Yearbook 75, pp. 555-561.

Arndt, N.T. (1977)
Ultrabasic magma and high-degree melting of the mantle. Contributions to Mineralogy and Petrology 64, pp. 205-221.

Arndt, N.T. (1983)
Role of a thin komatiitic-rich oceanic crust in the Archean plate-tectonic process. Geology 11, pp. 372-375.

Arndt, N.T. (1986a)
Differentiation of komatiite flows. Journal of Petrology 27, pp. 279-301.

Arndt, N.T. (1986b)
Komatiites: a dirty window to the Archean mantle. Terra Cognita 6, pp.59-66.

Arndt, N.T. and Jenner, G.A. (1986)
Crustally contaminated komatiites and basalts from Kambalda, Western Australia. Chemical Geology 56, pp. 229-255.

Arndt, N.T., Nesbitt, R.W. (1982)
Geochemistry of Munro Township basalts. In Komatiites, N.T. Arndt and E.G. Nisdet (eds.), George Allen and Unwin, London, pp. 309-329.

Arndt, N.T. and Nesbitt, R.W. (1984)
Magma mixing in komatiitic lavas from Munro Township, Ontario. In Archaean Geochemistry, A. Kroner, G.N. Hanson and A.M. Goodwin (eds.), Springer, Berlin, pp. 99-114.

Arndt, N.T. and Nisbet, E.G. (1982a)
What is a komatiite? In Komatiites, N.T. Arndt and E.G. Nisbet (eds.), George Allen and Unwin, London, pp. 19-27.

Arndt, N.T. and Nisbet, E.G. (1982b)
Komatiites. George Allen and Unwin, London, 526 p.

Arndt, N.T., Francis, D., and Hynes, A.J. (1979)
The field characteristics and petrology of Archean and Proterozoic komatiites. Canadian Mineralogist 17, pp. 147-163.

Arndt, N.T., Naldrett, A.J. and Pyke, D.R. (1977)
Komatiitic and Fe-rich tholeiitic lavas Munro Township, northeast Ontario. Journal of Petrology 18, pp. 319-369.

Arndt, N.T., Bickle, M.J., Jenner, G.A., Nisbet, E.G. and Zindler, A. (1986a)
The nature and composition of the Archean mantle. EOS, Transaction American Geophysical Union 67, pp.172-174.

Arndt, N.T., Chauvel, C., Brugmann, G., and Todt, W. (1986b)
Geochemistry of basalts from the Circum-Superior belt, Canada. Journal of the Geological Society of London, (submitted).

Arth, J.G. (1976)
Behavior of trace elements during magmatic processes - A summary of theoretical models and their applications. United States Geological Survey, Journal of Research 4, pp. 41-47.

Arth J.G. and Hanson, G.N. (1975)
Geochemistry and origin of the early Precambrian crust of northeastern Minnesota. Geochimica et Cosmochimica Acta 39, pp. 325-3t2.

Arth, J.G., Arndt, N.T. and Naldrett, A.J. (1977)
Genesis of Archean komatiites: trace element evidence from Archean komatiitic and theoleiitic lavas, Munro Township, Ontario. Geology 5, pp. 590-594.

Ashley, M., Ambler, E.P. and Flood, R.H. (1979)
Two occurences of ultramafic hornfels in the Biggenden Beds, Southeastern Queensland. Journal of the Geological Society of Australia 26, pp. 29-37.

Ashton, K.E. (1981)
Preliminary report on Geological Studies of the "Woodburn Lake Group" northwest of Tehek Lake, District of Keewatin. In Current Research, Part A, Geological Survey of Canada, Paper 81-1A, pp. 269-274.

Ashton, K.E. (1982)
Further geological studies of the "Woodburn Lake Group" northwest of Tehek Lake, District of Keewatin. In Current Research, Part A, Geological Survey of Canada, Paper 82-1A, pp. 151-157.

Ashton, K.E. (1985)
Archean orthoquartzites from the Churchill Structural Province near Baker Lake, N.W.T. Geological Association of Canada - Mineralogical association of Canada, Program with Abstracts 10, p. A2.

Ashton, K.E. (1988)
Precambrian geology of the southeast Amer Lake area (66H1), near Baker Lake, N.W.T.: a study of the Woodburn Lake Group, an Archean orthoquartzite-bearing sequence in the Churchill Structural Province. Unpublished Ph.D. thesis, Queen's University, Kingston, Ontario, (submitted).

Auvray, B., Blais, S., Jahn, B.M. et Piquet, D. (1982)
Komatiites and komatiitic series of the Finnish greenstone belts. In Komatiites, N.T. Arndt and E.G. Nisbet (eds.), Georges Allen & Unwin, London, 10, pp. 131-146.

Ayres, L.D. and Thurston, P.C. (1985)
Archean supracrustal sequences in the Canadian Shield: an overview. In Evolution of Archean Supracrustal Sequences, L.D. Ayres, P.C. Thurston, K.D. Card and W. Weber (eds.), Geological Association of Canada, Special Paper 28, pp.343-380.

Baragar, W.R.A. and Lamontagne, C.G. (1980)
The Circum-Ungava Belt in eastern Hudson Bay: The geology of Sleeper Islands and parts of the Ottawa and Belcher Islands. In Current Research, Part A, Geological Survey of Canada, Paper 80-1A, pp. 89-94.

Baragar, W.R.A. and McGlynn, J.C. (1976)
Early Archean basement in the Canadian Shield; a review of the evidence. Geological Survey of Canada, Paper 76-14, 20 p.

Baragar, W.R.A., Plant, A.G., Pringle, G.J., and Schau, M. (1979)
Diagenetic and postdiagenetic changes in the compositions of an Archean pillow. Canadian Journal of Earth Sciences 16, pp. 2102-2121.

Barnes, S.-J. (1985)
The petrography and geochemistry of komatiite flows from the Abitibi Greenstone Belt and a model for their formation. Lithos 18, pp. 241-270.

Barnes, S.-J., Gorton, M.P. and Naldrett, A.J. (1983)
A comparative study of olivine and clinopyroxene spinifex flows from Alexo, Abitibi Greenstone Belt, Ontario, Canada. Contributions to Mineralogy and Petrology 83, pp. 293-308.

Basaltic Volcanism Study Project (1981)
Basaltic Volcanism on the Terrestrial Planets. Pergamon Press, New York, 1,286 p.

Beaty, D.W. and Taylor, H.P.Jr. (1982)
The oxygen isotope geochemistry of komatiites: evidence for water-rock interaction. In Komatiites, N.T. Arndt and E.G. Nisbet (eds.), Georges Allen and Unwin, London, pp. 267-280.

Bell, R.T. (1970)
The Hurwitz Group - a prototype for deposition on metastable cratons. In Symposium on Basins and Geosynclines of the Canadian Shield, A.J. Baer (ed.), Geological Survey of Canada, Paper 70-40, pp. 159-169.

Bell, R.T. (1971)
Geology of Henik Lake (east half) and Ferguson Lake (east half) map-areas, Dictrict of Keewatin (with a contribution by J.L. Talbot). Geological Survey of Canada, Paper 70-61, 31 p.

Bellini, G.; Comin-Chiaramonti, P.; Marques, L.S.; Melfi, A.J.; Nardy, A.J.R.; Papatrechas, C.; Piccirillo, E.M.; Roisenberg, A.; and Stolfa, D. (1986)
Petrogenetic aspects of acid and basaltic lavas from the Parana Plateau (Brazil): geological, mineralogical and petrochemical relationships. Journal of Petrology 27, pp. 915-944.

Beswick, A.E. (1982)
Some geochemical aspects of alteration and genetic relations in komatiites suites. In Komatiites, N.T. Arndt and E.G. Nisbet (eds.), George Allen and Unwin, London, pp. 281-308.

Beswick, A.E. (1983)
Primary fractionation and secondary alteration within an Archaean ultramafic flow. Contributions to Mineralogy and Petrology 82, pp. 221-231.

Beswick, A.E. and Soucie, G. (1978)
A correction procedure for metasomatism in an Archaean greenstone belt. Precambrian Research 6, pp. 235-248.

Bickle, M.J. (1982)
The magnesium contents of komatiitic liquids. In Komatiites, N.T. Arndt and E.G. Nisbet, eds., George Allen and Unwin, London, pp. 479-494.

Bickle, M.J. (1986)
Implication of melting for stabilisation of the lithosphere and heat loss in the Archean. Earth and Planetary Science Letters 80, pp. 314-324.

Bickle, M.J., Ford, C.E. and Nisbet, E.G. (1977)
The petrogenesis of peridotitic komatiites: Evidence from high-pressure melting experiments. Earth and Planetary Science Letters 37, pp. 97-106.

Bickle, M.J., Martin, A. and Nisbet, E.G. (1975)
Basaltic and peridotitic komatiites and stromatolites above a basal unconformity in the Belingwe greenstone belt, Rhodesia. Earth and Planetary Science Letters 27, pp. 155-162.

Blackburn, C.E. (1980)
Towards a mobilist tectonic model for part of the Archean of northwestern Ontario. Geoscience Canada 7, pp. 64-72.

Blais, S. and Auvray, B. (1987)
Origine de l'olivine et du clinopyroxene dans les roches ultrabasiques komatiitiques de la ceinture archeenne de roches vertes de Kuhmo, Finlande orientale. Bulletin Mineralogique 110, pp. 73-92.

Blais, S., Auvray, B., Jahn, B. and Taipale, K. (1987)
Processus de fractionnement dans les coulees komatiitiques archeennes: cas des laves a spinifex de la ceinture de roches vertes de Tipasjarvi (Finlande orientale). Canadian Journal of Earth and Planetary Sciences 24, pp. 953-966.

Blake, D.H. (1980)
Volcanic rocks of the Paleohelikian Dubawnt Group in the Baker Lake-Angikuni Lake area, District of Keewatin, N.W.T.. Geological Survey of Canada, Bulletin 309, 39 p.

Brooks, C. and Hart, S. (1972)
An extrusive basaltic komatiite from a Canadian Archean metavolcanic belt. Canadian Journal of Earth Sciences 9, pp. 1250-1253.

Brooks, D.H. and Hart, S.R. (1974)
On the significance of komatiite. Geology 2, pp. 107-110.

Bryan, W., Finger, L. and Chayes, F. (1969)
Estimating proportions in petrogenic mixing equations by least squares approximation. Science 163, pp. 926-927.

Burke, K. and Dewey, J.F. (1973)
Plume generated triple junctions: key indicators in applying plate tectonics to old rocks. Journal of Geology 81, pp. 406-433.

Butler, J.C. (1986)
The role of spurious correlation in the development of a komatiite alteration model. Journal of Geophysical Research 91, B13, pp. E275-E280.

Cameron, W.E. and Nisbet, E.G. (1982)
Phanerozoic analogues of komatiitic basalts. In Komatiites, N.T. Arndt and E.G. Nisbet (eds.), George Allen and Unwin, London, pp. 29-50.

Campbell, I.H. and Arndt, N.T. (1982)
Pyroxene accumulation in spinifex-textured rocks. Geological Magazine 119, pp. 605-610.

Campbell, I.H. and Jarvis, G.T. (1984)
Mantle convection and early crustal evolution. Precambrian Research 26, pp. 15-56.

Canil, D. (1987)
The geochemistry of komatiites and basalts from the Deadman Hill area, Munro Township, Ontario, Canada. Canadian Journal of Earth Sciences 24, pp. 998-1008.

Cattell, A.C. (1987)
Enriched komatiitic basalts from Newton Township, Ontario: Their genesis by crustal contamination of depleted komatiite magma. Geological Magazine 124, pp. 303-309.

Cattell, A. and Arndt, N.T. (1987)
Low- and high-alumina komatiites from a Late Archean sequence, Newton Township, Ontario. Contributions to Mineralogy and Petrology 97, pp. 218-227.

Cattell, A., Krogh, T.E. and Arndt, N.T. (1984)
Conflicting Sm-Nd whole rock and U-Pb zircon ages for Archean lavas from Newton Township, Abitibi Belt, Ontario. Earth and Planetary Science Letters 70, pp. 280-290.

Cawthorn, R.G. (1975)
Degree of melting in mantle diapirs and the origin of ultrabasic liquids. Earth and Planetary Science Letters 27, pp. 113-120.

Chandler, F.W. (1988)
Quartz arenites: review and interpretation. Sedimentary Geology 58, pp. 105-126.

Compston, W., Williams, I.S., Campbell, I.H. and Gresham, J.J. (1986)
Zircon xenocrysts from the Kambalda volcanics: age constraints and direct evidence for older continental crust below the Kambalda-Norseman greenstones. Earth and Planetary Science Letters 76, pp. 299-311.

Condie, K.C. (1981)
Archean Greenstone Belts. Elsevier, Amsterdam, 434 p.

Condie, K.C. (1982)
Plate Tectonics and Crustal Evolution, 2nd edn., Pergamon Press, New York, 301 p.

Condie, K.C. and Hunter, D.R. (1976)
Trace element geochemistry of Archean granitic rocks from the Barberton region, South Africa. Earth and Planetary Science Letters 29, pp. 389-400.

Condie, K.C., Viljoen, M.J., and Kable, E.J.D. (1977)
Effects of alteration on element distributions in Archean tholeiites from the Barberton Greenstone Belt, South Africa. Contributions to Mineralogy and Petrology 64, pp. 75-89.

Cox, K.G. (1978)
Komatiites and other high-magnesium lavas: some problems. Philosophical Transactions of the Royal Society of London, Series A, 288, pp. 599-609.

Cox, K.G.; Bell, J.D. and Pankhurst, R.J. (1979)
The interpretation of igneous rocks. Allen and Unwin, London.

Davidson, A. (1970)
Precambrian geology, Kaminak Lake map-area, District of Keewatin. Geological Survey of Canada, Paper 69-51.

Davidson, A. (1972)
The Churchill Province. In Variations in Tectonic Styles in Canada, R.A. Price and R.J.W. Douglas (eds), Geological Association of Canada, Special Paper 11, pp. 381-433.

Deer, W.A., Howie, R.A., and Zussman, J. (1962)
Rock-forming minerals. Longman, London.

De Jongh, W.K. (1975)
Table of i uence coefficients. Unpublished report for Philip's a. .ication laboratory, Eindhoven, Holland.

De Wit, M.J. (1986)
Extensional tectonics during the igneous emplacement of the mafic-ultramafic rocks of the Barberton Greenstone Belt. In Workshop on the Tectonic Evolution of Greenstone Belts. M.J. de Wit and L.D. Ashwal (eds.), LPI Technical Report 86-10, Lunar and Planrtary Institute, Houston, pp. 84-85.

De Wit, M.J. and Hart, R. (1986)
A mid-Archean ophiolite complex, Barberton Mountain Land. In Workshop on the Tectonic Evolution of Greenstone Belts, M.J. de Wit and L.D. Ashwal (eds.), LPI Technical Report 86-10, Lunar and Planetary Science Institute, Houston, pp. 86-88.

De Wit, M.J., Hart, R.A. and Hart, R.J. (1987)
The Jamestown Ophiolite Complex, Barberton mountain belt: a section through 3.5 Ga oceanic crust. Journal of African Earth Sciences 6, pp. 681-730.

Donaldson, C.H. (1974)
Olivine crystal types in harrisitic rocks of the Rhum Pluton and in Archean spinifex rocks. Geological Society of America, Bulletin 85, pp. 1721-1726.

Donaldson, C.H. (1976)
An experimental investigation of olivine morphology. Contributions to Mineralogy and Petrology 57, pp. 187-213.

Donaldson, C.H. (1982)
Spinfex-textured komatiites: a review of textures, compositions and layering. In Komatiites, N.T. Arndt and E.G. Nisbet (eds.), George Allen and Unwin, London, pp. 213-244.

Donaldson, J.A. (1965)
The Dubawnt Group Districts of Keewatin and Mackenzie. Geological Survey of Canada, Paper 64-20, 11 p.

Donaldson, J.A. (1969)
Descriptive notes (with particular reference to the Late Proterozoic Dubawnt Group) to accompany a geological map of central Thelon Plain, Districts of Keewatin and Mackenzie (65M, NW1/2, 66B,C,D, 75P, E1/2, 76A, E1/2). Geological Survey of Canada, Paper 68-49 and Map 16-1968, 4 p.

Donaldson, J.A. and de Kemp, E. (1987)
The komatiite-quartz arenite association in Precambrian terranes: an Archean example from the Superior Province. Geological Association of Canada - Mineralogical Association of Canada, Program with Abstracts 12, Saskatoon, p. 37.

Dorsey, R.J. (1988)
Provenance evolution and unroofing history of a modern arc-continent collision: evidence from petrography of Plio-Pleistocene sandstones, eastern Taiwan. Journal of Sedimentary Petrology 58, pp. 208-218.

Dupre, B., Chauvel, C. and Arndt, N.T. (1984)
Pb and Nd isotopic study of two Archean komatiitic flows from Alexo, Ontario. Geochimica et Cosmochimica Acta 48, pp.1965-1972.

Eade, K.E. (1964)
Preliminary Report, Kognak River Map-area (east half), District of Keewatin. Geological Survey of Canada, Paper 64-27, 7 p.

Eade, K.E. (1966)
Kognak River (west half), District of Keewatin. Geological Survey of Canada, Paper 65-8.

Eade, K.E. (1976)
Geology of the Tulemalu Lake map area (65J), District of Keewatin. In Report of Activities, Part A, Geological Survey of Canada, Paper 76-1A, pp. 379-381.

Eade, K.E. (1986)
Precambrian geology of the Tulemalu Lake-Yathkyed Lake area, District of Keewatin. Geological Survey of Canada, Paper 84-11, 31 p.

Eade, K.E. and Blake, D.H. (1977)
Geology of the Tulemalu Lake map area, District of Keewatin. In Report of Activities, Part A, Geological Survey of Canada, Paper 77-1A, pp. 209-211.

Echeverria, L.M. (1980a)
Tertiary komatiites of Gorgona Island, Colombia. Carnegie Institution of Washington Yearbook 79, pp. 340-4.

Echeverria, L.M. (1980b)
Tertiary of Mesozoic komatiites from Gorgona Island, Columbia, Field relations and geochemistry. Contributions to Mineralogy and Petrology 73, pp. 253-266.

Elthon, D. (1986)
Komatiite genesis in the Archean mantle, with implications for the tectonics of Archean greenstone belts. In Workshop on the Tectonic Evolution of Greenstone Belts, M.J. de Wit and L.D. Ashwal (eds.), LPI Technical Report 86-10, Lunar and Planetary Institute, Houston, pp. 97-99.

Engel, A.E.G. (1968)
The Barberton Mountain Land: clues to the differentiation of the earth. Geological Society of South Africa, Annex. Volume 71, pp. 255-270.

Engi, M. (1978)
Mg-Fe exchange equilibria among Al-Cr spinel, olivine, orthopyroxene, and cordierite. Unpublished Ph.D. thesis, Swiss Federal Institute of Technology, Zurich.

Engi, M. (1983)
Equilibria involving Al-Cr spinel: Mg-Fe exchange with olivine. Experiments, thermodynamic analysis, and consequences for geothermometry. American Journal of Science 283-A, pp.29-71.

Engi, M., and Evans, B.W. (1980)
A re-evaluation of the olivine-spinel geothermometry: discussion Contributions to Mineralogy and Petrology 73, pp. 201-203.

Evans, B.W. (1977)
Metamorphism of alpine peridotite and serpentinite. Annual Review of Earth and Planetary Sciences 5, pp. 397-447.

Evans, B.W., and Frost, B.R. (1975)
Chrome-spinel in progressive metamorphism - a preliminary analysis; Geochimica et Cosmochimica Acta 39, pp. 959-972.

Ewart, A. (1979)
A review of the mineralogy and chemistry of Tertiary - Recent dacitic, latitic, rhyolitic and related salic volcanic rocks. In Trondhjemites, dacites and related rocks, F. Baker (ed.), The Hague: Elsevier, pp.113-121.

Ewart, A., Brothers, R.N. and Mateen, A. (1977)
An outline of the geology and geochemistry and possible petrogenetic evolution of the volcanic rocks of the Tonga-Kermadec-New Zealand arc. Journal of Volcanology and Geothermal Research 2, pp. 205-250.

Fabries, J. (1979)
Spinel-olivine geothermometry in peridotites from ultramafic complexes. Contributions to Mineralogy and Petrology 69, pp. 329-336.

Flower, M.F.J. and Levine, H.M. (1987)
Petrogenesis of a tholeiite-boninite sequence from Ayios Mamas, Troodos ophiolite: evidence for splitting of a volcanic arc? Contribution to Mineralogy and Petrology 97, pp. 509-524.

Francis, D.M. and Hynes, A.F. (1979)
Komatiite-derived tholeiites in the Proterozoic of New Quebec. Earth and Planetary Science Letters 44, pp. 473-481.

Francis, D., Ludden, J. and Hynes, A. (1983)
Magma evolution in a Proterozoic rifting environment. Journal of Petrology 24, pp. 556-582.

Fraser, J.A. (1964)
Geological notes on Northeastern District of Mackenzie, Northwest Territories. Geological Survey of Canada, Paper 63-40, 20 p.

Fraser, J.A. (1978)
Metamorphism in the Churchill Province, District of Mackenzie. In Metamorphism in the Canadian Shield, J.A. Fraser and W.W. Heywood (eds.), Geological Survey of Canada, Paper 78-10, pp. 195-202.

Fraser, J.A. (1988)
Geology of the Woodburn Lake map area, District of Keewatin. Geological Survey of Canada, Paper 87-11, 12 p.

Frey, F.A., Bryan, W.B., and Thompson, G. (1974)
Atlantic Ocean floor: Geochemistry and petrology of basalts from legs 2 and 3 of the Deep Sea Drilling Project. Journal of Geophysic Research 79, pp. 5507-5527.

Frisch, T. (1982)
Precambrian Geology of the Prince Albert Hills, Western Melville Peninsula, Northwest Territories. Geological Survey of Canada, Bulletin 346, 70 p.

Frisch, T., Annesley, I.R., and Gittins, C.A. (1985)
Geology of the Chantrey belt and its environs, Lower Hayes River and Darby Lake map areas, northern District of Keewatin. In Current Research, Part A, Geological Survey of Canada, Paper 85-1A, pp. 259-266.

Frost, B.R. (1975)
Contact metamorphism of serpentinite, chloritic blackwall and rodingite at Paddy-o-Easy Pass, Central Cascades, Washington. Journal of Petrology 16, pp. 272-313.

Fryer, B.J. and Jenner, G.A. (1978)
Geochemistry and origin of the Archean Prince Albert Group volcanics, western Melville Peninsula, Northwest Territories, Canada. Geochimica et Cosmochimica Acta 42, pp. 1645-1654.

Fujii, T. (1977)
Fe-Mg partitioning between olivine and spinel. Carnegie Institute of Washington, Yearbook 76, pp. 563-569.

Fuller, T. (1977)
Geology of a remnant greenstone belt - Amer Lake map-area, District of Keewatin, Northwest Territories. Unpublished B.Sc. thesis, University of Western Ontario, London, Ontario, 28 p.

Gansser, A., Dietrich, V.J. and Cameron, W.E. (1979)
Palaeogene komatiites from Gorgona Island. Nature 278, pp. 545-546.

Geist, D.J., Baker, B.H., and McBirney, A.R. (1985)
GPP: a program package for creating and using geochemical data files.

Gelinas, L., Lajoie, J. and Brooks, C. (1977)
The origin and significance of Archean ultramafic volcaniclastics from Spinifex Ridge, La Motte Township, Quebec. In Volcanic Regimes in Canada, W.R.A. Baragar, L.C. Coleman and J.M. Hall (eds.), Geological Association of Canada, Special Paper 16, pp. 297-309.

Gelinas, L. Mellinger, M. and Trudel, P. (1982)
Archaean mafic metavolcanics from the Rouyn-Noranda district, Abitibi greenstone belt, Quebec. 1. Mobility of the major elements. Canadian Journal of Earth Sciences 19, pp. 2258-2275.

Glikson, A.Y. (1972)
Earth Precambrian evidence of a primative ocean crust and island nucleii of sodic granite. Geological Society of America, Bulletin 83, pp. 3323-44.

Glikson, A.Y. (1979)
Siderophile and lithophile trace-element evolution of the Archean mantle. BMR Journal of Australian Geology and Geophysics 4, pp. 253-279.

Glikson, A.Y. and Lambert, I.B. (1976)
Vertical zonation and petrogenesis of the early Precambrian crust in Western Australia. Tectonophysics 30, pp. 55-89.

Gole, M.J., Barnes, S.J. and Hill, R.E.T. (1987)
The role of fluids in the metamorphism of komatiites, Agnew nickel deposit, western Australia. Contributions to Mineralogy and Petrology 96, pp. 151-162.

Goodwin, A.M. (1977)
Archean volcanism in Superior Province, Canadian Shield. in Volcanic Regimes in Canada, W.R.A. Baragar, L.C. Coleman, and J.M. Hall (eds.), Geological Association of Canada, Special Paper 16, pp. 205-241.

Gordon, T.M. (1988)
Precambrian geology of the Daly Bay area, District of Keewatin. Geological Survey of Canada, Memoir 422, 22 p.

Green, D.H. (1975)
Genesis of Archean peridotitic magmas and constraints on Archean geothermal gradients and tectonics. Geology 3, pp. 15-18.

Green, D.H. (1981)
Petrogenesis of Archean ultramafic magmas and implications for Archean tectonic. In Precambrian Plate Tectonics, A. Kroener (ed.), Elsevier, Amsterdam, pp. 469-490.

Green, D.H., Nicholls, I.A., Viljoen, M.J., and Viljoen, R.P. (1975)
Experimental demonstration of the existence of peridotite liquids in earliest Archaean magmatism. Geology 3, pp. 11-14.

Gruau, G. (1983)
Etude geochimique d'associations volcaniques basiques et ultrabasiques d'age superieur a 3.5 AE: consequences sur la structure du manteau archeen precose. Unpublished Ph.D. thesis, University of Rennes.

Gruau, G., Arndt, N.T., Chauvel, C. and Jahn, B.M. (1986)
Large scale compositional heterogeneity of the early Archean mantle: Hf isotopic evidence. Terra Cognita 6, p. 245.

Hallberg, J.A., Johnston, C., and Bye, S.M. (1976)
The Archean Marda igneous complex, Western Australia. Precambrian Research 3, pp. 111-136.

Hanson, G.N. (1978)
The application of trace elements to the petrogenesis of igneous rocks of granitic composition. Earth and Planetary Science Letters 38, pp. 26-43.

Hanson, G.N. and Langmuir, C.H. (1978)
Modelling of major elements in mantle-melts systems using trace element approaches. Geochimica et Cosmochimica Acta 42, pp. 725-741.

Heaman, L.M. and LeCheminant, A.N. (1988)
U-Pb baddeleyite ages of the Muskox intrusion and Mackenzie dyke swarm, N.W.T., Canada. Geological Association of Canada - Mineralogical Association of Canada, Program with Abstracts 13, p. A53.

Hellman, P.L. and Henderson, P. (1977)
Are rare earths modile during spilitisation? Nature 267, pp. 38-40.

Hellman, P.L., Smith, R.E., and Henderson, P. (1979)
The mobility of the rare earth elements: evidence and implications from selected terrains affected by burial metamorphism. Contributions to Mineralogy and Petrology 71, pp. 22-44.

Henderson, J.B. (1981)
Archean basin evolution in the Slave Province, Canada. In Precambrian Plate Tectonics, A. Kroener (ed.), Elsevier, Amsterdam, pp. 213-235.

Henderson, J.B. and Easton, R.M. (1977)
Archean supracrustal-basement rock relationships in the Keskarrah Bay map area, Slave Structural Province, District of Mackenzie. In Report of Activities, Part A, Geological Survey of Canada, Paper 77-1A, pp. 217-221.

Henderson, J.R., LeCheminant, A.N., Jefferson, C.W., Coe, K., and Henderson, M.N. (1986)
Preliminary account of the geology around Wager Bay, District of Keewatin. In Current Research, Part A, Geological Survey of Canada, Paper 86-1A, pp. 159-176.

Herzberg, C.T. (1983)
Solidus and liquidus temperatures and mineralogies for anhydrous garnet-lherzolite to 15 GPa. Physics of the Earth and Planetary Interiors 32, pp. 193-202.

Herzberg, C.T. (1986)
Origin of high-Mg komatiites: constraints from melting experiments to 8 GPa. EOS, Transactions American Geophysical Union 67, p.408.

Herzberg, C.T. (1987)
Lower-mantle composition: high-pressure melting studies. Nature 328, p.472.

Herzberg, C.T. and O'Hara, M.J. (1985)
Origin of mantle peridotite and komatiite by partial melting. Geophysical Research Letters 12, pp. 541-544.

Herzberg, C.T.; Hasebe, K. and Sawamoto, H. (1986)
Origin of high Mg komatiites: constraints from melting experiments to 8 GPa. Transaction American Geophysical Union 67, p.408.

Heywood, W.W. (1961)
Geological notes, northern District of Keewatin. Geological Survey of Canada, Paper 61-18, 9 p.

Heywood, W.W. (1967)
Geological notes, northeastern District of Keewatin and southern Melville Peninsula, District of Franklin, Northwest Territories (parts of 46, 47, 56, 57). Geological Survey of Canada, Paper 66-40, 20 p.

Heywood, W.W. (1977)
Geology of the Amer Lake map-area, District of Keewatin. In Report of Activities, Part A, Geological Survey of Canada, Paper 77-1A, pp. 409-410.

Heywood, W.W. and Schau, M. (1978)
A subdivision of the northern Churchill Structural Province. In Current Research, Part A, Geological Survey of Canada, Paper 78-1A, pp. 139-142.

Heywood, W.W., and Schau, M. (1981)
Geology of Baker Lake region, District of Keewatin. In Current Research, Part A, Geological Survey of Canada, Paper 81-1A, pp. 259-264.

Hoffman, P.F. (1986)
Crustal accretion in a 2.7-2.5 Ga "Granite-Greenstone" terrane, Slave Province, N.W.T.: a prograding trench-arc system? Geological Association of Canada - Mineralogical Association of Canada, Program with Abstracts 11, Ottawa, p. 82.

Hoffman, P.F. (1987a)
Tectonic subdivision of the Churchill Province. In Program with Abstracts, Current Activities Forum 1987, Geological Survey of Canada, Paper 87-8, p.A33.

Hoffman, P.F. (1987b)
Continental transform tectonics: Great Slave Lake shear zone (ca. 1.9 Ga), northwest Canada. Geology 15, pp. 785-788.

Humphris, S.E. and Thompson, G. (1978a)
Hydrothermal alteration of oceanic basalts by sea-water. Geochimica et Cosmochimica Acta 42, pp. 107-125.

Humphris, S.E. and Thompson, G. (1978b)
Trace element mobility during hydrothermal alteration of oceanic basalts. Geochimica et Cosmochimica Acta 42, pp. 127-136.

Humphris, S.E., Morrison, M.A. and Thompson, R.N. (1978)
Influence of rock crystallization history upon subsequent lanthanide mobility during hydrothermal alteration of basalts. Chemical Geology 23, pp. 125-137.

Huppert, H.E. and Sparks, R.S.J. (1985a)
Komatiites I: eruption and flow. Journal of Petrology 26, pp. 694-725.

Huppert, H.E. and Sparks, R.S.J. (1985b)
Cooling and contamination of mafic and ultramafic lavas during ascent through continental crust. Earth and Planetary Science Letters 74, pp. 371-386.

Huppert, H.E., Sparks, R.S.J., Turner, J.S., and Arndt, N.T. (1984)
Emplacement and cooling of komatiite lavas. Nature 309, pp. 19-22.

Irvine, T.N. (1965)
Chromian spinel as a petrogenetic indicator, part I: Theory; Canadian Journal of Earth Sciences 2, pp. 648-672.

Irvine, T.N. (1967)
Chromian spinel as a petrogenetic indicator, part II: Petrologic applications; Canadian Journal of Earth Sciences 4, pp. 71-103.

Irvine, T.N. and Baragar, W.R.A. (1971)
A guide to chemical classification of the common volcanic rocks. Canadian Journal of Earth Sciences 8, pp. 523-548.

Irving, A.J. and Ashley, P.M. (1976)
Amphibole-olivine-spinel, cordierite-anthophyllite and related hornfels associated with metamorphosed serpentinites in the Goobarragandra District, near Tumut, New South Wales. Journal of the Geological Society of Australia 23, pp. 19-43.

Jackson, E.D. (1969)
Chemical variation in coexisting chromite and olivine in chromitite zones of the Stillwater complex; In Magmatic Ore Deposits, Wilson, H.D.B. (ed.), Economic Geology 4, pp. 19-43.

Jahn, B.M., Gruau, G. and Glikson, A.Y. (1982)
Onverwacht Komatiites: REE geochemistry, Sm/Nd age and mantle evolution. Contributions to Mineralogy and Petrology 80, pp. 25-40.

Jahn, B.M., Auvray, B., Blais, S., Capdevila, R., Cornichet, J., Vidal, F. and Hameurt, J. (1980)
Trace element geochemistry and petrogenesis of Finnish greenstone belts. Journal of Petrology 21, pp. 201-244.

Jaques, A.L. and Green, D.H. (1980)
Anhydrous melting of peridotite at 0-15 kb pressure and the genesis of the tholeiitic basalts. Contributions to Mineralogy and Petrology 73, pp. 287-310.

Jarvis, G.T. and Campbell, I.H. (1983)
Archean komatiites and geotherms: solution to an apparent contradiction. Geophysical Research Letters 10, pp. 1133-1136.

Jenner, G.A. (1981)
Geochemistry of high-Mg andesites from Cape Vogel, Papua New Guinea. Chemical Geology 33, pp. 307-332.

Jensen, L.S. (1976)
A new cation plot for classifying subalkaline volcanic rocks. Ontario Division of Mines, Miscalleneous Paper 66, 22 p.

Jolly, W.T. (1980)
Development and degradation of Archean lavas, Abitibi area, Canada, in light of major element geochemistry. Journal of Petrology 21, pp. 323-363.

Jolly, W.T. (1982)
Progressive metamorphism of komatiites and related Archean lavas of the Abitibi area, Canada. In Komatiites, N.T. Arndt and E.G. Nisbet (eds.), George Allen and Unwin, London, pp. 245-266.

Jolly, W.T. (1987)
Lithophile elements in Huronian low-Ti continental tholeiites from Canada, and evolution of the Precambrian mantle. Earth and Planetary Science Letters 85, pp. 401-415.

Kinzler, R.J. and Grove, T.L. (1985)
Crystallization and differentiation of Archean komatiitic lavas from northeast Ontario: phase equilibrium and kinetic studies. American Mineralogist 70, pp. 40-51.

Kroener, A. ed. (1981)
Precambrian Plate Tectonics; Amsterdam: Elsevier, 781 p.

Kroener, A. (1984)
Evolution, growth and stabilization of the Precambrian lithosphere. In Structure and Evolution of the Continental Lithosphere, H.N. Pollack and J.R. Murthy (eds.), Pergamon Press, Oxford, Physics and Chemistry of the Earth 15, pp.69-106.

Kroener, A. (1985)
Evolution of the Archean continental crust. Annual Review of Earth and Planetary Sciences 13, pp. 49-74.

Lajoie, J. and Gelinas, L. (1978)
Emplacement of Archean peridotitic komatiites in La Motte Township, Quebec. Canadian Journal of Earth Sciences 15, pp. 672-677.

Langford, F.F. and Morin, J.A. (1976)
The development of the Superior Province of northwestern Ontario by merging island arcs. American Journal of Science 276, pp. 1023-1034.

Leake, B.E. (1978)
Nomenclature of amphiboles. The American Mineralogist 63, pp. 1023-1052.

LeCheminant, A.N., Miller, A.R. and LeCheminant, G.M. (1987)
Early Proterozoic alkaline igneous rocks, District of Keewatin, Canada: petrogenesis and mineralization. In Geochemistry and Mineralization of Proterozoic Volcanic Suites, T.C. Pharaoh, R.D. Beckinsale and D. Rickard (eds.), Blackwell Scientific Publications, Oxford, pp. 219-240.

LeCheminant, A.N., Blake, P.H., Leatherbarrow, R.W. and de Bie, L. (1977)
Geological Studies: Thirty Mile Lake and MacQuoid Lake map areas, District of Keewatin. In Report of Activities, Part A, Geological Survey of Canada, Paper 77-1A, pp. 205-208.

LeCheminant, A.N., Roddick, J.C., Tessier, A.C., and Bethune, K.M. (1987)
Geology and U-Pb ages of early Proterozoic calc-alkaline plutons northwest of Wager Bay, District of Keewatin. In Current Research, Part A, Geological Survey of Canada, Paper 87-1A, pp. 773-782.

Lesher, C.M., Arndt, N.T., and Groves, D.I. (1984)
Genesis of komatiite-associated nickel sulfide deposits at Kambalda, Western Australia: a distal volcanic-assimilation mode. in Sulfide Deposits in Mafic and Ultramafic Rocks, D.L. Buchanan and M.J. Jones (eds.), Institution of Mining and Metallurgy, London, pp. 70-80.

Lewis, J.D. and Williams, I.R. (1973)
The petrology of an ultramafic lava near Murphy Well, Eastern Goldfields, Western Australia. Western Australian Geological Survey Annual Report 1972, pp. 60-68.

Lewry, J.F., Sibbald, T.I.I., and Schledewitz, D.C.P. (1985)
Variation in character of Archean rocks in the western Churchill Province and its significance. In Evolution of Archean Supracrustal Sequences, L.D. Ayres, P.C. Thurston, K.D. Card and W. Weber (eds.), Geological Association of Canada, Special Paper 28, pp. 239-261.

Longhi, J., Wooden, J.L. and Coppinger, K.D. (1983)
The petrology of high-Mg dykes from the Beartooth Mountains, Montana: a search for the parent magma of the Stillwater Complex. Proceedings of the Fourteenth Lunar and Planetary Science Conference, part I, Journal of Geophysical Research, supplement 88, pp. B53-B69.

Lord, C.S. (1953)
Geological notes on southern District of Keewatin, Northwest Territories. Geological Survey of Canada, Paper 53-22.

Ludden, J.N. and Gelinas, L. (1982)
Trace element characteristics of komatiites and komatiitic basalts from the Abitibi greenstone belt of Quebec. In: Komatiites, N.T. Arndt and E.G. Nisbet (eds.), George Allen and Unwin, London, pp. 331-346.

Ludden, J.N. and Humphris, S.E. (1978)
Are the rare earth elements mobile during alteration processes? Geological Society of America, Abstracts and Programs 10, p. 447.

Ludden, J.N. and Thompson, G. (1978)
Behavior of rare earth elements during submarine weathering of tholeiitic basalt. Nature 274, pp. 147-149.

Ludden, J.N. and Thompson, G. (1979)
An evaluation of the behavior of the rare earth elements during the weathering of sea-floor basalt. Earth and Planetary Science Letters 43, pp. 85-92.

Ludden, J., Gelinas, L. and Trudel, P. (1982)
Archaean metavolcanics from the Rouyn-Noranda district. Abitibi greenstone belt, Quebec 2. Mobility of trace elements and petrogenetic constraints. Canadian Journal of Earth Sciences 19, pp. 2776-2287.

Ludden, J., Hubert, C. and Gariepy, C. (1986)
The tectonic evolution of the Abitibi belt, Canada. Geological Magazine 123, pp. 153-166.

Mack, G.H. (1984)
Exceptions to the relationship between plate tectonics and sandstone composition. Journal of Sedimentary Petrology 54, pp. 212-220.

Marsh, B.D. and Maxey, M.R. (1985)
On the distribution and separation of crystals in convecting magma. Journal of Volcanology and Geothermal Research 24, pp. 95-150.

McKenzie, D.P. (1984)
The generation and compaction of partially molten rock. Journal of Petrology 25, pp. 713-765.

Medaris, L.G.Jr. (1975)
Coexisting spinel and silicates in alpine peridotites of the granulite facies. Geochimica et Cosmochimica Acta 39, pp. 947-958.

Menzies, M., Seyfried, W. Jr. and Blanchard, D. (1979)
Experimental evidence of rare earth immobility in greenstones. Nature 282, pp. 398-399.

Mercier, J.-C.C. (1976)
Single pyroxene geothermometry and geobarometry. American Mineralogist 61, pp. 603-615.

Mercier, J.-C.C. and Nicolas, A. (1975)
Textures and fabrics of upper-mantle peridotites as illustrated by xenoliths from basalts. Journal of Petrology 16, pp. 454-487.

Moore, J.M.Jr. (1977)
Orogenic volcanism in the Proterozoic of Canada. In Volcanic Regime in Canada, W.R.A. Baragar, L.C. Coleman and J.M. Hall (eds.), Geological Association of Canada, Special Paper 16, pp. 127-148.

Mottl, M.J. and Holland, H.D. (1978)
Chemical exchange during hydrothermal alteration of basalt by sea-water. I. Experimental results for major and minor components of sea-water. Geochimica et Cosmochimica Acta, 42, pp. 1103-1115.

Myers, J.D. (1988)
Possible petrogenetic relations between low- and high-MgO Aleutian basalts. Geological Society of America Bulletin 100, pp. 1040-1053.

Nadeau, L. (1981)
The geology of Whitehills Lake map area, District of Keewatin. In Current Research, Part A, Geological Survey of Canada, Paper 81-1A, pp. 265-268.

Naldrett, A.J. and Goodwin, A.M. (1977)
Volcanic rocks of the Blake River Group, Abitibi greenstone belt, Ontario, and their sulfur content. Canadian Journal of Earth Sciences 14, pp.539-550.

Naldrett, A.J. and Arndt, N.T. (1976)
Volcanogenic nickel deposits with some guides for exploration. Transaction of the Society of Mining Engineering 260, pp. 13-15.

Nesbitt, R.W. (1971)
Skeletal crystal forms in the ultramafic rocks of the Yilgarn Block, Western Australia: evidence for an Archean ultramafic liquid. Geological Society of Australia, Special Publication 3, pp. 331-348.

Nesbitt, R.W. and Sun, S.-S. (1976)
Geochemistry of Archean spinifex textured peridotites and magnesian and low magnesian tholeiites. Earth and Planetary Science Letters 31, pp. 433-453.

Nesbitt, R.W., Jahn, B.M. and Purvis, A.C. (1982)
Komatiites: an early Precambrian phenoena. Journal of Volcanology and Geothermal Research 14 (1982), pp. 31-45.

Nesbitt, R.W., Sun, S.-S. and Purvis, A.C. (1979)
Komatiites: geochemistry and genesis. Canadian Mineralogist 17, pp. 165-186.

Nicholls, J. (1988)
The statistics of Pearce element diagrams and the Chayes closure problem. (submitted).

Nisbet, E.G. (1982)
The tectonic setting and petrogenesis of komatiites. In Komatiites, N.T. Arndt and E.G. Nisbet, (eds.), George Allen and Unwin, London, pp. 501-520.

Nisbet, E.G. (1987)
The Young Earth: an Introduction to Archean Geology. George Allen and Unwin, Boston, 402 p.

Nisbet, E.G. and Chinner, G.A. (1981)
Controls of the eruption of mafic and ultramafic lavas, Ruth Well Ni-Cu prospect, West Pilbara. Economic Geology 76, pp. 1729-1735.

Nisbet, E.G. and Fowler, C.M.R. (1983)
A model for Archean plate tectonics. Geology 11, pp. 376-379.

Nisbet, E.G. and Walker, D (1982)
Komatiites and the structure of the Archean mantle. Earth and Planetary Science Letters 60, pp. 105-116.

Nisbet, E.G., Bickle M.J. and Martin, A. (1977)
The mafic and ultramafic lavas of theBelingwe greenstone belt, Rhodesia. Journal of Petrology 18, pp. 521-566.

Nisdet, E.G.; Arndt, N.T.; Bickle, M.J.; Cameron, W.E.; Chauvel, C.; Cheadle, M.; Hegner, E.; Kyser, T.K.; Martin, A.; Renner, R.; and Roedder, E. (1987)
Uniquely fresh 2.7 Ga komatiites from the Belingwe greenstone belt, Zimbabwe. Geology 15, pp. 1147-1150.

O'Hara, M.J. (1968)
The bearing of phase equilibria studies in synthetic and natural systems on the origin and evolution of basic and ultrabasic rocks. Earth Science Reviews 4, pp. 69-133.

O'Hara, M.J., Saunders, M.J. and Mercy, E.L.P. (1975)
Garnet peridotite, primary ultrabasic magma and eclogite: interpretation of upper mantle processes in kimberlite. Physics and Chemistry of the Earth 9, pp. 571-604.

Ohtani, E. (1984)
Generation of komatiite magma and gravitational differentiation in the deep upper mantle. Earth and Planetary Science Letters 67, pp. 261-272.

Ohtani, E. (1985)
The primodial terrestrial magma ocean and its implication for stratification of the mantle. Physics of the Earth and Planetary Interiors 38, pp. 70-80.

Ohtani, E., Kato, T. and Sawamoto, H. (1986)
Melting of a model chondritic mantle to 20 GPa. Nature 322, pp. 352-353.

Oliver, R.L., Nesbitt, R.W., Hansen, D.M., and Franzen, N. (1972)
Metamorphic olivine in ultramafic rocks from Western Australia. Contributions to Mineralogy and Petrology 36, pp. 335-342.

Ozawa, K. (1983)
Evaluation of olivine-spinel geothermometry as an indicator of thermal history for peridotites. Contributions to Mineralogy and Petrology 82, pp. 52-65.

Paktunc, A.D. (1984a)
Petrogenesis of ultramafic rock of the Thompson Nickel Belt, Manitoba. Contributions to Mineralogy and Petrology 88, pp. 348-353.

Paktunc, A.D. (1984b)
Metamorphism of the ultramafic rocks of the Thompson Mine, Thompson Nickel Belt, northern Manitoba. Canadian Mineralogist 22, pp. 77-91.

Palme, H. and Nickel, K.G. (1985)
Ca/Al ratio and composition of the Earth's upper mantle. Geochimica et Cosmochimica Acta 49, pp. 2123-2132.

Patterson, J.G. (1981)
Amer Lake: An Aphebian fold and thrust complex. Unpublished M.Sc. thesis, University of Calgary, Calgary, Alberta, 105 p.

Pearce, T.H. (1968)
A contribution to the theory of variation diagrams. Contributions to Mineralogy and Petrology 19, pp. 142-157.

Pearce, T.H. (1987)
The identification and assessment of spurious trends in Pearce-type ratio variation diagrams: A discussion of some statistical arguments. Contributions to Mineralogy and Petrology 97, pp. 529-534.

Pearce, J.A. and Cann, J.R. (1973)
Tectonic setting of basic volcanic rocks determined using trace element analysis. Earth and Planetary Science Letters 19, pp. 290-300.

Percival, J.A. and Stern, R.A. (1984)
Geological synthesis in the western Superior Province, Ontario. In Current Research, Part A, Geological Survey of Canada, Paper 84-1A, pp. 397-408.

Pitcher, W.S.; Atherton, M.P.; Cobbing, E.J. and Beckinsale, R.D. (eds.) (1985)
Magmatism at a plate edge: The Peruvian Andes. Blackie - Halsted Press, New York, 328 p.

Purvis, A.C. (1978)
The geochemistry and metamorphic petrology of the southern

Cross-Forrestania Greenstone Belt at Digger's Rocks, Western Australia. Unpublished Ph.D thesis, University of Adelaine, Australia.

Pyke, D.R., Naldrett, A.J. and Eckstand, A.R. (1973)
Archean ultramafic flows in Munro Township, Ontario. Geological Society of America, Bulletin 84, pp. 955-978.

Rajamani, V., Shivkumar, K., Hanson, G.N. and Shirey, S.B. (1985)
Geochemistry and petrogenesis of amphibolites, Kolar Schist Belt, South India: evidence for komatiitic magma derived by low percentages of melting of the mantle. Journal of Petrology 26, pp. 92-123.

Redman, B.A. and Keays, R.R. (1985)
Archean basic volcanism in the eastern Goldfields Province, Yilgarn Block, Western Australia. Precambrian Research 30, pp. 113-152.

Reid, F.W. and Cole, J.W. (1983)
Origin of dacites of Taupo zone, New Zealand. Journal of Volcanology and Geothermal Research 18, pp. 191-214.

Roeder, P.L. and Emslie, R.F. (1970)
Olivine-liquid equilibrium. Contributions to Mineralogy and Petrology 29, pp. 275-282.

Roeder, P.L., Campbell, I.H., and Jamieson, H.E. (1979)
A re-evaluation of the olivine-spinel geothermometer; Contributions to Mineralogy and Petrology 68, pp. 325-334.

Rollinson, H.R. and Roberts, C.R. (1986)
Ratio correlations and major element mobility in altered basalts and komatiites. Contributions to Mineralogy and Petrology 93, pp. 89-97.

Roscoe, S.M. and Donaldson, J.A. (1988)
Uraniferous pyritic quartz pebble conglomerate and layered ultramafic intrusions in a sequence of quartzite, carbonate, iron formation and basalt of probable Archean age at Lac Sakami, Quebec. In Current Research, Part C, Geological Survey of Canada, Paper 88-1C, pp. 117-121.

Russell, J.K. (1986)
A fortran 77 computer program for the least-squares analysis of chemical data in Pearce variation diagrams. Computers and Geosciences 12, pp. 327-338.

Scarfe, C.M. and Takahashi, E. (1986)
Melting of garnet peridotite to 13 GPa: implications for the early history of the upper mantle. Nature 322, pp.354-356.

Schau, M. (1977)
Komatiites and quartzites in the Archean Prince Albert Group. In Volcanic Regimes in Canada, W.R.A. Baragar, L.C. Coleman and J.M. Hall (eds.), Geological Association of Canada, Special Paper 16, pp. 341-354.

Schau, M. (1982)
Geology of the Prince Albert Group in Parts of Walker Lake and Laughland Lake Map Areas, District of Keewatin. Geological Survey of Canada, Bulletin 337, 62 p.

Schau, M., Tremblay, F. and Christopher, A. (1982)
Geology of Baker Lake map area, District of Keewatin: a progress report; In Current Research, part A, Geological Survey of Canada, Paper 82-1A, pp. 143-150.

Schwerdtner, W.M., Sutcliffe, R.H. and Troeng, B. (1978)
Patterns of total strain within the crustal region of immature diapirs. Canadian Journal of Earth Sciences 15, pp. 1437-1447.

Schwarz, E.J. and Fujiwara, Y. (1977)
Komatiitic basalts from the Proterozoic Cape Smith range in northern Quebec, Canada. In Volcanic Regimes in Canada, W.R.A. Baragar, L.C. Colemen and J.M. Hall (eds.), Geological Association of Canada, Special Paper 16, pp. 193-201.

Seyfried, W.E.; Berndt, M.E. Jr. and Seewald, J. (1988)
Hydrothermal alteration processes at mid-ocean ridges: constraints from diabase alteration experiments, hot-spring fluids and composition of the oceanic crust. Canadian Mineralogist 26, pp. 787-804.

Smith, H.S., and Erlank, A.J. (1978)
Aspects of the geochemistry of Archean volcanic rocks: Lower Ultramafic Unit, Swaziland Sequence, South Africa. In Proceeding of the 1978 Archean geochemistry conference, I.E.M. Smith and J.G. Williams (eds.), Toronto, University of Tonronto Press.

Smith, H.S. and Erlank, A.J. (1982)
Geochemistry and petrogenesis of komatiites from the Barberton greenstone belt, South Africa. In Komatiites, N.T. Arndt and E.G. Nisbet (eds.), George Allen and Unwin, London, pp. 347-397.

Smith, R.E. and Smith S.E. (1976)
Comments on the use of Ti, Zr, Y, Sr, K, P, and Nb in classification of basaltic magmas. Earth and Planetary Science Letters 32, pp. 114-120.

Smith, H.S., Erlank, A.J., and Duncan, A.R. (1980)
Geochemistry of some ultramafic komatiite lava flows from the Barberton Mountain Land, South Africa; Precambrian Research 11, pp. 399-415.

Sparks, R.S.J. (1986)
The role of crustal contamination in magma evolution through geological time. Earth and Planetary Science Letters 78, pp. 211-223.

Srinivasan, R. and Ojakangas, R.W. (1986)
Sedimentology of quartz-pebble conglomerates and quartzites of the Archean Bababudan Group, Dharwar Craton, South India: evidence for early crustal stability. Journal of Geology 94, pp. 199-214.

Stamatelopoulou-Seymour, K. and Francis, D.M. (1980)
Metamorphic olivine in peridotitic komatiite flows, Lac Guyer, Quebec. Canadian Mineralogist 18, pp. 265-270.

Stamatelopoulou-Seymour, K., Francis, D.M. and Ludden, J.N. (1983)
The petrogenesis of the Lac Guyer komatiites and basalts and the nature of the komatiite-komatiitic basalt compositional gap. Contributions to Mineralogy and Petrology 84, pp. 6-14.

Staudigel, H. and Hart, S.T. (1983)
Alteration of basaltic glass: mechanisms and significance for the oceanic crust-seawater budget. Geochimica et Cosmochimica Acta 47, pp. 337-350.

Stockwell, C.H. (1982)
Proposals for time classification and correlation of Precambrian rocks and events in Canada and adjacent areas of the Canadian Shield, part 1: A time classification of Precambrian rocks and events. Geological Survey of Canada, Paper 80-19, 135 p.

Stolper, E. (1980)
A phase diagram for mid-ocean ridge basalts: Preliminary results and implications for petrogenesis. Contributions to Mineralogy and Petrology 74, pp. 13-27.

Stolper, E.M., Walker, D., Hager, B.H., and Hays, J.F. (1981)
Melt segregation from partially molten source regions: The importance of melt density and source region size. Journal of Geophysical Research 86, pp. 6261-6271.

Sun, S.-S and Nesbitt, R.W. (1978)
Petrogeneis of Archaean ultrabasic and basic volcanics: evidence from the rare earth elements. Contributions to Mineralogy and Petrology 65, pp. 301-325.

Sylvester, P.J., Attoh, K., and Schulz, K.J. (1987)
Tectonic setting of late Archean bimodal volcanism in the Michipicoten (Wawa) greenstone belt, Ontario. Canadian Journal of Earth Sciences, 24, pp. 1120-1134.

Takahashi, E. (1986)
Melting of a dry peridotite KLB-1 up to 14 GPa: implications on the origin of peridotite upper mantle. Journal of Geophysical Research 91, pp. 9367-9382.

Takahashi, E. and Kushiro, I. (1983)
Melting of a dry peridotite at high pressures and basalt magma genesis. American Mineralogist 68, pp. 859-879.

Takahashi, E. and C.M. Scarfe (1985)
Melting of peridotite to 14 GPa and the genesis of komatiite. Nature 315, 566 p.

Taylor, F.C. (1985)
Geology of the Half Way Hills map area. Geological Survey of Canada, Memoir 415, 19 p.

Tella, S. (1984)
Geology of the Amer Lake (NTS 66H), Deep Rose Lake (NTS 66G) and parts of the Pelly Lake (NTS 66F) map areas, District of Keewatin, N.W.T.. Geological Survey of Canada, Open file 1043.

Tella, S. and Annesley, I.R. (1987)
Precambrian geology of parts of Chesterfield Inlet map area, District of Keewatin. in Current Research, Part A, Geological Survey of Canada, Paper 87-1A, pp. 25-36.

Tella, S. and Annesley, I.R. (1988)
Hanbury Island Shear Zone, a deformed remnant of a ductile thrust, District of Keewatin, N.W.T.. in Current Research, Part C, Geological Survey of Canada, Paper 88-1C, pp. 283-289.

Tella, S. and Eade, K.E. (1986)
Occurrence and possible significance of high-pressure granulite fragments in the Tulemalu fault zone, District of Keewatin, N.W.T., Canada. Canadian Journal of Earth Science 23, pp. 1950-1962.

Tella, S. and Heywood, W.W. (1983)
Geology of the Amer Lake (N.T.S. 66H) map area, District of Keewatin; Northwest Territories. Geological Survey of Canada, Open File 942.

Tella, S., Heywood, W.W., and Loveridge, W.D. (1985)
A U-Pb age on zircon from a dacite porphyry, Amer Lake map area, District of Keewatin, NWT. in Current Research, Part B, Geological Survey of Canada, Paper 85-1B, pp. 371-374.

Tella, S., Annesley, I.R., Borradaile, G.J., and Henderson, J.R. (1986)
Precambrian geology of parts of Tavani, Marble Island and Chesterfield Inlet map areas, District of Keewatin, N.W.T.. Geological Survey of Canada, Paper 86-13, 20 p.

Thompson, G. (1973)
A geochemical study of the low-temperature interaction of sea-water and oceanic igneous rocks. Transaction American Geophysical Union 54, pp. 1015-1019.

Thirlwall, M.F. (1983)
Isotope geochemistry and origin of calc-alkaline lavas from a Caledonian continental margin volcanic arc. Journal of Volcanology and Geothermal Research 18, pp. 589-631.

Tippett, C.R. and Heywood, W.W. (1978)
Stratigraphy and structure of the northern Amer group (Aphebian), Churchill Structural Province, District of Keewatin. In Current Research, Part B, Geological Survey of Canada, Paper 78-1B, pp. 7-11.

Total Word (1988)
Word processing and publishing from the makers of Volkwriter. Lifetree Software Inc., Monterey.

Turner, F.J. (1981)
Metamorphic petrology: mineralogical, field and tectonic aspects. second edition, McGraw-Hill Book Company, New York, 524p.

Turner, J.S., Huppert, H.E. and Sparks, R.S.J. (1986)
Komatiites II: experimental and theoretical investigations of post-emplacement cooling and crystallization. Journal of Petrology 27, pp. 397-437.

Van Schmus, W.R., and Bowring, S.A. (1980)
Chronology of igneous events in the Wopmay orogen, Northwest Territories, Canada. 1980 Annual Meeting, Geological Society of America, Abstracts with Program 12, no.7, p. 540.

Velbel, M.A. (1985)
Mineralogically mature sandstones in accretionary prisms. Journal of Sedimentary and Petrology 55, pp. 685-690.

Viljoen, N.S. and Viljoen R.P. (1969a)
The geology and geochemistry of the lower ultramafic unit of the Onverwacht Group and a proposed new class of igneous rocks. Geological Society of South Africa, Special Publication 2, pp. 55-86.

Viljoen, M.J. and Viljoen, R.P. (1969b)
Evidence for the existence of a mobile extrusive peridotitic magma from the Komatii formation of the Onverwacht Group. Geological Society of South Africa, Special Publication 2, pp. 87-113.

Viljoen, M.J., Vilgoen, R.P., Smith, H.S. and Erlank, A.J. (1983)
Geological, textural and geochemical features of komatiitic flows from the Komati Formation. Geological Society of South Africa, Special Publication 9, pp. 1-20.

Walker, D. (1986)
Melting equilibria in multicomponent systems and liquidus/solidus convergence in mantle peridotite. Contributions to Mineralogy and Petrology 92, pp. 303-307.

Walker, D. and Cameron W.E. (1983)
Boninite primary magmas: evidence from the Cape Vogel Peninsula, PNG. Contribution to Mineralogy and Petrology 83, pp. 150-158

Walker, D., Stolper, E.M. and Hays, J.F. (1980)
Komatiite petrogenesis and melt segregation. EOS Transactions of American Geophysical Union, 61, pp. 385.

Warren (1984)
Primordial Degassing, Lithospheric Thickness, and Origin of Komatiites. Geology 12, pp. 335-338.

Whitford, D.J. and Arndt, N.T. (1978)
Rare earth element abundances in a thick, layered komatiite lava flow from Ontario, Canada. Earth and Planetary Science Letters 41, pp. 188-196.

Windley, B.F. (1977)
The Evolving Continents. John Wiley and Sons, New York, N.Y., 385 p.

Windley, B.F. (1984)
The Evolving Continents, 2nd edn., John Wiley and Sons, Chichester, 399 p.

Wood, C.P. (1980)
Boninite at a continental margin. Nature 288, pp. 692-694.

Wood, D.A., Gibson, I.L. and Thompson R.N. (1976)
Elemental mobility during zeolite facies metamorphism of the Tertiary basalts of eastern Iceland. Contributions to Mineralogy and Petrology 55, pp. 241-254.

Wood, J. and Thurston, P.C. (1986)
Ancient quartzites and carbonates in northwestern Ontario: evidence for early (Archean) crustal stability? Geological and Mineralogical Association of Canada, Program with Abstracts 11, Ottawa, p. 146.

Wright, G.M. (1955)
Geological notes on central District of Keewatin, Northwest Territories. Geological Survey of Canada, Paper 55-17, 17 p.

Wright, G.M. (1967)
Geology of the southeastern barren grounds, parts of the Districts of Mackenzie and Keewatin (Operation Keewatin, Baker, Thelon). Geological Survey of Canada, Memoir 350,

Symbols for minerals in Appendices A1.

Act/Hbl = actinolite and/or hornblende

Ap = apatite

Bt = biotite

Cb = carbonate

Chl = chlorite

Chr = chromite

Cr-Mag = chrome magnetite

Ep = epidote

Grn = garnet

Hm = hematite

Mag = magnetite

Mus = muscovite

Ol = olivine

Phl = phlogopite

Pl = plagioclase

Qtz = quartz

Srp = serpentine

Sp = spinel

Tlc = talc

Trm = tourmaline

Tr/Act = tremolite and/or actinolite

Appendix A1.a Modal composition of spinifex-textured komatiites, Woodburn Lake Group (Pipedream Lake belt)

	Tr/Act	Chl	Srp	Tlc	Cr-Mag/Mag	Chr	Cb	Hm
K-2a (spinifex)	60	25	-	-	15	-	-	tr
K-2b (spinifex)	60	25	-	-	15	-	-	tr
K-2d (randomly oriented spinifex)	55	30	-	-	15	-	-	tr
K-4a (randomly oriented spinifex)	45	30	15	-	10	-	-	-
K-4b (randomly oriented spinifex)	40	20	25	-	15	-	-	-
K-6a (spinifex)	60	30	-	-	10	-	-	-
K-6b (randomly oriented spinifex)	45	30	2	-	15	-	-	-
K-8a (spinifex)	65	25	-	-	10	-	-	-
K-18 (A-zone)	73	2	15	-	10	-	-	-
K-20 (spinifex)	77	15	2	-	5	-	1	-
K-22 (spinifex)	65	25	-	-	10	-	-	-
K-35 (spinifex)	55	35	-	-	10	-	-	-
K-37 (randomly oriented spinifex)	50	35	-	-	15	-	-	-
K-39 (randomly oriented spinifex)	50	5	30	-	15	-	-	-
K-42a (spinifex)	60	35	-	-	5	-	-	-
K-42b (spinifex)	65	25	-	-	10	-	-	-
K-42c (spinifex)	72	20	3	-	5	-	-	tr
K-42d (spinifex)	60	25	-	-	15	-	-	-
K-44a (spinifex)	65	25	5	-	5	-	tr	-
K-44b (spinifex)	65	15	10	-	10	-	-	-
K-44c (spinifex)	67	20	3	-	10	-	-	-
K-44d (spinifex)	55	25	10	-	10	-	-	-

Appendix A1.a (continued)

	Tr/Act	Chl	Srp	Tlc	Cr-Mag/Mag	Chr	Cb	Hm
K-44e (spinifex)	50	30	10	-	10	-	-	tr
K-44f (spinifex)	55	35	5	-	5	-	-	-
K-44g (spinifex)	55	15	20	tr	10	-	-	-
AK-14c (radiating spinifex)	45	10	40	-	5	-	-	-
AK-14d (spinifex top polyhedra)	50	10	25	-	15	tr	-	tr
AK-15c (spinifex)	59	35	-	-	5	-	-	1
AK-15d (radiating spinifex)	57	30	-	-	10	tr	-	3
AK-16c (spinifex)	65	20	5	-	10	-	-	tr
AK-22c (spinifex)	55	35	-	-	15	-	-	-
AK-23d-1 (spinifex)	49	35	-	-	15	-	-	1
AK-23d-2 (spinifex)	50	35	-	-	15	-	-	-
AK-23f (spinifex)	55	30	-	-	15	-	-	-
AK-24b (spinifex)	60	30	-	-	10	-	-	tr
AK-24c (spinifex)	70	30	-	-	10	-	-	-
AK-24e (spinifex)	65	25	-	-	10	-	-	tr
AK-25c (spnifex)	70	15	5	tr	10	-	-	tr
AK-28b (spinifex)	77	3	5	-	15	-	-	-
S-198b (spinifex)	65	25	tr	-	10	-	-	tr
S-198c (spinifex)	65	25	5	-	5	-	tr	-
S-198d (spinifex)	60	34	-	tr	5	-	-	tr
S-211c (spinifex)	65	30	-	-	5	-	-	-
S-211d (spinifex)	59	35	tr	tr	5	tr	-	tr

Appendix A1.a (continued)

	Tr/Act	Chl	Srp	Tlc	Cr-Mag/Mag	Chr	Cb	Hm
S-211e (spinifex)	62	30	3	-	5	-	-	tr
S-3a (spinifex)	70	29	tr	-	1	-	-	-
S-3b (spinifex)	65	32	-	-	3	-	-	-
S-3c (spinifex)	75	3	17	-	5	-	-	-

Appendix A1.b Modal composition of cumulate zone komatiites, Woodburn Lake Group (Pipedream Lake belt)

	Tr/Act	Chl	Srp	Cr-Mag/Mag	Chr	Cb	Hm
K-1a	43	5	50	2	-	-	tr
K-3a	45	15	30	10	-	-	-
K-7a	50	35	-	15	-	-	tr
K-7b	45	14	30	10	-	-	1
K-19	25	15	50	10	-	-	-
K-21	65	5	20	10	-	-	-
K-24	25	10	55	10	-	-	-
K-25	55	10	25	10	-	-	-
K-28	15	25	55	5	-	-	-
K-38	30	10	45	15	-	-	-
K-40	30	15	45	10	-	-	-
K-41	40	15	35	10	-	-	-
K-43a	13	10	65	10	-	2	-
K-43b	15	5	67	10	-	3	-
K-43c	20	10	55	8	-	5	2
K-43d	30	20	40	10	-	-	-
AK-13a	69	1	20	10	-	-	-
AK-14b	25	15	45	15	-	-	-
AK-15a	55	15	25	5	-	-	-
AK-15b	35	15	40	10	-	-	-
AK-16a	30	15	43	10	-	2	-
AK-16b	32	15	40	10	-	3	-

Appendix A1.b (continued)

	Tr/Act	Chl	Srp	Cr-Mag/Mag	Chr	Cb	Hm
AK-21a	40	10	35	15	-	-	-
AK-23a	45	30	-	25	-	-	-
AK-23b	30	20	35	15	-	-	-
AK-24a-1	30	10	47	10	-	2	1
AK-24a-2	5	3	82	10	-	-	-
AK-24d	40	17	30	10	-	2	1
AK-25b	45	15	25	15	-	-	-
AK-28a	42	3	40	15	-	-	-
S-190a	20	10	64	5	1	tr	-
S-211a	15	15	65	5	tr	-	-
S-211b	20	14	60	5	1	-	-
S-171a	24	10	45	10	-	-	1

Appendix A1.c Modal composition of massive and pillowed komatiites, Woodburn Lake Group (Pipedream Lake belt)

	Tr/Act	Chl	Srp	Cr-Mag/Mag	Chr	Cb	Hm	Ep
K-3a (massive)	44	15	35	5	1	-	tr	-
K-17a (massive)	70	25	-	5	-	-	-	-
K-34 (massive)	45	10	30	13	-	-	2	-
K-40 (massive)	40	10	36	10	-	1	-	3
AK-13b (sheared massive)	84	10	-	3-5	-	-	3	-
AK-18b (pillowed ?)	60	30	-	10	-	-	-	-
S-173c (massive)	45	30	10	15	-	-	-	-

Appendix A1.d Modal composition of contact metamorphosed komatiites, Woodburn Lake Group (Pipedream Lake belt).

	Ol	Tr/Act	Ath	Chl	Srp	Sp	Cr-Mag/Mag	Cb	Pl	Hm	Id
AK-8a (spinifex-textured flow)	15	75	-	-	-	5	5	-	-	-	3
AK-11a (massive)	3	75	10	5	-	-	5	-	-	2	-
AK-12a (pillowed ?)	5	50	-	25	-	3	15	-	-	2	-
AK-12b (pillowed ?)	25	47	15	3	2	5	-	-	3	-	-
S-200 (massive)	25	40	25	2	tr	2	5	tr	-	-	-

Appendix A1.e Modal composition of altered komatiites, Woodburn Lake Group (Pipedream Lake belt)

	Tr/Act	Chl	Srp	Cr-Mag/Mag	Cb
AK-3 (sheared, spinifex)	40	10	-	15	35
AK-29 (sheared komatiite)	25	2	58	15	-
AK-18c (sheared, cumulate)	45	15	25	15	-

Appendix A1.f Modal composition of komatiite dyke, Woodburn Lake Group (Pipedream Lake belt)

	Ol	Tr/Act	Ath	Chl	Sp	Cr-Mag/Mag	Hm
AK-7b	20	45	15	3	10	5	2

Appendix A1.g Modal composition of volcanoclastic (?) komatiite, Woodburn Lake Group (Pipedream Lake belt)

	Tr/Act	Chl	Cr-Mag/Mag	Cb
AK-18a	10	5	15	70

Appendix A1.h Modal composition of Esker Lake komatiites.

	Tr/Act	Ath	Chl	Srp	Tlc	Cr-Mag/Mag	Chr	Cb	Hm
R-216 (serpentinite)	-	-	20	65	-	10	-	5	-
R-220b-1 (serpentinite)	-	-	-	74	5	10	1	10	tr
R-220b-2 (serpentinite)	-	-	-	34	35	15	1	15	-
R-220c (serpentinite)	-	-	-	78	5	15	tr	2	-
R-226a (serpentinite)	5	-	-	80	-	15	-	-	-
R-228a (massive)	65	-	25	1	-	6	3	-	-
R-228c (massive)	50	-	5	35	-	10	-	-	-
R-228d (massive)	70	-	20	tr	-	10	-	-	-
R-238 (serpentinite)	54	-	10	30	-	5	1	-	tr
R-242a (spinifex-textured)	54	-	5	-	-	10	5	-	1
R-242b (cumulate)	55	5	2	15	tr	3	2	-	-

Appendix A1.i Modal composition of high-magnesium basalts, Woodburn Lake Group (Pipedream Lake belt)

	Tr/Act	Act/Tr	Hrn/Act	Chl	Mag	Cb	Pl	Qtz	Bt	Hm	Ep
AK-20-1 (tholeiitic basalt)	-	65	-	15	5	-	10	-	-	-	5
AK-20-2 (tholeiitic basalt)	-	65	-	15	2	-	10	-	-	-	8
AK-31 (komatiitic basalt)	-	62	-	30	-	-	3	-	-	-	5
S-99 (tholeiitic basalt)	35	-	-	7	2	-	20	1	-	tr	35
S-182 (tholeiitic basalt)	-	-	45	3	1	-	21	10	10	-	10
R-220d (komatiitic basalt)	17	-	-	-	5	2	75	tr	-	-	1
R-222 (komatiitic basalt)	2	-	55	3	1	tr	35	tr	2	-	2
R-232b (tholeiitic basalt)	25	-	-	5	15	1	52	2	-	-	-
R-232c (tholeiitic basalt)	-	-	34	10	-	-	55	5	-	tr	1
R-233 (komatiitic basalt)	55	-	15	-	1	-	24	tr	-	-	5

Appendix A1.j Modal composition of calc-alkaline suite, Woodburn Lake Group (Pipedream Lake belt)

	Chl	Mag	Cb	Pl	Qtz	Mus	Bt	Phl	Hm	Grn	Tm	Ep	Ap
AK-2 (rhyolite)	2	1	-	52	40	-	-	-	-	-	-	5	-
AK-6a (dacite)	-	2	-	30	40	-	15	-	-	-	-	10	3
AK-6b (sheared dacite/ andacite)	20	3	-	30	25	-	5	-	1	5	1	10	-
AK-6c (dacite)	15	2	5	20	30	-	-	-	-	-	1	25	2
AK-9 (rhyolite)	-	-	-	25	43	20	-	2	-	-	-	-	-
AK-11b (rhyolite)	-	-	25	20	40	13	-	2	-	-	-	-	-
AK-13c (rhyolite)	-	3	-	30	37	25	5	-	-	-	-	-	-

Legend to Appendices B1 to B6

Fe2O3T = total iron expressed as Fe2O3

Oxides and CIPW norms are presented in wt%

Trace elements are expressed in ppm

nd = not determined (analysed)

bl = below detection limit

\- = not calculated

AN = anorthite content of normative plagioclase

Mg# = [MgO/(MgO+FeO)]*100 (molecular)

(LOI) = loss on ignition determined at 1000 C for 1 hour

CIPW norms are calculated by adjusting the Fe2O3/FeO ratio (% Fe2O3 = % TiO2 + 1.5) and by recalculating the analysis to 100 % volatile-free

Values of chondritic ratios used for comparison:

CaO/Al_2O_3 = 0.82

CaO/TiO_2 = 16.7

Al_2O_3/TiO_2 = 20.4

Sc/Zr = 1.41

Ti/Zr = 110 (100?)

Ti/Sc = 78

Ti/V = 10

V/Zr = 11 (11.5?)

V/Sc = 8

Al/Zr = 1825

Al/Sc = 1410

Appendix B1.a (Woodburn Lake Group komatiites - area 1)

	K-41	K-41 (GSC)	K-42a	K-42a*	K-42a (GSC)	K-42a* (GSC)	K-42b	K-42b (GSC)	K-42c	K-42c (GSC)	K-42d
SiO2	43.47	43.10	43.06	43.20	42.30	42.70	43.20	43.10	44.68	44.00	41.34
TiO2	0.26	0.28	0.36	0.34	0.38	0.35	0.36	0.37	0.31	0.33	0.41
Al2O3	6.16	6.10	8.34	8.00	8.10	7.80	8.16	8.00	7.39	7.50	9.40
Fe2O3T	9.79	nd	11.72	11.90	nd	nd	11.90	nd	10.36	nd	12.23
Fe2O3	3.17	2.90	nd	nd	3.90	3.80	nd	4.50	nd	3.40	nd
FeO	5.96	6.10	nd	nd	6.80	7.00	nd	6.60	nd	6.00	nd
MnO	0.15	0.17	0.16	0.16	0.17	0.17	0.17	0.19	0.17	0.18	0.16
MgO	28.51	28.10	24.71	24.80	23.80	23.70	24.33	23.50	24.71	24.00	24.84
CaO	4.54	4.75	6.38	6.56	6.56	6.64	6.53	6.65	6.96	7.11	5.98
Na2O	0.59	0.20	0.74	0.87	bl	0.10	0.76	bl	0.87	0.20	0.83
K2O	0.05	0.07	0.04	0.04	0.03	0.04	0.04	0.04	0.04	0.06	0.05
P2O5	bl	0.01	bl	bl	0.01	0.01	bl	0.01	bl	bl	bl
H2O(LOI)	nd	6.90	nd	nd	5.40	5.70	nd	5.20	nd	5.30	nd
CO2	nd	0.30	nd	nd	0.30	0.10	nd	0.20	nd	0.10	nd
Total	93.52	98.90	95.51	95.15	97.75	98.11	95.45	98.36	95.49	98.10	95.32
B	nd	20	nd	nd	bl	bl	nd	bl	nd	22	nd
Ba	nd	26	nd	nd	13	11	nd	12	nd	10	nd
Co	62	110	84	nd	71	83	87	91	94	93	89
Cr	2607	2326	2910	2746	2805	2737	2913	2805	2689	2668	3223
Cu	nd	37	nd	nd	39	47	nd	58	nd	190	nd
Nb	bl	nd	bl	bl	nd	nd	bl	nd	bl	nd	bl
Ni	1494	1650	1125	1116	1130	1070	1123	1120	1373	1270	1033
Rb	bl	bl	bl	bl	20	10	bl	40	bl	40	bl
Sr	bl	bl	6	3	20	20	5	10	7	bl	9
V	162	83	215	206	110	130	205	140	174	110	256
Y	17	27	15	16	bl	22	19	25	19	31	21
Zn	71	100	108	58	100	60	55	90	79	80	91
Zr	10	10	12	13	bl	10	14	10	12	bl	20
Sc	24	nd	30	nd	nd	nd	31	nd	28	nd	36
AN	73.73		75.52				74.45		68.68		75.80
or	0.30		0.24				0.24		0.24		0.30
ab	4.99		6.26				6.43		7.36		7.02
an	14.81		19.32				18.74		16.14		22.00
C	-		-				-		-		-
di	6.73		9.81				10.87		14.50		6.10
hy	24.81		16.28				16.26		18.70		8.89
ol	38.73		39.00				38.47		34.06		46.07
mt	2.55		2.70				2.70		2.62		2.77
il	0.49		0.60				0.60		0.59		0.70
ap	-		-				-		-		-

	K-41	K-42a	K-42b	K-42c	K-42d
CaO/Al2O3	0.74	0.76	0.80	0.94	0.63
CaO/TiO2	17.5	17.7	18.1	22.5	14.6
Al2O3/TiO2	23.7	23.2	22.7	23.8	23.1
Sc/Zr	2.40	2.50	2.21	2.33	1.80
Ti/Zr	156	180	154	155	123
Ti/Sc	65	72	70	66	68
Ti/V	9.6	10.1	10.5	10.7	9.6
V/Zr	16.2	17.9	14.6	14.5	12.8
V/Sc	6.8	7.2	6.6	6.2	7.1
Al/Zr	3259	3677	3003	3258	2507
Al/Sc	1358	1471	1392	1396	1393
Mg#	86	83	82	84	82

Appendix B1.a (continued)

	K-42d (GSC)	K-42d (GSC)	K-43a	K-43a (GSC)	K-43b	K-43b (GSC)	K-43c	K-43c (GSC)	K-43d	K-43d (GSC)	K-44a
SiO2	48.90	48.80	42.10	41.80	40.80	40.70	41.10	40.50	41.59	40.80	43.02
TiO2	0.44	0.43	0.21	0.23	0.22	0.25	0.18	0.20	0.22	0.24	0.32
Al2O3	9.80	9.10	5.27	5.00	5.00	5.10	4.47	4.30	5.33	5.20	7.49
Fe2O3T	nd	nd	9.61	nd	10.55	nd	10.31	nd	10.37	nd	11.21
Fe2O3	3.60	3.50	nd	2.50	nd	2.50	nd	2.30	nd	2.50	nd
FeO	7.40	7.70	nd	6.20	nd	6.90	nd	6.90	nd	6.70	nd
MnO	0.17	0.18	0.14	0.16	0.13	0.14	0.13	0.14	0.13	0.13	0.15
MgO	24.10	24.00	29.55	29.30	32.24	32.00	33.36	33.20	31.96	31.60	25.49
CaO	6.12	6.12	4.05	4.11	2.00	2.04	1.27	1.30	2.12	2.14	6.27
Na2O	0.40	bl	0.31	bl	0.24	bl	0.20	bl	0.41	bl	0.89
K2O	0.00	0.06	0.05	0.05	0.03	0.04	0.01	0.03	0.01	0.02	0.04
P2O5	0.03	0.02	bl	bl	bl	0.01	0.01	0.01	bl	0.02	bl
H2O(LOI)	6.10	6.20	nd	8.20	nd	9.00	nd	9.50	nd	9.00	nd
CO2	0.40	0.40	nd	2.00	nd	0.80	nd	0.70	nd	0.30	nd
Total	99.54	98.51	91.29	99.55	91.29	99.48	91.04	99.00	92.14	98.65	94.88
B	25	nd	nd	22	nd	32	nd	27	nd	23	nd
Ba	15	20	nd	29	nd	11	nd	27	nd	25	nd
Co	110	nd	74	100	97	100	96	130	96	93	83
Cr	3079	3147	2310	2053	2707	2250	2373	1984	2565	2000	2019
Cu	18	nd	nd	16	nd	5	nd	bl	nd	4	nd
Nb	nd	nd	bl	nd	bl	nd	bl	nd	bl	nd	bl
Ni	970	970	1747	1690	2120	1860	2321	1980	2140	1790	1336
Rb	bl	10	bl	20	bl	bl	bl	bl	bl	20	bl
Sr	30	bl	19	30	4	20	1	bl	bl	bl	4
V	200	nd	141	55	110	69	106	47	124	60	202
Y	39	nd	22	20	17	26	1	26	4	23	22
Zn	120	70	84	70	89	80	89	90	60	70	49
Zr	10	10	10	bl	7	bl	6	20	10	10	13
Sc	nd	nd	20	nd	20	nd	10	nd	21	nd	29
AN			83.04		83.01		78.65		75.20		60.43
or			0.30		0.10		0.06		0.06		0.24
ab			2.62		2.03		1.69		3.47		7.53
an			12.04		9.92		6.24		10.52		16.33
C			-		1.02		1.05		0.79		-
di			5.73		-		-		-		11.74
hy			26.37		20.14		32.95		27.02		13.21
ol			39.57		45.06		44.29		45.32		41.50
mt			2.40		2.49		2.44		2.49		2.64
il			0.40		0.42		0.34		0.42		0.61
ap			-		-		0.02		-		-

	K-43a	K-43b	K-43c	K-43d	K-44a
CaO/Al2O3	0.77	0.39	0.28	0.48	0.84
CaO/TiO2	19.3	9.1	7.1	9.6	19.6
Al2O3/TiO2	25.1	23.1	24.8	24.2	23.4
Sc/Zr	2.00	2.86	3.00	2.10	2.23
Ti/Zr	126	189	180	132	148
Ti/Sc	63	66	60	63	66
Ti/V	8.9	11.2	10.2	10.7	9.5
V/Zr	14.1	16.9	17.7	12.4	15.5
V/Sc	7.1	5.9	5.9	5.9	7.0
Al/Zr	2788	3839	3941	2820	3048
Al/Sc	1394	1344	1314	1343	1366
Mg0	87	87	88	87	84

Appendix B1.a (continued)

	K-44a (GSC)	K-44b	K-44b	K-44b (GSC)	K-44c	K-44c	K-44c (GSC)	K-44d	K-44d	K-44d (GSC)	K-44e
SiO2	42.70	44.31	44.07	44.10	44.12	43.72	43.80	42.53	42.36	42.30	43.67
TiO2	0.34	0.27	0.27	0.31	0.32	0.32	0.34	0.30	0.30	0.32	0.32
Al2O3	7.20	6.35	6.35	6.10	7.40	7.38	7.40	7.09	7.04	6.80	7.26
Fe2O3T	nd	10.54	10.53	nd	10.77	10.84	nd	11.06	11.16	nd	9.28
Fe2O3	4.70	nd	nd	3.50	nd	nd	4.00	nd	nd	3.30	nd
FeO	5.70	nd	nd	6.10	nd	nd	5.90	nd	nd	7.00	nd
MnO	0.16	0.16	0.16	0.17	0.16	0.16	0.18	0.17	0.17	0.18	0.15
MgO	25.00	26.71	26.38	26.40	25.16	25.26	25.20	26.63	26.75	26.60	25.76
CaO	6.30	5.96	5.94	6.10	6.51	6.49	6.72	5.11	5.11	5.30	6.49
Na2O	bl	0.67	0.52	bl	0.91	0.75	bl	0.79	0.79	bl	0.90
K2O	0.04	0.02	0.02	0.03	0.04	0.04	0.05	0.07	0.08	0.07	0.03
P2O5	0.01	bl	bl	0.03	bl	bl	bl	bl	bl	bl	bl
H2O(LOI)	6.10	nd	nd	6.00	nd	nd	5.50	nd	nd	6.40	nd
CO2	0.50	nd	nd	0.20	nd	nd	0.20	nd	nd	0.10	nd
Total	98.03	94.99	94.24	99.04	95.39	94.96	99.29	93.75	93.76	98.37	93.86
B	bl	nd	nd	bl	nd	nd	bl	nd	nd	16	nd
Ba	11	nd	nd	10	nd	nd	10	nd	nd	12	nd
Co	81	65	nd	100	112	nd	87	95	nd	100	60
Cr	2668	2528	2522	2395	2912	2886	2885	2849	2854	2668	2848
Cu	7	nd	nd	19	nd	nd	24	nd	nd	44	nd
Nb	nd	bl	bl	nd	bl	bl	nd	bl	bl	nd	1
Ni	1230	1661	1596	1480	1188	1286	1200	1498	1420	1380	1413
Rb	50	bl	bl	30	bl	bl	bl	bl	1	10	bl
Sr	10	4	1	10	3	bl	bl	4	1	bl	8
V	110	134	154	83	172	177	110	183	190	120	182
Y	24	20	15	25	18	18	25	20	19	21	27
Zn	60	68	72	90	63	68	90	53	61	80	64
Zr	bl	10	10	10	14	12	10	10	12	10	14
Sc	nd	24	nd	nd	28	nd	nd	28	nd	nd	29
AN		71.55			67.50			69.99			67.31
or		0.12			0.24			0.41			0.18
ab		5.67			7.70			6.68			7.62
an		14.26			15.99			15.59			15.68
C		-			-			-			-
di		12.13			12.94			7.75			13.86
hy		22.50			16.86			16.77			16.21
ol		36.12			37.33			42.45			36.88
mt		2.57			2.64			2.61			2.64
il		0.51			0.61			0.57			0.61
ap		-			-			-			-

	K-44b	K-44c	K-44d	K-44e
CaO/Al2O3	0.94	0.88	0.72	0.89
CaO/TiO2	22.1	20.3	17.0	20.3
Al2O3/TiO2	23.5	23.1	23.6	22.7
Sc/Zr	2.40	2.00	2.00	2.07
Ti/Zr	162	137	100	137
Ti/Sc	68	69	64	66
Ti/V	12.1	11.2	9.8	10.6
V/Zr	13.4	12.3	10.3	13.0
V/Sc	5.6	6.1	6.5	6.3
Al/Zr	3359	2796	3751	2743
Al/Sc	1400	1398	1340	1324
Mg#	85	84	84	86

Appendix B1.a (continued)

	K-44e (GSC)	K-44f	K-44f (GSC)	K-44g	K-44g (GSC)	AK-14a	AK-14a (GSC)	AK-14a (GSC)	AK-14b	AK-14b (GSC)	AK-14c
SiO2	44.00	42.02	41.20	43.87	43.80	42.76	42.40	42.80	41.66	41.50	43.53
TiO2	0.34	0.36	0.37	0.30	0.33	0.29	0.31	0.32	0.24	0.25	0.30
Al2O3	7.30	8.14	8.20	6.97	7.40	6.90	6.70	6.90	5.65	5.50	7.32
Fe2O3T	nd	11.66	nd	10.55	nd	11.09	nd	nd	10.87	nd	10.20
Fe2O3	2.90	nd	4.40	nd	3.40	4.26	3.80	3.80	2.84	3.80	3.09
FeO	5.50	nd	6.00	nd	6.00	6.15	6.30	7.00	7.23	6.70	6.40
MnO	0.16	0.16	0.18	0.16	0.16	0.17	0.18	0.18	0.15	0.16	0.16
MgO	25.70	25.36	24.70	25.42	24.80	26.39	26.10	26.10	29.85	29.40	25.91
CaO	6.71	5.80	5.86	6.40	6.54	5.29	5.40	5.52	3.28	3.37	6.21
Na2O	bl	0.73	0.10	0.70	0.10	0.73	bl	bl	0.40	bl	0.76
K2O	0.02	0.04	0.07	0.02	0.05	0.00	0.07	0.00	0.02	0.02	0.07
P2O5	0.01	bl	0.01	bl	0.02	bl	0.03	0.02	bl	0.02	bl
H2O(LOI)	5.90	nd	6.00	nd	5.60	nd	6.60	6.60	nd	8.60	nd
CO2	0.20	nd	0.10	nd	0.20	nd	0.20	0.20	nd	0.40	nd
Total	98.74	94.27	97.99	94.39	98.40	93.70	98.17	98.72	92.12	98.92	94.46
B	20	nd	bl	nd	19	nd	bl	nd	nd	19	nd
Ba	11	nd	56	nd	12	nd	26	50	nd	17	nd
Co	77	90	86	89	94	71	94	nd	99	100	80
Cr	2737	3081	2942	2682	2600	2637	2532	2463	2600	2326	2865
Cu	6	nd	16	nd	5	nd	24	nd	nd	72	nd
Nb	nd	bl	nd	bl	nd	bl	nd	nd	bl	nd	bl
Ni	1350	1391	1240	1395	1290	1463	1430	1400	1882	1670	1320
Rb	30	bl	30	bl	10	1	20	bl	bl	10	bl
Sr	10	4	bl	7	bl	3	20	10	1	bl	3
V	110	222	130	166	120	163	100	nd	123	82	103
Y	23	21	20	17	20	10	22	nd	16	21	17
Zn	60	52	90	51	70	61	100	90	87	60	82
Zr	20	17	bl	11	20	13	20	bl	11	10	11
Sc	nd	31	nd	27	nd	27	nd	nd	21	nd	20
AN		75.29		72.76		71.26			80.03		71.70
or		0.24		0.12		0.47			0.12		0.41
ab		6.10		5.92		6.10			3.30		6.43
an		10.02		15.02		15.32			13.56		16.36
C		-		-		-			-		-
di		7.91		12.63		0.67			2.15		11.45
hy		15.07		21.04		10.69			25.40		17.02
ol		41.17		34.37		40.03			43.16		37.66
mt		2.70		2.61		2.60			2.52		2.61
il		0.60		0.57		0.55			0.40		0.57
ap		-		-		-			-		-

	K-44f	K-44g	AK-14a	AK-14b	AK-14c
CaO/Al2O3	0.71	0.92	0.77	0.58	0.85
CaO/TiO2	16.1	21.3	18.2	13.7	20.7
Al2O3/TiO2	22.6	23.2	23.8	23.5	24.4
Sc/Zr	1.82	2.45	2.08	1.91	2.55
Ti/Zr	127	164	134	131	164
Ti/Sc	70	67	64	69	64
Ti/V	9.7	10.8	10.7	11.7	9.8
V/Zr	13.1	15.1	12.5	11.2	16.6
V/Sc	7.2	6.2	6.0	5.9	6.5
Al/Zr	2533	3352	2808	2717	3520
Al/Sc	1389	1366	1352	1423	1383
Mg#	84	85	84	86	85

Appendix B1.a (continued)

	AK-14c (GSC)	AK-14d	AK-14d (GSC)	AK-15a	AK-15a (GSC)	AK-15b	AK-15b (GSC)	AK-15c	AK-15c (GSC)	AK-15c (GSC)	AK-15d
SiO2	43.20	42.14	42.80	43.22	43.00	42.10	42.20	40.97	40.90	41.80	43.35
TiO2	0.32	0.29	0.31	0.28	0.30	0.26	0.29	0.41	0.43	0.42	0.35
Al2O3	7.40	6.92	7.50	6.57	6.30	6.10	6.10	9.72	9.60	9.50	8.86
Fe2O3T	nd	11.63	nd	10.89	nd	10.80	nd	12.40	nd	12.40	11.70
Fe2O3	3.30	4.90	4.50	4.67	3.00	3.79	3.30	5.10	3.40	3.80	4.71
FeO	5.90	6.06	6.30	5.70	6.10	6.31	6.50	6.57	7.90	7.70	6.36
MnO	0.10	0.15	0.17	0.16	0.17	0.17	0.10	0.10	0.19	0.10	0.17
MgO	25.10	25.49	25.20	27.49	27.10	28.94	28.70	24.23	23.70	23.90	24.61
CaO	6.29	5.73	5.92	5.26	5.39	3.91	4.02	5.75	5.83	5.66	6.67
Na2O	0.20	0.29	0.20	0.64	bl	0.50	bl	0.77	0.20	0.60	0.81
K2O	0.09	bl	0.07	0.05	0.06	0.04	0.06	0.05	0.06	0.05	0.03
P2O5	0.02	bl	0.01	bl	0.02	bl	0.01	bl	0.03	0.03	bl
H2O(LOI)	6.10	nd	6.30	nd	7.00	nd	7.70	nd	6.30	7.10	nd
CO2	0.10	nd	0.10	nd	0.20	nd	0.10	nd	0.10	0.10	nd
Total	98.20	92.64	99.30	93.76	98.64	92.90	99.16	94.40	98.64	101.02	95.83
B	16	nd	21	nd	bl	nd	35	nd	bl	nd	nd
Ba	15	nd	19	nd	12	nd	32	nd	17	65	nd
Co	77	60	89	92	97	70	110	87	97	nd	50
Cr	2737	2736	2600	2737	2532	2790	2532	3300	3147	nd	2874
Cu	11	nd	13	nd	15	nd	19	nd	31	nd	nd
Nb	nd	bl	nd	bl	nd	bl	nd	bl	nd	bl	bl
Ni	1230	1296	1230	1549	1550	1707	1540	1037	980	nd	1224
Rb	30	bl	30	bl	20	bl	40	4	10	bl	4
Sr	bl	5	20	5	10	bl	10	1	10	bl	7
V	110	104	120	170	84	150	110	220	160	nd	193
Y	22	17	26	17	22	13	32	11	23	bl	10
Zn	80	57	90	99	70	94	80	105	100	nd	60
Zr	bl	12	bl	9	bl	10	10	10	40	49	15
Sc	nd	27	nd	25	nd	25	nd	35	nd	nd	30
AN		87.75		73.35		77.41		77.86			72.72
or		0.00		0.30		0.24		0.30			0.10
ab		2.45		5.42		4.23		6.52			6.05
an		17.50		14.91		14.50		22.92			10.27
C		-		-		-		-			-
di		0.62		0.05		3.00		4.47			11.79
hy		24.75		21.10		23.17		10.00			15.00
ol		34.99		30.00		42.60		44.61			39.10
mt		2.60		2.50		2.55		2.77			2.60
il		0.55		0.53		0.49		0.70			0.60
ap		-		-		-		-			-

	AK-14d	AK-15a	AK-15b	AK-15c	AK-15d
CaO/Al2O3	0.83	0.80	0.63	0.59	0.83
CaO/TiO2	19.8	18.8	15.0	14.0	19.1
Al2O3/TiO2	23.9	23.5	23.8	23.7	23.0
Sc/Zr	2.25	2.70	2.50	1.94	2.00
Ti/Zr	145	187	156	137	140
Ti/Sc	64	67	62	70	70
Ti/V	9.5	9.4	9.9	10.0	10.9
V/Zr	15.3	19.0	15.0	12.7	12.9
V/Sc	6.0	7.1	6.3	6.5	6.4
Al/Zr	3051	3862	3269	2857	2842
Al/Sc	1356	1390	1300	1469	1421
Mg#	83	86	86	81	83

Appendix B1.a (continued)

	AK-15d (GSC)	AK-16a	AK-16a (GSC)	AK-16b	AK-16b (GSC)	AK-16c	AK-18b	AK-18c
SiO2	43.30	41.47	40.90	41.12	40.60	43.19	44.17	41.13
TiO2	0.37	0.23	0.26	0.21	0.23	0.33	0.30	0.22
Al2O3	8.10	5.30	5.10	5.41	5.40	7.65	5.93	5.09
Fe2O3T	nd	10.48	nd	10.42	nd	11.03	13.00	10.44
Fe2O3	4.00	3.09	2.30	3.50	2.90	nd	nd	nd
FeO	6.70	6.65	6.90	6.23	6.50	nd	nd	nd
MnO	0.18	0.15	0.16	0.15	0.16	0.16	0.14	0.15
MgO	24.20	30.70	30.20	30.93	29.90	25.60	24.43	31.35
CaO	6.80	3.06	3.12	3.10	3.10	6.43	7.22	3.74
Na2O	bl	0.41	bl	0.36	bl	0.82	0.60	0.40
K2O	0.04	0.01	0.01	0.02	0.05	0.07	0.02	0.02
P2O5	0.02	bl	0.02	bl	0.01	bl	bl	bl
H2O(LOI)	4.90	nd	8.40	nd	8.50	nd	nd	nd
CO2	0.20	nd	1.10	nd	1.20	nd	nd	nd
Total	98.81	101.63	98.47	91.72	98.63	95.36	95.89	92.62
B	16	nd	bl	nd	30	nd	nd	nd
Ba	69	nd	19	nd	27	nd	nd	nd
Co	89	73	95	68	110	nd	74	102
Cr	2874	2561	2189	2471	2121	2896	2876	2623
Cu	290	nd	20	nd	10	nd	nd	nd
Nb	nd	bl	nd	bl	nd	bl	bl	bl
Ni	1190	1007	1690	1971	1710	1171	1133	1967
Rb	bl	bl	20	bl	10	bl	bl	bl
Sr	20	3	10	4	bl	1	7	12
V	150	130	72	127	79	194	195	133
Y	34	20	22	17	29	17	15	20
Zn	100	79	70	68	90	62	44	74
Zr	bl	9	bl	11	bl	13	16	9
Sc	nd	20	nd	21	nd	36	27	21
AN		78.40		81.12		71.00	72.57	74.19
or		0.06		0.12		0.41	0.12	0.12
ab		3.47		3.05		6.94	5.00	4.06
an		12.59		13.09		16.99	13.43	11.68
C		-		-		-	-	-
di		2.05		1.81		11.84	17.87	5.44
hy		24.46		23.00		13.20	19.36	16.22
ol		44.90		46.56		41.70	35.73	51.32
mt		2.51		2.40		2.65	2.61	2.49
il		0.44		0.40		0.63	0.57	0.42
ap		-		-		-	-	-

	AK-16a	AK-16b	AK-16c	AK-18b	AK-18c
CaO/Al2O3	0.58	0.57	0.84	1.22	0.73
CaO/TiO2	13.3	14.8	19.5	24.1	17.0
Al2O3/TiO2	23.0	25.8	23.2	19.8	23.1
Sc/Zr	2.22	1.91	2.77	2.70	2.33
Ti/Zr	153	115	152	180	147
Ti/Sc	69	60	55	67	63
Ti/V	10.6	9.9	10.2	9.2	9.9
V/Zr	14.4	11.6	14.9	19.5	14.8
V/Sc	6.5	6.1	5.4	7.2	6.3
Al/Zr	3115	2602	3113	3137	2992
Al/Sc	1402	1363	1124	1162	1282
MgO	87	87	87	84	89

Appendix B1.b (Woodburn Lake Group komatiites - area 2)

	K-1	K-2a	K-2b	K-2d	K-3a-1	K-3a-1 (GSC)	K-3a-2	K-3a-2 (GSC)	K-4a	K-4a (GSC)	K-4b
SiO2	41.00	43.00	42.92	42.34	42.79	42.20	43.04	42.20	42.71	42.50	42.20
TiO2	0.22	0.33	0.31	0.35	0.26	0.27	0.26	0.28	0.34	0.37	0.31
Al2O3	5.06	7.43	7.06	7.80	6.07	6.50	6.24	6.00	7.95	7.90	7.44
Fe2O3T	9.64	11.41	10.88	11.68	10.16	nd	10.22	nd	12.29	12.20	12.03
Fe2O3	nd	nd	nd	nd	nd	3.00	nd	3.10	nd	nd	nd
FeO	nd	nd	nd	nd	nd	6.10	nd	6.20	nd	nd	nd
MnO	0.15	0.15	0.15	0.16	0.17	0.19	0.17	0.17	0.17	0.19	0.15
MgO	33.25	25.76	26.04	25.35	29.10	28.40	28.77	27.60	24.33	23.80	25.13
CaO	1.48	6.38	6.37	6.19	4.29	4.40	4.73	4.73	6.70	6.85	6.42
Na2O	0.29	0.65	0.61	0.67	0.58	0.10	0.42	bl	0.96	bl	0.74
K2O	0.01	0.03	0.02	0.02	0.03	0.06	0.02	0.03	0.03	0.03	0.02
P2O5	bl	bl	bl	bl	bl	0.02	bl	0.01	bl	0.03	bl
H2O(LOI)	nd	nd	nd	nd	nd	7.40	nd	7.00	nd	5.70	nd
CO2	nd	nd	nd	nd	nd	0.30	nd	0.60	nd	0.30	nd
Total	91.18	95.14	94.36	94.56	93.45	98.94	93.87	97.92	95.48	99.87	94.44
B (AA)	nd	nd	nd	nd	nd	35	nd	29	nd	bl	nd
Ba (XRF)	nd	nd	nd	nd	nd	30	nd	20	nd	30	nd
Ba (AA)	nd	nd	nd	nd	nd	19	nd	20	nd	12	nd
Co (*)	nd	nd	nd	nd	72	110	nd	120	47	89	69
Cr (XRF)	2715	2855	2702	2851	2694	2395	2662	2463	2912	2942	2681
Cr (other)	nd	nd	nd	nd	2413	3100	nd	2700	2806	3000	2569
Cu (AA)	nd	nd	nd	nd	nd	15	nd	19	nd	bl	nd
Nb (XRF)	bl	bl	bl	bl	bl	nd	bl	nd	bl	nd	bl
Ni (XRF)	2250	1095	1546	1179	1672	1550	1760	1680	1110	1120	1333
Ni (other)	nd	nd	nd	nd	1633	1600	nd	1800	568	1100	1376
Rb (XRF)	bl	bl	bl	bl	bl	10	bl	bl	bl	10	bl
Sr (XRF)	bl	8	7	6	7	20	10	10	11	50	8
Sr (AA)	nd	nd	nd	nd	nd	17	nd	22	nd	21	nd
V (*)	110	180	169	198	151	110	148	93	203	120	188
Y (*)	18	19	19	18	16	34	22	28	20	23	18
Zn (XRF)	67	74	65	55	86	90	100	90	79	80	59
Zr (XRF)	6	13	12	14	7	20	13	10	13	20	11
Sc (INAA)	nd	nd	nd	nd	23	nd	nd	nd	29	nd	26
AN	74.95	75.84	76.14	76.27	73.87		80.93		68.04		72.99
or	0.06	0.10	0.12	0.12	0.10		0.12		0.10		0.12
ab	2.45	5.50	5.16	5.67	4.91		3.55		8.12		6.26
an	7.34	17.27	16.47	16.22	13.87		15.00		17.30		16.92
C	1.00	-	-	-	-		-		-		-
di	-	11.43	12.01	9.93	5.06		6.63		12.71		11.07
hy	30.19	16.03	16.91	14.94	22.69		24.61		9.53		12.97
ol	45.55	40.50	39.57	41.35	41.72		39.77		43.29		41.54
mt	2.49	2.65	2.62	2.60	2.55		2.55		2.67		2.62
il	0.42	0.63	0.59	0.66	0.49		0.49		0.65		0.59

	K-1	K-2a	K-2b	K-2d	K-3a-1	K-3a-2	K-4a	K-4b
CaO/Al2O3	0.29	0.86	0.90	0.79	0.71	0.76	0.84	0.86
CaO/TiO2	6.7	19.3	20.6	17.7	16.5	18.2	19.7	20.7
Al2O3/TiO2	23.0	22.5	22.8	22.3	23.4	24.0	23.4	24.0
Sc/Zr	-	-	-	-	3.29	-	2.23	2.36
Ti/Zr	220	152	155	150	223	120	157	169
Ti/Sc	-	-	-	-	68	-	70	72
Ti/V	12.0	11.0	11.0	10.6	10.3	10.5	10.1	9.9
V/Zr	18.3	13.9	14.1	14.1	21.6	11.4	15.6	17.1
V/Sc	-	-	-	-	6.6	-	7.0	7.2
Al/Zr	4461	3023	3112	2947	4587	2539	3235	3578
Al/Sc	-	-	-	-	1396	-	1450	1514
Mg#	91	86	87	86	87	86	85	83

Appendix B1.b (continued)

	K-4b (GSC)	K-6a	K-6b	K-7a	K-7a (GSC)	K-7b	K-7b (GSC)	K-8	K-9	K-10a	K-10b
SiO2	42.20	42.05	42.43	42.54	42.60	40.81	40.20	43.42	40.59	43.56	42.70
TiO2	0.37	0.35	0.33	0.30	0.32	0.23	0.26	0.31	0.21	0.36	0.35
Al2O3	7.30	8.01	7.40	7.06	6.90	5.52	5.40	7.21	4.92	8.58	8.26
Fe2O3T	nd	11.40	12.25	11.86	nd	10.85	nd	11.09	11.34	9.18	12.10
Fe2O3	4.90	nd	nd	nd	5.40	nd	3.50	nd	nd	nd	nd
FeO	5.90	nd	nd	nd	5.50	nd	6.30	nd	nd	nd	nd
MnO	0.16	0.16	0.17	0.16	0.17	0.17	0.18	0.16	0.16	0.16	0.19
MgO	24.80	25.76	24.75	25.40	25.20	31.24	30.60	25.00	31.78	25.21	23.60
CaO	6.46	6.06	6.69	6.30	6.44	2.29	2.31	6.94	1.90	6.48	6.43
Na2O	bl	0.62	0.74	0.69	bl	0.35	bl	0.69	0.27	0.72	0.78
K2O	0.04	0.03	0.02	0.02	0.02	0.03	0.03	0.03	0.01	0.03	0.10
P2O5	0.02	bl	bl	bl	bl	bl	bl	bl	bl	bl	bl
H2O(LOI)	6.80	nd	nd	nd	5.70	nd	8.90	nd	nd	nd	nd
CO2	0.30	nd	nd	nd	0.20	nd	0.40	nd	nd	nd	nd
Total	98.45	94.44	94.78	94.33	98.45	91.49	98.88	94.85	91.18	94.28	94.51
B (AA)	bl	nd	nd	nd	bl	nd	19	nd	nd	nd	nd
Ba (XRF)	30	nd	nd	nd	40	nd	30	nd	nd	nd	nd
Ba (AA)	14	nd	nd	nd	11	nd	20	nd	nd	nd	nd
Co (*)	87	nd	nd	88	90	54	100	nd	nd	nd	nd
Cr (XRF)	2600	2936	2700	2642	2658	2636	2250	2712	2676	3169	2934
Cr (other)	2600	nd	nd	2490	2400	2216	2200	nd	nd	nd	nd
Cu (AA)	51	nd	nd	nd	17	nd	17	nd	nd	nd	nd
Nb (XRF)	nd	bl	bl	bl	nd	bl	nd	bl	bl	bl	bl
Ni (XRF)	1210	1200	1289	1466	1340	1813	1690	1370	2093	1204	1131
Ni (other)	1200	nd	nd	1557	1500	1025	1700	nd	nd	nd	nd
Rb (XRF)	10	bl	bl	bl	bl	bl	30	4	bl	4	7
Sr (XRF)	20	8	12	5	bl	3	30	13	bl	12	12
Sr (AA)	17	nd	nd	nd	24	nd	14	nd	nd	nd	nd
V (*)	100	205	194	179	90	143	69	184	116	223	190
Y (*)	25	20	19	19	24	22	26	25	17	19	15
Zn (XRF)	70	78	60	82	70	92	70	72	94	88	91
Zr (XRF)	bl	13	13	14	bl	11	40	13	7	15	13
Sc (INAA)	nd	nd	nd	27	nd	21	nd	nd	nd	nd	nd
AN		78.35	72.86	73.40		79.32		73.85	80.49	76.73	73.96
or		0.18	0.12	0.12		0.18		0.18	0.06	0.18	0.59
ab		5.25	6.26	5.84		2.96		5.84	2.28	6.09	6.60
an		18.99	16.81	16.11		11.36		16.49	9.43	20.09	18.74
C		-	-	-		0.75		-	1.01	-	-
di		8.80	13.85	12.84		-		14.26	-	9.54	10.49
hy		14.53	12.33	15.34		26.80		16.15	27.54	19.19	15.38
ol		42.40	41.89	40.39		46.80		37.80	47.02	35.80	38.34
mt		2.68	2.65	2.61		2.51		2.62	2.48	2.70	2.68
il		0.66	0.63	0.57		0.44		0.59	0.40	0.68	0.66

	K-6a	K-6b	K-7a	K-7b	K-8	K-9	K-10a	K-10b
CaO/Al2O3	0.76	0.90	0.89	0.41	0.96	0.39	0.76	0.78
CaO/TiO2	17.3	20.3	21.0	10.0	22.4	9.1	18.0	18.4
Al2O3/TiO2	22.9	22.4	23.5	24.0	23.3	23.4	23.8	23.6
Sc/Zr	-	-	1.93	1.91	-	-	-	-
Ti/Zr	162	152	129	125	143	180	144	162
Ti/Sc	-	-	67	66	-	-	-	-
Ti/V	10.2	10.2	10.1	9.7	10.1	10.9	9.7	11.1
V/Zr	15.8	14.9	12.8	13.0	14.2	16.6	14.9	14.6
V/Sc	-	-	6.6	6.8	-	-	-	-
Al/Zr	3259	3011	2668	2655	2934	3718	3026	3361
Al/Sc	-	-	1383	1391	-	-	-	-
Mg#	86	85	83	87	86	89	88	84

Appendix B1.b (continued)

	K-11	K-12	K-13	K-14a	K-14b	K-15	K-16	K-17	K-17 (GSC)	K-18	K-19
SiO2	42.46	41.97	43.27	42.19	42.63	42.32	43.27	42.96	42.20	43.44	42.35
TiO2	0.26	0.34	0.28	0.36	0.30	0.24	0.34	0.26	0.27	0.29	0.19
Al2O3	6.89	7.91	6.59	8.26	7.86	5.75	7.99	6.10	5.90	6.95	4.51
Fe2O3T	10.46	11.10	11.11	10.02	13.20	9.50	11.75	10.14	nd	9.70	11.04
Fe2O3	nd	nd	nd	nd	nd	nd	nd	nd	3.40	nd	nd
FeO	nd	nd	nd	nd	nd	nd	nd	nd	5.80	0.00	0.00
MnO	0.16	0.15	0.16	0.15	0.15	0.16	0.18	0.16	0.17	0.16	0.18
MgO	28.79	25.61	25.97	25.51	26.40	29.50	24.70	28.56	27.80	27.10	31.52
CaO	4.50	6.33	6.23	6.19	5.69	4.41	6.53	4.70	4.77	5.81	2.72
Na2O	0.44	0.70	0.73	0.42	0.32	0.21	0.47	0.49	bl	0.32	0.00
K2O	0.02	0.03	0.07	0.03	0.02	0.01	0.04	0.05	0.04	0.03	0.00
P2O5	bl	bl	bl	bl	bl	bl	bl	bl	bl	nd	nd
H2O(LOI)	nd	nd	nd	nd	nd	nd	nd	nd	7.40	0.00	0.00
CO2	nd	nd	nd	nd	nd	nd	nd	nd	0.30	nd	nd
Total	93.18	94.22	94.41	93.13	95.77	92.10	95.27	93.42	98.05	93.96	92.59
B (AA)	nd	nd	nd	nd	nd	nd	nd	nd	19	nd	nd
Ba (XRF)	nd	nd	nd	nd	nd	nd	nd	nd	40	nd	nd
Ba (AA)	nd	nd	nd	nd	nd	nd	nd	nd	19	nd	nd
Co (*)	nd	nd	nd	nd	nd	nd	nd	81	120	nd	nd
Cr (XRF)	2664	2968	2667	2985	2777	2562	2841	2652	2463	2975	2435
Cr (other)	nd	nd	nd	nd	nd	nd	nd	2394	2500	nd	nd
Cu (AA)	nd	nd	nd	nd	nd	nd	nd	nd	35	nd	nd
Nb (XRF)	1	bl	bl	bl	bl	bl	bl	bl	nd	bl	1
Ni (XRF)	1613	1193	1362	1159	1295	1848	1141	1893	1750	1578	1981
Ni (other)	nd	nd	nd	nd	nd	nd	nd	2049	2000	nd	nd
Rb (XRF)	3	1	bl	bl	bl	bl	bl	bl	20	bl	bl
Sr (XRF)	13	12	9	13	9	21	12	6	20	5	1
Sr (AA)	nd	nd	nd	nd	nd	nd	nd	nd	20	nd	nd
V (*)	151	192	174	201	174	137	199	151	74	171	101
Y (*)	22	20	18	21	17	22	22	18	25	20	21
Zn (XRF)	64	71	79	63	65	84	8	135	120	42	17
Zr (XRF)	10	13	9	15	13	12	13	9	bl	10	5
Sc (INAA)	nd	nd	nd	nd	nd	nd	nd	24	nd	nd	nd
AN	79.66	75.60	70.12	85.27	86.78	89.23	83.11	77.52		86.56	94.64
or	0.12	0.18	0.41	0.18	0.12	0.06	0.24	0.30		0.18	-
ab	3.72	5.92	6.10	3.55	2.71	1.78	3.90	4.15		2.71	0.60
an	14.50	10.35	14.50	20.57	17.77	14.72	19.57	14.30		17.44	11.95
C	-	-	-	-	-	-	-	-		-	-
di	6.13	10.37	13.03	8.04	8.34	5.66	10.20	7.14		9.01	1.23
hy	23.06	12.00	16.35	20.14	21.20	27.03	21.14	23.72		25.40	33.05
ol	41.65	43.15	39.90	36.46	41.24	39.11	35.03	39.60		35.20	41.95
mt	2.55	2.67	2.50	2.70	2.61	2.52	2.67	2.55		2.60	2.45
il	0.49	0.65	0.53	0.60	0.57	0.46	0.65	0.49		0.55	0.36

	K-11	K-12	K-13	K-14a	K-14b	K-15	K-16	K-17	K-18	K-19
CaO/Al2O3	0.74	0.80	0.95	0.75	0.81	0.77	0.82	0.77	0.84	0.60
CaO/TiO2	17.3	18.6	22.3	17.2	19.0	18.4	19.2	18.1	20.0	14.3
Al2O3/TiO2	23.4	23.3	23.5	22.9	23.5	24.0	23.5	23.5	24.0	23.7
Sc/Zr	-	-	-	-	-	-	-	2.67	-	-
Ti/Zr	156	157	187	144	138	120	157	173	174	220
Ti/Sc	-	-	-	-	-	-	-	65	-	-
Ti/V	10.3	10.6	9.7	10.0	10.3	10.5	10.3	10.3	10.2	11.3
V/Zr	15.1	14.8	19.3	13.4	13.4	11.4	15.3	16.8	17.1	20.2
V/Sc	-	-	-	-	-	-	-	6.3	-	-
Al/Zr	3222	3219	3873	2913	2873	2535	3251	3585	3677	4772
Al/Sc	-	-	-	-	-	-	-	1345	-	-
Mg#	88	86	87	88	85	90	85	86	88	89

Appendix B1.b (continued)

	K-20	K-21	K-21 (GSC)	K-22	K-22 (GSC)	K-23	K-24	K-24 (GSC)	K-25	K-25 (GSC)	K-26
SiO2	43.33	42.85	42.60	43.38	43.10	40.84	41.93	41.70	41.27	40.70	40.96
TiO2	0.31	0.25	0.28	0.27	0.31	0.14	0.24	0.26	0.25	0.31	0.19
Al2O3	7.48	5.98	5.90	6.71	6.50	3.73	5.89	5.90	6.25	6.40	5.17
Fe2O3T	11.02	10.72	nd	11.61	nd	11.96	10.71	nd	12.20	nd	10.95
Fe2O3		4.67	4.50	5.49	5.00	nd	nd	3.80	nd	4.50	nd
FeO	0.00	5.44	5.40	5.51	5.70	nd	nd	6.10	nd	6.40	nd
MnO	0.16	0.16	0.18	0.15	0.16	0.20	0.17	0.19	0.18	0.18	0.18
MgO	25.36	28.10	27.60	25.17	24.80	34.10	31.04	30.50	27.95	27.00	31.94
CaO	7.03	5.12	5.19	7.09	7.22	0.70	3.06	3.17	4.48	4.53	2.00
Na2O	0.52	0.59	bl	0.49	bl	0.03	0.27	bl	bl	bl	0.20
K2O	0.03	0.04	0.05	0.02	0.02	bl	0.02	0.01	0.03	0.05	0.01
P2O5		bl	0.01	bl	bl	bl	bl	0.02	bl	0.01	bl
H2O(LOI)	0.00	nd	6.90	nd	5.30	nd	nd	6.90	nd	7.00	nd
CO2		nd	0.40	nd	0.50	nd	nd	0.20	nd	0.20	nd
Total	95.24	93.81	99.01	94.89	98.61	91.70	93.33	98.75	92.61	97.20	91.68
B (AA)	nd	nd	10	nd	15	nd	nd	22	nd	bl	nd
Ba (XRF)	nd	nd	30	nd	70	nd	nd	60	nd	30	nd
Ba (AA)	nd	nd	12	nd	29	nd	nd	17	nd	13	nd
Co (*)	nd	56	93	64	83	nd	95	110	75	82	nd
Cr (XRF)	2944	2674	2463	2557	2532	4181	2849	2463	2787	2600	2564
Cr (other)	nd	2604	2400	2526	2700	nd	2407	2500	2580	2300	nd
Cu (AA)	nd	nd	30	nd	60	nd	nd	23	nd	51	nd
Nb (XRF)	bl	bl	nd	bl	nd	bl	bl	nd	bl	nd	bl
Ni (XRF)	1322	1726	1550	1388	1240	2240	1961	1810	1626	1490	2002
Ni (other)	nd	2020	1500	800	1200	nd	2000	1700	1690	1500	nd
Rb (XRF)	bl	bl	bl	bl	10	bl	bl	bl	bl	bl	5
Sr (XRF)	9	8	30	12	30	bl	3	bl	6	10	1
Sr (AA)	nd	nd	21	nd	19	nd	nd	11	nd	12	nd
V (*)	182	158	89	178	110	99	139	75	152	67	110
Y (*)	20	21	26	17	27	18	18	20	23	25	19
Zn (XRF)	bl	80	70	43	70	bl	64	80	74	90	65
Zr (XRF)	10	9	bl	12	40	2	6	bl	7	bl	bl
Sc (INAA)	nd	26	nd	27	nd	nd	23	nd	25	nd	nd
AN	80.35	73.00		79.47		93.19	86.63		100.00		80.72
or	0.10	0.24		0.12		-	0.12		0.10		0.06
ab	4.40	4.99		4.15		0.25	2.20		-		2.37
an	17.99	13.55		16.05		3.47	14.00		16.97		9.92
C	-	-		-		2.41	-		-		1.06
di	13.41	9.39		15.20		-	0.30		4.10		-
hy	17.36	19.77		10.67		35.24	26.34		26.95		27.04
ol	37.77	41.76		36.39		46.65	45.61		40.20		46.69
mt	2.62	2.54		2.57		2.30	2.52		2.54		2.45
il	0.59	0.47		0.51		0.27	0.46		0.47		0.36

	K-20	K-21	K-22	K-23	K-24	K-25	K-26
CaO/Al2O3	0.94	0.86	1.06	0.19	0.52	0.72	0.39
CaO/TiO2	22.7	20.5	26.3	5.0	12.8	17.9	10.5
Al2O3/TiO2	24.1	23.9	24.9	26.6	24.5	25.0	27.2
Sc/Zr	-	2.89	2.25	-	3.83	3.57	-
Ti/Zr	186	167	135	420	240	214	-
Ti/Sc	-	58	60	-	63	60	-
Ti/V	10.2	9.5	9.1	8.5	10.4	9.9	10.4
V/Zr	18.2	17.6	14.8	49.5	23.2	21.7	-
V/Sc	-	6.1	6.6	-	6.0	6.1	-
Al/Zr	3957	3515	2958	9866	5193	4723	-
Al/Sc	-	1217	1315	-	1355	1323	-
Mg#	86	86	83	89	87	84	89

Appendix B1.b (continued)

	K-27	K-28	K-29	K-30	K-31	K-32	K-33	K-34	K-34 (GSC)	K-35	K-35 (GSC)
SiO2	42.41	42.58	41.74	43.92	41.92	42.87	42.75	41.85	41.80	41.97	41.90
TiO2	0.33	0.26	0.20	0.30	0.25	0.25	0.24	0.20	0.21	0.37	0.41
Al2O3	7.96	6.30	5.00	7.34	6.00	6.17	5.86	4.73	5.20	8.41	8.30
Fe2O3T	11.11	10.55	10.74	9.81	11.41	10.78	10.85	11.25	nd	11.94	nd
Fe2O3	nd	nd	nd	nd	nd	nd	nd	nd	4.00	nd	4.50
FeO	nd	nd	nd	nd	nd	nd	nd	nd	6.20	nd	6.40
MnO	0.17	0.16	0.18	0.15	0.18	0.17	0.18	0.16	0.17	0.17	0.17
MgO	24.86	28.16	32.34	26.52	29.74	28.90	29.42	31.59	31.00	24.75	24.40
CaO	6.63	4.92	2.51	6.75	3.75	4.45	4.86	2.56	2.62	6.19	6.36
Na2O	0.77	0.40	0.43	0.69	0.12	0.20	0.19	0.13	bl	0.67	bl
K2O	0.04	0.03	bl	0.02	0.01	0.02	bl	0.01	0.04	0.04	0.05
P2O5	bl	bl	bl	bl	bl	bl	bl	bl	bl	bl	0.02
H2O(LOI)	nd	nd	nd	nd	nd	nd	nd	nd	8.60	nd	6.00
CO2	nd	nd	nd	nd	nd	nd	nd	nd	0.40	nd	0.40
Total	94.28	93.36	93.11	95.50	93.46	93.81	93.55	91.68	99.44	94.51	98.91
B (AA)	nd	nd	nd	nd	nd	nd	nd	nd	10	nd	17
Ba (XRF)	nd	nd	nd	nd	nd	nd	nd	nd	30	nd	50
Ba (AA)	nd	nd	nd	nd	nd	nd	nd	nd	12	nd	11
Co (*)	nd	nd	nd	nd	nd	nd	nd	60	110	67	82
Cr (XRF)	3127	2802	2709	2861	3038	2863	2828	2658	2189	3297	3147
Cr (other)	nd	nd	nd	nd	nd	nd	nd	2210	2300	3271	3100
Cu (AA)	nd	nd	nd	nd	nd	nd	nd	nd	10	nd	39
Nb (XRF)	bl	bl	bl	3	bl	bl	bl	bl	nd	bl	nd
Ni (XRF)	1173	1576	1976	1324	1677	1685	1736	2020	1840	1056	1020
Ni (other)	nd	nd	nd	nd	nd	nd	nd	2110	2100	899	1000
Rb (XRF)	1	bl	11	6	bl	bl	bl	bl	bl	bl	10
Sr (XRF)	11	7	5	6	1	6	7	5	bl	10	40
Sr (AA)	nd	nd	nd	nd	nd	nd	nd	nd	11	nd	18
V (*)	220	157	144	186	135	147	151	110	50	226	130
Y (*)	17	21	8	14	18	21	24	17	20	18	25
Zn (XRF)	82	61	71	45	91	bl	91	60	110	84	80
Zr (XRF)	6	5	10	14	8	7	8	6	20	16	bl
Sc (INAA)	nd	nd	nd	nd	nd	nd	nd	20	nd	34	nd
AN	73.50	81.89	77.70	74.29	94.04	90.37	90.40	91.79		77.76	
or	0.24	0.10	-	0.12	0.06	0.12	-	0.06		0.24	
ab	6.52	3.30	3.30	5.04	1.02	1.69	1.61	1.10		5.67	
an	10.15	15.31	11.05	16.07	16.02	15.00	15.14	12.29		19.02	
C	-	-	-	-	-	-	-	-		-	
di	11.72	7.21	0.40	13.15	2.05	4.91	3.97	0.32		0.66	
hy	12.37	23.07	23.94	16.53	27.74	20.40	29.42	20.22		14.49	
ol	41.09	40.20	49.71	39.01	42.60	30.09	39.53	45.57		40.92	
mt	2.65	2.55	2.46	2.61	2.54	2.54	2.52	2.46		2.71	
il	0.63	0.49	0.30	0.57	0.47	0.47	0.46	0.30		0.70	

	K-27	K-28	K-29	K-30	K-31	K-32	K-33	K-34	K-35
CaO/Al2O3	0.83	0.78	0.50	0.92	0.62	0.72	0.69	0.54	0.74
CaO/TiO2	20.1	18.9	12.6	22.5	15.0	17.8	16.9	12.8	16.7
Al2O3/TiO2	24.1	24.2	25.0	24.5	24.3	24.7	24.4	23.7	22.7
Sc/Zr	-	-	-	-	-	-	-	3.33	2.13
Ti/Zr	330	312	120	129	180	214	100	200	139
Ti/Sc	-	-	-	-	-	-	-	60	65
Ti/V	9.0	9.9	8.3	9.7	11.1	10.2	9.5	10.9	9.8
V/Zr	36.7	31.4	14.4	13.3	16.9	21.0	10.9	18.3	14.1
V/Sc	-	-	-	-	-	-	-	5.5	6.7
Al/Zr	7010	6665	2645	2773	4020	4663	3875	4170	2781
Al/Sc	-	-	-	-	-	-	-	1251	1300
Mg#	86	88	89	88	88	88	88	87	83

Appendix B1.b (continued)

	K-36	K-36 (GSC)	K-37	K-37 (GSC)	K-38	K-38 (GSC)	K-39	K-39 (GSC)	K-40	K-40 (GSC)	AK-25a
SiO2	41.93	41.50	42.87	41.80	41.27	40.80	43.19	42.30	42.02	41.10	43.22
TiO2	0.26	0.27	0.31	0.33	0.23	0.26	0.29	0.30	0.24	0.25	0.27
Al2O3	6.12	6.00	6.82	6.70	5.45	5.30	6.67	6.40	5.50	5.30	6.45
Fe2O3T	11.20	nd	12.60	nd	10.85	nd	11.43	nd	10.81	nd	9.69
Fe2O3	nd	4.40	nd	6.40	nd	3.90	nd	5.20	nd	3.70	nd
FeO	nd	6.00	nd	5.40	nd	6.00	nd	5.40	nd	6.10	nd
MnO	0.18	0.19	0.16	0.18	0.19	0.21	0.16	0.16	0.19	0.21	0.17
MgO	29.18	28.50	26.04	25.70	31.24	30.60	26.42	25.80	30.62	29.40	27.69
CaO	4.32	4.44	6.28	6.47	3.06	2.14	6.43	6.64	3.62	3.70	5.34
Na2O	0.57	bl	0.69	0.10	0.36	bl	0.41	bl	0.37	bl	0.43
K2O	0.03	0.02	0.04	0.05	0.01	0.02	0.03	0.03	0.01	0.01	0.02
P2O5	bl	0.01	bl	0.03	bl	0.02	bl	bl	bl	0.01	bl
H2O(LOI)	nd	7.00	nd	5.00	nd	8.00	nd	5.70	nd	7.00	nd
CO2	nd	0.30	nd	0.10	nd	0.30	nd	0.50	nd	0.40	nd
Total	93.79	98.63	95.01	99.06	92.66	97.55	95.03	98.43	93.30	97.90	93.28
B (AA)	nd	17	nd	bl	nd	26	nd	20	nd	22	nd
Ba (XRF)	nd	60	nd	50	nd	30	nd	20	nd	20	nd
Ba (AA)	nd	67	nd	13	nd	21	nd	14	nd	8	nd
Co (*)	62	100	57	86	84	120	60	90	63	110	111
Cr (XRF)	2847	2532	2960	2874	2856	2395	2869	2660	2773	2395	2760
Cr (other)	2656	2400	2859	2600	2457	2600	2741	3000	2311	2600	nd
Cu (AA)	nd	16	nd	20	nd	25	nd	21	nd	13	nd
Nb (XRF)	bl	nd	bl	nd	bl	nd	bl	nd	bl	nd	bl
Ni (XRF)	1653	1570	1325	1320	1990	1720	1313	1240	1802	1750	1962
Ni (other)	1860	1700	962	1400	1732	2000	1326	1300	1597	1700	nd
Rb (XRF)	bl	bl	1	bl	bl	bl	bl	20	bl	10	bl
Sr (XRF)	bl	10	9	10	3	bl	5	10	5	10	8
Sr (AA)	nd	17	nd	17	nd	15	nd	24	nd	15	nd
V (*)	163	81	204	97	147	80	175	110	140	85	149
Y (*)	17	25	20	24	17	24	23	25	22	26	19
Zn (XRF)	61	100	49	60	100	80	42	40	107	90	111
Zr (XRF)	8	bl	7	10	8	20	9	bl	11	bl	9
Sc (INAA)	25	nd	28	nd	22	nd	26	nd	22	nd	25
AN	74.45		72.50		81.20		82.43		80.97		81.10
or	0.18		0.24		0.06		0.18		0.06		0.12
ab	4.82		5.84		3.05		3.47		3.13		3.64
an	14.85		15.39		13.23		16.27		13.32		15.61
C	-		-		-		-		-		-
di	5.85		12.55		1.55		12.42		3.60		8.61
hy	17.71		10.78		22.22		19.76		23.16		24.64
ol	47.19		45.92		48.71		38.83		46.16		36.79
mt	2.55		2.62		2.51		2.60		2.52		2.57
il	0.49		0.59		0.44		0.55		0.46		0.51

	K-36	K-37	K-38	K-39	K-40	AK-25a
CaO/Al2O3	0.71	0.92	0.56	0.96	0.66	0.83
CaO/TiO2	16.6	20.3	13.3	22.2	15.1	19.8
Al2O3/TiO2	23.5	22.0	23.7	23.0	22.9	23.9
Sc/Zr	3.13	4	2.75	2.89	2	2.78
Ti/Zr	195	266	173	193	131	180
Ti/Sc	62	66	63	67	65	65
Ti/V	9.6	207.0	9.4	9.9	10.3	10.9
V/Zr	20.4	1.3	18.4	19.4	12.7	16.6
V/Sc	6.5	0.3	6.7	6.7	6.4	6.0
Al/Zr	4047	5154	3604	3920	2645	3791
Al/Sc	1295	1288	1310	1357	1323	1365
Mg#	86	83	87	84	87	89

Appendix B1.b (continued)

	AK-25b	AK-25c	AK-25d	AK-26a	AK-26b	AK-27	AK-27	AK-28a	AK-28b	AK-29	S-3a
SiO2	43.13	42.96	42.95	42.76	42.29	42.69	42.74	39.77	44.73	38.84	42.65
TiO2	0.26	0.31	0.26	0.24	0.33	0.23	0.23	0.20	0.27	0.11	0.32
Al2O3	6.28	7.21	6.58	5.78	7.83	5.96	5.96	4.61	6.53	2.38	7.74
Fe2O3T	9.65	11.07	9.75	10.56	12.31	10.10	10.30	11.20	10.23	8.39	10.37
Fe2O3	nd	nd	nd	nd	nd	nd	nd	nd	nd	nd	nd
FeO	nd	nd	nd	nd	nd	nd	nd	nd	nd	nd	nd
MnO	0.17	0.16	0.17	0.16	0.16	0.18	0.18	0.15	0.15	0.10	0.17
MgO	28.16	25.62	28.14	29.40	25.46	29.37	29.36	32.31	25.34	37.19	25.38
CaO	4.91	6.36	4.90	4.17	6.25	4.85	4.85	2.21	7.88	1.42	6.28
Na2O	0.15	0.39	0.26	0.34	0.49	0.20	0.11	0.12	0.56	0.05	0.76
K2O	0.01	0.02	0.01	0.00	0.02	0.01	0.01	0.01	0.07	0.00	0.02
P2O5	bl	bl	bl	bl	bl	bl	bl	bl	bl	bl	bl
H2O(LOI)	nd	nd	nd	nd	nd	nd	nd	nd	nd	nd	(6.11)
CO2	nd	nd	nd	nd	nd	nd	nd	nd	nd	nd	nd
Total	92.72	94.10	93.82	93.41	95.14	92.79	92.94	90.58	94.96	87.68	99.80
B (AA)	nd	nd	nd	nd	nd	nd	nd	nd	nd	nd	nd
Ba (XRF)	nd	nd	nd	nd	nd	nd	nd	nd	nd	nd	nd
Ba (AA)	nd	nd	nd	nd	nd	nd	nd	nd	nd	nd	nd
Co (*)	nd	nd	nd	103	88	nd	nd	nd	nd	nd	nd
Cr (XRF)	2767	2866	2862	2856	2897	2632	2745	2469	2467	4629	2938
Cr (other)	nd	nd	nd	nd	nd	nd	nd	nd	nd	nd	nd
Cu (AA)	nd	nd	nd	nd	nd	nd	nd	nd	nd	nd	nd
Nb (XRF)	bl	bl	bl	bl	1	bl	bl	bl	bl	bl	bl
Ni (XRF)	1751	1357	1702	1765	1329	1900	1971	2035	1368	3384	1152
Ni (other)	nd	nd	nd	nd	nd	nd	nd	nd	nd	nd	nd
Rb (XRF)	bl	bl	bl	1	bl	bl	bl	bl	bl	bl	bl
Sr (XRF)	8	12	7	bl	13	7	8	9	7	16	8
Sr (AA)	nd	nd	nd	nd	nd	nd	nd	nd	nd	nd	nd
V (*)	157	178	151	154	193	136	150	112	171	57	186
Y (*)	19	22	17	16	20	12	21	18	22	8	19
Zn (XRF)	91	94	119	112	60	90	119	83	bl	104	87
Zr (XRF)	12	11	10	8	13	6	6	6	11	2	12
Sc (INAA)	nd	nd	nd	21	29	nd	nd	nd	nd	nd	nd
AN	92.83	84.41	88.40	83.20	82.17	90.86		91.52	76.11	93.68	73.29
or	0.06	0.12	0.06	-	0.12	0.06		0.06	0.41	-	0.12
ab	1.27	3.30	2.20	2.88	4.15	1.69		1.02	4.74	0.42	5.43
an	16.43	17.86	16.76	14.25	19.11	15.34		10.96	15.10	6.27	17.65
C	-	-	-	-	-	-		0.38	-	-	-
di	6.27	10.87	5.97	5.10	9.48	3.76		-	15.88	0.61	10.71
hy	30.97	21.90	28.01	26.57	16.62	29.05		24.19	22.61	16.51	15.35
ol	33.88	35.91	36.18	40.75	41.35	38.31		50.18	32.30	60.64	39.33
mt	2.55	2.62	2.55	2.52	2.65	2.51		2.46	2.57	2.33	2.64
il	0.49	0.59	0.49	0.46	0.63	0.44		0.38	0.51	0.21	0.61

	AK-25b	AK-25c	AK-25d	AK-26a	AK-26b	AK-27	AK-28a	AK-28b	AK-29	S-3a
CaO/Al2O3	0.78	0.88	0.74	0.72	0.80	0.68	0.48	1.08	0.60	0.81
CaO/TiO2	18.9	20.5	18.9	17.4	18.9	17.6	11.1	26.2	12.9	19.6
Al2O3/TiO2	24.2	23.3	25.3	24.1	23.7	25.9	23.1	24.2	21.6	24.2
Sc/Zr	-	-	-	2.63	2.23	-	-	-	-	-
Ti/Zr	130	169	156	180	152	230	200	147	330	160
Ti/Sc	-	-	-	69	68	-	-	-	-	-
Ti/V	9.9	10.5	10.3	9.4	10.3	10.2	10.7	9.5	11.6	10.3
V/Zr	13.1	16.2	15.1	19.3	14.9	22.7	18.7	15.6	28.5	15.5
V/Sc	-	-	-	7.3	6.7	-	-	-	-	-
Al/Zr	2760	3467	3401	3822	3186	5255	4064	3140	6295	3412
Al/Sc	-	-	-	1456	1420	-	-	-	-	-
Mg#	89	86	89	89	85	89	89	87	92	87

Appendix B1.b (continued)

	S-3a (UW)	S-3b	S-3b (UW)	S-3c	S-3c (UW)	S-211a	S-211a (UW)	S-211b	S-211b (UW)	S-211c	S-211c (UW)
SiO2	42.00	41.00	41.05	43.20	43.22	40.06	39.81	40.77	41.07	41.07	41.36
TiO2	0.32	0.32	0.32	0.30	0.30	0.23	0.24	0.22	0.22	0.35	0.35
Al2O3	7.27	7.90	7.77	7.20	7.16	5.30	5.01	5.20	5.00	8.05	8.64
Fe2O3T	10.49	12.69	12.37	10.02	10.50	11.32	11.19	10.30	10.25	12.00	12.01
Fe2O3	nd	nd	nd	nd	nd	nd	nd	nd	nd	nd	nd
FeO	nd	nd	nd	nd	nd	nd	nd	nd	nd	nd	nd
MnO	0.16	0.16	0.15	0.17	0.16	0.15	0.15	0.15	0.16	0.10	0.17
MgO	26.03	25.46	26.19	25.97	26.23	32.24	32.04	31.51	31.94	25.01	25.30
CaO	6.31	5.67	5.00	6.16	6.22	2.00	2.10	2.65	2.79	6.00	6.20
Na2O	0.22	0.71	0.29	0.79	0.31	0.34	bl	0.34	bl	0.60	0.31
K2O	0.03	0.04	0.04	0.02	0.03	0.01	0.02	0.01	0.02	0.03	0.03
P2O5	bl	bl	0.01	bl	0.01	bl	bl	bl	0.01	bl	bl
H2O(LOI)	(6.11)	(6.24)	(6.24)	(5.90)	(5.90)	(9.02)	(9.02)	(8.74)	(8.74)	(6.07)	(6.07)
CO2	nd	nd	nd	nd	nd	nd	nd	nd	nd	nd	nd
Total	99.01	100.27	100.23	100.69	99.99	101.47	101.00	100.05	100.27	101.20	100.52
B (AA)	nd	nd	nd	nd	nd	nd	nd	nd	nd	nd	nd
Ba (XRF)	13	nd	10	nd	15	nd	5	nd	7	nd	14
Ba (AA)	nd	nd	nd	nd	nd	nd	nd	nd	nd	nd	nd
Co (*)	44	nd	41	nd	44	nd	41	70	40	nd	45
Cr (XRF)	2273	3076	2510	2703	2262	2903	1576	2746	1427	3212	2500
Cr (other)	nd	nd	nd	nd	nd	nd	nd	2617	nd	nd	nd
Cu (AA)	nd	nd	nd	nd	nd	nd	nd	nd	nd	nd	nd
Nb (XRF)	2	bl	4	bl	2	bl	2	bl	1	bl	2
Ni (XRF)	906	1005	929	1416	1152	2434	1594	2103	1396	1070	911
Ni (other)	nd	nd	nd	nd	nd	nd	nd	nd	nd	nd	nd
Rb (XRF)	2	bl	4	bl	3	bl	2	bl	1	bl	2
Sr (XRF)	10	7	11	bl	13	bl	3	bl	4	5	10
Sr (AA)	nd	nd	nd	nd	nd	nd	nd	nd	nd	nd	nd
V (*)	23	195	101	105	90	131	52	127	54	212	101
Y (*)	9	19	9	bl	5	14	6	15	7	10	7
Zn (XRF)	nd	55	nd	74	nd	02	nd	90	nd	67	nd
Zr (XRF)	10	11	19	13	19	7	22	11	23	16	19
Sc (INAA)	nd	nd	nd	nd	nd	nd	nd	23	nd	nd	nd
AN		75.24		70.07		77.52		01.71		70.50	
or		0.24		0.12		0.06		0.06		0.10	
ab		5.01		5.60		2.00		2.00		5.75	
an		10.25		16.26		9.92		12.05		21.01	
C		-		-		1.09		-		-	
di		7.07		11.35		-		0.23		7.29	
hy		10.70		15.69		22.45		23.20		12.09	
ol		40.03		40.53		51.35		40.31		43.65	
mt		2.04		2.01		2.51		2.49		2.00	
il		0.01		0.57		0.44		0.42		0.00	

	S-3b	S-3c	S-211a	S-211b	S-211c
CaO/Al2O3	0.72	0.85	0.38	0.50	0.69
CaO/TiO2	17.7	20.5	8.7	12.1	17.4
Al2O3/TiO2	24.7	24.3	23.0	24.0	25.3
Sc/Zr	-	-	-	2.09	-
Ti/Zr	175	138	197	120	131
Ti/Sc	-	-	-	57	-
Ti/V	9.9	9.7	10.5	10.4	9.9
V/Zr	17.7	14.2	18.7	11.6	13.3
V/Sc	-	-	-	5.5	-
Al/Zr	3799	2962	4005	2539	2926
Al/Sc	-	-	-	1214	-
Mg0	85	87	89	89	85

Appendix B1.b (continued)

	S-211d	S-211d (UW)	S-211e	S-211e (UW)
SiO2	41.24	40.73	41.84	40.64
TiO2	0.31	0.30	0.33	0.32
Al2O3	8.65	8.48	8.25	7.88
Fe2O3T	10.17	10.21	11.18	11.09
Fe2O3	nd	nd	nd	nd
FeO	nd	nd	nd	nd
MnO	0.14	0.13	0.16	0.15
MgO	26.16	26.28	26.59	26.32
CaO	5.88	6.00	5.82	5.89
Na2O	0.58	0.28	0.67	0.27
K2O	0.02	0.03	0.04	0.04
P2O5	bl	0.02	bl	0.02
H2O(LOI)	(6.99)	(6.99)	(6.18)	(6.18)
CO2	nd	nd	nd	nd
Total	100.14	99.37	101.06	98.78
B (AA)	nd	nd	nd	nd
Ba (XRF)	nd	15	nd	25
Ba (AA)	nd	nd	nd	nd
Co (*)	nd	39	nd	42
Cr (XRF)	3092	2418	3136	2438
Cr (other)	nd	nd	nd	nd
Cu (AA)	nd	nd	nd	nd
Nb (XRF)	bl	3	bl	4
Ni (XRF)	1164	973	1300	1077
Ni (other)	nd	nd	nd	nd
Rb (XRF)	bl	2	bl	3
Sr (XRF)	6	8	9	12
Sr (AA)	nd	nd	nd	nd
V (*)	182	90	161	91
Y (*)	17	9	17	6
Zn (XRF)	62	nd	81	nd
Zr (XRF)	14	18	15	20
Sc (INAA)	nd	nd	nd	nd
AN	81.81		77.37	
or	0.12		0.24	
ab	4.91		5.67	
an	20.94		19.39	
C	-		-	
di	6.52		7.53	
hy	13.32		11.88	
ol	43.30		45.96	
mt	2.62		2.65	
il	0.59		0.63	

	S-211d	S-211e
CaO/Al2O3	0.68	0.71
CaO/TiO2	19.0	17.6
Al2O3/TiO2	27.9	25.0
Sc/Zr	-	-
Ti/Zr	133	132
Ti/Sc	-	-
Ti/V	10.2	12.3
V/Zr	13.0	10.7
V/Sc	-	-
Al/Zr	3268	2910
Al/Sc	-	-
Mg#	88	87

Appendix B1.c (Woodburn Lake Group komatiites - area 3)

	AK-3	AK-3 (GSC)	AK-7a	AK-7b	AK-8a	AK-8b	AK-11a	AK-11a (GSC)	AK-12a	AK-12b	AK-12b (GSC)
SiO2	39.07	38.60	45.49	42.86	43.31	39.09	42.13	41.20	44.41	44.43	44.70
TiO2	0.17	0.20	0.39	0.47	0.30	0.14	0.24	0.26	0.33	0.36	0.38
Al2O3	4.33	4.20	7.56	9.68	6.14	2.89	5.57	5.40	6.36	6.67	6.40
Fe2O3T	7.46	7.05	11.89	13.54	12.41	8.49	12.45	12.01	11.57	12.03	11.53
Fe2O3	nd	1.60	nd	nd	nd	nd	nd	4.90	nd	nd	4.20
FeO	nd	4.90	nd	nd	nd	nd	nd	6.40	nd	nd	6.60
MnO	0.31	0.32	0.20	0.19	0.17	0.14	0.18	0.20	0.17	0.18	0.20
MgO	26.61	26.30	27.09	25.71	28.87	37.47	28.94	28.20	25.88	26.20	25.90
CaO	6.78	6.90	4.34	4.96	4.97	1.48	5.86	5.14	5.81	5.45	5.60
Na2O	0.29	bl	0.70	0.98	0.45	0.19	0.49	bl	0.55	0.80	bl
K2O	0.02	0.02	0.11	0.35	0.08	0.01	0.10	0.10	0.11	0.11	0.10
P2O5	bl	0.02	bl	bl	bl	bl	bl	0.01	bl	bl	0.02
H2O(LOI)	nd	5.00	nd	nd	nd	nd	nd	5.80	nd	nd	4.10
CO2	nd	12.30	nd	nd	nd	nd	nd	0.30	nd	nd	0.40
Total	85.04	100.36	97.77	98.74	96.70	89.90	95.16	97.91	95.19	96.23	98.60
B (AA)	nd	nd	nd	nd	nd	nd	nd	50	nd	nd	nd
Ba (XRF)	nd	50	nd	nd	nd	nd	nd	60	nd	nd	160
Ba (AA)	nd	21	nd	nd	nd	nd	nd	20	nd	nd	140
Co (*)	61	110	nd	109	nd	90	74	110	nd	80	90
Cr (XRF)	2077	1916	3107	2627	2500	2359	2576	2395	2731	2793	2660
Cr (other)	2003	2000	nd	2257	nd	1837	2358	2300	nd	2693	2700
Cu (AA)	nd	5	nd	nd	nd	nd	nd	10	nd	nd	47
Nb (XRF)	bl	nd	bl	bl	bl	bl	2	nd	bl	bl	nd
Ni (XRF)	1743	1520	1367	604	1547	3017	1830	1690	1513	1485	1420
Ni (other)	1520	1600	nd	879	nd	2053	1747	1800	nd	2650	1500
Rb (XRF)	bl	20	4	31	bl	bl	4	30	4	6	bl
Sr (XRF)	50	70	96	71	33	2	22	40	37	30	60
Sr (AA)	nd	84	nd	nd	nd	nd	nd	34	nd	nd	49
V (*)	87	50	214	293	154	89	135	83	179	189	120
Y (*)	4	25	25	10	16	7	11	22	19	20	26
Zn (XRF)	130	130	75	124	73	97	125	150	62	82	80
Zr (XRF)	7	bl	24	21	16	7	11	bl	13	14	bl
Sc (INAA)	17	nd	29	34	nd	13	23	nd	nd	20	nd
AN	80.99		74.34	71.67	79.20	81.33	75.39		75.70	67.85	
or	0.12		0.65	2.07	0.47	0.06	0.59		0.65	0.65	
ab	2.45		5.92	0.29	3.81	1.61	4.15		4.65	6.77	
an	10.45		17.16	20.90	14.50	7.00	12.70		14.50	14.20	
C	-		-	-	-	-	-		-	-	
di	10.27		3.47	2.09	0.07	0.27	9.06		11.34	10.13	
hy	12.47		30.15	0.09	19.93	15.79	14.46		25.59	21.99	
ol	37.60		35.93	50.70	45.60	61.05	49.35		34.14	37.56	
mt	2.32		2.74	2.06	2.61	2.30	2.52		2.65	2.70	
il	0.32		0.74	0.09	0.57	0.27	0.46		0.63	0.60	

	AK-3	AK-7a	AK-7b	AK-8a	AK-8b	AK-11a	AK-12a	AK-12b
CaO/Al2O3	1.57	0.57	0.51	0.81	0.51	0.91	0.91	0.82
CaO/TiO2	39.9	11.1	10.6	16.6	10.6	21.1	17.6	15.1
Al2O3/TiO2	25.5	19.4	20.6	20.5	20.6	23.2	19.3	18.5
Sc/Zr	2.43	1.21	1.62	1.86	2.09	2.00	1.69	2.17
Ti/Zr	146	98	134	113	120	131	152	154
Ti/Sc	60	81	83	65	63	77	76	65
Ti/V	11.7	10.9	9.6	11.7	9.4	10.7	11.1	11.4
V/Zr	12.4	8.9	14.0	9.6	12.7	12.3	13.8	13.5
V/Sc	5.1	7.4	8.6	6.9	5.9	6.8	6.4	6.8
Al/Zr	3272	1666	2438	2030	2184	2679	2588	2520
Al/Sc	1347	1379	1506	1176	1281	1260	1264	1259
Mg#	89	86	84	87	92	87	86	83

Appendix B1.c (continued)

	AK-12c	AK-13a	AK-13a (GSC)	AK-13b	S-171a	S-171a (UW)	S-173c	S-173c (UW)	S-200	S-200 (UW)
SiO2	44.15	43.38	43.70	42.35	40.89	36.62	42.36	41.78	42.17	41.68
TiO2	0.34	0.28	0.29	0.28	0.22	0.23	0.33	0.33	0.36	0.36
Al2O3	6.45	6.19	6.20	6.38	5.33	5.05	7.57	7.28	8.23	8.14
Fe2O3T	11.70	10.79	10.57	10.67	11.97	12.31	11.99	11.94	11.83	11.47
Fe2O3	nd	nd	2.90	nd	nd	nd	nd	nd	nd	nd
FeO	nd	nd	6.90	nd	nd	nd	nd	nd	nd	nd
MnO	0.34	0.16	0.17	0.12	0.19	0.18	0.16	0.15	0.16	0.15
MgO	26.73	26.66	26.70	26.79	30.70	30.71	25.40	25.79	27.56	27.52
CaO	5.50	4.92	5.00	3.19	2.63	2.80	6.12	6.17	4.70	4.89
Na2O	0.63	0.00	0.10	0.27	0.21	bl	0.41	0.09	0.70	0.35
K2O	0.13	0.00	0.10	0.01	0.01	0.02	0.03	0.03	0.10	0.10
P2O5	bl	bl	0.03	bl	bl	0.01	bl	bl	bl	0.01
H2O(LOI)	nd	nd	7.00	nd	nd	(9.87)	nd	(6.03)	nd	(4.44)
CO2	nd	nd	0.54	nd	nd	nd	nd	nd	nd	nd
Total	95.97	93.26	99.71	90.06	92.15	97.00	94.45	99.59	95.97	99.12
B (AA)	nd	nd	31	nd	nd	nd	nd	nd	nd	nd
Ba (XRF)	nd	nd	220	nd	nd	8	nd	16	nd	52
Ba (AA)	nd	nd	190	nd	nd	nd	nd	nd	nd	nd
Co (*)	nd	59	100	nd	nd	46	nd	39	nd	49
Cr (XRF)	2911	2060	2737	2916	2441	1772	2499	2074	2419	1863
Cr (other)	nd	2696	2600	nd	nd	nd	nd	nd	nd	nd
Cu (AA)	nd	nd	7	nd	nd	nd	nd	nd	nd	nd
Nb (XRF)	bl	1	nd	bl	bl	1	bl	3	bl	2
Ni (XRF)	1265	1510	1430	1597	1573	1170	1102	953	1701	1330
Ni (other)	nd	719	1600	nd	nd	nd	nd	nd	nd	nd
Rb (XRF)	1	3	40	bl	bl	2	bl	4	1	7
Sr (XRF)	31	19	50	bl	bl	5	bl	11	27	34
Sr (AA)	nd	nd	32	nd	nd	nd	nd	nd	nd	nd
V (*)	172	157	110	106	131	66	201	96	177	95
Y (*)	16	22	27	bl	bl	0	7	9	25	11
Zn (XRF)	117	121	120	05	160	nd	70	nd	95	nd
Zr (XRF)	16	12	40	11	10	5	15	11	20	34
Sc (INAA)	27	26	nd	26	nd	nd	nd	nd	nd	nd
AN	72.97	65.07		07.30	00.01		04.37		73.07	
or	0.77	0.47		0.06	0.06		0.10		0.59	
ab	5.33	6.77		2.20	1.70		3.47		6.60	
an	14.39	13.06		15.03	13.05		10.73		10.66	
C	-	-		0.13	0.19		-		-	
di	10.25	9.00		-	-		9.26		4.01	
hy	22.00	21.91		30.20	26.42		19.50		12.04	
ol	30.94	37.03		29.56	46.72		30.94		40.09	
mt	2.67	2.50		2.50	2.49		2.65		2.70	
il	0.65	0.53		0.53	0.42		0.63		0.60	

	AK-12c	AK-13a	AK-13b	S-171a	S-173c	S-200
CaO/Al2O3	0.85	0.74	0.50	0.49	0.81	0.58
CaO/TiO2	16.2	17.6	11.4	12.0	18.6	13.3
Al2O3/TiO	19.0	22.1	22.8	24.2	22.9	22.9
Sc/Zr	2.36	-	-	-	-	-
Ti/Zr	120	140	153	132	132	100
Ti/Sc	65	-	-	-	-	-
Ti/V	11.9	10.7	9.0	10.1	9.9	12.2
V/Zr	10.0	13.1	16.9	13.1	13.4	8.9
V/Sc	7.2	-	-	-	-	-
Al/Zr	2133	2729	3060	2820	2670	2177
Al/Sc	1290	-	-	-	-	-
Mg#	86	84	87	88	85	87

Appendix B1.d (Woodburn Lake Group komatiites - area 4)

	AK-19c	AK-21a	AK-21b	AK-21c	AK-22a	AK-22b1	AK-22b2	AK-22c	AK-23a	AK-23b	AK-23c
SiO2	39.81	42.20	42.54	43.07	43.39	42.81	43.10	42.51	43.65	42.06	42.56
TiO2	0.09	0.21	0.32	0.33	0.26	0.33	0.30	0.31	0.29	0.21	0.31
Al2O3	1.70	5.20	7.52	7.83	6.33	7.84	7.24	7.18	7.10	5.19	7.25
Fe2O3T	9.22	9.90	11.70	11.90	9.50	11.74	11.64	12.17	10.48	11.36	11.31
Fe2O3	nd	nd	nd	nd	nd	nd	nd	nd	nd	nd	nd
FeO	nd	nd	nd	nd	nd	nd	nd	nd	nd	nd	nd
MnO	0.11	0.17	0.16	0.16	0.16	0.17	0.16	0.17	0.16	0.18	0.16
MgO	38.96	32.02	25.76	26.35	27.91	25.88	25.72	25.28	26.08	28.96	25.68
CaO	0.15	2.58	6.34	6.21	5.44	6.06	6.49	6.40	6.42	4.08	6.32
Na2O	0.29	0.03	0.55	0.47	0.46	0.48	0.48	0.49	0.51	0.33	0.36
K2O	bl	bl	3.04	0.02	0.02	0.03	0.02	0.03	0.02	0.01	0.01
P2O5	0.01	bl	bl	bl	bl	bl	bl	bl	bl	bl	bl
H2O(LOI)	nd	nd	nd	nd	nd	nd	nd	nd	nd	nd	nd
CO2	nd	nd	nd	nd	nd	nd	nd	nd	nd	nd	nd
Total	90.34	92.39	94.93	96.42	93.47	94.54	95.15	94.54	94.71	92.38	93.96
Ba (XRF)	nd	nd	nd	nd	nd	nd	nd	nd	nd	nd	nd
Ba (AA)	nd	nd	nd	nd	nd	nd	nd	nd	nd	nd	nd
Co (*)	116	nd	94	nd	nd	nd	85	nd	84	126	108
Cr (XRF)	3039	2668	2920	2982	2691	3045	2840	2922	2759	2669	2916
Cr (other)	2254	nd	2717	nd	nd	nd	2658	nd	2509	2341	2673
Cu (AA)	nd	nd	nd	nd	nd	nd	nd	nd	nd	nd	nd
Nb (XRF)	2	bl	bl	bl	1	bl	bl	bl	bl	bl	bl
Ni (XRF)	3021	2070	1242	1206	1651	1248	1224	1213	1294	2254	1288
Ni (other)	2538	nd	1141	nd	nd	nd	1035	nd	803	2198	933
Rb (XRF)	bl	bl	bl	bl	bl	bl	bl	bl	bl	bl	bl
Sr (XRF)	bl	1	14	10	10	14	12	14	9	9	9
Sr (AA)	nd	nd	nd	nd	nd	nd	nd	nd	nd	nd	nd
V (*)	42	121	194	196	166	167	195	193	178	133	152
Y (*)	13	19	22	15	18	18	18	20	18	19	17
Zn (XRF)	41	89	51	45	110	71	57	55	60	92	63
Zr (XRF)	4	8	11	11	11	15	12	10	11	9	12
Sc (INAA)	9	nd	29	32	26	29	31	27	27	20	27
AN	23.27	98.06	79.40	82.84	79.56	82.50	81.20	80.67	79.78	81.92	85.62
or	-	-	0.24	0.12	0.12	0.18	0.12	0.18	0.12	0.06	0.06
ab	2.45	0.25	4.65	3.98	3.89	4.06	4.06	4.15	4.32	2.79	3.05
an	0.74	12.80	17.93	19.20	15.15	19.15	17.54	17.30	17.03	12.65	18.14
C	0.95	0.46	-	-	-	-	-	-	-	-	-
di	-	-	10.75	9.23	9.36	8.68	11.65	11.50	11.76	6.02	10.50
hy	21.28	34.01	15.88	18.02	23.88	16.35	18.96	17.67	21.38	25.38	20.91
ol	61.74	41.17	41.24	41.58	37.25	41.85	38.66	39.49	36.18	41.63	37.14
mt	2.31	2.48	2.64	2.65	2.55	2.65	2.61	2.62	2.60	2.48	2.62
il	0.17	0.40	0.61	0.63	0.49	0.63	0.57	0.59	0.55	0.40	0.59

	AK-19c	AK-21a	AK-21b	AK-21c	AK-22a	AK-22b1	AK-22b2	AK-22c	AK-23a	AK-23b	AK-23c
CaO/Al2O3	0.09	0.50	0.84	0.79	0.86	0.77	0.90	0.89	0.90	0.79	0.87
CaO/TiO2	1.7	12.3	19.8	18.8	20.9	18.4	21.6	20.7	22.1	19.4	20.4
Al2O3/TiO2	18.9	24.8	23.5	23.7	24.4	23.8	24.1	23.2	24.5	24.7	23.4
Sc/Zr	2.25	-	2.64	2.91	2.36	1.93	2.58	2.70	2.45	2.22	2.25
Ti/Zr	135	158	175	180	142	132	150	186	158	140	155
Ti/Sc	60	-	66	62	60	68	58	69	64	63	69
Ti/V	12.9	10.4	9.9	10.1	9.4	10.1	9.2	9.6	9.8	9.5	12.2
V/Zr	10.5	15.1	17.6	17.8	15.1	13.1	16.3	19.3	16.2	14.8	12.7
V/Sc	4.7	-	6.7	6.1	6.4	6.8	6.3	7.2	6.6	6.7	5.6
Al/Zr	2240	3439	3616	3766	3044	2765	3192	3798	3414	3051	3196
Al/Sc	999	-	1372	1294	1288	1430	1235	1407	1391	1373	1420
Mg#	92	90	86	86	89	86	86	85	87	88	86

Appendix B1.d (continued)

	AK-23d1	AK-23d2	AK-23e	AK-23f	AK-23g	AK-24a1	AK-24a2	AK-24b	AK-24b (GSC)	AK-24c	AK-24d
SiO2	43.13	42.94	41.52	44.21	43.00	41.09	40.39	42.99	42.70	43.47	45.06
TiO2	0.29	0.28	0.17	0.29	0.32	0.21	0.17	0.31	0.34	0.29	0.17
Al2O3	6.88	6.46	4.22	6.68	7.74	5.04	4.13	7.50	7.80	7.08	4.30
Fe2O3T	11.70	10.83	10.63	9.79	10.84	9.70	10.39	11.70	nd	9.87	10.33
Fe2O3	nd	nd	nd	nd	nd	nd	nd	nd	4.50	nd	nd
FeO	nd	nd	nd	nd	nd	nd	nd	nd	6.10	nd	nd
MnO	0.16	0.16	0.18	0.17	0.18	0.16	0.19	0.17	0.18	0.16	0.16
MgO	26.03	26.51	33.79	26.78	26.35	30.19	33.60	25.88	25.80	25.98	28.17
CaO	6.29	6.17	1.27	6.18	5.92	3.13	1.26	6.47	6.65	6.51	5.75
Na2O	0.47	0.45	0.23	0.15	0.41	0.28	0.21	0.67	bl	0.43	0.34
K2O	0.02	0.03	0.01	0.01	0.05	0.03	0.01	0.03	0.07	0.01	0.02
P2O5	bl	bl	bl	nd	bl	bl	bl	bl	0.02	bl	bl
H2O(LOI)	nd	nd	nd	nd	nd	nd	nd	nd	5.60	nd	nd
CO2	nd	nd	nd	nd	nd	nd	nd	nd	0.10	nd	nd
Total	94.97	93.83	92.02	94.26	94.81	89.83	90.35	95.72	99.06	93.80	94.30
Ba (XRF)	nd	nd	nd	nd	nd	nd	nd	nd	30	nd	nd
Ba (AA)	nd	nd	nd	nd	nd	nd	nd	nd	15	nd	nd
Co (*)	82	90	95	nd	104	110	nd	77	93	97	100
Cr (XRF)	2793	2742	2596	2784	3159	2600	2589	2910	2805	2749	2140
Cr (other)	2571	2569	1999	nd	2855	2280	nd	2804	2700	2563	1847
Cu (AA)	nd	nd	nd	nd	nd	nd	nd	nd	66	nd	nd
Nb (XRF)	bl	bl	bl	bl	bl	bl	bl	bl	nd	bl	bl
Ni (XRF)	1131	1489	2010	1716	1286	1587	2355	1412	1300	1441	1893
Ni (other)	979	1320	1517	nd	1391	1427	nd	1310	1100	1300	1760
Rb (XRF)	bl	bl	bl	bl	bl	bl	1	bl	20	bl	bl
Sr (XRF)	13	13	3	12	7	8	8	12	20	17	21
Sr (AA)	nd	nd	nd	nd	nd	nd	nd	nd	25	nd	nd
V (*)	104	106	114	101	197	121	99	109	130	171	106
Y (*)	23	22	13	12	21	19	19	15	27	19	19
Zn (XRF)	51	45	90	9	70	84	80	65	90	102	56
Zr (XRF)	13	9	4	9	12	8	7	13	40	12	7
Sc (INAA)	27	27	17	nd	29	21	10	20	nd	20	17
AN	00.60	00.30	76.40	93.25	04.71	04.03	77.07	75.33		02.62	77.96
or	0.12	0.10	0.06	0.06	0.12	0.06	-	0.30		0.10	0.06
ab	3.90	3.01	1.95	1.27	3.47	2.37	1.70	5.67		3.64	2.00
an	16.60	15.52	6.30	17.53	19.22	12.47	6.25	17.31		17.30	10.10
C	-	-	1.52	-	-	-	1.49	-		-	-
di	11.61	11.90	-	10.40	0.05	2.42	-	11.76		11.00	14.54
hy	19.02	20.29	31.70	30.77	21.95	27.20	29.17	14.03		22.55	30.42
ol	30.70	30.05	46.05	30.29	37.02	41.62	40.03	42.40		34.32	32.61
mt	2.60	2.50	2.42	2.60	2.64	2.40	2.42	2.62		2.60	2.42
il	0.55	0.53	0.32	0.55	0.61	0.40	0.32	0.59		0.55	0.32

	AK-23d1	AK-23d2	AK-23e	AK-23f	AK-23g	AK-24a1	AK-24a2	AK-24b	AK-24c	AK-24d
CaO/Al2O3	0.91	0.96	0.30	0.93	0.76	0.62	0.31	0.86	0.92	1.34
CaO/TiO2	21.7	22.0	7.5	21.3	18.5	14.9	7.4	20.9	22.5	33.8
Al2O3/TiO2	23.7	23.1	24.0	23.0	24.2	24.0	24.3	24.2	24.4	25.3
Sc/Zr	2.00	3.00	4.25	-	2.42	2.63	2.63	2.15	2.33	2.43
Ti/Zr	134	107	255	193	160	150	120	143	145	146
Ti/Sc	64	62	60	-	66	60	49	66	62	60
Ti/V	9.5	10.1	9.0	10.0	9.0	10.4	10.3	11.0	10.2	9.6
V/Zr	14.2	10.4	28.5	17.9	16.4	15.1	12.4	13.0	14.3	15.1
V/Sc	6.0	6.2	6.7	-	6.0	5.0	4.7	6.0	6.1	6.2
Al/Zr	2000	3797	5501	3926	3412	3333	2731	3052	3121	3250
Al/Sc	1340	1266	1313	-	1412	1270	1040	1417	1330	1330
Mg#	06	07	90	00	07	90	90	06	00	00

Appendix B1.d (continued)

	AK-24e	S-198a	S-198a (UW)	S-198b	S-198b (UW)	S-198c	S-198c (UW)	S-198d	S-198d (UW)
SiO2	42.32	40.98	40.86	41.56	41.47	42.70	42.12	42.16	41.21
TiO2	0.31	0.18	0.18	0.35	0.35	0.30	0.29	0.32	0.32
Al2O3	7.52	4.53	4.46	8.28	8.23	7.20	6.93	8.42	8.17
Fe2O3T	11.59	10.65	10.60	11.46	11.27	11.65	11.99	10.62	10.89
Fe2O3	nd	nd	nd	nd	nd	nd	nd	nd	nd
FeO	nd	nd	nd	nd	nd	nd	nd	nd	nd
MnO	0.17	0.17	0.17	0.16	0.15	0.16	0.16	0.16	0.16
MgO	25.62	32.11	32.75	25.75	26.44	25.69	25.30	26.61	26.43
CaO	6.20	1.95	2.09	5.83	5.98	6.21	6.30	5.66	5.70
Na2O	0.55	0.22	bl	0.46	0.08	0.55	0.14	0.43	0.06
K2O	0.04	0.01	0.02	0.02	0.03	0.04	0.05	0.01	0.02
P2O5	bl	bl	0.02	bl	bl	bl	0.01	bl	0.01
H2O(LOI)	nd	nd	(9.09)	nd	(6.23)	nd	(6.02)	nd	(6.29)
CO2	nd	nd	nd	nd	nd	nd	nd	nd	nd
Total	94.32	90.80	100.23	93.87	100.23	94.50	99.31	94.39	99.26
Ba (XRF)	nd	nd	7	nd	18	nd	13	nd	14
Ba (AA)	nd	nd	nd	nd	nd	nd	nd	nd	nd
Co (*)	nd	nd	40	nd	41	87	45	86	41
Cr (XRF)	2935	2723	1365	3091	2356	2859	2431	3351	2419
Cr (other)	nd	nd	nd	nd	nd	2709	nd	3127	nd
Cu (AA)	nd	nd	nd	nd	nd	nd	nd	nd	nd
Nb (XRF)	bl	bl	1	bl	4	bl	2	bl	1
Ni (XRF)	1280	1967	1572	1178	1001	1315	1051	1232	1011
Ni (other)	nd	nd	nd	nd	nd	1304	nd	1027	nd
Rb (XRF)	bl	bl	1	bl	2	bl	3	bl	2
Sr (XRF)	11	bl	7	10	13	18	16	bl	12
Sr (AA)	nd	nd	nd	nd	nd	nd	nd	nd	nd
V (*)	188	118	47	196	97	190	93	211	96
Y (*)	19	14	6	18	8	21	8	13	8
Zn (XRF)	70	154	nd	99	nd	73	nd	102	nd
Zr (XRF)	14	7	26	12	29	12	21	13	19
Sc (INAA)	28	19	nd	nd	nd	27	nd	30	nd
AN	79.42	83.86		84.02		78.57		85.24	
or	0.18	0.06		0.12		0.24		0.06	
ab	4.65	1.86		3.89		4.65		3.64	
an	17.96	9.67		20.47		17.06		21.02	
C	-	0.61		-		-		-	
di	10.17	-		6.72		10.93		5.60	
hy	16.48	29.39		16.88		17.69		19.15	
ol	48.67	45.53		41.48		39.77		48.80	
mt	2.62	2.44		2.68		2.61		2.64	
il	0.59	0.34		0.66		0.57		0.61	

	AK-24e	S-190a	S-190b	S-190c	S-190d
CaO/Al2O3	0.82	0.43	0.70	0.86	0.67
CaO/TiO2	20.0	10.8	16.7	20.7	17.7
Al2O3/TiO2	24.3	25.2	23.7	24.0	26.3
Sc/Zr	2.00	2.71	-	2.25	2.31
Ti/Zr	133	154	175	150	148
Ti/Sc	66	57	-	67	64
Ti/V	9.9	9.2	10.7	9.5	9.1
V/Zr	13.4	16.9	16.3	15.8	16.2
V/Sc	6.7	6.2	-	7.0	7.0
Al/Zr	2841	3423	3650	3174	3426
Al/Sc	1421	1261	-	1411	1485
Mg#	86	89	86	86	87

Appendix B1.e (Woodburn Lake Group komatiites - Esker Lake and No-Name Lake belts)

	R-216	R-216 (UW)	R-220b-1	R-220b-2 (UW)	R-220b-2	R-220b-2 (UW)	R-220c	R-220c (UW)	R-226a	R-226a (UW)	R-228a (UW)
SiO2	39.49	39.15	38.84	37.74	35.98	35.91	38.84	38.63	38.47	38.11	42.82
TiO2	0.09	0.08	0.10	0.10	0.11	0.10	0.12	0.11	0.14	0.13	0.40
Al2O3	2.16	1.90	2.56	2.27	2.45	2.17	2.53	2.36	3.25	2.90	8.16
Fe2O3T	7.19	7.16	9.48	9.24	9.99	9.82	10.57	10.43	10.14	10.40	11.02
Fe2O3	nd	nd	nd	nd	nd	nd	nd	nd	nd	nd	nd
FeO	nd	nd	nd	nd	nd	nd	nd	nd	nd	nd	nd
MnO	0.06	0.06	0.08	0.37	0.05	0.38	0.06	0.05	0.16	0.16	0.17
MgO	38.13	39.84	36.99	37.71	34.11	34.73	36.68	38.84	36.05	36.83	25.37
CaO	0.77	0.81	0.75	0.81	1.65	1.74	0.28	0.33	0.17	0.28	6.96
Na2O	0.18	bl	bl	bl	0.24	bl	0.18	bl	0.21	0.01	0.28
K2O	0.01	0.02	bl	0.01	0.01	0.01	0.01	0.01	0.02	0.03	0.05
P2O5	bl	bl	bl	0.01	bl	bl	bl	bl	0.01	0.01	bl
H2O(LOI)	(12.47)	(12.47)	(12.06)	(12.06)	(15.77)	(15.77)	(11.55)	(11.55)	(11.37)	(11.37)	(5.02)
CO2	nd	nd	nd	nd	nd	nd	nd	nd	nd	nd	nd
Total	100.55	101.49	100.86	100.01	100.48	100.31	100.02	101.52	99.99	100.14	100.25
Ba	nd	6	nd	2	nd	2	nd	3	nd	11	20
Cr	1912	796	2467	836	2227	830	2230	774	3343	1295	2134
Nb	bl	1	bl	bl	bl	2	bl	2	bl	bl	3
Ni	4178	2733	3315	2555	3270	2231	3221	2222	3024	2168	1083
Rb	bl	1	bl	1	bl	1	bl	2	3	1	4
Sr	6	9	3	9	4	7	bl	5	bl	3	33
V	51	20	70	20	58	21	71	27	81	29	180
Y	13	1	9	2	8	1	4	2	bl	bl	6
Zn	75	nd	107	nd	80	nd	101	nd	270	nd	nd
Zr	5	24	bl	26	4	20	4	26	bl	30	15
AN	71.49		100.00		73.31		47.70		30.45		
or	0.06		-		0.06		0.06		0.12		
ab	1.52		-		2.03		1.52		1.78		
an	3.82		3.72		5.58		1.39		0.78		
C	0.45		1.20		-		1.71		2.60		
di	-		-		2.06		-		-		
hy	22.27		24.07		10.43		23.37		24.34		
ol	56.92		56.52		61.09		57.75		55.49		
mt	2.31		2.32		2.33		2.35		2.38		
il	0.17		0.19		0.21		0.23		0.27		
ap	-		-		-		-		0.02		

	R-216	R-220b-1	R-220b-2	R-220c	R-226a
CaO/Al2O3	0.36	0.29	0.67	0.11	0.05
CaO/TiO2	8.6	7.5	15.0	2.3	1.2
Al2O3/TiO2	24.0	25.6	22.3	21.1	23.2
Sc/Zr	-	-	-	-	-
Ti/Zr	100	165	100	139	128
Ti/Sc	-	-	-	-	-
Ti/V	10.6	8.6	11.4	10.1	10.4
V/Zr	10.2	14.5	17.0	9.4	11.7
V/Sc	-	-	-	-	-
Al/Zr	2285	3240	3346	1964	2719
Al/Sc	-	-	-	-	-
Mg#	94	92	90	91	91

Appendix B1.e (continued)

	R-228c	R-228c (UW)	R-228d	R-228d (UW)	R-238	R-238 (UW)	R-242a	R-242a (UW)	R-242b	R-242b (UW)	F-115
SiO2	41.68	41.16	42.79	42.58	41.51	41.89	42.77	42.29	41.54	42.02	50.37
TiO2	0.37	0.37	0.32	0.32	0.22	0.23	0.37	0.37	0.25	0.25	nd
Al2O3	5.94	5.71	7.71	7.55	5.37	5.24	8.44	8.27	6.21	5.99	6.25
Fe2O3T	11.13	11.11	10.89	10.91	9.84	9.70	11.58	11.26	10.64	10.45	11.95
Fe2O3	nd	nd	nd	nd	nd	nd	2.81	nd	4.15	nd	nd
FeO	nd	nd	nd	nd	nd	nd	7.89	nd	5.84	nd	nd
MnO	0.20	0.21	0.18	0.18	0.12	0.12	0.16	0.16	0.16	0.18	0.14
MgO	29.88	29.05	25.33	25.80	33.23	34.19	23.83	24.38	29.34	30.33	22.09
CaO	3.31	1.77	6.87	6.20	0.48	0.28	6.30	3.63	4.34	4.46	4.20
Na2O	0.30	bl	0.61	0.20	0.24	0.03	0.44	bl	0.51	0.17	0.42
K2O	0.06	0.07	0.07	0.08	0.02	0.03	0.01	0.02	0.10	0.11	bl
P2O5	bl	0.02	bl	0.01	0.01	0.02	bl	0.02	bl	0.02	bl
H2O(LOI)	(8.13)	(8.13)	(5.77)	(5.77)	(9.65)	(9.65)	(5.78)	(5.78)	(7.57)	(7.57)	(5.30)
CO2	nd	nd	nd	nd	nd	nd	nd	nd	nd	nd	nd
Total	100.20	97.74	99.74	99.59	100.69	101.37	99.68	96.18	100.66	101.54	100.72
Ba	nd	20	nd	13	nd	12	nd	16	nd	16	nd
Cr	3374	2097	2472	2014	2341	1853	2357	1958	2672	1685	1600
Nb	bl	bl	bl	2	bl	1	bl	3	1	3	nd
Ni	1647	1348	1465	1110	2454	1811	986	827	1839	1462	1040
Rb	bl	4	4	3	bl	3	bl	3	bl	6	nd
Sr	7	12	31	21	bl	3	17	18	17	20	nd
V	151	67	176	94	123	47	180	101	160	64	nd
Y	17	4	21	8	17	3	16	10	16	6	nd
Zn	90	nd	67	nd	91	nd	114	nd	101	nd	nd
Zr	16	17	15	16	9	19	21	14	9	22	nd
AN	85.26		77.80		53.20		84.96		76.89		81.02
or	0.35		0.41		0.12		0.06		0.59		-
ab	2.54		5.16		2.03		3.72		4.32		3.55
an	14.68		18.09		2.32		21.03		14.36		15.17
C	-		-		4.10		-		-		-
di	1.38		9.55		-		8.14		5.68		4.53
hy	27.96		18.70		39.80		23.78		16.69		68.46
ol	48.82		37.91		38.85		32.79		47.56		0.49
mt	2.71		2.64		2.49		2.71		2.54		2.17
il	0.70		0.61		0.42		0.70		0.47		-
ap	-		-		0.02		-		-		-

	R-228c	R-228d	R-238	R-242a	R-242b	F-115
CaO/Al2O3	0.56	0.79	0.09	0.75	0.70	0.67
CaO/TiO2	9.0	19.0	2.2	17.0	17.4	-
Al2O3/TiO2	16.1	24.1	24.4	22.8	24.8	-
Sc/Zr	-	-	-	-	-	-
Ti/Zr	147	106	167	-	-	-
Ti/Sc	-	-	-	-	-	-
Ti/V	14.7	10.9	10.7	12.3	9.4	-
V/Zr	13.7	8.6	17.8	-	-	-
V/Sc	-	-	-	-	-	-
Al/Zr	3156	2126	3650	-	-	-
Al/Sc	-	-	-	-	-	-

Appendix B1.e (continued)

	F-150c	F-150f	F-169a
SiO2	49.54	41.96	40.41
TiO2	nd	nd	nd
Al2O3	6.00	4.19	5.55
Fe2O3T	10.07	14.55	8.68
Fe2O3	nd	nd	nd
FeO	nd	nd	nd
MnO	0.17	0.16	0.10
MgO	23.56	27.22	27.66
CaO	7.03	6.74	5.02
Na2O	0.40	0.61	0.19
K2O	bl	bl	bl
P2O5	bl	bl	bl
H2O(LOI)	(5.45)	(6.48)	(12.00)
CO2	nd	nd	nd
Total	102.22	101.91	99.61
Ba	nd	nd	nd
Cr	1143	805	1127
Nb	nd	nd	nd
Ni	1006	632	1493
Rb	nd	nd	nd
Sr	nd	nd	nd
V	nd	nd	nd
Y	nd	nd	nd
Zn	nd	nd	nd
Zr	nd	nd	nd
AN	81.16	62.75	89.89
or	-	-	-
ab	3.38	5.16	1.61
an	14.58	8.70	14.29
C	-	-	-
di	16.14	19.79	8.39
hy	48.13	5.87	22.86
ol	11.51	52.43	37.56
mt	2.17	2.17	2.17
il	-	-	-
ap	-	-	-

	F-150c	F-150f	F-169a
CaO/Al2O3	1.17	1.61	0.90
CaO/TiO2	-	-	-
Al2O3/TiO2	-	-	-
Sc/Zr	-	-	-
Ti/Zr	-	-	-
Ti/Sc	-	-	-
Ti/V	-	-	-
V/Zr	-	-	-
V/Sc	-	-	-
Al/Zr	-	-	-
Al/Sc	-	-	-

Appendix B1.f (Woodburn Lake Group komatiitic basalts)

	R-22ød	R-22ød (UW)	R-222	R-222 (UW)	R-232b	R-232b (UW)	R-232c	R-232c (UW)	R-233	R-233 (UW)	AK-20
SiO2	51.35	51.77	46.93	46.88	44.15	44.60	53.34	53.33	46.22	46.43	50.97
TiO2	1.09	1.17	0.66	0.67	1.84	1.90	1.14	1.10	0.57	0.55	0.65
Al2O3	13.58	14.24	13.59	13.93	14.50	14.20	13.80	14.56	12.03	12.09	11.05
Fe2O3	8.07	8.44	12.29	11.83	11.60	11.24	10.05	10.33	12.15	11.74	15.10
MnO	0.08	0.09	0.16	0.19	0.15	0.10	0.14	0.17	0.25	0.29	0.17
MgO	13.02	14.40	13.35	13.64	8.96	9.35	7.09	7.50	12.73	13.12	8.74
CaO	2.57	2.66	5.22	6.24	6.51	4.70	5.26	5.35	9.04	8.96	8.30
Na2O	3.24	0.21	2.41	bl	2.59	1.92	3.93	3.30	2.00	1.30	1.66
K2O	0.14	0.14	1.01	0.90	2.42	2.36	1.39	1.40	1.60	1.57	1.10
P2O5	0.22	0.21	bl	0.02	0.16	0.19	0.10	0.15	bl	0.01	bl
H2O(LOI)	(5.56)	(5.56)	(3.42)	(3.42)	(4.06)	(4.06)	(1.00)	(1.00)	(2.45)	(2.45)	nd
Total	99.72	90.90	100.14	97.79	97.02	95.50	90.04	99.15	99.12	90.50	97.90
Ba	nd	135	nd	157	nd	364	nd	432	nd	206	nd
Cr	475	422	730	790	151	101	245	320	1033	1274	370
Nb	0	13	3	4	bl	0	5	0	bl	4	bl
Ni	207	250	207	213	105	170	143	143	301	207	130
Rb	9	4	42	36	55	54	42	40	66	66	60
Sr	207	205	299	291	102	176	372	373	221	207	140
V	102	122	302	174	147	166	140	131	270	177	209
Y	20	21	25	10	30	27	17	14	20	15	12
Zn	109	nd	70	nd	04	nd	190	nd	161	nd	60
Zr	129	103	43	bl	52	12	112	70	31	bl	45
Sc	nd	nd	nd	nd	nd	nd	nd	nd	nd	nd	27
AN	29.21		53.60		50.30		35.10		56.11		50.07
Q	4.09		-		-		1.37		-		2.24
or	0.03		5.97		14.30		0.21		9.46		6.50
ab	27.42		20.39		20.40		33.25		14.60		14.05
an	11.31		23.56		20.79		17.90		10.76		19.45
ne	-		-		0.70		-		1.50		-
C	3.95		-		-		-		-		-
di	-		5.09		0.40		6.03		21.07		10.22
hy	39.60		11.99		-		23.10		-		31.70
ol	-		23.53		19.11		0.00		26.03		-
mt	3.76		3.13		4.04		3.03		3.00		3.12
il	2.07		1.25		3.49		2.17		1.00		1.23
ap	0.51		-		0.37		0.23		-		-

	R-220d	R-222	R-232b	R-232c	R-233	AK-20
CaO/Al2O3	0.19	0.45	0.45	0.36	0.75	0.76
CaO/TiO2	2.4	9.4	3.5	4.6	15.9	12.9
Al2O3/TiO2	12.5	20.7	7.9	12.8	21.1	17.0
Sc/Zr	-	-	-	-	-	0.6
Ti/Zr	51	92	212	61	110	87
Ti/Sc	-	-	-	-	-	144
Ti/V	35.9	13.1	75.1	48.9	12.3	13.5
V/Zr	1.4	7.0	2.8	1.3	9.0	6.4
V/Sc	-	-	-	-	-	10.7
Al/Zr	557	1684	1475	688	2053	1299
Al/Sc	-	-	-	-	-	2165
Mg#	83	75	68	66	74	61

Appendix B1.f (continued)

	AK-31	S-99	S-99 (UW)	S-182	S-182 (UW)
SiO2	50.71	46.38	47.33	53.91	53.40
TiO2	0.56	0.57	0.56	1.06	1.08
Al2O3	12.43	15.53	16.46	16.77	17.00
Fe2O3	11.05	12.08	12.48	11.77	11.78
MnO	0.18	0.23	0.26	0.17	0.18
MgO	12.72	8.79	8.97	3.83	3.94
CaO	6.55	9.79	9.97	6.19	6.28
Na2O	3.20	1.78	1.38	4.36	4.04
K2O	0.08	1.29	1.28	0.85	0.83
P2O5	bl	bl	0.02	0.08	0.16
H2O(LOI)	nd	(2.34)	(2.34)	(1.21)	(1.21)
Total	97.48	99.58	101.85	100.20	99.89
Ba	nd	nd	157	nd	304
Cr	1093	441	660	45	77
Nb	1	bl	5	4	7
Ni	353	163	145	34	28
Rb	bl	29	50	20	20
Sr	117	288	289	456	429
V	255	269	173	199	135
Y	9	7	14	22	25
Zn	91	123	nd	132	nd
Zr	45	42	bl	104	66
Sc	nd	nd	nd	nd	nd
AN	41.64	67.00		39.09	
Q	-	-		2.64	
or	0.47	7.62		5.02	
ab	27.08	15.06		36.89	
an	19.32	30.58		23.68	
ne	-	-		-	
C	-	-		-	
di	10.60	14.72		5.42	
hy	24.51	7.20		18.51	
ol	10.55	16.89		-	
mt	2.99	3.00		3.71	
il	1.06	1.08		2.01	
ap	-	-		0.19	

	AK-31	S-99	S-182
CaO/Al2O3	0.53	0.63	0.37
CaO/TiO2	11.7	17.2	5.8
Al2O3/TiO2	22.2	27.3	15.8
Sc/Zr	-	-	-
Ti/Zr	75	81	61
Ti/Sc	-	-	-
Ti/V	13.2	12.7	32.8
V/Zr	5.7	6.4	1.9
V/Sc	-	-	-
Al/Zr	1461	1956	853
Al/Sc	-	-	-
Mg#	76	65	47

Appendix B2. (Rare Earth Element (REE) analyses)

	AK-2 (GSC)	AK-2 (GSC)	AK-3	AK-6a (GSC)	AK-6a (GSC)	AK-9 (GSC)	AK-9 (GSC)	AK-11a	AK-12b *	AK-13a *	AK-14a
La	17	18	1.1	17	16	6.8	6.8	1.2	3.6	11	1.3
Ce	32	32	3.2	37	35	12	12	1.8	7.4	18	4.2
Nd	16	16	1.1	23	23	8.3	8.8	3.5	4.7	5.6	1.9
Sm	2.0	1.9	bl	3.6	3.5	1.3	0.8	bl	0.7	0.7	0.5
Eu	0.6	0.6	bl	1.4	1.4	0.3	0.3	0.1	0.3	0.2	0.1
Gd	1.7	1.6	nd	4.1	3.9	1.7	1.6	nd	nd	nd	1.7
Dy	0.9	1.1	0.5	3.4	3.5	1.5	2.0	1.0	1.5	1.0	1.1
Er	nd	nd	1.4	nd	nd	nd	nd	1.0	1.1	1.3	1.2
Yb	0.3	0.3	0.5	1.3	1.4	0.3	0.9	1.0	1.0	0.9	0.7
Y	4.6	4.5	nd	17	16	5.6	9.9	nd	nd	nd	nd

	AK-14a (GSC)	AK-14a (GSC)	AK-14b	AK-14b (GSC)	AK-14b (GSC)	AK-14c	AK-14c (GSC)	AK-14c (GSC)	AK-14d	AK-14d (GSC)	AK-14d (GSC)
La	1.4	1.4	0.8	0.8	0.8	0.7	0.7	1.2	0.6	0.6	0.6
Ce	2.7	2.6	5.0	1.7	1.6	3.2	1.6	2.1	6.2	1.8	1.7
Nd	3.2	3.0	1.2	2.6	2.6	1.7	2.5	2.9	1.4	2.6	3.1
Sm	0.3	0.5	0.5	0.3	0.4	0.9	0.2	0.6	0.4	0.5	0.9
Eu	0.2	0.2	bl	0.1	0.1	0.1	0.2	0.2	0.1	0.2	0.2
Gd	1.1	0.9	1.5	0.8	0.6	2.2	1.0	0.9	1.6	0.9	0.9
Dy	1.4	1.5	0.8	1.0	1.1	1.2	1.2	1.5	1.0	1.2	1.5
Er	nd	nd	1.2	nd	nd	1.3	nd	nd	1.4	nd	nd
Yb	0.7	0.5	0.5	0.4	0.3	0.7	0.5	0.5	0.7	0.6	0.6
Y	7.4	6.0	nd	4.8	4.0	nd	6.0	6.3	nd	6.2	6.1

Appendix B2. (continued)

	AK-15a	AK-15b	AK-15c	AK-15d	AK-16a	AK-16b	AK-20 (GSC)	AK-20 (GSC)	AK-23a	AK-23b	AK-23c
La	2.3	2.6	0.7	1.8	1.3	0.9	4.0	4.9	0.6	0.7	0.5
Ce	4.9	5.3	5.4	5.7	5.9	5.4	9.3	9.6	1.6	1.9	2.3
Nd	2.2	2.5	1.6	2.2	1.4	1.4	7.8	10	1.6	1.7	nd
Sm	bl	bl	0.5	0.5	bl	bl	1.6	1.1	0.3	bl	bl
Eu	0.1	0.1	0.2	0.1	0.1	0.2	0.7	0.7	0.1	0.1	0.2
Gd	nd	nd	1.7	1.7	1.4	1.7	2.3	2.4	nd	nd	nd
Dy	1.0	1.0	1.2	1.1	0.7	0.9	2.3	2.9	1.2	1.2	0.9
Er	1.5	1.4	1.4	1.3	1.2	1.4	nd	nd	1.2	1.3	1.3
Yb	0.9	0.9	0.6	0.6	0.5	0.7	nd	1.5	0.9	0.9	0.6
Y	nd	nd	nd	nd	nd	nd	10	15	nd	nd	nd

	AK-23g	AK-23e	AK-24b	AK-24c	AK-24d	AK-24e	AK-26a	AK-26b	AK-31 (GSC)	AK-31 (GSC)	AK-31 (GSC)
La	0.6	0.9	0.5	0.5	0.6	0.6	0.9	1.6	3.3	3.2	3.6
Ce	2.2	2.9	4.5	2.6	1.7	bl	3.1	3.4	8.3	8.1	8.3
Nd	1.7	1.0	1.3	nd	nd	nd	bl	bl	7.2	6.7	7.5
Sm	0.4	bl	0.6	bl	bl	bl	nd	bl	1.2	1.7	1.2
Eu	0.1	bl	0.1	0.2	0.2	0.2	0.2	0.2	0.5	0.5	0.5
Gd	nd	nd	1.6	nd	nd	nd	nd	nd	2.1	2.0	2.1
Dy	1.5	0.7	0.9	0.9	0.8	1.2	1.0	0.9	2.1	2.2	2.5
Er	1.4	1.5	1.4	1.4	1.1	1.0	1.3	1.3	nd	nd	nd
Yb	1.0	0.7	0.6	0.6	0.5	0.7	0.6	0.6	0.6	0.5	1.3
Y	nd	nd	nd	nd	nd	nd	nd	nd	9.1	7.9	13

Appendix B2. (continued)

	AK-31 (GSC)	K-3a-1	K-3a-1	K-3a-1	K-3a-1	K-3a-1	K-4a	K-4b	K-7b	K-17a	K-21
La	3.2	1.1	1.1	1.0	1.1	1.0	1.0	1.0	1.0	1.2	0.8
Ce	7.9	nd	nd	nd	nd	nd	3.1	5.5	nd	3.7	2.3
Nd	6.8	1.4	1.5	1.4	1.5	1.6	3.0	2.1	1.6	2.1	1.3
Sm	1.4	nd	bl	nd	0.8	nd	bl	bl	bl	0.3	0.4
Eu	0.5	0.1	0.1	0.1	0.1	0.1	0.2	0.1	0.1	0.2	0.2
Gd	2.0	nd	nd	nd	nd	nd	nd	nd	nd	nd	1.1
Dy	2.6	0.8	0.7	0.7	1.1	1.1	1.1	0.8	0.7	1.0	1.0
Er	nd	1.5	1.6	1.2	0.9	0.9	1.5	1.6	1.8	1.8	0.8
Yb	1.1	0.6	0.4	0.4	0.5	0.5	1.0	0.9	1.0	0.9	0.7
Y	12	nd	nd	nd	nd	nd	nd	nd	nd	nd	nd

	K-22	K-24	K-24 (GSC)	K-24 (GSC)	K-25	K-34	K-35	K-36	K-37	K-38	K-39
La	2.2	1.4	1.2	1.1	1.3	0.8	0.7	0.8	0.7	0.9	0.9
Ce	6.0	5.1	2.4	2.4	3.8	2.4	4.3	4.9	3.5	4.8	3.6
Nd	2.5	2.5	2.7	3.0	3.0	2.2	2.4	2.4	2.2	1.7	2.4
Sm	bl	bl	0.4	0.9	bl	bl	bl	bl	bl	bl	bl
Eu	0.1	0.1	0.2	0.2	0.2	0.1	0.2	0.1	0.2	0.1	0.1
Gd	nd	nd	0.9	0.8	nd	nd	nd	nd	nd	nd	nd
Dy	0.9	1.0	1.2	1.4	1.2	0.8	1.1	0.9	1.0	0.7	1.0
Er	1.3	1.5	nd	nd	1.7	0.8	1.5	1.5	1.4	1.4	1.4
Yb	0.9	1.0	0.6	0.6	1.1	0.8	0.9	0.9	0.9	0.7	0.8
Y	nd	nd	6.6	6.5	nd	nd	nd	nd	nd	nd	nd

Appendix B2. (continued)

	K-40	K-41	K-42a	K-42a INAA	K-42b	K-42b INAA	K-42c	K-42c INAA	K-42d	K-42d INAA	K-43a
La	0.5	0.9	0.7	1.4	0.5	0.4	0.7	0.8	0.6	0.8	nd
Ce	bl	4.6	7.1	6.0	1.9	2.9	3.6	1.7	4.3	2.5	7.2
Nd	1.5	2.4	1.5	3.2	1.4	1.9	2.4	1.9	1.5	2.2	1.9
Sm	bl	bl	bl	0.6	0.4	0.6	bl	0.6	bl	0.6	bl
Eu	0.1	0.2	0.1	0.3	0.2	0.3	0.2	0.3	0.2	0.3	0.1
Gd	nd	nd	nd	nd	1.3	nd	nd	nd	0.7	nd	0.9
Dy	0.9	1.0	1.1	nd	1.3	nd	1.2	nd	1.3	nd	0.6
Er	0.9	1.5	1.0	nd	1.1	nd	1.0	nd	1.1	nd	1.0
Yb	0.8	0.8	0.8	1.3	0.8	1.2	0.9	1.4	0.9	1.4	nd
Y	nd	nd	nd	nd	nd	nd	nd	nd	nd	nd	nd

	K-43a	K-43a	K-43a	K-43a	K-43a INAA	K-43b	K-43b INAA	K-43c	K-43c INAA	K-43d	K-43d INAA
La	nd	nd	nd	nd	2.8	0.4	0.4	1.5	2.3	0.5	0.3
Ce	8.3	8.2	7.9	9.2	8.8	3.8	1.5	3.3	5.6	bl	2.4
Nd	2.5	2.5	2.4	2.7	4.4	0.6	1.3	2.3	2.1	1.3	1.5
Sm	0.3	bl	bl	bl	0.8	bl	0.3	bl	0.4	bl	0.2
Eu	0.1	0.2	0.2	0.1	0.3	0.2	0.2	0.1	0.2	0.1	0.1
Gd	1.0	1.0	0.9	0.9	nd	1.3	nd	nd	nd	nd	nd
Dy	0.6	0.6	0.6	0.6	nd	0.5	nd	0.7	nd	0.7	nd
Er	1.2	1.2	1.1	1.0	nd	1.0	nd	1.1	nd	0.9	nd
Yb	nd	nd	nd	nd	0.9	0.6	0.8	0.8	0.8	0.7	0.9
Y	nd	nd	nd	nd	nd	nd	nd	nd	nd	nd	nd

Appendix B2. (continued)

	K-44a	K-44a INAA	K-44b	K-44b INAA	K-44d	K-44d INAA	K-44e	K-44e INAA	K-44f	K-44f INAA	K-44g
La	0.6	0.6	0.8	2.2	0.5	1.0	0.9	1.2	0.7	0.3	0.6
Ce	1.9	2.4	6.0	8.7	6.5	3.4	3.4	6.6	3.1	3.6	5.2
Nd	1.4	1.1	2.3	3.1	1.4	1.9	2.4	4.9	2.0	1.8	1.2
Sm	0.5	0.6	0.3	0.6	0.3	0.6	0.3	0.7	bl	0.7	bl
Eu	0.2	0.3	0.1	0.2	0.2	0.3	0.3	0.3	0.2	0.4	0.1
Gd	nd	nd	nd	nd	1.2	nd	nd	nd	nd	nd	1.3
Dy	1.1	nd	1.0	nd	1.0	nd	1.3	nd	1.2	nd	0.9
Er	1.0	nd	1.0	nd	1.5	nd	1.5	nd	1.5	nd	1.4
Yb	0.8	1.2	1.0	0.9	0.6	1.2	1.1	1.5	1.0	1.5	0.5
Y	nd	nd	nd	nd	nd	nd	nd	nd	nd	nd	nd

	K-44g INAA	K-44g (GSC)	K-44g (GSC)	R-222 (GSC)	R-222 (GSC)	R-232b	R-232b (GSC)	R-232b (GSC)	R-232c	R-233	R-233 (GSC)
La	0.9	1.4	0.7	3.0	2.8	nd	17	15	nd	nd	1.4
Ce	4.4	2.0	1.5	7.1	6.4	42	32	30	57	5.5	3.7
Nd	1.9	3.6	2.5	7.3	nd	nd	20	22	nd	nd	5.2
Sm	0.6	0.2	0.5	1.8	nd	nd	3.8	3.6	4.2	nd	0.8
Eu	0.3	0.2	0.2	0.5	0.5	1.4	1.4	1.4	0.7	0.4	0.4
Gd	nd	1.0	0.8	2.5	2.7	7.0	5.0	5.0	4.0	2.1	2.1
Dy	nd	1.3	1.3	3.0	3.0	4.7	4.6	5.1	2.9	1.9	2.5
Er	nd	nd	nd	nd	nd	2.3	nd	nd	1.4	1.6	nd
Yb	1.2	0.7	0.4	1.5	1.6	2.0	1.5	2.0	1.3	1.5	1.3
Y	nd	6.0	5.2	16	16	nd	22	24	nd	nd	14

Appendix B2. (continued)

	R-233 (GSC)	R-242a (GSC)	R-242a (GSC)	S3-0126F	S3-0126F (GSC)	S3-0126F (GSC)	S3-0126G	S3-0126G (GSC)	S3-0126G (GSC)	S3-0126H (GSC)	S3-0126H (GSC)
La	1.2	1.3	1.2	1.5	1.6	1.4	1.7	1.5	1.5	2.0	1.7
Ce	3.3	3.4	3.3	5.4	4.6	4.3	3.8	3.1	3.2	4.6	4.3
Nd	nd	4.8	5.5	3.6	6.0	7.2	nd	4.8	6.3	5.0	nd
Sm	nd	0.5	0.6	nd	1.3	0.8	nd	0.5	0.1	0.4	nd
Eu	0.4	0.2	0.2	0.6	0.6	0.7	0.3	0.3	0.4	0.6	0.7
Gd	2.2	1.6	1.5	nd	2.5	2.5	nd	1.4	1.4	1.7	2.0
Dy	2.7	1.9	2.1	2.8	3.1	3.3	1.4	1.7	1.8	1.7	2.4
Er	nd	nd	nd	2.1	nd	nd	1.3	nd	nd	nd	nd
Yb	1.6	0.9	1.0	1.4	1.5	1.8	0.8	0.9	0.9	0.4	1.4
Y	15	9.5	9.7	nd	17	18	nd	9.6	9.4	7.4	13

	T-8 (GSC)	T-8 (GSC)	T-4 (GSC)	T-4 (GSC)	T-13 (GSC)	T-13 (GSC)
La	26	25	5.4	5.4	3.9	3.9
Ce	58	54	16	15	10	9.8
Nd	32	31	15	16	10	12
Sm	6.1	5.0	4.3	3.3	2.7	1.6
Eu	1.6	1.5	1.4	1.4	0.9	0.9
Gd	5.3	5.2	5.7	5.6	3.4	3.4
Dy	4.3	4.4	6.4	6.7	3.8	3.9
Er	nd	nd	nd	nd	nd	nd
Yb	1.6	1.7	2.9	3.4	1.9	1.9
Y	20	19	34	34	21	20

Appendix B3. (Prince Albert Group komatiitic suite)

	S3-0126H	S3-0126F	S3-0126G	S3-0126A	S3-356A	S3-0101	S3-0125	S3-515B	S3-78	S3-430	S2-208C (GSC)
SiO2	44.93	45.94	45.98	44.72	48.71	45.20	51.03	42.88	41.98	42.77	39.00
TiO2	0.47	0.43	0.32	0.49	0.62	0.73	0.07	0.14	0.45	0.37	0.10
Al2O3	9.65	8.82	7.11	10.26	13.25	10.55	3.00	3.11	5.95	6.28	2.70
Fe2O3T	11.70	12.00	9.48	12.40	11.38	20.67	7.66	8.59	17.25	11.92	nd
Fe2O3	nd	nd	nd	nd	nd	nd	nd	nd	nd	nd	3.10
FeO	nd	nd	nd	nd	nd	nd	nd	nd	nd	nd	7.70
MnO	0.17	0.15	0.17	0.17	0.18	0.23	0.10	0.13	0.15	0.17	0.33
MgO	18.70	19.39	23.79	17.76	12.93	4.77	19.16	34.97	24.49	24.92	37.00
CaO	5.96	5.66	7.56	6.58	6.10	6.40	13.02	2.40	5.90	6.62	0.44
Na2O	0.66	0.64	0.46	1.39	3.58	0.60	1.01	bl	0.15	0.15	0.04
K2O	4.63	5.01	0.02	4.33	1.54	0.21	0.04	0.02	0.03	0.02	0.01
P2O5	bl	bl	bl	bl	bl	bl	bl	bl	nd	nd	0.03
H2OT	nd	nd	nd	nd	nd	nd	nd	nd	nd	nd	8.20
CO2	nd	nd	nd	nd	nd	nd	nd	nd	nd	nd	bl
Total	96.95	98.12	94.89	98.18	98.29	97.44	95.97	91.44	96.35	93.22	99.45
Ba	nd	nd	nd	nd	nd	nd	nd	nd	nd	nd	nd
Co	84	79	80	84	72	112	59	72	nd	nd	100
Cr	2082	1382	1929	1673	719	420	135	1595	374	2379	2000
Cu	nd	nd	nd	nd	nd	nd	nd	nd	nd	nd	bl
Nb	bl	bl	bl	bl	1	bl	bl	bl	bl	3	nd
Ni	492	396	1334	591	289	414	346	2045	341	1244	2100
Rb	136	163	bl	132	60	bl	bl	bl	bl	bl	nd
Sr	15	16	15	13	243	373	93	bl	48	56	bl
V	236	196	161	253	313	172	51	74	147	186	71
Y	13	21	21	16	23	21	17	16	15	21	nd
Zn	82	77	61	72	71	225	48	bl	18	121	92
Zr	21	24	15	26	38	58	1	8	22	18	nd
Sc	34	31	22	35	43	26	3	15	nd	nd	16
AN	100.00	100.00	81.61	100.00	37.58	84.66	29.26	100.00	92.42	92.82	85.44
Q	-	-	-	-	-	6.93	-	-	-	-	-
or	18.67	20.01	0.12	12.68	9.10	1.24	0.24	0.12	0.18	0.12	0.06
ab	-	-	3.89	-	25.81	5.75	8.55	-	1.27	1.27	0.34
an	9.69	6.48	17.28	8.97	15.54	31.75	3.53	8.43	15.47	16.48	1.99
lc	6.82	7.52	-	10.12	-	-	-	-	-	-	-
ne	3.03	2.93	-	6.37	2.43	-	-	-	-	-	-
C	-	-	-	-	-	5.57	-	-	-	-	1.90
di	15.89	17.34	16.83	18.99	11.85	-	51.55	2.74	11.89	13.88	-
hy	-	-	31.21	-	-	39.73	21.13	30.39	22.55	26.19	21.17
ol	38.14	39.28	22.35	36.19	28.39	-	7.96	46.42	48.57	31.74	63.07
mt	2.86	2.88	2.64	2.89	3.87	3.23	2.28	2.38	2.83	2.71	2.32
il	0.89	0.82	0.61	0.93	1.18	1.39	0.13	0.27	0.85	0.78	0.19
ap	-	-	-	-	-	-	-	-	-	-	0.07

	S3-0126H	S3-0126F	S3-0126G	S3-0126A	S3-356A	S3-0101	S3-0125	S3-5158	S3-70	S3-430	S2-208C (GSC)
CaO/Al2O3	0.62	0.64	1.06	0.64	0.46	0.35	4.61	0.77	0.99	1.05	0.16
CaO/TiO2	12.7	13.2	23.6	13.4	9.8	8.8	197	17.1	13.1	17.9	4.4
Al2O3/TiO2	20.5	20.5	22.2	20.9	21.3	25.4	42.8	22.2	13.2	17.0	27.0
Sc/Zr	1.62	1.29	1.47	1.35	1.13	0.45	3.00	1.00	-	-	-
Ti/Zr	134	100	120	113	98	76	420	105	123	123	-
Ti/Sc	83	83	87	84	87	168	140	56	-	-	30
Ti/V	12.0	13.2	11.9	11.6	11.9	25.5	8.2	11.4	17.2	11.9	8.5
V/Zr	11.2	8.2	10.7	9.7	8.2	3.0	51.0	9.3	7.1	10.3	-
V/Sc	6.9	6.3	7.3	7.2	7.3	6.6	17.0	4.9	-	-	4.4
Al/Zr	2431	1944	2507	2000	1044	1692	15870	2056	1431	1845	-
Al/Sc	1501	1505	1710	1551	1630	3774	5290	1097	-	-	893
Mg#	82	82	87	80	76	39	87	92	80	85	87

Appendix B3. (continued)

	S2-205A (GSC)	S2-201A (GSC)	S2-208D (GSC)	S2-201C (GSC)	S2-210A (GSC)	S2-203C (GSC)	S2-169 (GSC)	S2-183B (GSC)	S2-130 (GSC)	S2-176A (GSC)	S2-147D (GSC)
SiO2	40.70	38.40	38.40	41.10	40.30	40.60	38.20	40.80	43.30	42.50	43.10
TiO2	0.18	0.15	0.34	0.17	0.34	0.33	0.38	0.17	0.29	0.29	0.22
Al2O3	4.10	3.60	11.40	3.70	6.90	5.40	7.40	4.40	6.90	7.50	7.60
Fe2O3T	nd	nd	nd	nd	nd	nd	nd	nd	nd	nd	nd
Fe2O3	5.30	4.80	3.20	3.10	3.00	4.30	4.40	3.90	0.35	2.10	1.40
FeO	4.20	4.60	8.90	4.80	7.40	6.60	7.10	4.80	7.60	6.30	6.80
MnO	0.19	0.19	0.22	0.24	0.21	0.25	0.16	0.14	0.19	0.17	0.21
MgO	38.50	34.70	24.10	33.70	28.10	33.40	27.90	31.60	26.70	26.80	26.90
CaO	1.50	1.70	6.90	3.50	5.50	2.50	4.10	4.10	7.10	7.50	7.60
Na2O	0.01	0.08	0.16	0.07	0.11	0.03	0.09	0.10	0.13	0.32	0.13
K2O	0.01	0.03	0.02	0.01	0.02	0.01	0.03	0.01	0.04	0.05	0.01
P2O5	0.04	0.03	0.05	0.02	0.04	0.03	0.04	0.04	0.04	0.04	0.04
H2OT	5.50	11.40	5.10	9.80	7.20	5.80	8.70	9.30	5.00	5.70	5.60
CO2	0.03	0.05	bl	0.07	bl	0.05	bl	0.14	bl	bl	bl
Total	100.23	99.68	98.79	99.41	99.12	99.25	98.50	99.36	98.44	99.27	99.61
Ba	nd	nd	nd	nd	nd	nd	nd	nd	nd	nd	nd
Co	95	94	71	88	78	100	96	90	50	74	74
Cr	2300	2500	2100	2900	3100	4500	3800	3400	2500	2600	2800
Cu	14	32	bl	37	23	35	610	bl	90	45	bl
Nb	nd	nd	nd	nd	nd	nd	nd	nd	nd	nd	nd
Ni	1900	1800	700	2300	1100	1400	1300	1500	770	1200	1000
Rb	nd	nd	nd	nd	nd	nd	nd	nd	nd	nd	nd
Sr	bl	15	bl	18	31	bl	bl	25	21	58	43
V	110	110	230	100	200	160	250	130	170	210	140
Y	nd	nd	nd	nd	nd	nd	nd	nd	nd	nd	nd
Zn	83	59	76	90	91	84	64	44	66	64	68
Zr	nd	nd	nd	nd	nd	nd	nd	nd	nd	nd	nd
Sc	20	18	33	16	23	22	31	15	25	25	23
AN	92.84	92.41	95.73	94.27	95.15	97.96	96.28	93.16	94.28	87.46	94.82
Q	-	-	-	-	-	-	-	-	-	-	-
or	0.06	0.18	0.12	0.06	0.12	0.06	0.18	0.06	0.24	0.30	0.06
ab	0.08	0.68	1.35	0.59	0.93	0.25	0.76	0.85	1.10	2.71	1.10
an	7.18	8.24	30.33	9.75	18.28	12.21	19.70	11.53	18.13	10.88	20.13
lc	-	-	-	-	-	-	-	-	-	-	-
ne	-	-	-	-	-	-	-	-	-	-	-
C	1.44	0.42	-	-	-	0.87	-	-	-	-	-
di	-	-	2.85	5.88	6.94	-	0.30	6.75	13.36	14.28	13.71
hy	28.61	19.23	4.66	23.82	16.59	23.91	16.24	21.89	21.34	14.13	18.59
ol	62.13	56.48	50.81	46.57	45.54	52.56	48.83	45.93	37.33	40.01	37.89
mt	2.44	2.39	2.67	2.42	2.67	2.65	2.73	2.42	0.51	2.60	2.83
il	0.34	0.28	0.65	0.32	0.65	0.63	0.72	0.32	0.55	0.55	0.42
ap	0.09	0.07	0.12	0.05	0.09	0.07	0.09	0.09	0.09	0.09	0.09

	S2-205A (GSC)	S2-201A (GSC)	S2-208D (GSC)	S2-201C (GSC)	S2-210A (GSC)	S2-203C (GSC)	S2-169 (GSC)	S2-183B (GSC)	S2-130 (GSC)	S2-176A (GSC)	S2-147D (GSC)
CaO/Al2O3	0.37	0.47	0.61	0.95	0.80	0.46	0.55	0.93	1.03	1.00	1.00
CaO/TiO2	8.3	11.3	20.3	20.6	16.2	7.6	10.0	24.1	24.5	25.9	34.6
Al2O3/TiO2	22.8	24.0	33.5	21.8	20.3	16.4	19.5	25.9	23.8	25.9	34.6
Sc/Zr	-	-	-	-	-	-	-	-	-	-	-
Ti/Zr	-	-	-	-	-	-	-	-	-	-	-
Ti/Sc	54	50	62	64	89	90	74	60	70	70	57
Ti/V	9.0	8.2	8.9	10.2	10.2	12.4	9.1	7.9	10.2	8.3	9.4
V/Zr	-	-	-	-	-	-	-	-	-	-	-
V/Sc	5.5	6.1	7.0	6.3	8.7	7.3	8.1	8.7	6.8	8.4	6.1
Al/Zr	-	-	-	-	-	-	-	-	-	-	-
Al/Sc	1004	1050	1827	1223	1587	1290	1263	1552	1460	1587	1740
Mg#	90	89	80	91	84	86	83	89	86	86	86

Appendix B3. (continued)

	S2-163A (GSC)	S2-120F (GSC)	S2-150A (GSC)	S2-162A (GSC)	S2-174 (GSC)	S2-150B (GSC)	S2-158B (GSC)	S2-208B (GSC)	S2-178A (GSC)	S2-120K (GSC)	S2-70 (GSC)
SiO2	41.90	41.80	42.10	42.10	45.00	41.40	43.40	44.60	45.00	45.50	44.60
TiO2	0.30	0.27	0.32	0.26	0.27	0.36	0.30	0.28	0.27	0.30	0.28
Al2O3	7.00	7.00	5.40	6.20	7.20	6.00	5.80	5.90	6.70	5.60	4.50
Fe2O3T	nd	nd	nd	nd	nd	nd	nd	nd	nd	nd	nd
Fe2O3	2.80	2.90	4.10	2.70	2.50	3.00	3.10	1.60	1.20	1.80	5.00
FeO	6.40	7.10	5.90	7.00	5.90	6.00	6.30	6.20	8.30	7.60	8.30
MnO	0.10	0.22	0.25	0.21	0.19	0.17	0.22	0.19	0.17	0.10	0.20
MgO	26.90	26.30	28.20	27.40	27.40	32.90	27.20	27.00	25.90	23.90	23.00
CaO	7.10	6.80	6.90	5.80	8.10	7.90	6.50	6.70	5.70	8.10	8.20
Na2O	0.00	0.10	0.24	0.11	0.10	0.23	0.20	0.00	0.09	0.02	0.35
K2O	0.03	0.02	0.05	0.02	0.03	0.07	0.05	0.02	0.02	0.29	0.11
P2O5	0.03	0.03	0.04	0.04	0.03	0.06	0.04	0.04	0.05	0.04	0.00
H2OT	5.90	6.50	6.20	7.40	2.00	9.60	6.70	6.70	5.90	5.30	4.60
CO2	bl	bl	bl	bl	bl	0.00	bl	bl	bl	bl	bl
Total	98.62	99.12	99.70	99.24	98.80	107.69	99.81	99.31	99.31	98.63	99.22
Ba	nd	nd	nd	nd	nd	nd	nd	nd	nd	nd	nd
Co	62	61	77	62	74	74	82	56	58	64	67
Cr	2400	2400	2800	2200	2500	2500	1800	2300	2000	290	1600
Cu	10	70	40	69	30	32	47	13	45	50	110
Nb	nd	nd	nd	nd	nd	nd	nd	nd	nd	nd	nd
Ni	820	790	1500	1200	1300	1000	1200	700	820	260	110
Rb	nd	nd	nd	nd	nd	nd	nd	nd	nd	nd	nd
Sr	23	56	25	55	74	360	bl	bl	320	110	bl
V	170	170	160	150	200	170	220	170	160	130	140
Y	nd	nd	nd	nd	nd	nd	nd	nd	nd	nd	nd
Zn	56	500	67	57	64	70	72	69	65	63	61
Zr	nd	nd	nd	nd	nd	nd	nd	nd	nd	nd	nd
Sc	24	35	19	24	20	29	24	20	30	20	21
AN	96.50	92.29	86.93	94.62	92.49	100.00	89.73	95.86	95.90	98.83	77.81
Q	-	-	-	-	-	-	-	-	-	-	-
or	0.10	0.12	0.30	0.12	0.10	-	0.30	0.12	0.12	1.71	0.65
ab	0.60	1.52	2.03	0.93	1.52	-	1.69	0.60	0.76	0.17	2.96
an	10.65	10.23	13.51	10.37	10.75	15.13	14.70	15.60	17.02	14.33	10.30
lc	-	-	-	-	-	0.32	-	-	-	-	-
ne	-	-	-	-	-	1.05	-	-	-	-	-
C	-	-	-	-	-	-	-	-	-	-	-
di	12.97	12.15	16.21	9.63	16.79	16.96	13.63	13.66	0.00	20.31	23.06
hy	10.14	10.00	14.12	24.39	20.09	-	24.46	32.05	30.95	31.99	23.26
ol	30.76	39.26	43.77	37.10	35.45	60.32	34.06	27.40	26.17	21.54	29.09
mt	2.61	2.57	2.64	2.55	2.57	2.70	2.61	2.32	1.74	2.61	2.50
il	0.57	0.51	0.61	0.49	0.51	0.60	0.57	0.53	0.51	0.57	0.53
ap	0.07	0.07	0.09	0.09	0.07	0.14	0.09	0.09	0.14	0.09	0.19

	S2-163A (GSC)	S2-120F (GSC)	S2-150A (GSC)	S2-162A (GSC)	S2-174 (GSC)	S2-150B (GSC)	S2-158B (GSC)	S2-200B (GSC)	S2-178A (GSC)	S2-120K (GSC)	S2-70 (GSC)
CaO/Al2O3	1.01	0.97	1.28	0.94	1.13	1.32	1.12	1.14	0.85	1.45	1.82
CaO/TiO2	23.7	25.2	21.6	22.3	30.0	21.9	21.7	23.9	21.1	27.0	29.3
Al2O3/TiO2	23.3	25.9	16.9	23.9	26.7	16.7	19.3	21.1	24.8	18.7	16.1
Sc/Zr	-	-	-	-	-	-	-	-	-	-	-
Ti/Zr	-	-	-	-	-	-	-	-	-	-	-
Ti/Sc	75	46	101	65	58	74	75	84	54	64	80
Ti/V	10.6	9.5	12.0	10.4	8.1	12.7	8.2	9.9	10.1	13.9	12.0
V/Zr	-	-	-	-	-	-	-	-	-	-	-
V/Sc	7.1	4.9	8.4	6.3	7.1	5.9	9.2	8.5	5.3	4.6	6.7
Al/Zr	-	-	-	-	-	-	-	-	-	-	-
Al/Sc	1543	1058	1503	1367	1360	1894	1278	1561	1181	1058	1134
Mg#	85	84	85	85	87	88	85	87	84	83	78

Appendix B3. (continued)

	S2-204 (GSC)	S3-506 (GSC)	S3-4009 (GSC)	S3-4010 (GSC)	S3-4011 (GSC)	S2-1206 (GSC)	S2-147A (GSC)	S2-215B (GSC)	S2-120C (GSC)	S3-003 (GSC)	S2-147A (GSC)
SiO2	47.80	47.80	40.64	43.67	44.14	40.30	38.70	39.00	38.90	48.30	46.10
TiO2	0.25	0.35	0.15	0.18	0.15	0.30	0.29	0.15	0.09	0.39	0.28
Al2O3	4.20	6.10	2.13	1.93	1.77	8.00	5.90	2.20	1.90	6.20	5.80
Fe2O3T	nd	nd	nd	nd	nd	nd	nd	nd	nd	nd	nd
Fe2O3	1.00	1.60	4.00	2.67	2.26	1.00	3.30	2.60	3.60	0.80	1.30
FeO	7.90	7.40	4.20	4.30	4.40	8.00	7.70	7.10	4.00	9.60	6.10
MnO	0.15	0.22	0.20	0.17	0.15	0.22	0.23	0.24	0.23	0.18	0.17
MgO	24.80	26.00	36.57	36.04	35.98	25.50	28.70	27.70	26.50	23.20	27.20
CaO	7.10	5.62	0.48	0.61	0.67	7.30	5.10	2.30	11.80	6.34	6.20
Na2O	0.06	0.30	0.02	0.03	0.06	0.29	0.07	0.05	0.07	0.10	0.20
K2O	0.02	0.01	0.01	0.01	0.01	0.02	0.02	0.01	0.02	0.09	0.02
P2O5	0.04	0.05	0.03	0.03	0.03	0.04	0.04	0.03	0.03	0.05	0.03
H2OT	6.00	5.20	10.90	9.60	9.60	6.70	6.00	5.00	5.70	1.10	6.50
CO2	bl	bl	0.44	0.29	0.17	1.30	1.90	13.00	7.30	2.20	6.30
Total	99.32	100.65	99.41	99.24	99.22	98.47	96.85	86.38	92.84	96.35	93.90
Ba	51	9	nd	9	nd	nd	nd	nd	nd	nd	nd
Co	94	85	nd	72	nd	84	85	94	74	75	79
Cr	2000	1700	nd	1300	nd	2400	2200	4100	2500	1800	2700
Cu	110	9	nd	13	nd	35	33	36	32	bl	52
Nb	nd	nd	nd	nd	nd	nd	nd	nd	nd	nd	nd
Ni	1490	2200	nd	1800	nd	1200	1500	990	1000	700	1300
Rb	bl	9	nd	3	nd	nd	nd	nd	nd	nd	nd
Sr	36	bl	nd	bl	nd	49	72	24	360	53	43
V	72	120	nd	89	nd	200	150	100	170	80	100
Y	nd	nd	nd	nd	nd	nd	nd	nd	nd	nd	nd
Zn	100	69	nd	58	nd	66	79	80	32	bl	61
Zr	24	64	nd	19	nd	nd	nd	nd	nd	nd	nd
Sc	20	15	nd	12	nd	27	31	13	29	18	19
AN	95.64	85.74	92.81	91.77	86.04	89.29	96.37	93.15	100.00	95.04	89.70
Q	-	-	-	-	-	-	-	-	-	-	-
or	0.12	0.06	0.06	0.06	0.06	0.12	0.12	0.06	-	0.53	0.12
ab	0.51	2.54	0.17	0.25	0.51	2.45	0.59	0.42	-	0.85	1.69
an	11.13	15.27	2.19	2.83	3.13	20.47	15.73	5.75	4.81	16.20	14.87
lc	-	-	-	-	-	-	-	-	0.09	-	-
ne	-	-	-	-	-	-	-	-	0.32	-	-
C	-	-	1.29	0.83	0.51	-	-	-	-	-	-
di	18.94	9.74	-	-	-	12.29	7.40	4.33	32.59	11.92	12.40
hy	46.38	46.23	33.93	46.10	47.10	9.37	12.40	37.26	-	51.05	16.59
ol	14.23	18.52	47.89	36.62	35.51	43.80	50.35	30.72	42.70	12.60	39.25
mt	1.45	2.32	2.39	2.44	2.39	2.61	2.60	2.39	2.31	1.16	1.80
il	0.47	0.66	0.28	0.34	0.28	0.57	0.55	0.20	0.17	0.74	0.53
ap	0.09	0.12	0.07	0.07	0.07	0.09	0.09	0.07	0.07	0.12	0.07

	S2-204 (GSC)	S3-506 (GSC)	S3-4009 (GSC)	S3-4010 (GSC)	S3-4011 (GSC)	S2-1206 (GSC)	S2-147A (GSC)	S2-215B (GSC)	S2-120C (GSC)	S3-003 (GSC)	S2-147A (GSC)
CaO/Al2O3	1.69	0.92	0.23	0.32	0.38	0.91	0.86	1.05	6.21	1.02	1.07
CaO/TiO2	28.4	16.1	3.2	3.4	4.5	24.3	17.6	15.3	131.1	16.3	22.1
Al2O3/TiO2	16.8	17.4	14.2	10.7	11.8	26.7	20.3	14.7	21.1	15.9	20.7
Sc/Zr	0.03	0.23	-	0.63	-	-	-	-	-	-	-
Ti/Zr	63	33	-	57	-	-	-	-	-	-	-
Ti/Sc	75	140	-	90	-	67	56	69	19	130	88
Ti/V	20.8	17.5	-	12.1	-	9.0	11.6	9.0	3.2	29.3	9.3
V/Zr	3.0	1.9	-	4.7	-	-	-	-	-	-	-
V/Sc	3.6	8.0	-	7.4	-	7.4	4.8	7.7	5.9	4.4	9.5
Al/Zr	926	504	-	537	-	-	-	-	-	-	-
Al/Sc	1111	2151	-	851	-	1567	1007	895	347	1022	1615
Mg#	84	85	91	91	92	83	84	85	88	88	88

Appendix B3. (continued)

	S3-4033 (GSC)	S3-4034 (GSC)	S3-4035 (GSC)	S3-4036 (GSC)
SiO2	41.20	41.63	40.88	43.35
TiO2	0.07	0.06	0.06	0.05
Al2O3	1.97	1.06	0.69	0.41
Fe2O3T	nd	nd	nd	nd
Fe2O3	1.68	1.15	1.59	1.23
FeO	4.50	5.10	5.10	4.40
MnO	0.24	0.24	0.27	0.17
MgO	41.46	41.94	42.40	39.84
CaO	0.02	0.03	0.07	0.06
Na2O	bl	0.03	bl	0.01
K2O	1.56	0.76	0.38	0.16
P2O5	0.03	0.04	0.03	0.02
H2OT	7.40	8.00	8.50	9.60
CO2	bl	bl	bl	bl
Total	100.13	100.04	99.97	99.30
Ba	36	23	15	13
Co	85	83	91	100
Cr	1400	1300	1300	2500
Cu	98	6	10	23
Nb	nd	nd	nd	nd
Ni	2200	2300	2100	2600
Rb	222	117	61	25
Sr	bl	17	15	14
V	21	26	25	36
Y	nd	nd	nd	nd
Zn	71	82	96	98
Zr	bl	bl	bl	bl
Sc	56	8	8	5
AN	0.00	79.58	100.00	66.37
Q	-	-	-	-
or	9.22	4.49	2.25	0.95
ab	-	0.25	-	0.00
an	0.10	0.11	0.15	0.17
lc	-	-	-	-
ne	-	-	-	-
C	0.32	0.23	0.22	0.16
di	-	-	-	-
hy	9.00	18.21	19.01	38.25
ol	71.72	67.10	66.59	48.17
mt	2.28	1.67	2.26	1.78
il	0.13	0.11	0.11	0.09
ap	0.07	0.09	0.07	0.05

	S3-4033 (GSC)	S3-4034 (GSC)	S3-4035 (GSC)	S3-4036 (GSC)
CaO/Al2O3	0.01	0.03	0.10	0.15
CaO/TiO2	0.3	0.5	1.2	1.2
Al2O3/TiO2	28.1	17.7	11.5	8.2
Sc/Zr	-	-	-	-
Ti/Zr	-	-	-	-
Ti/Sc	70	45	45	50
Ti/V	20.0	13.9	14.4	8.3
V/Zr	-	-	-	-
V/Sc	3.5	3.3	3.1	6.0
Al/Zr	-	-	-	-
Al/Sc	1737	701	456	361
Mg#	93	93	93	93

Appendix B4. (Aberdeen Lake komatiites)

	L245-1	L245-3	L245-12	L245-18	L245-24	L245-27	L57-2	L57-3	L57-5
SiO2	40.77	39.69	41.41	46.04	38.59	38.36	46.34	45.14	42.87
TiO2	0.31	0.09	0.17	0.11	0.22	0.20	0.16	0.35	0.11
Al2O3	6.00	2.02	1.70	2.33	2.14	2.42	4.03	8.40	2.77
Fe2O3	8.54	8.69	9.87	7.37	8.59	12.10	11.22	10.21	10.10
MnO	0.34	0.07	0.07	0.07	0.10	0.10	0.22	0.14	0.12
MgO	15.79	36.60	35.21	33.52	36.39	34.16	31.62	23.96	34.70
CaO	9.72	0.14	0.16	0.10	0.36	0.09	1.04	6.73	0.13
Na2O	0.22	0.19	0.26	0.20	0.14	0.23	0.35	0.03	0.19
K2O	0.03	bl	0.01	0.01	0.01	0.02	0.02	0.09	0.02
P2O5	bl	bl	bl	0.10	0.02	bl	bl	bl	bl
H2O(LOI)	nd	nd	nd	nd	nd	nd	nd	nd	nd
CO2	nd	nd	nd	nd	nd	nd	nd	nd	nd
Total	81.72	87.57	88.86	89.93	86.56	88.40	95.00	95.05	90.37
Co	nd	49	64	nd	75	100	90	70	63
Cr	2334	2362	1800	1802	1930	1776	2076	2574	1039
Nb	2	bl	1	1	bl	2	bl	4	bl
Ni	607	2071	2013	2492	2536	2519	2499	1029	2722
Rb	bl	bl	bl	bl	bl	bl	bl	3	1
Sr	7	1	bl	bl	bl	bl	4	29	4
V	147	79	33	40	40	33	52	172	71
Y	34	11	10	15	10	10	16	21	15
Zn	39	50	49	55	31	72	00	49	77
Zr	39	7	4	3	3	6	12	23	6
Sc	nd	10	9	nd	12	14	13	26	10
AN	09.15	30.17	26.51	12.41	50.29	69.41	75.50	72.94	20.63
or	0.10	-	0.06	0.06	0.06	0.12	0.12	0.53	0.12
ab	1.06	1.61	2.20	1.69	1.10	1.95	2.96	7.02	1.61
an	15.30	0.69	0.79	0.24	1.66	4.42	9.13	10.93	0.64
C	-	1.45	0.97	1.90	1.29	0.40	0.09	-	2.20
di	26.22	-	-	-	-	-	-	11.47	-
hy	20.47	29.40	36.20	61.13	26.29	20.90	46.53	22.72	40.56
ol	5.01	51.23	45.00	21.55	52.43	56.01	33.31	30.99	41.04
mt	3.00	2.00	2.00	2.00	2.00	2.00	2.00	3.00	2.00
il	0.59	0.17	0.32	0.21	0.42	0.30	0.30	0.66	0.21
ap	-	-	-	0.23	0.05	-	-	-	-
CaO/Al2O3	1.62	0.07	0.09	0.07	0.17	0.37	0.46	0.00	0.05
CaO/TiO2	31.4	1.6	0.9	1.6	1.6	4.5	11.5	19.2	1.2
Al2O3/TiO2	19.4	22.4	10.0	21.2	9.7	12.1	25.2	24.0	25.2
Mg#	04	92	91	93	92	09	09	07	90

Appendix B5. (Woodburn Lake Group calc-alkaline suite)

	AK-2	AK-9	AK-9	AK-11b	AK-13c	AK-5a	AK-6a (GSC)	AK-6a (GSC)	AK-6c	K326A (GSC)	K347 (GSC)
SiO2	70.99	75.83	75.70	76.00	72.49	63.65	58.32	58.50	62.25	70.50	76.50
TiO2	0.31	0.01	0.04	0.12	0.06	0.45	1.00	1.12	0.45	0.26	0.09
Al2O3	15.05	13.85	14.00	14.40	13.26	14.63	16.10	16.00	14.81	14.90	14.40
Fe2O3T	1.90	1.02	nd	0.67	1.61	4.03	9.41	nd	6.26	nd	nd
Fe2O3	nd	nd	0.30	nd	nd	nd	nd	1.60	nd	1.00	0.40
FeO	nd	nd	0.60	nd	nd	nd	nd	6.50	nd	0.70	0.50
MnO	0.03	0.02	0.03	0.02	0.05	0.11	0.15	0.17	0.20	0.13	0.03
MgO	1.02	0.15	0.25	0.00	0.27	2.30	2.61	2.79	1.85	0.44	0.24
CaO	0.69	0.52	0.55	0.46	0.71	3.76	4.40	4.66	4.95	2.92	0.69
Na2O	6.40	3.33	2.90	1.04	4.43	2.57	2.95	2.20	5.00	4.10	3.50
K2O	1.62	3.97	4.01	3.70	2.52	3.64	2.99	3.02	0.65	1.79	3.26
P2O5	0.09	bl	0.02	0.04	0.04	0.12	0.00	0.13	0.10	0.11	0.07
H2O(LOI)	nd	nd	1.10	nd	nd	nd	nd	2.40	nd	0.00	0.50
CO2	nd	nd	1.00	nd	nd	nd	nd	1.40	nd	2.20	0.30
Total	98.10	98.70	100.50	97.33	95.44	95.26	98.10	100.49	96.61	99.85	100.40
B	nd	nd	20	nd	nd	nd	nd	72	nd	nd	nd
Ba	nd	nd	1120	nd	nd	nd	nd	600	nd	nd	nd
Co	nd	1	nd	nd	nd	26	12	15	31	nd	nd
Cr	12	18	nd	17	8	101	20	20	40	137	137
Cu	nd	nd	6	nd	nd	nd	nd	3	nd	nd	nd
Nb	bl	4	nd	7	7	nd	4	nd	nd	nd	nd
Ni	41	17	00	20	35	62	30	100	75	nd	nd
Rb	30	115	130	129	110	135	140	140	10	nd	nd
Sr	250	121	130	117	93	233	509	530	429	nd	nd
V	34	bl	19	3	bl	94	bl	75	70	nd	nd
Y	7	9	21	bl	bl	13	16	26	16	nd	nd
Zn	23	22	20	45	166	55	129	130	01	nd	nd
Zr	111	50	50	02	57	97	110	100	107	nd	nd
Sc	nd	1	nd	nd	nd	14	13	nd	10	nd	nd
AN	4.97	0.39		10.67	0.00	44.70	45.97		26.74	20.41	9.10
Q	24.31	39.53		53.24	34.66	22.40	13.00		16.55	33.07	41.00
or	9.57	23.46		22.34	14.09	21.51	17.67		3.04	10.50	19.27
ab	54.16	20.10		0.00	37.49	21.75	25.05		42.99	34.69	29.62
an	2.04	2.50		2.02	3.26	17.63	21.31		15.69	13.77	2.97
C	1.73	3.13		7.06	2.05	-	0.19		-	1.17	4.03
di	-	-		-	-	0.19	-		6.06	-	-
hy	3.66	1.24		2.39	2.00	0.43	14.15		6.34	1.37	1.09
mt	0.92	0.49		0.32	0.70	1.95	3.74		2.03	1.45	0.50
il	0.59	0.02		0.23	0.11	0.05	2.05		0.05	0.49	0.17
ap	0.21	-		0.09	0.09	0.20	0.19		0.23	0.25	0.16
F/(F+M)	0.63	0.06		0.44	0.05	0.62	0.77		0.76	0.00	0.79

Appendix B5. (continued)

	K759C (GSC)	K0006A (GSC)	K567D (GSC)	K793 (GSC)
SiO2	67.00	56.00	62.80	64.10
TiO2	0.64	0.66	0.83	0.52
Al2O3	15.70	15.80	13.40	14.70
Fe2O3T	nd	nd	nd	nd
Fe2O3	2.10	1.70	2.00	1.00
FeO	1.70	5.90	4.80	3.40
MnO	0.06	0.16	0.11	0.12
MgO	1.11	5.69	4.47	3.54
CaO	6.27	6.74	6.05	6.28
Na2O	1.60	3.40	1.60	2.00
K2O	2.09	1.03	1.05	1.17
P2O5	0.28	0.14	0.21	0.16
H2O(LOI)	1.30	2.20	1.70	1.80
CO2	0.10	0.50	0.60	1.40
Total	99.95	99.92	100.42	00.19
B	nd	nd	nd	nd
Ba	nd	nd	nd	nd
Co	nd	nd	nd	nd
Cr	205	205	234	137
Cu	nd	nd	nd	nd
Nb	nd	nd	nd	nd
Ni	nd	nd	nd	nd
Rb	nd	nd	nd	nd
Sr	nd	nd	nd	nd
V	nd	nd	nd	nd
Y	nd	nd	nd	nd
Zn	nd	nd	nd	nd
Zr	nd	nd	nd	nd
Sc	nd	nd	nd	nd
AN	68.38	46.30	66.00	62.06
Q	35.19	7.48	27.36	28.05
or	12.35	6.09	6.21	6.91
ab	13.54	28.77	13.54	16.92
an	29.28	24.81	26.28	27.68
C	0.00	-	-	-
di	-	6.28	5.14	1.97
hy	3.21	19.75	14.63	12.64
mt	3.04	2.46	2.90	1.45
il	1.22	1.25	1.50	0.99
ap	0.65	0.32	0.49	0.37
F/(F+M)	0.77	0.57	0.60	0.56

Appendix B6. (Ketyet River Group basalts, Taylor, 1985)

	T-1	T-2	T-3	T-4	T-5	T-6	T-7	T-8	T-9	T-10	T-11	T-12
SiO2	56.40	55.80	55.20	47.40	54.90	53.80	53.00	57.30	52.80	53.30	51.50	54.20
TiO2	0.89	1.54	1.00	1.76	2.10	0.84	1.53	1.60	2.47	2.20	2.39	2.09
Al2O3	13.60	14.20	14.00	12.40	13.40	14.70	13.30	14.50	12.60	13.50	13.00	13.00
Fe2O3	1.80	8.10	2.30	3.90	8.00	2.30	4.90	4.90	6.80	5.30	12.00	9.40
FeO	7.70	4.50	8.00	12.60	5.60	8.10	7.70	7.00	6.90	5.80	3.50	4.40
MnO	0.15	0.14	0.18	0.21	0.14	0.18	0.12	0.15	0.20	0.10	0.17	0.15
MgO	5.43	2.39	5.04	5.17	2.44	5.52	4.08	2.26	3.30	3.26	3.33	2.53
CaO	4.36	5.63	7.35	8.10	5.81	6.91	3.51	2.52	6.05	4.33	3.75	5.14
Na2O	4.00	4.50	3.00	1.00	3.90	4.20	5.20	5.20	2.70	4.40	3.70	3.80
K2O	0.99	1.57	1.02	0.09	1.87	0.88	3.10	1.20	1.45	2.23	2.56	1.71
P2O5	0.13	0.17	0.12	0.16	0.24	0.10	0.20	0.18	0.35	0.23	0.24	0.25
H2O(LOI)	2.90	2.20	2.30	4.50	2.10	2.20	2.30	2.70	2.70	2.30	2.90	2.30
CO2	1.40	0.20	0.20	3.20	0.10	0.10	1.70	0.50	0.50	1.90	0.20	0.20
Total	99.75	100.14	100.51	100.49	100.60	99.83	100.64	100.89	98.82	98.85	99.24	99.17
Ba	290	270	360	100	490	190	510	600	420	760	480	300
Rb	50	50	60	bl	bl	70	150	40	bl	70	bl	70
Zn	100	130	110	130	140	100	160	130	150	210	170	140
AN	32.41	26.76	46.11	77.46	29.09	34.43	8.17	20.47	44.04	22.00	26.53	29.36
Q	8.04	5.07	8.04	10.15	7.43	1.05	-	8.93	12.04	4.64	3.18	8.48
or	5.85	9.28	6.03	0.53	11.05	5.20	18.32	7.56	8.57	13.18	15.13	10.11
ab	33.85	38.08	25.39	8.46	33.00	35.54	42.67	44.00	22.85	37.23	31.31	32.15
an	16.23	13.91	21.72	29.08	13.54	18.66	3.79	11.33	17.98	10.50	11.30	13.37
ne	-	-	-	-	-	-	0.72	-	-	-	-	-
C	-	-	-	-	-	-	-	0.41	-	-	-	-
di	3.74	10.93	11.56	8.43	11.59	12.33	10.26	-	8.13	7.80	4.82	8.87
hy	23.14	12.24	19.76	27.63	11.58	19.59	-	16.53	14.52	11.07	10.86	13.36
ol	-	-	-	-	-	-	12.93	-	-	-	-	-
mt	2.61	4.41	3.33	4.73	5.22	3.33	4.39	4.49	5.76	5.36	5.64	5.21
il	1.69	2.92	1.90	3.34	3.99	1.60	2.91	3.04	4.69	4.18	4.54	3.97
ap	0.30	0.39	0.28	0.37	0.56	0.23	0.46	0.42	0.81	0.53	0.56	0.58
CaO/Al2O3	0.32	0.32	0.21	0.08	0.29	0.29	0.39	0.36	0.21	0.33	0.28	0.29
CaO/TiO2	4.49	2.92	3.00	0.57	1.86	5.00	3.40	3.25	1.09	2.00	1.55	1.82
Al2O3/TiO2	15.3	9.2	14.0	7.0	6.4	17.5	8.7	9.1	5.1	6.1	5.4	6.2

Appendix B6. (continued)

	T-13	T-14	T-15
SiO2	46.40	62.40	55.80
TiO2	1.81	0.20	1.55
Al2O3	15.50	11.20	13.90
Fe2O3	1.60	4.40	7.80
FeO	8.80	11.80	4.60
MnO	0.22	0.03	0.15
MgO	7.92	1.60	2.22
CaO	7.55	0.23	5.57
Na2O	4.80	2.10	3.60
K2O	0.25	1.11	1.60
P2O5	0.10	0.10	0.19
H2O(LOI)	3.50	3.30	2.20
CO2	2.10	0.20	0.10
Total	99.75	98.75	99.36
Ba	140	200	380
Rb	50	60	50
Zn	130	80	150
AN	41.26	2.67	35.56
Q	-	32.09	10.55
or	1.48	6.56	9.93
ab	28.49	17.77	30.46
an	20.01	0.49	16.81
ne	6.57	-	-
C	-	6.37	-
di	13.73	-	8.13
hy	-	28.64	12.90
ol	19.41	-	-
mt	2.32	2.46	4.42
il	1.92	0.38	2.94
ap	0.23	0.23	0.44
CaO/Al2O3	0.31	0.19	0.26
CaO/TiO2	4.75	10.50	2.32
Al2O3/TiO2	15.3	56.0	9.0

Appendix C1. DCP-AES analytical technique used in determining REE in rocks

The rare earth elements (REE) were analyzed using quantitative direct current plasma atromic emission spectrometry (DCP-AES) within the geochemical laboratory at the University of Ottawa. Samples and standards were prepared for analysis by low temperature multiacid digestion (i.e. HF, HNO_3, $HClO_4$ acids). After the dissolution is complete the remaining solutions of each sample are evaporated to dryness. The resulting salts are then dissolved in 50 ml of 1 N nitric acid. This 50 ml solution is then loaded onto a 1 x 20 cm gradient exchange column of 100 - 200 mesh AG50W-X8 cation resin that has been preequilibrated with 1 N nitric acid. Then, the sample within the column is eluted with 120 ml of 2 N nitric acid. The resulting elute contains most of the major elements and is discarded. Next, the sample is eluted with 50 ml of 6 N nitric acid, followed by another elution with 50 ml of 8 N nitric acid. These two elutes are saved for determination of REE. The columns are then washed and preequilibrated with 100 ml 1 N nitric acid in readiness for the next sample. A flow rate of 1-2 ml/min was maintained during the cation exchange procedure. The saved elutes from each sample are evaporated to dryness on a hot plate. The remaining salts are then brought back into solution with 25 ml of dilute hydrochloric acid. This 25 ml is then analyzed for REE with the DCP instrument.

The instrument used for analyzing the solutions is a Beckmann/Spectrametrics SpectraSpan III atomic emission spectrometer with a single analytical channel and a dynamic background compensator. The plasma source is a Spectrajet III direct current plasma with two spectrographic carbon anodes and a tungsten cathode in an inverted Y configuration. The output of the spectrometer's microprocessor is sent to a microcomputer. The analyses were performed by John Loop (University of Ottawa). The sample solutions were introduced into the plasma through a nebulizer system. The instrument was calibrated through an autocalibration system which needs both a high and a low standard. Calibration standards were prepared for REE analysis by dissolving accurately determined quantities of pure REE oxides in dilute hydrochloric acid. However, these solutions do not take into consideration the matrix effects introduced by various rock types. To compensate for matrix effects, a standard solution with REE contents like BCR-1 was prepared and used as a high standard. This solution was calibrated with extreme care against BCR-1. The REE spectral lines used were chosen on the basis of high sensitivity and minimum line interference. Background corrections were made to minimize spectral noise and interelement corrections. Precision and accuracy of the technique were monitored by running several standards of silicate rocks and a sample of komatiite with known values (INAA by Barnes, 1985). Problems were encountered with the REE determinations of this study, mostly because of the low levels of REE in most samples.

Appendix D1. Source list of mineral and rock data used in mass balance calculations (Table 20, 21, 22, and 23).

For-92 - olivine, grain 1, Smith et al. (1980)

For-91 - olivine, AX-21, Barnes et al. (1983)

For-90 - olivine, grain 2, Smith et al. (1980)

For-89 - olivine, AX-65, Barnes et al. (1983)

For-88 - olivine, AX-48, Barnes et al. (1983)

For-85 - olivine, AX-58, Barnes (1985)

For-83 - olivine, AX-56, Barnes (1985)

Pig - pigeonite, AX-56, Barnes (1985)

Pig-1 - pigeonite, AX-58, Barnes (1985)

Pig-2 - pigeonite, AX-19, Barnes (1985)

Aug - augite, AX-19, Barnes et al. (1983)

Aug-1 - augite, AX-19, Barnes et al. (1983)

Aug-2 - augite, AX-56, Barnes (1985)

Aug-3 - augite, AX-58, Barnes (1985)

Chr-1 - chromite, AX-56, Barnes (1985)

Chr-2 - chromite, AX-58, Barnes (1985)

Mt-1 - magnetite, calculated from stoichiometry

Mt-2 - magnetite, calculated from stoichiometry

Plag-60 - plagioclase (AN_{60}), calculated from stoichiometry

Plag-70 - plagioclase (AN_{70}), calculated from stoichiometry

AK-2 - low-SiO_2 rhyolite, from this study

AK-9 - high-SiO_2 rhyolite, from this study

667642 - Brown River Gneiss, Schau (1982)

667636 - Brown River Gneiss, Schau (1982)